" MEANDERING COMPOUND FLOW "

BY

MANUEL LUIS MAGALHÃES DE LIMA DA SILVEIRA E LORENA

A THESIS SUBMITTED IN FULFILMENT OF THE
REQUIREMENTS FOR THE DEGREE OF
DOCTOR IN PHILOSOPHY
IN CIVIL ENGINEERING
JUNE 1992

UNIVERSITY OF GLASGOW
DEPARTMENT OF CIVIL ENGINEERING
GLASGOW
UNITED KINGDOM

ProQuest LLC.
789 East Eisenhower Parkway
P.O. Box 1346
Ann Arbor, MI 48106 – 1346

"This is for Célia and Leonora"

ACKNOWLEDGEMENTS

I would like to thank the **Science and Engineering Research Council** for their financial support towards the investigation presented in this thesis.

I wish to express my sincere thanks my supervisor **Dr. D. A. Ervine** for his guidance, patience, encouragement and help throughout the course of this work. I would also like to thank all the other members of my working group S.E.R.C. Series B, **Prof. B. Willetts** and **Mr. R. Hardwick** from Aberdeen University, **Prof. R. Sellin** and **Miss. R. Greenhill** from Bristol University, **Dr. D. Knight** and **Dr. Yuen** from Birmingham University, **Dr. Y. Fares** from Surrey University, **Dr. Y. Guymer** from Sheffield University, **Dr. N. Brockie** from Herriot-Watt University and **Dr. K. Shiono** from Bradford University.

The Author is grateful to **Mrs Mary Jonhstone, Mr. David Wilmer** and **Mr. David Ramsbottom** from the Hydraulic Research Ltd, for their invaluable technical assistance in the S.E.R.C. flume Series B, Wallingford.

I would like to express my gratitude to **Prof. Muir Wood(Cormack Professor and Head of the Department), Professor Green(previous Head of the Department) and Professor A. Coull** for allowing the use of the Glasgow University facilities.

I would like to thank **Mr. A. Burnett**, superintendent, for his help and assistance in the procurement of materials used in the Glasgow flume. Special thanks for **Mr. A. Gray** who build the Glasgow flume and gave substantial contributions in the design stage and **Mr. Ian Dickson, Mr. Ken Ryan and Mr. A. Yuill** who gave the technical assistance for electrical and electronic components of the Glasgow flume.

My appreciation to **Miss L. Drysdale** from the Computer Centre of

Glasgow University for her suggestions concerning the choice of the graphics software used in this Thesis.

The Author wishes to acknowledge to all the remainder staff of Civil Engineering Department for their support and understanding that made very pleasant the three years of research work.

The Author is grateful to all his fellow researchers in special, Dr. W. Withers, Paul Addison, Libor Jendele, Russell Manson, James Wark, Dr. K. Jasem, Dr. A. Khan, K. Belkheir, Q. Li and Dr. Liu.

Gratitude to my family and friends by the encouragement without which this thesis would not have been possible.

SUMMARY

The work of this thesis is an experimental study of flow behaviour in meandering compound channels. The work was carried out as part of an S.E.R.C. Research Grant(GR/E/75783) and a large component of the data was measured at the S.E.R.C. Flood Channel Facility located at H.R. Wallingford Ltd. A smaller component of the project was carried out in a flume at the University of Glasgow.

The purpose of the research was to identify the main flow mechanisms in meandering compound flow, to carry out detailed measurements of all the flow parameters, to provide refined flow data for numerical models, and to provide a framework for understanding such complex three dimensional flows so that hydraulic engineers would be more able to predict stage-discharge relationships, design two-stage channels and improve understanding of morphology of river forms during overbank flow.

The Flood Channel Facility at Hydraulic Research Wallingford Ltd is 10 m wide and 50 m long with discharge rates in excess of 1 m^3/s. The main experimental parameters varied were main channel sinuosity(1.374 and 2.04), main channel cross-section(trapezoidal and natural cross-section), depth ratios(floodplain depth/main channel depth) varying between 0 and 0.5 as well as several variations of floodplain roughness. The measurement programme included discharge measurements, local water levels by digital gauges, streamline angle measurements, velocity measurements in two dimensions by mini-propellers, Reynolds shear stress and turbulence intensities by Laser Doppler Velocimeter, boundary shear stress measurements by Preston tube, producing a large comprehensive data set.

A smaller scale complementary physical model study was also conducted at the University of Glasgow investigating the behaviour of one channel bend during overbank flow.

The research has shown very clearly that meandering compound flow behaviour bears little or no resemblance to straight parallel compound flow. Large secondary flow structures are developed which are driven by floodplain flow crossing the main

channel. These cells are transmitted to the bend regions where they completely overcome conventional bend secondary flows causing reversal of cell direction at the bends. Beyond the apex of each bend these cells decay and dump fluid from the main channel on the floodplain on the downstream side.

A detailed parametric study in this thesis also reveals that discharge conveyance in meandering compound flows depends on sinuosity of the main channel, floodplain roughness, main channel aspect ratio and cross-sectional shape, as well as the ratio of meander belt width to total floodway width.

Analysis of results in this thesis also reveals the energy distribution and loss system in meandering compound flows, the flow discharge distribution in each sub-section of the flow field as well as how the force-momentum balance can be applied in such flows, although the later analysis shows the difficulty in producing any trends in apparent shear force, comparable to straight/parallel cases. The thesis concludes with some pointers to one-dimensional model which might be adopted for discharge conveyance calculations.

TABLE OF CONTENTS

INDEX OF TABLES

CHAPTER 4

CHAPTER 5

CHAPTER 6

LIST OF FIGURES

CHAPTER 3

CHAPTER 4

CHAPTER 7

INDEX OF THE APPENDIXES

NOMENCLATURE

A = Total cross-section area

A_c = Main channel cross-sectional area

A_f = Floodplain cross-sectional area

AST_S = Apparent shear stress

a = The meander double amplitude

B_c = Main channel top width

B_f = Floodplain bottom width

BW_i = Body weight component

BSF_i = Boundary shear force component

C = The Chezy roughness coefficient

COH = Section coherence

CL = Cross-over length

D = Local flow depth

d = Diameter of the Preston tube.

F_1 = Actual discharge/theoretical discharge for inbank flows

F4 = Actual discharge/theoretical discharge for overbank flows using imaginary vertical walls method

F5 = Actual discharge/theoretical discharge for overbank flows using imaginary horizontal walls method

f = The Darcy-Weisbach friction factor

f_c = Friction coefficient for a flow around a bend

f_d = Frequency of the Doppler shift

f_s = Frequency of scattered light

f_i = Frequency of incident light

g = The acceleration of gravity

H = Total flow depth

h = Floodplain flow depth

h_L = Head loss

K = Turbulent kinetic energy per unit mass

k_m = Main channel roughness

k_f = Floodplain roughness

l_s = Length scale related to the width of the lateral shear layer

M_{ij} = Momentum flux

n = The Manning's roughness coefficient

P = Wetted perimeter of the total cross-section

P_c = Wetted perimeter of the main channel

P_f = Wetted perimeter of the floodplain

PF_i = Pressure force component

ΔP_p = The Preston tube reading

p = Pressure

q = Longitudinal unit flow(discharge per unit width)

R = The hydraulic radius

$\mathbb{R}$ = The Reynolds Number($4Q/P\nu$)

R_c = Central radius of a river bend

r = Sinuosity of a river meander

r = General radius of a river bend

S_0 = Bed slope

s_x = Longitudinal slope of channel bed

s_y = Lateral slope of channel bed

U = Average Streamwise Velocity

U_* = Shear velocity ($\sqrt{(\tau_0/\rho)}$)

u'= Fluctuation velocity component in the longitudinal direction

$-\rho\overline{uv}$ = Reynolds stress

$-\rho\overline{uw}$ = Reynolds stress

V = Average transverse velocity

V_R = The resultant velocity

Δ V = Velocity difference across the lateral shear layer

v'= Fluctuation velocity component in the transverse direction

W = Average vertical velocity

W_t = Total channel width of a compound cross-section

W_m = Meander belt width

w'= Fluctuation velocity component in the vertical direction

x = Longitudinal coordinate direction

y = Lateral coordinate direction

z = Vertical coordinate direction

z_p = the lateral distance across floodplain

α = Cross-over angle of a meander

δ = Width of the shear layer

δ_f = Distance between fringes

τ_0 = Local bottom shear stress

τ_{as} = Depth averaged apparent shear stress at the interface main channel/floodplain

τ_b = Shear stress for channel bottom

τ_{bj} = Bottom shear stress at the junction floodplain/main channel

τ_c = Bottom shear stress on the main channel

τ_f = Bottom shear stress on the floodplain

τ_w = Shear stress for channel side wall

τ_∞ = The plateau shear stress on the bed of a wide floodplain

τ_{xy} = Depth averaged transverse shear stress

ε = Rate of dissipation of the turbulent kinetic energy

ϕ = Index of the relative flow depth

Θ_1 = Angle between laser beams

Φ = Index of the degree of interaction between main channel and floodplain for straight compound channels

υ = Kinematic viscosity

υ_s = eddy viscosity arising from secondary currents

υ_t = eddy viscosity arising from turbulence

λ_m = The meander wave length

λ_1 = Wave length of incident light

ρ = Fluid density

γ = Specific weight

Θ = Angle of the current in relation to the streamwise direction

CHAPTER 1

INTRODUCTION

1.1 RIVERS and FLOODPLAINS

1.2 CONTROLLING FLOODS

1.3 THE COMPOUND CROSS-SECTION - A BETTER SOLUTION

1.4 BACKGROUND AND PURPOSE OF THE WORK

1.5 LAYOUT OF THE THESIS

CHAPTER 1

INTRODUCTION

1.1 RIVERS and FLOODPLAINS

Rivers have always been a focus of ancient and modern civilisations. Many benefits can be obtained from rivers such as a supply of drinking water, water for irrigation, access routes to the sea and a possible source of power. Rivers also perform a primary function in land drainage and a secondary more dubious role in waste disposal. Benefits such as these explain why communities settled near rivers on the adjacent floodplains, where the soil is naturally excellent for farming. However, there is at least one significant hazard associated with human settlement on the floodplains adjacent to rivers, the risk of flooding. Another risk is meander migration and development.

The occurrence of river-floods can have serious consequences to such communities, occasionaly resulting in the loss of lives and damage of property. As industry, electricity and water supply are disrupted by floods, the financial consequences are very high. Flooding can also pose serious health risks, especially if the sewage system becomes completely drowned, resulting in sewage backing-up and possible contamination of the water supply system. In order to minimise these adverse impacts, it is important to have efficient floodplain and river management. This will benefit communities and will maintain the balance of the natural environment.

It is common practice of river engineers to use floodplains(which are low lying areas adjacent to the river) as flood storage, forming wetland environments. With the progressive growth of the urban communities, these wetlands should be adequately protected from development and land use. River management should also include a careful control on the degree of river water contamination, including sewage and other kinds of hazardous wastes. Another key area of management is flood

defence, flood alleviation and flood control.

1.2 CONTROLLING FLOODS

Flood control in rivers can take many forms. These include
(i) The construction of regulating reservoirs in the upstream reaches of a river, which can attenuate the peaks of major floods and generally act to smooth-out fluctuations in river flows.
(ii) The construction of floodplain temporary storage areas, where floods are diverted during the rising and peak floods, and drain back to the river during the falling leg of a flood hydrograph.
(iii) The use of sluice gates on a river reach can also prove effective in controlling flood levels and minimising flooding effects.
(iv) Other more localised measures include the raising of flood defense walls especially in urban areas and the use of flood relief channels to bye-pass very sinuous meanders.
(v) Perhaps one of the most common solutions adopted by river engineers is the straightening, widening and deepening(dredging) of a river course, allowing a more efficient passage of a flood. This can have very serious environmental consequences such as removal of trees, natural vegetation, as well as disturbing wild life and fish life. This is further compounded by the introduction of gabions in many cases which can be an eyesore.

A new solution has been developed, namely, the two-stage channel and its concept is described below.

1.3 THE COMPOUND CROSS-SECTION - A BETTER SOLUTION

The term "compound cross-section" or " two-stage channel is defined as a channel with a cross-section whose berms (or floodplains) are normally dry, but in a period of high flood, the berms become inundated. The cross-section shape of a compound

channel contains a central deep channel with symmetrical side berms with horizontal or shallow side slopes. The side berms can be symmetrical on either side of the main channel, or asymmetrical, rough or smooth boundaries. In essence, the main river is allowed to remain in its original condition preserving natural habitat, and the only disruption is the creation of side berms, which can be quickly grassed over retaining a natural look.

Sellin(1991) points out that the concept of a compound channel as shown in **Fig(1.1(a))** is not new, but the construction of the type shown in **Fig(1.1(b)** has become widespread only in recent years. The old concept of straightening rivers has become discredited, because it affects the landscape and destroys the wildlife habitats.

Pursglove(1989) considers that the construction of the two-stage channel is an environmentally sensitive method of coping with river floods. With this solution, the river is allowed to meander more or less as before and the wild habitat vegetation and trees left unaltered. **Figs(1.2(a))** and **Fig(1.2(b))** shows the two-stage channels constructed for the River Roding in Essex and River Ray in Oxfordshire(U.K.). Both cases have been discussed in detail by **Pursglove(1989)**, particularly the River Roding, for which **Sellin and Giles(1988)** have carried out a detailed experimental investigation. In **Fig(1.2(a))** the berms are cut-back as far as the limits of the meanders, replanted in grass, forming an upper confined channel(or floodplain) which inundates with some regularity during the winter high flows. In **Fig(1.2(b))** an existing tree-line is retained by forming the upper channel on one side only.

Ackers(1991) emphasises the environmental, ecological and hydraulic advantages of two-stage channels. He pointed out that, compound cross-sections show more natural appearance and the berms or floodplains provide useful habitats for waterside vegetation and wildlife. However their use should be compatible with inundation from time to time. Therefore precautions should be taken in which concerning the forecast and duration of the

inundations. The hydraulic advantage of compound cross-section stems for the increase of conveyance for a given stage. This benefit is not as great as expected because there is an interaction mechanism between the zones of different depths and consequently the discharge is slightly reduced at flows depths slightly greater than bankfull level. The deep section inserted in the compound cross-section is likely to be self-maintained in sediment point of view than a single wider section with same discharge capacity.

1.4 BACKGROUND AND PURPOSE OF THE WORK

In a world where the public is more and more concerned about the ecological aspects of the planet, the utilization of two-stage channel could be a more sensitive approach for dealing with river floods without damaging the natural environment.

The mechanics of flow in such two-stage channels presents the hydraulic engineer with several problems. How can the stage discharge-curve relationship be predicted with accuracy? What are the most significant main channel/floodplain interactions? What is the effect of the floodplain(upper channel) roughness? What is the effect of sinuosity and planform of the main(lower) channel? What is the effect of main channel size, shape and aspect ratio? What is the long term behaviour of such two-stage channels in view of the fact that larger floods carry most of the annual sediment transport load, and will now carry part of that load onto the side berms(**Ervine and Jasem(1992)**).

As shown schematically in **Fig(1.3)**, two-stage channels can be classified into three main groups:

(i) Straight/parallel compound channels, where the main channel is straight.

(ii) Skewed compound channels, where the main channel is skewed in relation to the floodplain direction.

(iii) Meandering compound channels, where the main channel presents a certain degree of sinuosity.

By the mid eighties, it was felt that the general area of river flooding, overbank flow in natural rivers, as well as two stage channels warranted an extensive research programme at a larger scale than previous model studies.

A strategy report, entitled " The Report of Research Committee Consultative on Flood Protection " published by **MAFF**(Ministry of Agriculture, Food and Fisheries) in April of 1985 recommended the construction of a large Scale Facility at Hydraulics Research Ltd, Wallingford U. K., with the research conducted by academic teams, and research grants sponsored by the Science and Engineering Research Council(S.E.R.C.).

The strategy was to investigate straight and skewed cases, in (i) and (ii) above in the period 1986-89, meandering compound flow, (iii) above, from 1989-91, and finally sediment transport studies in compound flows from 1991-94. These sub-divisions were known as Series A tests(1986-89), Series B tests(1989-91) and Series C tests(1991-94). Series C tests have not yet started due to lack of S.E.R.C. funding.

The work of this thesis is firmly in the realm of Series B tests and was carried out between 1988-1991 with the first year spent solely at Glasgow University and remaining two years alternating between Glasgow and S.E.R.C. flume at Wallingford.

The initial Series A involved four Universities, namely Birmingham(**Dr. Knight and Dr. Shiono**), Bristol(**Dr. Sellin and Dr. Elliot**), Ulster(**Dr. Myers and Dr. Brennan**) and Queen Mary and Westfield College(**Dr. Wormleaton and Dr. Merrett**), respectively. The results obtained from this project were decisive in providing deeper insights into the flow mechanisms and modelling of straight compound channels. Today it is already possible to design straight compound channels with a good degree of confidence. However, the flow mechanisms that develop in meandering compound channels present a degree of complexity much greater than the straight case. The interaction mechanism between the main channel flow and the floodplain flow is complicated by the presence of bends and cross-over regions in plan form. With the exception of **U.S.Army Corps of Engineers(1956)**, experimental

studies of meandering compound flows have been performed in flumes of modest size and with instrumentation of limited capacity. Therefore the knowledge of mechanics of the flow in meandering compound channels was quite limited, and the Series B programme was therefore a natural progression from Series A. Five Universities were involved in the project: Aberdeen (**Prof. Willetts and Mr. Hardwick**), Bristol(**Prof. Sellin and Miss Greenhill**), Birmingham(**Dr. Knight and Dr. Fares**), Glasgow(**Dr. Ervine and the Author**), as well as more specialised tests by Sheffield(**Dr. Guymer and Mr. Brockie**). The project was performed in the same facility 10m wide by 50 m long, with discharges up to $1m^3/s$, and equipped with sophisticated measurement devices, such as orifice meters for flow discharge measurement, digital gauges for stage recording, vane for streamline measurement, mini-propellers for flow velocity measurement, Preston tube for boundary shear stress measurement, Churchill Probes for water surface level measurement and Laser Doppler Velocimeter(L.D.V.) for Reynolds shear stress measurement and turbulence intensity measurement. This flume was located at Hydraulic Research Ltd, Wallingford, U.K..

The list of objectives of this research work were:

a) To investigate the behaviour of sinuous and meandering river channels during episodes of overbank flow onto adjacent floodplains.

b) To investigate the behaviour of sinuous and meandering two-stage channels with flow on the adjacent side berms, in terms of stage-discharge, flow resistance, discharge distribution and momentum exchange.

c) To identify the physical flow mechanisms existing in both cases above, for a range of meandering geometries, overbank flow depths, bed formation, floodplain roughness values and discharge rates.

d) To determine the influence of flow depth, main channel sinuosity, main channel shape, size and aspect ratio, floodplain roughness, floodplain width, and local water levels on the conveyance of meandering compound flows.

e) To determine the magnitude of energy loss distribution in meandering compound flows, including losses due to bed friction, losses due to bend sinuosity, losses due to floodplain flow shearing over the main channel and losses due to turbulent co-flowing shear layers.
f) To carry out detailed measurements of stage, discharge, water surface levels, velocities, boundary shear stress and turbulent flow structure for a range of geometries and parameters.
g) To provide accurate and refined flow data for use in numerical river models, both one-dimensional, two-dimensional and also turbulence models.
h) To analyse scale effects, when comparing S.E.R.C. flume Series B data with data from small scale flumes and field measurements..
(i) To use the boundary shear stress and velocity data for analysis of sediment deposition and scour as well as broader river morphological effects.
j) To propose a theory or model predicting stage discharge in meandering compound flows.
k) To complement the work at the SERC flood channel facility (Series B) with the information obtained from smaller scale studies at Aberdeen, Bristol, Glasgow, Birmingham and Sheffield Universities. Aberdeen concentrated on overall flow structures, Bristol cross-over effects where flood plain flow passes over the main channel at the inflexion points. Glasgow investigated the behaviour of bends during overbank flow and Sheffield dispersion in complex river flow situations. The role of Birmingham centred on the turbulence and boundary shear stress measurements.

In order to accomplish list of objectives presented above, the following parameters were varied in S.E.R.C. flume Series B:
- Sinuosity: 1.37 and 2.04, corresponding to cross-over angles of 60^{o} and 110^{o}.
- Main Channel Cross-Section: Trapezoidal and "Natural"
- Floodplain Roughness: Smooth and Fully Roughened Cases.
- Stage: between 50mm and 300.0 mm(inbank and overbank cases).
- Discharge: between 50 l/s and 1000.0 l/s.

This programme has now provided the largest and most comprehensive data set available in the world on the meandering compound flows. It is not possible to present all the data in this thesis. Instead the data of this thesis is limited to representative examples of the data and detailed analysis carried out by the Author.

1.5 LAYOUT OF THE THESIS

This thesis sets out primarily to present data from the S.E.R.C. flume Series B test programme, to present data from smaller scale model study at the University of Glasgow, and to carry out analysis of the data for more general use in the field of river engineering and also numerical modelling.

Chapter 2 presents a literature review covering straight, skewed and meandering compound flows. Each topic includes the description of

- Flow mechanisms that develop in meandering compound flows.
- The parameters that affect the conveyance of meandering compound channels.
- Physical and numerical models of meandering compound flows.

Chapter 3 describes the design, construction, calibration and running of the S.E.R.C. flume at Wallingford during Series B test and the small scale Glasgow flume. This includes the choice of meander geometries, flow parameters, instrumentation, calibration tests, cross checking, research programme, methodology followed in the tests and a detailed description of each instrument used in the measurement programme.

Chapter 4 presents the stage-discharge data from a range of geometries tested on the S.E.R.C. Series B. The flow resistance in meandering compound channels is made in terms of the relationship between the Manning's n resistance coefficient against the stage and in terms of the Darcy-Weisbach friction factor with the Reynolds number. This analysis was performed with data from S.E.R.C. Series B and compared with data obtained from

S.E.R.C. Series A. The first parametric analysis on the influence of a range of parameters on conveyance in meandering compound flows is also presented in this chapter.

Chapter 5 presents detailed velocity data, description of flow mechanisms, analysis of flow structures such as secondary currents and longitudinal velocities and the implications of these flow mechanisms for sediment transport in meandering compound flows. The data used in the analysis was from S.E.R.C. flume Series B and from Glasgow flume.

Chapter 6 presents a detailed analysis of the S.E.R.C. flume data in terms of the distribution of the discharge in each sub section of the flow, distribution of energy and energy loss in meandering compound flows, as well as force-momentum balance and apparent shear stress approximation.

The purpose of Chapter 6 is to provide the background and basis of a new model being developed at the University of Glasgow, which aims to provide a simplified modelling technique for meandering compound flows in general.

Chapter 7 proposes new ideas towards a model of meandering compound flows, summarises the conclusions presented in Chapters 4, 5 and 6 and indicates new topics for further research in meandering compound flows.

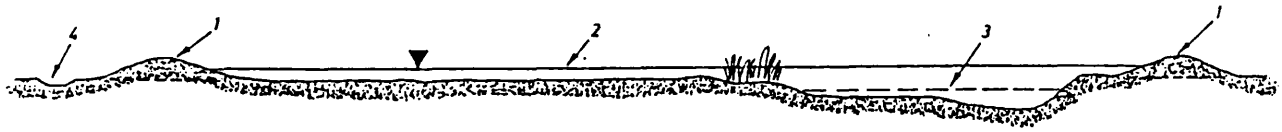

1 -Levee
2 -Flood water level
3 -Summer river level
4 -Back drain

a) Compound channel incorporating natural floodplain

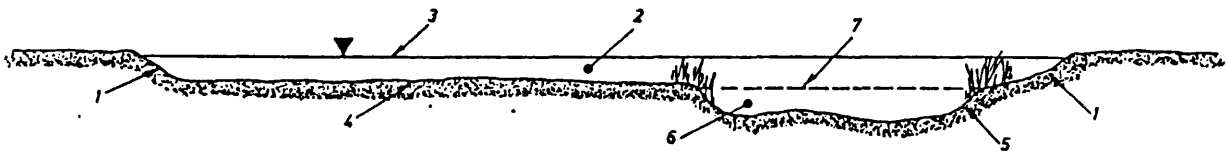

1 -Upper channel bank
2 -Upper channel
3 -Upper bankfull
4 -Berm
5 -Lower channel bank
6 -Lower channel
7 -Lower bankfull

b) Compound channel with berm constructed below natural floodplain level

Fig (1.1) - Types of Compound River Channels in Rural Areas(After Sellin(1991).

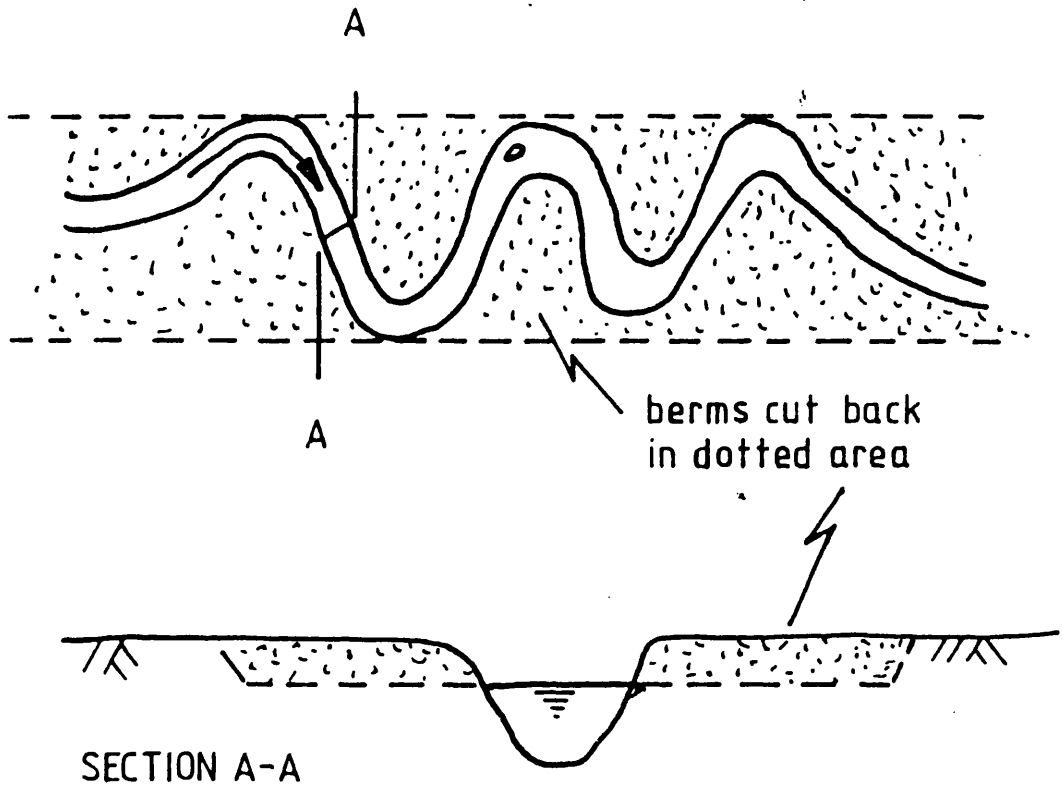

Fig (1.2 a) - Two-Stage Channels(After Pursglove(1989)).

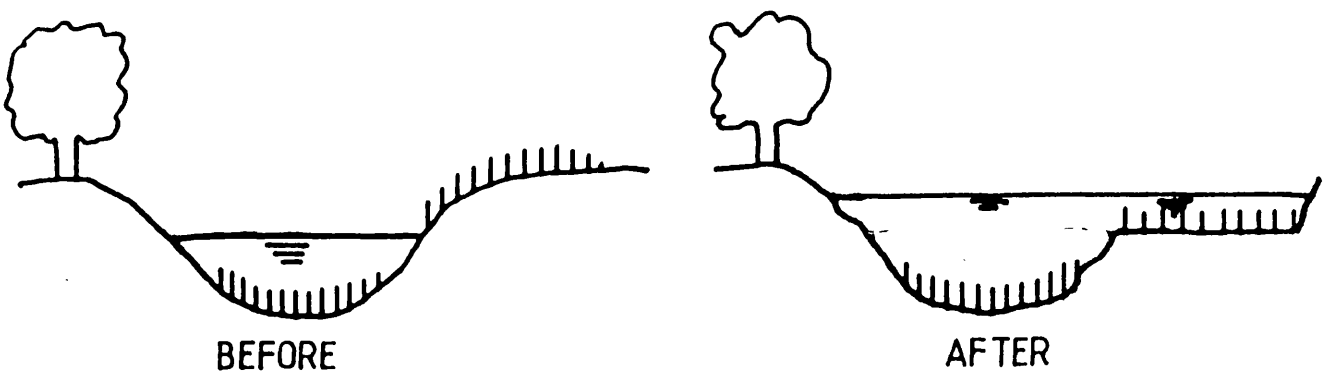

Fig (1.2 b) - River Ray in Oxfordshire(After Pursglove (1989)).

a) Straight Compound Channel.

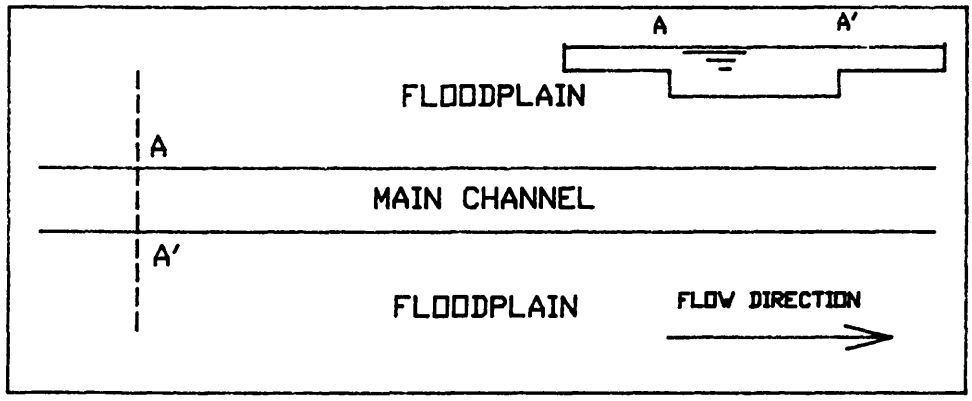

b) Skew Compound Channel.

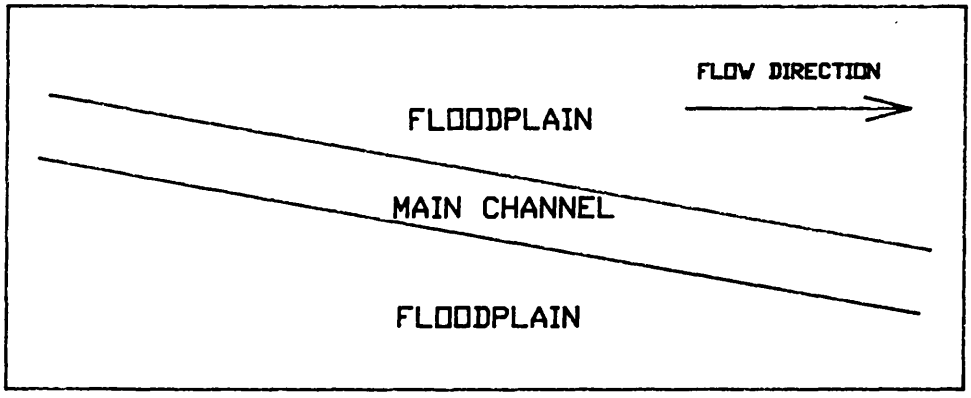

c) Meandering Compound Channel.

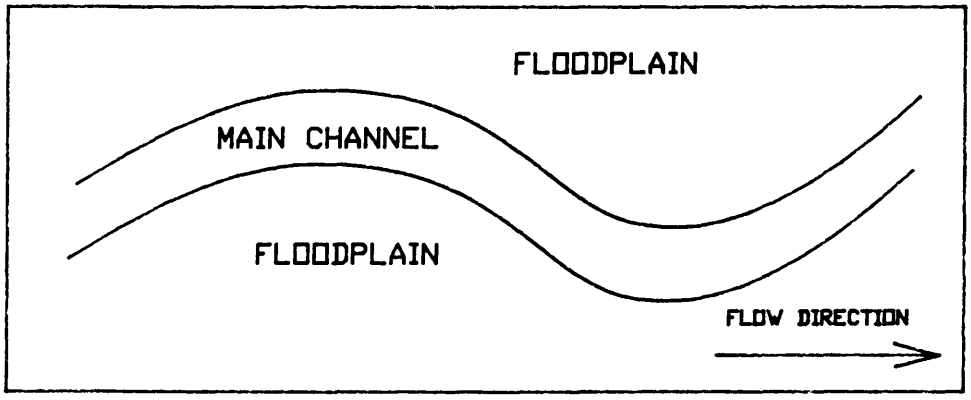

Fig (1.3) - Plan View of Compound Channels. a) Straight Case, b) Skewed Case and c) Meandering Case.

CHAPTER 2

LITERATURE REVIEW

CHAPTER 2

LITERATURE REVIEW

2.1 INTRODUCTION

For more than thirty five years, experiments and calculation methods for the flow field in compound open channels have been carried out experimentally and numerically. Because the flow behaviour in compound channels is a complex phenomenon, the investigation of this subject has concentrated on the least complex case, namely that of straight compound flow. In the last few years skew compound flow has been investigated and most recently meandering compound flow, which is the subject of this thesis. Progress in electronics measurement instrumentation, as well as large increases in computational power has led to a significant extension and shift in compound channels flow research. Secondary currents, the distribution of turbulence quantities and the complex three-dimensional character of the flow situation are now focal topics of recent experimental work on compound channels. The progressive refinement of one-dimensional stage/discharge relationship and empirical friction factor formulae by 2-D and 3-D numerical models have become recent research topics of mathematical modellers worldwide.

In this chapter the Author summarizes the most important findings of research on flow behaviour on compound channels carried out worldwide. The literature review is organized into three main topics:

- Straight Compound Channels
- Skew Compound Channels
- Meandering Compound Channels

reflecting the increase in complexity in each case.

Each topic is subdivided into the following points:

- Flow Mechanisms
- Stage-Discharge Relationships

- Flow Resistance
- Primary Velocities
- Secondary Currents
- Discharge Assessment

For the particular case of straight compound channels the review includes also the following topics:

- Boundary Shear Stress
- Turbulence Intensities and Reynolds Shear Stress

2.2 STRAIGHT COMPOUND CHANNELS

2.2.1 Flow Mechanisms in Straight Compound Channels

It was mentioned by **Goncharov(1964)**, that research into the interaction between the flow in a straight channel and a parallel flood plain started in 1953 by **T.L.Zheleznyakov**, who reported the occurrence of the reduction of flow velocity in the main channel bordered by a submerged floodplain.

Since that date, the investigation of flow mechanisms in straight compound channels has been carried out almost continuously worldwide, mostly in flumes of modest size.

The most recent effort started in 1986 in the U.K. and sponsored by the Science and Engineering Research Council (S.E.R.C.). The research program, entitled Series A, had a duration of three years with an aim to investigate overbank flow behaviour in straight compound channels with a view to providing refined data for numerical models. The research was carried out in a large flume facility, 50 metres length and 10 metres wide located at Hydraulics Research Ltd, Wallingford. The experimental programme included detailed measurements of stage, discharge, velocity boundary shear stress, turbulent velocities and turbulent shear stress. During the test program, several parameters were varied including the aspect ratio of the main channel(top width/bankfull depth); aspect ratio of floodplain width to main channel width; the number of floodplains; the side

slope of main channel; and the roughness of floodplain compared with the roughness of main channel. This research programme was supervised by **Dr. D. Knight** from Birmingham University, **Prof. R. Sellin** from Bristol University, **Dr. Myers** from University of Ulster and **Dr. Wormleaton** from Queen Mary and Westfield College. **Fig(2.1)** illustrates a typical cross-section used in S.E.R.C. flume.

The main flow mechanism in straight compound channels is the appearance of higher velocities in the main channel and smaller velocities on the floodplain. This disparity can lead to large velocity gradients in the region of the interface between the main channel and floodplains, which will create turbulence and produce momentum transfer from the faster moving fluid to slower. This phenomenon, as presented in **Fig(2.2)**, by **Knight(1991)** is better visualised as being a vertical shear layer at the channel/floodplain interface. **Sellin(1964)** presented photographic evidence of banks of vertical vortices generated in this region, which suggested a mechanism of momentum transfer from the fasting moving layers to slower moving layers. These vertical vortices, shown in **Fig(2.3)**, are considered to cause substantial energy loss and to induce secondary currents, as well.

Momentum transfer consists of two components, namely advection by secondary currents and turbulent diffusion. The latter consists of bed and wall friction and shear due to velocity gradients. **Kawara and Tamai(1989)**, have investigated experimentally the momentum transfer across the interface main channel/floodplain in straight compound channels. They suggested that secondary currents play a dominant role in the resulting flow characteristics of momentum transfer to floodplain from main channel. **Fig(2.4)** shows the relative magnitude of advection and diffusion components.

2.2.2 Flow Resistance in Straight Compound Channels.

The equations of **Manning** and **Chezy** have been used widely by

River Engineers for the analysis of flow resistance in prismatic open-channels. However the **American Society of Civil Engineers Task Force Report on Friction Factors** has recommended the adoption of the **Darcy-Weisbach** equation for scientific work. The advantages of using the Darcy-Weisbach friction factor are that it is a non-dimensional parameter and it can be compared with results of pipe flow experiments. The three resistance equations can be related by the following equation:

$$C = R^{1/6} / n = (8\ g / f)^{1/2} \qquad (2.1)$$

where C is the Chezy roughness coefficient, n is the Manning's roughness coefficient, R is the hydraulic radius, g is the acceleration of gravity and f is the Darcy-Weisbach friction factor.

Compound channel behaviour is complicated by the presence of momentum transfer mechanism which affects the conveyance of the channel considerably. This mechanism takes the form of a bank of vertical vortices that spread along the interface of main channel with floodplain. **Sellin(1964)** and **Zheleznyakov(1965)** reported the presence of this mechanism and demonstrated its effects in terms of reduction of deep section discharge and velocity at depths just above bankfull.

Knight et al.(1989), **Myres and Brennan(1989)** and **Ervine and Ellis(1987)** have carried out research on flow resistance on compound channels. These have shown that simple resistance relationships developed for single cross sections can not be applied for compound channels, particularly in view of large changes in hydraulic radius R for flow depths just above bankfull level.

Myers and Brennan(1989) have presented the most exhaustive study of flow resistance in straight smooth compound channels, as part of the SERC Series A research program already mentioned in point 2.2.1. They established flow resistance relationships for compound sections and for the main channel itself and floodplain itself, both in terms of Manning's and Darcy-Weisbach resistance coefficients simple channel shapes. Their results are presented in **Fig (2.5)** and show that both resistance coefficients reduce

significantly in value at depths just above bankfull but increase to simple channel values with increasing depths of flow on the floodplain. They conclude that resistance relationships for compound channels are of more complex nature than those applicable to simple channels, indicating the presence of other variables relating to the influence of momentum transfer mechanism.

Based on field measurements at Montford bridge on the river Severn(**Fig(2.6(a))**), **Knight(1989)** noticed similar behaviour for the variation of Manning coefficient against stage. He also refers the existence of a loop for the variation of Darcy Weisbach friction factor against Reynolds Number, as shown in **Fig(2.6(b))**, for the same River.

Ackers(1991) in his" Design Manual for Straight Compound Channels", gives an explanation for the behaviour of Manning's and Darcy coefficients. As the flows spread to cover the floodplain the **Manning's** n value drops by approximately a third, despite the fact that in reality the roughness of the floodplain is not greater than the main channel. This spurious reduction in resistance is due to the form of **Manning's** equation. The hydraulic mean depth falls as the floodplain becomes inundated. This effect is the result of treating such a complex section as one single section. In relation to the ocurrence of the loop in the variation of friction factor against Reynolds number, as shown in **Fig(2.6(b))**, are two explanations:

- as the floodplains become inundated, the reduction of R with increase of stage, yields a reduction in friction factor not related to the actual increase of flow resistance.
- by expressing Reynolds number as $4Q/P\upsilon$, the rapid increase of P as the floodplain becomes inundated over-rides any increase in discharge.

These two effects combined together produce a looped function that does not have any physical meaning. This demonstrated that both P and R are not monotonic functions with stage. He concludes his remarks by recommending that: the cross-section should not be

treated as a single section; the floodplains berms should be treated separately from the main channel. Ackers also proposes that Manning's n should be used only as a roughness element related to the physical roughness of the channel. All other influences on channel resistance must be quantified separately by appropriate factors.

In general, the S.E.R.C. flume study showed that flow resistance and flow interaction in straight compound flows:

- decrease with increasing relative flow depth;
- decrease with increasing aspect ratio of the main channel;
- increase with increasing ratio of flood plain width to main channel width;
- decrease with increasing main channel side slope;
- increase with increasing ratio between flood plain roughness and main channel roughness.

2.2.3 Stage-Discharge Relationships in Straight Compound Channels.

Many researchers such as **Sellin(1964)**, **Bhowmik and Demissie(1982)**, **Myers and Brennan(1989)**, **Kiely(1989)**, and **Nalluri and Judy(1985)** have analysed the behaviour of the stage/discharge curve of a straight compound channel in detail.

Sellin(1964) was amongst the earliest to identify the anomaly or discontinuity in the stage discharge curve relationship. He observed that as the flow just overtops the bankfull level, the overbank flow reduces the velocities of the flow contained within the normal inbank channel. Hence the measured overbank discharge for low depths was found to be less than the inbank one. As the floodplain depth continues to increase the discharge starts to increase again.

In order to determine the distribution of flow in the main channel and in the floodplains **Bhowmik and Demissie(1982)** carried out measurements in real rivers. They observed, as shown in

Fig(2.7), the average velocity on the flood plain increases as the stage increases. The average velocity for total flow section shows a sharp decrease as the stage starts to increase above bank-full condition. After a certain stage this average velocity attains a minimum value and then it starts to increase with a rate and magnitude much like that on the floodplain. They reported that the minimum averaged velocity for the composite section in real rivers was reached at a stage where the averaged depth in the floodplain was about 10-20% of the depth in the main channel.

Myers and Brennan(1989) carried out, in S.E.R.C. flume, extensive research of channel carrying capacity of compound cross sections. Their work on the S.E.R.C. flume at HR Ltd Wallingford, tested four ratios of B/b(total width of the compound channel divided by the base width of the main channel) over the range 1.2, 2.2, 4.2 and 6.67 respectively. The stage/discharge curve was plotted in log-log scale as shown in Fig 2.8 and the linear correlation obtained was excellent. They pointed out that the most notable feature of these relationships was the discontinuity at bankfull depth, with reduction in discharge as depth rises just above bankfull value. The reduction of discharge at low overbank depths is produced by the presence of highly turbulent shear layer with associated energy losses at the junction location between floodplain and main channel. It can be seen from **Fig(2.8)** that increasing the ratio B/b has the effect of increasing the interaction effect.

Nalluri and Judy(1985) investigated the effect of varying the shape of the main channel cross section as well as the flood plain roughness on the stage/discharge curve of straight compound channels. The two cross sections studied were trapezoidal and rectangular, respectively. The presence of dense and partially submerged (tall vegetation) roughness on flood plain of natural rivers was simulated in their tests using flexible roughness. **Fig(2.9(a))** shows a plan view of the flume and the cross-sections used by **Nalluri and Judy(1985)**. The resistance coefficient Manning's n, shown in **Fig(2.9(b))**, was found to be widely

affected by the roughness distribution as well as the relative depth ratio y_f/y_c, where y_f is the floodplain flow depth and y_c is the total flow depth. They conclude that the rectangular cross section for stages just above bankfull shows a more pronounced effect in decreasing the discharge than the trapezoidal section. In which concerns the effect of flexi roughness, they noticed a reduction in the carrying capacity of full and sub-sections of compound channels.

2.2.4 Secondary Currents in Straight Compound Channels.

In open channels two types of secondary currents can occur:

i) Skew induced secondary currents that derive their origin to changes in channel plan geometry. River bends are a typical example of this phenomenom with secondary currents induced by non-uniform centrifugal pressure.

ii) Stress induced secondary currents. These usually stem from non-uniform shear stress distribution with resultant momentum transfer to lower velocity and shear stress regions often towards the lower two corners of a channel base.

The accurate measurement of the secondary velocity components in open channel flows is very difficult, because their magnitude is only 1-3% of primary mean velocity. With the advent of Laser Doppler Velocimetry (L.D.V.), the accuracy of measurements of velocity field and turbulence characteristics of compound open channels flows have been improved considerably.

Shiono and Knight(1989) and **Tominaga and Nezu(1991)** have measured the secondary currents in straight compound channels by using of the two-component fibre-optic Laser Doppler velocimeter.

Tominaga and Nezu(1991) carried out experiments in an asymmetrical cross section. It can be seen in **Fig(2.10(a))**, that strong, upward inclined secondary currents are generated from the junction edge toward the free surface in compound channels. The maximum magnitude of this inclined secondary upflow is about 4% of the maximum main-stream velocity. A pair of longitudinal

vortices was recognized on both sides of inclined upflow. When the floodplain bed was rough, the structure of secondary currents was almost the same.

Shiono and Knight(1989) undertook measurements of secondary flow structures in a symmetrical compound channel by using a 2 component LDV. They identified, as shown in **Fig(2.10(b))**, the existence of two major cells in the main channel region, one in the upper layer with a strong upflow and another one in the lower corner with a downflow. These cells vary in strength with the side slope of the main channel section. In the floodplain only one large cell exists, which extends across the majority of the width.

2.2.5 Primary Velocities in Straight Compound Channels.

Several researchers have investigated experimentally the distribution of the longitudinal velocity in straight compound channels, including **Myers(1987)**, **Shiono and Knight(1989)**, and **Tominaga and Nezu(1991)**.

Myers(1987) data, based on smaller scale model studies, produced lateral distribution of depth averaged longitudinal velocity. At low overbank depths, as shown in **Fig(2.11)** the depth averaged velocity profile shows a steep velocity gradient across the interface between the main channel and the floodplain. This gradient reduces when the floodplain depth increases. According to Myers, higher flow depths on the floodplain, a reverse phenomenom can occur with higher velocities on the floodplain than in the main channel. This is usually only true for smooth floodplain boundaries.

Shiono and Knight(1989) normalised profiles of primary velocity by the local shear velocity. **Fig(2.12)** shows experimental velocities across the main channel and floodplain in the S.E.R.C. flume, compared with the standard 2-D logarithmic law. The profiles agree closely with the 2-D logarithmic law in the centre of the main channel and at remote distances on the

floodplain. In the shear layer region on the floodplain region the velocity gradient in respect to z seems to be smaller than that given by the standard logarithmic profile. They also analysed the effect of main channel side slope s=0, 1.0 and 2.0. They verified that the isovels become more distorted in the main channel as the main channel side slope steepens. The interaction effect increases as the main channel side slopes become more rectangular.

Tominaga and Nezu(1991) analysed distributions of primary velocities normalised by the maximum streamwise velocity. From **Fig(2.13)** it can be seen that isovels lines bulge significantly upward in the vicinity of the main channel/floodplain junction. The velocity in this region is decelerated due to momentum transport by secondary currents away from the wall. On both sides of this deccelerated region, the isovel lines bulge towards the solid boundaries due to high momentum transport by secondary currents. They conclude that the structure of the primary mean velocity is affected by the momentum transport due to secondary currents.

Samuels(1989) developed an analytical model to predict the depth-averaged velocity as it varies laterally across main channel and floodplain. This will be discussed in Section 2.2.8 and the method is based on the ability to predict the width of a lateral shear layer at the main channel flood plain junction. This is shown schematically in **Fig(2.14)** with a typical distribution of depth averaged velocity across a compound channel. The relationship proposed for the width of the shear layer was:

$$\delta = 5.7 \left(ghS_0/f \right)^{1/4} \varepsilon^{1/2} \qquad (2.2)$$

Where h is the local flow depth and f is Darcy-Weisbach friction factor, ε is the turbulent eddy viscosity which may be roughly approximated considering only bed generated shear, as $\varepsilon = C_1 U_* h$. U_* is the shear velocity and C_1 is a coefficient.

2.2.6 Boundary Shear Stress in Straight Compound Channels

Myers and Elsawy(1975), Rajaratnam and Ahmadi(1981), Baird and Ervine(1984) Radojkovic(1985) and Shiono and Knight(1989) measured boundary shear stress in straight compound channels using a Preston tube. **Myers and Elsawy(1975)** observed distorted shear stress profiles in compound channels. **Baird and Ervine(1984)** maintained that it is important to be able to predict the bed shear stress profiles on a floodplain for different flow conditions in order to model sediment transport processes. **Radojkovic(1985)** pointed out the dependence of shear stress distribution on the velocity difference between main channel and floodplain flows. **Fig(2.15)** compares the distribution of bed shear stress in a single straight channel with a straight compound channel. Typical values of the boundary shear stress are:

- In a single channel:

$$\tau_b = 0.97\ \rho g y S_0 \text{ for channel bottom}$$

$$\tau_w = 0.75\ \rho g y S_0 \text{ for channel side wall}$$

where τ_b is the maximum boundary shear stress in the channel bottom; y is the flow depth; S_0 is the channel slope; ρ is the fluid density; g is the acceleration of gravity; τ_w is the maximum boundary shear stress on the channel side wall.

- In a compound channel:

$$\tau/\tau_b < 1.0 \text{ in the main channel}$$

$$\tau/\tau_b > 1.0 \text{ in the floodplain channel}$$

where τ is the local value of the boundary shear stress with interacting effect(main channel flow/floodplain flow); τ_b is the value of boundary shear stress with non-interacting effect.

Rajaratnam and Ahmadi(1981) noticed that the bed shear stress on the floodplain increases rapidly as the junction edge is approached. This increase of the bed shear stress on the floodplain was greater with a decrease of h/H(h is the floodplain depth; and H is the main channel depth). They developed the following predictive relationship for floodplain

shear stress using smooth, asymmetrical compound channels,

$$(\tau_b - \tau_{b\infty})/(\tau_{bj} - \tau_{b\infty}) = e^{-0.693 x^2} \qquad (2.3)$$

in which τ_b is the local boundary shear stress on the bed of the floodplain; τ_{bj} is the boundary shear stress on the floodplain bed at the junction of the main channel and the floodplain; $\tau_{b\infty}$ is the plateau shear stress on the bed of a wide floodplain, sufficiently far from the turbulent interface not to be influenced by the momentum transfer mechanism($\tau_{b\infty} = \rho g S_0 y$); $x = z_p / b_p$, z_p is the lateral distance across flood plain and b_p is the value of z_p when the right hand side of equation 2.3 has a value of 0.5. However this relationship is a function of flow depth only and cannot account for different roughness and geometries.

Shiono and Knight(1989) stated that the boundary shear stress distribution in compound channels is affected by secondary flow and lateral shear effects, resulting in additional shear stresses. They based their deduction in the following equation,

$$\rho g H S_0 - \tau_b \left(1 + \frac{1}{S^2} \right)^{1/2} = \frac{\partial}{\partial y} [H((\rho UV)_d - \tau_{yx}] \qquad (2.3a)$$

where $\rho g H S_0$ is the standard two-dimensional value of bottom shear stress, τ_b is the bottom shear stress, $\overline{UV}_1$ is the secondary flow term, τ_{yx} is the depth averaged transverse shear stress, S_0 is the bed slope and S is the side slope (1:S, vertical : horizontal)

As it will be mentioned in section 2.2.8 **Shiono and Knight(1991)** and **Wark et al.(1990)** developed numerical models that can predict bottom shear distribution in compound channels. In general both models fit experimental data quite well. **Fig(2.16)** illustrates the applicability of Shiono's analytical model to S.E.R.C. flume Series A data. The relative importance of the terms of equation 2.3 a will be shown in next section.

2.2.7 Turbulence Intensities and Reynolds Shear Stress in Straight Compound Channels.

Measurements of turbulence characteristics in straight compound channels have been conducted by making use of hot-film anemometers[**Prinos et al.(1985)**], a one-component Laser Doppler Anemometer(LDA)[**McKeogh et al.(1985)**] and more recently by two-component Laser Doppler Velocimeter(LDV)[**Shiono and Knight(1990)** and **Tominaga** and **Nezu(1991)**].

McKeogh et al.(1985) measured turbulent intensities for different depth ratios of flood plain flow depth to main channel flow depth in a straight compound channel with a symmetric cross section. It was discovered that as the depth ratio increases the longitudinal turbulent intensity decreases. From the contours of turbulence intensity (**Fig(2.17)**) it can be seen that there is a transfer of turbulence from the floodplain to the main channel.

Tominaga and **Nezu(1991)** carried out measurements of Reynolds shear stresses and turbulence intensities in an asymmetric compound channel. From the experimental results they verified that the distribution of Reynolds stresses of $-\overline{uv}$ and $-\overline{uw}$, shown in **Fig(2.18)**, is affected by the strong momentum exchange between the main channel and the floodplain. The sign of $-\overline{uv}$ and $-\overline{uw}$ corresponds to the signs of $\frac{\partial U}{\partial y}$ and $\frac{\partial U}{\partial z}$, respectively. All the three components of turbulence intensities present a strong anisotropic behaviour near the free surface and near the main channel/floodplain junction edge.

Shiono and Knight(1990) measured the turbulence intensities u', v' and w' and Reynolds shear stresses τ_{xy} and τ_{zx} in a symetric compound channel. In which turbulence intensities are concerned, they found that the turbulence is not isotropic and the gradient of $[(w')^2 - (v')^2]$ induces secondary flow. As the flow depth ratio decreases both components u' and v' increase whereas the vertical w 'component does not. **Fig(2.19)** shows one of the plots of vertical profiles of turbulence intensities u', v' and w' normalised by the local friction velocity U*. Experimental measurements of Reynolds shear stresses τ_{zx} and τ_{yx}

are shown in **Fig (2.20)** and **Fig (2.21)**, respectively. At the centre of the main channel and in remote zones of the floodplain, they noticed that the vertical distribution of τ_{zx} was approximately linear, indicating the flow was in these regions predominantly 2-D with normal turbulence structure. In the shear layer region, the distribution of τ_{zx} was non linear, especially near the edge of the main channel/floodplain. This effect becomes more pronounced with a decrease of relative flow depth. The value of lateral shear τ_{yx} is presented in **Fig(2.21)** reaching a maximum at the main channel-floodplain interface. Outside the lateral shear layer the values of τ_{yx} are practically zero, indicating no transverse turbulence effects and very little lateral momentum transfer. The gradient of τ_{yx} in respect to y was negative in the main channel and positive on the floodplain. Further insights into the relative magnitude of each of the shear stress terms can be obtained by considering the **x** component of the steady uniform flow of **Reynolds** equation:

$$\frac{\partial\ \rho UV}{\partial\ y} + \frac{\partial\ \rho WU}{\partial\ z} = \rho\ g\ \sin\ \Theta_1 + \frac{\partial\ \tau_{yz}}{\partial\ y} + \frac{\partial\ \tau_{xz}}{\partial\ z} \qquad (2.4)$$

where $\sin\Theta_1$ = bed slope, $\tau_{yx} = -\rho\overline{uv}$, $\tau_{zx} = -\rho\overline{uw}$, ρ is the density of water and g is the gravitational acceleration. Integration from any point z to the water surface H, gives:

$$\underbrace{\int_0^H \frac{\partial\ \rho UV}{\partial\ y}\, dz}_{\text{Term I}} + \underbrace{\rho UW}_{\text{Term II}} + \underbrace{\rho g\ (\ H-z)\sin\Theta_1}_{\text{Term III(a)}} + \underbrace{\int_0^H \frac{\partial\ \tau_{yx}}{\partial\ y}\, dz}_{\text{Term III(b)}} - \tau_{zx} = 0 \qquad (2.5)$$

considering $\bar{w} = 0$ and $\tau_{zx} = 0$ at $z = H$. The first two terms(I) represent the contribution from the secondary flow, the third term(II) is the contribution from the water surface slope and the fourth term(III) is the contribution from the lateral shear turbulence. The individual contributions of several terms are shown in **Fig(2.22)** and when summed give the resultant of vertical distribution of Reynolds shear stress τ_{zx}(dotted line). The non-linearity of τ_{zx} is highlighted.

2.2.8 Methods for Discharge Assessment in Straight Compound Channels.

The design of two stage-channels or compound channels has been an area of increasing interest to river engineering. In general rivers have compound sections, possessing a main channel which usually carries flow and one or two floodplains that transport flow during the occurrence of a major flood. The application of artificial compound channels in flood relief schemes has become a more common technique used by the river engineers. Basically the berms are cut on either side of the existing channel. This allows the conveyance of compound channel to be increased and the downstream water levels to be decreased, during the occurrence of floods. **Sellin(1989)** presents an example of application of this method to the river Roding, as described in **Chapter 1.**

In the design of compound channels it is fundamental to have a method that enables estimates of the stage-discharge relationship. Methods for stage/discharge assessment in straight compound channels can be arranged in three main groups:

- Empirical methods subdivided into:
  - The Single Channel Method
  - The Division Line Methods
  - The Apparent Shear Force Method
  - The Method of Correction Factors
- Mathematical Models subdivided into :

Numerical methods

Analytical procedures

- The New Method Purposed by **Ackers(1991)**
- Single Channel Method

In this case the complete channel is treated as a single unit. Usually no account is taken of roughness variation across the channel, although composite friction factors have been employed. **Wark(1990)** verified that this method underpredicts flows by up to 30% at low overbank stages.

- Division Line Methods

The main channel and the floodplains are sub-divided and the flow is calculated in each sub-area separately. Variations in roughness can be included and the total flow is obtained by summation. There are many sub-division methods which differ in position and direction of dividing lines, and whether or not these lines are included when calculating the wetted perimeters of sub-areas. Some of the dividing lines used in the application of this method are sketched in **Fig(2.23)**

Chow(1959) and Posey(1967) advocate the application of this method for the calculation of stage-discharge curve for a straight compound channel. Because this method neglects the turbulent shear interaction and momentum transfer it tends to overpredict the total flow by significant margins, **Ramsbottom(1989)**. In **Fig (2.24) James and Brown(1977)** compare the stage-discharge curve obtained by the single method and the division line method against the actual curve. It is clear that errors induced by both methods will considerably affect the estimation of the conveyance of a compound section.

- Apparent Shear Force Method

This method is based in the consideration of the force momentum equilibrium equation applied to a compound channel. Assuming that the flow is in steady and uniform, the body weight is in balance by the boundary shear stress integrated along the wetted perimeter.

$$\tau_{av}*(B_m+2B_f+2H)=\rho g A_T S_0 \qquad (2.6)$$

Where τ_{av} is the averaged boundary shear stress, B_m is the bottom width of the main channel, B_f is bottom width of the floodplain, H is the depth of flow in the main channel and A_T is the total cross section area of the compound section.

Ervine and Baird(1982) considered both main channel and floodplain areas(as presented in **Fig(2.25)**) are separated by imaginary vertical walls. Applying the momentum equation to each zone, they obtained the following equation:
For the main channel

$$\tau_c(B_m+h) = \rho g A_c S - \int_0^y \rho uv \, dy - \int_0^y \rho u'v' \, dy \qquad (2.7)$$

where the second term of the right part of the equation 2.7 represents the momentum transfer due to secondary currents and the third term represents the momentum transfer by the turbulent diffusion effect. Neglecting the effect of secondary currents and replacing the effect of turbulent diffusion by the concept of depth averaged apparent shear stress τ_{as}, equation 2.7 becomes:

$$\tau_c(B_c+h) = \rho \; g \; A_c S_0 - \tau_{as}(H-h) \qquad (2.8)$$

For the floodplains:

$$\tau_f(B_f+ H - h) = \rho \; g \; A_f S_0 + \tau_{as}(H-h) \qquad (2.9)$$

τ_{as} is the depth averaged apparent shear stress that acts in the interface of the main channel with the floodplain and it is assumed to assist floodplain flow and to resist main channel flow.

Based on the results obtained in the S.E.R.C. flume **Wormleaton and Merrett(1990)** carried out extensive correlation work in order to relate the depth-averaged apparent shear stress against the lateral variation of mean velocity between the main channel and the floodplain regions ΔV, the depth of flow on the floodplain(H-h) and the floodplain width bf. A simple exponential

least square regression was found for τ_{as} in terms of the above parameters, using data from three smooth and one rough geometry. The resulting regression equation was :

$$\tau_{as} = 3.325\ \Delta V^{1.451}\ (H-h)^{-0.354}\ B_f^{0.519} \qquad (2.10)$$

Ervine and Baird(1984) undertook also correlation work from data obtained in sixteen different cross sections with smooth boundaries. They also deduced an empirical relationship for the depth averaged apparent shear stress,

$$\frac{\tau_{as}}{\rho\ g\ (H-h)\ S_0} = (H/(H-h) - \phi)^{1.5} (B_m/h)^{0.5} (0.5+0.31\ \ln(B_f/h) \qquad (2.11)$$

where ϕ is the relative flow depth at which velocities either side of the division between main and floodplain are close enough for τ_{as} to be negligible.

It must be stressed that equations are empirical relationships and so their domain of application could not be extended outside those for which they were obtained.

- Method of Correction Factors

The compound cross section is divided into main channel and flood plain sub-sections using vertical divisions lines at boundaries. A conventional open channel formula is applied to each section and simultaneously empirical correction coefficients are introduced in the formulae to take into account the interaction effect. **Radojkovic(1976)** was the first to recommend the application of this method. As an index of the degree of interaction between the main channel and floodplain, he deduced the following Φ coefficients for main channel and floodplains :

$$\Phi_c = \tau_c P_c / \rho\ g\ A_c\ S = \tau_c / (\ \tau_c + \tau_a\ (H-h)/\ P_c\ ) \qquad (2.12)$$

$$\Phi_f = \tau_f\ P_f\ /\ \rho\ g\ A_f\ S = \tau_f / (\ \tau_f + \tau_a\ (H-h)\ /\ P_f\ ) \qquad (2.13)$$

In order to calculate discharge, he deduced the following formula:

$$Q_T = Q_c' \sqrt{\Phi_c} + Q_f' \sqrt{\Phi_f} \qquad (2.14)$$

where Q_c' and Q_f' represent the discharges obtained in the main channel and floodplain assuming that they are treated as separated zones without the interference shear.

This method was further developed by **Ervine and Baird(1982)** and most recently by **Wormleaton and Merret(1990)**, who produced ϕ factors for the SERC flume Series A data. Values of ϕ_c generally vary from 0.4 to 1.0 while values of ϕ_f vary in the range of 1.2 to 1.6.

The methods above are largely empirical and require calibration. However the main reason that the above methods fail to give accurate results, when applied to compound channels, is that the flow distribution and shear stress distribution is non-uniform. The simple 1-D theory is based on the underlying assumption of uniform flow and bed generated shear stress only, which do not apply to two-stage channels. The above empirical approach does not take this non-uniformity into account, being based on simplistic analysis and inadequate understanding of the basic flow mechanisms occurring in compound channels. In recent years work has been concentrated on gaining an accurate picture of the physical processes taking place and has stimulated interest in methods of discharge estimation based on 2-D depth averaged flow theory. Two different areas of investigation has been developed in modelling these complex flow mechanisms mathematically for the case of straight compound channels:

(a) The numerical approach undertaken by **Wark et al.(1991)** uses the lateral distribution method of discharge estimation.

(b) The analytical approach carried out by **Knight and Shiono(1988)**.

- The Lateral Distribution Method

Considering first the numerical by **Wark et al.(1991)**, the method is based on calculating the distribution of flow within the channel. The governing equation is derived from the general

2-D, shallow water equations, neglecting the secondary current term and assuming the flow is steady and uniform(in longitudinal direction) and the water surface is horizontal. Considering the assumptions mentioned, the 2-D dynamic equation can be written

$$gDS_{xf} - \frac{B\, f \mid q \mid q}{8\, H^2} + \frac{\partial}{\partial y}\left[\nu_t D \frac{\partial q}{\partial y} \right] = 0 \qquad (2.15)$$

Gravity Bed shear Lateral shear

Where

$B = (1 + s_x^2 + s_y^2)^{1/2}$: A factor relating boundary shear stress on an inclined surface to stress in the horizontal plane.

D = Local Flow depth

f = Darcy-Weisbach friction factor

g = Gravitational acceleration

S_x = Longitudinal slope of channel bed

S_y = Lateral slope of channel bed

x = Longitudinal coordinate direction

y = Lateral coordinate direction

q = Longitudinal unit flow(discharge per unit width)

υ_t = Lateral eddy viscosity

Given estimates of the bed and lateral shears it is possible to solve equation for the distribution of flow within the channel. The bed shear is calculated by local application of 1-D theory, for example by using Manning's equation or the Darcy Weisbach equation. The evaluation of the lateral shear term is more complicated. Various models have been proposed for the estimation of the lateral eddy viscosity term. **Vreugdenhil and Wijbenga(1982)** suggested the use of a constant value of υ_t but they did not compare the solution with measured data. Based on dimensional analysis, the lateral eddy viscosity relating to bed roughness generated turbulence is given by the equation

$$\upsilon_t = C_2\, U_*\, D \qquad (2.16a)$$

Where

U_* - The shear velocity = $(\tau_b / \rho)^{1/2}$

C_1 - The non-dimensional eddy viscosity(NEV)

ρ - Fluid density

τ_b - Bed shear stress

According to **Samuels(1985)** C_1 is a constant that is likely to lie in the range 0.25 to 0.7. Other researchers such as **Wormleaton(1988)**, suggested that shear layer driven turbulence may be an important source of lateral shear in compound channels. In this case the lateral eddy viscosity is given by the expression:

$$\upsilon_t = C_2 \, l_s \, \Delta U \qquad (2.16b)$$

Where

C_2 - A constant

l_s - A length scale related to the width of the shear layer

ΔU - Velocity difference across the shear layer

Wark et al.(1990) have argued that in real rivers, floodplains bed generated shear dominates, and in view of other uncertainties have opted for a simple expression for ν_t given by equation 2.16 a.

Wark et al.(1990) have solved the equation by an appropriate finite difference scheme with the lateral shear term computed at the mid-node positions(staggered grid). Equation 2.15 is non-linear and the solution is obtained by iteration procedure using Newton method. The required boundary conditions are that q = 0 at the solid channel boundaries. The input values are channel geometry, bed roughness and eddy viscosity parameters in each sub-area of the channel. Comparisons between the computational model and measurements conducted in a physical model were made and the findings showed that the eddy viscosity can be modelled with adequate precision using only the bed generated shear model. The factor C_1 was found to lie within the range 0.16 ± 0.08. They also recommend the use of constant values of C for each sub-area.

Fig(2.26) represents the comparison of experimental results, obtained by **Kiely(1989)** in a small scale model, and the numerical

values, generated by **Wark et al.(1990)** mathematical model. The comparison was made in terms of velocity distribution and stage/discharge curve. The non-dimensional eddy viscosity was assumed as zero on the floodplains, while in the main channel the calculations were carried out for a range of non-dimensional eddy viscosity between 0 and 0.5. As it can been seen the best agreement was achieved when C_1 is in the range 0.16 to 0.24.

A more detailed analysis of the Lateral Distribution Method(LDM) is given in **Wark, Slade and Ramsbottom(1991)**, which applies the method successfully to a series of natural rivers and floodplains, as well as the SERC flume Series A data.

- The Analytical Approach

Shiono and Knight(1990) emphasized the importance of momentum exchange arising from secondary currents as well as from the Reynolds stress. They deduced the depth averaged streamwise momentum equation for a steady uniform flow in a channel of depth, H, at any point in the cross section. After making certain assumptions, the governing equation assumes the form,

$$\rho g D S_0 + \frac{\partial}{\partial y}\left[\rho D\left(\nu_s + \nu_t\right)\frac{\partial U_d}{\partial y}\right] - \tau_0 = 0 \qquad (2.17)$$

Where,

D is the local flow depth

S_0 is the channel gradient

g is the gravitational acceleration

U_d is the depth averaged at position y

τ_0 is the bed shear stress

υ_s eddy viscosity arising from secondary currents

υ_t eddy viscosity arising from turbulence

y is the lateral direction.

Shiono and Knight(1990) found an analytical solution for this partial differential equation. They used experimental data from the S.E.R.C. flume Series A tests to determine the dimensionless eddy viscosity for a two-stage channel. In general, good correlation was found between experimental data and model

values of depth averaged velocities across the width for a typical value of eddy viscosity equal to

$$\upsilon_s+\upsilon_t = 0.16\ U_* D \qquad (2.18)$$

Fig(2.27) ilustrates the comparison of depth-averaged velocities across the width, obtained experimentally from the S.E.R.C. flume Series A tests and by the **Shiono and Knight(1991)** analytical model. In general there is a good level of agreement between experimental and model results. The maximum velocity in the main channel is very similar in both cases and discharge distribution across the width is also quite well simulated. There are some discrepancies close to the upper edge of the bank between the main channel and floodplain.

The numerical solution presented by **Wark et al.(1990)**, and the analytical solution found by **Shiono and Knight(1990)**, allow calculation not only the stage/discharge curve of a straight compound channel, but also the lateral distribution of depth averaged longitudinal velocity, U_d as well as the lateral distribution of the boundary shear stress, τ_b.

The numerical solution presented by **Wark et al(1990)** and the analytical approach deduced by **Shiono and Knight(1991)** can be regarded as very promising methods for dealing with the design of two-stage channels. However there is still a lack of information of the turbulent eddy viscosity values to use in different flow zones. Thus more research in this area is needed in order to improve and refine these design methods.

Keller and Rodi(1988) and **Kawara and Tamai(1988)** have developed two-dimmensional and three-dimensional numerical models to give the depth-averaged flow characteristics. Their work has involved the use of more sophisticated turbulence models.

Much more sophisticated models of compound flows are now being developed as part of the SERC Flood Channels initiative. **Younis(1992)** is developing k-ε, algebraic stress models and Reynolds stress models applied to compound flows, whereas **Williams(1992)** is developing large eddy simulation techniques in the same area.

- The New Method Proposed by **Ackers(1991)**

From the point of view of the practical river engineer the knowledge of the stage/discharge curve is of primary importance. The mathematical models recommended by **Wark et al(1990)** and **Shiono et al(1991)** need a certain amount of computing expertise as well as the fact that there is not, at present, a reliable method of determining values of turbulence coefficients for ν_t. Thus it was necessary to develop a method much simpler and faster than the previous ones, but also with a certain degree of accuracy. Based on these ideals of simplicity and accuracy, **Ackers(1991)** developed a new empirical method that allows calculation of the stage/discharge curve of a straight compound channel. The methodology is based on the analysis of all the experimental data of S.E.R.C. flume Series A through a comparison of the measured discharge with the computed total discharge. In order to represent the depth variation on the floodplain, **Ackers(1991)** recommended two parameters:

-Relative Depth, (H-h)/H

-Channel Coherence, COH

Where

H: is total flow depth

h: is bankfull depth

COH is the coherence of channel section, expressed as the ratio of the theoretical conveyance calculated by treating it as a single unit, to that calculated by summing the conveyances of the separate zones. **Fig(2.28)** shows the coherence of river Severn at Monford Bridge. In its general form the section coherence is defined as being

$$COH = \frac{\sum_{i=1}^{i=n} A_i \quad \sqrt{\left(\sum_{i=1}^{i=n} A_i / \sum_{i=n}^{i=n} \left(f_i P_i \right) \right)}}{\sum_{i=1}^{i=n} \left(A_i \left[A_i / f_i P_i \right] \right)} \qquad (2.19)$$

The discrepancy between the basic calculation and the

measured flow was expressed by different non-dimensional parameters such as DISADF which represents the ratio of measured discharge against basic calculation. The degree of interference between the channel flow and the main channel presents different trends. **Fig(2.29)** shows DISDAF plotted against relative depth. Four distinct regions of flow behaviour were identified, each of them with a different mathematical function for the assessment of discharge. For each region a predictive function based on the results from large S.E.R.C. flume was established. The effects of flow depth, floodplain width, channel side slope, asymmetry, width/depth ratio and floodplain roughness were also taken into consideration in these predictive functions.

As mentioned by **Ackers(1991)**, the results produced by this method were compared against field data giving excellent results. For example for river Severn stage/discharge curve obtained by the method shows an average discrepancy in relation to the actual value in the order of +0.3%.

At present time it seems that the empirical method, proposed by **Ackers(1991)**, could be the best solution for the practical river engineers, at least for non-meandering compound flows. As a long term solution it is more likely however that turbulence methods will replace empirical ones.

2.3 SKEWED COMPOUND CHANNELS

2.3.1 Introduction.

The skewed compound channel idealised in **Fig(2.30)** represents the cross-over region of a meandering compound channel, containing an element of the floodplain flow passing over the main channel below with an angle between the two flows. **James and Brown(1977)**, **Elliot and Sellin(1990)** and **Ervine and Jasem(1991)** have investigated experimentally the flow behaviour in skewed compound channels. The skewed compound channel investigated by **Elliot and Sellin(199)** and **Ervine and Jasem(1991)**

did not contain any bend effect.

James and Brown(1977) conducted an investigation on skewed compound channels reproduced in a tilting flume 26.8 metres long and 1.5 metres wide. Three single cross-overs with skew angles 7.2, 11.0 and 24.0 degrees respectively were studied. Each cross-over length started and finished through a bend. This is sketched in **Fig(2.34)**.

Elliot and Sellin(1990) carried out experimental work in the SERC Flood Channel Facility at HR Ltd, Wallingford where the main channel was skewed in relation to the floodplain direction. Two skew angles were studied 5.1 and 9.2 degrees, respectively.

Ervine and Jasem(1991) conducted experimental work in a physical model much smaller than the S.E.R.C. flume, with plan dimensions 8.5 m long and 0.8 m wide. The flume incorporated a main channel skewed 5.84 degrees in relation to the floodplain direction. Two floodplain roughnesses were studied, namely the smooth case and the roughened case,respectively. The roughened case was simulated by means of vertical rods each 10.0mm diameter, equally spaced (100.0 mm) and penetrating through the free surface.

2.3.2 Flow Mechanisms in Skewed Compound Channels.

Ervine and Jasem(1991) advocate that the flow in a skewed compound channel, even at a small skew angle of the order of 6 degrees, presents several characteristics which are totally dissimilar to straight parallel compound channels. Dye tests carried out by them, reveal that flood plain flow approaching the main channel can bifurcate with part of the floodplain flow being entrained down into the main channel and part crossing to opposite flood plain. **Fig(2.30)** ilustrates the development of this flow mechanism.

Elliot and Sellin(1990) point out that velocity distribution, both in the main channel and over the two floodplains, are distorted by this cross-flow. This is sketched

in **Fig(2.31)**, where the maximum velocity filaments move in the same direction as the flood plain cross-flow.

2.3.3 Flow Resistance in Skewed Compound Channels.

Using the relationship between the Darcy Weisbach friction factor and Reynolds number, **Ervine and Jasem(1991)** compared their data against the **Elliot and Sellin(1990)** skewed channel data, and also the straight compound channel data of S.E.R.C. Series A data. They verified, as it can be observed in **Fig(2.32)**, that increasing skew angle increases resistance to flow, for the same bed friction losses.

James and Brown(1977) also verified that the resistance coefficient increased with cross-over angle.

2.3.4 The Stage-Discharge Relationship in Skewed Compound Channels.

Ervine and Jasem(1991) observed that, when the floodplain roughness is increased, the conveyance of skewed compound channels diminishes significantly.

Elliot and Sellin(1990) demonstrated that the skewness of the channel reduces the total capacity of the cross section in comparison with the straight compound channel. The maximum reduction in capacity, as it is indicated in **Fig(2.33)**, is 12% and it occurs at the relative depth of 0.2.

James and Brown(1977) pointed out that the conveyance of skewed compound channels is significantly affected by the skew angle.

2.3.5 Secondary Currents in Skewed Compound Channels.

Ervine and Jasem(1991) observed in the skewed compound

channel that floodplain flow passing over the main channel generates a large secondary cell whose recirculating velocity is up to 20% -30% of the normal component of the oncoming floodplain flow velocity and 3%-5% of the streamwise main channel velocity. Comparing their results with **Elliot and Sellin(1990)**, it was noticed that as the skew angle increases, the values of recirculation secondary velocities also increases. This has significant implications in terms of numerical models of skewed compound channels. The values of $V\frac{\partial U}{\partial y}$ and $W\frac{\partial U}{\partial z}$, which represent the effect of the secondary currents, can not be neglected in any numerical simulation.

2.3.6 Primary Velocity in Skewed Compound Channels.

James and Brown(1977) pointed out that normalized velocity profiles of floodplain flow, as shown in **Fig(2.34)**, were highly distorted by skewed channels. Velocities accelerated in diverging floodplain areas and decelerated in converging floodplain areas. Surface currents indicate flow was exchanged between floodplain and skewed channel.

Ervine and Jasem(1991) observed, as it is sketched in **Fig(2.35)**, that the depth averaged lateral velocity profile in a skewed compound flow is asymmetric with no shear layer on the right narrowing floodplain and a wide shear layer on the left floodplain. For low depths on the floodplain the maximum velocity filament is pushed to the left side of the main channel and for high depths it moves to left floodplain.

2.3.7 Boundary Shear Stress in Skewed Compound Channels.

By using Preston tube, **Elliot and Sellin(1990)** carried out measurements of boundary shear stress over the skewed channel test length. They noticed, as shown in **Fig(2.36)**, the occurrence of peak values of boundary shear stress in the region where the

cross-flow leaves the main channel. The floodplain that receives flow from the main channel presents values of bottom shear stress significantly larger than the other.

2.3.8 Methods for Discharge Assessment in Skewed Compound Channels.

Ervine and Jasem(1991) applied the sub-division method for discharge assessment in skewed compound channels, both with smooth floodplains and also with roughened floodplains. The sub-division method applied was the one recommended by **Chow(1959)** using imaginary vertical walls. They verified, as it is evidenced in **Fig(2.37)**, that errors up to 25% for the smooth floodplain case(and up to 50% for the rough floodplain case) can be reached if this method is applied. Thus the sub-division method is not accurate in assessing discharge in skewed compound channels because it does not take into consideration losses produced by secondary cells, lateral and horizontal shear which are not associated with bed friction.

For the roughened floodplain case, a horizontal sub-division method would be most appropriate, with a horizontal division at bankfull level and with floodplain roughness extending 2 to 3 floodplain depths of flow, into the main channel.

Because the flow behaviour in skewed compound channels is highly three dimensional, its simulation should be made only in three dimensional numerical models where the effects of bed friction for main channel and floodplains, secondary currents and the turbulent shear are present.

2.4 MEANDERING COMPOUND CHANNELS

2.4.1 Introduction.

Research into meandering rivers with the flow confined to

the main channel has been continuing for over a century. **Thompson(1876)** appears to have been the first to have pointed out the existence of spiral motion in a curved open channel. Since that date, the phenomena associated with flow in bends of open channels has been studied almost continuosly experimentally by researchers such as **Mockmore(1944)**, **Shukry(1950)**, **Chow(1957)** and many others. With the advent of computers, flow around bends can now be modelled by numerical procedures.

The mechanics of flow in meandering rivers with overbank flow is a highly three-dimensional and chaotic problem. Although it is complicated, it is now receiving considerable attention from the river hydraulic community, especially through the SERC Series B programme. The research of river meanders with overbank flow has been carried out experimentally (**Toebes and Sooky(1967)**; **Rajaratnam and Ahmadi(1989)**; **Kiely(1989)**; **U.S.A. Corps of Engineers(1956)**) and numerically(**Ervine and Ellis(1987)**; **Samuels(1985)**; **Stein and Rouve'(1989)**). With the exception of S.E.R.C. flume(Series B), located at H.R. Ltd Wallingford(where the author carried out the research described here) and the U.S. Army Corps of Engineers study, most of the flumes where the experimental studies took place were of modest size. Numerical modelling of meandering compound How has been made by using one dimensional or two-dimensional depth averaged equations.

2.4.2 Geometry of Rivers Meanders.

Leopold and Wolman(1957;1960) made an extensive study of river morphology. Their study was based on several rivers in U.S.A., where they developed empirical equations relating the wavelength and amplitude of meander bends to bankfull width of the channel. They also related meander wavelength to bend radius of curvature. The following equations are due to **Leopold and Wolman(1960)**:

$$\lambda_m = 10.9\ B_c^{1.01} \qquad (2.20)$$

$$a = 2.7\ B_c^{1.1} \qquad (2.21)$$

$$\lambda_m = 4.7\ R_c^{0.98} \qquad (2.22)$$

where λ_m is the meander wavelength, a is the amplitude, R_c is the river bend radius of curvature and B_c is the top width of the main channel. All are expressed in feet. A definition sketch of regular meander path is shown in **Fig(2.38)**. Assuming the exponents above are approximately 1.0, the following relationship between the centre-line bend radius and bankfull width can be obtained

$$R_c = 2.4\ B_c \qquad (2.23)$$

which was corroborated by the results found by **Leopold and Wolman(1957;1960)** in river meanders in U.S.A.. However **Hey(1976)** found that the above equation did not fit data obtained in several rivers in U.K. where, for sinuosity 1.5(sinuosity is defined as the ratio of channel length along the curved "thalweg divided by the straight line "valley" length), the ratio R_c/B_c was considerably greater than 2.4 and 3.0. Thus equation 2.23 can only be applied if the meander is fully developed. For other cases **Hey(1976)** presented a relationship between the radius of curvature,bankfull width and the arc angle that it is shown in **Fig(2.39)**. For the same bankfull width the radius increases with the arc angle. He found however good correlation between the meander arc length with channel width.

Yalin(1971) postulated that meanders could be attributed to the law governing the spatial correlation of perturbations in turbulent flows. He explained that macroturbulent eddies would produce periodical reverses along the flow direction and proposed the wavelength could be related to the bankfull width through the following expression

$$\lambda_m = 2\pi B_c \qquad (2.24)$$

Based on compilation of the research carried out worldwide on river morphology, **Ervine and Ellis(1987)** had

prepared the following summary of some typical geometric parameters of river meanders,

Typical Geometric Parameters for Meandered Rivers

Sinuosity: r		
Description :	Straight,	r = 1.0 to 1.05
	Sinuous,	r = 1.05 to 1.5
	Meandering,	r > 1.5
Meander wave length(λ_m)		$\lambda_m \cong 10B_c$
Main Channel width (B_c)		$B_c \cong 5 \rightarrow 20$ h
Average bend radius of curvature(R_c)		$R_c \cong 2.7\ B_c$
Floodplain width(W_t)		$W_t \cong 10 \rightarrow 20B_c$(or >a + B_c)
Meander double amplitude(a)		$a \cong 0.5\ \lambda_m$ when r = 1.5
		$a \cong 0.8\ \lambda_m$ when r = 2.0
		$a \cong 2.0\ \lambda_m$ when r = 4.0

2.4.3 Flow Behaviour at River Bends(inbank only).

Flow in curved channels tends to result in secondary currents. They are developed as the result of centrifugal forces $\rho U^2/r$ acting on fluid filaments producing superelevation of the free water surface at the outer wall, and accompanied by a corresponding diminution of the depth at the inner wall. This situation can be described simply by the following equation,

$$\rho g S_y = \rho \frac{U^2}{r} \qquad (2.25)$$

In each vertical, the resultant of the transverse gravity force directed inwards should equali the resultant centrifugal force directed outwards. But within the vertical there is not a static equilibrium because the actual velocity distribution with depth is not everywhere equal to the average velocity. At the surface U is larger than the average, whereas S_y (the transverse slope) produces a pressure that is identical for all particles in the vertical and which is adapted to the averaged velocity. This implies that at the

surface, the centrifugal force is larger than the counteracting transverse gravity force, resulting in net resulting force outwards. Along the bed the reverse takes place,namely the low velocity produces a low centrifugal force lower than the transverse gravity force, so that there is a net force inwards. This produces a rotating cell, as sketched in **Fig(2.40)**, where the particles at the surface are moving outwards and near the bottom moving inwards.

Bathurst(1979) observed in actual river bends with steep outer banks, that besides the main cell, as shown in **Fig(2.41)**, another cell can develop, near the outer bank, with reverse circulation.

The basic equations governing the dynamics of the flow in curved channels were derived by **Rozovskii(1957)**, **Rouse(1959)**, and **Schiliting(1988)** among others. In general they assume that the flow is steady the pressure distribution is hydrostatic, the depth is generally smaller in comparison with width and radius of curvature and the channel is sufficiently wide so that bank effects can be neglected. Based in the above conditions and considering that transverse and vertical velocities V and W, are small in comparison to streamwise velocity U, **Chang(1987)** deduced in polar-cylindrical coordinates, the following dynamic equation of the flow around the bend in the radial direction:

$$\underset{\text{I}}{U\frac{dV}{ds}} = \underset{\text{II}}{\frac{U^2}{r}} \underset{\text{III}}{- g S_r} + \underset{\text{IV}}{\frac{\partial}{\partial z}\left(\varepsilon \frac{\partial V}{\partial z}\right)} \qquad (2.26)$$

This equation represents in analytical form the growth and decay of secondary currents. The spatial variation of transverse velocity(V), expressed by term I, is related to the balance of centrifugal acceleration(term II), transverse water surface slope(term III) and turbulent shear(term IV). The transverse circulation grows when the summation of terms II, III, and IV is positive. This can happen when the centrifugal force is larger than the resistance induced by transverse water surface slope and

fluid friction. The transverse circulation decays when opposite situation occurs. An equilibrium can be reached if the summation of these three terms is zero.

Analytical equations of transverse or secondary velocity profiles for steady, fully developed flow in curved channels have been deduced by **Rozovskii(1957)**, **Kondrat'ev et al.(1959)** **Kikkawa et al.(1976)**, among others. Most relationships are obtained based on the semi-empirical theories of turbulence, using equations of motion as the analytical basis. **Fig(2.42)** shows the comparison of **Rozovskii's(1957)** experimental data against the theoretical velocity profiles of **Kondrat'ev et al.(1959)**. Both theories reproduce the experimental data reasonably well.

From the experimental results obtained by **Shuckry(1950)**, shown in **Fig(2.43(a))**, it can be seen that the path of the maximum streamwise velocity in a curved channel, gradually deviates its course from the inner bank to the outer bank of the bend. **Ippen**(1962) and many other researchers explained that at the bend entrance, the horizontal components of the forward velocity are greater near the convex bank than the concave bank and vary across the channel in close agreement with the law of a free vortex (Vr = constant). However, in the bend, secondary circulation develops, thus breaking down the free vortex. The circulation carries the core of maximum velocities across the channel towards the outer bank.

In the case of rivers with larger aspect ratio B/y (channel width/depth), and at very sharp turns, the streamlines cannot follow the boundaries, and separation, as sketched in **Fig(2.43(b))**, will usually occur accompained by additional secondary currents. **Rozovskii(1957)** pointed out that there is not a definitive rule for flow separation. There is however some connection with the braking effect of the side wall, depth of flow, the form of the banks and particularly the angle of bank slope. Flow separation produces energy losses in the flow and causes sediment deposition in the zones of low circulation.

The energy losses dissipated in a curved channel are greater than those in a straight channel of the same depth, velocity, and

energy surface roughness. At subcritical flow conditions this increment in resistance will cause a diminution of flow velocities and increased depths upstream, creating a backwater effect, as shown in **Fig(2.44)**. The flow is accumulating potential energy, in the upstream reach, in order to overcome the excess of energy expenditure introduced by the bend. **Chang(1987)** noted that the increase in power expenditure in curved channels can be attributed to:

- Internal friction produced by secondary currents
- Boundary resistance due to transverse shear
- Eddy losses due to flow separation

Head losses in bends are function of Froude number(**Yen(1965)**) as well as Reynolds number and bend geometry (**Shukry(1950)**). **Shukry(1950)** found that Reynolds number effect on energy loss can be neglected for values beyond $3*10^4$. The energy loss due to resistance of a bend h_b has usually been expressed in terms of velocity head:

$$h_b = f_c \frac{U^2}{2g} \qquad (2.27)$$

where U is the streamwise average velocity at a cross section upstream of the bend where the flow is uniform, and f_c is the friction coefficient. **Raju(1937)**, and later **Shukry(1950)** found that the coefficient f_c varies considerably with each of the parameters Reynolds of the approach flow, the ratio of the central radius of curvature of the channel to channel width(R_c /b), the ratio of flow depth to channel width of the channel(y/b) and total central angle of the bend($2\alpha/180^0$). Both researchers produced several mathematical design curves to obtain f_c(using experimental data in a rectangular channel with width b=0.30m) as function of Reynolds number, R_c/b, y/b and $(2\alpha)/180^0$.

Shukry(1950) also found that the kinetic energy of the secondary currents in a bend is relatively small compared with the energy in the longitudinal direction, and consequently, plays only a minor part in the energy loss due to bend resistance.

The magnitude of the boundary shear stress that develops

around the bend depends on the velocity gradient close to bed and consequently on the pattern of the primary velocity. It was observed by **Bathurst(1989)** and shown in **Fig(2.45)** that peak values of shear stress occur in the regions of downwelling where the isovels are compressed, and in regions where the primary velocity is relatively high. In the bend region the pattern of primary isovels is affected by secondary circulation and consequently the magnitude and position of the shear stress peaks are influenced as well. It is seen in **Fig(2.46)**, taken from **Ippen et al.(1962)**, that the region of high shear stress crosses the channel to the outer wall following the core of maximum velocity.

Numerical simulation of flow behaviour in curved channels has been carried out by several researchers such as **Rozovskii(19579, Leschziner and Rodi(1979), Kalkwijk and De Vriend(1980), Chang(1987)** and more recently by **Fares(1990)**. **Fares(1990)** developed a quasi three-dimensional model for the integration of the flow equations at bends. In general, 3-D procedures yield good predictions of the main and secondary flows and water levels.

2.4.4 Flow Behaviour for Overbank Case.

Flow behaviour in meandering compound channels is highly three-dimensional with intensive mass and momentum exchange between the inner meander channel and the floodplains. The flow process is more complicated than the straight compound channel and also the skewed compound channel. The complexity of the problem can be gauged from **Fig(2.47)** where the three-dimensional nature of the flow is evidenced by the presence of secondary cells in the bend region, high shear rates at the main channel/floodplain interface and likely large differential friction between the main channel and floodplain boundaries.

Meandering compound channels have been investigated experimentally[**U.S.A. Corps of Engineers(1956), Goncharov(1962) Toebes and Sooky(1967), James and Brown(1977), Ahmadi(1979),**

Stein and Rouve(1989), McKeogh and Kiely(1989), Willets and Hardwick(1990)] and numerically[Yen(1983), Samuels(1985), Ervine and Ellis(1987) and Stein and Rouve(1989)].

Flow Mechanisms in Meandering Compound Channels.

Additional flow mechanisms above the straight and skewed cases were identified for multiple meander compound channels:

- Secondary currents [Toebes and Sooky(1967), Kiely(1989) and Stein and Rouve (1989)]
- Horizontal shearing [Ervine and Ellis(1987), Kiely(1989)]
- Flow expansion and contraction [Ervine and Ellis(1987), Kiely(1989)]].

Based on small scale experimental work, Toebes and Sooky(1967) were among the first researchers to notice that during overbank flow the secondary cell rotational the bend apex, was in opposite direction to those of in-bank flow. This is shown in Fig(2.48). This cell represents the remnant of the secondary currents which are generated in the upstream reach of the bend by flood plain cross the main channel and are transported downstream to the apex. These secondary currents are driven by flood plain flow when it impinges on the main channel flow.

The essential direction of floodplain flow is longitudinal and parallel to the outer floodplain walls, whereas the main channel flow, below the bank level is parallel to the main channel walls. Therefore a nearly horizontal shear layer appeared between the upper and the lower parts of the main channel as shown in Fig(2.49). Its strength develops between the bend apex and the cross-over region, where it reaches the maximum value. Downstream of the cross-over, it starts decreasing and reaches a minimum value, at the bend apex.

It was postulated by Ervine and Ellis(1987) that, when floodplain flow crosses the deeper main channel and re-enters on the opposite floodplain, an expansion-contraction phenomenom

takes place generating significant energy losses. This is shown schematically in **Fig(2.49)**.

Kiely(1989) carried out experimental research in meandering compound flows(sinuosity : 1.25). He found secondary currents of strong magnitude throughout the full length of the meander channel. He noticed that, at the bend apex, the direction of the secondary currents were in opposite to those of an in-bank case and that the strength of secondary currents were about 30% of the streamwise velocity. At cross-over region, he observed the appearance of secondary currents with magnitude almost the same as the primary velocities.

Flow Resistance in Meandering Compound Channels.

In straight compound channels, flow resistance is basically produced by the lateral shear and bed friction. In meandering compound channels, besides the bed friction and the lateral shear layer, additional flow mechanisms such as secondary currents, horizontal shear and flow expansion-contraction increase flow resistance. It was described in section 2.3 that all these flow mechanisms are also present in skewed compound channels, with the exception of the effect of the bend.

James and Brown(1977) conducted laboratory tests in a tilting flume to study the effects of overbank flow on the resistance coefficient. Testing was carried out on skewed and meandering main channels bounded by straight floodplains. Results indicated that resistance coefficients increased with the degree of skewness of the cross-over and sinuosity.

Ervine and Jasem(1991), compared data from S.E.R.C. flume straight compound case, the S.E.R.C. flume 9^{o}skewed compound channel and the S.E.R.C. flume meandering compound channel(sinuosity:1.37), tested during Phase B of the Flood Channels programme. All three geometries have very similar bed friction characteristics, but increased skewness and sinuosity significantly affects the flow resistance coefficient. This is shown if **Fig(2.50)**.

The Stage-Discharge Relationship in Meandering Compound Channels.

U.S.A. Corps of Engineers(1956) carried an extensive study of the various factors affecting conveyance in meandering compound channels. Specific objectives were to determine the effects of the following factors on conveyance; radius curvature of bends; sinuosity of channel; depth of overbank flow; ratio of overbank area to channel area; and floodplain roughness. In a flume 9.0 metres wide and 30.0 metres long, straight compound channels and regular meander compound channels were reproduced. Two floodway widths, three depths of overbank flow and three degrees of boundary roughness were used in testing channels of various degrees of sinuosity and various meander belt widths. The work concentrated on stage-discharge relationships. From the results obtained in this experimental investigation, the following conclusions were made:

- Where the main-channel top width is relatively narrow(and small) compared to the total width of the meandering compound channel(meander belt width plus floodplain width), the effect of main channel sinuosity on the conveyance of the meandering compound channel is small. The ratio of the main channel top width to the total width of the compound channel tested was approximately 9% - 5.0% .

- In the case of the ratio between the main channel top width to the total width of the meandering compound channel(meander belt width plus floodplain width) be equal or greater than 15.6%, the effect of increasing the channel sinuosity on the conveyance of meandering compound channels becomes a critical factor.

- When the total width of the meandering compound channel exceeds the meander-belt width by about 300 per cent, the effect of channel sinuosity on the floodway capacity becomes relatively small.

- Channel discharge is reduced about 8-10 per cent by increasing the main channel sinuosity from 1.2 to 1.4 and from

1.4 to 1.57. A typical example of the relationship between channel sinuosity and channel discharge for various overbank flow depths, obtained by U.S.Army Corps of Engineers is shown in **Fig(2.51)**.

Willetts and Hardwick(1990) investigated experimentally the effects of the main channel cross-section shape on the stage-discharge curve of a meandering compound flow. The comparison was done for a uniform trapezoidal cross-section and for a cross-section produced naturally by bed erosion and deposition. Stage-discharge graphs obtained are shown in **Fig(2.52)** for the case of the two different cross-over angles. This graph shows that for higher stages, both the 60^0 and 110^0 cross-over with natural cross-section, produce greater conveyance than the corresponding trapezoidal cross-section even though the cross-sectional area is smaller. The reason for this is probably due to the fact that for higher stages, the conveyance of the meander main channel is insignificant in comparison with the floodplain contribution, and the flow streamlines are practically parallel to the floodplain walls. In these circumstances, the meander channel acts in a similar manner to "groves" in relation to the floodplain flow with energy losses produced by the expansion-contraction phenomenom when the floodplain flow passes over the main channel. Expansion-contraction losses in open channels vary with the main channel aspect ratio (top-width/bankfull depth).

Sellin and Giles(1988) carried out a detailed study of a two-stage length of the river Roding in Essex. **Fig(2.53)** shows a plan of the 3 km reach of the river that was modelled in the form of a two-stage channel. This experimental study differs from previous ones because it is site-specific and reproduces an actual river containing irregular meanders which are confined by irregular floodplain berms. **Sellin and Giles** investigated the capacity of the river Roding with particular attention to the effect of the roughness of different parts of the cross-section and the seasonal effect of the vegetation that grows along the channel berms. They found that floodplain roughness has a

dominant role in the conveyance of two-stage channels. **Fig(2.54)** shows the effect of uncut berm and cut berm on the stage-discharge curve of River Roding in Essex. From measurements of stage-discharge taken in the actual river, they conclude that conveyance of channel can be improved approximately 50% if berm vegetation is removed.

Secondary Currents in Meandering Compound Channels.

The investigation of secondary currents in meander compound channels has been carried out by **Toebes and Sooky(1967)**, **Ahmadi(1980)**, **Kiely(1989)** and **Stein and Rouve'(1989)**. All these researchers found that at a bend apex, the main secondary cell, for overbank case, rotates in opposite to the direction of a secondary cell that develops in a meandering channel without floodplain flow, (inbank flow only).

Using a 2-component Laser Doppler, **Stein and Rouve'(1989)** measured secondary currents in a physical model of a meandering compound channel. **Fig(2.55)** shows the production and destruction of secondary cells along the meander channel. At bend apex two secondary cells are spiralling one against the other, being the larger one rotating in opposite direction when compared to a bend with inbank flow. They note the existence of smaller depth-averaged main channel velocities, large energy losses due to occurring of turbulence, and the appearance of an horizontal shear between the upper and lower part of the main channel.

Ervine and Jasem(1991) reveal that recirculating secondary velocities, measured in the meandering compound channel of S.E.R.C. Flume, Series B in the cross over region, reached values of 20% to 30% of the normal component of approaching flood plain velocity.

Primary Velocity in Meandering Compound Channels.

Primary velocities (in the streamwise direction) in meandering compound channels have been investigated in detail by

Goncharov(1957), Toebes and Sooky(1967), Ahmadi(1979) and Kiely(1989).

By using a physical model, Goncharov(1957) investigated the flow mechanism and the flow structures that develop in a compound channel bend. He found out that the distribution of depth-averaged primary velocity in a meander compound channel with overbank flow differs greatly from the distribution for inbank flow. The primary velocity decreases considerably and its distribution across the channel width is smoother than for the inbank case. Fig(2.56) shows the distribution of depth averaged primary velocity in the compound channel for three degrees of submergence, obtained by Goncharov. He noticed that, as the degree of floodplain submergence increases, the role of the main channel in carrying the high-water discharge is reduced considerably. In order to have a better visualization of the interaction between the main channel and floodplain flows, Goncharov(1957) plotted the flow patterns for the same submergence depths, which are shown in Fig(2.57). As it can be observed when the degree of submergence increases the path lines inside of the meander belt start to be less affected by the main channel and tend to be almost parallel to the floodplain walls.

Toebes and Sooky(1967) carried out experimental work of compound flow in meandering channels with sinuosity 1.13. They observed that vectors of the resultant velocity show divergent and convergent patterns, indicating flow exchange between the main channel and the floodplain, as well as also strong vertical velocity components. Fig(2.58) shows the distribution of the resultant velocity vectors. Toebes and Sooky Calculated the discharge in several subsections of the meander, and managed to quantify the mass exchange between meander and floodplain flows. Fig(2.59) shows one of the plots obtained by these researchers where the flow distribution in each sub-section is expressed in terms of percentage of total flow. It is clear from Fig(2.59) that discharge is not steady and there is a significant discharge exchange between the main channel and the floodplain regions.

Ahmadi(1979) pointed out that the maximum velocity near the

surface occurred just outside the limits of the meandering main channel in the region of the inner bend as shown in **Fig(2.60)**.

McKeogh and Kiely(1980) carried out model studies of meandering compound flow, and found that below bankfull the resultant velocity vectors were in a direction parallel to the channels walls. At the bends, the maximum velocity filament (**Fig(2.61a)** was located at the inner wall. Above bankfull, as shown in **Fig(2.61b)**, they observed the velocity vectors in the main channel region did not follow the main channel walls but tended to be approximately parallel to the floodplain walls. In the floodplain, the flow direction was essentially longitudinal. Most of **Kiely's** work was carried out at relative depth ratio (H-h)/H of 0.38.

Methods for Discharge Assessment in Meandering Compound Channels.

Until now, numerical modelling of compound flows of river meanders has been made by one-dimensional models [**Yen(1983)**, **Pender(1985)**,and **Ervine and Ellis(1987)**] and also two-dimensional models [**Samuels(1985)**, **Stein and Rouve'(1989)**].

Pender(1985) used a finite difference technique to discretize the one-dimensional flow equations. His model simulates side flows into adjacent floodplains and subsequent side flows back unto the main channel some distance downstream. This approach did not take into consideration any effect of the lateral shear interaction between the main channel and the floodplain.

Yen(1983) proposed an approximate method to compute the flow capacity for meandering compound flow. The combined channel is considered as one-dimensional unit, while the meandering channel is treated as imposing additional resistance to the flow.

Ervine and Ellis(1987), developed a method for predicting stage-discharge curves for meandering rivers with compound flows, based on the energy equation. They identified five main sources of energy loss, including: frictional head loss in the main channel, flow resistance on the floodplain due to grass, trees

and hedges, flow resistance due to secondary currents at river bends, flow resistance due to floodplain flow components passing normally over the main channel flow encountering sudden expansions and contractions and flow resistance due to co-flowing turbulent shear between the faster moving main channel and the slower moving floodplain flow-parallel to the main channel. They quantified the magnitudes of each element of energy loss, except the co-flowing turbulent shear term. The results predicted by this method, as shown in **Fig(2.62)**, were compared with experimental data of U.S.Army Corps of Engineers, giving reasonable correlation.

Samuels(1985) used a finite element technique to discretize the two-dimensional flow equations excluding turbulent shear stress terms. He compared his numerical results with experimental data of **Toebes and Sooky(1967)**, giving an acceptable correlation. His work has been by **Wark(1989)** who has developed a two-dimensional finite element model with lateral turbulent shear terms included.

For simulation of flow behaviour in a meandering compound channel, **Stein and Rouve'(1989)** applied a two-dimensional depth-averaged numerical model with constant eddy viscosity. They compared numerical results against experimental data yielding reasonable results for the prediction of primary velocities, water elevation and discharge distribution. **Fig(2.63)** shows the comparison between experimental and calculated primary velocities. Qualitative distribution of discharge throughout the model is illustrated in **Fig(2.64)**. **Stein** and **Rouve** recognize however, that due to the three-dimensional behaviour of the flow, the prediction of velocity profiles is unsatisfactory and needs to be refined, probably through the use of a more sophisticated turbulence model.

Because the flow behaviour in meandering compound channels is highly three-dimensional, its numerical simulation needs to be by 3D models. **Manson and Pender(1992)** (Glasgow University) are presently developing a 3D K-ε model for meandering compound channels. The mathematical model will be tested by using data

from a skewed compound channel, obtained by **Jasem(1990)**, and later will be compared with data from meandering compound channels, obtained in the S.E.R.C. flume Series B programme.

2.5 SUMMARY

The main findings of this literature review can be summarized as follows:

(i) In straight compound channels the flow behaviour is dominated by the lateral shear that develops at the junction of the main channel/floodplain as a result of the gradient of velocities.

(ii) There is already a good understanding of flow structures and flow mechanisms that develop in straight compound channels. The experience and the knowledge gained from S.E.R.C. flume experiments, (Series A Straight Compound Channels) contributed decisively for this success.

(iii) The 2D analytical approach recommended by **Shiono and Knight(1991)** and the 2D numerical method presented by **Wark et al.(1990)** for calculation of stage-discharge curves and boundary shear stress distribution in straight compound flows give results that fit well actual data, obtained either in physical models either in rivers.

(iv) Flow in the skewed and in the meandering compound channels have several characteristics that are total dissimilar to the straight parallel compound flow case.

(v) Flow resistance in the skewed compound channels increases with increasing angle of skew.

(vi) Flow resistance in meandering compound channels increases with the cross-over angle of the meander, with sinuosity and with floodplain roughness.

(vii) Some flow mechanisms were identified in skewed and in meandering compound channels:

. The development of secondary currents in the main channel whose magnitude is greater than the inbank

case.

. The appearance of flow expansion in the main channel region and flow contraction in the floodplain region.

. The occurrence of an horizontal shear in the main channel region.

(viii) In skewed and in meandering compound channels the energy losses are caused by:

. Bed friction

. Secondary Currents

. The horizontal shear

. The lateral shear

(ix) Flow structures in skewed and in meandering compound channels are highly three dimensional. Thus they need to be modelled by 3D numerical procedures.

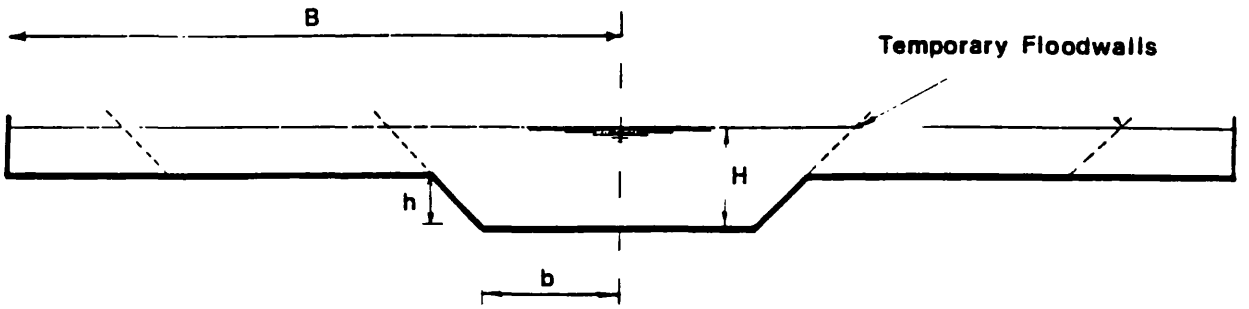

Total length of channel		L = 49 67m	Ratios of B/b investigated	B/b = 6·667, 4 2, 2 5 22,12,Asym 27
Half base width of channel		b = 750 mm		
Half total width of compound			Longitudinal bed slope	S = 1·027x10^{-3}
section	(L.H.S.)	B = 4 964 mm	Maximum Discharge capacity	Q = 11 m^3/s
	(R.H.S.)	B = 5008 mm	Relative Depth $\frac{H-h}{h}$ range	0·05;0·1;0·15;0·2; 0·25;0·3;0·4,0·5
Bankfull depth		h = 150mm		
Main channel side slope		S = 1 1		

Fig (2.1) - Typical Cross-Section of a Compound Channel Used in S.E.R.C. Flume Series A Tests : Definitions and Terminology by Myers and Brennan(1990).

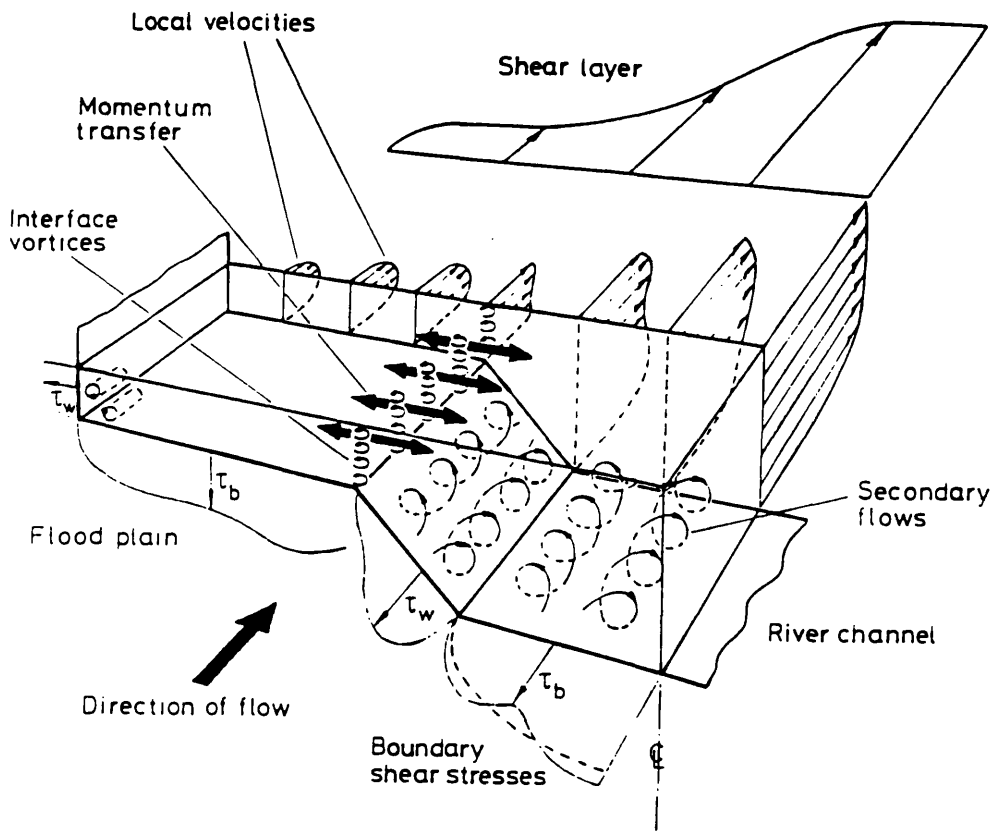

Fig (2.2) - Flow Mechanisms in Straight Compound Channels by Knight(1991).

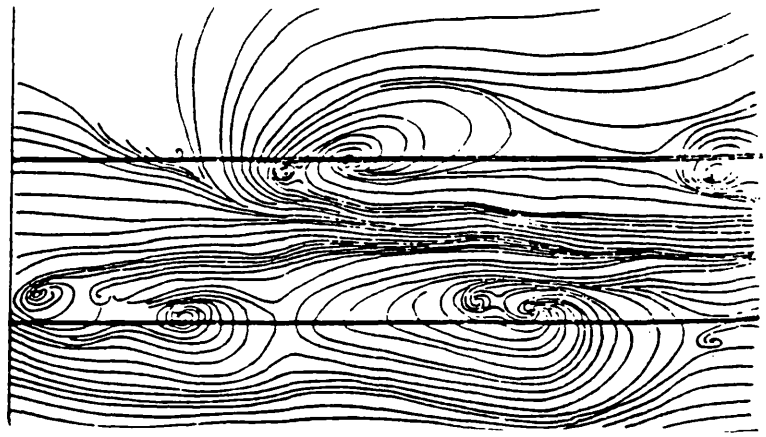

Fig (2.3) - Plan View of Vertical Vortices in a Straight Compound Channel by Sellin(1964)

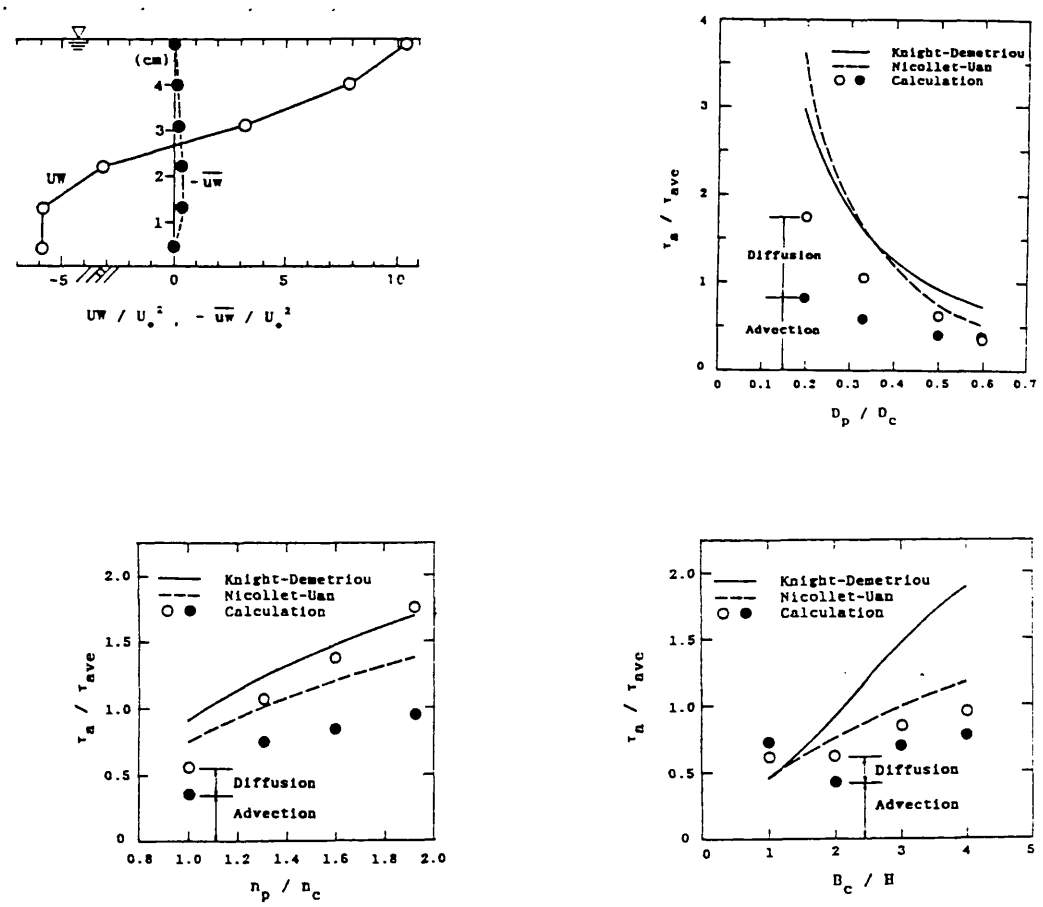

Fig (2.4) - Effect of Water Depth, Floodplain Roughness and Main Channel Width on the Mechanics of the Lateral Momentum Transfer in Straight Compound Channels(After Kawara et. al.(1989)).

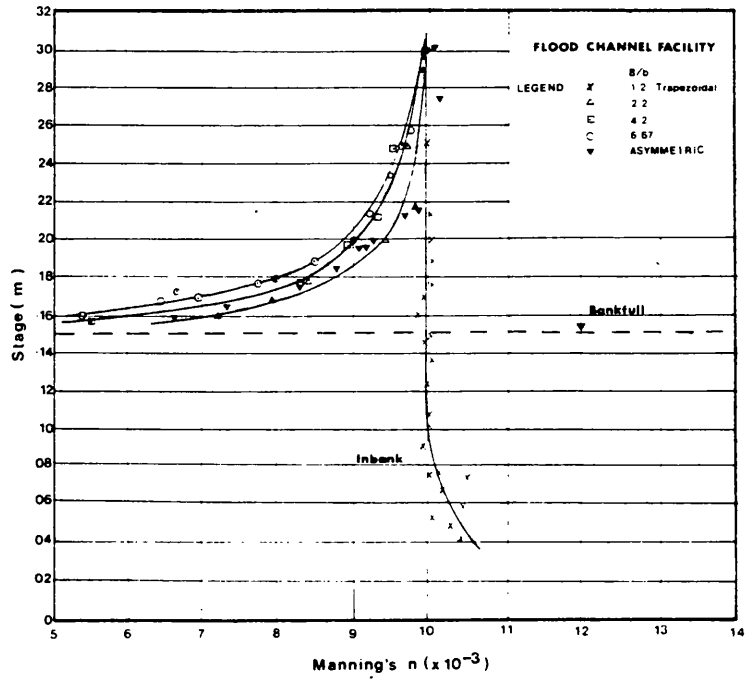

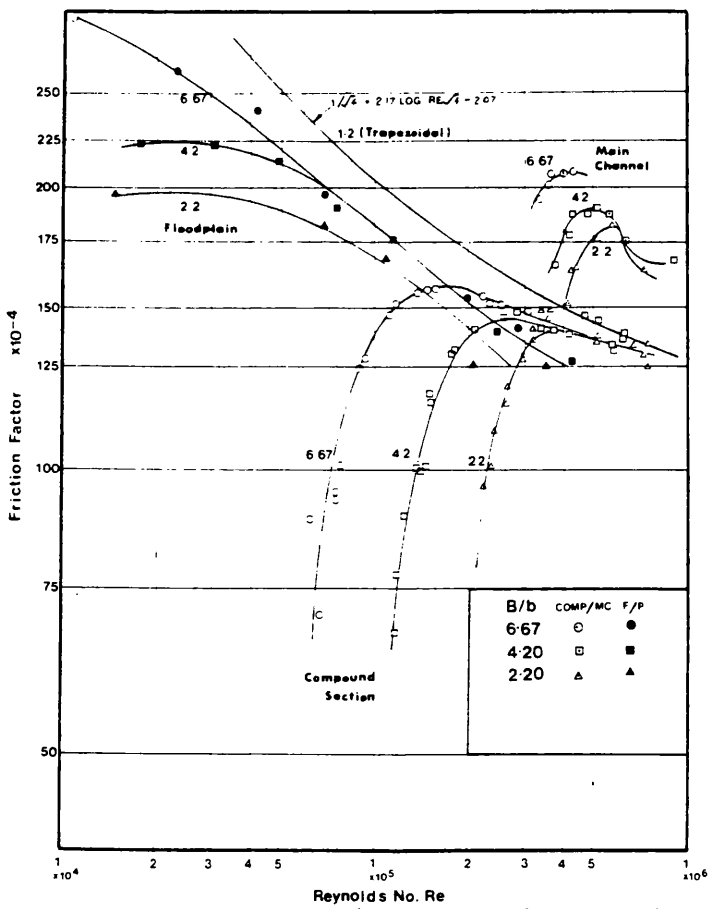

Fig (2.5) - Flow Resistance Coefficients in Straight Compound Channels by Myers and Brennan(1990)

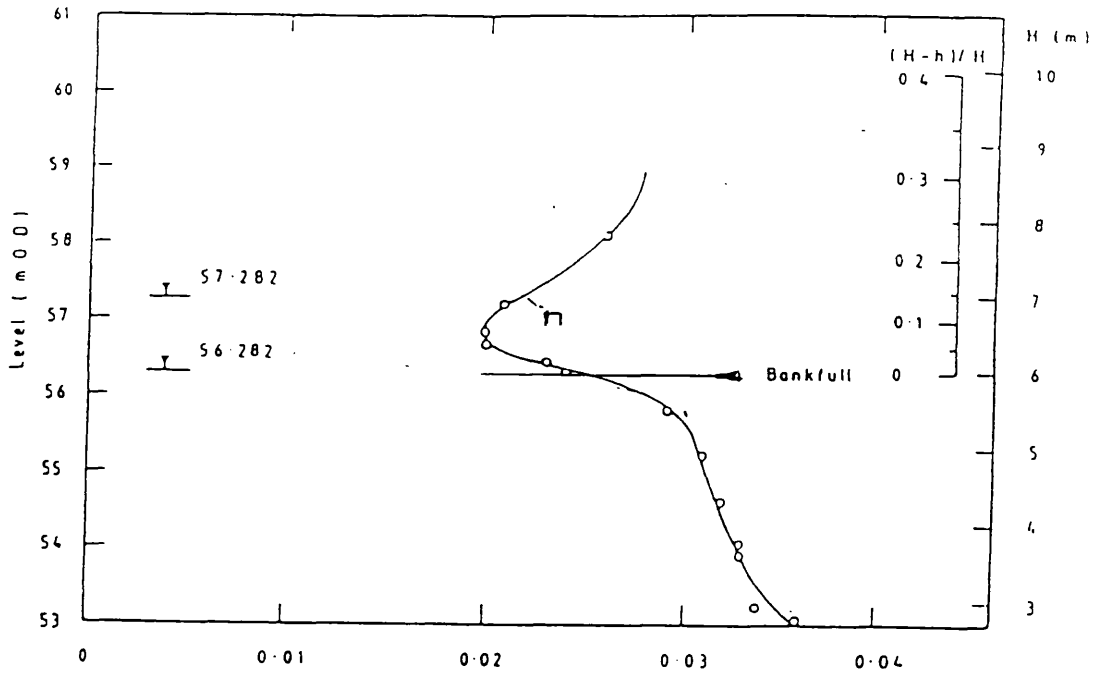

Fig (2.6(a)) - River Severn at Monford Bridge. Variation of Manning's n with Stage (after Knight(1989))

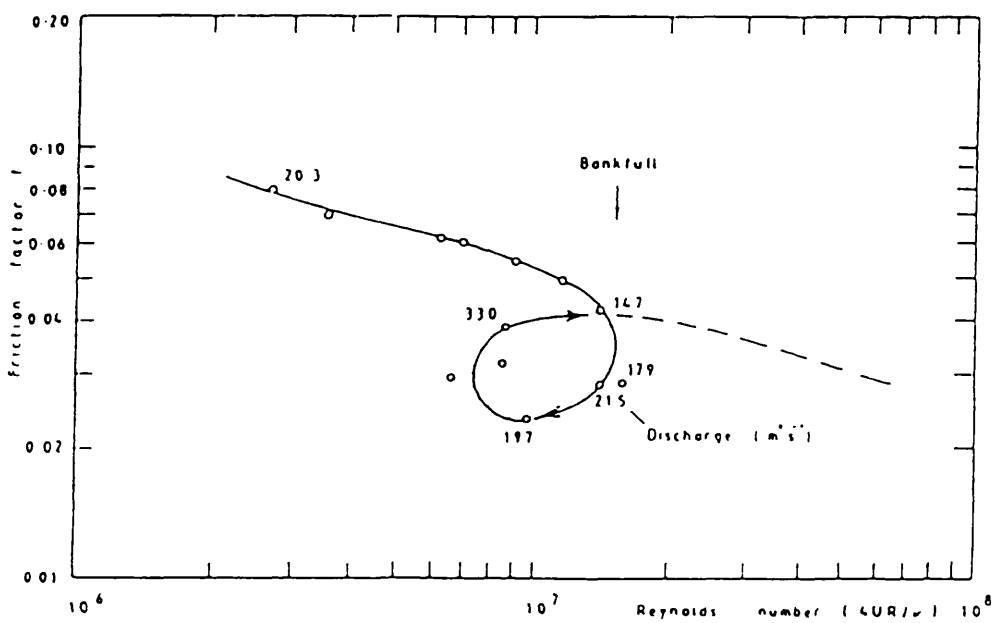

Fig (2.6(b)) - River Severn at Monford Bridge. Variation of friction factor with Reynolds number(after Knight(1989)).

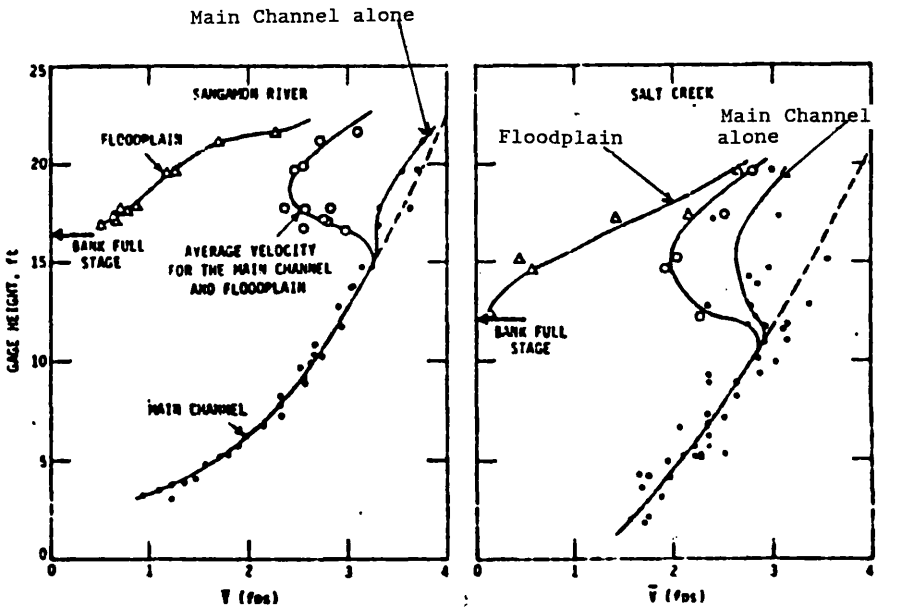

Fig (2.7) - Variation of Average Velocity with Stage in Main Channel, on Floodplain and Considering Composite Cross Section(after Bhowmik 1982)

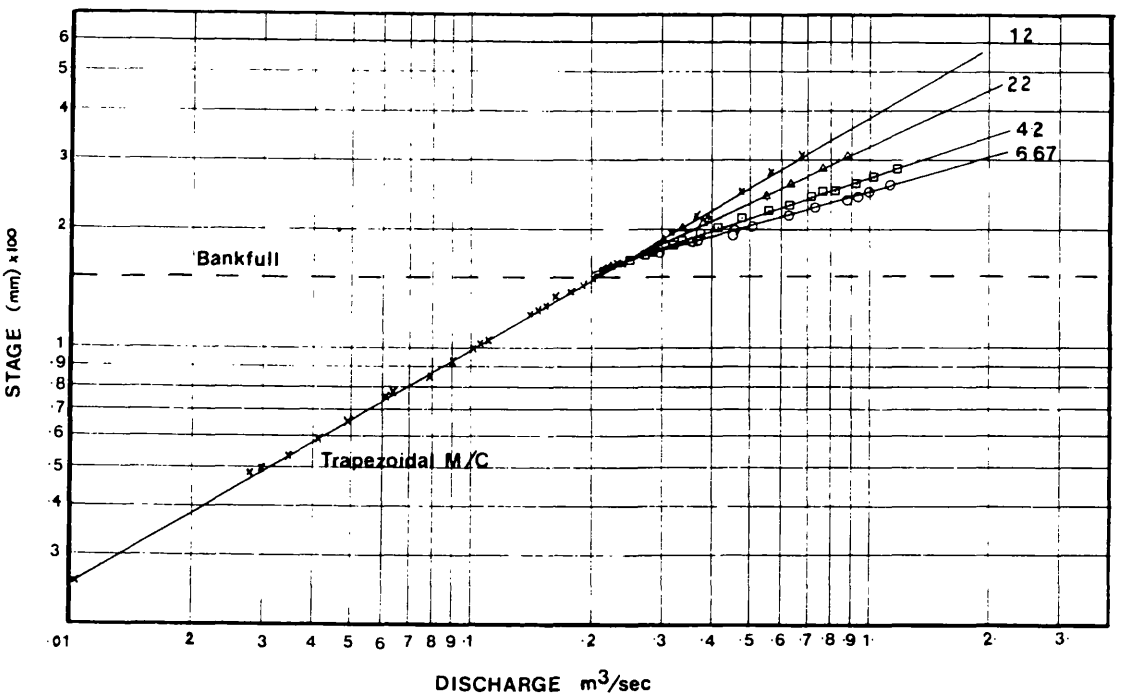

Fig (2.8) - Typical Rating Curves of Straight Compound Channels by Myers(1989).

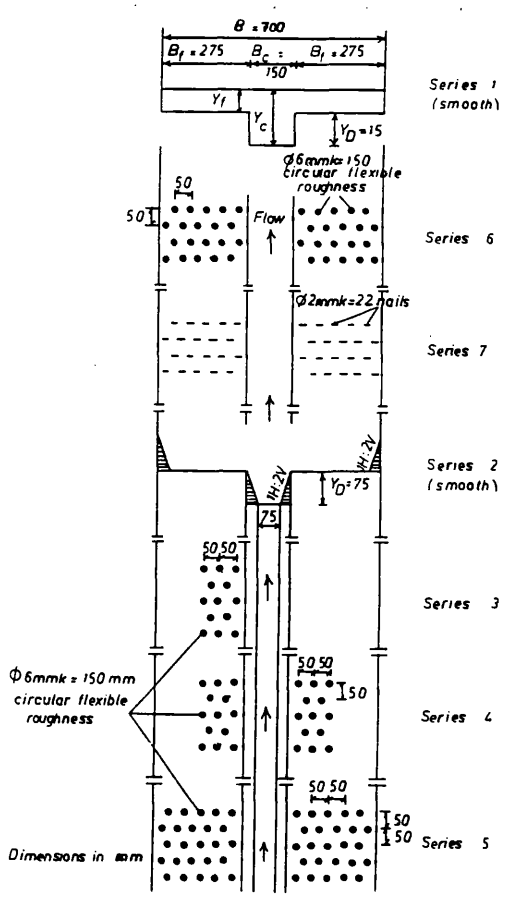

Fig(2.9(a)) - Plan View and Cross-Sections of the Flume Used by Nalluri and Judy(1985) in the Study of Compound Channels with Vegetated Floodplains.

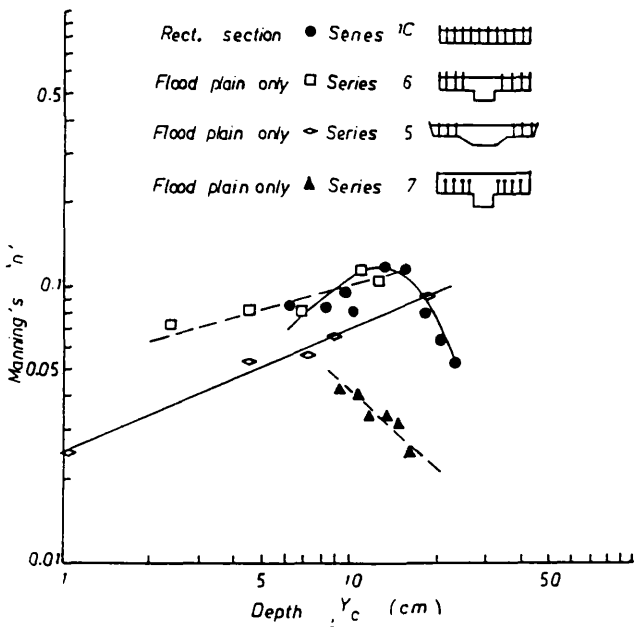

Fig(2.9(b)) - Comparison of Manning's n(floodplain only) for Different Cross-Sections and Roughness(After Nalluri and Judy(1985)).

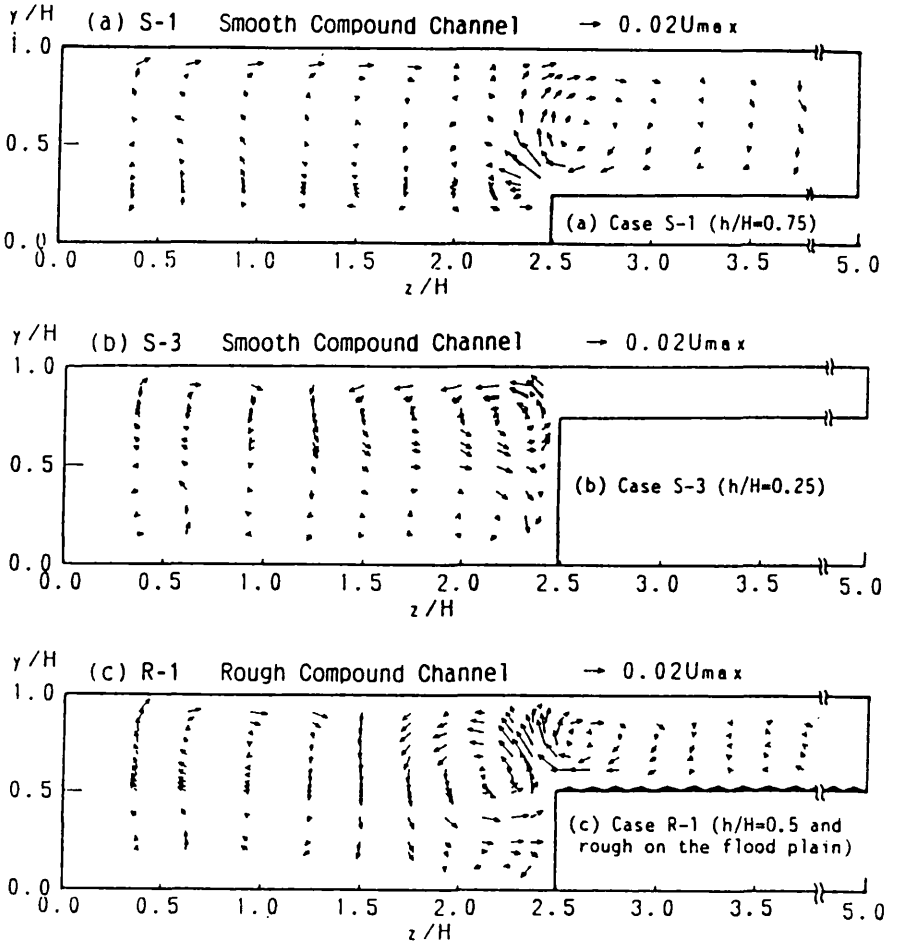

Fig (2.10(b)) - Secondary Currents in a Symmetrical Compound Cross-Section by Shiono(1991).

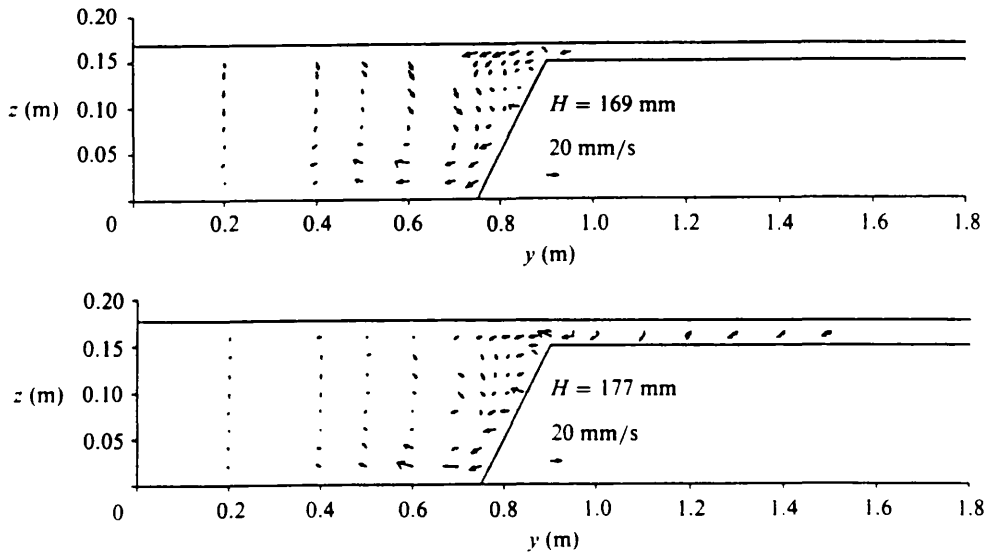

Fig (2.10(a)) - Secondary Currents in an Asymmetrical Compound Cross-Section by Tominaga(1991).

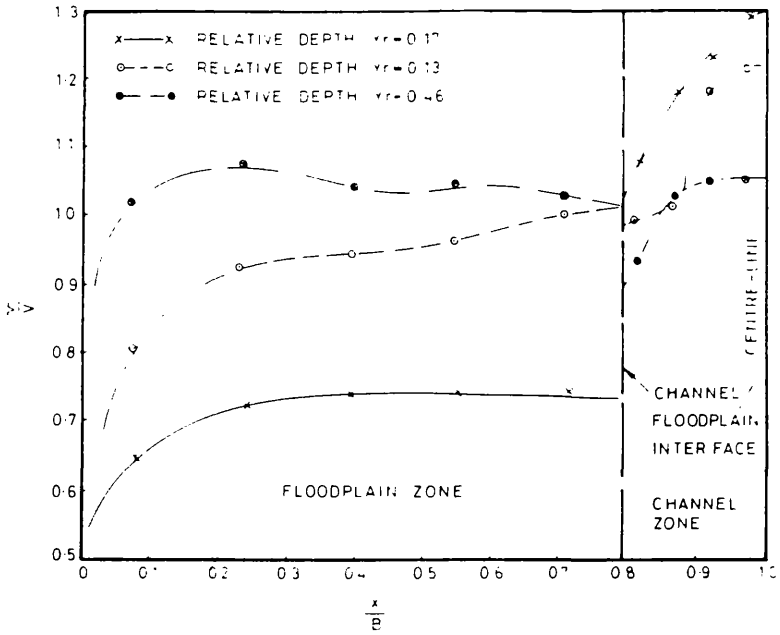

Fig (2.11) - Variation of Depth Averaged Velocity in a Straight Symmetrical Compound Channel by Myers(1987)

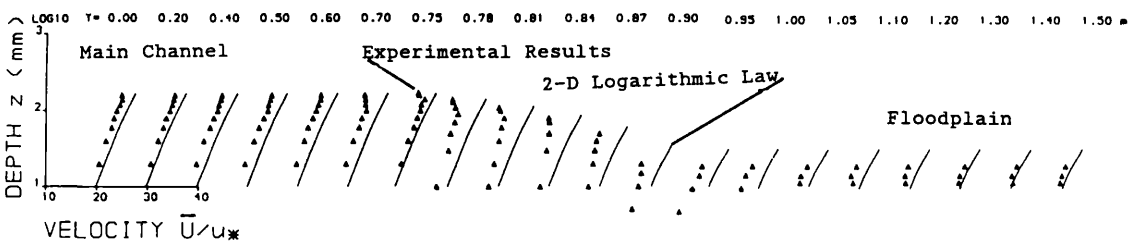

Fig (2.12) - Non-Dimensional Profiles of Longitudinal Velocity in a Symmetrical Cross Section of a Compound Channel by Shiono(1989)

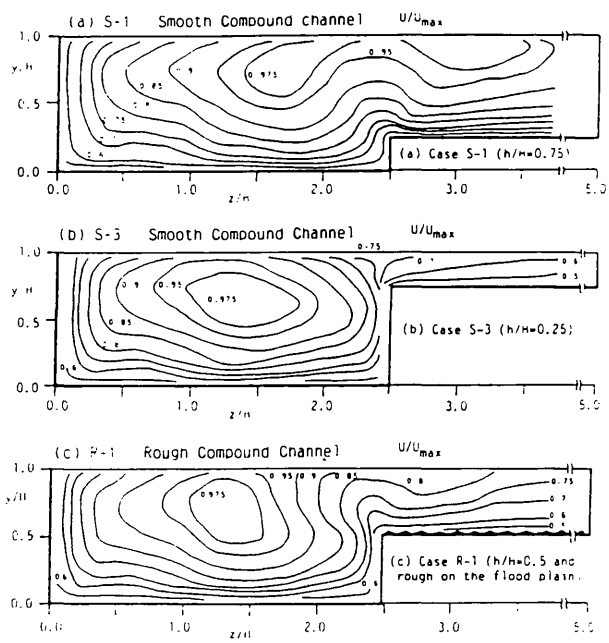

Fig (2.13) - Non-Dimensional Profiles of Longitudinal Velocity in an Asymmetrical Cross Section of a Compound Channel by Tominaga(1991)

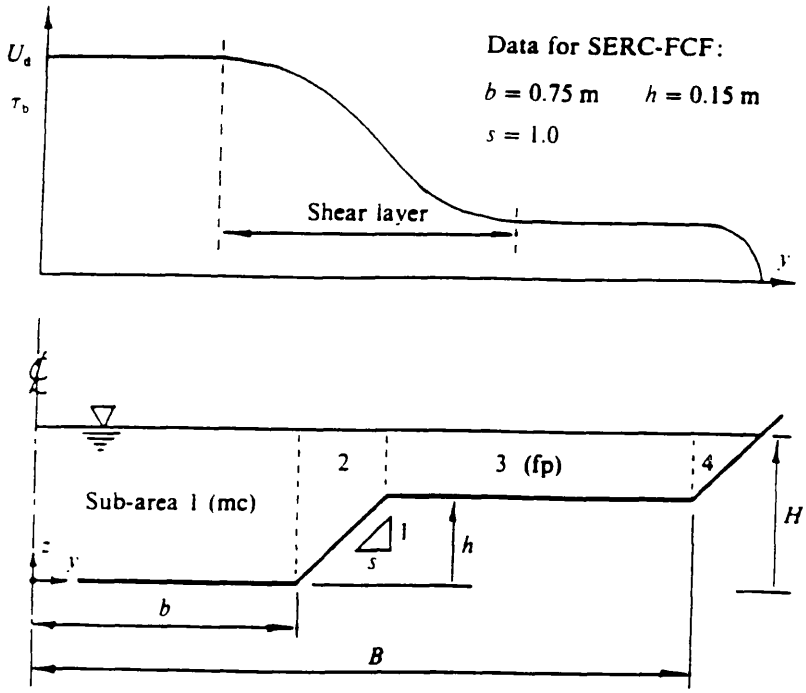

Fig (2.14) - Width of Lateral Shear Layer in Straight Compound Channels by Knight(1991)

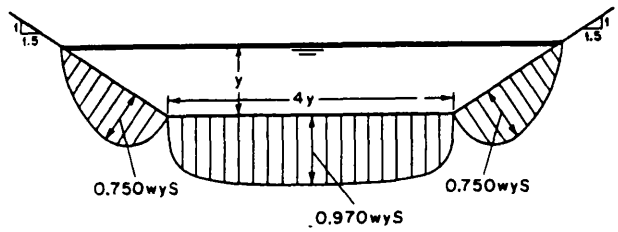

a) Sketch of Distribution of Boundary Shear Stress in a Straight Single Open Channel(After **Chow (1959)**

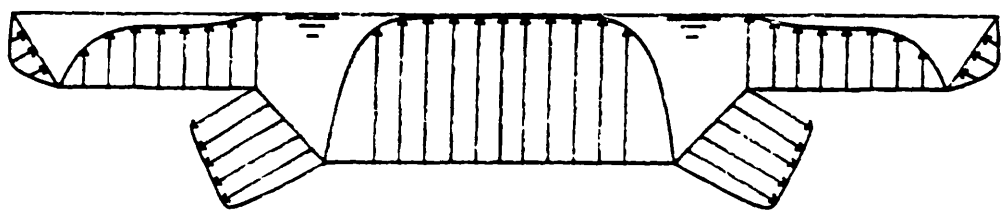

b) Sketch of Distribution of Boundary Shear Stress in a Straight Compound Channel.

Fig (2.15) - Typical Distribution of Boundary Shear Stress in Straight Open Channels. a) Single Channel b) Compound Channel.

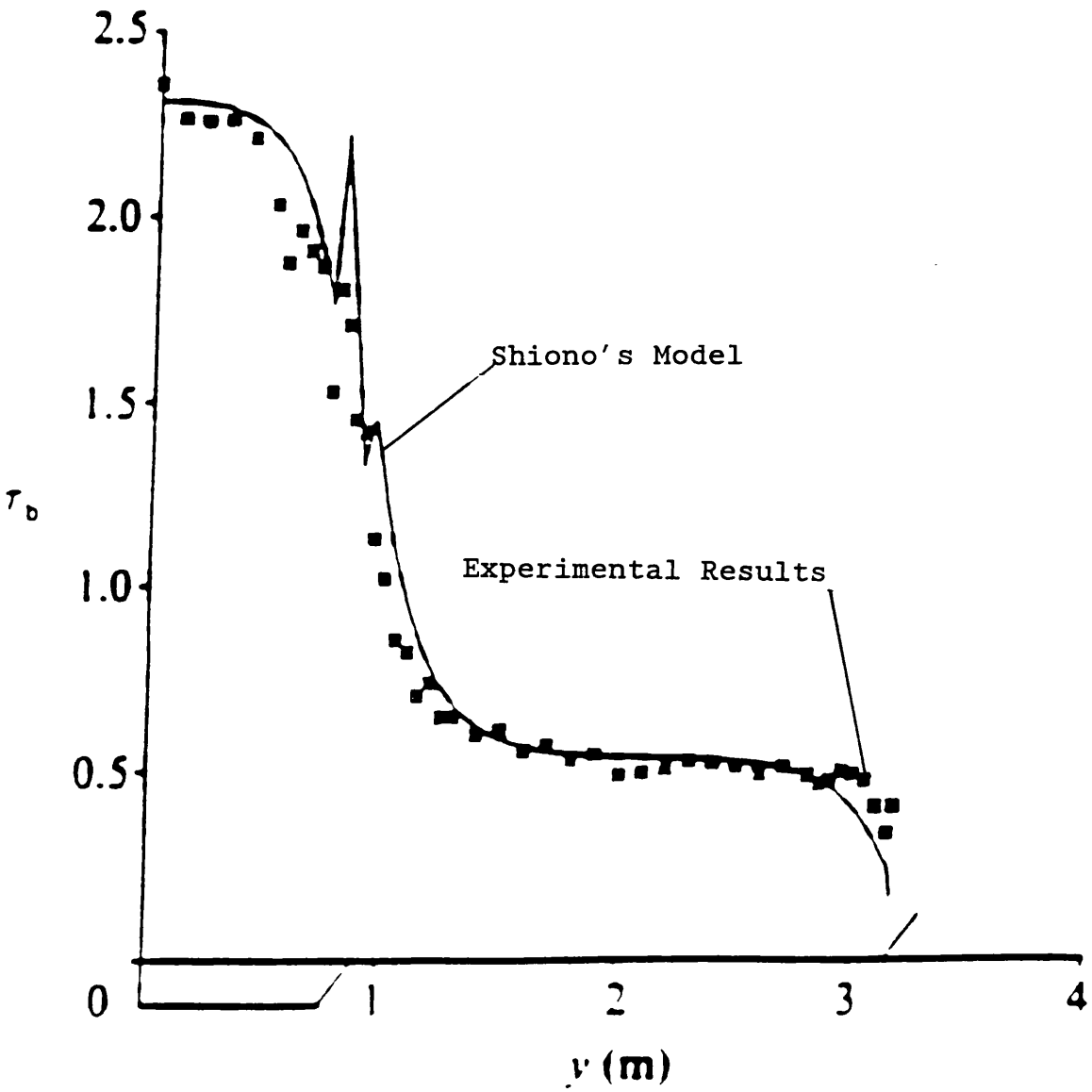

Fig (2.16) - Boundary Shear Stress in a Straight Compound Channel. Comparison Between Experimental Data and Shiono(1991) Model.

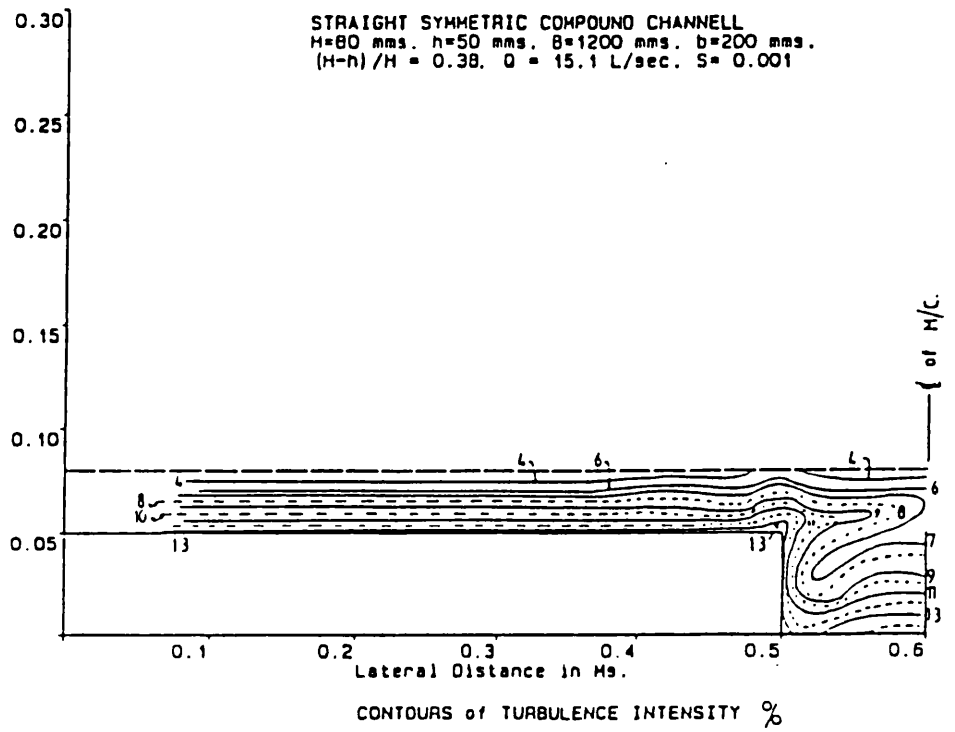

Fig (2.17) - Contours of Turbulence Intensity in a Straight Compound Channel by Mckeogh(1989).

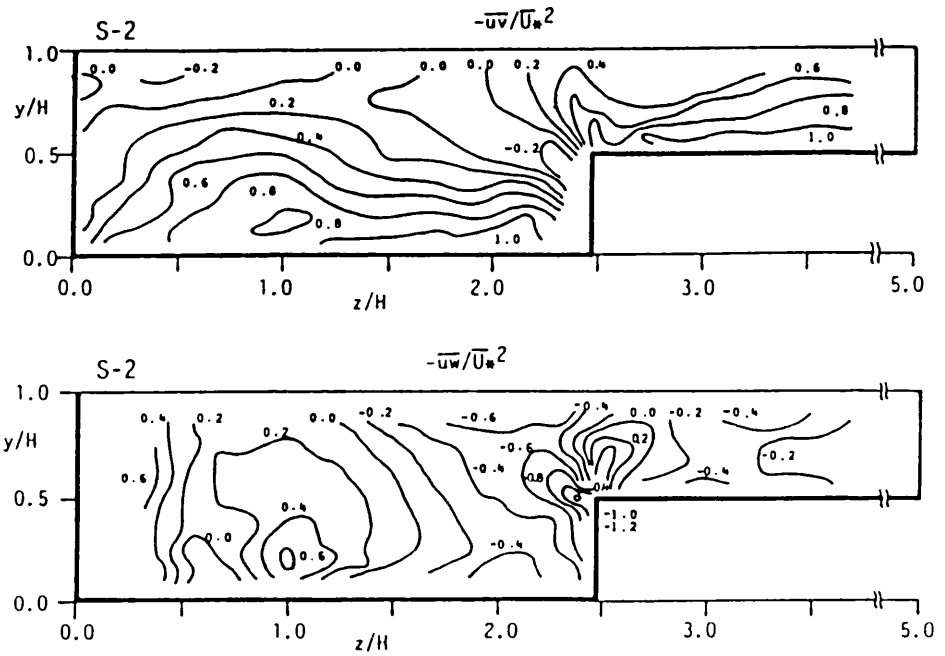

Fig (2.18) - Distribution of Reynolds Shear Stress in an Asymmetrical Cross-Section of a Compound Channel by Tominaga(1990).

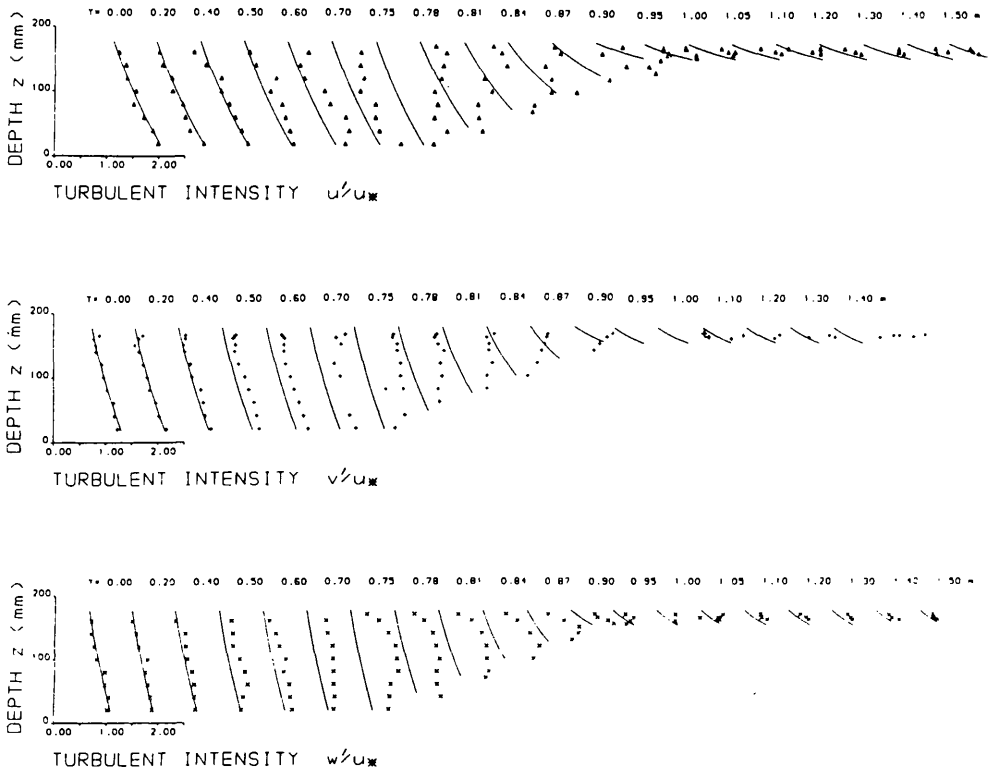

Fig (2.19) - Non-Dimensional Profiles of Turbulent Intensities in a Symmetrical Cross-Section of a Compound Channel by Shiono(1989).

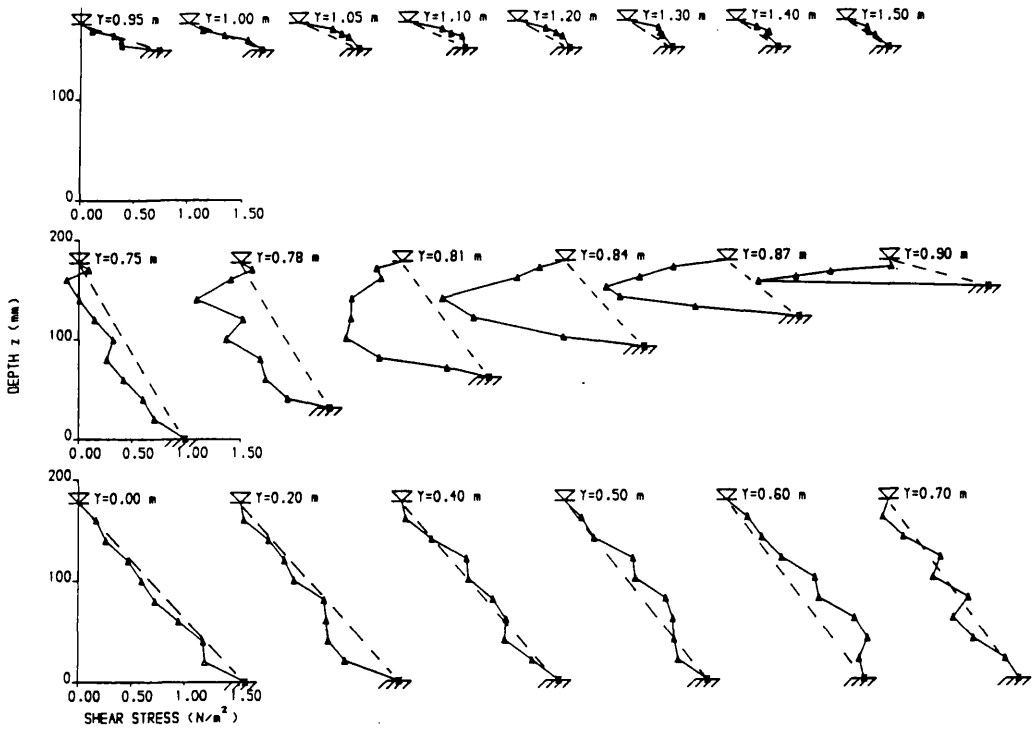

Fig (2.20) - Distribution of τ_{zx} in a Straight Compound Channel by Shiono(1989).

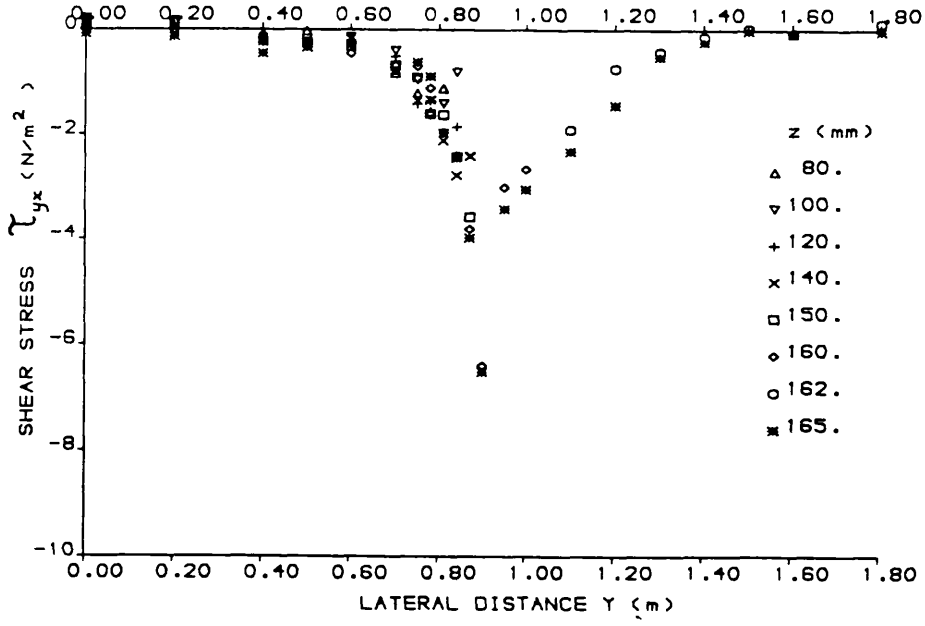

Fig (2.21) - Distribution of τ_{xy} in a Straight Compound Channel by Shiono(1989).

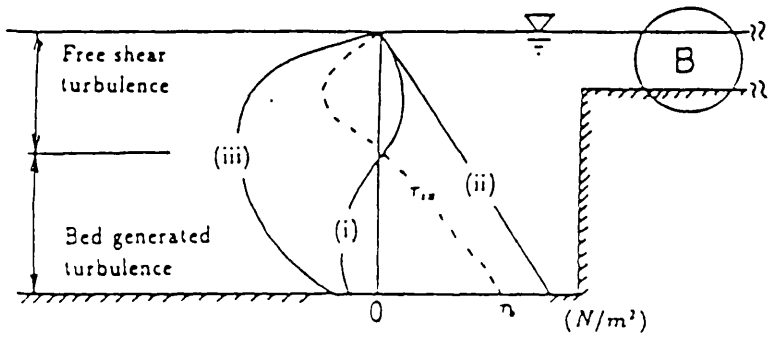

Shear stress distribution in main channel

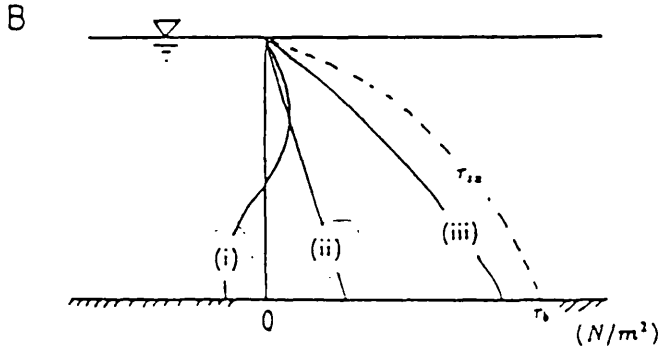

Shear stress distribution in flood plain

Fig (2.22) - Ilustrative Explanation of Shear Stress Distribution in a Straight Compound Channel by Knight(1989)

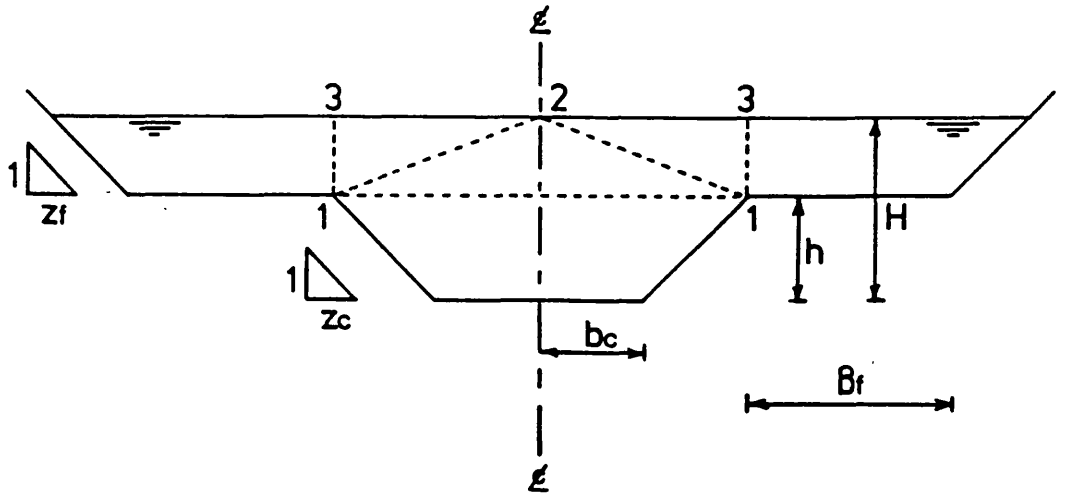

Fig (2.23) - Division Line Method Applied to Compound Channels.

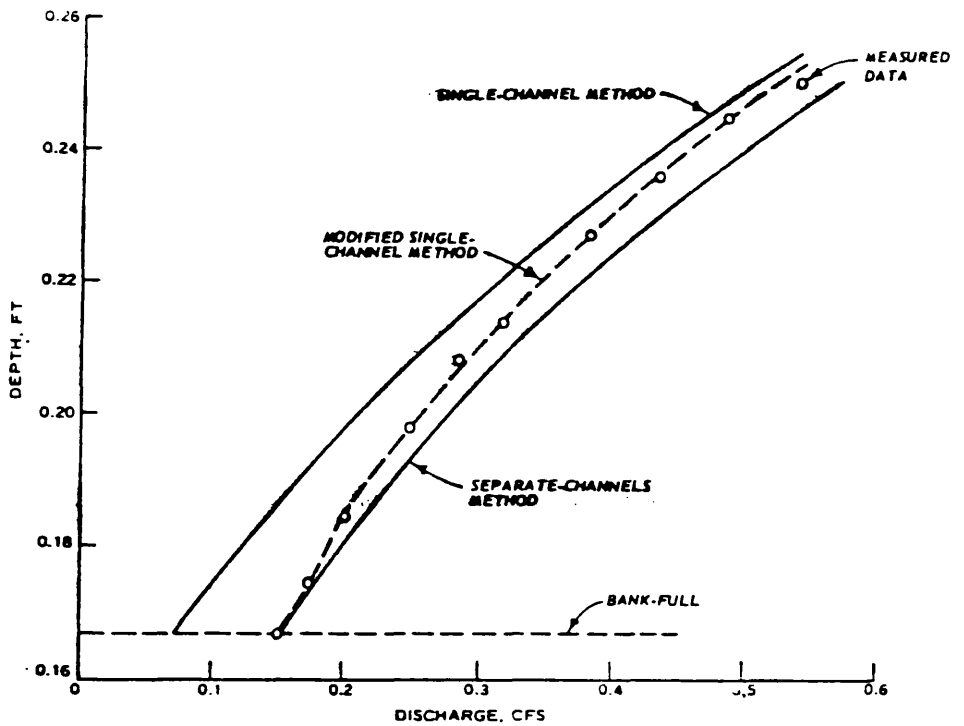

Fig (2.24) - Comparison of Measured Data and Theoretical Methods for Prediction of Stage-Discharge Relationship by Brown(1977).

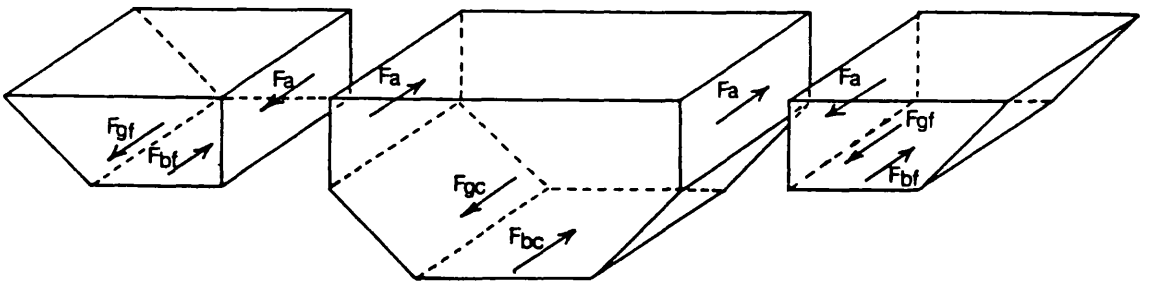

Fig (2.25) - The Out Balance of Forces in a Straight Compund Channel.

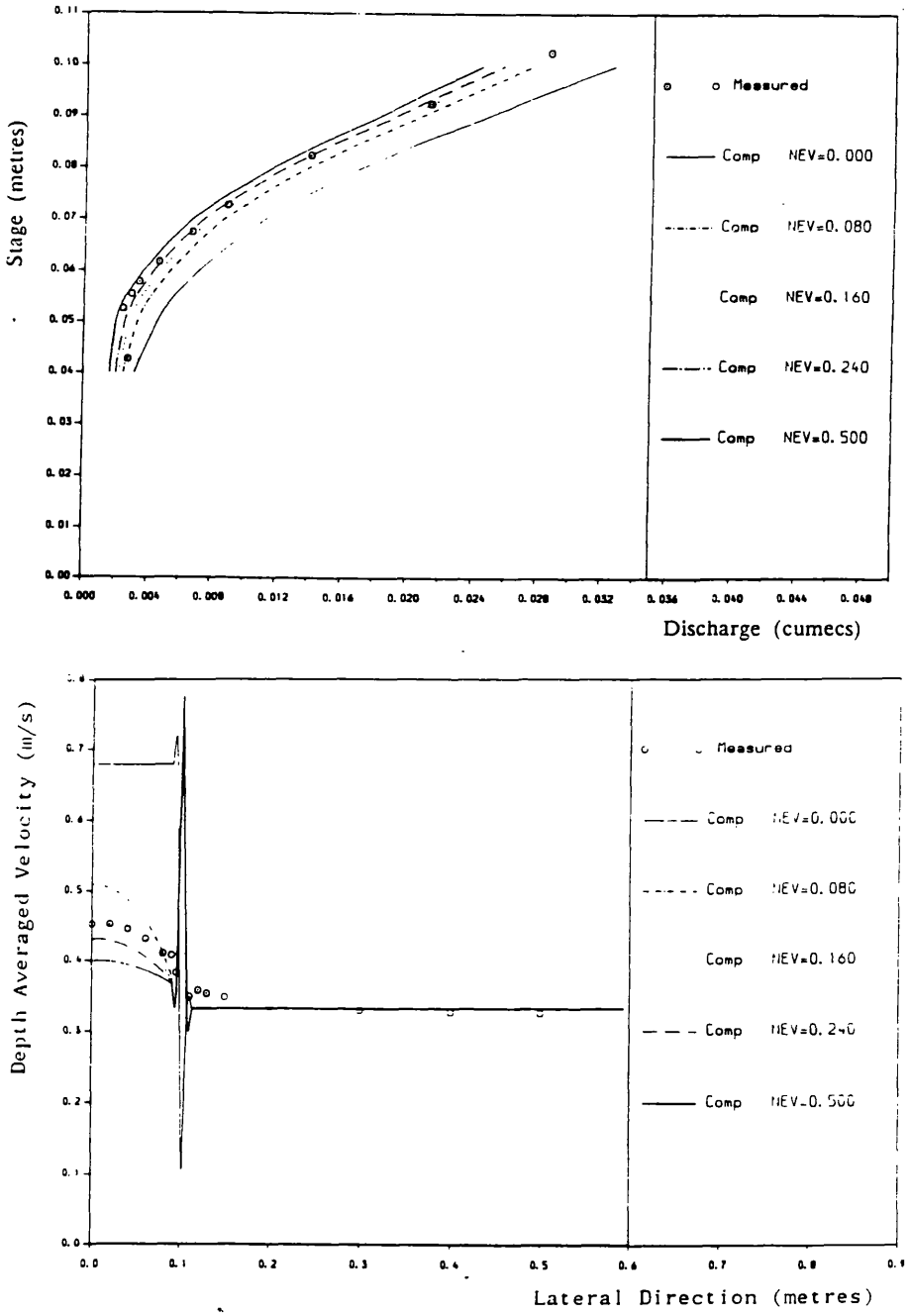

Fig (2.26) - Comparison of Kiely(1990) Experimental Results with Wark(1990) Numerical Model.

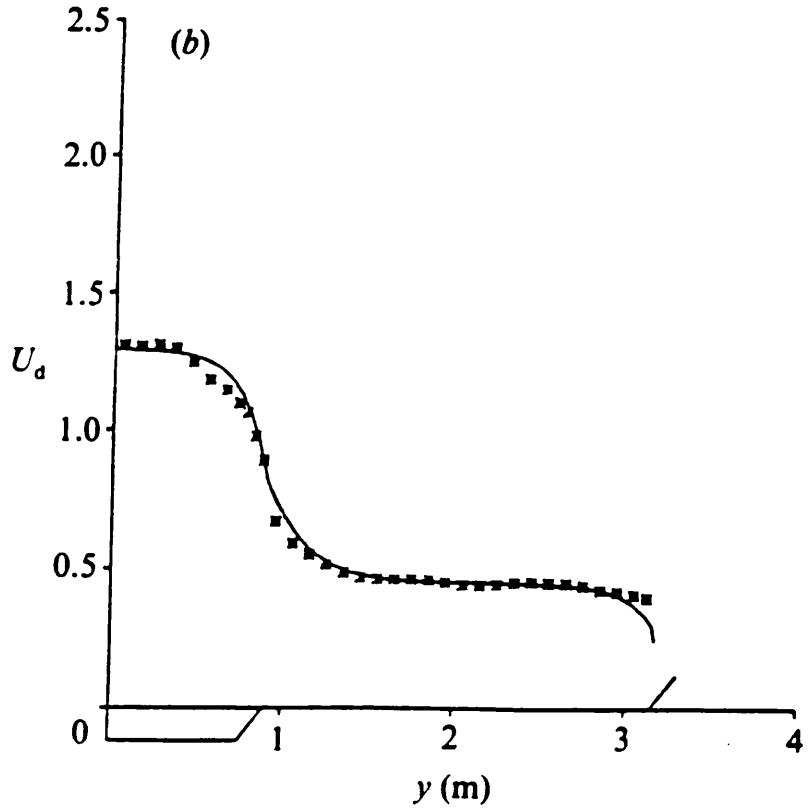

Fig (2.27) - Comparison of S.E.R.C. Experimental Results with Shiono(1991) Numerical Model.

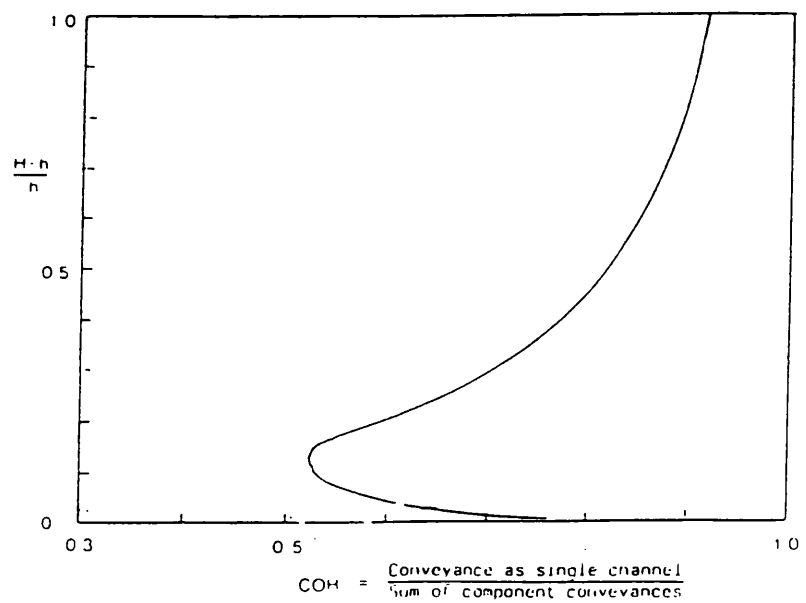

Fig (2.28) - Coherence of River Severn by Ackers(1991).

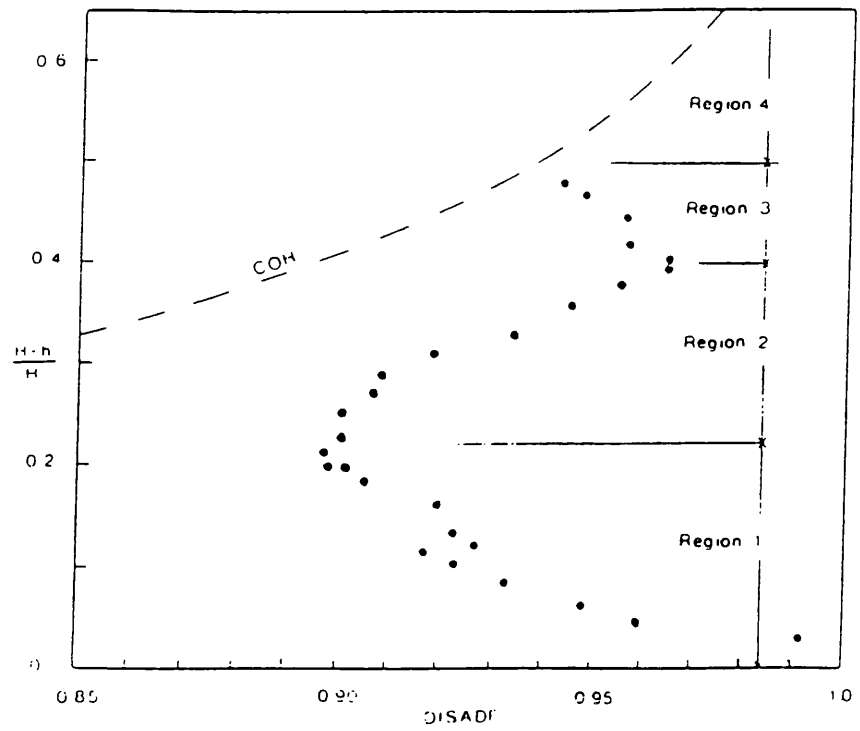

Fig (2.29) - Variation of DISADF with Depth Ratio by Ackers(1991)

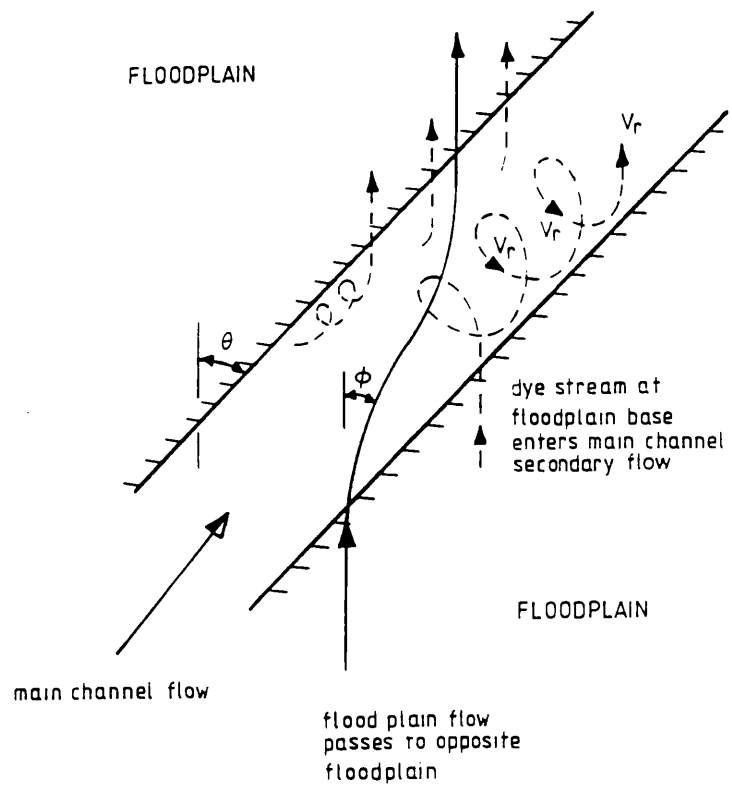

Fig (2.30) - Ocurrence of Flow Bifurcation in Skewed Compound Channels by Ervine and Jasem(1991).

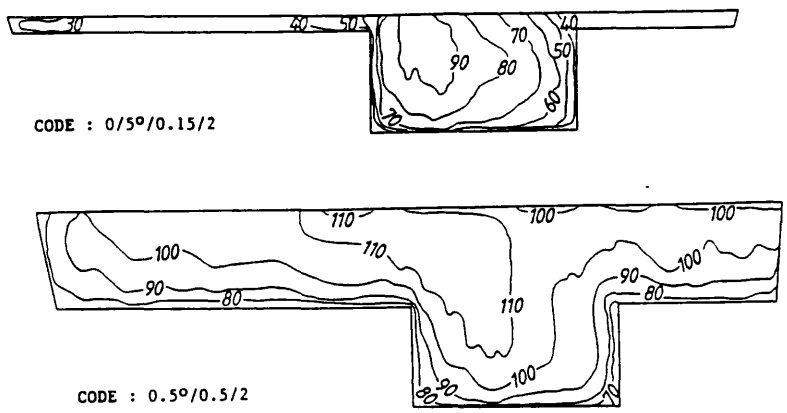

Fig (2.31) - Distribution of Longitudinal Velocities in Skew Compound Channels by Elliot and Sellin(1990).

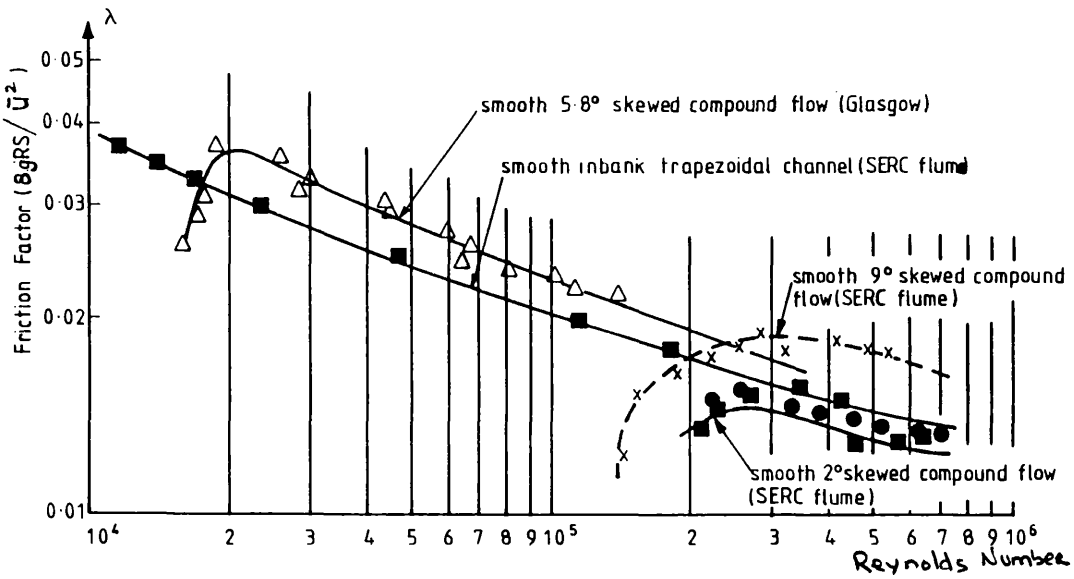

Fig (2.32) - Friction Factors for Skewed Compound Channels by Ervine and Jasem(1991).

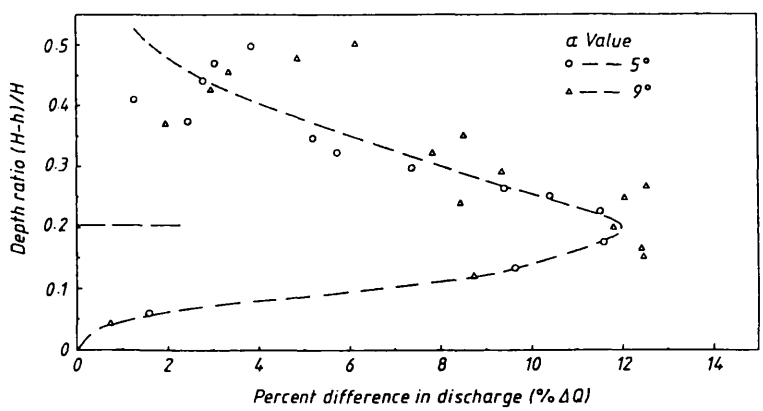

Fig (2.33) - Percent Reduction in Discharge in Skewed Compound Channels in Comparison with Straight Compound Channels by Elliot and Sellin(1991)

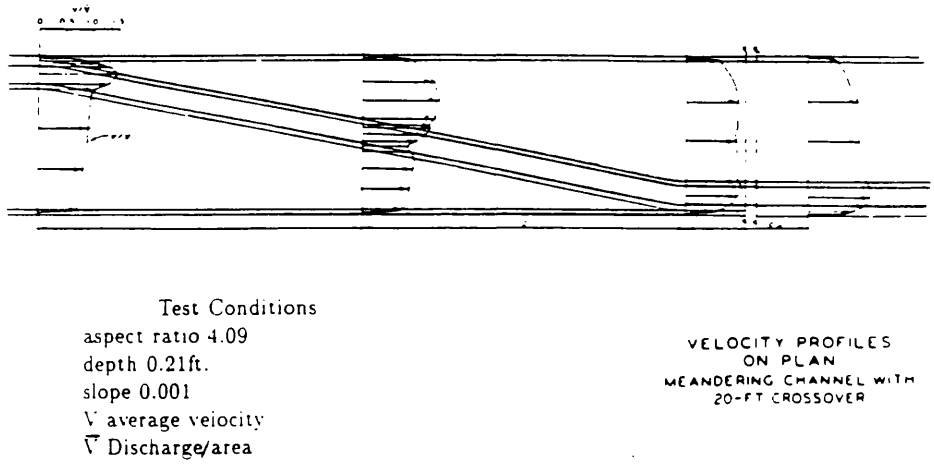

Fig (2.34) - Velocity Profiles in a Skewed Compound Channel by James and Brown(1977).

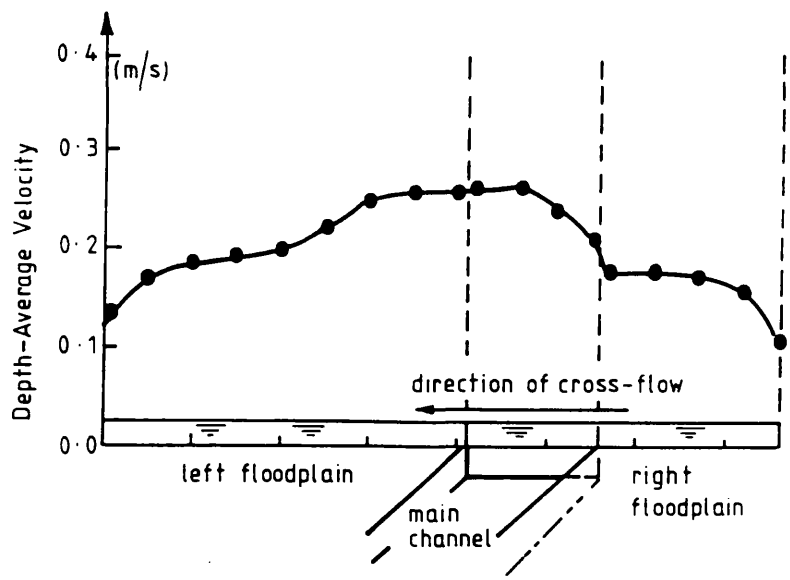

Fig (2.35) - Lateral Distribution of Depth Averaged Velocity in a Skewed Compound Channel by Ervine and Jasem(1991).

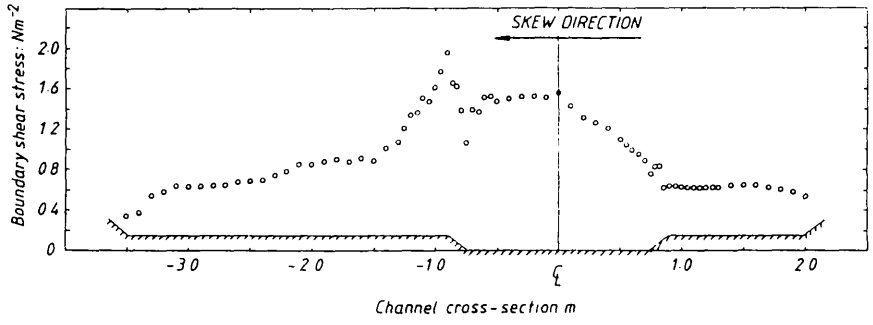

Fig (2.36) - Variation of Longitudinal Boundary Shear Stress Values Across The Skewed Channel by Elliot and Sellin(1990).

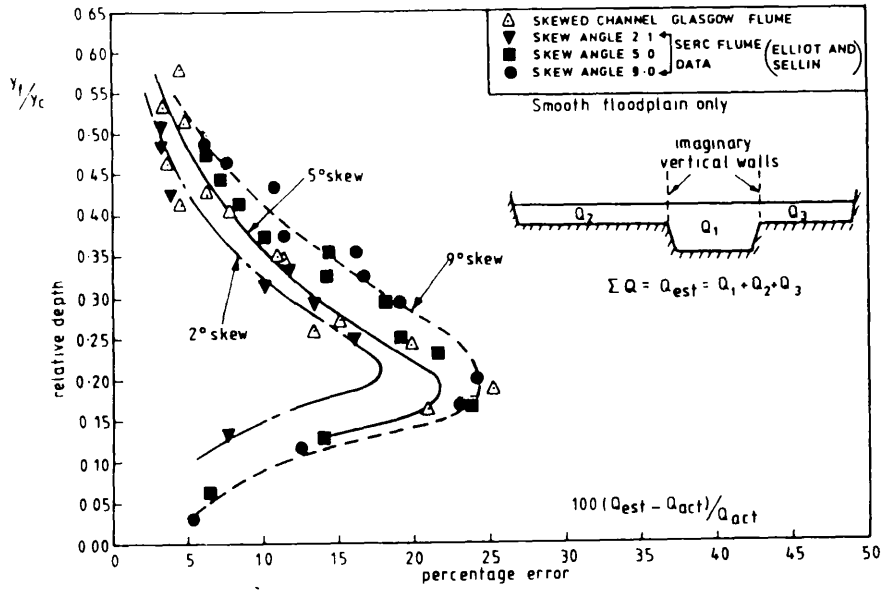

Fig (2.37) - Percentage of Error Between The Estimated and Experimental Discharge with Relative Depth by Ervine and Jasem(1991).

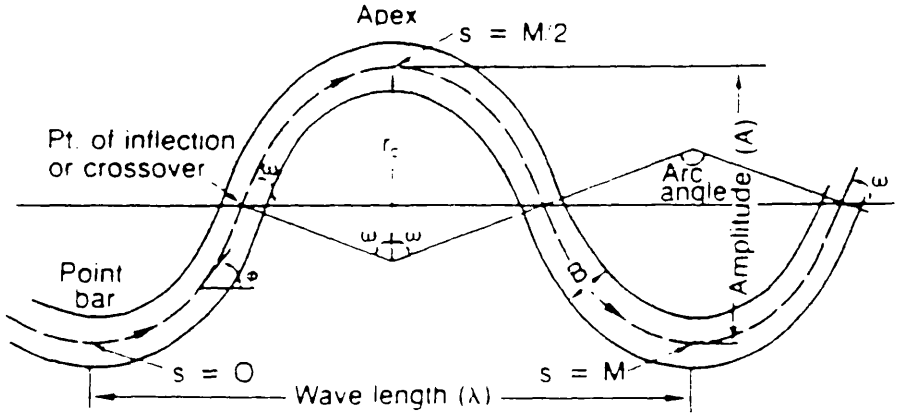

Fig (2.38) - Plan Geometry of a Regular Meander: Definitions and Terminology(After Chang(1987)

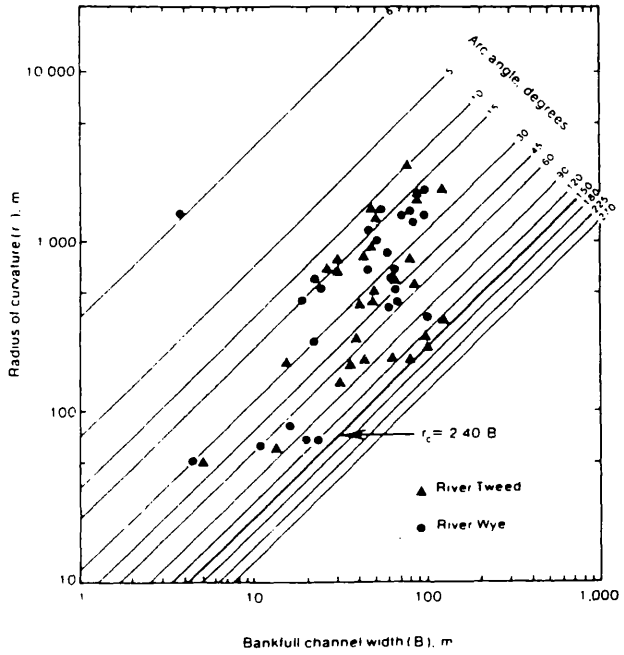

Fig (2.39) - Relationship between Radius of Curvature, Bankfull Width and Arc Angle by Hey(1976).

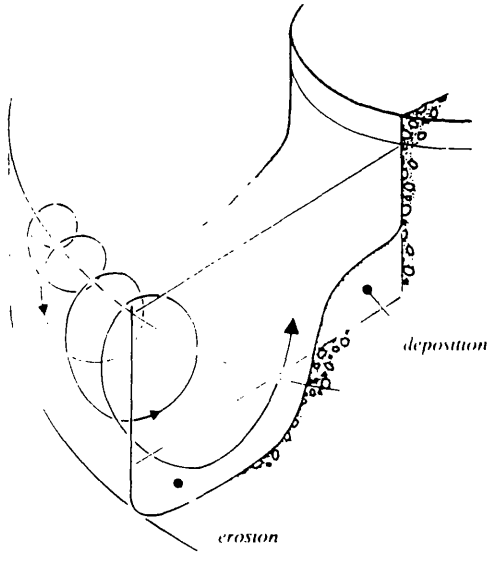

Fig (2.40) - Development of Secondary Currents around the Bend.

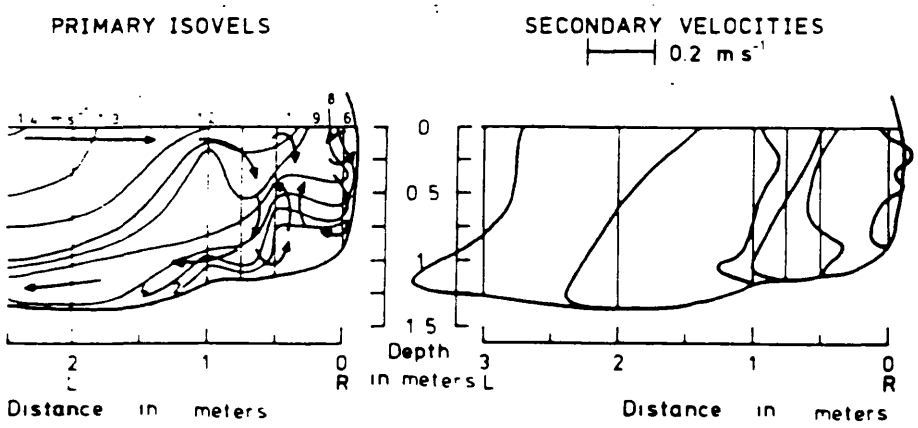

Fig (2.41) - Distribution of Primary and Secondary Velocities at Bend Apex at Maes Mawr River by Bathurst et al.(1979)

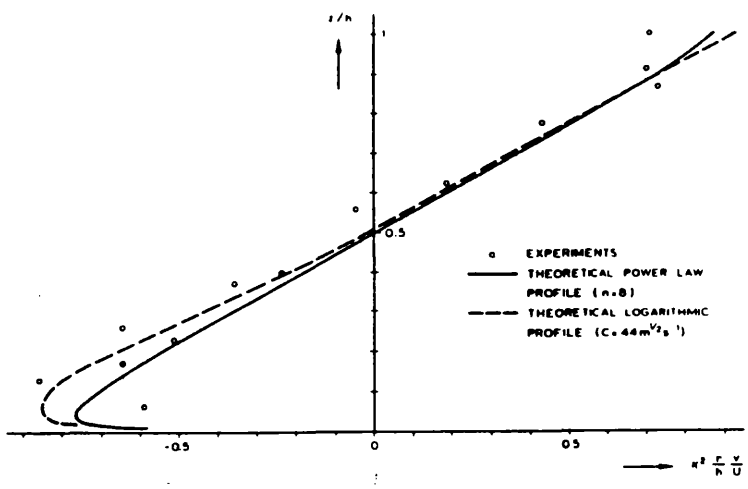

Fig (2.42) - Theoretical and Experimental Velocity Profiles for Secondary Flow in River Bends after Kondrat'ev(1959).

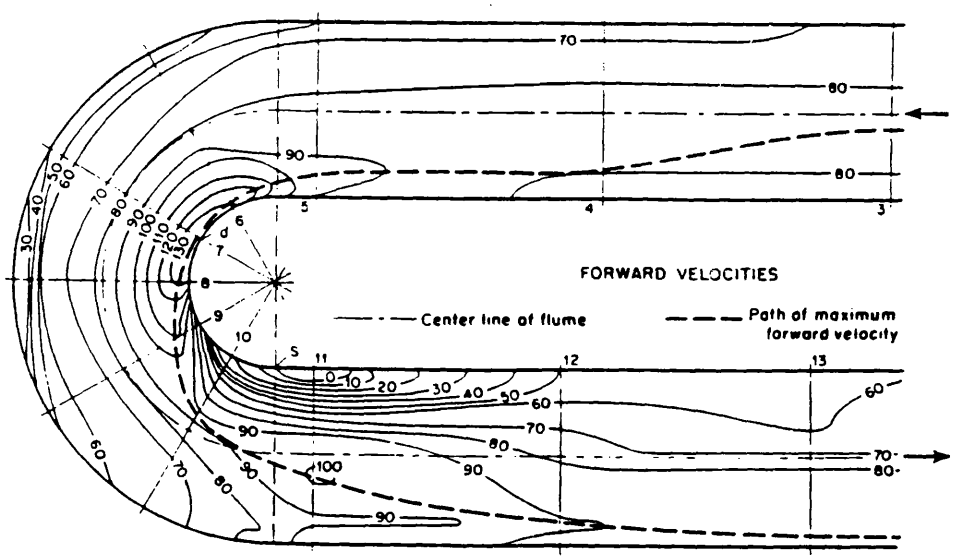

Fig (2.43(a)) - Contour Lines of Primary Velocities in a Flow Around the Bend(After Shukry(1950))

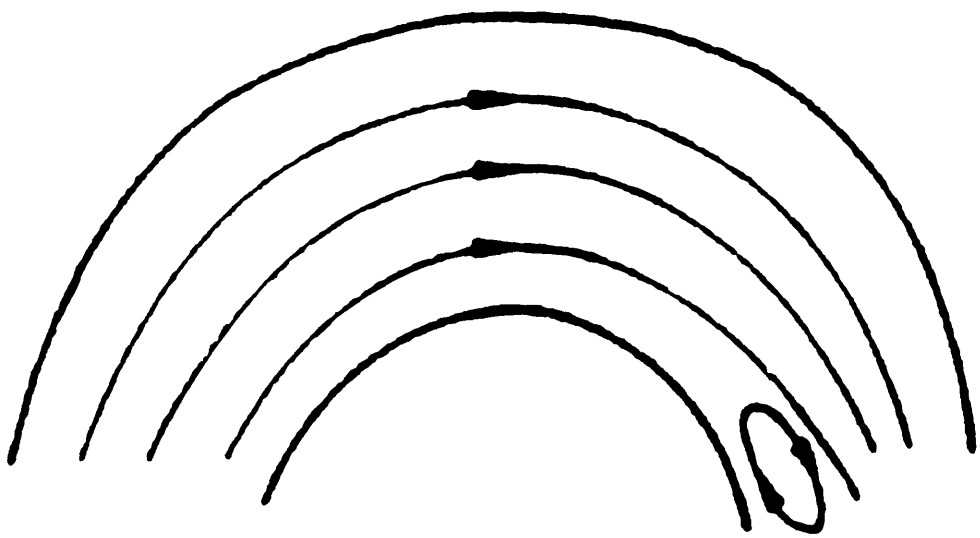

Fig (2.43(b)) - Sketch of Flow Separation in a River Bend.

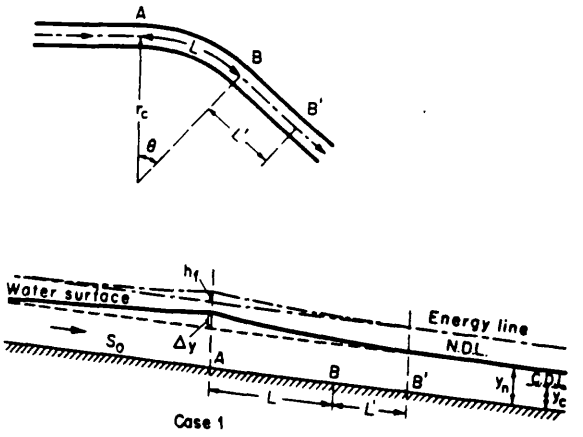

Fig (2.44) - Energy Line and Flow Profile around the Bend for Sub-Critical Flow(After Chow(1957)).

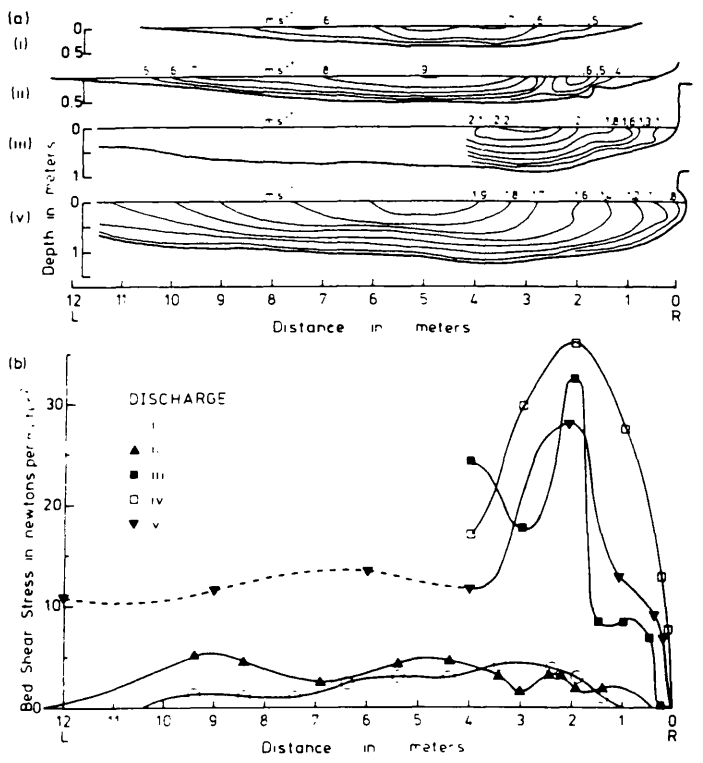

Fig (2.45) - Pattern of Primary Velocities Isovels and Distribution of Ratio of Boundary Shear Stress at Maes Mawr Bend at Discharges of: i) 5.25 m3/s ii) 6.84 m3/s iii) 15.48 m3/s (After Bathurst et al.(1962))

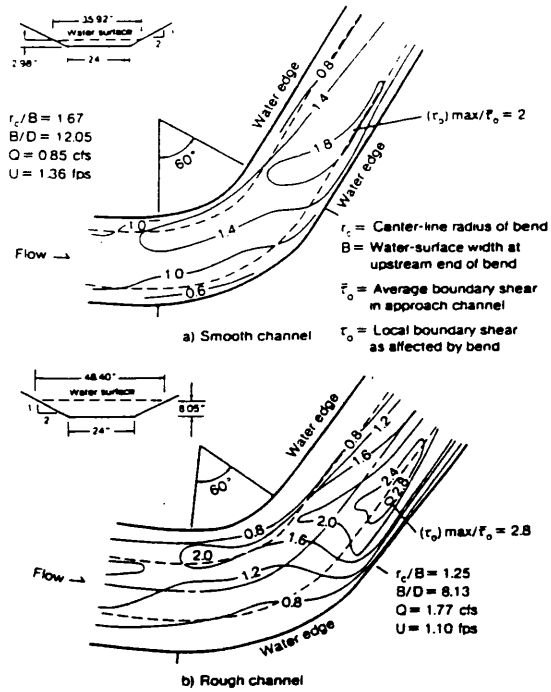

Fig (2.46) - Boundary Shear Stress Distribution in Curved Trapezoidal Channels obtained experimentally by Ippen and Drinker(1962).

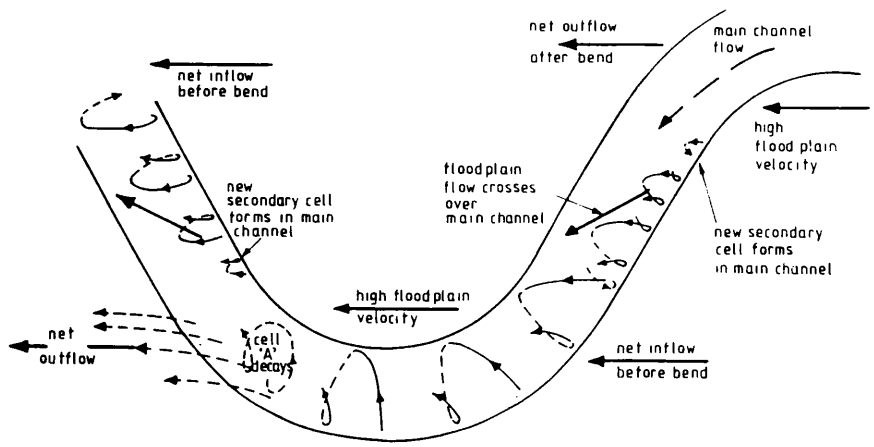

Fig (2.47) - Flow Mechanisms for Meandering Compound Channels(After Ervine and Jasem(1991))

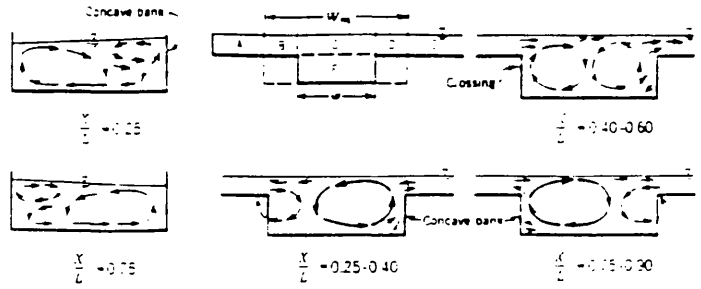

Fig (2.48) - Helicoidal Currents for Inbank Case and Overbank Case in Meandering Compound Channels(After Toebes and Sooky(1967))

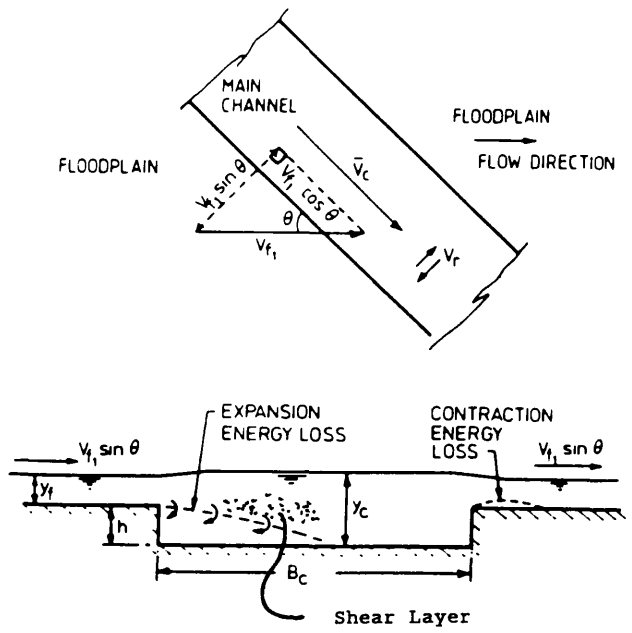

Fig (2.49) - Expansion and Contraction Phenomenom in Meandering Compound Channels(After Ervine Ellis(1987))

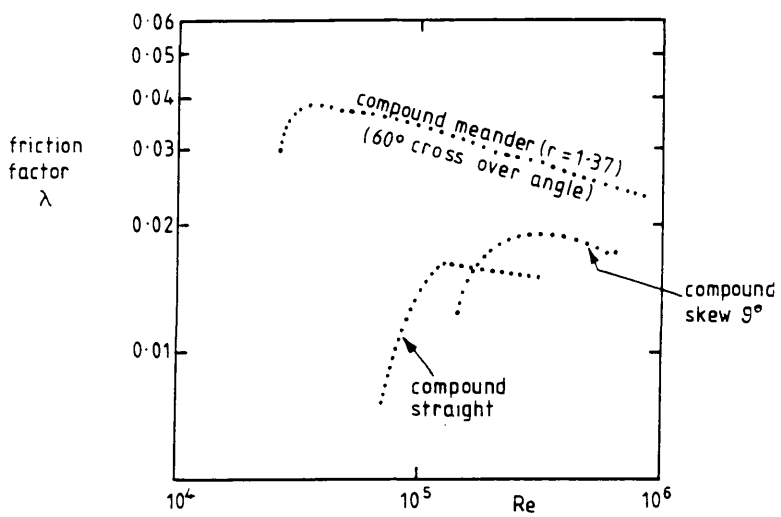

Fig (2.50) - Friction Factors for Various Types of Smooth Compound Flow(After Ervine and Jasem(1991))

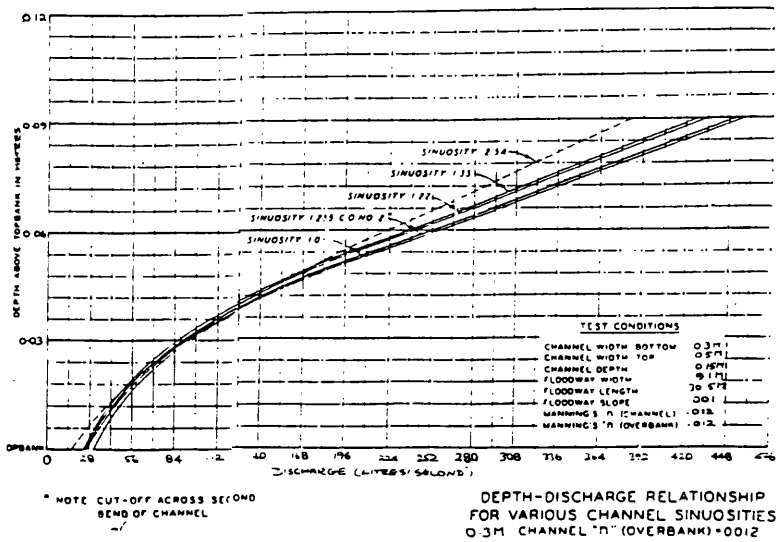

Fig (2.51) - Stage-Discharge Relationship for Various Channel Sinuosities from U.S. Army Corps of Engineers(1956).

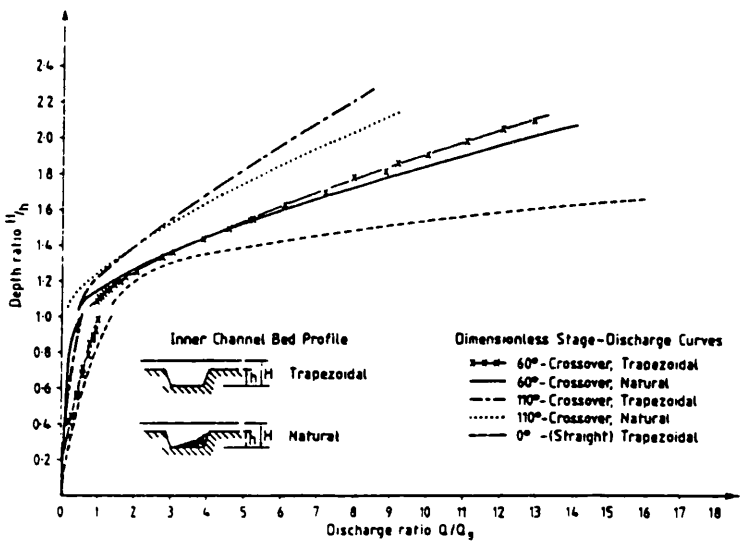

Fig (2.52) - Effect of Cross-Section Geometry on Stage-Discharge Relationship for Meandering Compound Channels from Willetts and Hardwick(1990).

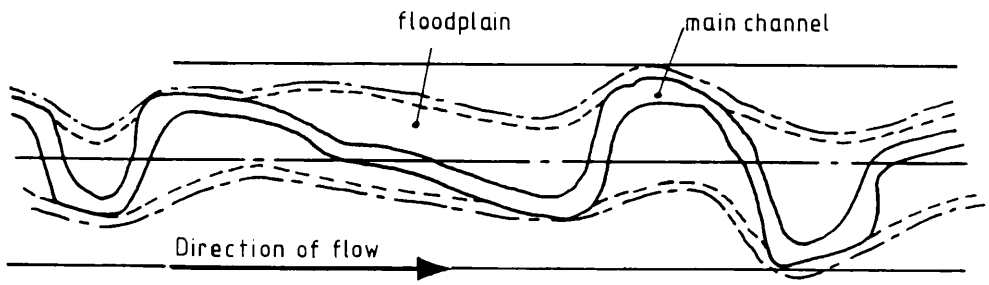

Fig (2.53) - Plan of the Reach of River Roding Modelled by Sellin and Giles(1988).

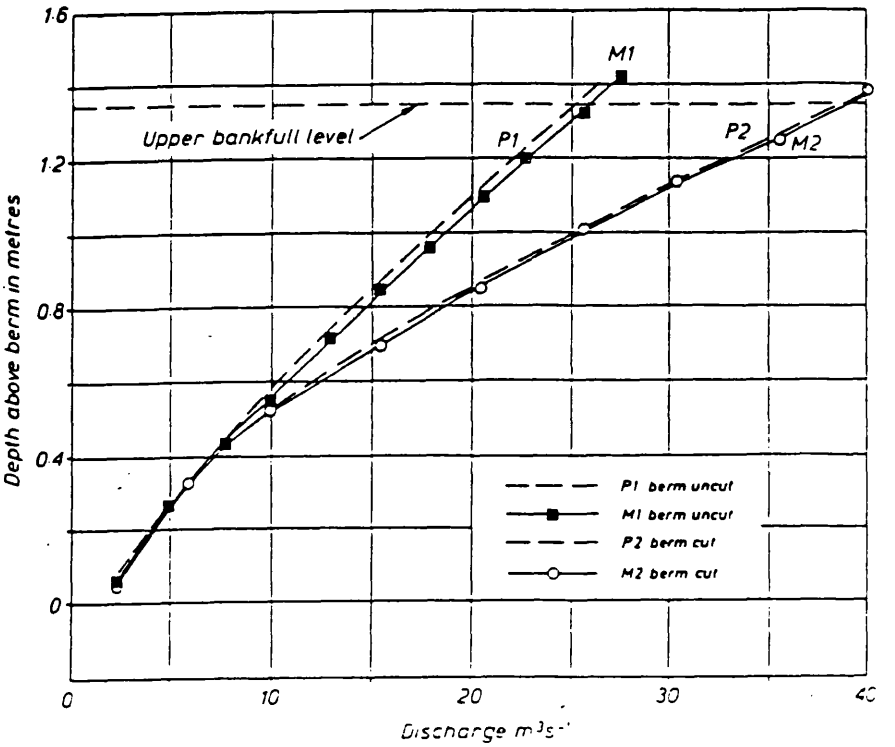

Fig (2.54) - Effect of Floodplain Roughness on the Stage-Discharge Curve of River Roding in Essex from Sellin and Giles(1988).

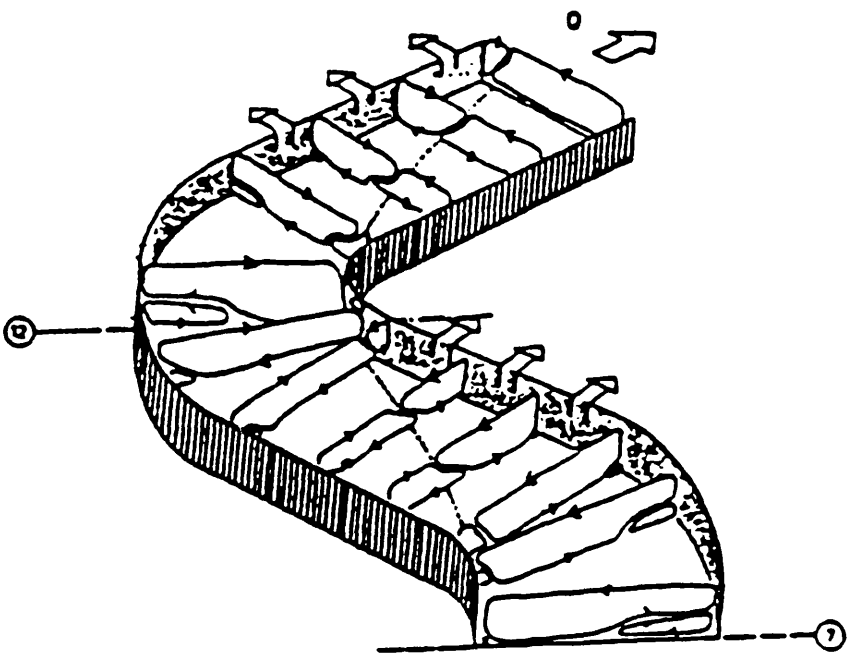

Fig (2.55) - Growth and Decay of Secondary Cells in Meandering Compound Channels by Stein and Rouve'(1989).

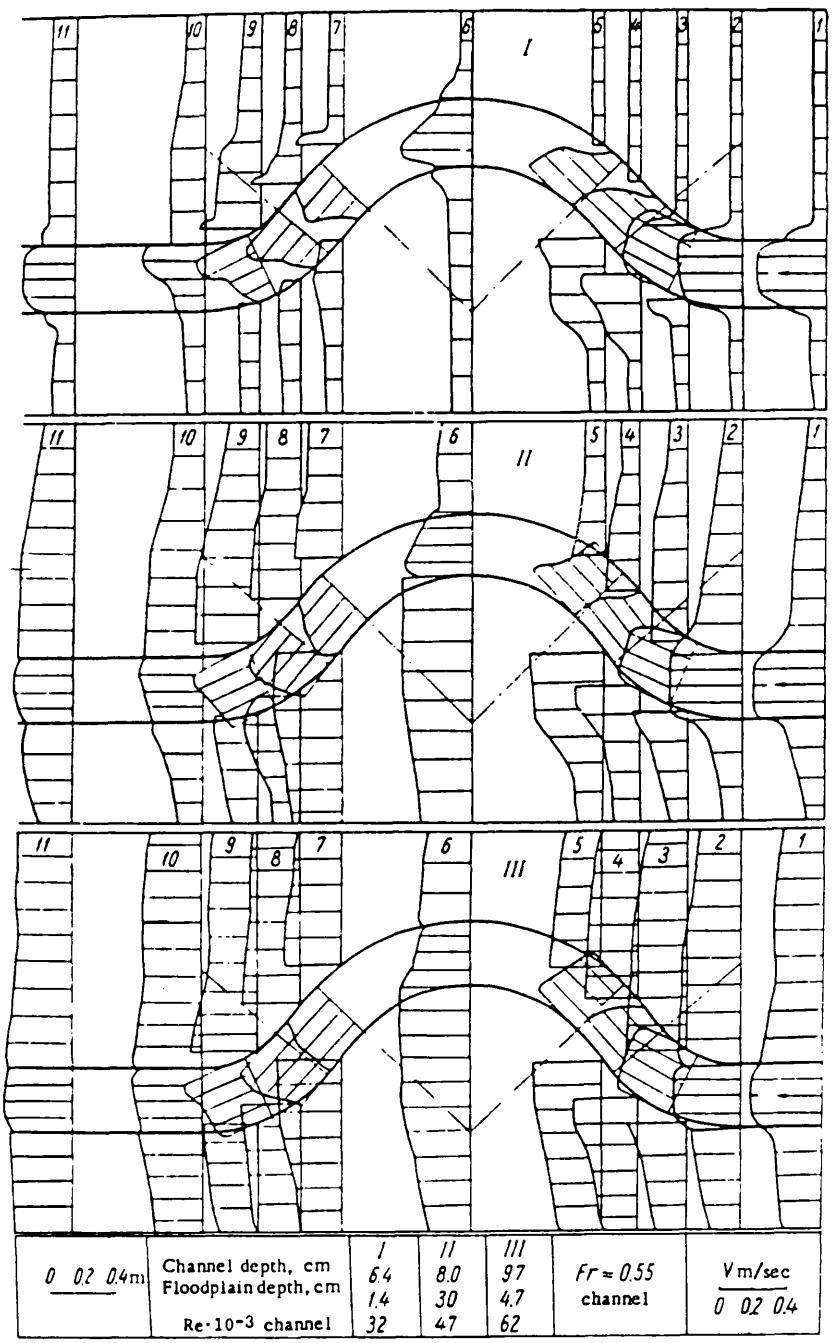

Fig (2.56) - Distribution of Depth Averaged Longitudinal Velocity across the Main Channel and Floodplain in a Compound Bend(After Goncharov(1957)).

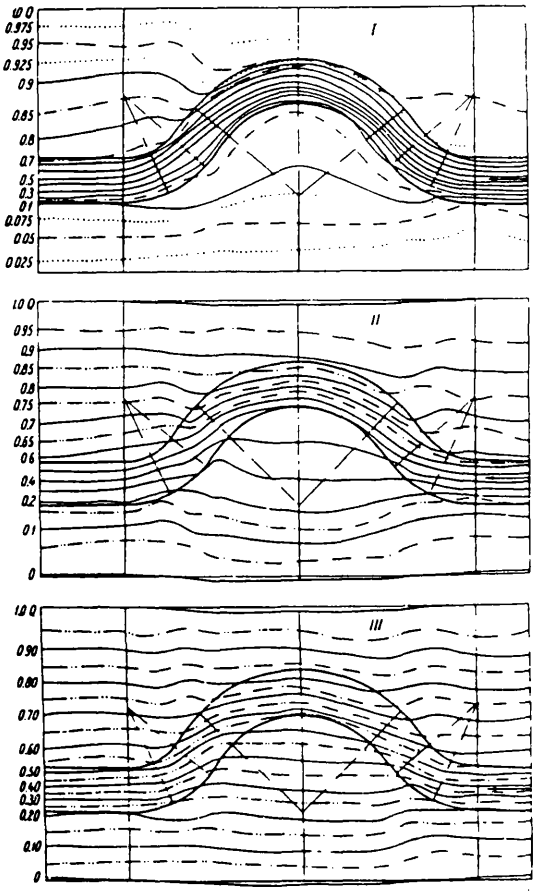

Fig (2.57) - Flow Patterns in a Compound Bend by Goncharov(1957).

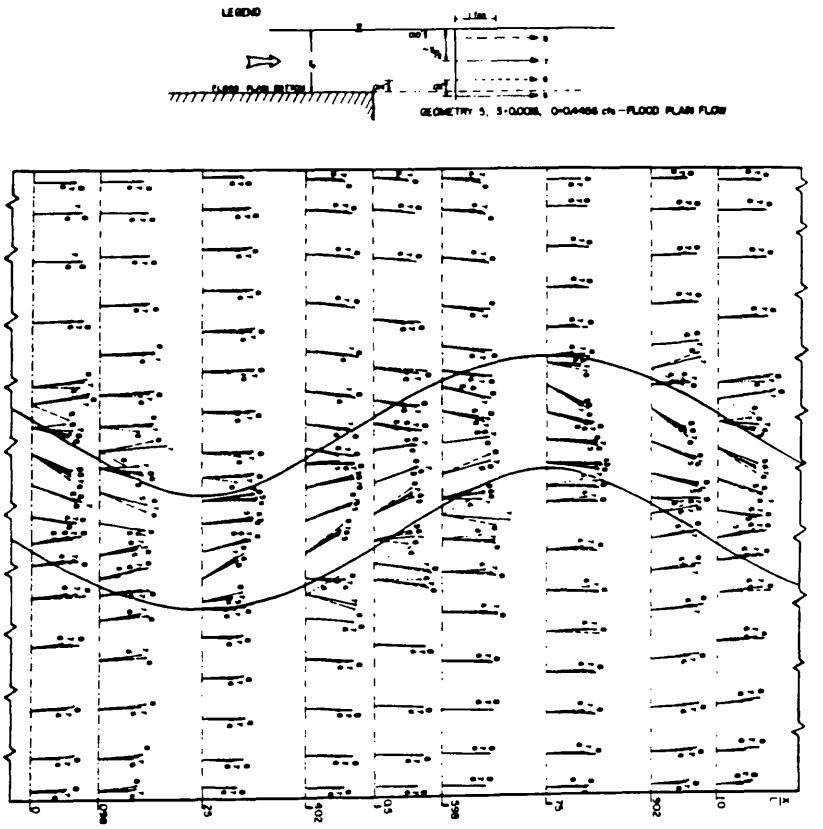

Fig (2.58) - Distribution of Resultant Velocity in a Meander Compound Channel by Toebes and Sooky(1967).

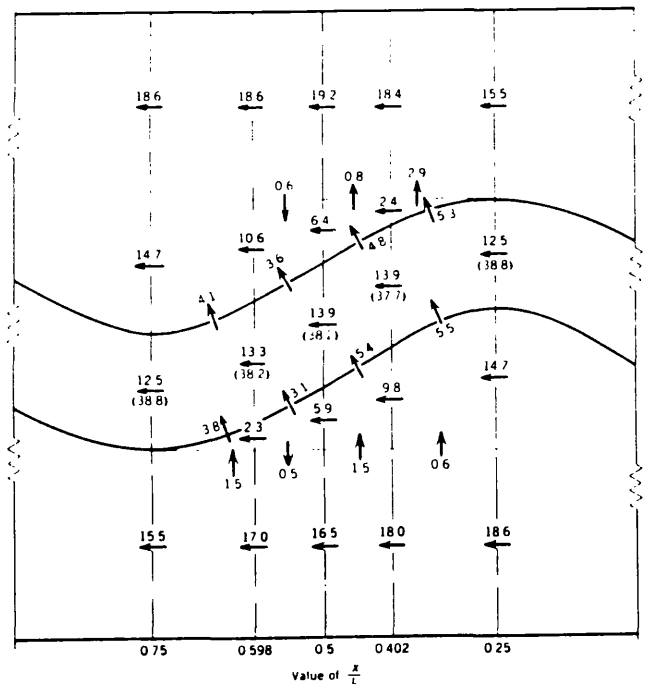

Fig (2.59) - Discharge Distribution in a Meander Compound Channel(After Toebes abd Sooky(1967)).

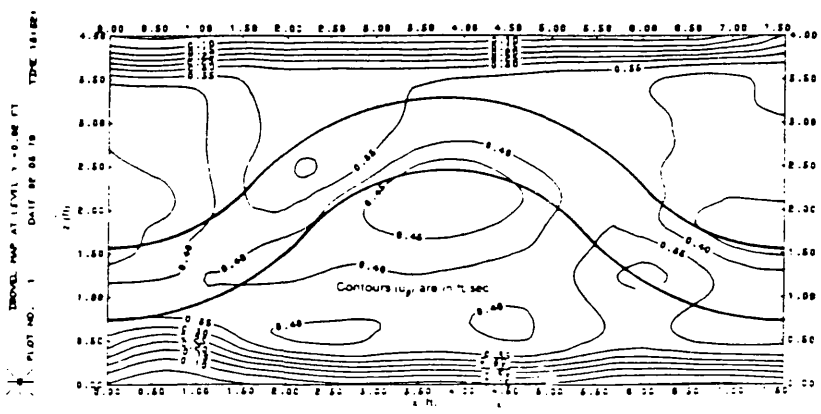

Fig (2.60) - Isolines of Primary Velocities in a Meander Compound Channel by Ahmadi(1979).

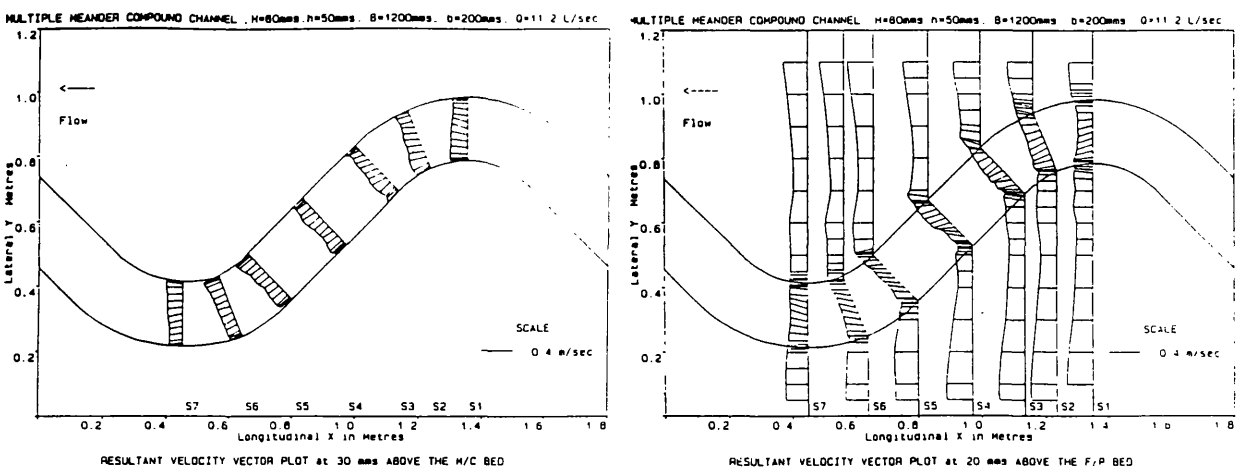

Fig (2.61) - Distribution of Resultant Velocity Vector in a Meander Compound Channel: a) 30 mm above main channel b) 20 mm above floodplain(After McKeogh and Kiely(1989)).

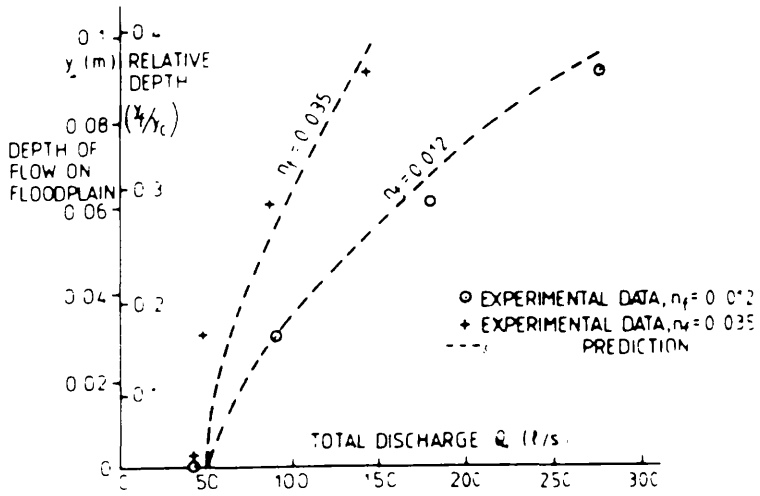

Fig (2.62) - Comparison between Experimental Data(U.S. Corps of Engineers) and Ervine and Ellis(1987) Model for Sinuosity: 1.2.

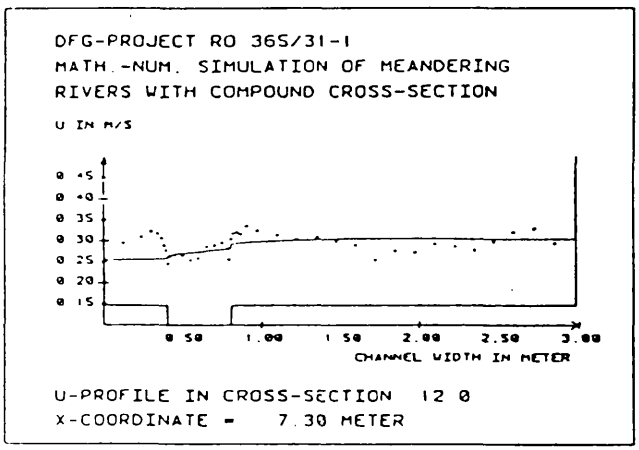

Fig (2.63) - Comparison between Measured and Calculated Values of Primary Velocities, obtained by Stein and Rouve'(1989)

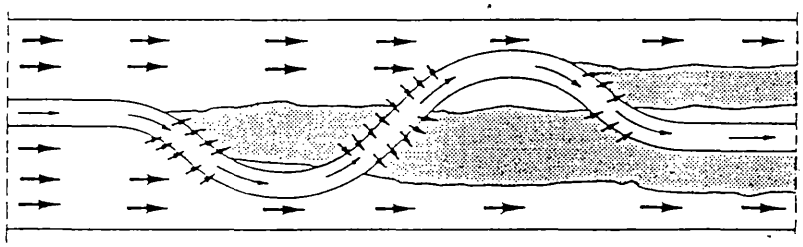

Fig (2.64) - Qualitative Distribution of Discharge in a Meander Compound Channel(After Stein and Rouve'(1989)).

CHAPTER 3

EXPERIMENTAL APPARATUS

3.8 INSTRUMENTATION FOR THE GLASGOW FLUME

- 3.8.1. Introduction
- 3.8.2. Discharge Measurement
- 3.8.3 Pointer Gauges
- 3.8.4. Streamline Angle Measurement
- 3.8.5. Pitot Tubes and Velocity Measurement
- 3.8.6. Program of Testing
- 3.8.7. Methodology of Testing
- 3.8.8. Scale Effects in Glasgow Flume.

3.9 SUMMARY

CHAPTER 3

EXPERIMENTAL APPARATUS

3.1 INTRODUCTION

The work described in this Chapter concerns the design, construction, calibration, instrumentation and running of the S.E.R.C. flume facility at Hydraulics Research Ltd, Wallingford. It concentrates on the parts of the work carried out by the Author of the thesis. It also concerns the design, construction and running of a smaller complementary flume at the University of Glasgow, designed to run in parallel with the S.E.R.C. flume studies, and designed to produce more detailed data of the behaviour of a single river bend during overbank flow.

The initial problem in the physical modelling of meandering overbank flow is the large number of parameters which affect the behaviour and which give a degree of complexity far beyond straight or skewed compound flows. As a first guess, these might be listed as:

(1) Depth Ratio: $(H - h)/(H)$ (see page 62)

(2) Main Channel Aspect Ratio: (B_c / h)

(3) Floodplain Aspect Ratio: $(B_f/(H-h)$

(4) Sinuosity: $r = \frac{\text{channel length along curved thalweg}}{\text{straight length of valley line}}$

(5) Non-dimensional ratio of main channel roughness:

$$k_{sc}/ H$$

(6) Non-dimensional ratio of floodplain roughness:

$$k_{sf}/(H - h)$$

(7) Side slope of main channel: s_c

(8) Side slope of floodplain: s_f

(9) Longitudinal slope of the floodplain: S_o

(10) Ratio of bend radius to main channel top width R_c/B_c

(11) Ratio of meander wavelength to main channel width λ_m/B_c

(12) Cross-over angle (α) between main channel and floodplain flow

(13) Meander belt width / total flume width ratio

(14) Cross section of the main channel, whether artificial or naturally formed.

to name only some of the key parameters in this type of flow, where H is the total depth; h is the bankfull depth; b_c is the mean main channel width; b_f is the mean floodplain width.

Until now, experimental investigations on meandering compound channels have been conducted in flumes of modest size with the main channel aspect ratio distorted in relation to natural values. For example, main channel aspect ratios of previous physical models have varied usually between 3 and 5, while in nature the values are usually between 5 and 20. Such distortions have significant implications for development of the flow mechanisms in meandering compound channels, as it will be demonstrated in **Chapter 4**. This explains part of the reason for the need for an experimental programme on meandering channels to be performed in a large facility.

Because construction, maintenance and operation costs of a large facility are very high, the experimental programme of Meandering Compound Channels, Series B, was jointly funded by the Science and Engineering Research Council(S.E.R.C.) and Hydraulic Research Ltd, located at Wallingford, and some contributions have been made by the MAFF and a number of Water Authorities. This research project, with a duration of three years, is a the continuation of the Straight Compound Channels Project, Series A, which was funded by the same bodies, roughly from 1986 to 1989.

Due to its experience and worldwide prestige, Hydraulic Research Ltd(H.R. Ltd) Wallingford was the place chosen to install such a large facility. H.R. Ltd was responsible for the construction, maintenance and part of the operation of the facility. Mrs **M. Johnstone**, from H.R. Ltd, was responsible for the day-to day running of the flume facility.

The experimental work was funded by S.E.R.C. through research grants and supervised by **Prof. B. Willetts** (Aberdeen University), **Prof. R. Sellin** (Bristol University), **Dr. A. Ervine** (Glasgow University), and Dr. D. **Knight** (Birmingham University)

and **Dr. I. Guymer** (Sheffield University). Because the experimental program was very extensive, the tests were sub-divided into various parts, with each part performed by a Research Assistant from each University. Miss **R. Greenhill** from Bristol University, Mr. **R. Hardwick** from Aberdeen University and the **Author** from Glasgow University conducted flow measurements of velocities, stream angles and water surface levels in the main channel and floodplain as well as tests of stage-discharge. **Dr. Y. Fares** and more recently **Dr. Yuen**, both from Birmingham University carried out measurements of flow turbulence. **Dr.N. Brockie** conducted the tests related to dye dispersion.

The organization of the experimental program was sub-divided between each of the Universities, being approximately,

- Glasgow University with hydraulic design of the flume, specialising in stage/discharge, flow conveyance and flow resistance.
- Bristol University with the instrumentation of the flume including data collection and data analysis of flow velocity and stream angles.
- Aberdeen University with the design of a Churchill probe for measurement of water surface levels.
- Birmingham University in charge of running the Laser Doppler system and boundary shear stress.
- Sheffield University with the running of the dye dispersion apparatus.

It was decided that the experimental programme on the S.E.R.C. flume would cover the widest possible range of scenarios in the time available. This included:

(i) Two sinuosities of the main channel, namely 1.374 and 2.04 corresponding to cross-over angles 60^0 and 110^0 respectively.

(ii) A range of flow depths covering both inbank and overbank flows.

(iii) Two different cross-sectional geometries of the main channel namely trapezoidal and natural. Trapezoidal was done for sinuosity 1.374 only and natural for both sinuosities.

(iv) Seven Types of Floodplain Boundary Roughness:

Smooth Case(for both sinuosities)

Fully Roughened(for both sinuosities)

Width Reduced at Meander Belt Limits but with smooth floodplains(for both sinuosities)

Partially Roughened(for sinuosity 1.37)

Brick Blocks(for both sinuosities)

Wall(only for sinuosity 2.04)

(v) The aspect ratio of the main channel was varied slightly as a consequence of changing cross-sectional shape in (iii). Model studies at the Aberdeen University were conducted with a greatly reduced aspect ratio, thus allowing variation of this parameter.

(vi) The side slopes of the main channel and floodplains were held constant, as was the longitudinal slope of the floodplains. In the case of the total channel width reduced at the limits of the meander belt, the side wall slope of the floodplain was 45^{o}.

(vii) The bend centre line radius was kept constant for all tests, although the meander wavelength λ_m was reduced in moving from sinuosity 1.374 to 2.04.

The stage-discharge curve was determined for all the above case studies. Besides the stage-discharge curve tests, the experimental program at the S.E.R.C. flume also involved measurement of streamline angles by a specially designed vane, local flow velocities by mini-propeller, water surface levels by the Churchill probe, Reynolds shear stress and turbulence intensities by the Laser Doppler Velocimeter, and boundary shear stress by the Preston tube.

As already mentioned, the **Author** designed and operated a complementary flume at the University of Glasgow. This will be described in Section 3.7. Despite being smaller in size than the S.E.R.C. flume, the Glasgow flume had a few advantages not available to the S.E.R.C. flume.

The first of these was the ability to vary the ratio of floodplain discharge to main channel discharge (Q_f/Q_{mc}) to any

ratio between 0 and ∞ . This is not the case for the S.E.R.C. flume whose Q_f/Q_{mc} ratio is pre-determined by geometry and uniform flow considerations. The Glasgow flume therefore had independent controls on the floodplain flow and main channel flow, for any given stage.

The Glasgow flume also contained greater flexibility in bend design including bend radius, bend angle, bend cross-sectional shape etc, although time did not permit a comprehensive variation of these parameters.

The range of experiments on the Glasgow flume included tests of stage-discharge, local velocities, streamline angles and detailed water level measurements.

3.2 THE S.E.R.C. FLUME, WALLINGFORD

3.2.1. Introduction

The main part of the experimental programme of meandering channels (Series B was performed in the S.E.R.C. flume, located in Hydraulic Research Ltd, Wallingford. The S.E.R.C. flume is a very large facility, probably the largest in the world, measuring 56 metres long and 10 metres wide, with the effective moulded channel length 49 metres long. Two meander channels with sinuosities 1.374 and 2.04 were investigated experimentally. Both models were of the fixed bed type and moulded in mortar, producing a smooth finish similar to the Series A tests. **Fig (3.1)** and **Fig(3.2)** show a general view of both models.

For the initial sinuosity 1.374 (and cross-over angle 60^0), two cross-sections were studied. A trapezoidal cross section with 45^0 side slopes, a natural cross-section, based on data from 17 real rivers outlined in Section 3.2.1. For sinuosity 2.04 only the natural cross-section was investigated. With a natural cross-section it was intended to simulate a more realistic cross section similar to the ones that are developed in natural rivers.

The longitudinal slope of the floodplain was $0.996 * 10^{-3}$for

sinuosity 1.374 and 1.02 * 10^{-3} for sinuosity 2.04.

Water was delivered to the model by six pumps, totalling approximately 1.1 m^3/s. Four pumps had a capacity of 0.125 m^3/s each, one had a lower capacity of 0.059 m^3/s and the sixth pump had the largest capacity, reaching 0.565 m^3/s. The set of pumps delivered water from a common sump to the inlet tank of the model.

Discharge from the pumps flows through measurement orifices to the inlet tank of the model and from there to a still basin as the upstream end of the moulded flume. A stilling boom smoothed any flow disturbances before entering the moulded sections of the flume. At the downstream end of the flume, flow enters a further stilling basin and then flows over five parallel tail gates finally returning to the original sump, completing the cycle.

Each tail gate can be set individually and the opening is controlled by a reading taken from a vernier, graduated in millimetres.

The flume is spanned by two moveable bridges which carry instrument carriages.

The facility is very well equipped with instrumentation. The following instruments were available in S.E.R.C. flume:

- Orifice Meters for flow discharge measurement;
- Digital Gauges for stage recording;
- Vane for streamline angle measurement;
- Mini-Propeller, for flow velocity measurement;
- Preston Tube for boundary shear stress measurement;
- Churchill Probes for water surface level measurement;
- LDA for Reynolds stress and turbulence intensity measurements.

The following floodplain roughness cases were studied:

- Smooth case(both sinuosities)
- Fully roughened(both sinuosities)
- Reduced Floodplain Width at Meander Belt Limits with smooth floodplains(both sinuosities)
- Partially roughened(sinuosity 1.37)
- With brick blocks(both sinuosities)

With a wall(only sinuosity 2.04)

Fig(3.3) sketches the eleven different formulations of floodplain roughness investigated in this project. These eleven formulations were used for stage-discharge measurements only. The cases of fully roughened and partially roughened floodplain were simulated through a set of rod frames (that had been used in the Series A tests) covering the complete floodplain in the first case and only the meander belt width in second and third cases. **Fig(3.4)** shows a plan view of the roughness rod the frame used in the tests. **Fig(3.5)** shows the S.E.R.C. flume with sinuosity 1.374 with the floodplain fully roughened.

With tests performed with brick blocks and walled floodplain it was intended to study the effect produced by bridge piers and roads that cross river valleys on the conveyance of a river when a flood occurs. **Fig(3.6)** and **Fig(3.7)** present the plan view of the location of brick blocks in both meander channels. **Fig(3.8)** shows the location of the floodplain wall in the meander channel with sinuosity 2.04.

3.2.2. The Design Concept.

The design of the plan geometry of the two meander channels and their cross-sections were carried out by the **Author** under the supervision of **Dr. A. Ervine.**

At the start of the project, when the experimental program of meander channels was defined, it was already intended to investigate two sinuosities, one less than 1.5 and other one around 2.0. At the same time, it was thought that the plan geometry and the cross-section of each meander channel, moulded in S.E.R.C. flume, should have a pattern similar to the ones found in nature. Based on studies of river morphology, researchers such as **Leopold and Wolman(1960), Chang(1987), Zeller(1967)** and **Jansen(1979)** (already mentioned in **Chapter II**), several key indicators were found that describe the trends of the plan geometry and the cross-section of natural river meanders.

These key indicators were followed in the design of both plan geometry and cross-section of each meander channel.

3.2.3. Design of Plan Geometry of the Meander Channel

The criteria followed in the design of the plan geometry of the FIRST meander was:

- Bends composed by circular arcs, joined with straight cross-over lengths.
- Number of meander wavelengths at least 4 to allow flow development.
- Length of each straight cross-over : > 2.5 m
- Cross-Over angle: 60 degrees
- Bankfull Depth(h) : 150.0 mm
- Top Channel Width(B_c) : 5h → 20h
- Sinuosity < 1.5
- Meander Wavelengths $\lambda_m \cong$ 10 B_c(where B_c is the top width)
- Bend radius $R_c \cong 2.5\ B_c$
- Double Amplitude of Meander(a) $a \cong 0.5\lambda_m$ for sinuosity <1.5.
- Floodplain Width(Wt): Wt≅ 10 → 20 B_c
- Width of floodplain outside the meander belt to be wide enough to allow shear layers to develop.

The equations involved in the optimisation design of the plan geometry were:

$$CL = 2\ [\ \lambda_m/4 - R_c \cos(\ 90 - \alpha\ )]/\ (\ \cos\alpha\ ) \qquad (3.1)$$

$$a = 2(R_c - b_1) \qquad (3.2)$$

$$b_1 = [\ \lambda_m/4 - (CL/2)/(\cos\alpha)]/\ \tan\alpha \qquad (3.3)$$

$$W_m = a + B_c \qquad (3.4)$$

$$W_f = [10 - W_m\ ]/2 \qquad (3.5)$$

$$r = \left[\ \frac{2\ \pi\ R_c}{360}\ 2\ \alpha + CL\ \right]\ /\ (\lambda_m/2) \qquad (3.6)$$

where,

λ_m is the meander wave length

R_c is the central radius of the meander

a is the double amplitude of the meander

W_m is the width of meander belt
W_f is half of floodplain width outside W_m
CL is the cross-over length
B_c is the top width
r is sinuosity of the meander
α is half of centre angle of the meander
These parameters are sketched in **Fig(3.9a)**.

Based on the above equations, a computer program was prepared which allowed the simulation of several hypotheses of meander geometries. After some trials it was decided to consider the following input values :

Flume Area for Moulding the Meander Channels:

- Total Length of The Model: 49.0 m
- Width of The Model: 10.0 m
- Meander Wave-length : 12.0 m
- Bend Central Radius : 2.743 m
- Cross-over Angle : 60 degrees
- Top Width of main channel: 1.2 m
- Bankfull Depth: 150.0 mm

The output results were:

- Cross-Over Length : 2.5 m
- Double Amplitude of The Meander : 4.91 m
- Width of Meander Belt : 6.11 m
- Half Width of Floodplain Outside Meander Belt: 1.95 m
- Sinuosity : 1.374
- Number of Wavelengths : 4.0

Checking if the geometry of the first optimised meander is in agreement with the key indicators we obtain,

S.E.R.C. Model Ratio	Key Indicator
$\lambda_m/B_c = 12/1.2 = 10$	$\lambda_m/B_c = 10$(**Zeller(1967)**)
$R_c/B_c = 2.74/1.2 = 2.3$	$R_c/B_c = 2.4$ (**Chang(1987)**)
$\lambda_m/R_c = 12/2.74 = 4.38$	$\lambda_m/R_c = 4.6$ (**Leopold(1960)**)
$a/\lambda_m = 4.91/12 = 0.4$	$a/\lambda_m = 0.5$(**Jansen(1979)**) when
$B_c/h = 8$	$5 < B_c/h < 20$

The level of agreement between the proposed ratios and the key indicators appears to be acceptable.

Taking into account the flume length, the number of meander wavelengths chosen was four.

Fig(3.9b) shows a plan view of the proposed meander with sinuosity 1.374. **Fig(3.10)** shows four wavelengths of this meander inserted in the layout of S.E.R.C. flume. This design was adopted for the test programme.

Similar steps and criteria were followed in the design of the SECOND meander channel with sinuosity approximately 2.0. The criteria adopted was:

- Flume Area for Moulding the Meander Channels:
- Length: 49.0 m
- Width: 10.0 m
- Channel Top width : between 0.8 and 1.2 m
- Maximum Bankfull Depth : 150.0 mm
- Cross-Over Angle: 110 ^{0}
- Central Radius: between 1.8 and 2.743 m
- Meander channel composed by circular arcs and straight lengths(as before)
- Number of Wavelengths(λ_m):at least 4(as before)
- Sinuosity: Approx. 2.0
- Straight Cross-Over Length: between 0 and 0.5 m.
- Amplitude to be approximately 0.8 λ_m for sinuosity around 2.
- Width of floodplain outside the meander belt to be wide enough to allow shear layers to develop.

It was realized that in the case of this high sinuosity, the floodplain width outside of the meander belt was much smaller than in the first case of sinuosity 1.374. In order to achieve the final criterion for the need of normal development of the lateral shear layers outside the meander belt, it was necessary to compute what shear layer width would be developed.It was decided to use the formula derived by Samuels(1985) for the width of lateral shear layers in straight compound channels, which could give an approximate value. The formula derived by Samuels(1985) is in the form

$$\delta = 5.7 \left[D / (g S_f) \right]^{1/4} \varepsilon^{1/2} \qquad (3.7)$$

where

D is the flow depth

g is the gravity force

S_f is the friction slope

f is the friction factor

ε is the eddy viscosity which can be expressed by the formula suggested by **Cunge (1980)**:

$$\varepsilon = C U_\infty (f / 8)^{1/2} D \qquad (3.8)$$

where

C is a coefficient that varies between 0.23 and 0.6

U_∞ is the free stream velocity

In this case the values considered were D = 0.10 m, g = 9.8 m/s^2, f = 0.035, S_f= 1/1000, ε ranges between 0.0004 and 0.0011 m, and U_∞ = 0.265 m/s. For this set of input values δ ranges between 0.47 m and 0.76 m so it was agreed to make the width of the floodplain outwits the meander belt, at least 0.7 m wide.

The other equations used in design of the second sinuosity plan geometry were:

$$\lambda_m = 4 \left[R_c \cos (\alpha - 90) - CL / 2 \sin (\alpha - 90) \right] \qquad (3.9)$$

$$a = 2 \left[R_c + R_c \sin(\alpha - 90) + CL / 2 \cos (\alpha - 90) \right] \qquad (3.10)$$

$$W_m = a + B_c \qquad (3.11)$$

$$r = 2 \left[2 \pi R_c (2 \alpha) / 360 + CL \right] / \lambda_m \qquad (3.12)$$

where all the parameters have meaning previously defined.

Based on the above equations, simulation of several plan geometries of meanders with sinuosities near 2.0 was carried out by a computer programme. This analysis produced four versions of meanders whose characteristics are presented in **Table(3.1)**.

Version number 2 was the one chosen to be modelled in S.E.R.C. flume with an important advantage in that the central radius, the top width, and the bankfull depth have the same values as in the first meander with sinuosity 1.374, thus allowing comparison between the experimental results obtained with both sinuosities. Besides that, the floodplain width outside

the meander belt was 0.72 m, which is, following the results obtained with **Samuels(1985)** equation, wide enough to allow the shear layer to be fully developed.

Checking if the second geometry of this meander is in agreement with the key indicators:

S.E.R.C. Model Ratios	Key Indicator
$\lambda_m/B_c = 9.97/1.2 = 8.3$	$\lambda_m/B_c = 10$(**Zeller(1967)**)
$R_c/B_c = 2.74/1.2 = 2.4$	$R_c/B_c = 2.4$ (**Chang(1987)**)
$\lambda_m/R_c = 9.97/2.74 = 3.63$	$\lambda_m/R_c = 4.6$ (**Leopold(1960)**)
$a/\lambda_m = 7.8/9.97 = 0.8$	$a/\lambda_m = 0.8$(**Jansen(1979)**) when r = 2.0
$B_c/h = 8$	$5 < B_c/h < 20$

The level of agreement between the proposal and the key indicators seems to be acceptable.

Taking into consideration the flume length, the number of meander wavelengths chosen was four and a half.

Fig(3.11) shows a plan view of the proposed meander with sinuosity 2.04. **Fig(3.12)** shows four and a half wavelengths of this meander inserted in the layout of S.E.R.C. flume. This design was adopted during the test program with sinuosity 2.04.

3.2.4. Design of the Main Channel Cross-Sectional Geometry

Two types of cross-sections were moulded inside the meander channel with sinuosity 1.374. The first cross-section studied, shown in **Fig(3.13)**, was trapezoidal with dimensions 0.9 m bottom width, side walls inclined 1:1, 0.15 m bankfull depth, and 1.2 m main channel top width. With this particular cross-section, it was intended to establish a comparison with previous results of Series A tests performed with straight compound trapezoidal channels. The second cross-section was achieved by putting concrete inserts into the trapezoidal cross-section, thus giving a "natural" cross-section moulded into the main channel. Here it was intended to represent a more realistic cross-section, similar to those rivers usually develop in nature, with pools at the

bends and riffles at the cross-over region.

The method of the insert design is illustrated in **Table (3.2)** and **Table (3.3)**. Seventeen data sets of natural river bends, shown in **Fig(3.14)**, were used in the analysis with each bend apex idealised into ten non-dimensional ratios as shown in **Table(3.3)**. This data were averaged for all 17 cases to produce a typical bend apex cross-section, which is sketched in **Fig(3.15)**.

Fig(3.15) shows the 17-bend average as well as the chosen bend design used on the S.E.R.C. flume. This cross section applies to the bend apex only, with dimensions shown in detail in **Fig(3.16)**.

The remainder of the main channel cross-sections were determined by simple rules:

(i) The flowing cross-sectional area below bankfull level is constant at all cross sections.

(ii) The main channel cross section at the cross-over region is trapezoidal.

(iii) All changes in cross-sectional geometry between bend apex and cross-over region are linear.

Table(3.4) shows the equations, the method applied and the area of each sub section in the design of the inserts of the natural channel with sinuosity 1.374. **Table(3.5)** presents the geometric elements of each section. The inserts of the natural cross-section of the meander channel with sinuosity 1.374 are sketched in **Fig(3.17)**.

Because of time constraints, sinuosity 2.04 was studied only with the natural cross-section. The inserts were designed following a procedure similar to one used above

Table(3.6) shows the equations, the method applied as well as the area of each cross section. **Table(3.7)** presents the geometric elements of each section. The inserts of the natural cross-section of the meander channel with sinuosity 2.04 are sketched in **Fig(3.18)**.

3.2.5. Construction of Main Channel Meander and Floodplains

Based on design drawings of the plan geometry of the meander channel with sinuosity 1.374 and assuming a rectangular cross-section of 1.2 metres wide and 0.15 metres deep, the carpentry section of the H.R. Ltd workshop prepared the main channel templates in wood for a complete meander wave-length.

As a reference for the construction of the meander model, three datum points were implanted into one side of the S.E.R.C. flume, one at the upstream end, the second in the middle and the third at the downstream end of the flume. The zero datum was chosen to be the upstream one. All three were levelled by an automatic level.

To produce the first meander channel, the floodplain of the previous straight compound channel Series A test was cut away to expose the bottom of the S.E.R.C. flume, over a width of approximately 6.5 metres.

After removing all demolition material, the flume centre line was marked on the bottom bed. On this line the tapping points were marked at 6 metre intervals to indicate the centre of each cross-over and the position of each bend apex was marked as well. These two points give the references to which the wood moulds of the meander channel could be accurately placed on the flume bed. Hard board were also placed at each bend apex cross-over section perpendicular to the flume side walls. By using an automatic level, each hard board and the mould of meander channel were levelled in the longitudinal direction with slope 1/1000, which was the specified longitudinal slope for the floodplain. The hard board and the moulds of the meander channel gave support for the levelling procedure of the mortar. Simultaneously with this process, 2 inch diameter steel pipes were laid between the middle point of each cross-over and the side wall of the flume. These acted as the conduits from tapping points prepared at each middle point of the cross-over for the purpose of carrying out stage and water level measurements.

Once the moulds of the meander channel and the wood forms were positioned in S.E.R.C. flume and levelled, the next step was the construction of the floodplain. This was done by filling the floodplain areas with hardcore, leaving a thickness of 20-30 mm for the mortar layer. The hardcore was wet and compacted, and upon which a layer of mortar was laid down. With the help of a screening board, the mortar was levelled to a slope 1/1000. **Fig(3.19)** shows a photographic view of this phase of S.E.R.C. flume's construction.

Once the mortar was laid, the moulds of the meander channel were carefully removed to leave a rectangular cross-section. Templates with the trapezoidal configuration were then positioned at regular intervals against channel sides which, when moulded, produced a trapezoidal section with side walls inclined 1:1.

This process was repeated over the remaining meander wave-lengths.

Once the construction was finished, the entire floodplain and the main channel were surveyed using an automatic level. In the survey a grid 1m per 1m was used. The floodplain and main channel levels were referenced to the upstream datum. In order to obtain the floodplain slope, a best fit plan was adjusted to the complete set of levels at 1mx1m intervals. For the sinuosity 1.374, the slope of the best fit plan found was 0.996/1000. All flume areas with discrepancies greater than 1.5 mm were corrected.

After finishing the test program with sinuosity 1.374 and trapezoidal cross-section, the inserts of natural cross-section were inserted into the main channel. In the bend region, the inserts were placed at 20 degree intervals, together with three inserts in the cross-over region. The process of moulding was basically to fill with mortar the volume limited by two inserts tied-in with the bed of the previous meander channel.

After modelling the entire meander channel with natural cross-section, the geometry of each cross-section was surveyed. The check included the verification of levels, lengths and slopes. In some sections level discrepancies as high as 5.0 mm

were noticed. **Fig(3.20)** shows the heavy inserts built in S.E.R.C. flume, after the survey has been carried out which differ slightly from the design. However, the cross sectional area of all sections was practically constant. A view of bend region of the natural meandering channel for sinuosity 1.37, after construction, is shown in **Fig(3.21)**.

Similar process was followed in the construction of the second sinuosity (2.04). The only difference was in relation to the moulding procedure followed for the natural cross-section. The **Author** suggested a different moulding procedure using a system of male-female, as shown in **Fig(3.22)**. Significant improvements in accuracy were achieved with this new method of moulding. After the survey of the resulting cross-sections, discrepancies found were less than 1.5 mm. The slope of best fit plan for sinuosity 2.04 was 1.02/1000.

In all cases the finishing of the mortar was excellent. In hydraulic terms the mortar surface can be considered smooth.

The test program included also tests where the floodplain was roughened, simulating the presence of trees in a natural floodplain. This kind of roughness was reproduced by wood frames, containing vertical rigid rod elements in wood, 25.0 mm diameter with a triangular distribution of an angle of $60^{0}$and with a density of 12 rods per m^{2}. **Fig(3.4)** shows a plan view of a large roughness frame applied in S.E.R.C. flume. All these frames were built by the carpentry section of H.R. Ltd.

This pattern of rods was used also in Series A tests therefore allowing the results obtained in both programs to be compared. Detailed analysis of the rod roughness can be obtained from **Ackers(1991)**.

3.3 INSTRUMENTATION

3.3.1. Introduction

S.E.R.C. flume Series B was equipped with:

- Orifice Meters for flow discharge measurement;
- Digital Gauges for stage recording;
- Vane for streamline angle measurement;
- Mini-Propeller, for flow velocity measurement;
- Preston Tube for boundary shear stress measurement;
- Churchill Probes for water surface level measurement;
- LDA for Reynolds stress and turbulence intensity measurements.

This section presents a detailed description of above instruments used in the experimental programme of S.E.R.C. Series B, including calibration procedures, mode of operation, cross-checks and test program.

3.3.2. Orifice Meter and Differential Manometers for Discharge Measurement

The discharge delivered by each pump was measured by an orifice plate meter connected to differential water pressure manometers. These orifice meters were inserted in a long straight pipe reach, downstream of the pumps and before the inlet tank Both the orifice plate and length of the pipe, upstream and downstream of the plate location, were designed in agreement with the British Standard BS1042. The differential pressure generated by the orifice meter was read in a differential water manometer. Tables of values of the calibration curves for each orifice meter were prepared by Hydraulic Research Ltd.

The orifice plate and the differential pressure manometer were connected by transparent tubes which were carefully purged each day to remove any bubbles inside the tubes which would significantly affect the readings in the differential manometer.

When the Flood Channels Program started, the first task the Author was involved with, was to check the validity of the calibration curves for each orifice plate. The check was done by verifying if the same discharge, when delivered by different pumps, and measured by different orifice plates produced the same

uniform depth. An error was found in the orifice plate for pump No. 1 which was corrected and gave good agreement with discharges measured by pumps number 2,3,4 and 5.

Besides this check, discharges measured by each orifice meter were compared with discharges obtained by the velocity integration method carried out from the measurements of streamline angles, velocities and water depths, at bend apex. The difference between discharges obtained by both procedures is shown in **Table(3.8)**. The error between both methods was always less than 4 % demonstrating that the calibration curves of the orifice meter were correct.

3.3.3 Stage Measurement

The water levels in the meandering channel, were measured by using digital gauges in stilling pots, as shown in **Fig(3.23)**. At the mid-way point of each cross-over length (**Fig(3.10)** and **Fig(3.12)**), there was a tapping point which was connected to a stilling pot at the side of the flume. The connection from the tapping point was made by a 2 inch pipe tube until the flume side-wall was reached, followed by a 10 mm transparent rubber tube into the stilling pot. The digital gauge runs inside the stilling pot and reads the water levels to an accuracy of 0.01 mm. In fact, the water level reading inside the stilling pot corresponds to the water pressure in the point where the tapping point is located. During the test program it was assumed that the pressure distribution for both inbank and overbank cases was hydrostatic. This assumption was verified as being reliable later on.

The calibration procedure involved not only the digital gauges themselves, but also the physical measurement of the water level that is associated with the reading given by each digital gauge.

The calibration of digital gauges was carried out by the Electrical Services of H.R. Ltd.

The determination of the zero of each digital gauge was made with the assistance of a special kind of tripod containing a shaft that rotates freely.

A calibration procedure developed by H.R. Ltd was used in the calibration of the zero of each digital gauge.

Each day, before uniform depth was set up in S.E.R.C. flume, two operations were carried out. First, the pointer of each digital gauge was cleaned with a special acid. Second, the stilling pots were filled with water, in order to purge the tubes that connect them with the tapping points.

The water levels taken from the digital gauge were averaged from four readings. In order to record all these readings, there was a standard sheet where these values were filled in.

Water temperature was taken with a centigrade thermometer, with an accuracy of 1 degree. The temperature was measured inside the inlet tank, at the beginning of the tests and at the end of the tests. Significant increases of temperature were noticed between both readings, reaching, sometimes, three to four degrees. This seems to be attributed to the continuous circulation of water through the pumps.

The water temperature was measured because its value affects the calculation of water viscosity, and Reynolds Number which is a decisive parameter in the study of flow resistance.

3.3.4. Vane for Measurement of Streamline Angle

Measurements of the stream angle in the three-dimensional compound meandering flows in S.E.R.C. flume, were carried out by a vane connected to a rotary potentiometer. Two different systems were used for the measurements. The first system was designed to measure the stream angle in the main channel, although covering also a narrow strip of the floodplain, 300 mm out from both edges of the main channel. This system will be named the "Main Channel System". The second system was designed to carry out measurements of stream angles on the floodplain region. In order to

distinguish this system from the previous one it will be named as the "Floodplain System".

In the "Main Channel System", the measurements of the streamline angle of the current were carried out using a connected to a rotary potentiometer as shown in **Fig(3.24)**. The vane and the potentiometer run along a 2 metres wide traverse, as part of a rigid instrument carriage. Two different instrument carriages were designed for the Series B S.E.R.C. programme. One, for the meander channel with sinuosity 1.374 and other for the higher sinuosity 2.04. In order to carry out measurements of the streamline angle in the bend region, the instrument carriage has to have the facility to rotate thus aligning it normal to the main channel walls. This is seen more clearly in **Fig(3.25)** for Sections 1 to 6. Unfortunately in the case of the smaller sinuosity, the instrument carriage could rotate only by $\pm 40^{0}$, thus measurements at Section 6 and in fact up to Section 11 carried out with traverse running parallel to the cross-over direction(30 degrees). For the higher sinuosity case the instrument carriage did not have any restriction in relation to the angle of rotation of the traverse. Both instrument carriages were supported by a large rigid beam and they could slide manually along one of the edges of the large beam. The carriage was manually positioned in the section where the measurements would take place.

The coordinates of the grid of streamline angle measurements (undertaken with the vane in the main channel), were previously defined in a computer file. Simultaneously the movements of the vane were robotised by two motors, controlled by a computer programme. This program, written in Turbopascal, ran on a PC Vanilla computer. After sampling the data over 30 seconds, the computer program calculated average values of streamline angles and stored the results in the same file containing the coordinates of the grid. This file is then used in the next stage of velocity measurements with the mini-propeller. The conception and the design of this system was made by Miss **R. Greenhill** from Bristol University.

The "Floodplain System", included a bank of three vanes with the respective potentiometers, mounted in a horizontal line on a carriage supported by a small beam. The instrument carriage and the bank of vanes were both moved manually. The vanes were separated horizontally by 500 mm and vertically they could be moved manually by increments of 10.0 mm. This instrument carriage was modified from a previous one that existed in Series A tests. The data, after passing through an A/D converter, was collected by a PDP 11/73 computer, where a program in Fortran 77 calculated time-average values of stream angles. The sampling time was 50 seconds.

Calibration Procedures

Each potentiometer receives a constant input voltage of 10 volts. As the vane rotates the rotary potentiometer changes its output voltage, which can vary between 0 and 10 volts. For each degree of rotation of the vane, the potentiometer responds by a certain variation of voltage. This ratio is called the calibration constant whose value is provided by the supplier. The domain of application of the calibration constant is restricted to a rotational amplitude that generally can not be greater than 330.0 degrees. The calibration constant of each potentiometer was checked by Bristol University.

The vane, sketched in **Fig(3.24a)**, was composed by a fin attached to a small rod. Each fin and the respective rod, used during the test program, were balanced dynamically by Bristol University. The balance was performed in two steps. First it was attached to the shaft an eccentrically small weight, as shown in **Fig(3.26a)**. Secondly the vane was spinned and the corresponding angle read. The spinning process was repeated at least one hundred times to check if there was any kind of statistical bias. If there was, the position of the eccentric weight was adjusted.

Mode of Operation

During the initial test programme carried out with the vane in the "Main Channel" system, it was realized that an angular

error(4 to 5 degrees) could be made quite easily, if the vane was not set up correctly. Thus a special method was developed jointly by the Author and Mrs. M. Johnstone, from H.R.Ltd., for setting up the vane. The steps were:

a) The motors were de-energised by switching off the power at the control box.

b) The vane and the rotary potentiometer were fixed to the instrument carriage.

c) Cables were attached from the rotary potentiometer to both the 10 Volt supply and the signal output marked "vane".

d) The vane was lowered into the water and the carriage was adjusted so that the vane was over the required point.

e) At this stage, a voltameter is required for checking the output voltage of the potentiometer.

f) The voltameter cable was connected to the voltage output of potentiometer.

g) A calibrating ruler with groves inserted 100 mm apart, was placed on the bed of the flume, parallel with the section line and with the grooves coinciding with the vertical lines marked on the bed of the flume.

h) The vane was lowered on the required groove(generally the section where the measurements started was 200 mm from the edge of the main channel).

i) The potentiometer and the attached protractor were rotated to the required angle.

j) A reading was taken from the voltameter. This reading was called the zero reading(around 5 volts).

k) The vane was raised and the ruler removed.

l) The vane was lowered and by small movements, the fin was placed in same position as previously, giving the same voltage reading in the voltameter. If it was not the case, by moving slowly the fin it was possible to reach the required value.

m) The voltameter was unplugged and the cable that conveys the output signal to the computer was connected.

n) The motors were switched on and the test could start.

The zero reading voltage in the voltameter, mentioned in

point j, corresponds to a zero angle which is referenced as the streamwise direction of each section where the measurements were performed. Thus all angles were referenced in relation to the streamwise direction of the section.

Another aspect of the angle results that need to be explained, is the reference system used to define what is the meaning of a positive or a negative angle value. Looking downstream, in streamwise direction when the vane rotates in clockwise direction (or to the right) the angle value, given by the computer programme was negative. If the vane rotates anti-clockwise, the angle value was positive.

Miss. R. Greenhill prepared a manual that explains in detail how to run the computer program for the angle and velocity measurements in the main channel system.

Test Program.

The test program of the measurements of the streamline angles in main channel and on the floodplain is presented in **Table (3.9).**

In the main channel region, the sections and the verticals where measurements were performed for both sinuosities are shown in **Fig(3.25)** to **Fig(3.28)**. In **Fig(3.25)**, a total of eleven cross sections were chosen covering half of a complete meander. In **Fig(3.26)** for the higher sinuosity a total of 14 cross sections were chosen covering just over a half meander. The half meander concept was allowable on the grounds of flow symmetry.

The distribution of vertical slices at each cross-section is shown in **Fig(3.27)** for the lower sinuosity and **Fig(3.28)** for the higher sinuosity. There were typically 21 vertical slices at each cross-section, extending 300mm on to the floodplains on either side of the main channel. In each vertical slice the first measurement was taken 10.0 mm from the bed and the others with increments of 15.0 mm.

On the floodplain the measurements were made in a square grid of 0.5m by 0.5m, and the increments in each vertical were 10.0 mm.

Cross-Checks

The stream line angle measurements were directly and indirectly cross-checked with results produced by other instruments. The direct method used, was to compare (for the bend apex section), angle values obtained by the vane with those from the laser Doppler velocimeter(LDV) values, calculated from the velocities components U and V. Both values presented an excellent level of agreement.

The indirect method used was to check if there was a mass balance for both inbank and overbank cases. This also involves the verification of the accuracy of the other measurements such as velocities by the mini-propellers and surface water levels by Churchill probe. The mass balance for both for inbank and overbank showed that the variation of the streamwise discharge was in agreement with the variation of transverse discharge. This analysis was carried out by the Author in some detail and submitted to the Series B Grantholders in the form of a detailed report. The analysis of the discharge distribution in S.E.R.C. flume, both for inbank and overbank cases, will be detailed in Chapter 6.

3.3.5. Minipropellers for Velocity Measurement

Introduction.

Measurements of velocities in S.E.R.C. flume were carried out using mini-propellers which were mounted on the same instrument carriage as that for the angular vanes. However, the methodology of measurement followed in the main channel was different to the one adopted on the floodplain. On the floodplain, three mini-propellers were fixed, recording only the velocity in the longitudinal flow direction. In the main channel, the mini-propellers was positioned at the same level as the streamline angle direction, thus measuring the resultant component of velocity along the streamline filament. **Fig(3.29)**

shows the mini-propeller mounted on the "Main Channel" instrument carriage of S.E.R.C. flume.

Principles

H.R. Ltd has investigated the performance of mini-propellers, when they are not aligned with longitudinal direction of the current. This study, published in report SM3, concludes that the "Cosine Law" can not be applied for streamline angles larger than 10 degrees. At the beginning of this project, it was realized that the angle of streamlines in the main channel region would be often much greater than the limit value of 10 degrees. Thus the system for measurements of velocities was designed in order to measure the resultant component of velocity. To convert the resultant velocity and the stream angle into spanwise and streamwise components of velocity, the following equations were applied:

$$U = VR \cos \circledast \qquad (3.13)$$

$$V = VR \sin \circledast \qquad (3.14)$$

where:

U is the streamwise component of velocity

V is the spanwise component of velocity

VR is the resultant velocity

$\circledast$ is the angle of current in relation to the streamwise direction.

The "Cosine Law" was applied in the case of measurements of velocities on the floodplain, which were taken far away(more than 500 mm) from the influence of the main channel region. In this case the angle of the streamlines was always less then 10 degrees.

Calibration Procedures

As the flow passes through the blades of the mini-propeller, it starts spinning. Each time the blade completes a turn, a pulse is conveyed to the computer in form of frequency. The frequency of the mini-propeller rotation is associated to the local velocity. Each mini-propeller has a calibration curve that

relates its frequency with the local flow velocity. The mini-propellers were periodically calibrated in a special calibration canal designed by H.R.Ltd. The results were satisfactory.

Mode of Operation

The mode of operation was similar to the procedure described in relation to the vane. However in this case the movements of the mini-propeller were controlled by the computer file containing the coordinates of the grid and also the average angle of the streamlines previously measured by the vane. Two motors (mentioned already in the case of the vane), moved the minipropeller to the required position in the grid. An additional motor rotated the mini-propeller in agreement with the value of the stream angle of the corresponding grid point previously stored in the file.

The principles followed in the set-up procedure, data acquisition and analysis were similar to the vane case.

The test program, presented in **Table(3.9)**, for the case of the vane measurements, was exactly the same for velocity measurements.

3.3.6. Churchill Probe for Water Surface Levels

Introduction

In S.E.R.C. flume, local measurements of water surface levels were achieved by a Churchill probe, mounted on to the traverse. The probe is essentially a conductivity type probe with varying resistance (and voltage), as the water level varies. Thus it was necessary to determine the calibration curve that relating the water surface level variation with voltage variation. Mr. **R. Hardwick** (Aberdeen University), was the Research Assistant responsible for the measurements with the Churchill probe. **Fig(3.30)** shows the Churchill probe mounted in the instrument

carriage.

The data acquisition and data analysis was jointly done by an A/D interface card and by a PDP 11/73 computer.

The movements of the probe were controlled by an Amstrad 1512 computer,which is the same that controls the movement of the LDV(laser Doppler velocimeter).

Data Acquisition and Data Analysis

The electrical signal generated by the Churchill probe, was received by an A/D interface card of the PDP 11/73 mini-computer, which digitized the information. A computer programme in Fortran 77 collected the data until the time of 50 seconds was exceeded. The same programe analysed the data and time-averaged values of local water surface levels were obtained.

Calibration

After achieving the uniform flow condition in S.E.R.C. flume, the Churchill probe was immersed and placed on the vertical that coincides with one of the cross-over tapping points, usually located in middle of the section. The reading of water level of the corresponding stilling pot and the voltage generated by the probe will give the initial values. By using the Amstrad computer, the Churchill probe was moved in increments of 1 mm and the corresponding average voltage was registered. Thus a calibration curve that relates increments of vertical displacements against the increments of voltage was produced.

The calibration procedure was carried out at the start of the test and at the end, because there was some changes in the voltage, introduced probably by temperature variations. The mean of the two calibrations was considered for determination of the water surface level.

The calibration curve was checked with values of water levels given by other stilling pots. No apparent discrepancies were noted.

Test Program

In the main channel water surface levels were measured at the same verticals as in the test program of the stream angles and resultant velocities. On the floodplain, measurements of water surface levels took place in a square grid of 0.5 metres.

3.3.7. Preston Tube for Boundary Shear Stress Measurement

Introduction

Measurements of boundary shear stress were carried out by 4.02 mm diameter Preston tube, connected to a 5 millibar pressure transducer. The Preston tube and pressure transducer were mounted in the instrument carriage are shown in **Fig(3.31)**.

The Preston tube was placed manually on the bottom surface of the flume, and boundary shear stress was measured for a sinuosity 1.374 and 2.04 main channel and floodplain, natural section and trapezoidal section, inbank and overbank cases with smooth floodplains. In the main channel the Preston tube was placed parallel to the main channel walls direction while on the floodplain it was parallel to the longitudinal direction.

Principles of The Preston Tube

Preston(1954) invented a method for measuring boundary shear stress in pipe flows and in boundary layers, by using of a Preston tube, whose operating principles are exactly the same as a Pitot tube.

His method is an indirect method of measuring turbulent skin friction. It depends upon the assumption of a universal inner law(or law of the wall) common to boundary layers and fully developed pipe flow. A non-dimensional and empirical relationship was established between the Preston tube reading and skin friction, which was expressed as,

$$\frac{\tau_0 \, d^2}{4 \rho \, \nu^2} = F \left[\frac{\Delta p_p \, d^2}{4 \rho \, \nu^2} \right] \qquad (3.15)$$

where Δp_p is the Preston tube reading(i.e. difference between the dynamic pressure and static pressure), d is the diameter of the Preston tube, τ_0 is the wall shear stress , ρ is the fluid density and ν is the kinematic viscosity and F is the function that can be determined from measurements in fully developed pipe flow. Based in the above relationship **Preston(1954)** obtained experimentally a calibration curve that relates differential pressure with the skin friction.

Further investigations, carried out in this field by other researchers, pointed out that the original calibration curve proposed by **Preston(1954)** was in error. **Patel(1965)** (Cambridge University), carried out experimental work and following the same procedure as suggested by **Preston(1954)**, obtained a revised calibration curve. From his work, **Patel(1965)** identified three regions where the experimental data fits the calibration curve within ± 1.5 %.τ_0. Assuming the non-dimensional parameters X^* and Y^* are defined as being,

$$X^* = \log_{10} \left[\frac{\Delta p_p d^2}{4 \rho \nu^2} \right] \qquad (3.16)$$

$$Y^* = \log_{10} \left[\frac{\tau_0 \, d^2}{4 \rho \, \nu^2} \right] \qquad (3.17)$$

Patel(1965) derived the following empirical non-dimensional equations

a) Region 1, for $X^* < 2.96$

$$X^* = 2Y^* - 0.037 \qquad (3.18)$$

b) Region 2, for $2.96 < X^* < 5.6$

$$Y^* = 0.8287 - 0.138X^* + 0.1437X^{*2} - 0.006X^{*3} \qquad (3.19)$$

c) Region 3 for $5.6 < X^* < 7.6$

$$Y^* = X^* - 2 \log (1.95 Y^* + 4.10) \qquad (3.20)$$

In the second equation Y^* is calculated by an iterative procedure. This method (as reported by **Preston(1954)**), presents a restriction in relation to the diameter chosen for the Preston tube. The tube diameter must not be greater than 1/5 of the boundary layer thickness. For the Preston tube used in this study with a diameter 4.02 mm, the above condition implies that measurements of shear stress should be done for flow depths greater than 20.00 mm.

Data Acquisition and Data Analysis

In the Preston tube, the pressure differential between the dynamic pressure and the static pressure which activates the pressure transducer, producing an analog electrical signal. This signal is received by the interface card of the PDP 11/73 mini-computer and is digitalized in milli-volts, which are averaged during 50 seconds.

This data coming from the pressure transducer is analysed by a program which calculates the average boundary shear stress. The computer program was written by **Dr. K. Shiono** (Bradford University), in Fortran 77, containing some instructions in machine code that activate the A/D interface card. The procedure followed in using the program as follows:

a) To initiate the program, input file name, temperature, static voltage, diameter of the Preston tube and the identification of the pressure transducer.

b) To start sampling, the input values are coordinates of the vertical where the readings were taken, number of scans(eg. 20), sampling time(eg. 0.5 seconds), number of cycles(eg. 5.0).

The program itself was basically structured in three main parts. In the first part, the A/D interface card transforms an input electrical signal in digits and sequently a calibration curve changes these digits into milli-volts. In the second part (using the calibration curve of the pressure transducer), the

average value of milli-volts is transformed into differential pressure. From the input value of temperature, water viscosity is calculated through the correlation equation that relates both parameters. In the third part, the non-dimensional parameter X^* is computed. This allows identification of the flow region and the corresponding equation that calculates Y^*. Once Y^* is calculated, the value of τ_0 can be immediately obtained.

The program gives the following outputs namely coordinates of the point where the measurements took place, average value of voltage coming from the pressure transducer, average value of boundary shear stress.

Mode of Operation

The connection between the pressure transducer and the Preston tube was made by two rubber tubes, one linked to the static head pressure and the other one connected to dynamic head pressure. Both connections could be controlled in the pressure transducer through two valves. There is an additional valve in the pressure transducer which facilitates the purging of the system(Preston tube, small tubes, and pressure transducer). This third valve is also connected by a small rubber tube, which is filled with water and immersed in a bucket.

During the test programme a lot of care was taken to ensure that the Preston tube, the three rubber tubes, and the pressure transducer were fully purged. From previous experience it was known that small air bubbles in the system could affect significantly the results.

The procedure followed in operating the system was the following:

a) Three rubber tubes were connected to each pressure transducer valve and were maintained tightened by application of special type of screw which does not allow any air to come inside the tubes.
b) All three valves of the pressure transducer were open.

c) The rubber tube connected to the third valve(the one made specially to facilitate the purging procedure) was immersed inside of the bucket with 3/4 filled of water.
d) The valve connected to the dynamic head pressure tube is closed.
e) The tube connected to the static head pressure is sucked until water starts flowing freely without any bubble.
f) There is now flow circulating between the third tube, which is immersed in the bucket, and the static head tube.
g) The extremity of the static tube is left free in the air, and water is flowing from the bucket, through the third tube, pressure transducer and discharging into the SERC Flume.
h) The valve connected to the dynamic tube is open.
i) The steps e, f and g are repeated for the dynamic head tube.
j) At this stage there is water circulating from the bucket, third tube, pressure transducer, static head tube or dynamic head tube and discharging to the SERC flume.
k) The static head tube and dynamic tube are connected to the Preston tube, by using the same kind of screws already described in a).
l) At this stage, there is water coming out from the Preston tube through the static head hole and the dynamic head hole.
m) The Preston tube is immersed in water that is flowing in the flume.
Although it is not possible to see, because the pressure transducer box is enclosed, there is often some air bubbles inside the pressure transducer. A method was devised to eliminate these small air bubbles namely,
o) The bucket is positioned in a level much higher than the pressure transducer and flow circulation between the bucket and the Preston tube is increased, eliminating any remaining air bubbles.
p) At this stage all the system is fully purged and conditions are prepared to make the test for the measurement of static voltage.

To run the boundary shear programe, first it was necessary

to obtain the static voltage of the pressure transducer. The static voltage is the voltage that the pressure transducer generates when the Preston tube is immersed in static water, that is the differential pressure is zero. The procedure followed to obtain the static voltage was the following:

q) The Preston tube is immersed in a second bucket with 3/4 of water(in a level lower than the first bucket) and the additional valve is closed.

r) The computer programme runs and the static voltage is measured.

s) An average value of static voltage was calculated from five runs.

t) With the value of static voltage known, the additional valve is open and Preston tube(that is placed in a level lower than the first bucket) is transferred and immersed in water that is flowing in the SERC flume.

u) The Preston tube is manually placed in position to start measuring the boundary shear stress of that point.

v) The additional valve is closed and the computer programme can restart to run.

x) The first set of average values of boundary shear stress and milli-volts appear in screen of the computer.

Calibration

Before the start of each test programme, the A/D interface card was checked and calibrated. The procedure used was to introduce a known voltage inside the interface card, run the computer and verify if the result coming from the programme was giving the same voltage. By this process the curve that relates digit numbers with milli-volts was recalibrated and this instruction in the computer program was corrected. This work was done jointly by the **Author** and Mr. **D. Wilmer**, from the H. R. Ltd.

The 5 millibar pressure transducer was periodically calibrated in Bristol University.

Test Program

The test programme of measurements of boundary shear stress with Preston tube included two series of measurements. In the first series, measurements were made at the same verticals and sections as the turbulence measurements with the laser. In the second series, measurements of boundary shear stress were performed also to cover the complete main channel and floodplain region. Tests were done for natural cross-section; sinuosity 1.374 and 2.04; and smooth floodplains. The test program of boundary shear stress is shown in **Table(3.10)**. In the main channel, the verticals where the measurements of boundary shear stress took place, were approximately the same as the ones used for the measurements of the stream angles and the resultant velocities. On the other hand, the floodplain was covered by a rectangular grid of 1.0 * 0.5 metres, in the longitudinal and in transversal directions respectively.

Cross-Checks

As will be explained in section **3.3.8**, the laser Doppler velocimeter can only work down to 12 mm from the bottom surface of flume. Therefore, the boundary shear stress values taken with the Preston tube were inserted as bottom values of the profile of Reynolds shear stress τ_{xz}. Although there is not a direct check between both values, the bottom shear stress Preston tube measurements showed an excellent degree of correlation with the Reynolds shear profile τ_{xz}. Another cross-check carried out was to compare the boundary shear stress values obtained on the floodplain region outside of the meander belt with the average bottom shear stress of a straight channel with same bed slope(S_0) and flow depth(H) which is calculated through $\tau_0 = \rho g R S_0$. The agreement between both results was also excellent.

3.3.8. Laser Doppler Velocimeter

Introduction

A Laser Doppler velocimeter(LDV) is an optical instrument which allows the measurement of the instantaneous velocity of the tracer particles suspended in the fluid without disturbing the fluid.

The turbulence measurements of instantaneous velocity and Reynolds shear stress in the S.E.R.C. flume (Series B) were undertaken using two component argon-ion laser Doppler Velocimeter(LDV) system, which was supplied by TSI(model 9273). The components of the LDV system installed in the S.E.R.C. flume are shown in **Fig(3.32)**. This type of LDV was operated by using the fringe model in backscater mode.

The measurements were taken using a 15 mm diameter submersible fibre-optic probe, which has a focal length of 80 mm from the front lens and was connected to the laser and processing system through 20 metres of fibre optic cable. The cable contains five separate cables, four transmitting fibre links and one receiving fibre links. **Fig(3.33)** shows the fibre optic cable as well as the submersible probe of the LDV, installed in the instrument carriage. **Fig(3.33)** also shows the probe emitting four laser beams, two blue and two green ones, respectively.

The optical and electronic equipment used in the laser velocimeter were two beam splitters, two Brag cells, lenses, apertures, two photodetectors and counter processors as well as microprocessors units.

The measurements of turbulent velocities and Reynolds shear stress were carried out mainly at the bend apex and in some cases also at a section 40 degrees downstream of bend apex. The measurements were carried for both sinuosities 1.374 and 2.04, for the trapezoidal cross section and natural cross section, for inbank and overbank flows and with smooth floodplains.

To operate this laser, it was necessary to have it seeded with an appropriate amount of scattering particles. Titanium

dioxide(T_iO_2) was used as particle tracer and was manually injected in the flow, in a continuous way, 1.0 metre upstream from the test section. The concentration used was 25 grammes of T_iO_2 per 25 litres of water or 1 part per thousand(1 PPT).

Principles of Laser Velocimetry

The Laser Doppler velocimeter uses the Doppler shift of light scattered by moving particles to determine particle velocity and thus find the fluid flow velocity. The principle of Doppler shift is sketched in **Fig(3.34)**. The general equation expressing the Doppler shift, f_d, as a function of particle velocity $\underline{U}$ is:

$$f_d = f_s - f_i = \frac{1}{\lambda_1} \underline{U} \left(\hat{e}_s - \hat{e}_i \right) = \frac{2\, U_x}{\lambda_1} \sin(\theta_1/2) \qquad (3.21)$$

where:

f_s is the frequency of scattered light

f_i is the frequency of incident beam light

$\hat{e}_s$ $\hat{e}_i$ are the unit vectors of scattered and incident light

λ_1 is wave length of incident light

$\underline{U}$ (U,V,W) velocity vector

U velocity along x-axis(U_x)

V velocity along y-axis(U_y)

W velocity along z-axis(U_z)

U $\overline{U} + u'$

u' is the fluctuating component of velocity

$\overline{U}$ is the mean velocity

θ_1 is the angle between the beams

Because the laser beams use a monochromatic coherent light source, it makes possible to determine the values of f_i and λ $\hat{e}_s$ $\hat{e}_i$, if the geometry of the laser system is known. Once these values are determined, the velocity of particle can be calculated from equation **3.21**.

This laser, as mentioned in the introduction, operates with a fringe model in backscatter mode. The interference fringe is sketched in **Fig(3.35)**, and offers a convenient method to

visualizing the basis of Laser Doppler Velocimetry. As two monochromatic and coherent laser beams with planar wave front meet, they yield a interference pattern of fringes at the beam crossing.

The distance between fringes δf can be calculated from the half-angle $\oplus/2$ between two beams and wave length of the laser light.

$$\delta f = \frac{\lambda 1}{2 \sin \oplus 1 /2} \qquad (3.22)$$

A particle moving across the fringe pattern with velocity component U_x perpendicular to the fringe planes will scatter light at a frequency of f_d

$$f_d = \frac{U_x}{\delta f} = U_x / \left[\frac{\lambda 1}{2 \sin \oplus_1 /2} \right] = \frac{2\, U_x}{\lambda_1} \sin \frac{\oplus 1}{2} \qquad (3.23)$$

An LDV system can distinguish velocity direction when it is equipped with a Bragg cell. The Bragg cell emits an acoustical wave that shifts the incident beam wave length in multiples of the Bragg shift, f_B. As soon as the incident beam is shifted by the Bragg cell, the fringes move rather than remain stationary. The result is a non-zero frequency for zero velocity. Without the Bragg cell, a measured frequency, f_m, would give a velocity result of $\pm V_m$. With the Bragg cell, the measured frequency would give velocities V_{m1} or V_{m2}. If knowledge of flow behaviour eliminates V_{m1}, the system is able to identify the velocity direction.

The counter processor measures the time taken for a given number of cycles in a Doppler burst using a high resolution clock. The Doppler frequency is calculated based in the following equation,

$$f_d = \frac{\text{Number of cycles}}{\text{Time}} \qquad (3.24)$$

Mode of Operation

The laser was operated at the power of 300mW, generating four monochromatic coherent beams of light(two blue and two green), which, after passing all the laser components and the fibre optic cable, reached the head of optical probe . The four beams are focused to cross in an ellipsoidal measurement volume which is approximately 1mm long and 50 μm in diameter. In the measurement volume the two green beams intersect in a plane that is perpendicular to the plane formed by the two blue beams. The scattered light coming from the measurement volume is collected by the probe and the signal is transmitted through the fifth fibre optic cable to the photodetectors and further on to the processor units. The blue beam with a wavelength of 488nm and a fringe space 4.17μm was used for measurement of the longitudinal component of velocity since the back scattered signal of the blue beam was more attenuated than the green beam which has a wavelength of 514.5nm and a fringe space equal to 4.36 μm. The green beam was used for measurement of either the vertical or the lateral component of velocity.

The frequency of shifting was 100kHz for the green beams and 50kHz for the blue beams. The filter ranges in the signal processors were set at 30kHz to 200kHz for the green beam(U velocity component) and 100kHz to 400kHz for the blue beam(W and V component.

The input conditions were set as 8 cycles per burst, a single measurement per burst, with 1ms as the minimum time between data points and coincident window of 100μs.

Because one of the aims of the work was also to calculate Reynolds shear stress which is a cross-correlation event, the measurements of instantaneous velocity needed to be carried out at the same time. Thus both counter processors were synchronised to operate in coincidence mode.

Before the test program started the laser signal was optimized with a slow oscilloscope, by adjusting the optics for maximum amplitude and frequency of the burst.

Data Acquisition System and Data Analysis.

The data transfer to a direct memory access(DMA) of the PDP 11/73 mini computer was processed through the master signal processor. The data was collected until the time of 60 seconds was exceeded. The data rate of sampling was between 20Hz and 100Hz and generally set at 50Hz for most of the time sampling.

Two computer programs were developed by **Dr. Shiono** (Bradford University), one for collecting data from the laser and other for analysis. Both programmes were written in Fortran 77, containing some sub-routines in machine code which activate the interface card. Both the raw data and the analysis were stored in cassettes.

The first program calculates the instantaneous velocity in two directions and stores the time taken for each number of cycles in a Doppler burst for both directions. The equations used in the programme are,

$$f_{d1} = \frac{\text{No. cycles}}{\text{Time}}_{1} \qquad (3.25)$$

$$f_{d2} = \frac{\text{No. cycles}}{\text{Time}}_{2} \qquad (3.26)$$

$$U_1 = (f_{d1} - f_{s1})\, f_{r1} \qquad (3.27)$$

$$U_2 = (f_{d2} - f_{s2})\, f_{r2} \qquad (3.28)$$

where

f_{d1} and f_{d2} are the Doppler frequencies in directions 1 and 2.

U_1 and U_2 are the instantaneous velocity in directions 1 and 2.

f_{s1} and f_{s2} are the frequency shiftings applied in directions 1 and 2.

f_{r1} and f_{r2} are the distance between fringes in directions 1 and 2.

The instantaneous velocity and the sampling time are stored in a file of PDP 11 memory.

Based on data obtained in the first program, the second program calculates average flow velocity, turbulence intensity and Reynolds shear stress. The recommendation from TSI, was that the time used as a weighting function for bias correction. The following equations were used in the program

Average Velocity

$$\bar{u}_i = \frac{\sum u_i \, t_i}{\sum t_i} \qquad (3.29)$$

Turbulence Intensity

$$\sqrt{(\overline{u_i'^2})} = \sqrt{\frac{\sum \left(u_i - \bar{u} \right)^2 t_i}{\sum t_i}} \qquad (3.30)$$

Reynolds Shear Stress

$$\tau_{ij} = \rho \frac{\sum u_i' \, u_j' * t_i t_j}{\sum t_i t_j} \qquad (3.31)$$

where subscripts i and j refer the direction of measurement.
All the data analysis made by the second program has been stored in cassette.

Mode of Control.

The probe head shown in **Fig(3.33)** was fixed on a 90^0 streamlined elbow shape which ran on a TSI two-axis transversing system. The transversing system used for the laser probe was exactly the same utilized for the measurements of the resultant streamline angle and velocity in the main channel, already described in section **3.3.4**. This system was itself mounted on a bridge that covers the entire width of flume. The TSI transversing system could rotate and be positioned manually at any location along the flume. Once the probe was in position, movements were controlled by an Amstrad 1512 computer, covering

2.0 metres in transverse direction and 0.5 metres in vertical direction, with a spatial resolution to within 2mm in the transverse direction and 0.5mm in the vertical direction. The probe head could rotate 90^0 in vertical plan in any direction.

During the tests, the elbow shape that holds the laser probe was kept in horizontal position for the measurements of velocity components U and W, and in the vertical position for the measurements of velocity components U and V. When the probe is in the horizontal position a special reference panel was used to set the blue beams parallel to the longitudinal direction of the flume. When the probe is in vertical position the green beams were set coinciding with the direction of a line marked on the slab of the flume that defines the main channel cross section.

For measurements near the free surface of the water, part of the laser beams were outside of the water and were reflected by the wavy surface water/air. This produces too much noise in the resulting laser signal. A solution found was by covering the probe by a cylindrical perspex tube full of water. Using this method the beams were always crossing the same medium(water), and also avoiding the effect of reflections. Before any test programme started, the tube was fully filled with water and was carefully purged through a small rubber tube connected to the cylindrical tube, eliminating any of air bubbles.

Test Programme

The test programme of turbulence measurements with the Laser Doppler velocimeter is presented in **Table (3.11)**.

The methodology adopted in defining the grid points for the laser measurements was,

a) to measure along the same verticals as those chosen for the measurements of streamline angles and velocities as already discussed in Section 3.3.4 and

b) to place a vertical in each corner of section and some near this area, as well.

The first condition allows a check on results obtained by different systems. This procedure can detect if there is

something wrong with the equipment or if the flow was not set up correctly or for errors in measurement. In fact, when the test program started, the **Author** compared the results of velocity distribution given by the LDV system against the velocity distribution from the angle and velocity measurements taken by the vane and mini-propeller. After careful examination, it was noticed that there was a constant discrepancy between both values. With the help of **Dr. D. Knight**, and **Dr. Y.Fares** (Birmingham University), the entire procedure was carefully re-examined. It was discovered that in the program of the PDP, the instruction that tells the computer the value of frequency shifting was wrong for one of the beams. Thus this instruction in the computer program was altered and the results in both systems become almost the same.

With the second condition it was envisaged that a detailed study would be made of the effects of abrupt changes in the geometry of the cross-section in relation to the velocity and turbulent field. This is particularly true for the natural cross-section geometry with a number of abrupt geometry changes.

The laser presents some restrictions in relation to the highest(near the water surface) and deepest point(near the bottom of the flume) where measurements can be carried out without noise interference. The recommendation of TSI was that the highest point should be distanced 15 mm from the water surface and 12 mm from the bottom of the flume.

Cross-Checks

The results produced by the LDV were cross checked with results produced by other instruments:

- Velocities(U and V components) obtained by the laser, against the velocities(U and V components) calculated from the streamline angle and resultant velocity using the vane and mini-propeller.

-The trend evidenced in the vertical profile of Reynolds shear stress obtained by LDV was compared with the bottom shear stress values measured by the Preston tube.

The cross-check on both cases showed an excellent level of agreement.

3.4 GENERAL CALIBRATION AND CROSS-CHECKING

As a general rule, the Series B tests on the S.E.R.C. flume were subject to a rigorous regime of calibration of the instruments and cross-checking of results in as many ways as possible.

This is important in such a data set as this, where data will be used extensively for some years to come, especially in the field of calibrating numerical models.

The calibration procedures have already been outlined in the description of each instrument. The instruments subjected to the most rigorous calibration procedures were,

Vane
Mini-propeller
Differential Pressure Transducer
Churchill Probe
Orifice Plates

Whenever possible the measurements given by an instrument were cross checked by another instrument or by some different method. This has already been discussed in the description of each instrument but is also summarised in below.

3.5 SETTING-UP UNIFORM FLOW IN THE S.E.R.C. FLUME

The entire testing programme for Series B was based on steady "uniform" flow in the flume. The concept of uniform flow in this case, is better defined as "quasi-uniform" flow in the sense that meandering compound flow is so disturbed and wary and with local variations in water level, that a constant flow depth is not possible.

It was therefore decided to make the definition of uniform

flow based on a best-fit line through tapping point measurements along the flume centre-line and at fixed points in each meander wavelength.

The steps followed in setting up the uniform flow were:

- A known discharge was set up.
- The tailgate position was read.
- The surface levels in each tapping point were measured.
- The best fit line was adjusted to the water surface levels and the surface slope was calculated by a computer program..
- Another tailgate position was chosen, and after repeating the process again, a new surface slope was calculated usually 2 points in M_2 backwater curve and 2 points in M_1 backwater curve as sketched in **Fig(3.36)**.
- After carrying out this process a total of 4 times surface slope and normal depth were plotted against tail gate position(normal depth chosen was the one of the measuring section).
- By a graphical procedure, the normal depth and the tail gate position were obtained for the required surface slope S_o(longitudinal slope of the floodplain which in this case was 1/1000).
- The entire process was repeated for another discharge.
- Based in values of discharge and uniform depth the normal depth-discharge curve was built up as the Rating curve for the flume.
- For a precise setting of normal depth and discharge to give a certain depth ratio(H-h)/H (ex. 0.25, 0.40), the normal depth-discharge curve and normal depth-tail gate curve were interpolated.

This process is sketched in **Fig(3.36)**.

As was previously mentioned, each tail-gate had a scale which allowed accurate control of its opening. Before each test programme was started, all the tail gates were levelled by an automatic level and the reading on each scale was adjusted to the same value.

During the process of getting the uniform flow in S.E.R.C. flume Series B for inbank case, only one tail-gate was operated

while all the others were maintained in closed position and levelled. For sinuosity 1.374 the tail gate used was the second from the left bank(**Fig(3.10)**, while for the other sinuosity it was the first from the right bank(**Fig(3.12)**).

For the overbank case the uniform flow conditions were achieved by operating all five tail gates. In this case the crest of each tail gate was approximately positioned at the same level. The position of each tail gate was controlled by a reading taken from a ruler.

3.6 PROGRAM OF TESTING (S.E.R.C. FLUME)

The complete programme of testing for the Series B, S.E.R.C. flume study is given in **Appendix I-a**. This is in the form of a schedule prepared by **Professor Sellin** (University of Bristol) covering the entire two year testing period. The schedule of testing shows the programme on a weekly basis, giving details of the work involved and which Research Assistants were involved at any given time. This is a useful record of the work done.

As well as this form of record, we have already discussed the streamline angle measurement programme (Section 3.3.4), the miniature propeller meter velocity programme (Section 3.3.5), the Churchill probe water level recording programme (Section 3.3.6), the Preston tube boundary shear stress programme (Section 3.3.7), and the LDV turbulence and Reynolds shear stress programme(Section 3.3.8) (as well as this there was a dye dispersion programme which the Author was not involved in).

The other main programme was that of stage-discharge measurement, already mentioned in Sections 3.3.2 with the programme summarised in **Table(3.13)**.

Fig(3.3) shows a sketch of all eleven case studies of stage-discharge tests. In the case of fully roughened floodplain, the floodplain was fully covered with rod frames. In the case of partially roughened floodplain, only the meander belt was filled with rod frames. **Fig (3.4)** shows a plan view of a typical rod

frame used in the tests. **Fig(3.6)** presents a plan view of the location of brick blocks on the floodplain of the sinuosity 1.374. The plan view of sinuosity 2.04 with brick blocs and with the floodplain walled are presented in **Fig(3.7)** and **Fig(3.8)**, respectively. During the tests with floodplain fully or partly roughened, the rods pierced the water surface. On the other hand, in the tests made with brick blocks or with a walled floodplain, the flow never overtopped these obstacles. In the width reduced case, the floodplain was fully roughened and the floodplain walls were placed at the limits of the meander belt.

The tests performed with brick blocks in the floodplain of the meander simulate the effect of bridge piers on river flood conveyance, while the walled floodplain reproduces the reduction in conveyance introduced by roads that cross river valleys.

The program of stage-discharge tests was carried out for inbank case and overbank case. For inbank case the flow was confined to the main channel and the only test restriction was the bankfull depth. For overbank case the test program was limited by the delivery capacity of all six pumps which could reach 1.1 m^3/s.

3.7 THE GLASGOW FLUME

3.7.1. Introduction

The whole rationale for the Glasgow Flume was to provide a complementary study to that going on at the main S.E.R.C. flume at H.R. Ltd Wallingford. The Glasgow flume was intended to investigate the behaviour of one river channel bend during overbank flow, where the geometry of the river bend could be changed more easily than the S.E.R.C. flume, and where the ratio of the floodplain flow to main channel flow could be set at any ratio, which is not the case in the S.E.R.C. flume where this ratio is essentially fixed. The Glasgow flume study was also meant to be complementary to smaller scale studies of the

cross-over region (Bristol) and general flow development studies at Aberdeen.

The intention for the Glasgow flume was to have it designed, constructed, and up-and-running during the first ten months of the research programme between December 1988 and September 1989, at which time access to the S.E.R.C. flume would be available. The intention after September 1989 was for the Author to spend some time at the S.E.R.C. flume study at Wallingford and the remaining time running the Glasgow flume, so that both studies continued in parallel.

However it was difficult to run both studies in parallel because of the time-consuming nature of the Wallingford work, both in terms of checking data but also plotting and analysis of results. Thus few results than expected were obtained from the Glasgow Flume.

The Glasgow rig, shown in **Fig(3.37)** and **Fig(3.38)**, is composed of two flumes in one, the main channel flume and the floodplain flume, connected together at the bend and cross-over region. The main channel flume and the floodplain flume simulate the main channel flow and the floodplain flow of a river meander with a sinuosity around 1.28. However this rig has a particularity that distinguishes it from S.E.R.C. flume. The discharge control in both flumes is done independently, therefore allowing the ratio of main channel discharge/floodplain discharge to vary between 0 and ∞. Several combinations of main-channel/floodplain discharges could be studied in this rig while in S.E.R.C. flume these conditions could not be varied.

Water was pumped from a common sump tank and the discharge was delivered to each flume by a different pump. The main channel and the floodplain pumps could deliver 40 l/s and 60 l/s respectively. After the discharge has been conveyed through the piped circuit, it enters the inlet tank of each system. On leaving each inlet tank the flow reaches the beginning of each flume where a set of small tubes smoothed any flow disturbance. At the exit of each flume, the flow through a control structure(a vertical tail gate, in the case of the main channel flume), or

over the hinge tail gate (as in the case of the floodplain flume), returning to the common sump, thus closing the loop. A view of the sump, the pump and the gate valve of the main channel system is shown in **Fig(3.39)**. The main channel and the floodplain channel sumps were linked to form a common sump as sketched in **Fig(3.40)**. This figure shows a view of the sump tank, the pump, the gate valve and the differential manometers of the "Main Channel" system.

In the Glasgow rig the test programme included measurements of water depths by pointer gauge, discharge by orifice meter linked with differential manometer, streamline angles by vane linked with potentiometers, local flow velocities by Pitot static tubes connected to pressure transducers and temperature by thermometer. Boundary shear stress was not measured, nor was the turbulent flow structure.

3.7.2. Design Concept

As explained in the introduction, the Glasgow flume was designed in such a way that the floodplain and the main channel flows could be simulated simultaneously and controlled independently. Thus the model is composed of two flumes, one simulating the main channel flow and the other one reproducing the floodplain flow of a meander compound channel. Both flumes are connected at bend and in the cross-over regions as sketched in **Fig(3.40)**. This kind of model allows any combination of main channel/ floodplain discharges which can vary between zero to infinite.

The criteria followed in the design of the floodplain and main channel flume were:

- Both flumes should be accommodated in area 6.0m * 9.0 m
  Floodplain slope 1/1000
- Width of floodplain outside the meander belt to be wide enough to allow shear layers to develop.
- Main channel sinuosity < 1.5

- The cross over angle of the main channel to be different from S.E.R.C. flume. 45^0 was chosen.
- The upstream reaches of the floodplain flume and of the main channel flume should have sufficient length to allow the development of turbulent boundary layer.
- Meander Wavelength $\lambda_m \cong 10$ Bc
- Top channel width Bc ≅ 5 h →10 h where h is the bankfull depth
- Bend radius Rc ≅ 2.5 Bc
- Total width of the Floodplain(Wt) ≅ 10 Bc

Fig(3.40) shows a plan view of the Glasgow flume with the dimensions chosen in agreement with the above criteria. The sinuosity of the main channel is

$$r = \frac{\text{curved channel length}}{\text{straight valley length}} = \frac{3995.06}{3128.47} = 1.277$$

Meander wavelength (λ_m): 6256.8 mm
Main channel width (Bc): 450.0 mm
Bankfull depth(h): 67.00 mm
Bend radius of curvature(Rc): 1000.0 mm
Half of the meander amplitude (a/2): 1150.0 mm
Half of the total channel width(Wt/2) :1650.0 mm

The Glasgow flume plan geometry was checked against the key indicators recommended by several researchers:

Key indicators	Glasgow Flume Values
Rc/Bc = 2.4 (**Chang (1987)**)	Rc/Bc = 2.2
λ_m/Bc = 10.0 (**Zeller(1967)**)	λ_m/Bc = 14.0
λ_m/Rc = 4.6 (**Leopold (1960)**)	λ_m/Rc = 6.3
a/λ_m = 0.5 (**Jansen(1979)**)	a/λ_m = 0.4
Wt/Bc = 10 → 20(**Ervine(1987)**)	Wt/Bc = 7.3
Bc/h = 5 → 20(**Ervine(1987)**)	Bc/h = 6.7

Taking into account the limitation in available area, the dimensions chosen for the plan geometry of the meander, when compared with key indicators, can be considered as acceptable.

The upstream reach of both flumes were designed taking into

account the development of the turbulent layer. The equation applied was

$$\delta_1 = \frac{0.37}{\left[\frac{V}{\nu}\right]^{0.2}} \quad X^{0.8} \qquad (3.32)$$

where δ_1 is the depth of the boundary layer; V is the average velocity, ν is water viscosity and X is the length of the turbulent layer. For the main channel for maximum flow depth around 120 mm the length of turbulent layer was calculated to be approximately X = 6.3m.

For the floodplain flume the length of turbulent layer was calculated for flow depths of 50 mm is approximately:

Considering the area available for both flumes, the dimensions chosen for upstream and the downstream lengths were:

Floodplain Flume:	Main Channel Flume:
Upstream Reach : 2000.0 mm	4000.0 mm
Downstream Reach : 1900.0 mm	2000.0 mm

As it can be seen, the upstream length of the main channel flume was 2.0 m shorted than that required for fully developed turbulent flow at maximum depth.

Once the plan geometry of the flume was defined, the next step was to choose suitable pumps for the main channel and floodplain flumes. In the exercise it was necessary to calculate the maximum discharge to be delivered in each flume as well as the total head loss.

The maximum discharge in the floodplain system was calculated by Manning's equation, with floodplain depth as 60.0 mm and channel width as 1.65 m and longitudinal bed slope 0.001.

$$Q = (1/n)\ (A)^{5/3}/\ (P)^{2/3}\ \sqrt{S_0} \qquad (3.33b)$$

$$Q = 100\ (0.099)^{5/3}/(1.77)^{2/3}\sqrt{10^{-3}}$$

$$Q = 46\times10^{-3}\ m^3/s$$

$$V = 46\times10^{-3}/\ 0.099 = 0.46\ m/s$$

The head losses that occur in the floodplain flume and recirculating pump system are due to flow measurement orifice

plate, losses through gate valve, friction in supply pipe, entry to inlet tank, entry loss to flume, friction along flume, exit from flume and entry to pipe system again.

Based on estimates of all these values the pump chosen was a Myson MS, model 150-4210, with bronze impeller which can deliver a discharge of 60 l/s at the head of 6.0 m.

The estimate of the maximum discharge that occur in the main channel flume was performed by a procedure similar to the one used for the floodplain system. This time the flow depth was 150 mm, bed slope 1/1270 and channel width 450 mm giving,

$Q = 100 (0.0575)^{5/3} / (0.75)^{2/3} \sqrt{(1/1270)} \cong 38.0 \times 10^{-3}$ m^3/s

$V = 38.0 \times 10^{-3} / 0.0575 = 0.56$ m/s

The head losses were calculated by a procedure similar to the one followed for the floodplain system allowing for flow measurement orifice plate, valve loss, pipe bends, pipe friction, entry to inlet tank, flume losses etc.and the result was

$$\sum h_L \cong 2.0 \text{ m}$$

Based on the results of the maximum discharge and head loss the pump chosen for the main channel system was a Myson MS, model 125-4210 with bronze impeller which can deliver a discharge of 40 l/s at the head of 6.0 m.

Once the pumps were chosen the next step of the design procedure was to size the outlet and inlet tanks of both systems. The sketch shown in **Fig(3.41)** illustrates the method followed in sizing the tanks for both systems. For the floodplain system the volumes needed were:

(Maximum storage available in outlet tank: 0.7 * 1.82 * 1.82 = 2.3 m^3)

Water depth in the flume: 0.05 m

Volume in the flume: 1.65 * 7.2 * 0.05 = 0.6 m^3

Volume in the inlet tank:

1.82 * 1.22 * (1.4 - 1.15) = 0.8m^3

The total volume needed is: 0.6 + 0.8 = 1.4 m^3

The storage volume of the inlet tank is 2.3 m^3, which is greater than the required volume of 1.4 m^3. However, the inlet

tank needed to be placed at a level approximately 0.3 m higher than the level of the outlet tank.

The final dimensions of the tanks were:

Outlet tank: 1.82m * 1.82m * 1.22m

Inlet tank: 1.82m * 1.22m * 1.22m

For the main channel system the volumes needed were:

Maximum storage available in outlet tank: 0.7 * 1.22 * 1.82 = 1.5 m^3

Water depth in the flume: 0.117 m

Volume in the flume: 0.45 * 10.0 * 0.117 = 0.53 m^3

Volume in the inlet tank:

1.22 * 1.22 * (1.4 - 1.15) = 0.4m^3

The total volume needed is: 0.52 + 0.4 = 0.92 m^3

The storage volume of the inlet tank is 1.5 m^3, which is greater than the required volume of 0.92 m^3, having an extra capacity of 0.6 m^3. However, the inlet tank again needed to be placed at a level approximately 0.3 m higher than the level of the outlet tank.

The final dimensions of the tanks were:

Outlet tank: 1.82 m * 1.22 m * 1.22 m

Inlet tank: 1.22 m * 1.22 m * 1.22 m

3.7.3. Construction.

The main channel flume (450 mm wide) and the base of the floodplain flume (1650 mm wide) were built with 18.00 mm thick plywood. The floodplain was moulded in polystyrene sheet, 62 mm thick, covered by a 5.00 mm plywood sheet, giving a total bankfull depth of 67 mm. The side walls of the floodplain flume were made in aluminium plate because it is a non-corrosive properties as well as its stiffness which allowed the walls to act as rails for the instrument carriage. The side walls of main channel flume, built in plywood, had the function of also acting as the rails for the smaller instrument carriages. Both flume

were painted with oil based paint.

Both the floodplain and main channel flumes were supported by substantial frames built with 30.0 * 30.0 * 3.2 mm thick square section steel. The legs of the supporting system had a special levelling device which allowed up or down movement, thereby placing the channel bed at the required level.

The access platform, shown in **Fig(3.38)** straddled the floodplain flume and was able to roll along a second supporting frame independently of the first. This platform was used to give access over the full flume width.

The recirculating pvc pipe system for both floodplain and main channel flumes were composed on the following elements:

	Main Channel System:	Floodplain System:
Diameter of pipe	5"	6"
Type of pipe	PVC	PVC
Flanges	11	4
Gaskets	11	4
Backing rings	11	2
Butterfly valve	1	1
Gate valve	1	1
45^{o} bends	2	0
PVC pipe length	10 m	8.0 m
Pump	1 MSK 125-4210	1 MSK 150-4210

Some electrical equipment was ordered jointly with pumps which included one star delta starter for each pump and the corresponding electrical panel.

Fig(3.39) shows the pump and the gate valve of main channel system and the electrical panels of both systems.

The orifice flow meters installed in each piped circuit were made of perspex. **Fig(3.42)** shows the location of the orifice meter used for measurements of the discharge delivered to the floodplain flume.

The storage tanks for both flumes had the following dimensions:

No.	Size in metres	Identification
1	1.82 * 1.82 * 1.22	Sump of the floodplain system
1	1.82 * 1.22 * 1.22	Inlet of the floodplain system
1	1.82 * 1.22 * 1.22	Sump of main channel system
1	1.22 * 1.22 * 1.22	Inlet of main channel system

The tanks are of galvanised steel and painted with anti-corrosive paint. The sump tanks of both flumes were inter-connected giving a common sump.

Following construction of both systems, the bottom level of both flumes were levelled by an automatic level. The floodplain flume was levelled with the slope 1/1000 and the main channel flume with the slope 0.78/1000.

In order to perform detailed measurements in the Glasgow flume, three instrument carriages were made. The main instrument carriage was for the floodplain flume (1650 mm wide) as well as two identical carriages for the inlet and outlet channel of main channel flume, respectively. The instrument carriage used in the floodplain flume, shown in detail in **Fig(3.43)** was equipped with a pointer gauge, a bank of three vanes with angular potentiometers as well as one Pitot static tube and the respective pressure transducer. This instrument carriage, performs measurements not only on the floodplain area but also in the cross-over and bend region of the main channel.The other two instrument carriages were designed for measurement of water depths in the inlet and outlet of the main channel flume were equipped with a pointer gauge only. The right hand side of **Fig(3.37)** shows the small instrument carriage used in the inlet of the main channel flume.

The construction and the set up of Glasgow flume was done by **Mr. A. Gray**, technician of the Civil Engineering Department.

3.8 INSTRUMENTATION FOR THE GLASGOW FLUME

3.8.1. Introduction

Considerable time and effort was spent on the development, calibration and automatisation of the instrumentation in the Glasgow flume. It was considered that well calibrated accurate instruments would provide data quality on a par with the S.E.R.C. flume. It was also considered important that data acquisition, processing and storage be as efficient as the S.E.R.C. flume, and hence considerable effort was expended on automatic transfer of signals from the instruments IG A/D converters and on to micro processors with sophisticated software for analysis and graphical routines.

The Glasgow flume was equipped with following measurement instruments:

- Orifice meter and Differential manometers.
- Thermometer.
- Pointer gauge.
- Vanes with potentiometers.
- Pitot tubes and Pressure transducers.

3.8.2. Discharge Measurement

The discharge delivered by the main channel system and by the floodplain system were measured by two different orifice meters connected to differential manometers. In each case the orifice meter was located in a straight reach of pipe between the outlet tank and the inlet tank. The design and the location of each orifice meter was done in agreement with B.S. 1042, From the calibration curves proposed by B.S. 1042 discharges were calculated as a function of pressure differential. The procedure followed was:

For Main Channel System

Input Conditions:

Orifice Characteristics:

Pipe Diameter

$D = 0.127$ m

Orifice Diameter

$d = 0.088$ m

Viscosity

$\nu = 1.14 * 10^{-6}$ m^2/s

Method of Calculation following B.S. 1042

a) Diameter Ratio

$$\beta = d/D = 0.693 \qquad (3.38a)$$

b) Velocity of Approach Factor:

$$E = (1 - \beta^4)^{-1/2} = 1.147 \qquad (3.39a)$$

c) Expansion Factor

$\varepsilon = 1.0$ for incompressible liquids

d) Flow Coefficient

$$\alpha = (E \varepsilon \pi d^2 / 4) \sqrt{} (2 g) \qquad (3.41)$$

e) Reynolds Number

$$\mathbb{R} = 4 Q / (\pi D \nu) \qquad (3.37a)$$

e) Discharge Coefficient

$$C_d = 0.599 + 0.0312 \beta^{2.1} - 0.184 \beta^8 + 0.0029 \beta^{2.5} [10^6 / \mathbb{R}]^{0.75} + 0.039 L_1' \beta^4 (1 - \beta^4)^{-1} + 0.0337 L_2' \beta^3 \qquad (3.42)$$

where in this case $L_1' = 1$ and $L_2' = 0.47$, because the tapping points were located on D and D/2.

f) Discharge Q(in m^3/s) that passes through the orifice meter, was expressed on function of pressure difference Δh(in metres of water) which is read on the differential manometer.

$$Q = \alpha C_d \Delta h^{1/2} \qquad (3.42)$$

Fig(3.44) shows the cross section of the orifice meter used in

the main channel system.

For Floodplain System

Input Conditions:

Orifice Characteristics:

Pipe Diameter

D = 0.1524 m

Orifice Diameter

d = 0.11 m

Viscosity

$\nu = 1.14 * 10^{-6}\ m^2/s$

Method of Calculation following B.S. 1042

a) Diameter Ratio

$$\beta = d/D = 0.722 \qquad (3.37b)$$

b) Velocity of Approach Factor:

$$E = (1 - \beta^4)^{-1/2} = 1.17 \qquad (3.38b)$$

All other steps are exactly the same as the ones followed for the main channel system.

The best fit line procedure was applied to these results and the correlation curves relating discharge with pressure difference were developed for both cases.

For the main channel system, the theoretical calibration curve derived from B.S. 1042 was,

$$\text{Log } Q = a_0 + a_1 \text{ Log } (\Delta h) \qquad (3.44)$$

where

$a_0 = -1.726$

$a_1 = 0.494$

Correlation Coefficient: 0.999

For the floodplain system the theoretical calibration curve derived from B.S. 1042 was,

$$\text{Log } Q = a_2 + a_3 \text{ Log } (\Delta h) \qquad (3.45)$$

where

$a_2 = -1.521$

$a_3 = 0.493$

Q is discharge in m^3/s

Δh is the pressure difference in metres of water

Correlation Coefficient: 0.999

Each orifice meter was provided with two differential manometers: one filled with water for low flow measurements, covering 1m of pressure differential; other filled with mercury for high discharges measurements, covering also 1m of mercury pressure differential. Each differential manometer was provided with a system of valves and by-pass which allowed the system to be purged of air bubbles. **Fig(3.39)** shows the differential manometer used for measurements of the discharged delivered by the main channel system.

Due to insufficient space of the hydraulic laboratory, the length of straight reach upstream and downstream of the orifice meter did not comply with all requirements of the B.S. 1042. Thus a calibration procedure was carried out to compare the results given by the method proposed by B.S. 1042 against the discharge obtained by depth integration method where velocities were measured using a mini-propeller and water depths through a pointer gauge. The measurements taken with the mini-propeller and pointer gauge were performed in downstream region of the floodplain. **Table(3.14)** shows the comparison of discharges obtained by both procedures. The discharges obtained by the orifice meter and by the velocity integration method present a good level of agreement, being the difference between both results around 5%. The calibration results are plotted in **Fig(3.44a)**, for the main channel flume and in **Fig(3.44b)**, for the floodplain flume, revealing experimental data close enough to accept the B.S. 1042 correlation. The maximum difference was ± 5%.

Thermometer

Water temperature in Glasgow model was taken by centigrade thermometer thus providing accurate estimates of fluid viscosity for each test-run.

3.8.3 Pointer Gauges

Water levels were measured by pointer gauges with accuracy ± 0.5 millimetres. For measurements of water levels in the inlet and in the outlet of main channel and on the floodplain region there is a pointer gauge mounted on each instrument carriage. **Fig(3.43)** shows a detail of the instrument carriage with the pointer gauge for measurements of flow depths in the floodplain, cross-over and bend region of the main channel.

It was important to obtain detailed local water levels in the cross-over and bend apex regions in view of local acceleration and deceleration of the flow as well as centrifugal effects at the bend. It was originally envisaged that Churchill probes would be used for water level recording in this area, although initial test runs showed that pointer gauge data was just about as accurate and less time consuming.

3.8.4. Streamline angle measurement

The stream angles were measured by a bank of three rotating vanes, each one connected to a potentiometer through a small shaft. The shafts of the vanes were aligned and distanced 50.0 mm apart. The bank of vanes, shown in **Fig(3.45)**, was mounted on a rigid plate. Through a specially designed bearing system the bank could rotate 180^{0}, the rotation angle measured by a protractor. The reading of the angle was taken by a pointer that was linked to the bank of vanes. The bank of vanes were able to move up and down vertically over the flow depth, to move across the flume width transversely, and to move longitudinally along the flume length, thus providing full three dimensional movement.

Access to the instrument carriage is gained by a straddling platform, shown in **Fig(3.37)** and in **Fig(3.38)**, specially built up for this purpose.

The potentiometers used in Glasgow flume were the Penny and Giles type, exactly of the same kind as those used in S.E.R.C. flume. Although each potentiometer has its calibration curve

given by the supplier, each was submitted to a rigorous calibration procedure. **Table(3.15)** shows the calibrations constants obtained by the **Author** compared with those given by the supplier.

The calibration constants calculated by the **Author** were the ones used in the sampling procedure of the stream angles of the flow.

All three potentiometers were stabilised by a constant input 10 d.c. volts. The output current in d.c. voltage is governed by the angular position of the vane and shaft in relation to the transducer body. These potentiometers have a rotational range of 300 degrees and care was taken never to be operating in the out-of range 60^{0}.

The d.c. voltage generated by each potentiometer was collected by an A/D interface card MC-MIO-16/L/9 containing 8 differential input channels, 4 analog output channels, and 2 ports for digital input/output. Four different input channels (± 10 volts range) were used, three for the output signal of the three potentiometers and one for the output signal of the pressure transducer, from the pitot tube which will be described in next point.

Data acquisition and data analysis was carried out by software named **Labtech Notebook**, Version 6, connected to a graphical interface, named Iconview, run on an IBM PC, version PS/2, shown in **Fig(3.46)**.

After setting up the interface card and connecting all three output channels from the potentiometers, significant noise was noticed coming to the computer. After some trials, the found to eliminate this noise used two resistors 100 kΩ connected between input signals and earth. A check on the accuracy of the data was carried out by comparing the signal received by the A/D card and the software with the readings taken direct from a digital voltameter. The results produced by both systems were exactly the same.

The graphical interface, Iconview, allows displays of the data and controls the setups by moving and connecting icons.

Fig(3.47) shows the display screen of the computer with icons connections for streamline angle measurement in Glasgow flume. For the sampling procedure of the stream angles, nine channels were used, three per each vane. The first three channels receive the analog input signal and convert into degrees. In the conversion process, the main aspects of control set-up were defined in the following way:

Interface Device:[0 : MC-MI016H/A]
Channel Type: Analog Input
Channel Units: Volts
Scale Factor : Calibration Constant of Each Potentiometer(ex. 28.57 for pot. No. 1)
Offset Constant: Volts reading that corresponds to Zero Angle(usually around 5.0 volts)
Sampling Rate :10 Hertz
Stage Duration: 60 seconds

The second set of three channels calculates the average angle measured by each vane. The last set of three channels determines the standard deviation of the angle measured by each vane. For each test run, the results of the three average angles and the three standard deviation angles appeared in computer screen in six windows, as shown in **Fig(3.48)**.

3.8.5. Pitot Tube and Velocity Measurement

Flow velocity in Glasgow flume was measured by using a 4.0 mm diameter Pitot tube connected to an ultra low head pressure transducer. Preference was given to a Pitot static tube system for velocity measurements instead of a mini-propeller. The reasons for this is that a mini-propeller needs flow depths of at least 10-12 mm to operate satisfactorily. In some cases this may be purely achieved on the floodplain. Also the external diameter of the Pitot static tube is only 4 mm, implying that area averaging of the local velocity is over a much smaller area than the miniature propeller meter.

The Pitot static tube, shown in **Fig(3.49)**, is a L shaped

tube that measures the kinetic energy of the flow. It is an measurement instrument composed by two tubes. The inner tube records the kinetic energy plus the pressure energy($U^2/(2g) + p/\gamma$). The outer tube, running parallel to the inner tube, has several small holes around the Pitot tube and registers the pressure energy(p/γ). The difference between the two energies gives the value of kinetic energy of the flow. If this difference is read in appropriate device such as a differential pressure transducer, the flow velocity of the particular point, where the Pitot static tube is located, can be determined.

The pressure transducer, shown in **Fig(3.49)**, used in the test program was a Validyne type DP45, with a diaphragm dash number 18. This pressure transducer is designed to measure very low differential pressures. The diaphragm chosen, measures differential pressures up to 56.00 mm of water. The pressure difference activates the diaphragm through two female pressure ports connections which can be tapered by American Standard Pipe Thread. The transducer bleeding is carried out by a bleed port which facilitates cleaning or filling the pressure cavities.

In order to calibrate the pressure transducer a special device, shown in **Fig(3.50)**, was built in the workshop of the Civil Engineering Department. This calibration device is composed basically of two graduated tubes with four valves. Two shutoff valves allowed the connection of the pressure transducer tubes to the calibration device. The third is a by-pass valve, which when open levels the water contained in both tubes. The fourth and last valve is a drain valve which is connected to one of the graduated tubes and enabling a variation in the water level in this tube, creating a pressure difference between the two tubes. A sketch of the calibration device with the identification of the valves is shown in **Fig(3.51)**. The steps in the calibration procedure were as follows:

a) By opening the by-pass valve, the water in tubes of the calibration device were levelled.

b) The readings of the water levels in both tubes were taken as the zero reading.

c) The computer program was run and the result of average voltage was obtained; this is the zero voltage.
d) The by-pass valve was closed.
e) The drain valve was opened in order to give a certain variation of water level in the corresponding tube and a reading was taken.
f) The computer programme was run again and a new average voltage was obtained.
g) The drain valve was open again to give another increment(usually around 2.0 mm of water) in water level in tube and the process e) and f) was repeated until the range of 54 mm of water level variation was complete.
h) The variation of water levels in the tubes in relation to the zero reading were correlated with voltage variation in relation to the zero voltage.
A sketch of the apparatus used in the calibration procedure of the pressure transducer is shown in graphical form in **Fig(3.51)**. The calibration curve of the pressure transducer model DP 45-18 is presented in **Fig(3.52)**. The calibration constant obtained was 1 mm of water for 8.02 milli-volts variation

The software and hardware used for data acquisition and data analysis process were the same as previously described for the vane system. In this case four channels were used for data acquisition and data analysis of the analog input signal generated inside the pressure transducer box.

The Pitot static tube and pressure transducer, were mounted on the same horizontal plate where the three potentiometers with vanes were fixed in the instrument carriage. **Fig(3.49)** shows the Pitot tube and the pressure transducer mounted on the instrument carriage.

Some results produced by the Pitot tube were cross-checked with values given by mini-propellers. In general a good agreement between both results was found.

3.8.6. Program of Testing.

The test program in Glasgow flume involved the study of two cases. In the first case the floodplain system was closed and the main channel system was delivering a flow of 0.0175 m^3/s. Measurements of stream angles, velocities and water surface levels were carried out in five sections around the bend. The flow velocity measurement performed with the Pitot tube were carried out in the streamwise direction, as in this particular test condition, the stream angles were always less than $10^0$and the " Cosine Law" is applicable. In the grid of measurements, the verticals were distanced 50.0 mm apart and in the vertical direction the measurements were taken in increments of 10.0 mm. **Fig(3.53)** shows the location of the sections and the vertical slices where the measurements were conducted.

In the second case the main channel system was closed and the floodplain system was on. In this condition the stage-discharge curve of the system was obtained. **Appendix I** contains the values of the stage-discharge curve of the floodplain system. The uniform depth was varied between 11.0 mm to 62.0 mm while the discharge was varied between 0.0024 to 0.0371 m^3/s. It was not possible to test for higher discharges than 0.0371 m^3/s because the water surface was already very wavy.

3.8.7. Methodology of Testing.

As explained in point 3.3.7, in the test program of the Glasgow flume two cases were analysed and the methodology adopted for testing in both cases, was also different.

In the first case the uniform conditions were achieved in the inlet of the main channel by varying the vertical tail gate, located in the downstream end of the outlet of the main channel. The steps followed in choosing the correct uniform depth were the followings:

Bankfull Depth of Main Channel(h) : 67.0 mm

Total Flow Depth (H) : 88.0 mm

$$D_R = \frac{88 - 67}{88} = 0.24$$

Area : $0.088 * 0.45 = 0.0395\ m^2$

Perimeter : $0.45 + 2 * 0.088 = 0.626$ m

Hydraulic Radius: 0.063 m

Slope: $0.78 * 10^{-3}$

Manning's n : 0.01

Discharge following Manning's equation:

$$Q = 100 * (0.0631)^{2/3} * (0.78 * 10^{-3})^{1/2} * 0.0395 = 0.0175\ m^3$$

Average depths in the inlet channel:

88.3 mm

Average depths in the outlet channel:

80.0 mm

Thus there is a difference in depth between the inlet and outlet channel. This can be explained by the disturbance that the floodplain area introduces in the flow.

In the second case the main channel system was shutt and the floodplain system was on. The uniform flow was established in the inlet and outlet channel of the floodplain system by varying the hinge gate, located at the downstream end of the flume. The flow depths were measured in three vertical of a section located in the middle point of each straight reach and then averaged.

It is considered important to clarify what is meant by shutting the main channel system. When the main channel system was off the following steps were taken before the floodplain system was putting on:

- the pump of the main channel system was off.
- the valve downstream of the main channel pump was closed.
- the vertical gate, located in the downstream end of the outlet channel was putted down, preventing any water leakage.

When the floodplain system was off and the main system was on similar steps were taken.

3.8.8 Scale Effects in The Glasgow Flume.

In small scale flumes such as the Glasgow flume, the Reynolds Number is much smaller than the prototype case and the flow although turbulent, is not rough turbulent. This means that viscous scale effects may have some influence particularly in the floodplain region were the flow depths were much smaller than in the main channel region, producing smaller Reynolds numbers. The only way to investigate the magnitude of scale effects is by comparing results of discharge velocity and shear stresses produced by smaller scale models against ones obtained in prototypes. Although, the study carried out at the Glasgow flume could not be compared with any prototype, it was considered important to consider at least qualitatively the likely scale effects in this model.

Gravity is the predominant factor influencing fluid motion wherever a free surface gradient is present. Model studies of river meanders are included in this category. In order to achieve similarity, the Froude number($\mathbb{F}= V/(gH)^{1/2}$of the model and prototype must be identical. However the viscous forces cannot be neglected in view of their role in the boundary friction and as the origin of fluid turbulence.

Viscous effects in fluid dynamics are represented by the Reynolds number($\mathbb{R} = 4 V R / \nu$). The effect of the Reynolds number on the flow resistance for instance can be visualised through the Moody diagram, where the flow resistance is expressed through the relationship between the Darcy-Weisbach friction factor and the Reynolds number. **Weber(1974)** produced a similar diagram for open channel flow. He considers $\mathbb{R}$=2000 as an arbitrary upper limit for the transition from laminar flow to turbulent flow in open channels. This criterion was easily achieved on the floodplain of the Glasgow flume.

Despite reaching the turbulent flow criterion, there are still likely to be scale effects considering both the smoothness of the boundaries in the Glasgow flume(main channel and floodplain) and also considering the model Reynolds number(

10^4-10^5) compared to typical prototype Reynolds numbers(10^6-10^7).

The Moody diagram reveals the turbulent zone with its characteristics smooth and rough low features. The dividing line between these features is given approximately by $U*k/\nu>50$ showing that prototypes with substantial k values are much more likely to have floodplain flow in the rough turbulent zone, and models with smooth boundaries are certainly in smooth turbulent zone. When this is combined with the ratio of the protype to model Reynolds number being of the order of 100-200 typically, then scale effects are inevitable and hence the rationale for the S.E.R.C. Flume study, where the Reynolds number ratio is more likely to be around 20-30 rather than 100-200.

Table(3.16a)(Main channel) and **Table(3.16b)**(Floodplain) contain the values of the Darcy Weisbach friction factor($f= 8gRS/V^2$), the Reynolds number($\mathbb{R}=4VR/\nu$) and the Froude number($\mathbb{F}=V/(gH)^{1/2}$) for flow depths varying between 10mm-60mm in the main channel and in the smooth floodplain regions of the Glasgow flume.

Both tables show that:

(i) The range of Reynolds numbers for inbank flow, and also floodplain flow is generally 10^4- 10^5.

(ii) Flow is smooth turbulent in both main channel and floodplain regions, as the Reynolds number is always greater than 2000.0 and the boundaries are very smooth(plywood).

(iii) The Darcy-Weisbach friction factor reduces with increasing Reynolds number.

(iv) The **Author's** results fit quite well the f-$\mathbb{R}$ relationship of the smooth law curve of the Moody diagram. This is shown in **Fig(3.54)**.

From the above findings it can be concluded that some scale effects will occur in the Glasgow flume, particularly in the floodplain region. The most likely effect is viscous damping on the floodplain, increasing the friction factor, reducing turbulence levels and momentum transfer in the model. However it should be remembered that the main features, such as secondary

cells, which dominate this type of bend overbank flow will remain largely unaffected. That is, viscous damping will have little effect on large flow structures, but a lot of effect on finer scale turbulence such as the lateral shear turbulence found in straight/parallel compound flows.

The Manning's equation was derived for the fully rough turbulent flow condition. In the Glasgow flume, the flow is smooth turbulent, therefore the Manning's equation should not be applied. Instead it is recommended that the Darcy-Weisbach equation be used, which has a much greater range of application, covering the smooth and the fully turbulent flow conditions.

In actual rivers where the boundaries of main channel and floodplain are very rough, the flow regime will be rough turbulent and the Manning's equation in this case can be applied.

3.9. SUMMARY

This chapter presents a detailed description of S.E.R.C. and Glasgow flumes, the instrumentation used in both flumes for collecting and analysing data, including the calibration procedure followed and the cross-checks and the experimental program with the explanation of the methodology followed in the tests.

Data obtained in both flumes, as demonstrated by the results of the cross-checks, was very accurate and reliable. In particular the S.E.R.C. data, because it was obtained in such a large model, will allow to analyse the internal structure of a meander compound flow in a very detailed way, never reached until now, and consequently to calibrate mathematical models. The Glasgow flume data will complement the information of S.E.R.C. flume.

Table(3.1)

Design of Plan Geometry of 2nd Meandering Channel of the S.E.R.C. Flume Series B.

Version Number	Cross-Over Length	Central Radius	Top Width	R_c/B_c	B_c/h
	m	m	m		
1	0.5	2.743	1.2	2.29	8.0
2	0.0	2.743	1.2	2.29	8.0
3	0.0	1.98	0.8	2.5	8.0
4	0.423	1.83	0.8	2.3	8.0

Design of Plan Geometry of 2nd Meandering Channel of The S.E.R.C. Flume Series B.

Wave Length	Width of Meander Belt	Sinuosity	Bankfull Depth	Number of Wave Lengths
m	m		mm	
9.97	9.03	2.21	150	4.5
10.31	8.56	2.04	150	4.5
7.44	6.106	2.04	100	6.5
6.586	6.107	2.26	100	7.0

Table(3.2) - 17 References Used in the Design of Apex Section of the Natural Meandering Channel of The S.E.R.C. Flume Series B.

No.	River Name	Source	Year	Page
1	Dommel	A.S.C.E. J. HYD. DIV.	1983	996
2	Dommel	A.S.C.E. J. HYD. DIV.	1983	996
3	Sacramento	A.S.C.E J. HYD. DIV.	1981	1686
4	Sacramento	A.S.C.E. J. HYD. DIV.	1981	1686
5	Fall	River Meand. Conference	1983	679
6	Fall	River Meand. Conference	1983	681
7	Chislehampton	A.S.C.E J. HYD. DIV.	1986	660
8	Tanana	River Meand. Conference	1983	209
9	Grande del Rancho	River Meand. Conference	1983	646
10	East Fork	River Meand. Conference	1983	837
11	Magdalena	Princ. of River Engin.		142
12	Wall	Princ. of River Engin.		144
13	Wall	Princ. of River Engin.		144
14	Mississipi	River Meand. Conference	1983	633
15	Mudy Creek	River Meand. Conference	1983	633
16	Snov	River Mechanics (Vol.2)		20-30
17	Severn	River Meand. Conference		37

Table(3.3) - Geometric Data from 17 River Bends.

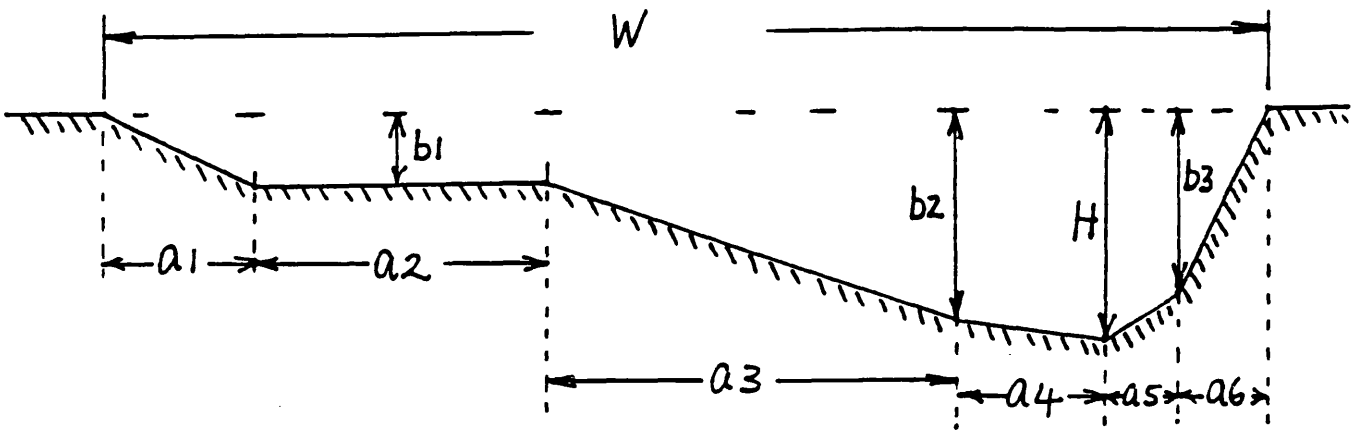

No.	River	a1/w	a2/w	a3/w	a4/w	a5/w	a6/w	b1/H	b2/H	b3/H	W/H
1	Dommel	0.03	0.25	0.52	0.05	0.08	0.05	0.17	0.93	0.83	5
2	Dommel	0.04	0.25	0.41	0.12	0.08	0.10	0.37	0.74	0.70	6.7
3	Sacramento	0.08	0.16	0.63	0.06	0.05	0.02	0.40	0.93	0.67	41.3
4	Sacramento	0.00	0.22	0.51	0.07	0.17	0.0	0.20	0.89	0.5	16.7
5	Fall	0.11	0.43	0.29	0.10	0.05	0.02	0.25	0.93	0.92	7.7
6	Fall	0.13	0.27	0.22	0.08	0.12	0.17	0.11	0.70	0.61	6.3
7	Chislehampton	0.18	0.12	0.35	0.08	0.08	0.20	0.47	0.99	1.0	2.6
8	Tanana	0.21	0.19	0.35	0.12	0.06	0.08	0.28	0.68	0.80	20
9	Grande del Rancho	0.34	0.15	0.14	0.24	0.07	0.06	0.54	0.85	0.72	12.5
10	East Fork	0.08	0.10	0.37	0.21	0.19	0.04	0.40	0.95	0.80	14.3
11	Magdalena	0.08	0.53	0.17	0.10	0.0	0.12	0.20	0.83	1.0	33.3
12	Wall	0.23	0.22	0.38	0.08	0.06	0.03	0.52	0.86	0.72	50
13	Wall	0.16	0.34	0.30	0.10	0.07	0.03	0.29	0.78	0.63	33.3
14	Mississippi	0.17	0.28	0.31	0.14	0.035	0.05	0.23	0.54	0.76	33.3
15	Mudycreek	0.20	0.17	0.29	0.14	0.07	0.10	0.33	0.73	0.80	7.7
16	Snov	0.03	0.34	0.38	0.15	0.0	0.08	0.17	0.72	1.0	
17	Severn	0.21	0.16	0.36	0.22	0.04	0.01	0.27	0.73	0.95	16.7
	AVERAGE VALUES	0.13	0.25	0.35	0.12	0.07	0.07	0.30	0.92	0.79	19.2

Table(3.4) - Design of the Natural Inserts of the Meander Channel with Sinuosity 1.374.

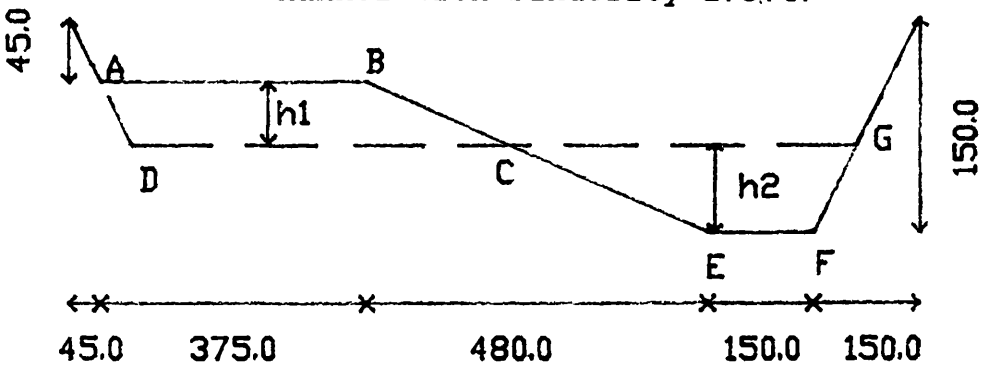

ABCD = AREA A1

CEFG = AREA A2

AREA A1 = (375-h1) * h1 + h1*h1/2 + (h1/tan(12.339) *h1/2

AREA A2 =(150*h2) + h2*h2/2 + (h2/tan(12.339) * h2/2

TABLE

VARIATION OF h1 AND h2 WITH BEND ANGLE

α ANGLE degrees	h1 mm	AREA A1 mm2	h2 mm	AREA A2 mm2
0.0	0.0	0.0	0.0	0.0
12.0	8.8	3438.0	17.0	3355.0
20.0	14.7	5898.0	26.0	5783.0
24.0	17.6	7153.0	30.0	7007.0
36.0	26.4	11144.0	42.0	11214.0
40.0	29.3	12521.0	45.0	12391.0
48.0	35.2	15413.0	52.0	15333.0
60.0	44.0	19957.0	61.0	19517.0

Table(3.5) - Geometric Parameters of the Natural Inserts for Sinuosity 1.374.

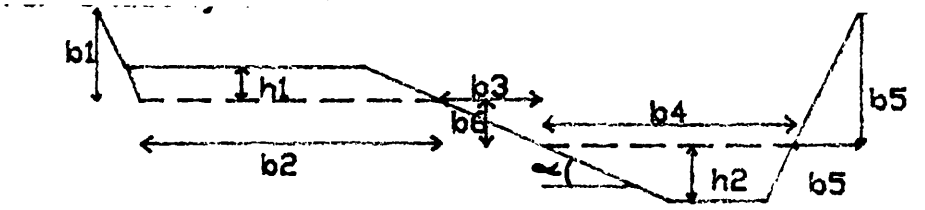

$\alpha = \tan^{-1}(105/480) = 12.339^{\circ}$

b1 = 45.0 + h1

b2 = 375.0 -h1 + h1/tan(12.339)

b3 = 480-h1/tan(12.339) -h2/tan(12.339)

b4 = 150+ h2/tan(12.339) + h2

b5 = 150- h2

b6 = b3 * tan(12.339)

ANGLE degrees	b1 mm	b2 mm	b3 mm	b4 mm	b5 mm	b6 mm
0.0	45.0	375.0	480.0	150.0	150.0	105.0
12	53.8	406.4	362.0	245.0	133.0	79.2
20.0	59.7	427.5	293.9	294.9	124.0	64.3
24.0	62.6	438.0	262.4	317.0	120.0	57.4
36.0	71.4	469.2	167.31	384.0	108.0	36.6
40.0	74.3	479.6	140.2	400.7	105.0	30.6
48.0	80.2	500.7	81.4	439.7	98.0	17.8
60.0	89.0	532.1	0.0	489.9	89.0	0.0

Table(3.6) - Design of the Natural Inserts of the Meander Channel with Sinuosity 2.04.

INSERTS FOR 110 DEGREES MEANDER

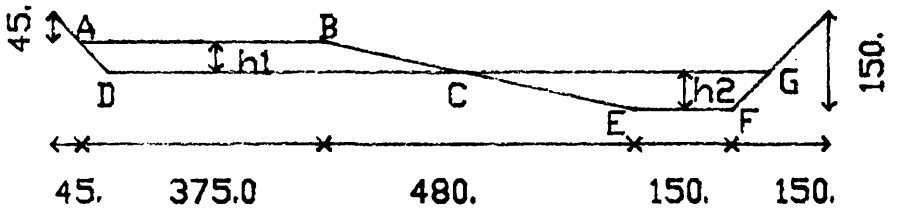

ABDC = AREA A1

CEFG = AREA A2

AREA A1 = (375 - h1) * h1 + h1 * h1 / 2 +
+ (h1 / tan (12.34)) * h1 / 2

AREA A2 = (150 - h2) + (h2 * h2) /2 +
+ (h2 / tan (12.34) * h2 / 2

ANGLE Degrees	h1 mm	AREA A1 mm2	h2 mm	AREA A2 mm2
0.0	0.0	0.0	0.0	0.0
10.0	4.0	1528.9	9.0	1576.0
20.0	8.0	3114.3	16.0	3113.0
30.0	12.0	4757.0	22.0	4648.0
40.0	16.0	6457.0	28.0	6384.0
50.0	20.0	8214.0	34.0	8320.0
60.0	24.0	10029.0	39.0	10087.0
70.0	28.0	11900.0	44.0	11993.0
80.0	32.0	13829.0	48.0	13618.0
90.0	36.0	15814.0	53.0	15775.0
100.0	40.0	17857.0	58.0	18071.0
110.0	44.0	19957.0	61.0	19516.0

Table(3.7) - Geometric Parameters of the Natural Inserts for Sinuosity 2.04.

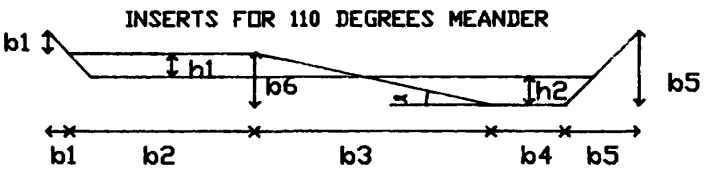

$\alpha = \tan^{-1}(105/480) = 12.339^{0}$

b1 = 45 + h1

b2 = 375.0 - h1 + h1/tang(12.339)

b3 = 480.0 - h1/tan(12.339) - h2/tan(12.339)

b4 = 150.0 + h2/tan(12.339) - + h2

b5 = 150.0 - h2

b6 = b3 * tan(12.339)

ANGLE Degrees	b1 mm	b2 mm	b3 mm	b4 mm	b5 mm	b6 mm
0.0	45.0	375.0	480.0	150.0	150.0	105.0
10.0	49.0	389.0	421.0	200.0	141.0	92.0
20.0	53.0	404.0	370.0	239.0	134.0	81.0
30.0	57.0	418.0	325.0	273.0	128.0	71.0
40.0	61.0	432.0	279.0	306.0	122.0	61.0
50.0	65.0	446.0	233.0	339.0	116.0	51.0
60.0	69.0	461.0	192.0	367.0	111.0	42.0
70.0	73.0	475.0	151.0	395.0	106.0	33.0
80.0	77.0	489.0	114.0	417.0	102.0	25.0
90.0	81.0	504.0	73.0	445.0	97.0	16.0
100.0	85.0	518.0	32.0	473.0	92.0	7.0
110.0	89.0	532.0	0.0	489.0	89.0	0.0

Table(3.8)

Comparison of Discharge Measurements between Orifice Meter and Velocity Integration Method in The S.E.R.C.Flume Series B.

Sinuosity: 1.374 Trapezoidal Section Smooth Floodplains

Stage	Discharge in l/s		Difference
mm	Orifice Meter	Integration Method	%
100.0	47.0	46.3	1.5
200.0	253.0	251.0	0.8
250.0	640.0	663.0	3.6

Sinuosity: 1.374 Natural Section Smooth Floodplains

Stage	Discharge in l/s		Difference
mm	Orifice Meter	Integration Method	%
140.0	32.5	33.0	1.5
165.0	57.5	57.5	0.0
200.0	226.0	222.0	1.8
250.0	614.0	637.0	3.8

Sinuosity: 2.04 Natural Section Smooth Floodplains

Stage	Discharge in l/s		Difference
mm	Orifice Meter	Integration Method	%
140.0	25.0	25.0	0.0
200.0	179.0	183.0	2.2

Table(3.9)

Test Program of Measurements of Stream Angles and Velocities in The S.E.R.C. Flume Series B.

Trapezoidal Cross-section with Smooth Floodplains

Sinuosity: 1.374

Depth mm	Case	Area Covered
100	Inbank	Main Ch.
200	Overbank	Main Ch.+ Floodplain
250	Overbank	Main Ch.+ Floodplain

Natural Cross-section with Smooth Floodplains

Sinuosity: 1.374

Depth mm	Case	Area Covered
140	Inbank	Main Ch.
165	Overbank	Main Ch.
200	Overbank	Main Ch.+ Floodplain
250	Overbank	Main Ch.+ Floodplain

Natural Cross-section with Fully Roughened Floodplains

Sinuosity: 1.374

Depth mm	Case	Area Covered
165	Overbank	Main Ch.
200	Overbank	Main Ch.+ Floodplain
250	Overbank	Main Ch.+ Floodplain

Table(3.9)

(Continued)

Test Program of Measurements of Stream Angles and Velocities in The S.E.R.C. Flume Series B.

Natural Cross-section with Smooth Floodplains

Sinuosity: 2.04

Depth mm	Case	Area Covered
140	Inbank	Main Ch.
165	Overbank	Main Ch.
200	Overbank	Main Ch.+ Floodplain

Natural Cross-section with Fully Roughened Floodplains

Sinuosity: 2.04

Depth mm	Case	Area Covered
165	Overbank	Main Channel
200	Overbank	Main Channel

In the main channel the following sections were measured:

Sinuosity	Sections
1.374	1 to 11
2.04	1 to 14

Table(3.10)

Test Program of Measurements of Boundary Shear Stress in The S.E.R.C. Flume Series B.

Natural Cross-section with Smooth Floodplains

Sinuosity: 1.374

Depth mm	Case	Area Covered
140	Inbank	Main Ch.
200	Overbank	Main Ch.+ Flood.

Natural Cross-section with Smooth Floodplains

Sinuosity: 2.04

Depth mm	Case	Area Covered
140	Inbank	Main channel
165	Overbank	Main Ch. + Flood.
200	Overbank	Main Ch. + Flood.

Table(3.11)

Test Program of Measurements of Flow Turbulence in The S.E.R.C. Flume Series B.

Sinuosity: 1.374

Type of Cross Section	Depth mm	Case	Section
Trapezoidal	100	Inbank	Apex
Trapezoidal	200	Overbank	Apex
Natural	140	Inbank	Apex
Natural	140	Inbank	$+40^{o}$
Natural	165	Overbank	Apex
Natural	200	Overbank	Apex
Natural	200	Overbank	$+40^{o}$

Sinuosity: 2.04

Type of Cross Section	Depth mm	Case	Section
Natural	140	Inbank	Apex
Natural	165	Overbank	Apex
Natural	200	Overbank	Apex

Table(3.12)

Cross-Checks of The S.E.R.C. Series B.Flume Results

Instrument No.1	Instrument No.2	Method of Cross-Check
Orifice Meter	Vane, Mini-Propeller Churchill Probe	Discharge by Integration
Vane	LDV	Streamline Angles
Mini-Propeller	LDV	Velocity
Preston Tube	LDV	Boundary Shear

Table(3.13)

Case Studies of Stage-Discharge in S.E.R.C. Flume Series B.

Case	Sinuosity	Main Channel Cross-Section	Floodplain Roughness
1	1.374	Trapezoidal	Smooth
2	1.374	Natural	Smooth
3	1.374	Natural	Fully Rough.
4	1.374	Natural	Part. Rough.
5	1.374	Natural	Brick Blocks
6	1.374	Natural	Width Reduced
7	2.04	Natural	Smooth
8	2.04	Natural	Fully Rough.
9	2.04	Natural	Width Reduced
10	2.04	Natural	Brick Blocks
11	2.04	Natural	With a Wall

Table(3.14)

Comparison of Discharge Measurements by The Orifice Meter and by The Velocity Integration Method in the Glasgow Flume

Floodplain System

Discharge in m^3/s

Orifice	Integr. Met.	Error %
0.0175	0.0169	- 3.6
0.0216	0.0206	- 4.8
0.0281	0.0283	+ 1.0
0.041	0.039	- 5.0
0.051	0.052	+ 2.0

Main Channel System

Discharge in m^3/s

Orifice	Integr. Met.	Error %
0.0155	0.016	+ 3.0
0.0205	0.0199	- 3.0
0.0289	0.0282	- 2.5
0.042	0.043	+ 2.4

Table(3.15)

Calibration Constants of the Potentiometers of Glasgow Flume

millivolts/degree

Potentiometer No.	Author	Supplier
1	35	35.8
2	38.0	39.94
3	37.0	36.12

Table(3.16a)

Analysis of Scale Effects in The Main Channel of The Glasgow Flume

Stage mm	Reynolds Number	The Darcy-Weisbach Friction Factor	Froude Number
10.0	$4.9*10^3$	0.0369	0.404
20.0	$1.4*10^4$	0.0297	0.44
30.0	$2.64*10^4$	0.0267	0.46
40.0	$4.0*10^4$	0.0242	0.47
60.0	$9.18*10^4$	0.0205	0.54

Table(3.16b)

Analysis of Scale Effects in The Floodplain of The Glasgow Flume

Stage mm	Reynolds Number	The Darcy-Weisbach Friction Factor	Froude Number
10.0	$5.8*10^3$	0.0365	0.47
20.0	$1.8*10^4$	0.0291	0.52
30.0	$3.5*10^4$	0.0255	0.55
40.0	$5.5*10^4$	0.0233	0.58
60.0	$1.03*10^5$	0.0205	0.60

Fig (3.1) - General View of The S.E.R.C. Flume Series B with Sinuosity 1.374 and Smooth Floodplains.

Fig (3.2) - General View of The S.E.R.C. Flume Series B with Sinuosity 2.04 and Smooth Floodplains.

SINUOSITY 1.374

MAIN CHANNEL CROSS SECTION : TRAPEZOIDAL

FLOODPLAIN ROUGHNESS : SMOOTH

MAIN CHANNEL CROSS SECTION : NATURAL

FLOODPLAIN ROUGHNESS : SMOOTH

FLOODPLAIN ROUGHNESS : FULLY ROUGH.

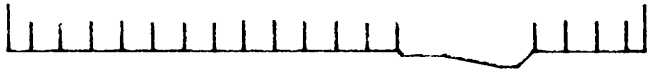

FLOODPLAIN ROUGHNESS : PART. ROUGH.

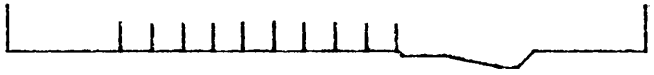

FLOODPLAIN WIDTH REDUCED AND SMOOTH

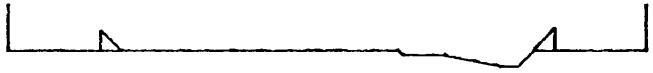

FLOODPLAIN ROUGHNESS : BRICK BLOCKS

SINUOSITY 2.04

MAIN CHANNEL CROSS SECTION : NATURAL

FLOODPLAIN ROUGHNESS : SMOOTH

FLOODPLAIN ROUGHNESS : FULLY ROUGH.

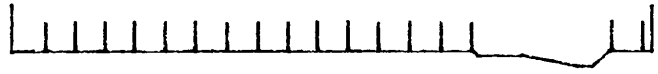

FLOODPLAIN WIDTH REDUCED AND SMOOTH

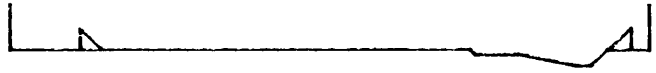

FLOODPLAIN ROUGHNESS : BRICK BLOCKS

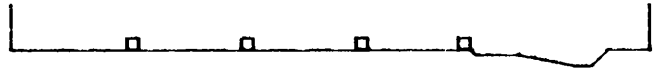

FLOODPLAIN ROUGHNESS : WITH A WALL

Fig. 3.3 - Case Studies of The S.E.R.C. Flume Series B Tests.

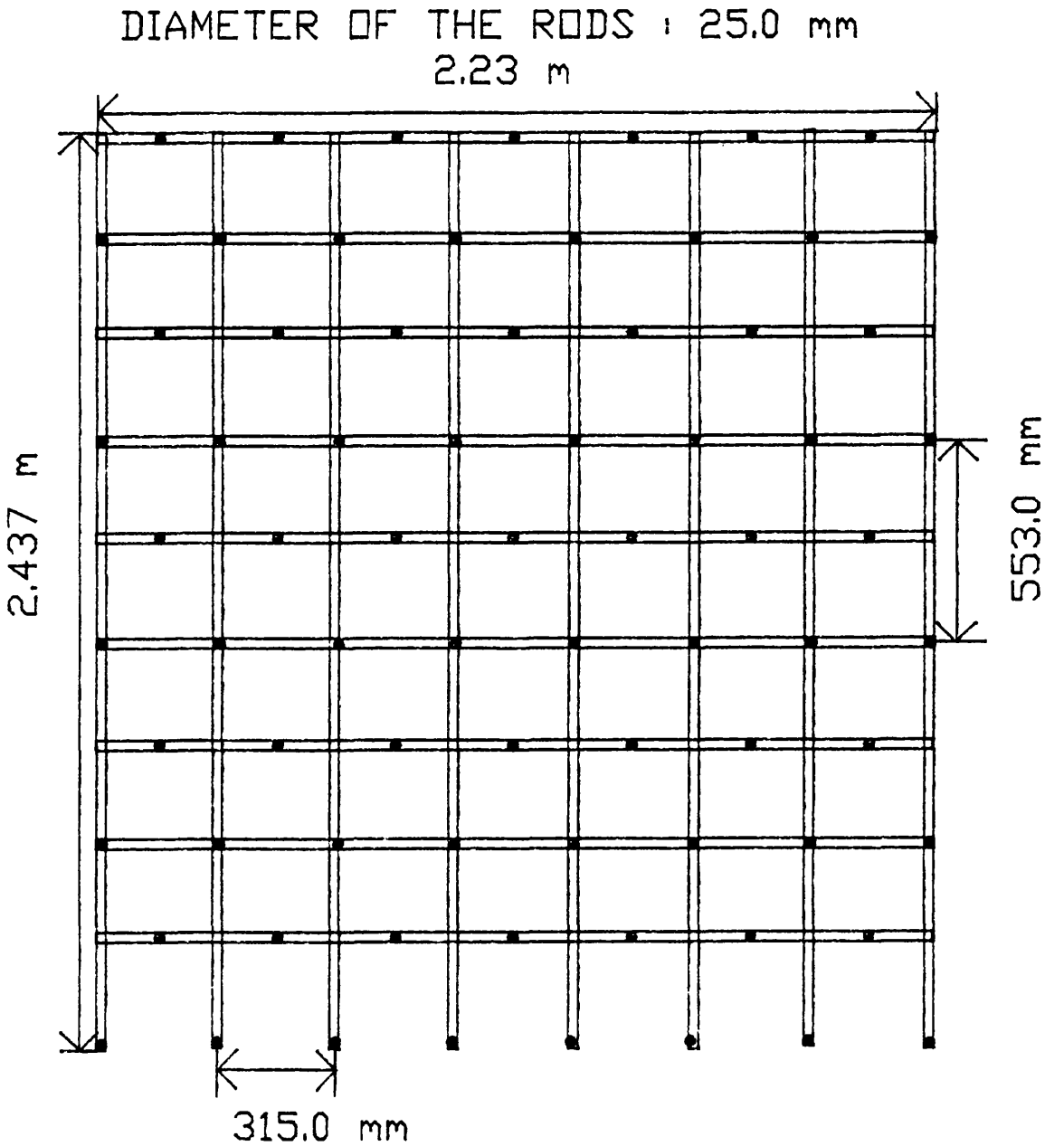

Fig 3.4 - Roughness Frame Used in The S.E.R.C. Flume Series B.

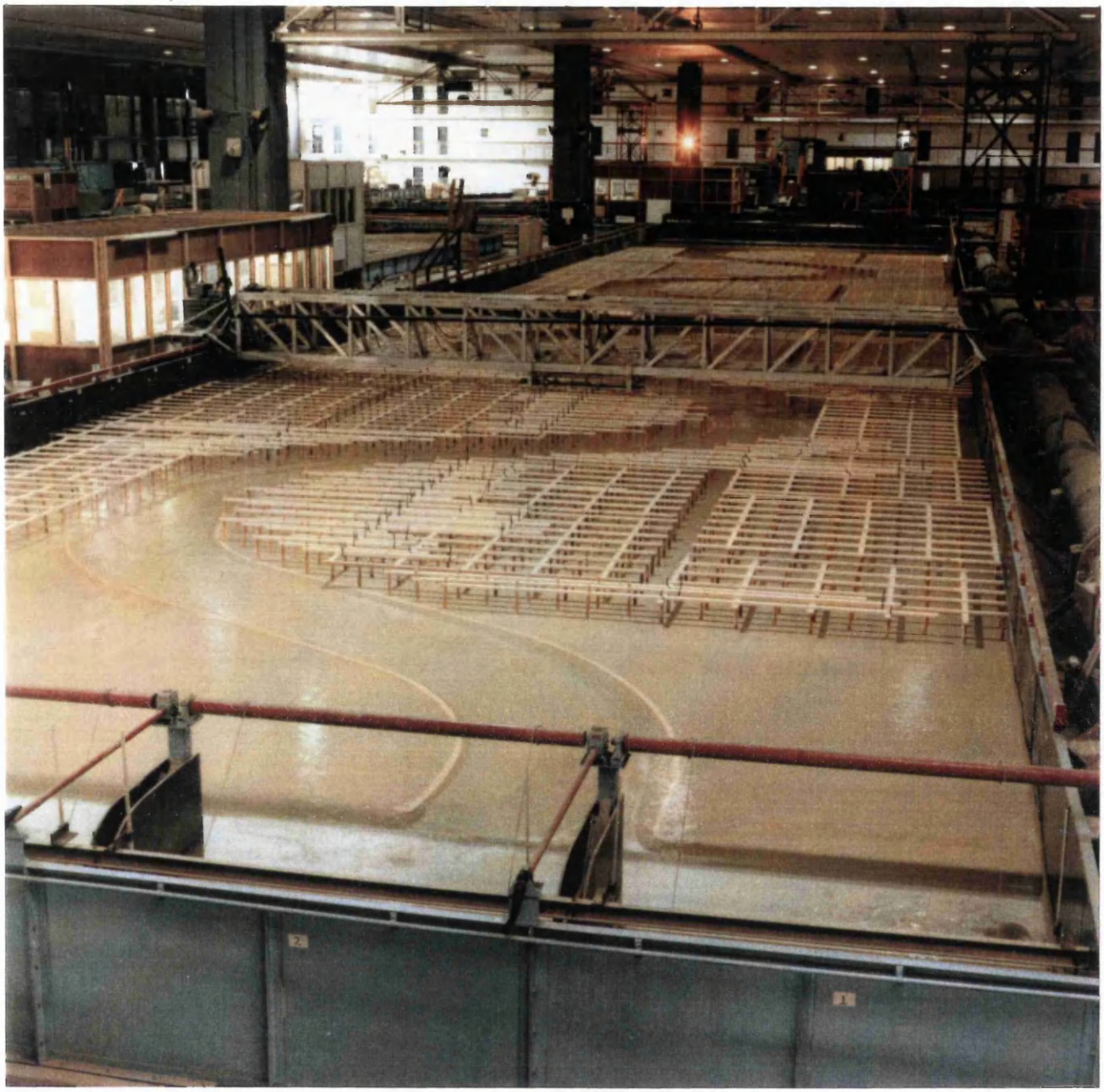

Fig (3.5) - General View of The S.E.R.C. Flume Series B with Sinuosity 1.374 and Fully Roughened Floodplains.

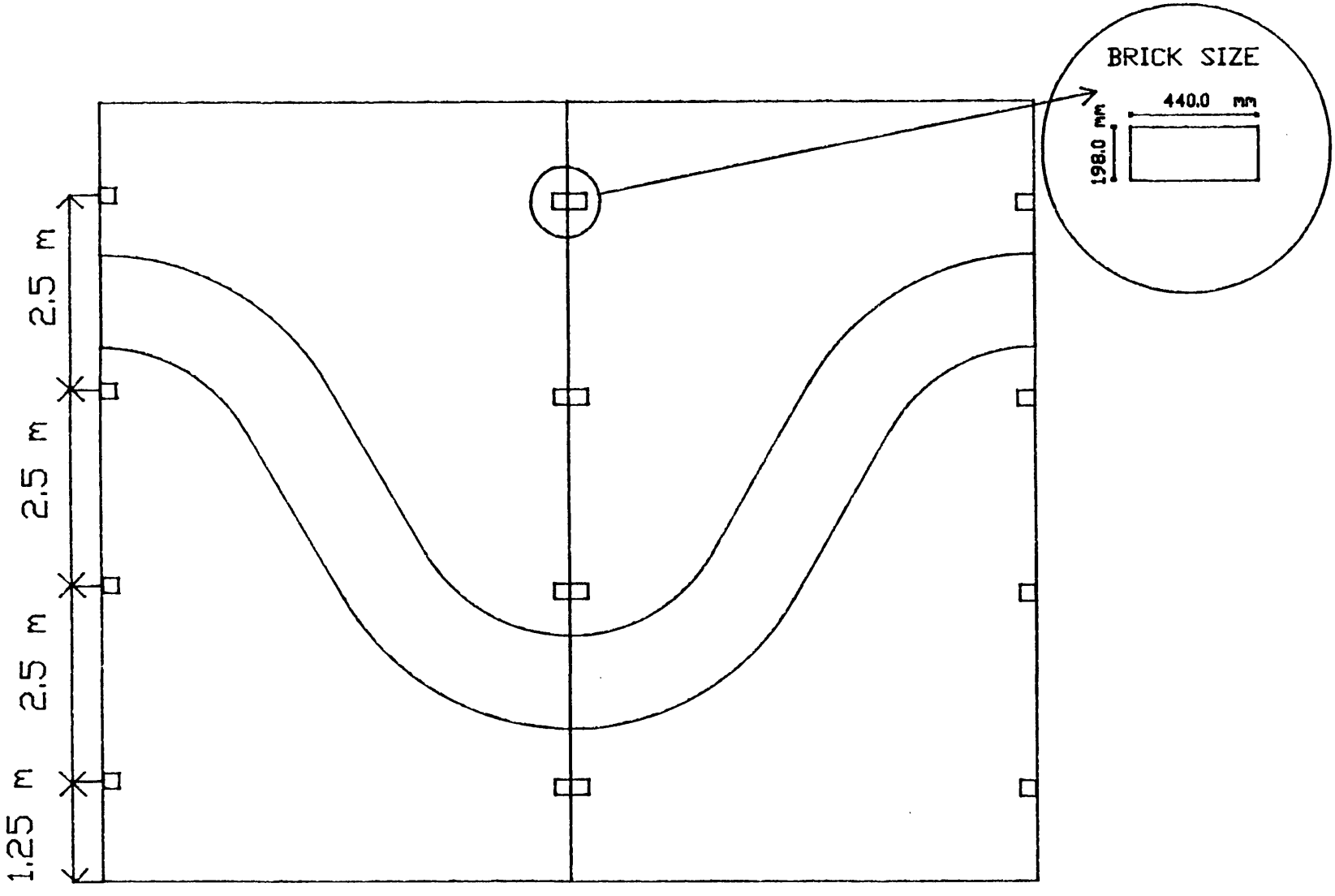

Fig. 3.6 - Plan View of the Location of the Brick Blocks in The S.E.R.C. Flume Series B with Sinuosity 1.374.

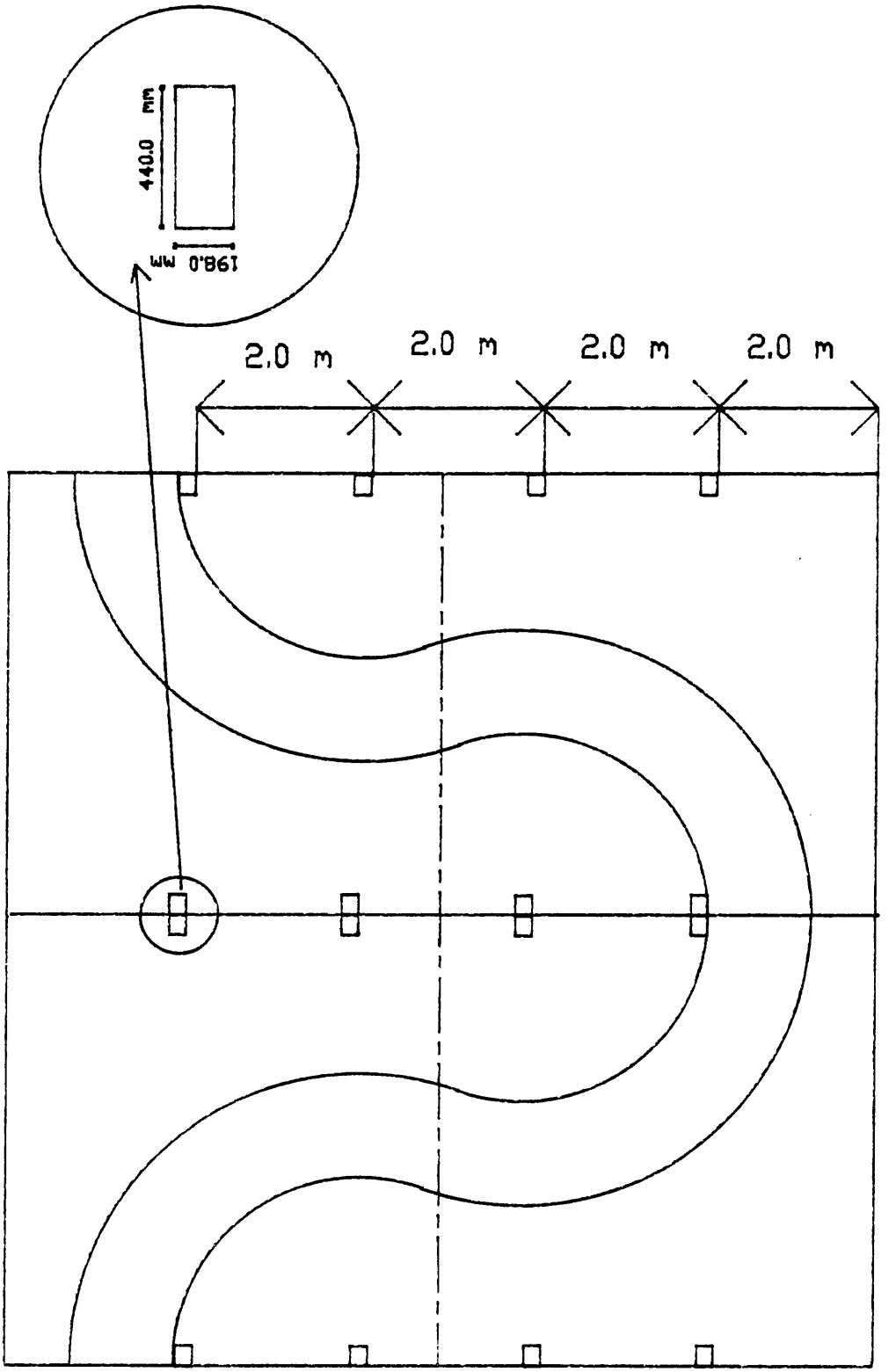

Fig. 3.7 – Plan View of the Location of the Brick Blocks in The S.E.R.C. Flume Series B with Sinuosity 2.04.

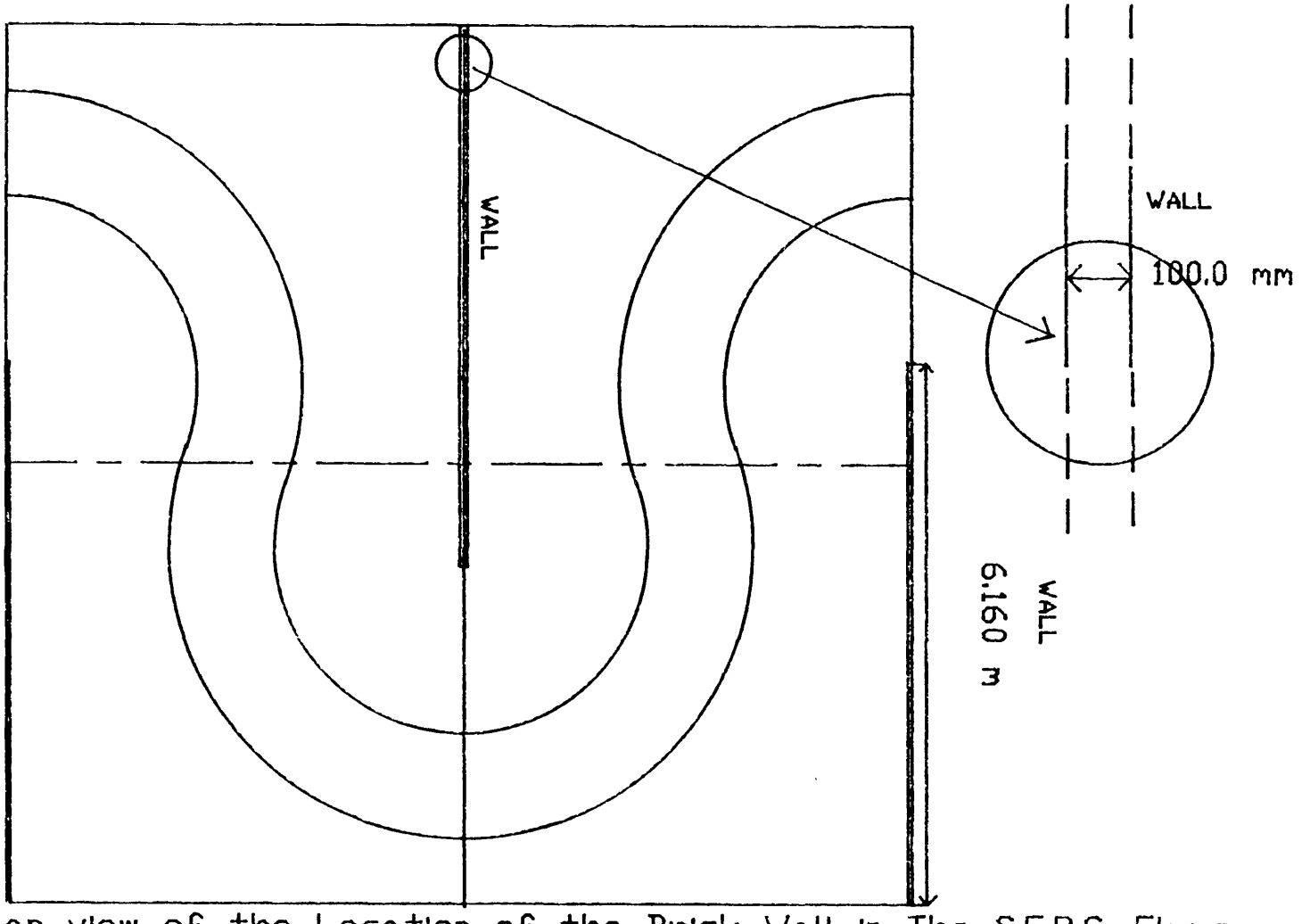

Fig 3.8 - Plan view of the Location of the Brick Wall in The S.E.R.C. Flume Series B with Sinuosity 2.04.

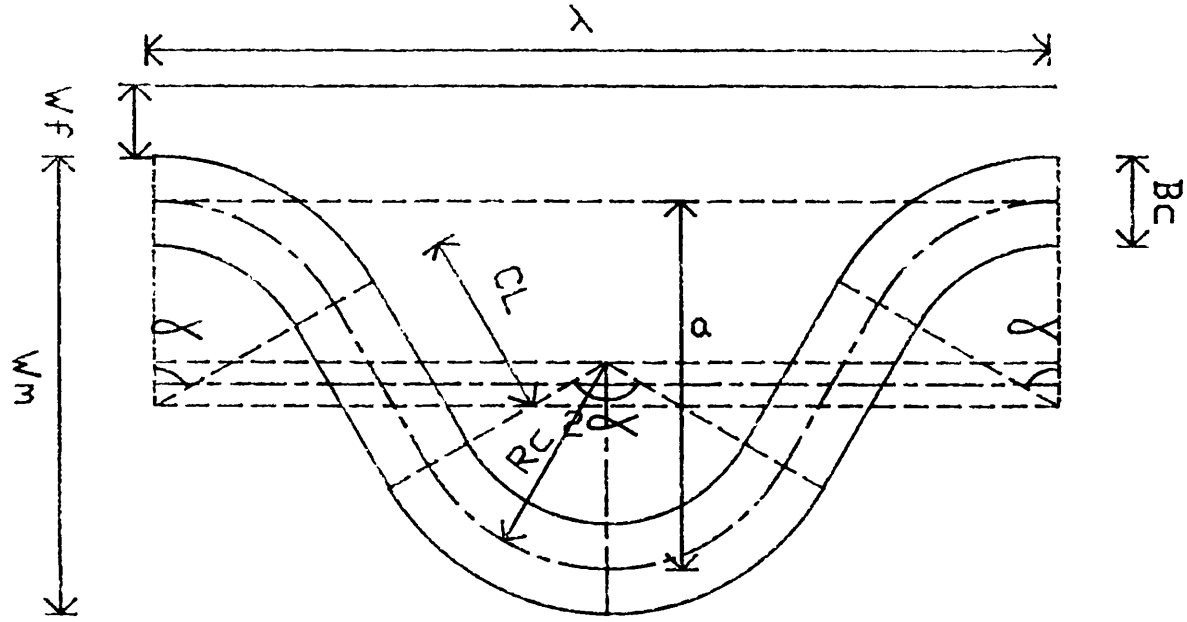

λ : MEANDER WAVE LENGTH
Rc: THE CENTRAL RADIUS OF THE MEANDER.
a: THE DOUBLE AMPLITUDE OF THE MEANDER.
Wm: THE WIDTH OF THE MEANDER BELT.
Wf: HALF OF THE FLOODPLAIN WIDTH OUSIDE THE MEANDER BELT.
CL: THE CROSS-OVER LENGTH.
Bc: THE TOP WIDTH.
α: HALF OF CENTRE ANGLE OF THE MEANDER.

Fig 3.9a - Definition of the Parameters of a Meandering Compound Channel.

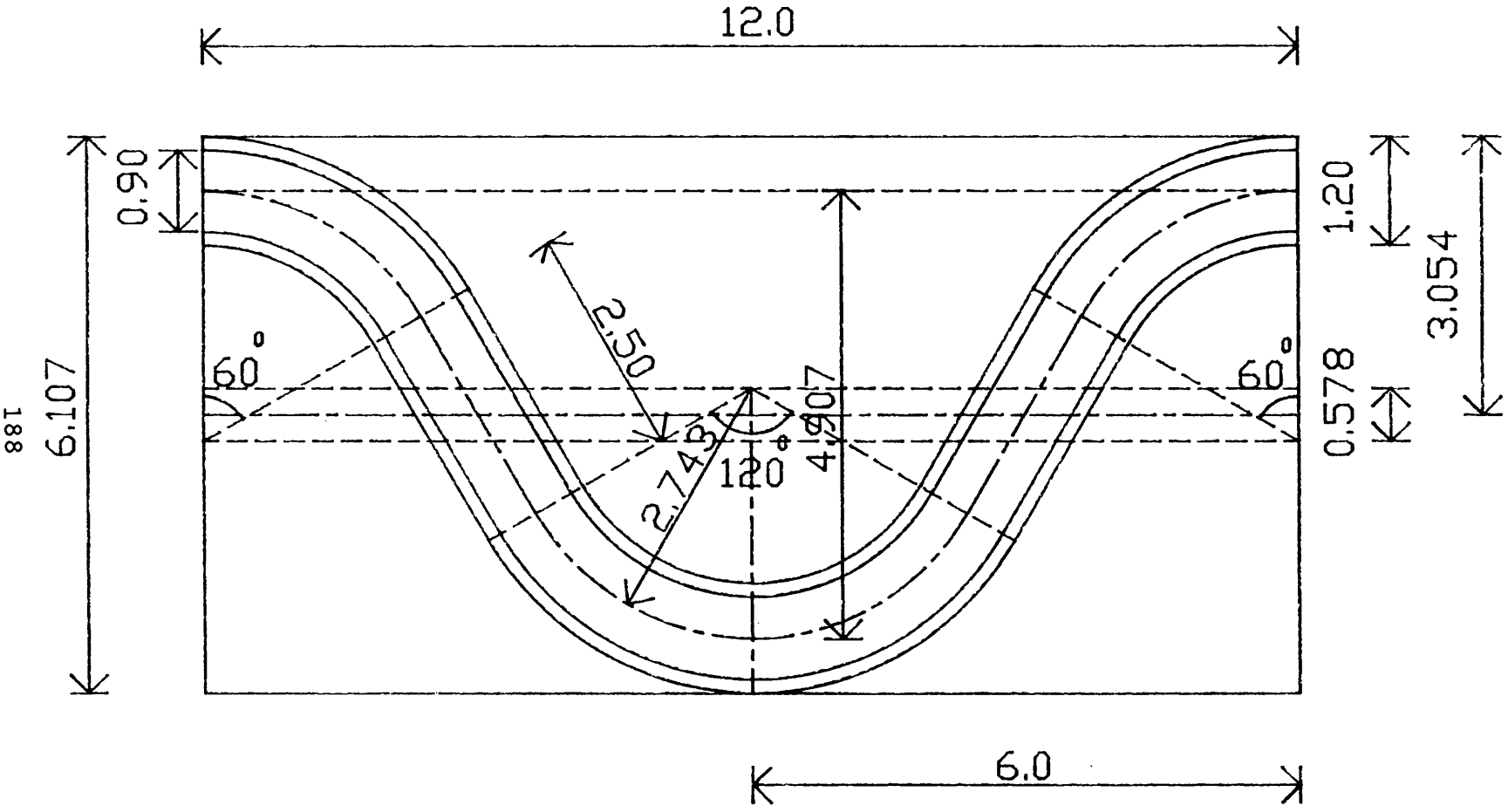

Units : Length in metres and angle in degrees

Fig. 3.9b – Definition of The Geometry of The Meandering Channel of S.E.R.C. Flume Series B with Sinuosity 1.374.

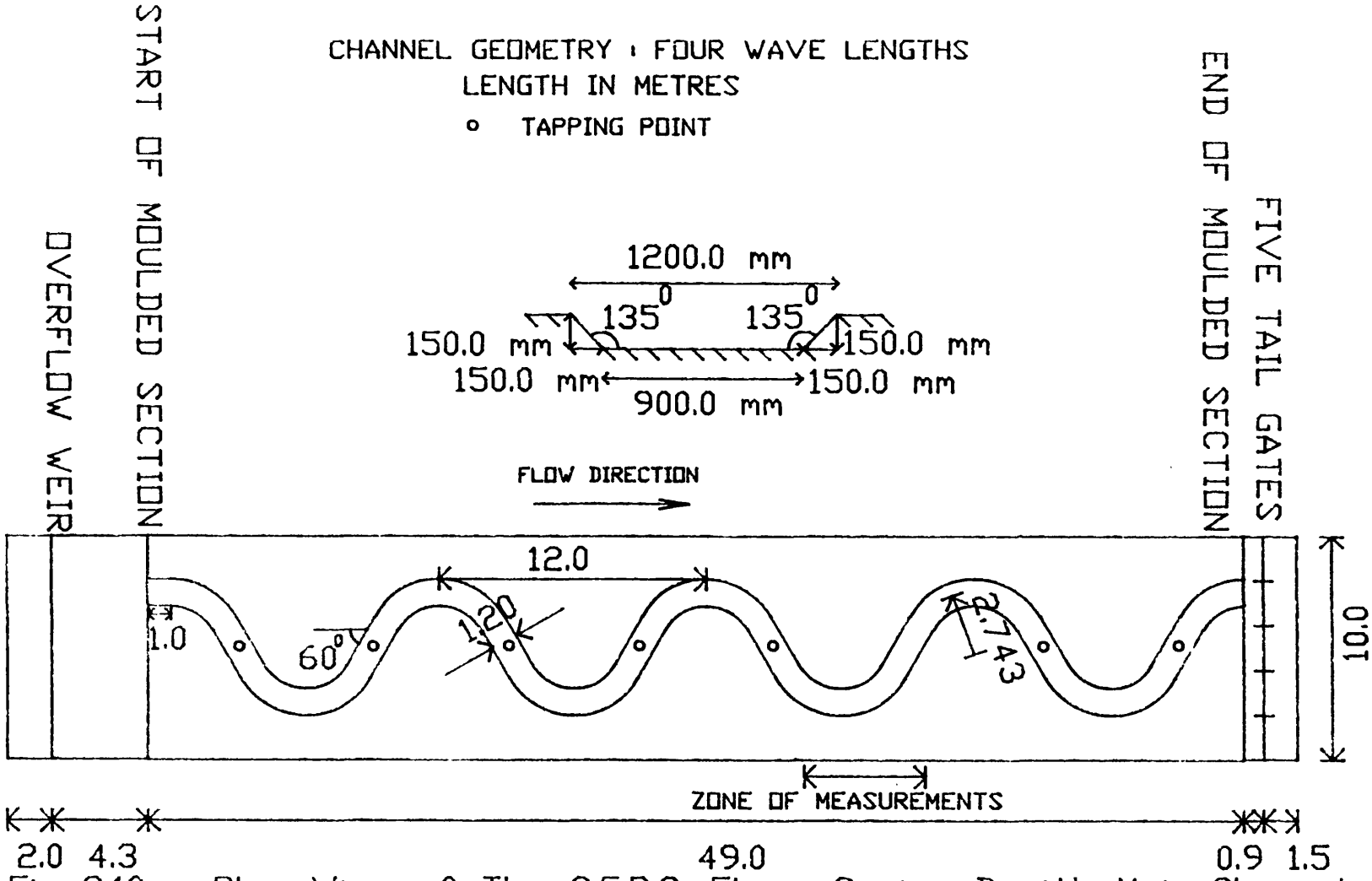

Fig 3.10 - Plan View of The S.E.R.C. Flume Series B with Main Channel Sinuosity equal to 1.374.

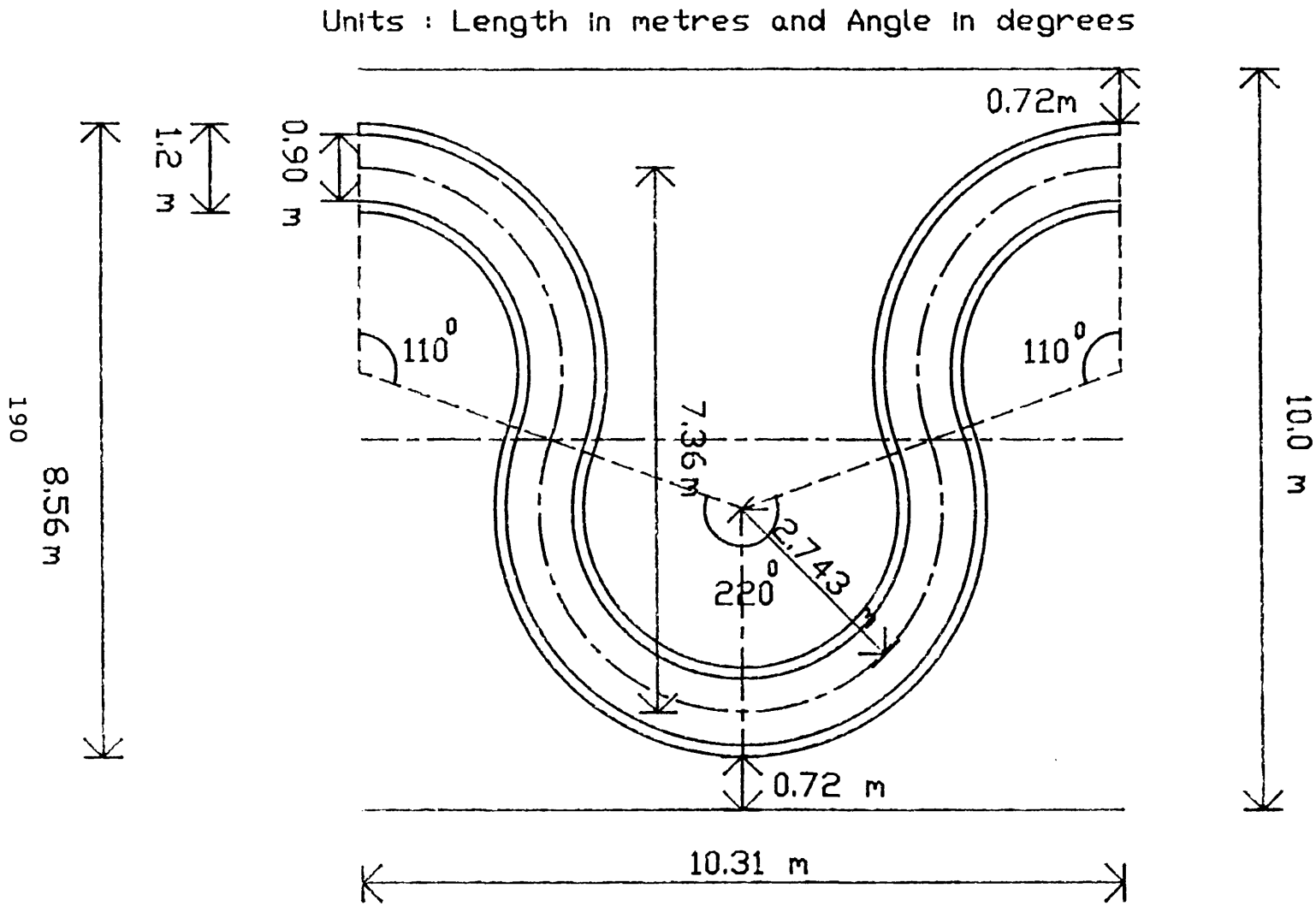

Fig 3.11 - Definition of The Geometry of The Meandering Channel of The S.E.R.C. Flume Series B with Sinuosity 2.04.

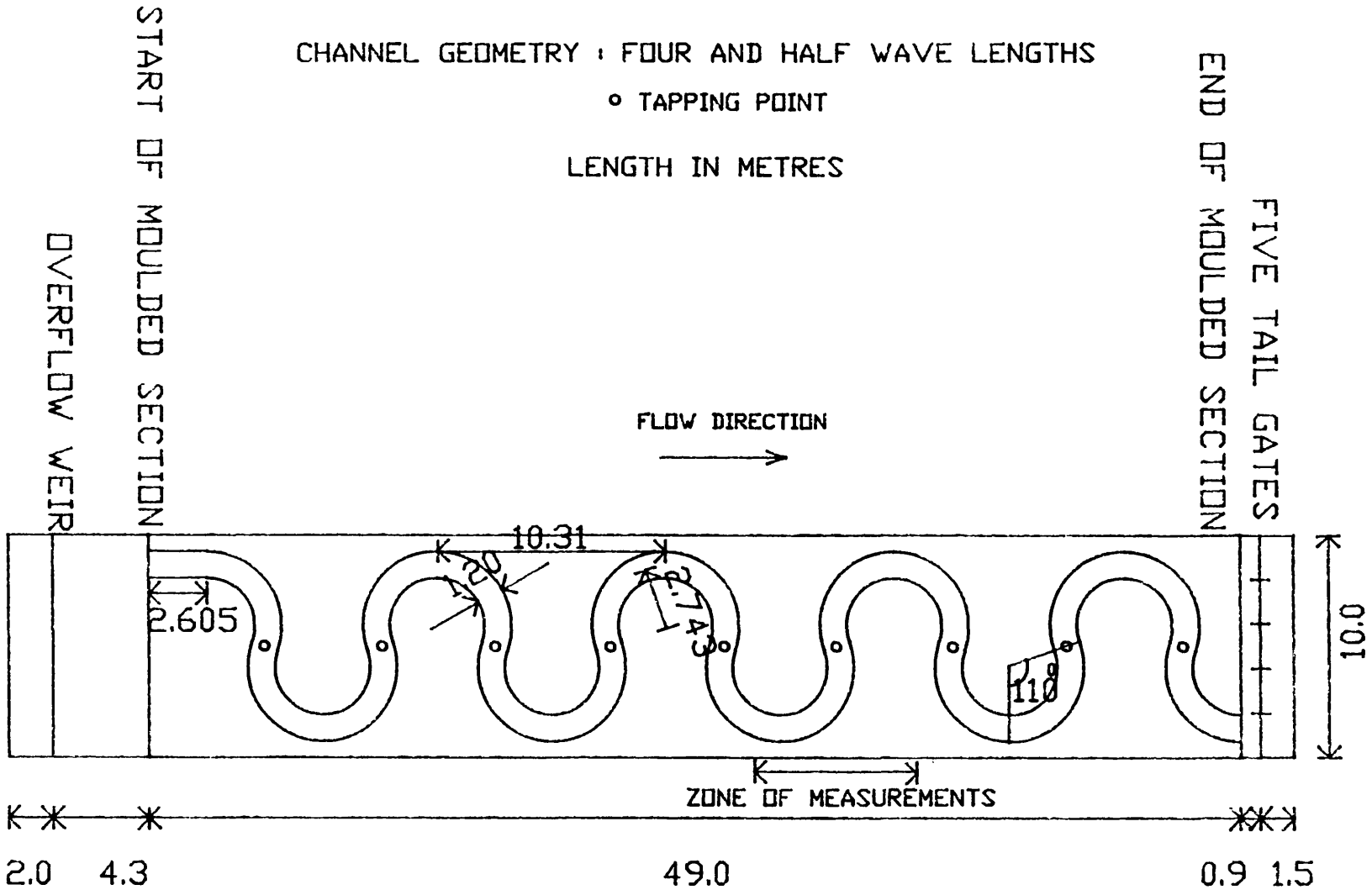

Fig 3.12 - Plan View of The S.E.R.C. Flume Series B with Main Channel Sinuosity equal to 2.04.

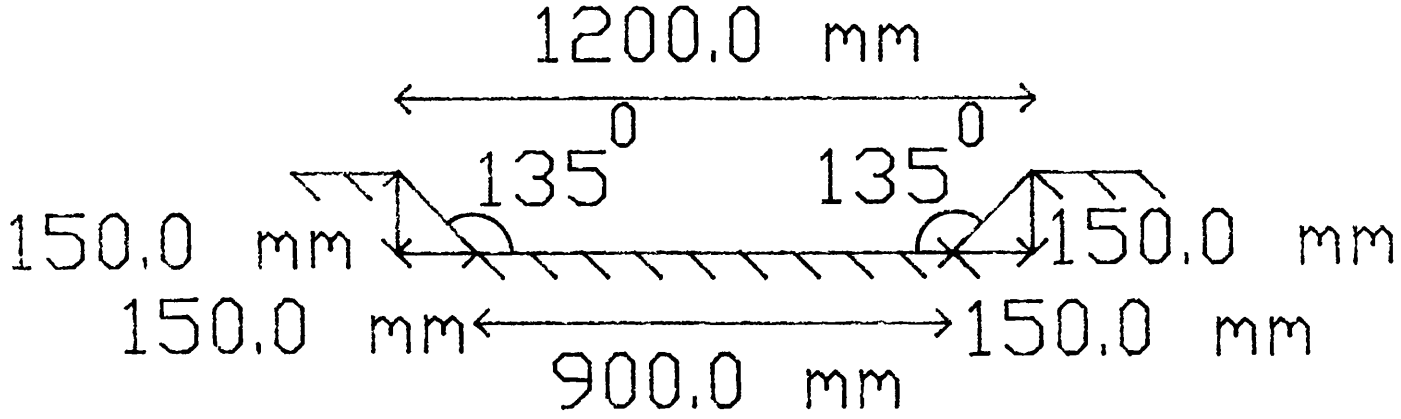

Fig. 3.13 - Trapezoidal Cross-Section Used in S.E.R.C. Flume with Sinuosity 1.374.

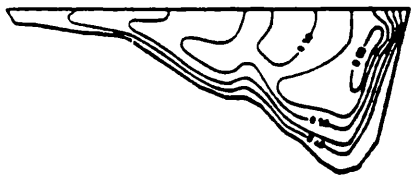

Bend No. 1

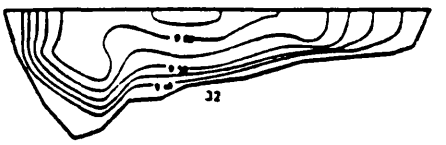

Bend No. 2

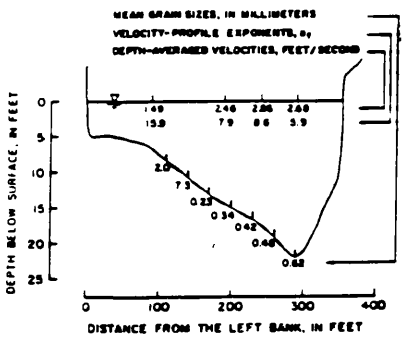

Bend No. 3

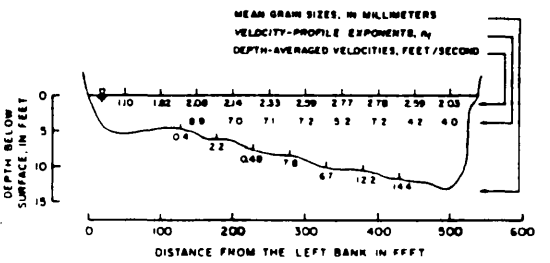

Bend No. 4

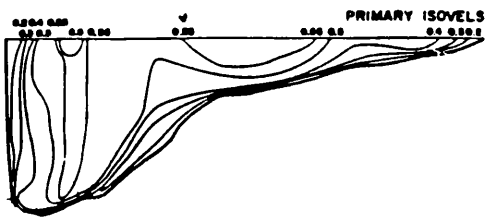

Bend No. 5

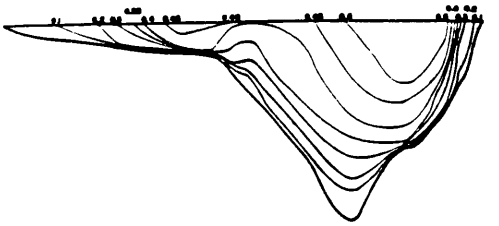

Bend No. 6

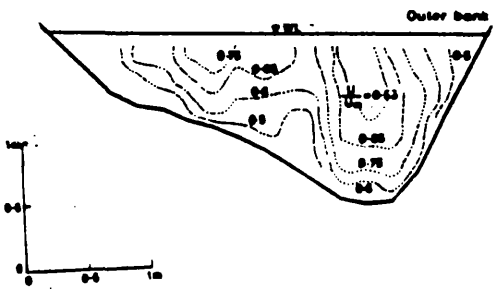

Bend No. 7

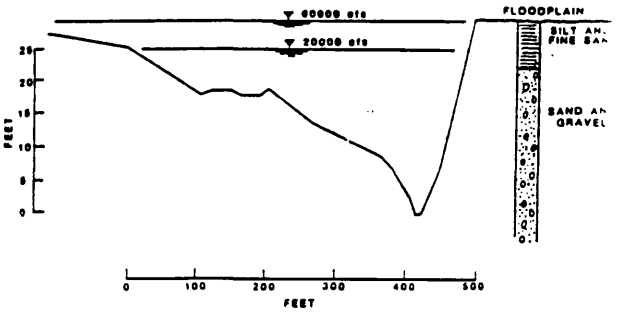

Bend No. 8

Fig (3.14) - Bend Apices of Natural River Meanders.

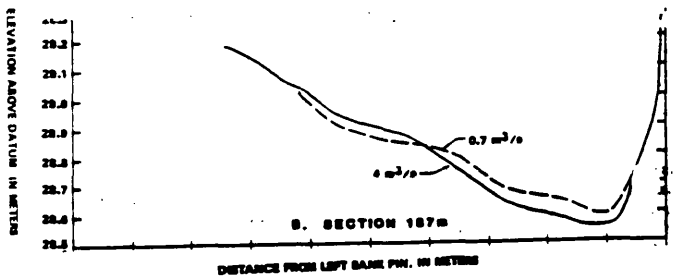

Bend No. 9

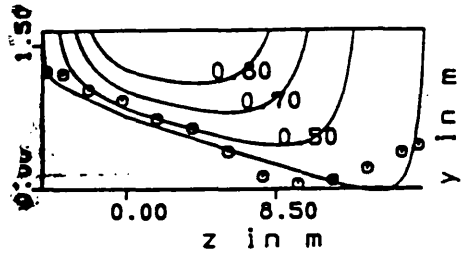

Bend No. 10

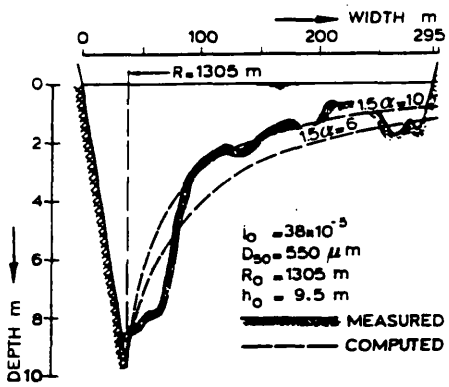

Bend No. 11

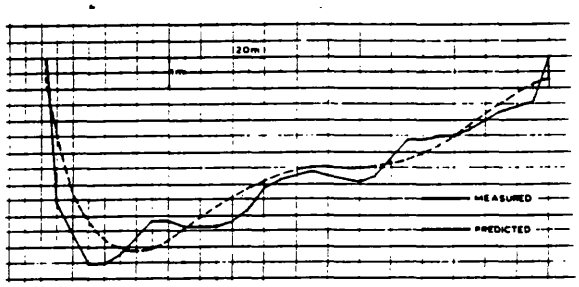

Bend No. 12

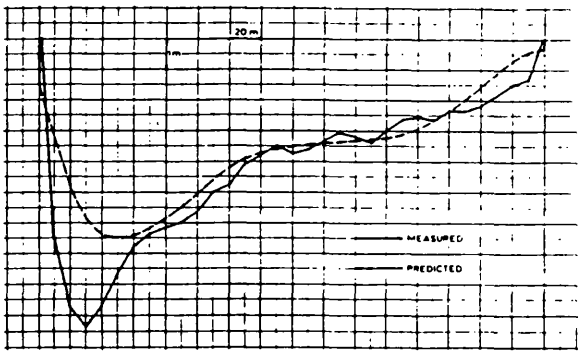

Bend No. 13

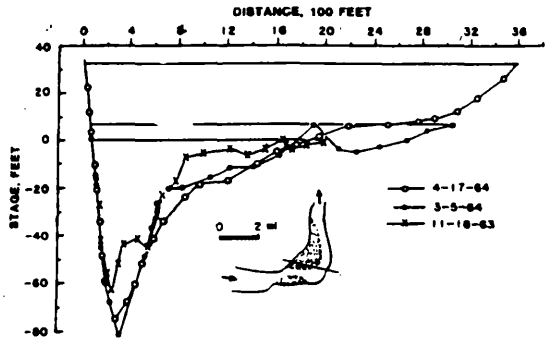

Bend No. 14

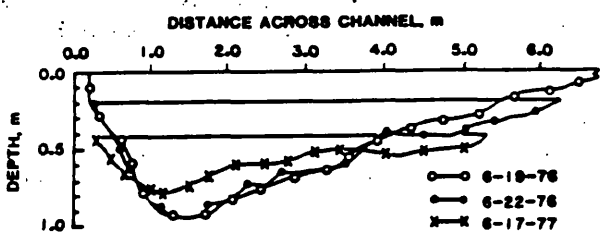

Bend No. 15

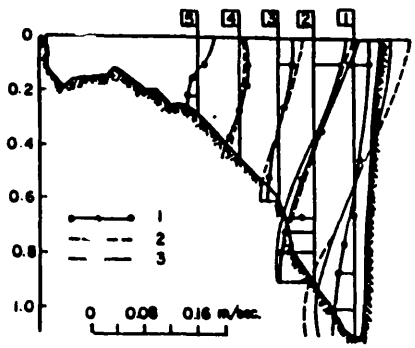

Bend No. 16

Fig (3.14) - Bend Apices of Natural River Meanders. (Continuation)

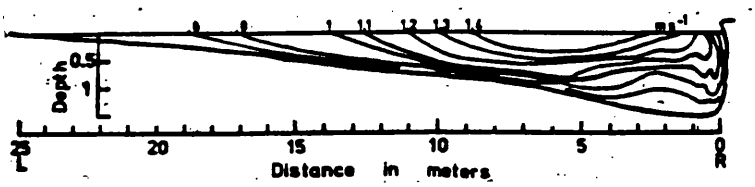

Bend No.17

Fig (3.14) - Bend Apices of Natural River Meanders. (Continuation)

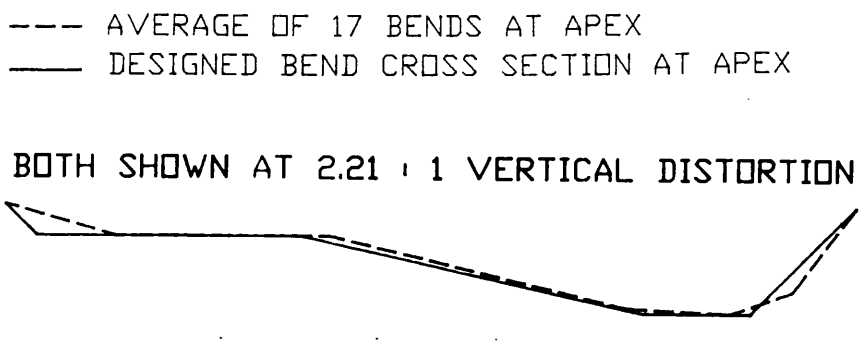

Fig (3.15) - Typical Bend Apex of a River Bend Based in Average Values of Bend Apices of Natural River Meanders.

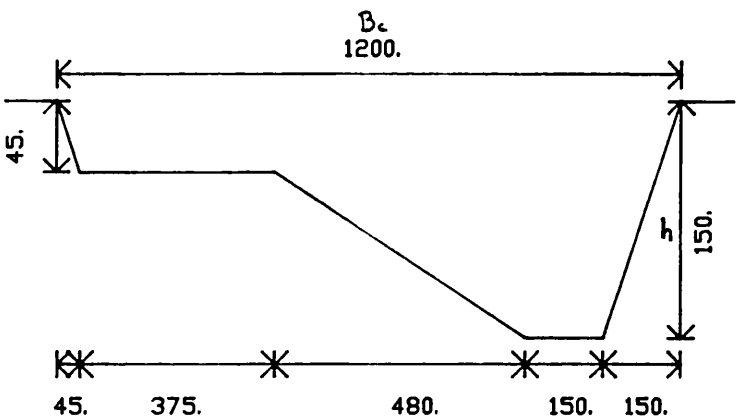

UNITS IN MILLIMETRES

AREA REDUCTION : 37.5 %

$B_c / h = 8.0$(min.)

Fig (3.16) - Bend Apex of the Natural Meander Channel of S.E.R.C. Flume Series B Tests.

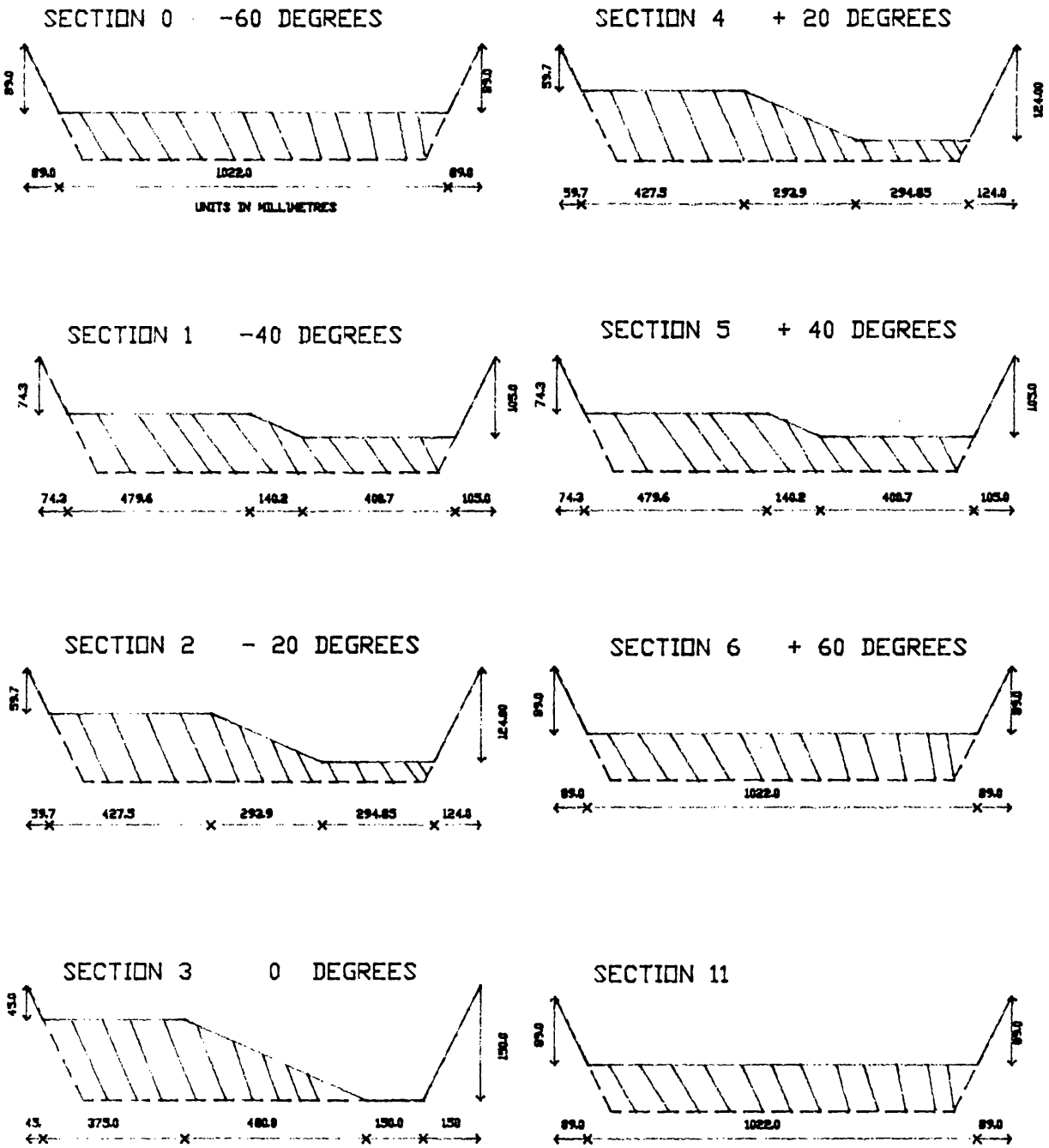

UNITS IN MILLIMETRES

Fig. 3.17 - Design of the Inserts of the Natural Meander Channel of S.E.R.C. Flume with Sinuosity 1.374.

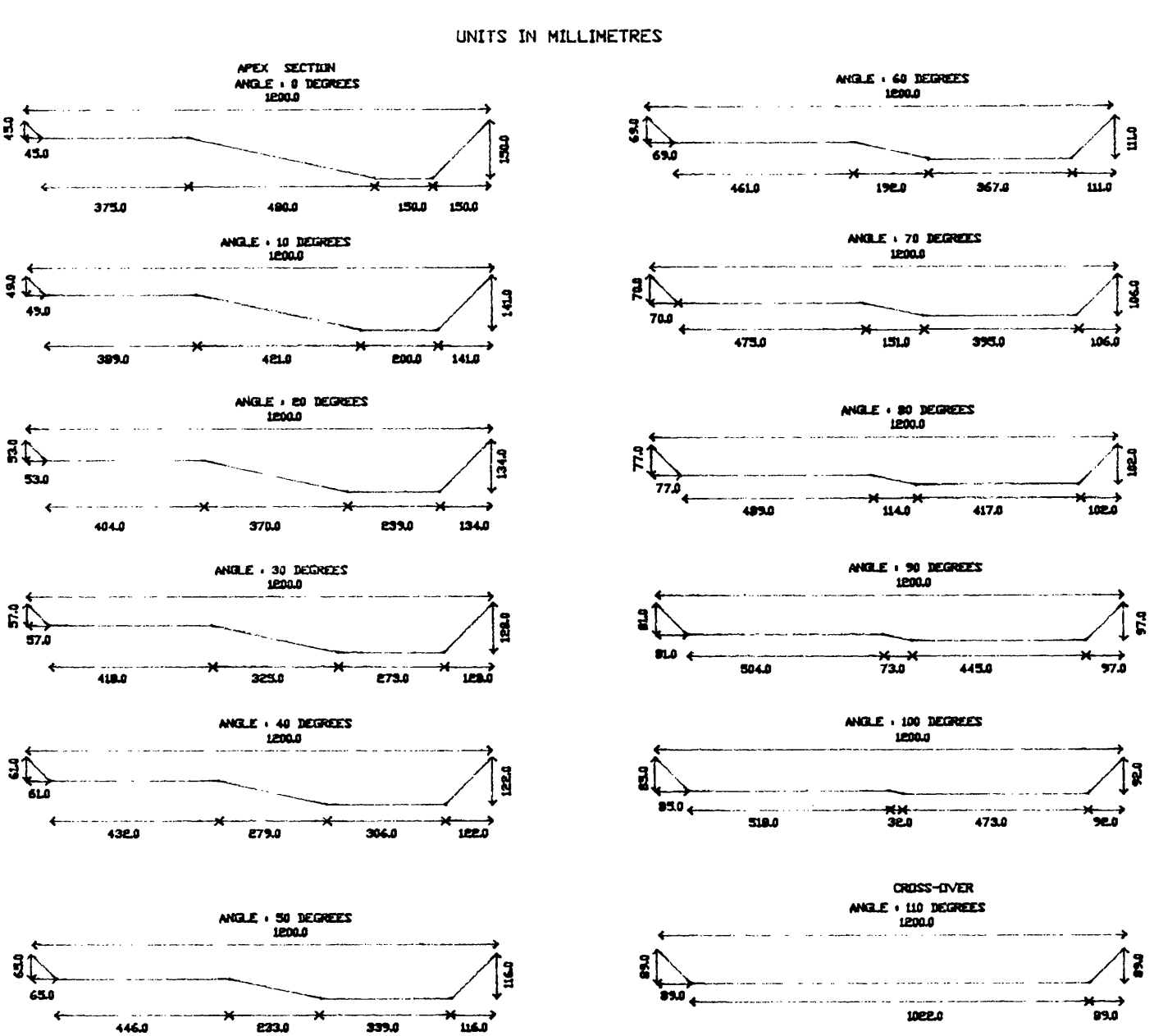

Fig. 3.18 Design of the Inserts of the Natural Meander Channel of S.E.R.C. Flume with Sinuosity 2.04.

Fig (3.19) - Phase of Construction of The S.E.R.C. Flume Series B with Sinuosity 1.374 and Trapezoidal Cross-Section.

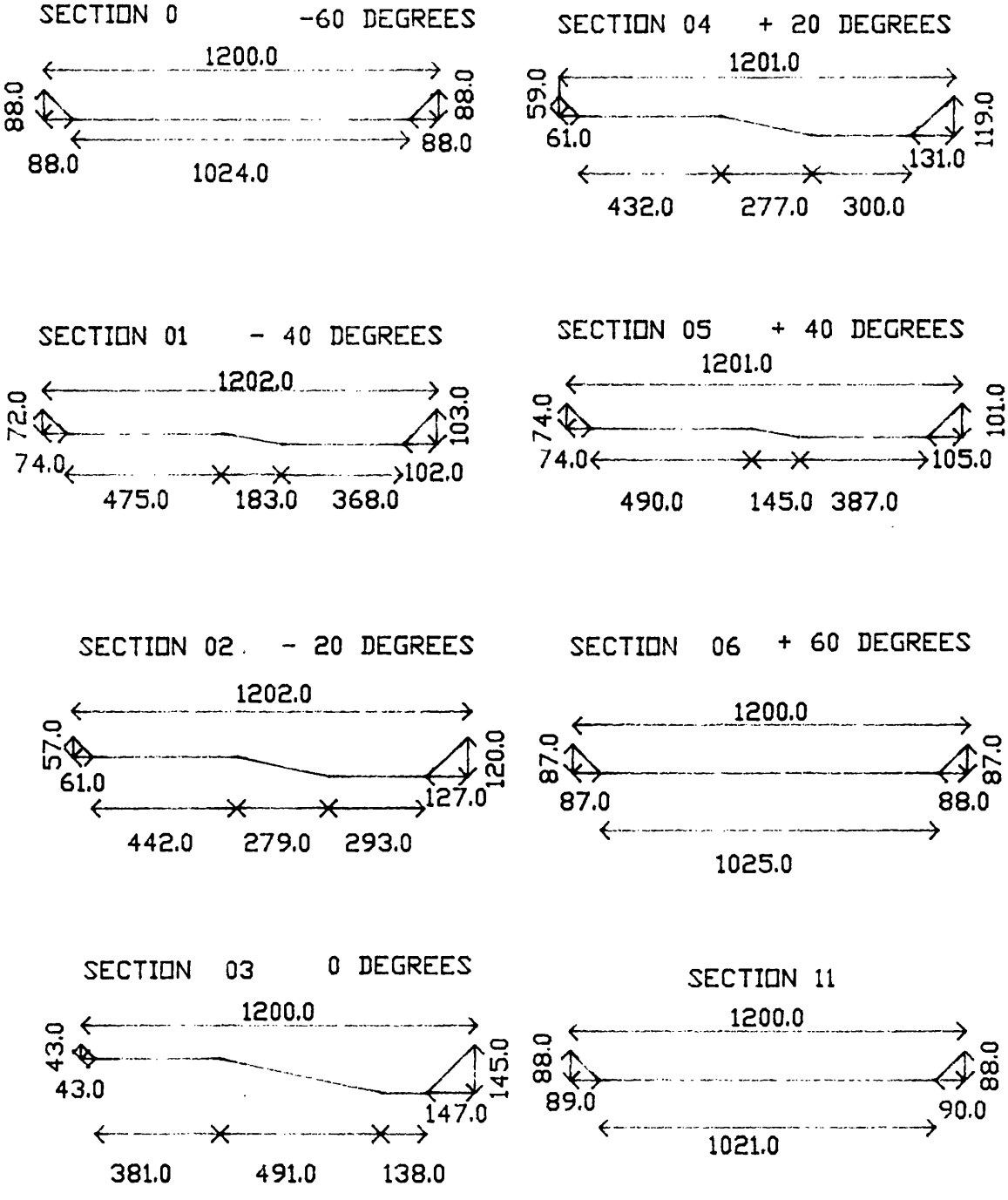

Fig. 3.20 - Insert as Built of the Natural Meander Channel with Sinuosity 1.374 of S.E.R.C. Flume.

Fig (3.21) - A View of the Bend Region of the Natural Meandering Channel(sinuosity 1.37), after Construction. S.E.R.C. Series B.

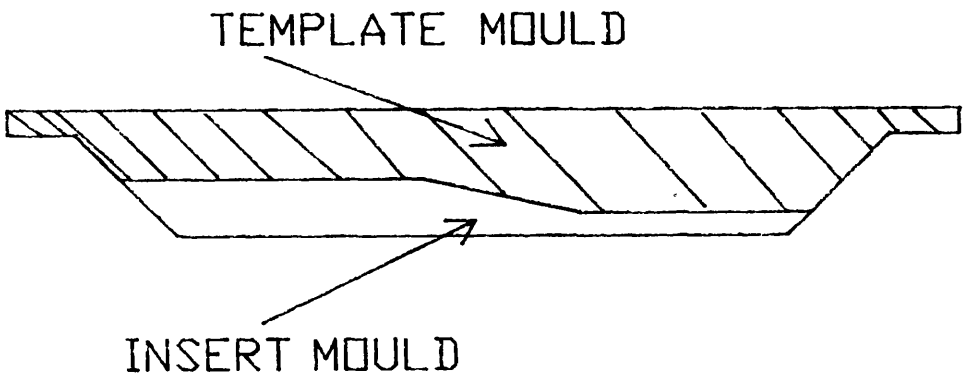

Fig. 3.22 - Moulding Procedure of the Inserts of the Natural Meandering Channel with Sinuosity 2.04 of the S.E.R.C. Flume Series B.

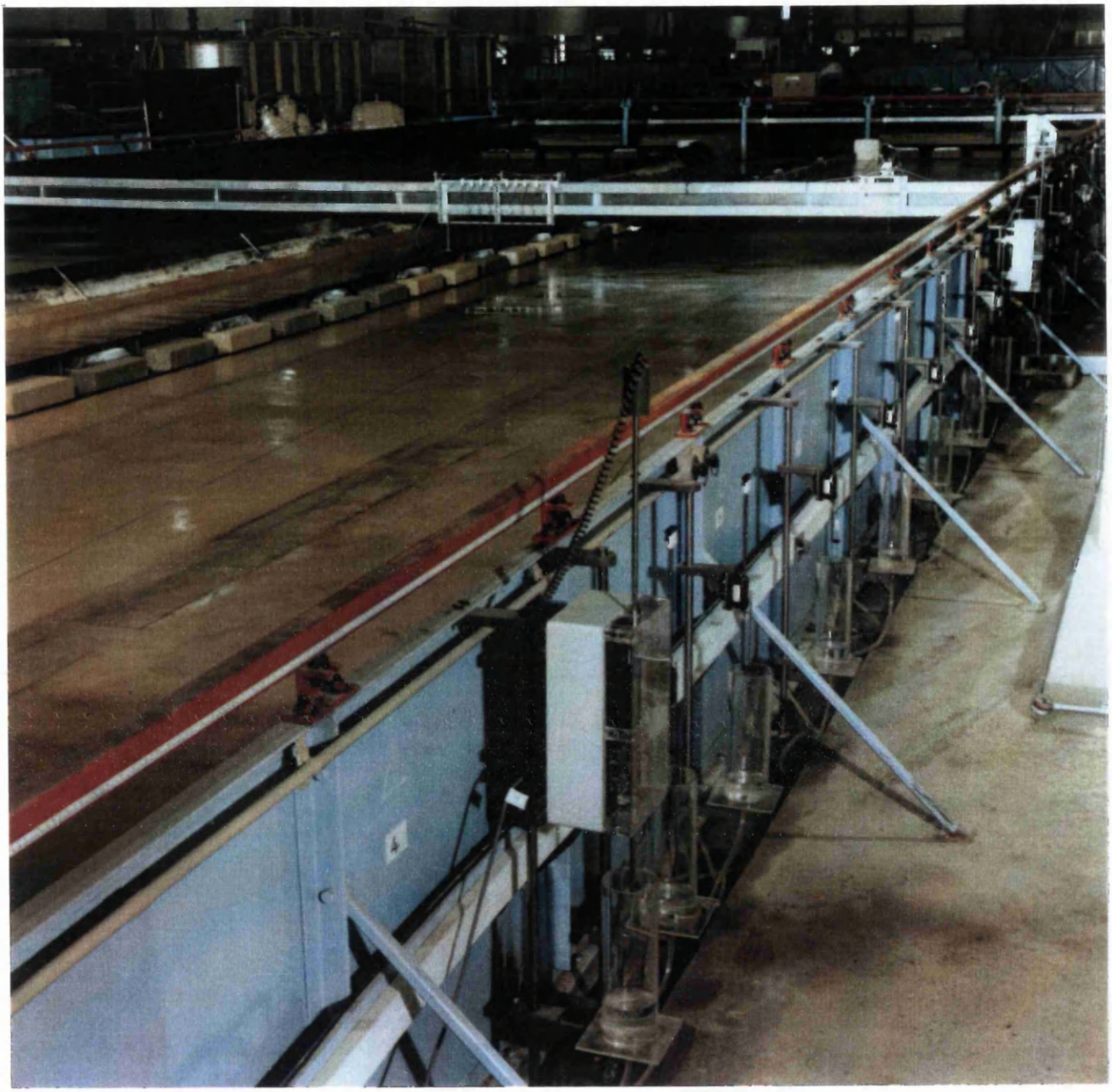

Fig (3.23) - Digital Gauge Used for Measurements of Water Levels in The S.E.R.C. Flume.

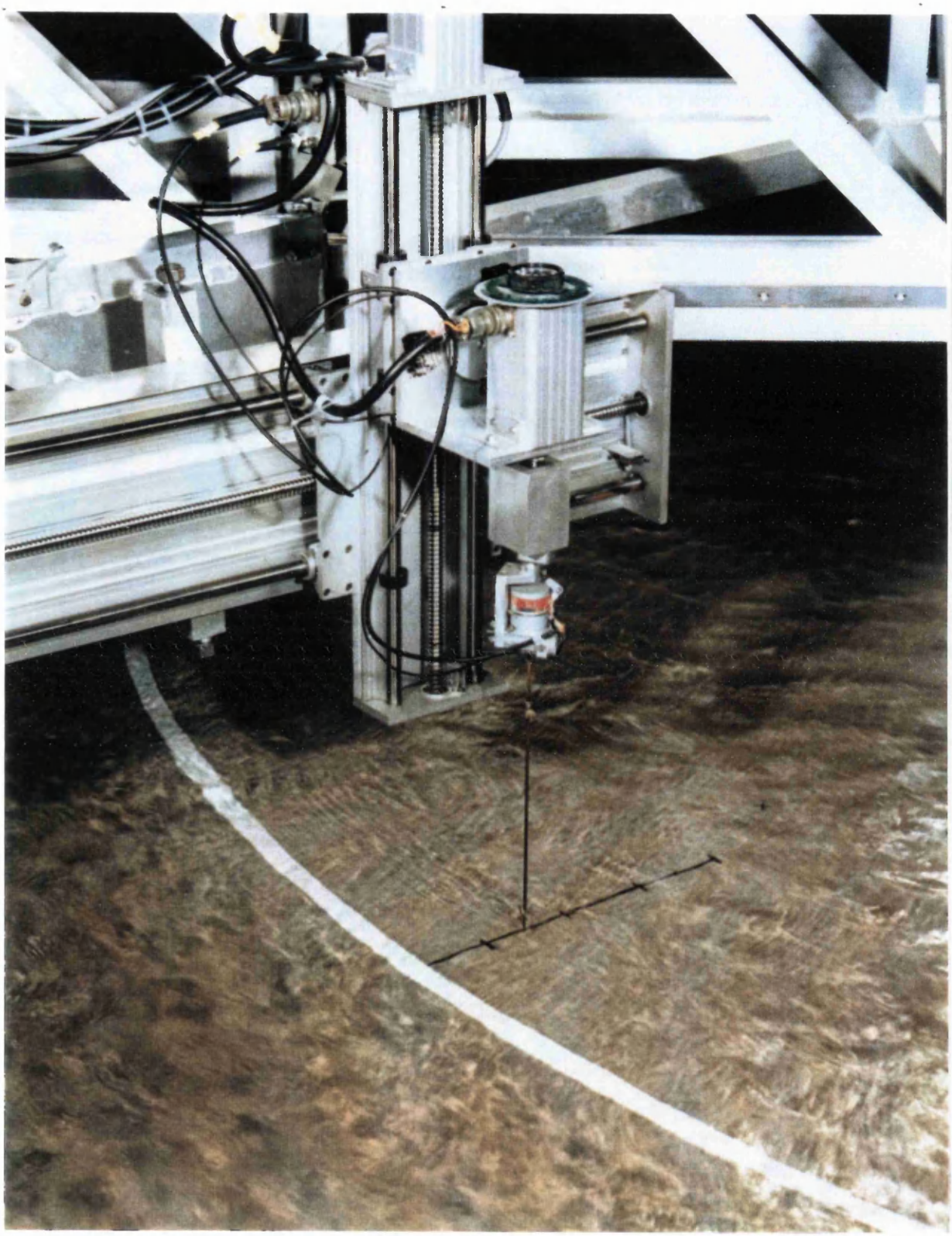

Fig (3.24) - Vane Used for Measurements of Streamline Angles in The S.E.R.C. Flume Series B.

SKETCH OF THE VANE USED IN S.E.R.C. FLUME SERIES B

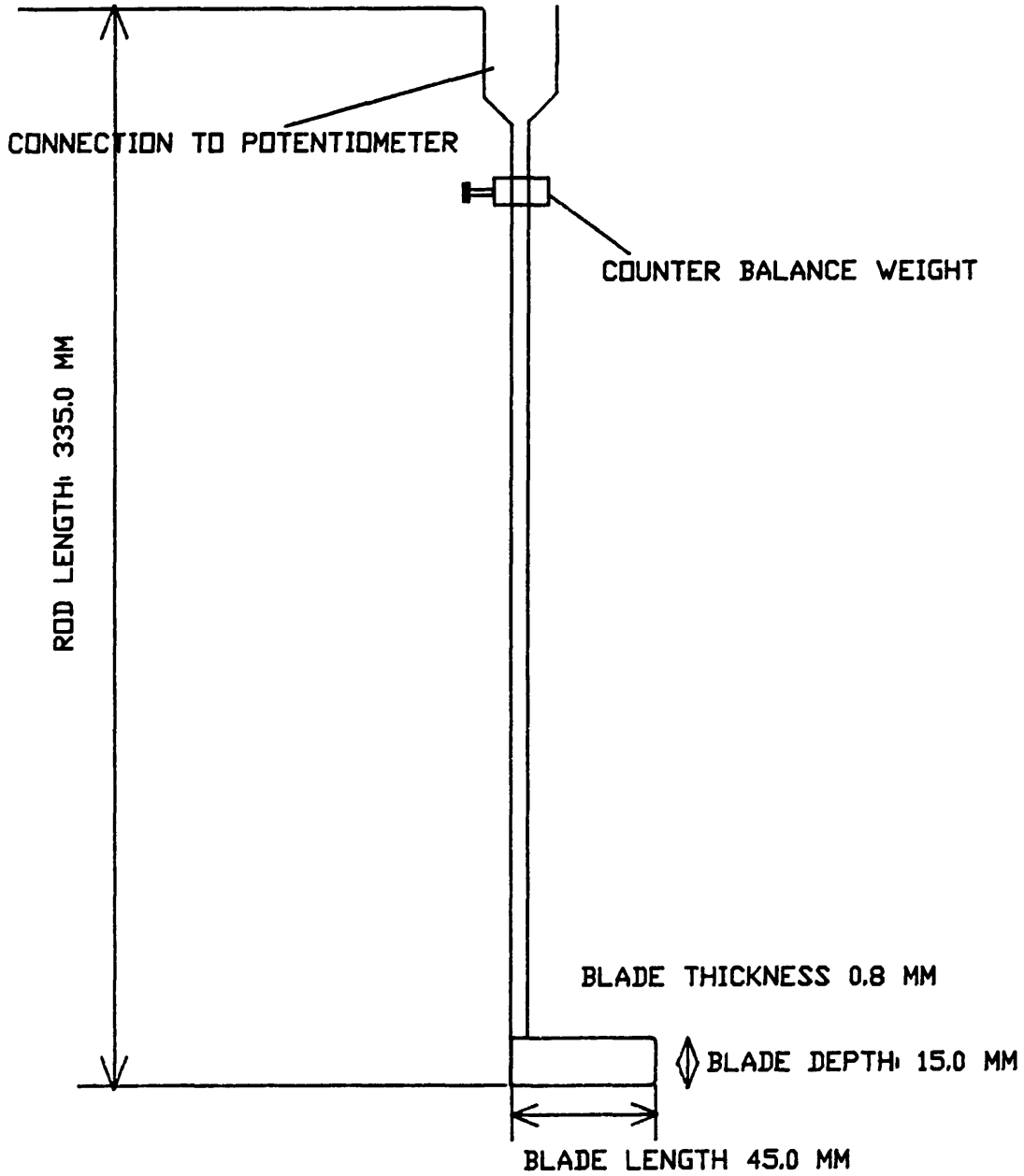

THESE ARE AVERAGE VALUES OF THE VANES USED IN S.E.R.C. SERIES B.

Fig (3.24a) - Sketch of the Vane used in The S.E.R.C. Flume Series B.

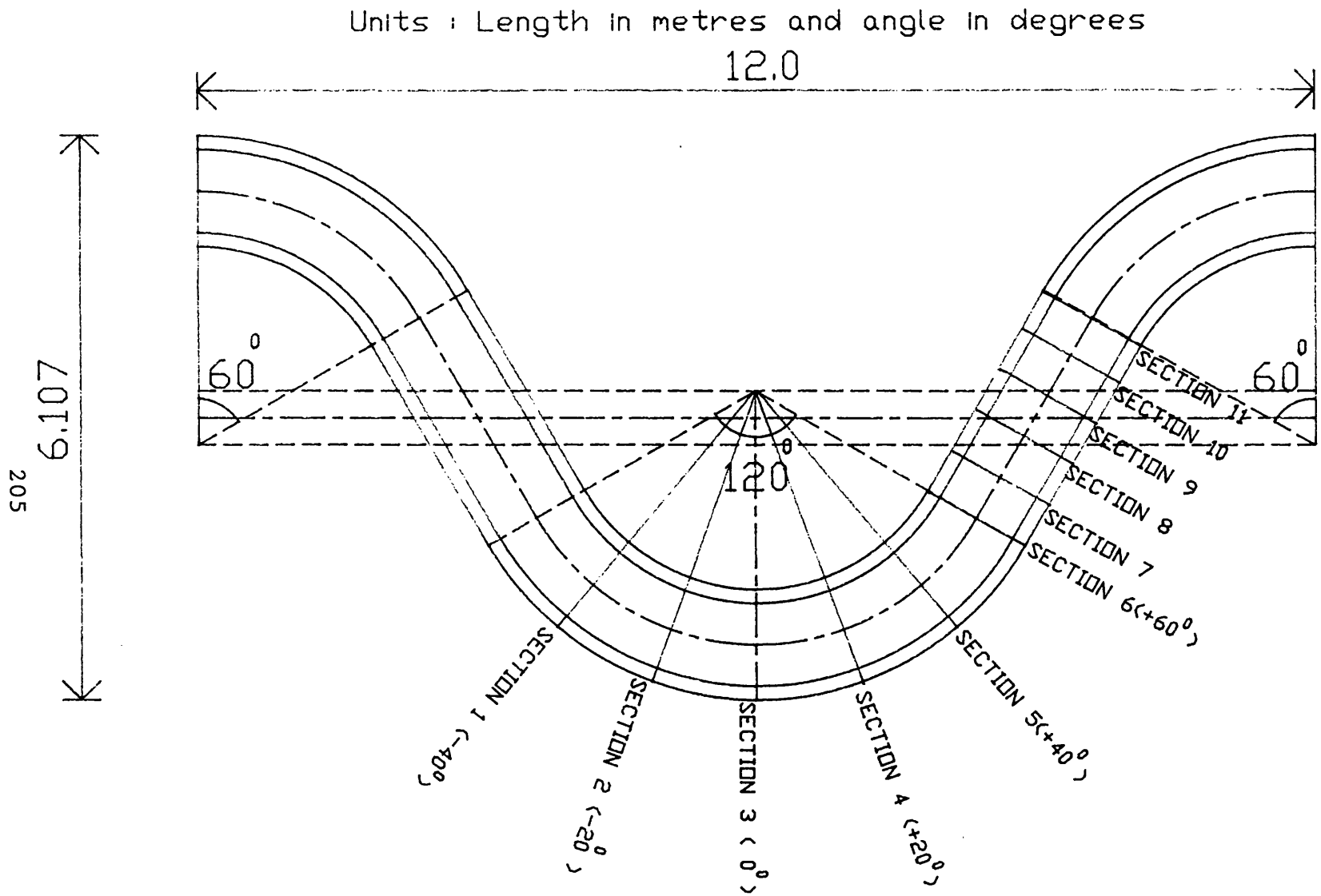

Fig. 3.25 - Location of the Measurement Sections in S.E.R.C. Flume with Sinuosity 1.374.

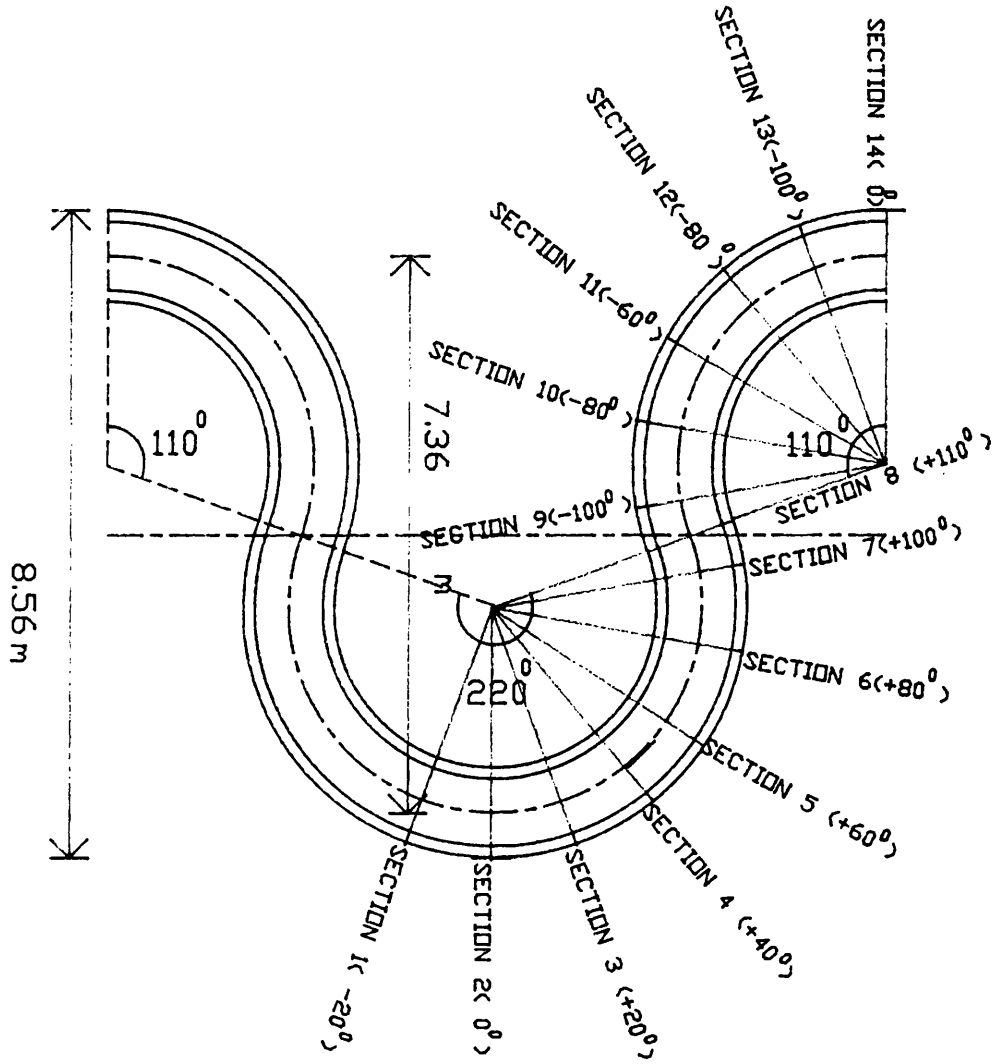

Fig. 3.26 - Location of the Measurements Sections in S.E.R.C. Flume with Sinuosity 2.04.

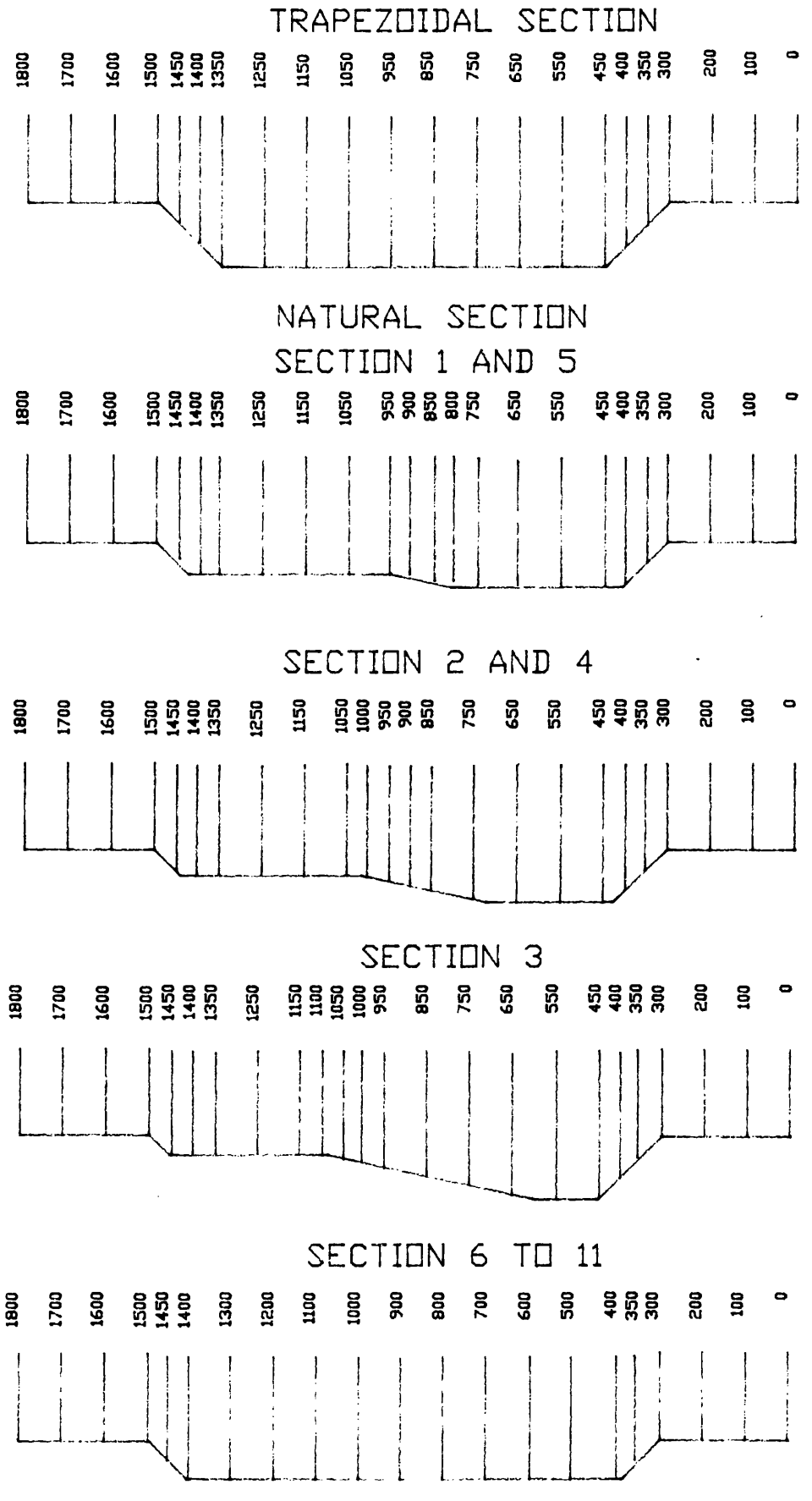

Fig. 3.27 - Grid of Measurements in the Main Channel of S.E.R.C. Flume with Sinuosity 1.374.

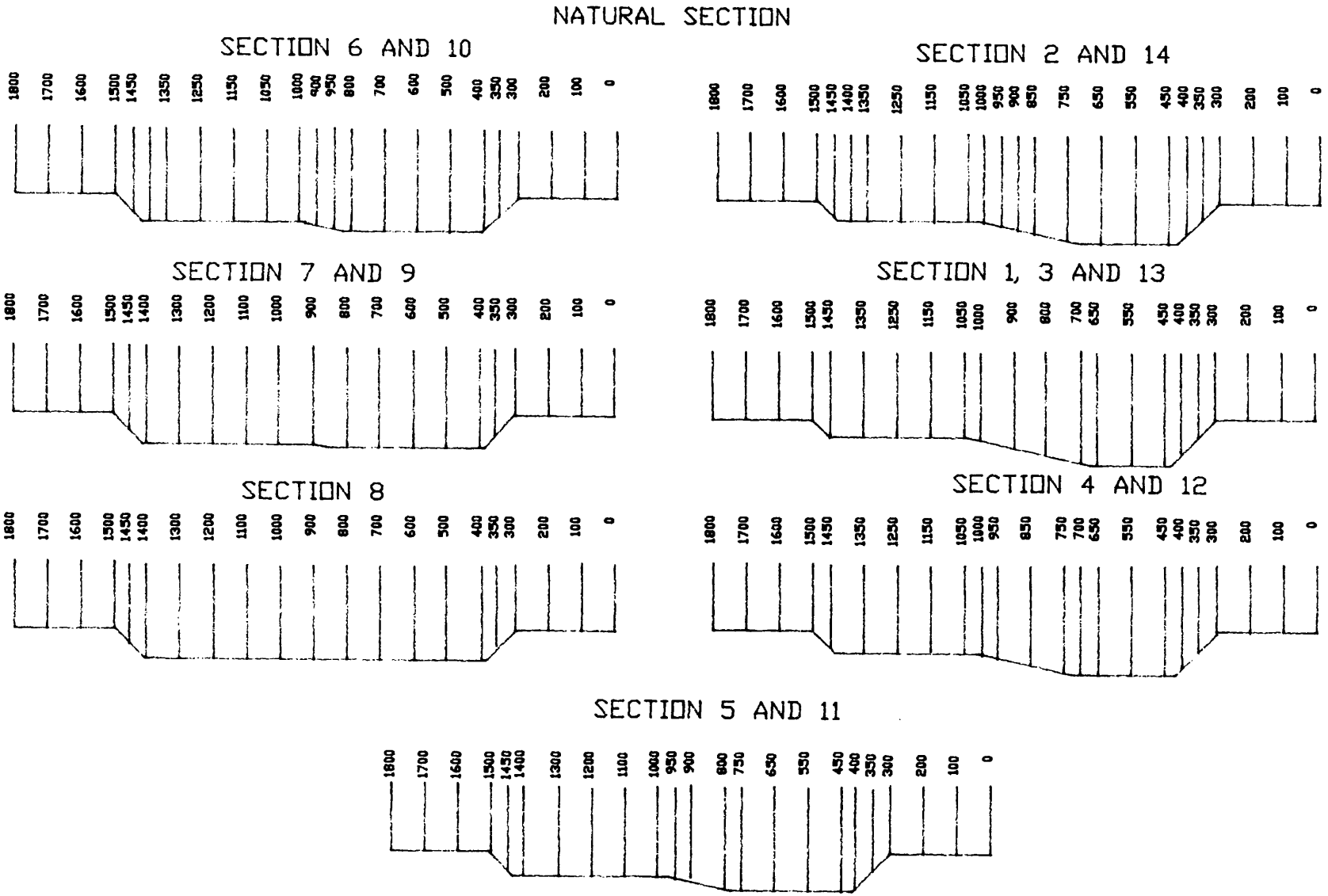

Fig. 3.28 - Grid of Measurements in the Main Channel of S.E.R.C. Flume with Sinuosity 2.04.

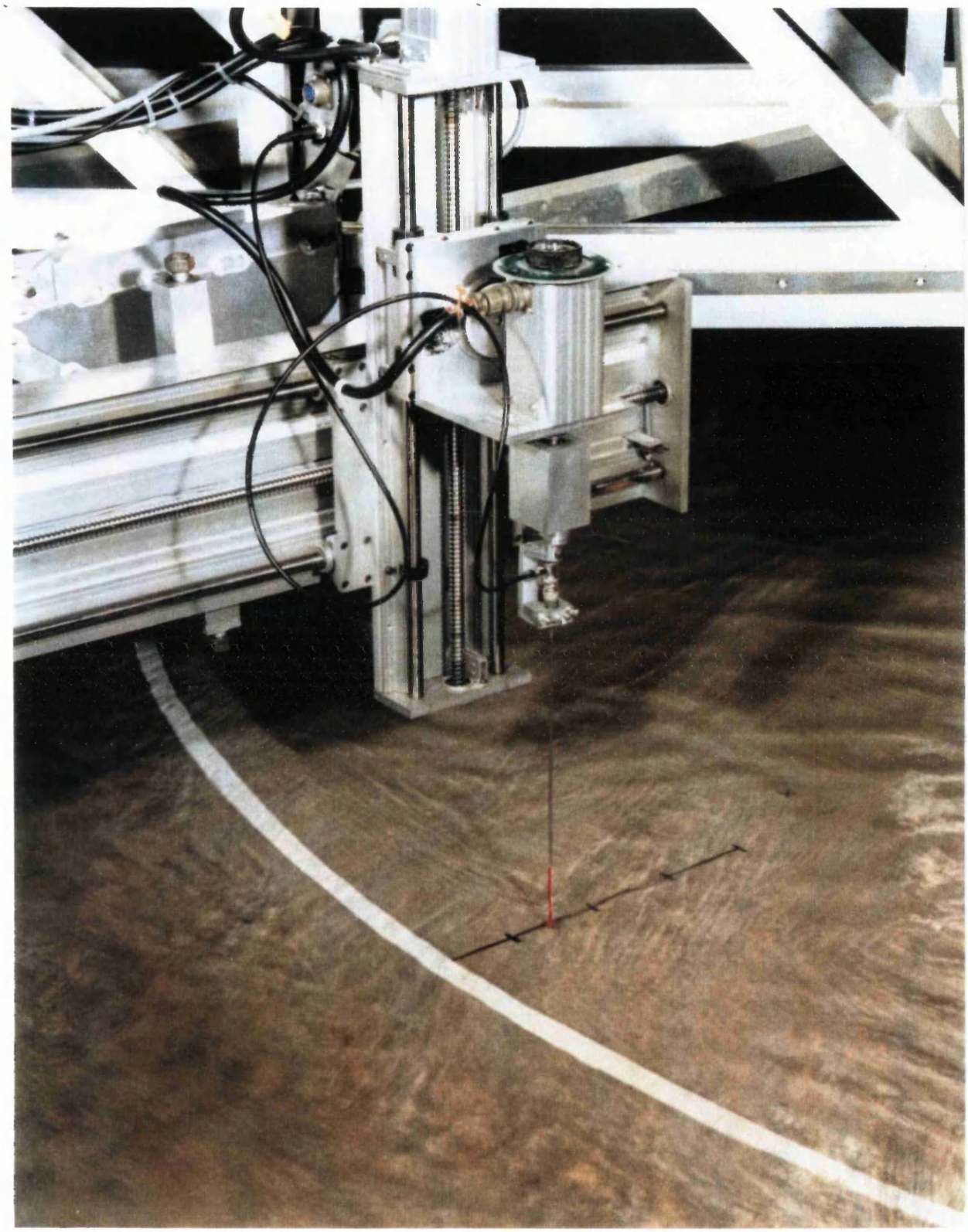

Fig (3.29) - Mini-Propeller Mounted in the Main Channel Instrument Carriage of The S.E.R.C. Flume Series B.

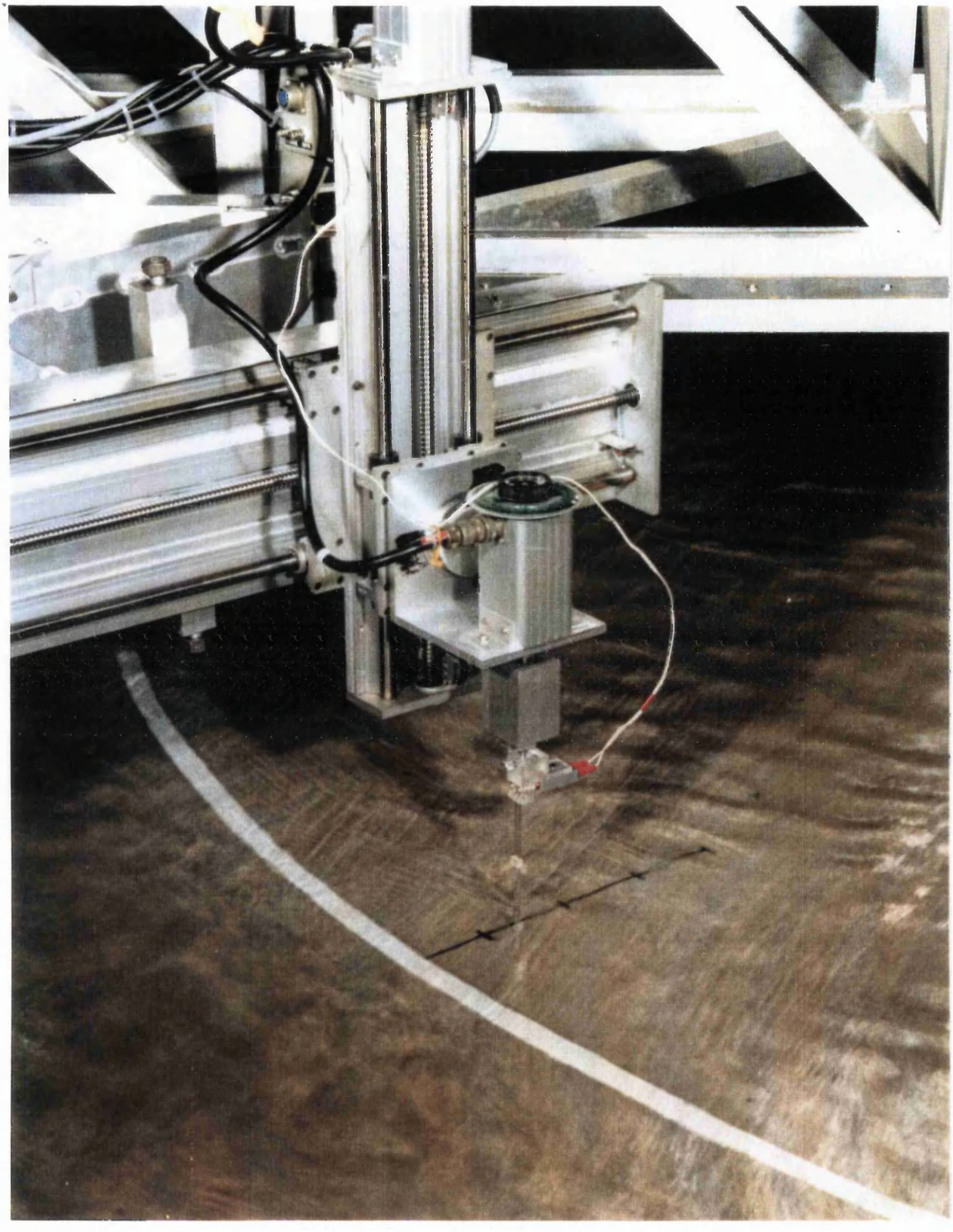

Fig (3.30) - Churchill Probe Used in The S.E.R.C. Flume Series B for Water Surface Levels Measurements.

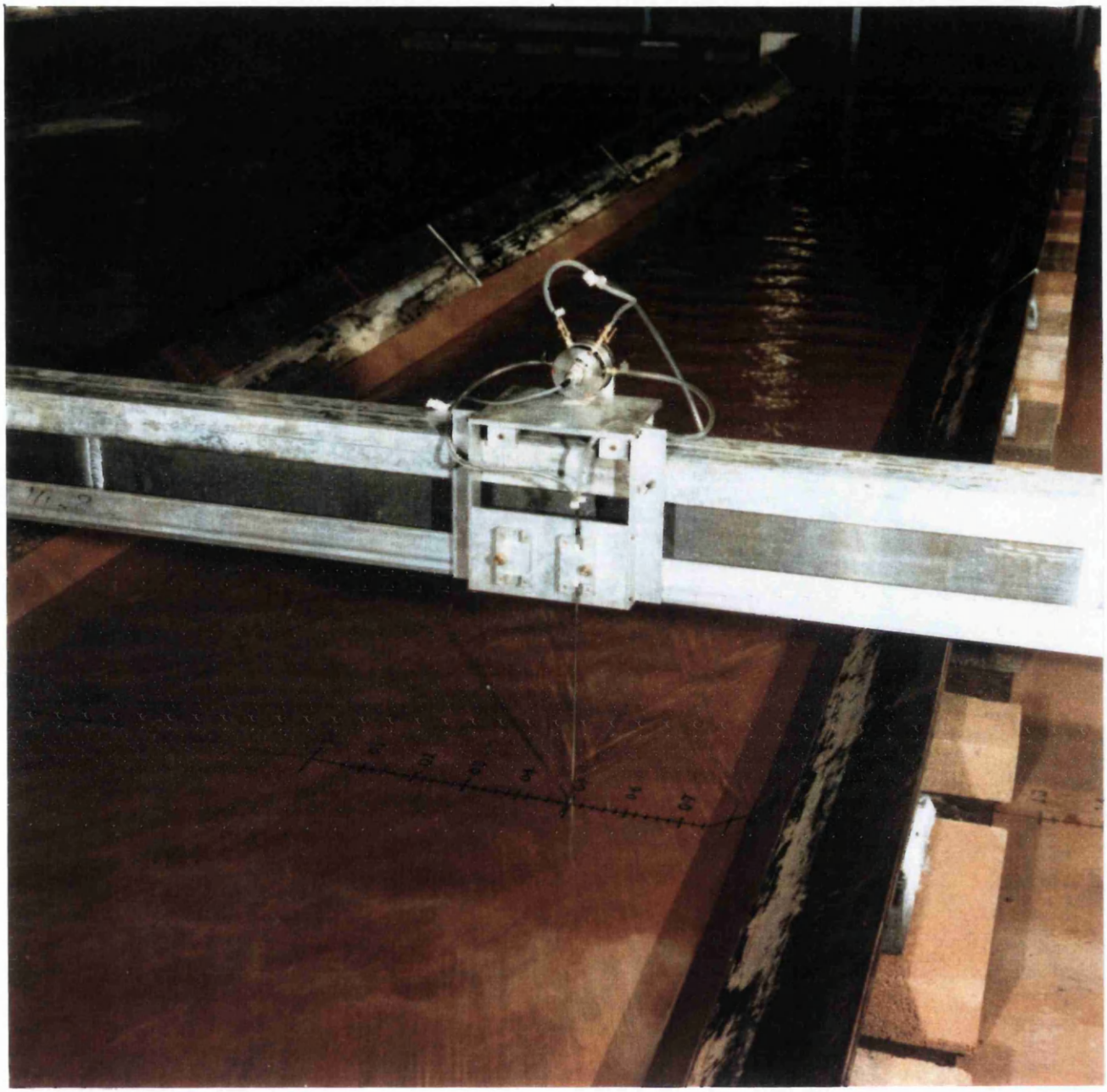

Fig (3.31) - Preston Tube and Pressure Transducer Used in The S.E.R.C. Flume for Boundary Shear Stress Measurements.

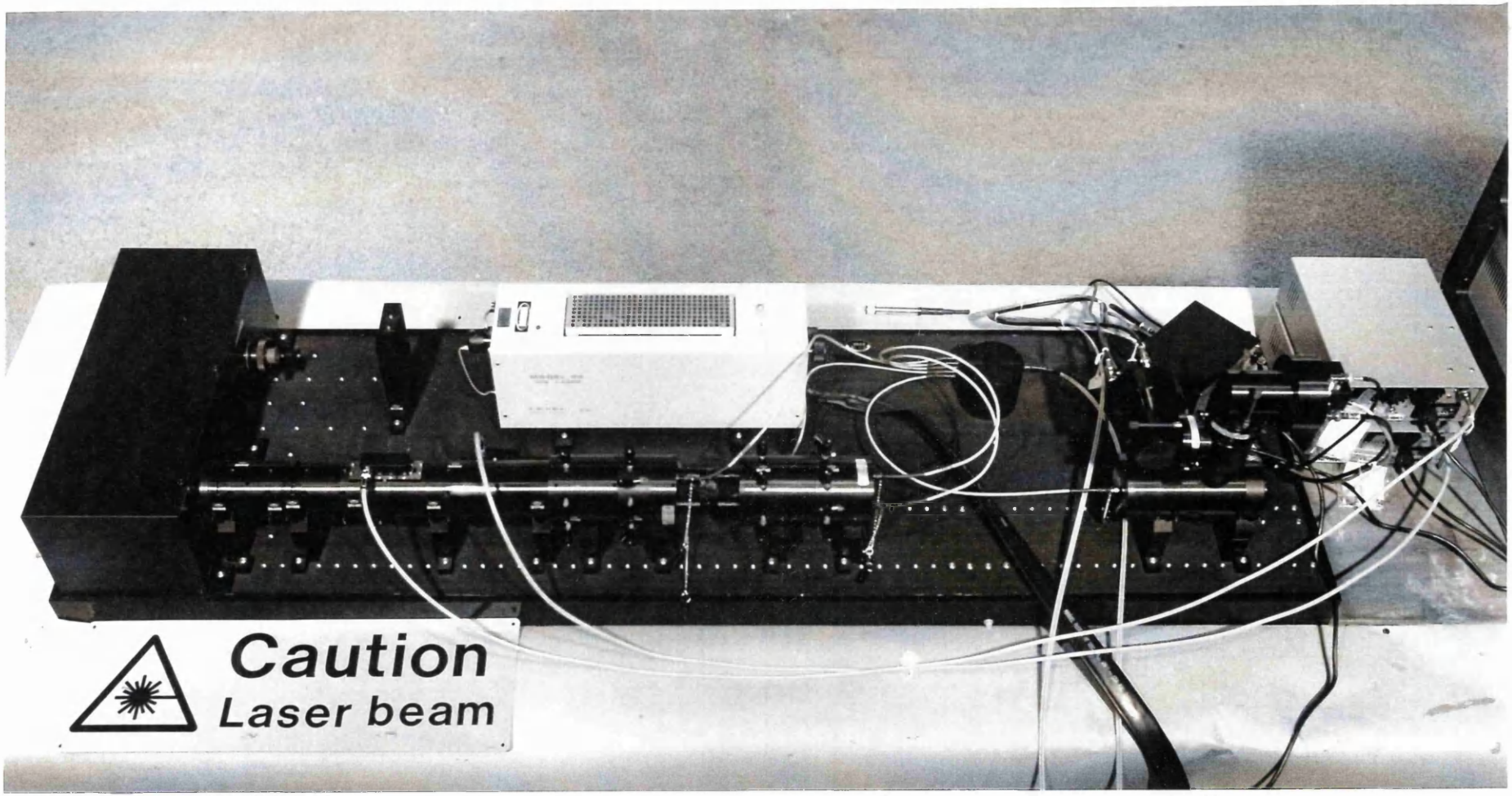

Fig (3.32) - Components of the Laser Doppler Velocimeter Installed in The S.E.R.C. Flume for Measurements of Flow Turbulence.

Fig (3.33) - Submersible Probe of the LDV Installed in the Main Channel Instrument Carriage of The S.E.R.C. Flume Series B.

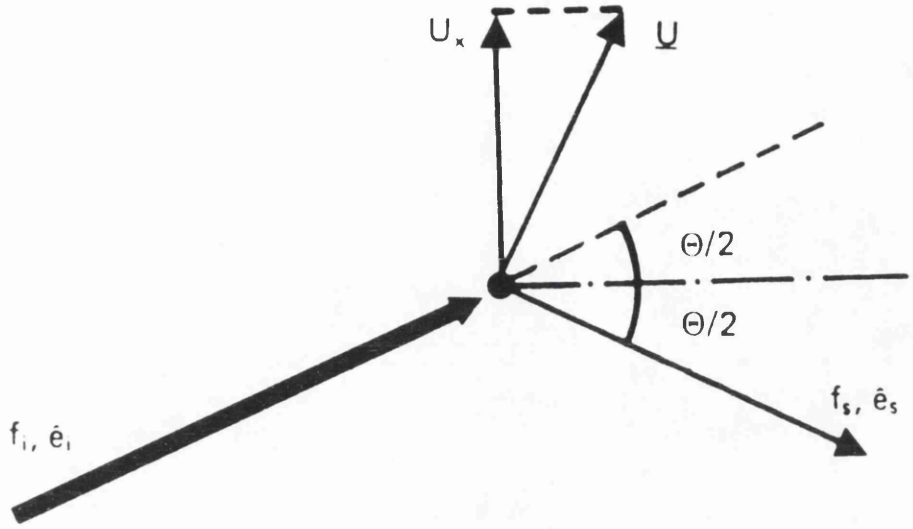

Fig (3.34) - Diagram Showing the Doppler Shift.

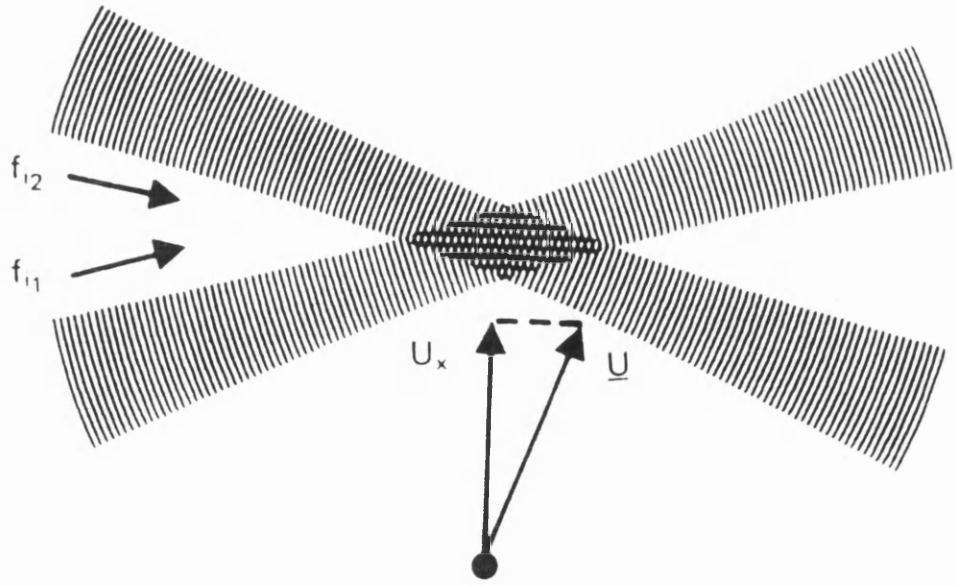

Fig (3.35) - Diagram of the Fringe Model.

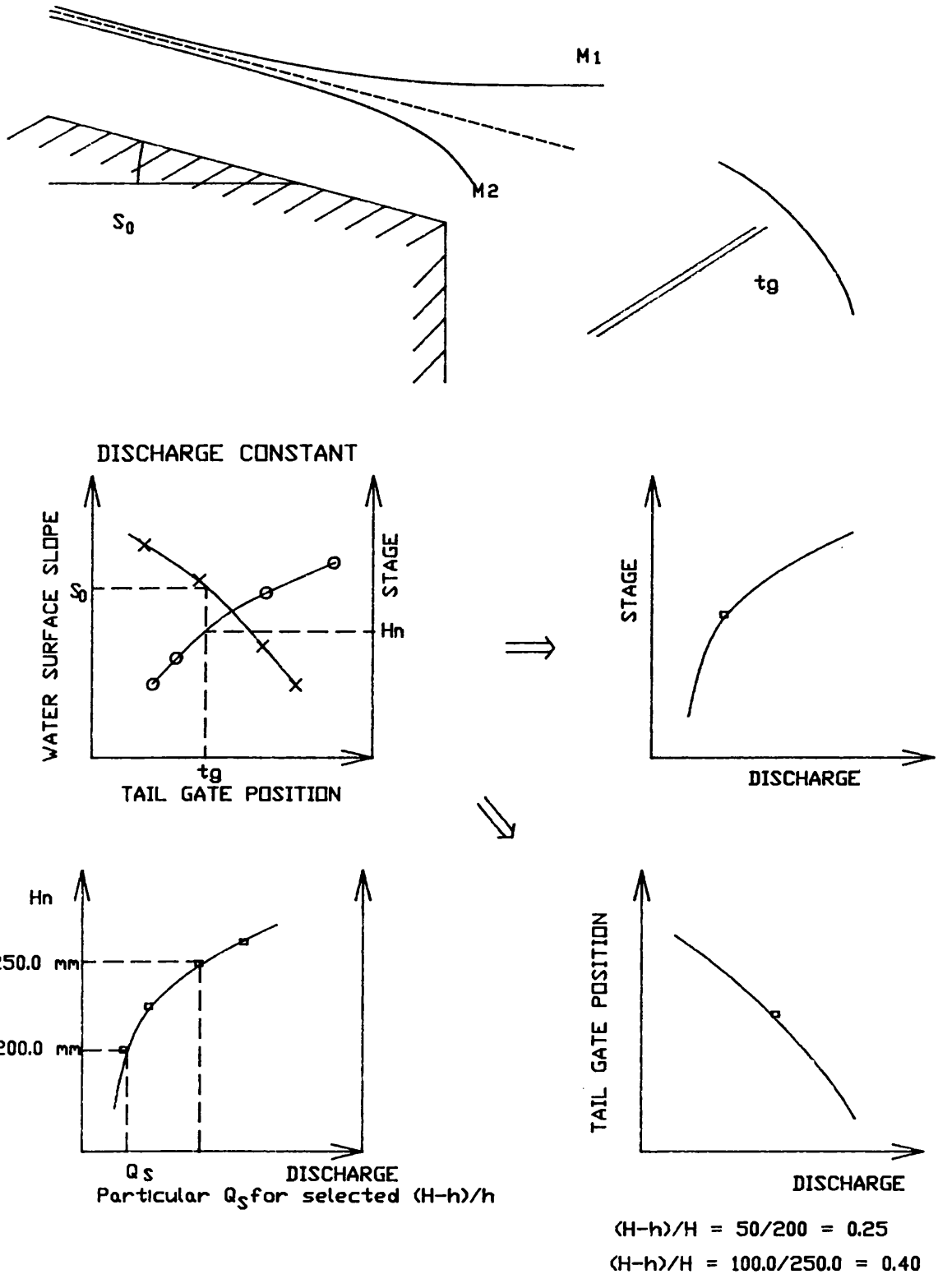

FIG. 3.36 - HOW TO SET UP UNIFORM FLOW IN S.E.R.C. FLUME.

Fig (3.37) - Lateral View of The Glasgow Flume.

Fig (3.38)

Upstream View of
The Glasgow Flume.

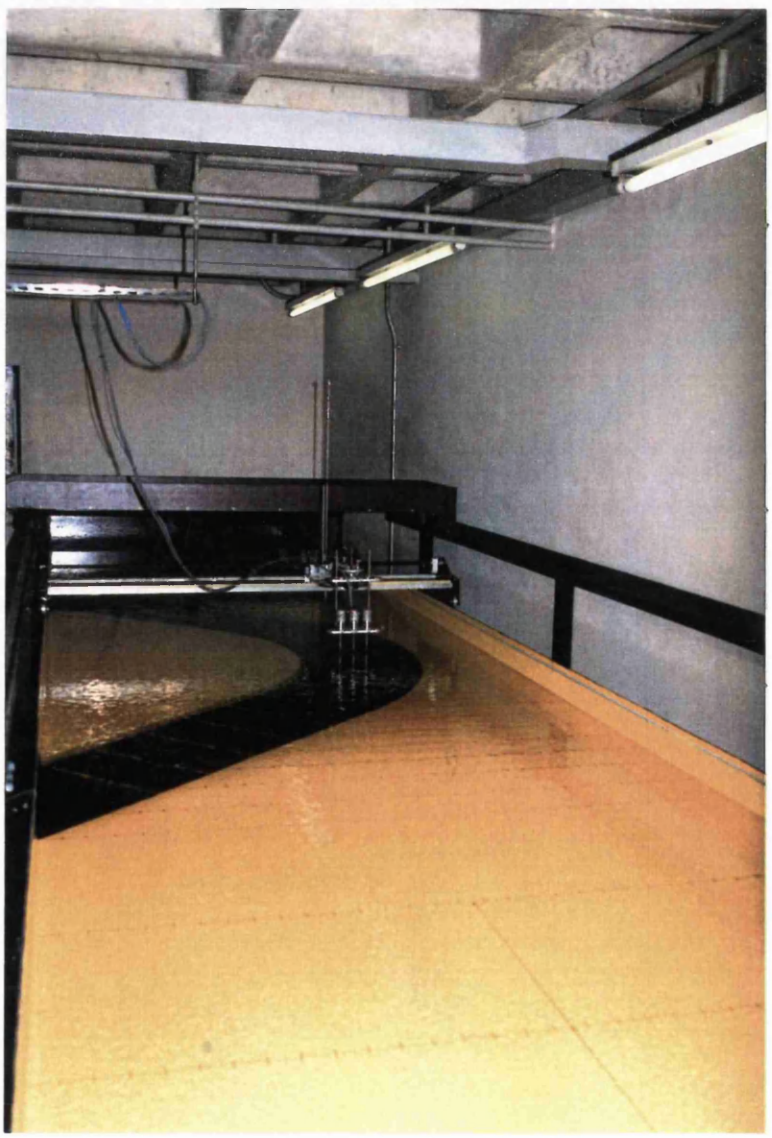

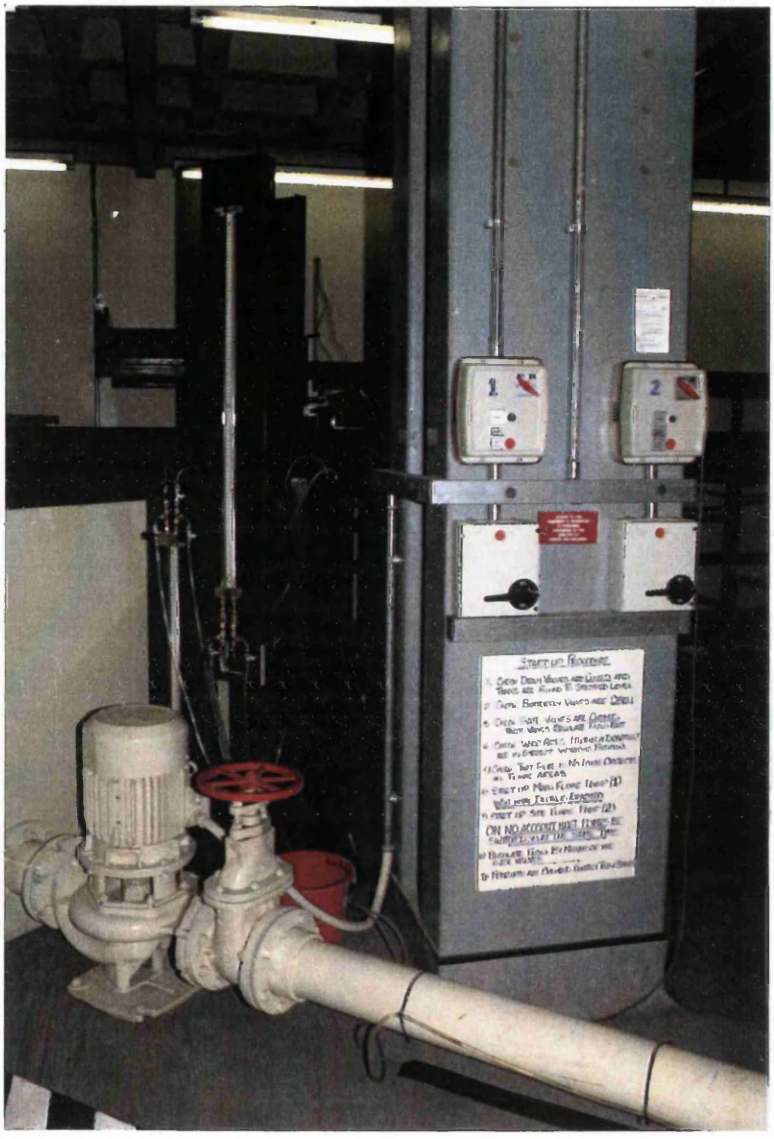

Fig (3.39) - View of the Sump, the Pump, the Gate Valve and the Differential Manometers of the Main Channel System of The Glasgow Flume.

UNITS IN MILLIMETRES

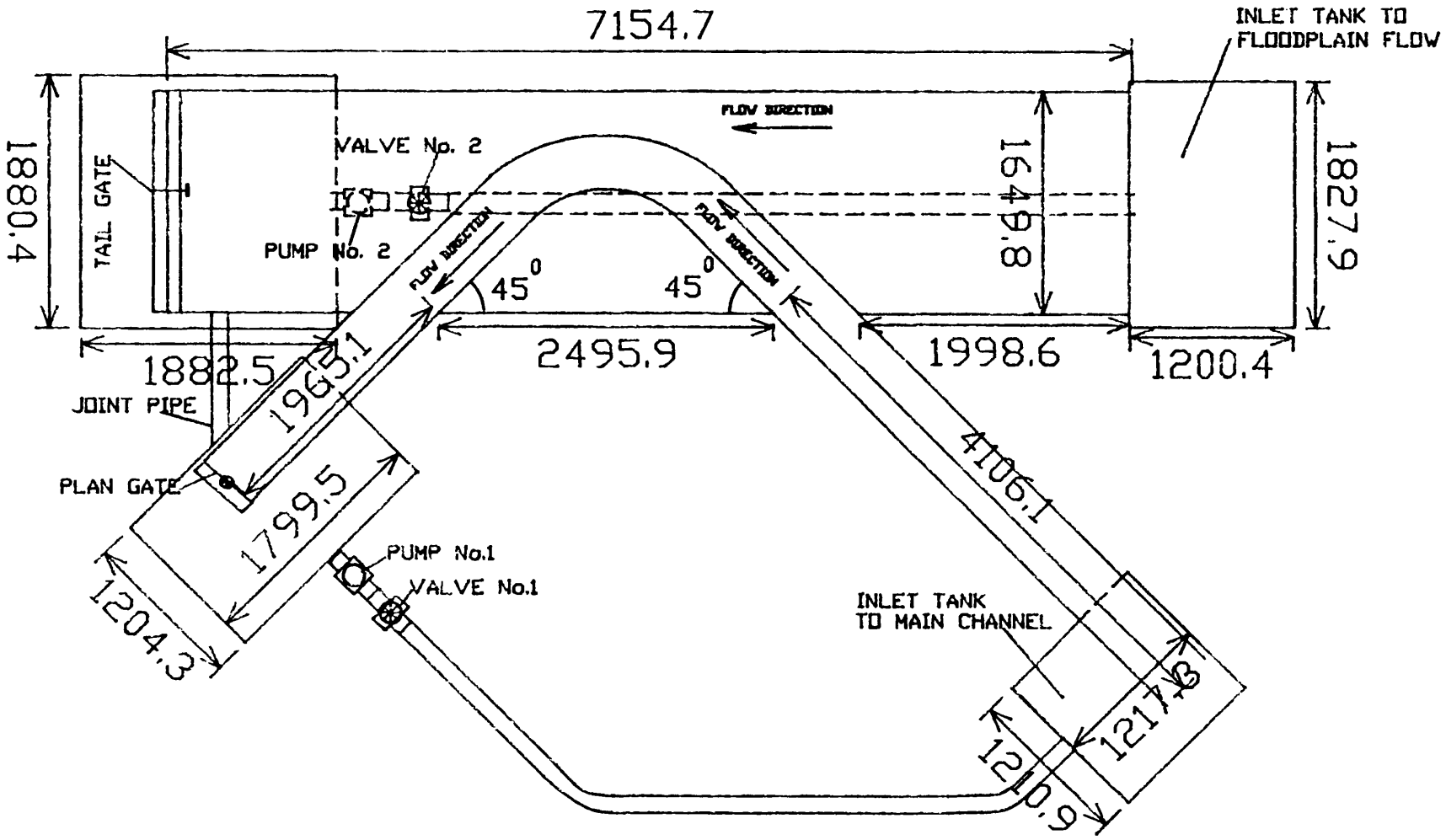

Fig. 3.40 - Plan of The Glasgow Flume

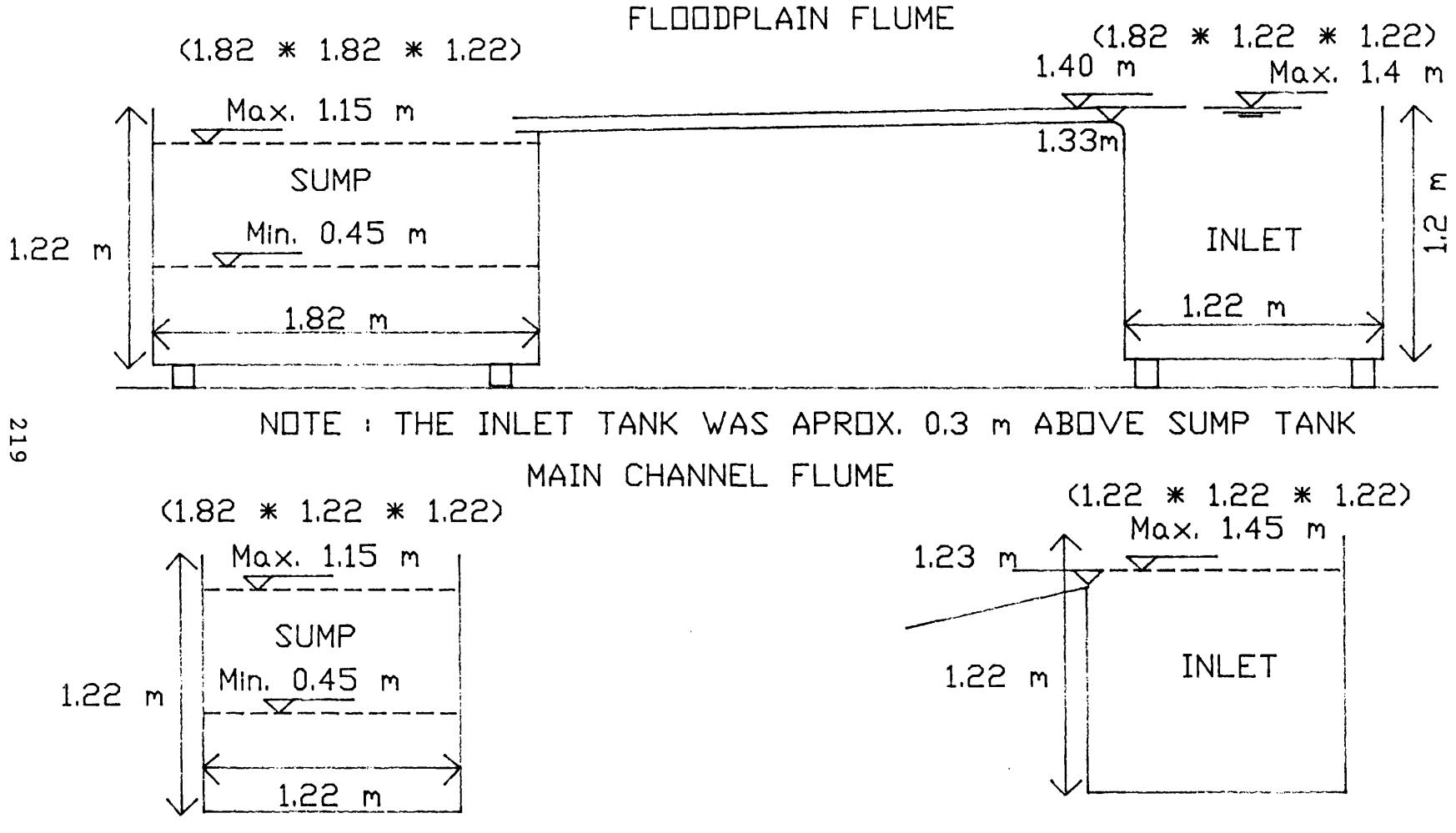

Fig. 3.41 - Ilustrative Sketch of the Design of the Size of the Glasgow Flume's Tanks.

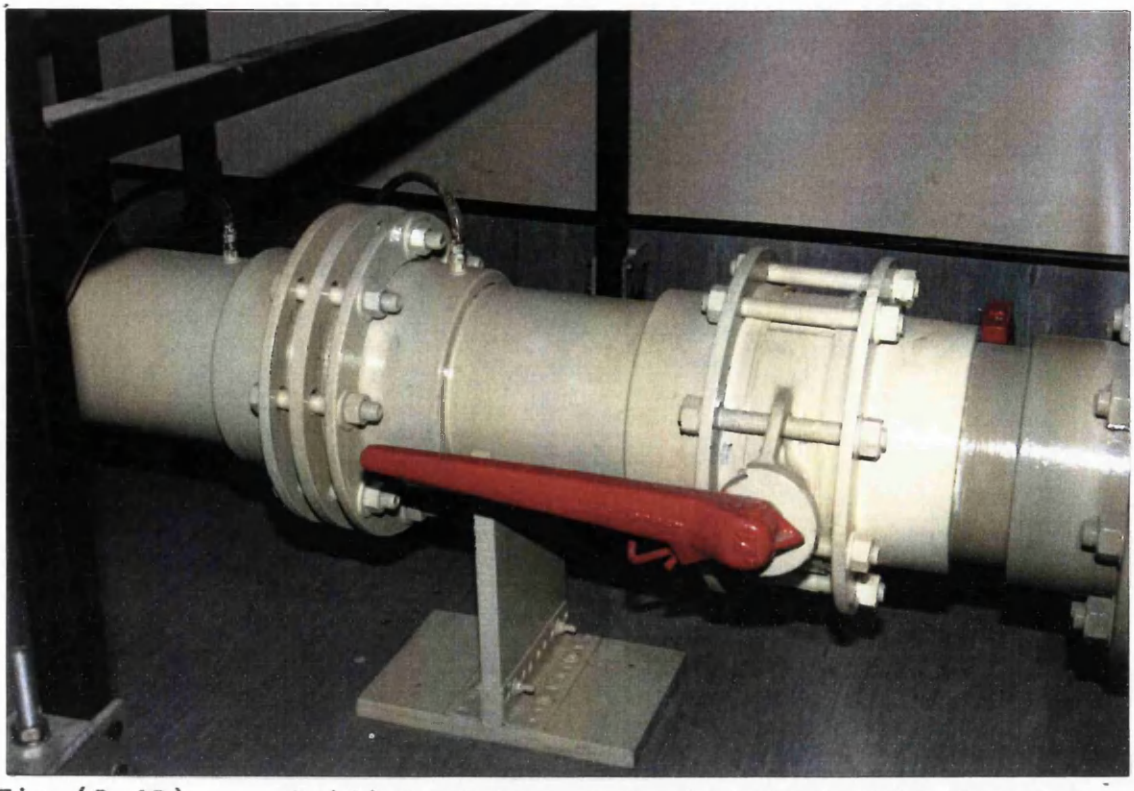

Fig (3.42) - Orifice Meter and the Butterfly Valve.

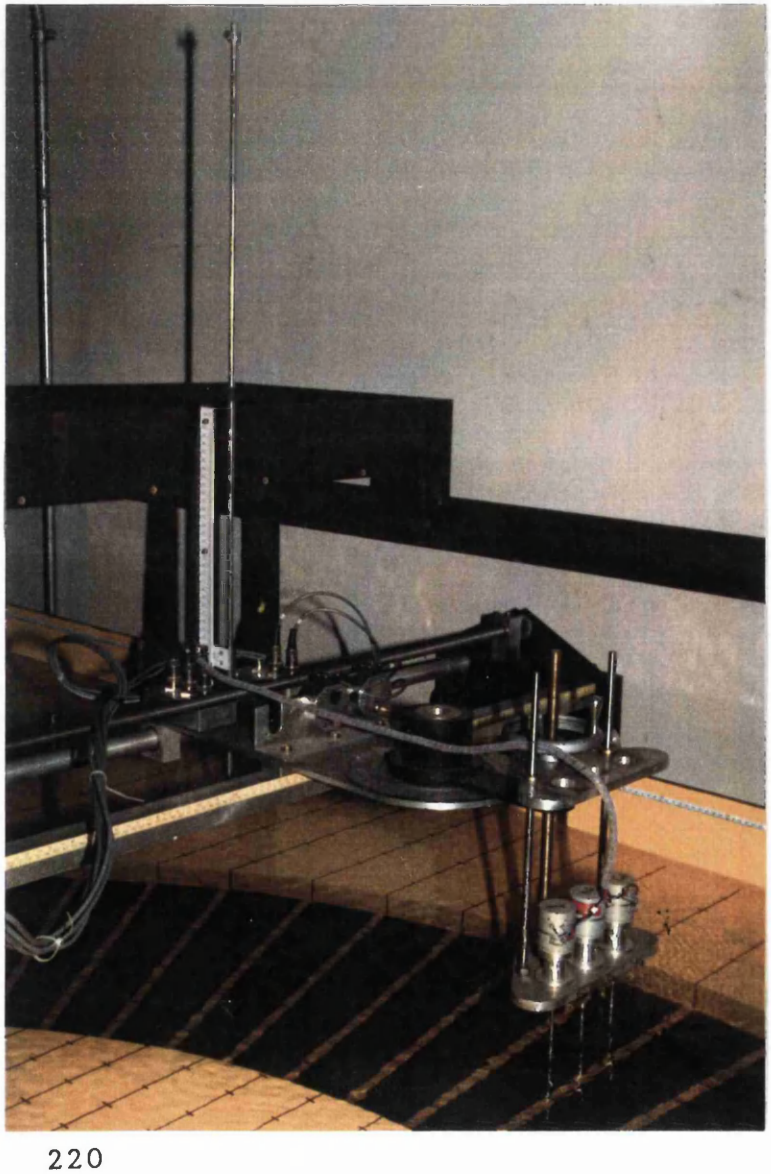

Fig (3.43)
Instrument Carriage of
The Glasgow Flume.

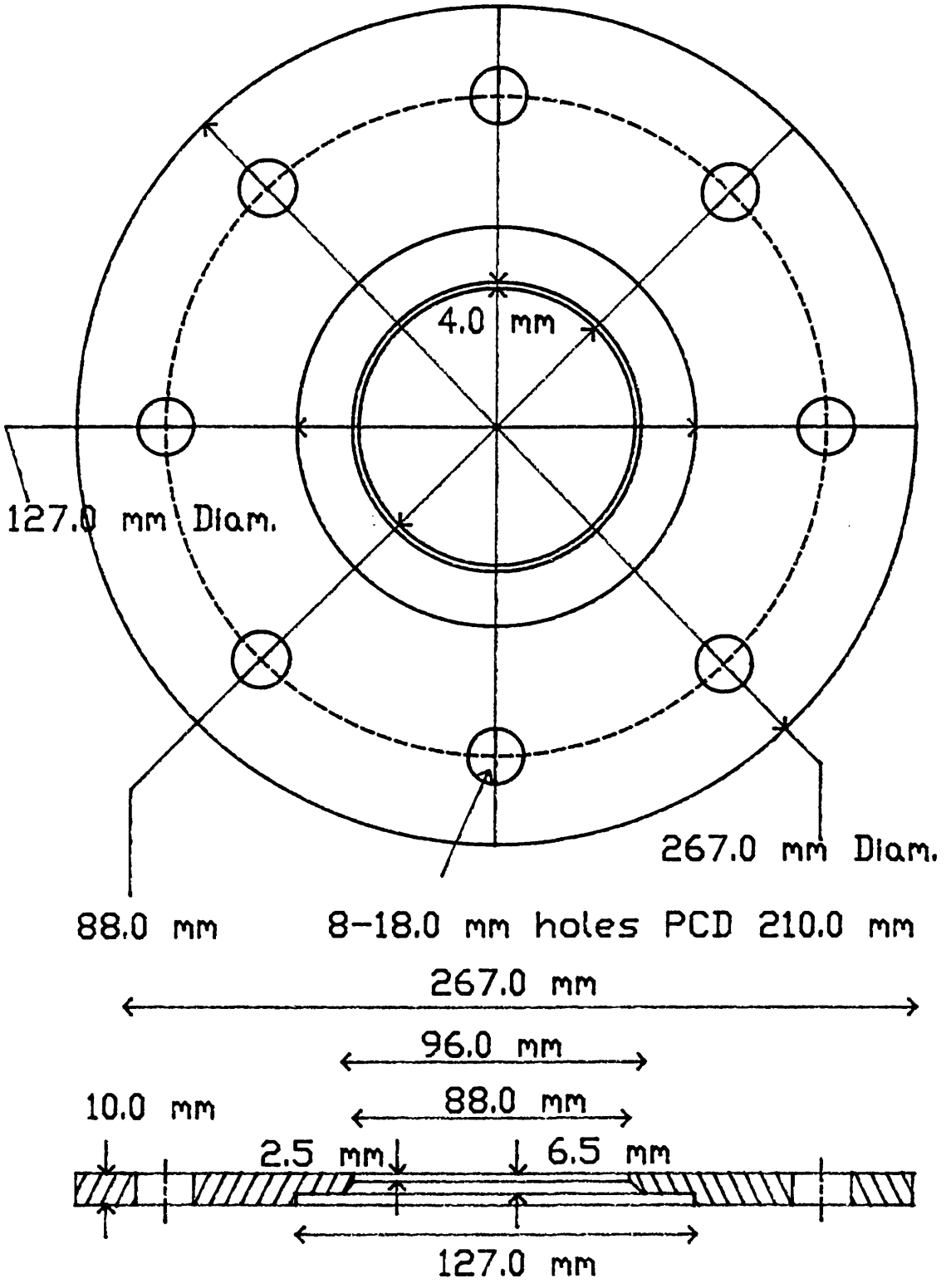

Fig. 3.44 - Cross-Section of the Orifice Plate Used in the Measurement of the Discharge of the Main Channel System of Glasgow Flume.

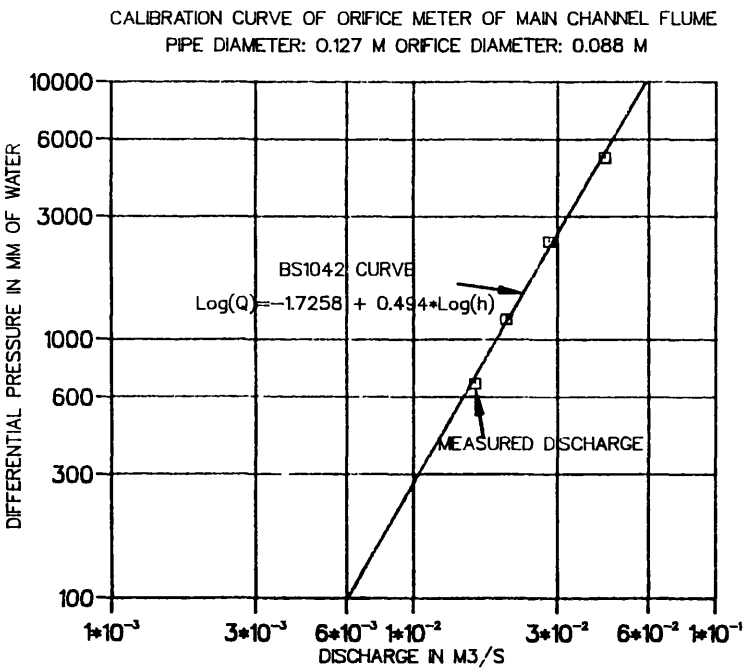

Fig (3.44a) - Calibration Curve of the Orifice Meter of The Main Channel of The Glasgow Flume.

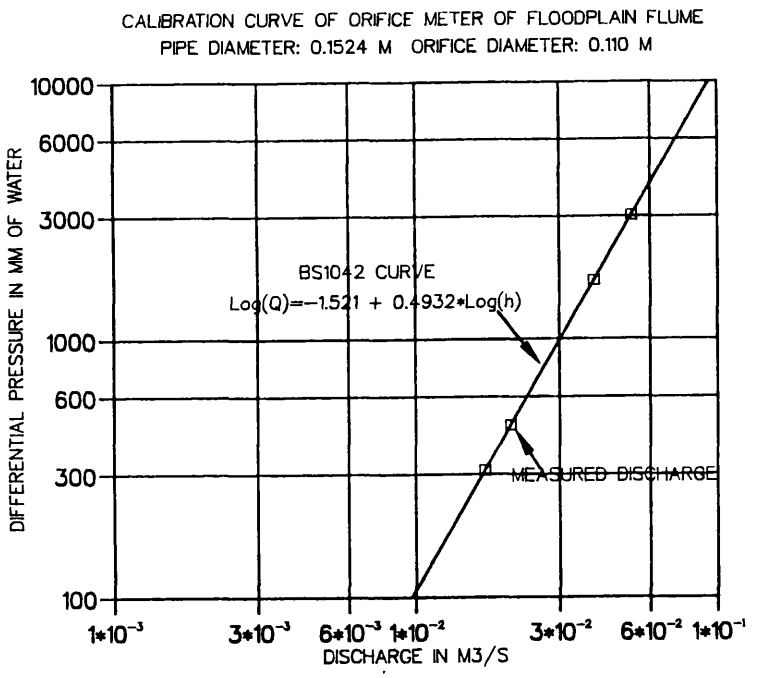

Fig (3.44b) - Calibration Curve of the Orifice Meter of The Floodplain Channel of The Glasgow Flume.

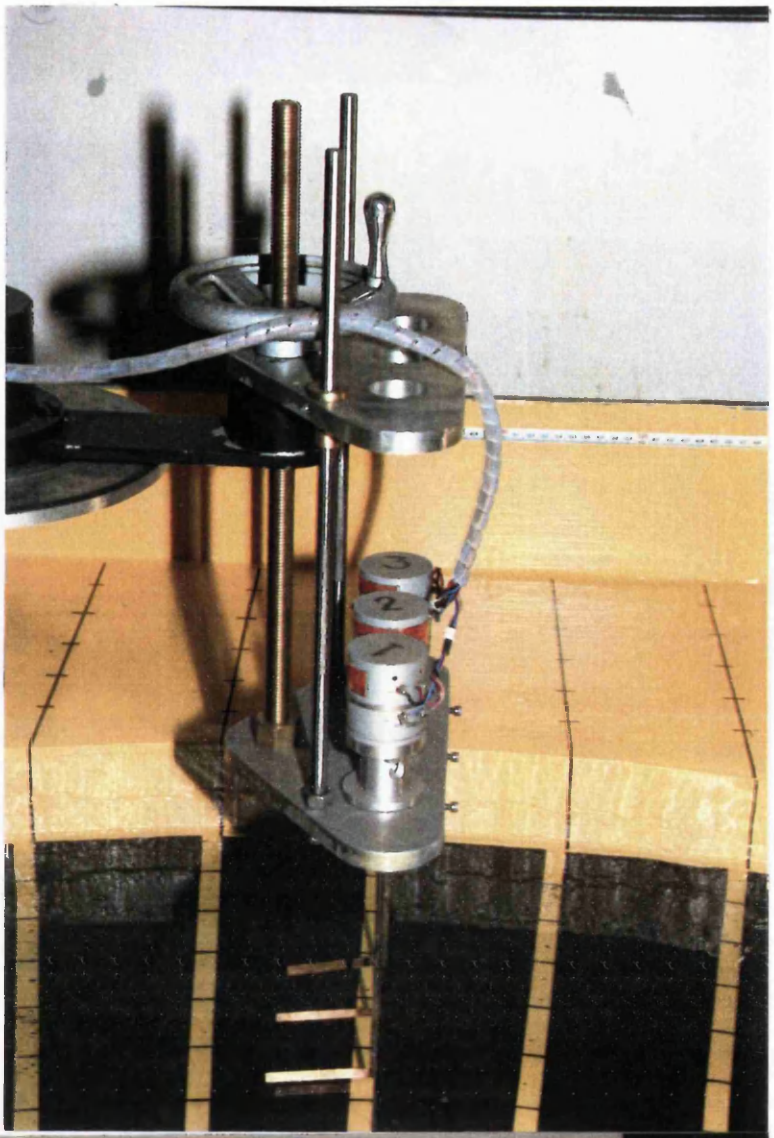

Fig (3.45)

Bank of Three Vanes Mounted on Instrument Carriage

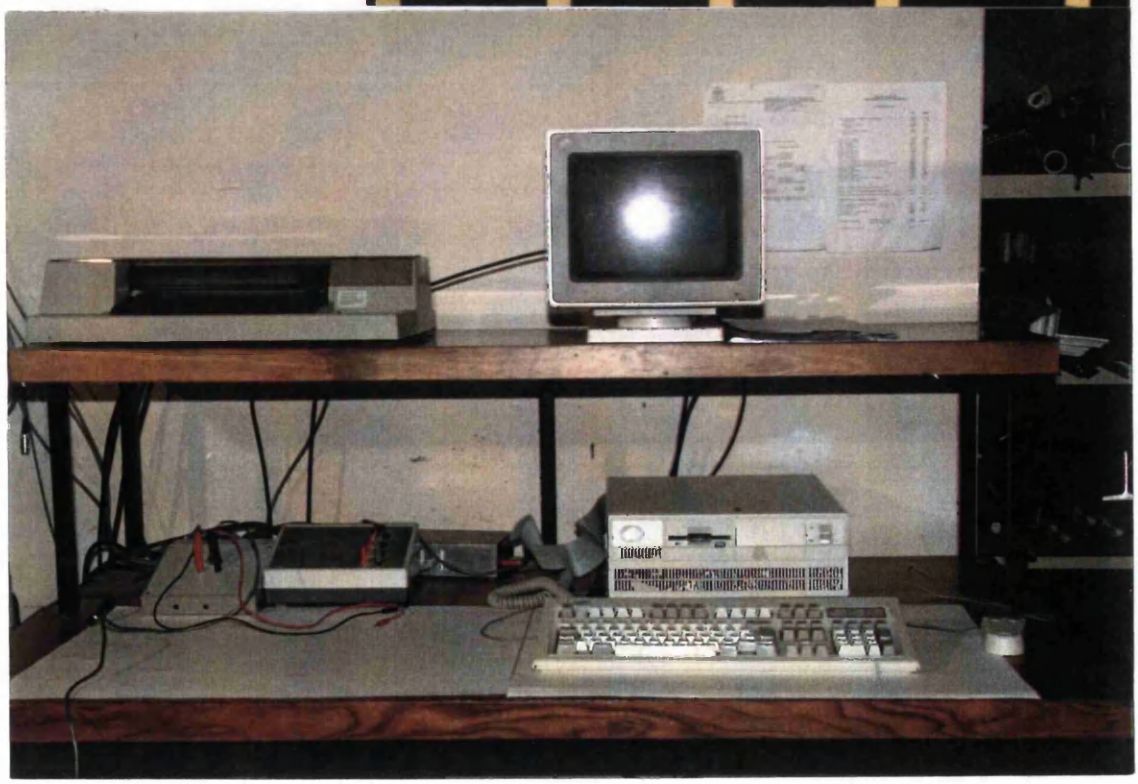

Fig (3.46) - Computer System of The Glasgow Flume.

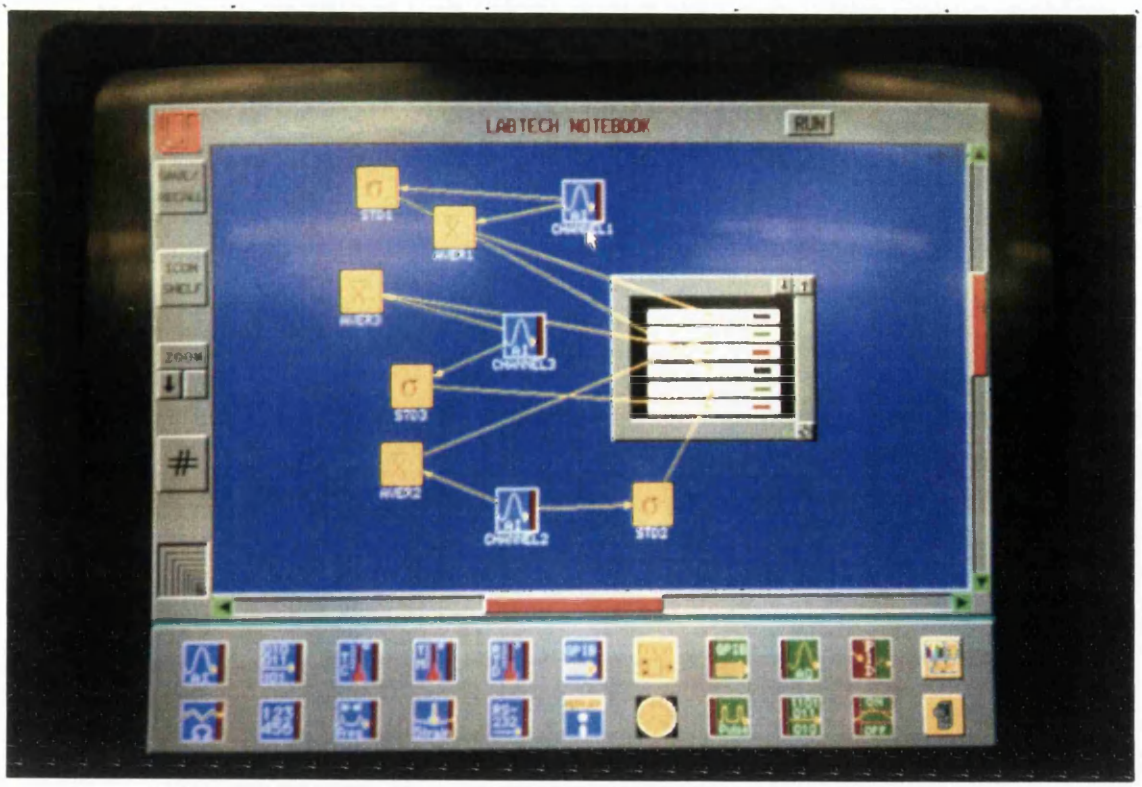

Fig (3.47) - Display Screen Showing Icons Connections for the Angle Measurements at The Glasgow Flume.

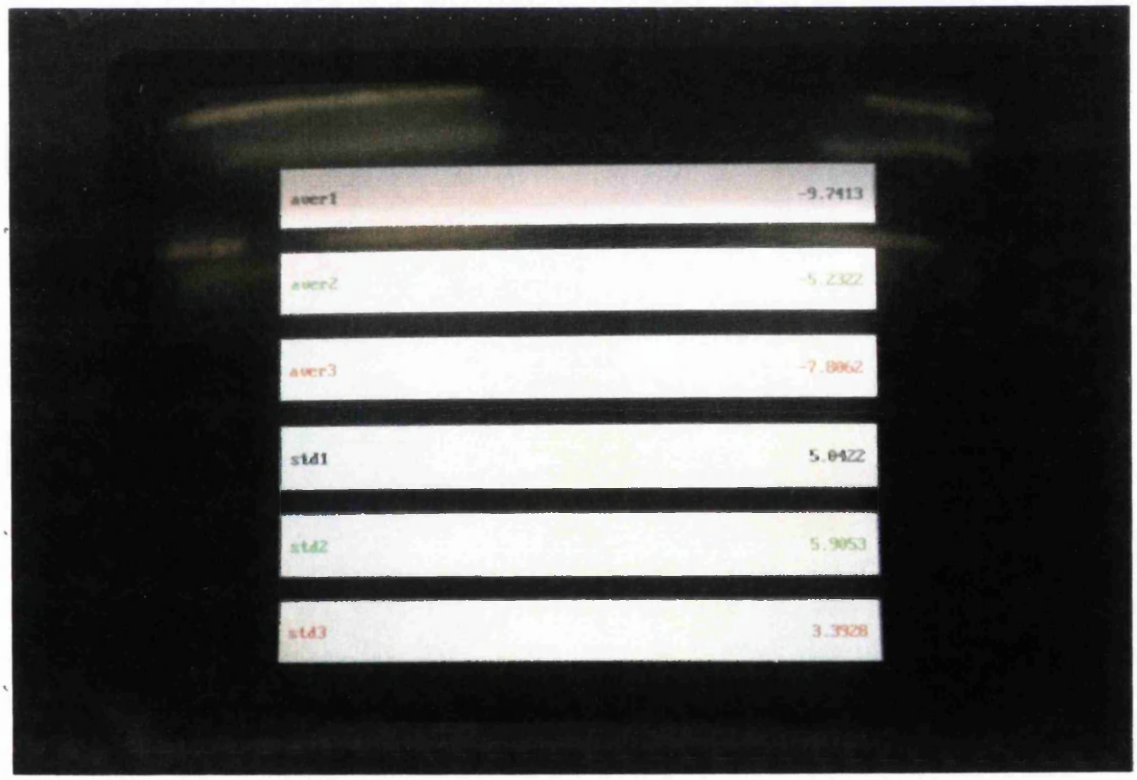

Fig (3.48) - Display Screen Showing Six Windows with Results of Three Average and Three Standard Deviation Angles at the Glasgow Flume.

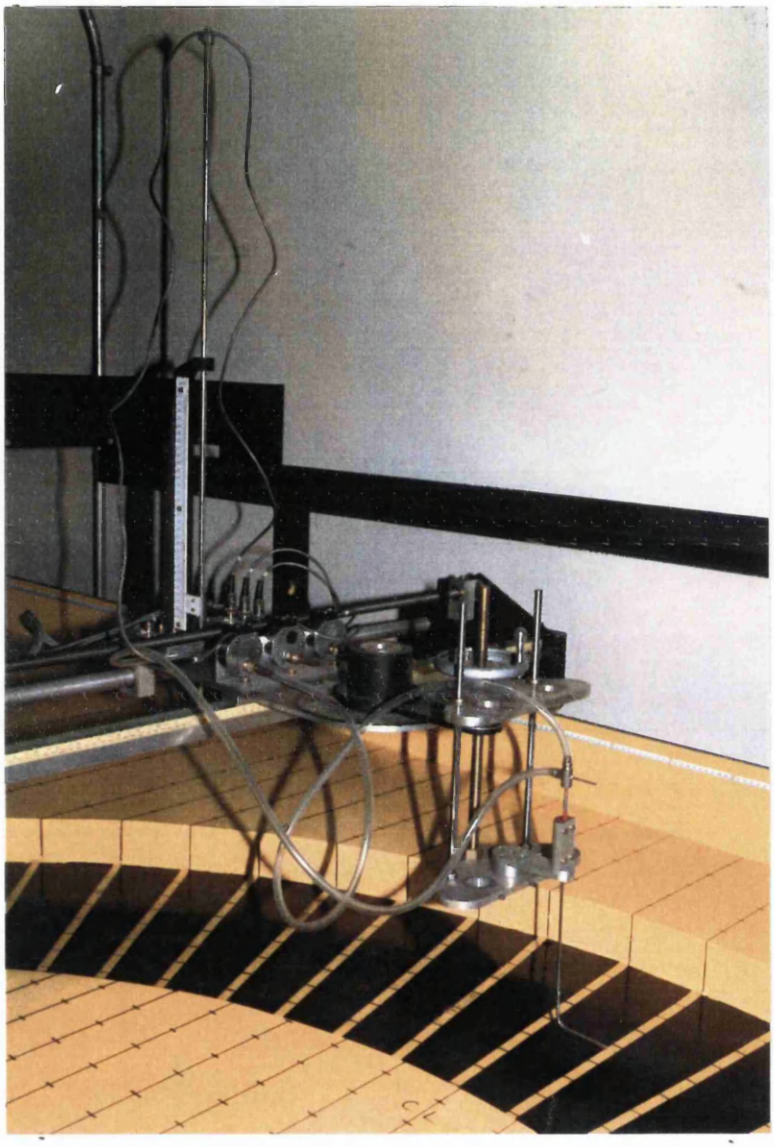

Fig (3.49) - The Pitot Static Tube and The Pressure Transducer Mounted on the Instrument Carriage of The Glasgow Flume.

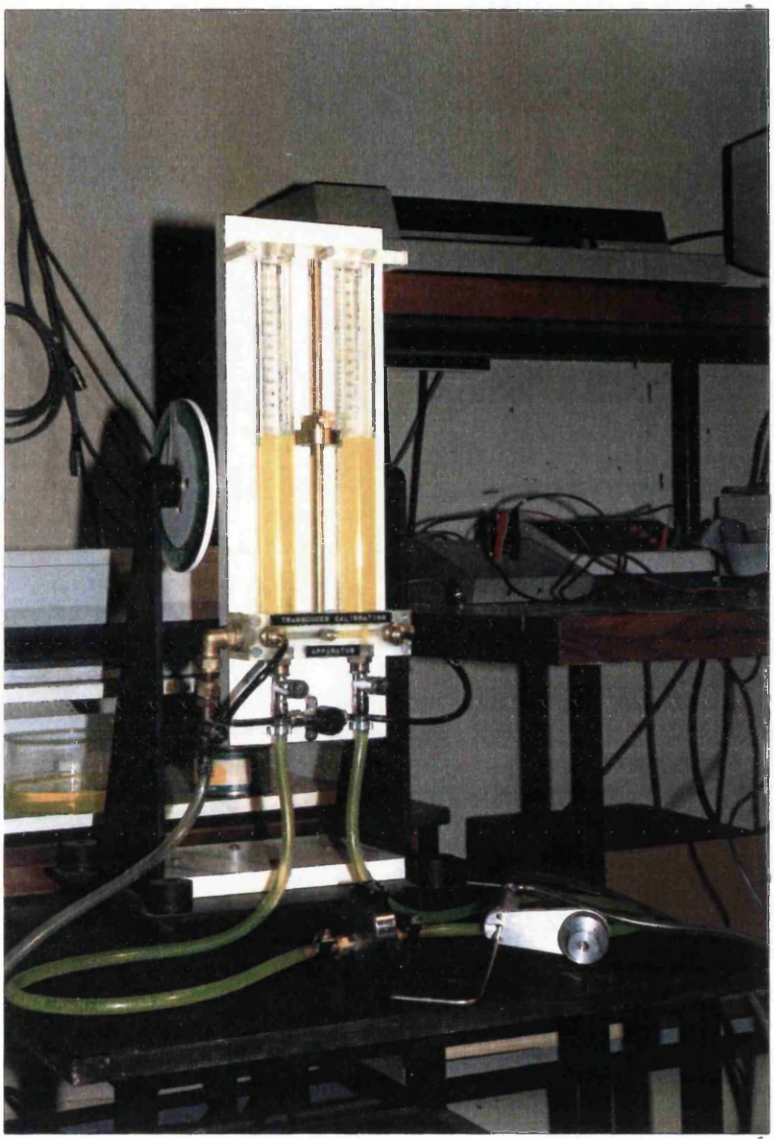

Fig (3.50) - Calibration Device for the Pressure Transducer of the Glasgow Flume.

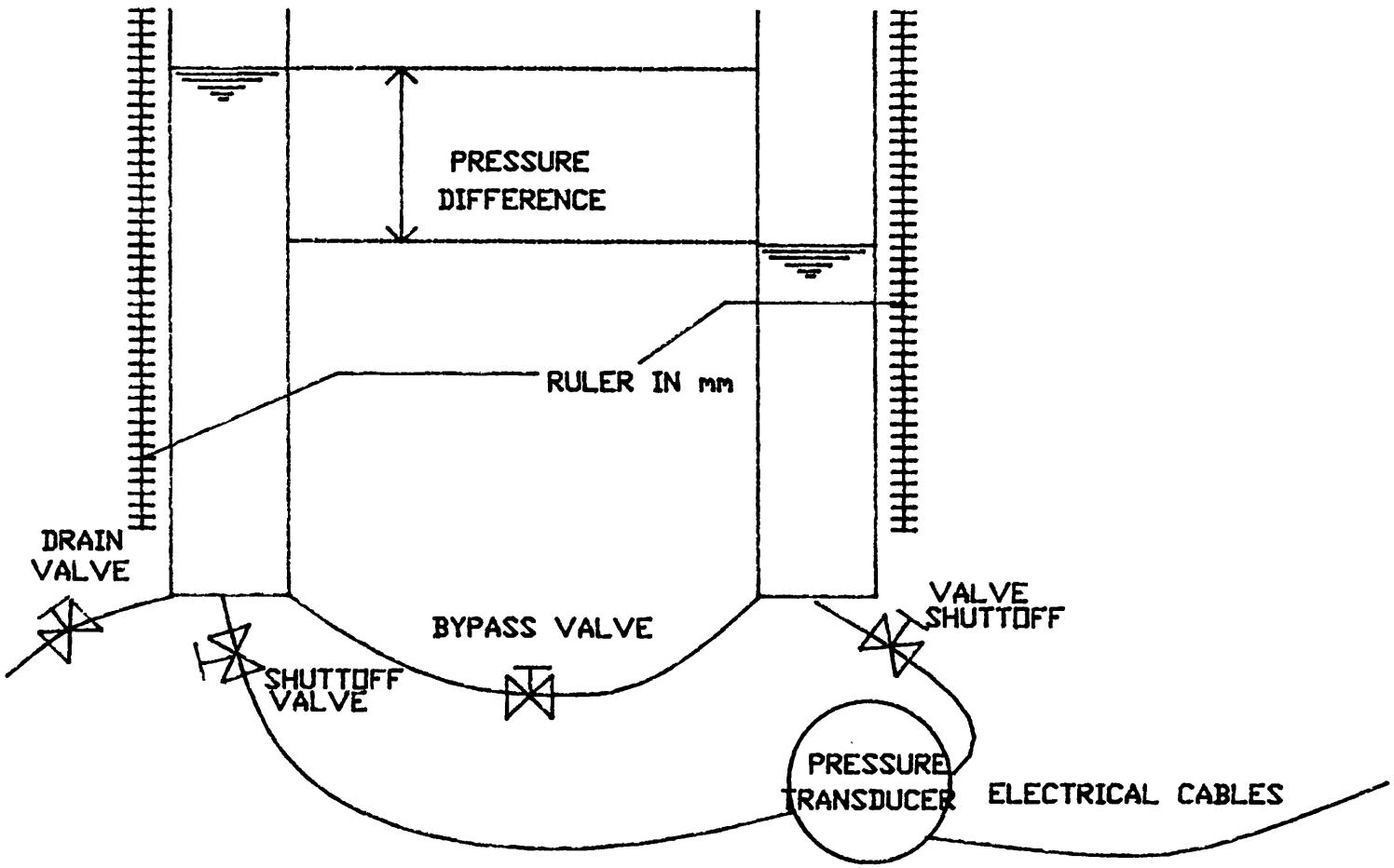

Fig. 3.51 - Sketch of the Calibration Device with Valve Arrangement.

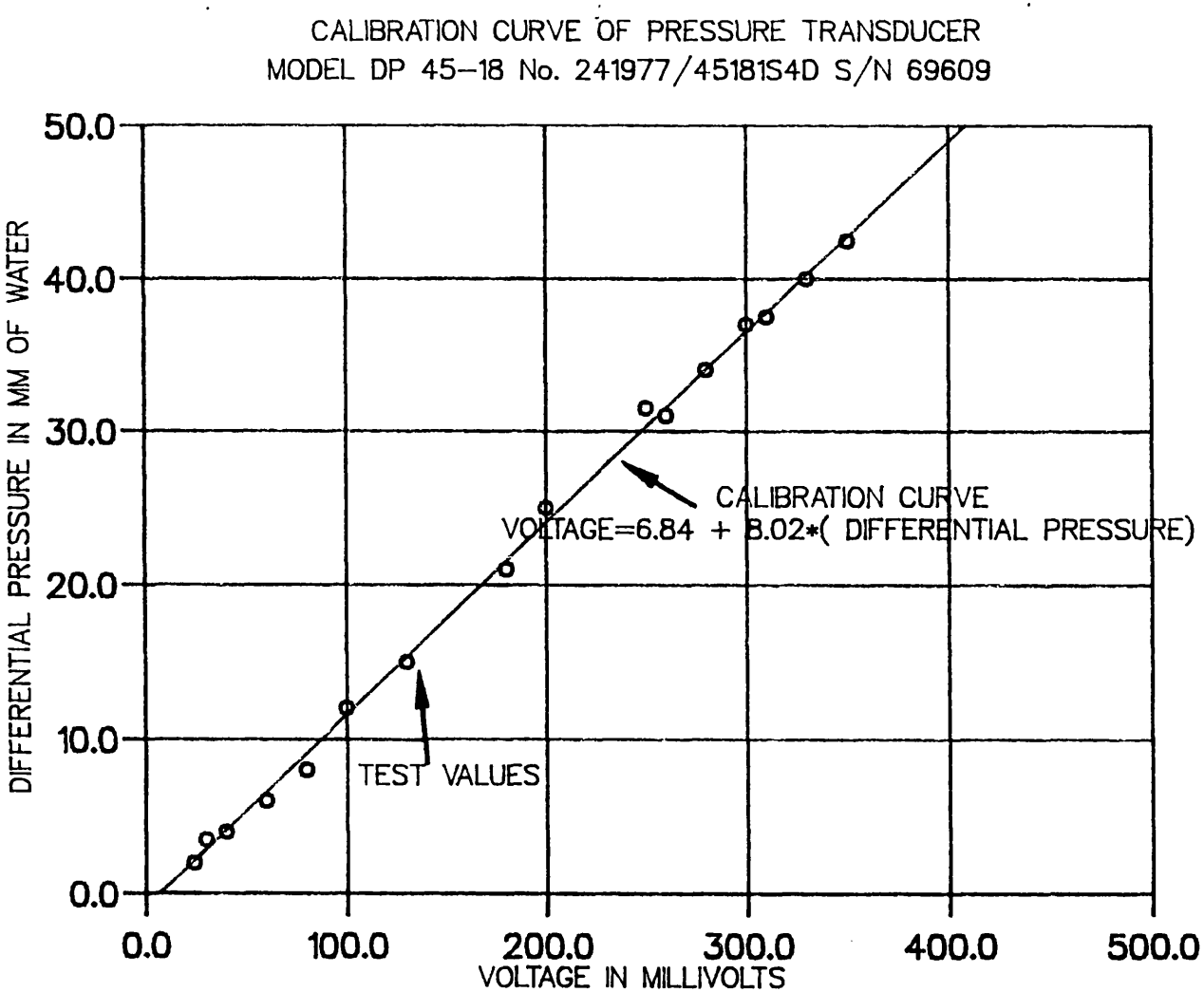

Fig (3.52) - Calibration Curve of the Pressure Transducer of The Glasgow Flume.

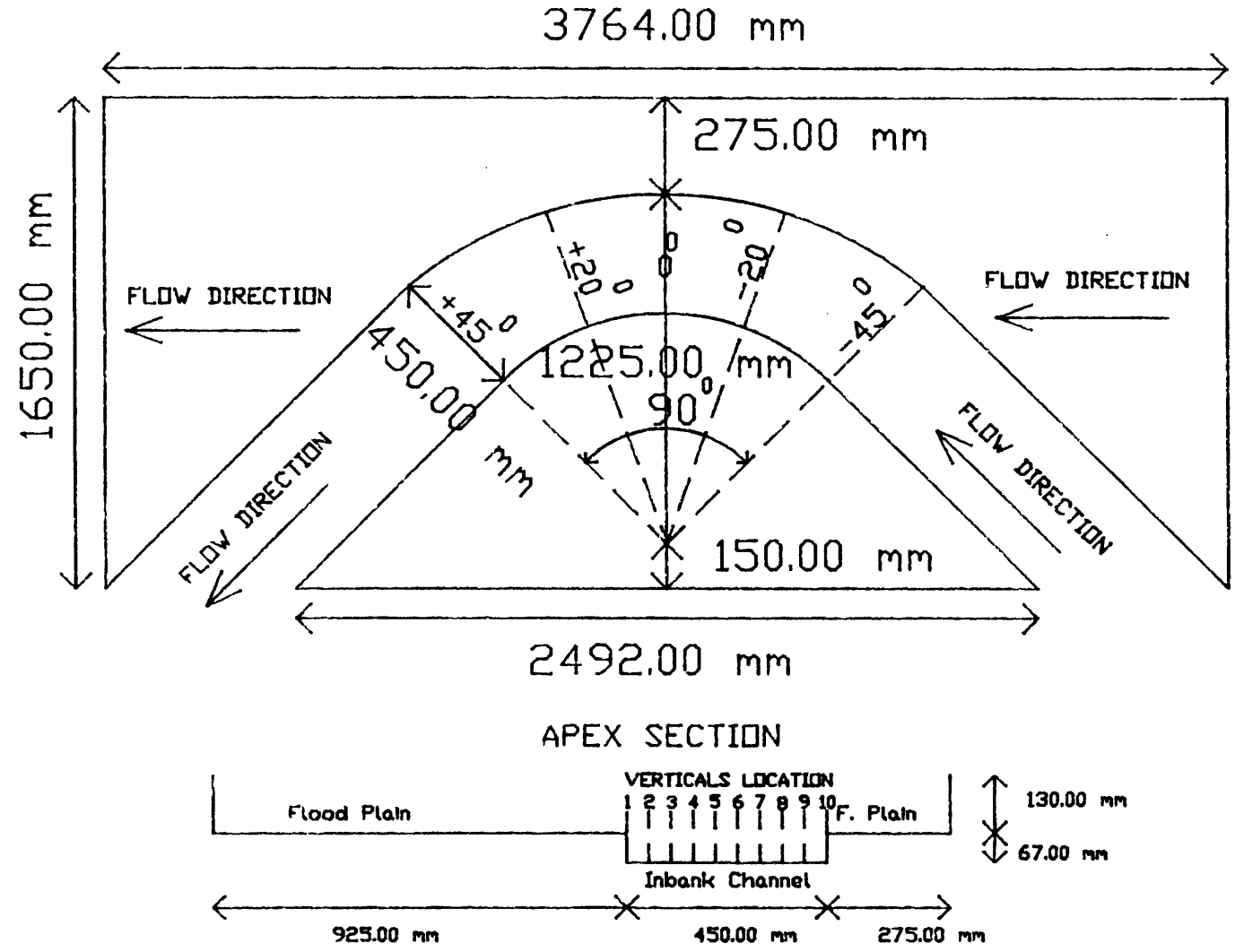

Fig. 3.53 - Test Sections and Verticals of The Glasgow Flume.

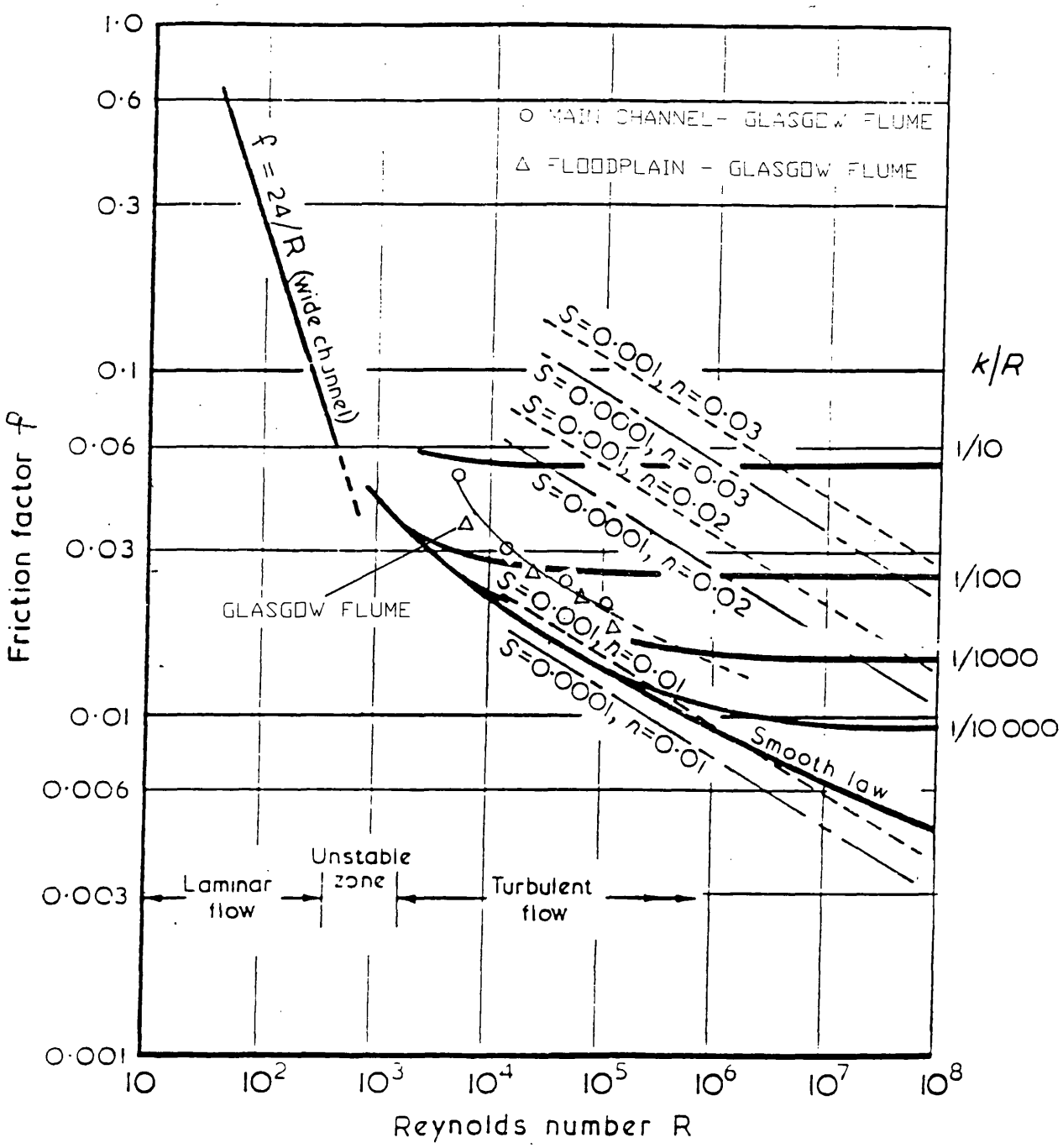

Fig (3.54) - Moody Diagram for Open Channels(from Weber(1974))

CHAPTER 4

STAGE-DISCHARGE, FLOW CONVEYANCE AND ENERGY LOSSES IN MEANDERING COMPOUND FLOWS

CHAPTER 4

STAGE-DISCHARGE, FLOW CONVEYANCE AND ENERGY LOSSES IN MEANDERING COMPOUND FLOWS

4.1 INTRODUCTION

Several parameters affect the conveyance of meandering compound channels. Previous research on this subject has shown that:

- Increasing the main channel sinuosity considerably diminishes the conveyance(**U.S.Army Corps of Engineers(1956)**. Typically the discharge reduces 30%-40% for increasing sinuosity from 1.0 to 1.57.
- Floodplain roughness reduces conveyance substantially **(Sellin and Giles(1988))**. Typically a 30% reduction in the total conveyance is found comparing compound channels with cut and uncut floodplain vegetation.
- The geometry of the main channel's cross-section seems to have a considerable effect on conveyance. This is true both for the shape of the main channel(**Willetts and Hardwick(1990))** but also for the aspect ratio of the main channel(**Ervine and Jasem(1992))**.
- The relative depth of flow(**Kiely(1989))** is also a significant parameter. For instance the strength of the secondary currents that develop in the main channel are much greater for an overbank case than for an inbank case. These secondary currents, as shown by **Ervine and Ellis(1987)**, introduce significant energy losses and reduce the conveyance of meandering compound channels.

Chapter 4 is concerned with the parametric analysis of the conveyance of meandering compound channels. In this analysis the following parameters were varied:

- Main Channel Cross-Section
- Sinuosity
- Floodplain Roughness
- Stage(relative depth of flow)

- Main channel aspect ratio
- Ratio of the meander belt width to the total channel width.

Chapter 4 is divided into five main sections:

(i) Stage-Discharge

The conveyance of the meandering compound channels is examined in terms of the stage-discharge relationship. This analysis is based in data collected from S.E.R.C. flume Series B tests.

(ii) Flow-Resistance

The flow resistance of meandering compound channels of S.E.R.C. Series B was examined in terms of the variation of the resistance coefficient Manning's n with stage, and the relationship between the Darcy-Weisbach friction factor with the Reynolds number. Two different approaches are presented. First, a one-dimensional approach was used, where both resistance coefficients were calculated, at bend apex section, considering the main channel and the floodplain cross-sections as a single section. Second, a three dimensional approach was used, where detailed contour maps of the Darcy-Weisbach friction factor were determined from boundary shear stress and velocity measurements. In the one-dimensional approach, the analysis included comparison with data from S.E.R.C. Series A(the straight and the skew compound channel).

(iii) Boundary shear distribution

The resistance developed by the flow near the river bed can be expressed in terms of the boundary shear stress distribution. Based on data from S.E.R.C Series B, the effects of the stage and of the main channel sinuosity on the boundary shear distribution will be shown for the case of smooth floodplains.

(iv) Parametric analysis

Following on the work of **Ackers(1991)**, the parametric

analysis of the conveyance of meandering compound channels was carried out using a non-dimensional functions F_1, F_4 and F_5, which represent the ratio between actual discharge divided by the theoretical discharge. The theoretical discharge was computed, considering only energy loss produced by skin friction. Function F_1 was derived for the inbank case while the other two functions F_4 and F_5 were developed for the overbank case. Function F_4 was calculated considering the vertical wall division method while function F_5 was computed, considering the combination of both, the horizontal and the vertical wall division methods as discussed by **Ervine and Ellis(1987)**. This analysis included data from S.E.R.C. Series B, from S.E.R.C. Series A and data from other flumes.

(v) Separation of energy losses

A method was developed to separate main channel energy losses from floodplain energy losses, that occur in the meandering compound channels of S.E.R.C. Series B.

4.2 STAGE-DISCHARGE CURVES FOR S.E.R.C. SERIES B TESTS

In S.E.R.C. flume Series B tests, stage-discharge curves for the meandering compound flows were determined in the following cases:

- Inbank and overbank cases(for sinuosities 1.37 and 2.04)
- Main Channel Cross-Sections:
  - Trapezoidal section(for sinuosity 1.37)
  - Natural section(for sinuosities 1.37 and 2.0)

Floodplain Roughness:

- Smooth Case(for sinuosities 1.37 and 2.0)
- Floodplain Width Reduced but Smooth(for sinuosities 1.37 and 2.0)
- Fully Roughened(for sinuosities 1.37 and 2.0)
- Partially Roughened(for sinuosities 1.37)
- Floodplain with Pier Blocks(for sinuosities 1.37 and 2.0)

Floodplain Walled(for sinuosity 2.0)

The actual data from the S.E.R.C. flume Series B is shown. in Tabular form in Appendix I, giving detailed values of stage, discharge and temperature.

A distribution of 12 rods per square metre with each rod 25 mm diameter and spaced 315 mm apart(**Fig(3.4)** was used in the cases of fully or partially roughened floodplain. Fully details have already been given in Chapter 3, Section 3.2.1.

Fig(4.1) shows the S.E.R.C. flume Series B stage-discharge curves for both inbank and overbank cases, for sinuosities 1.37 and 2.0, and when the floodplains were smooth and fully roughened. Considering the inbank cases only the following points can be noted:

(i) The meander channel with sinuosity 1.37 with trapezoidal cross-section, presents higher conveyance than the natural case with same sinuosity. This is due to the greater area of the trapezoidal cross-section(40% greater) compared to the cross-sectional area of the natural meander channel.

(ii) Comparison of the conveyance of the two natural meander channels with different sinuosities shows a slight reduction in conveyance as the sinuosity increases.

These findings should be reviewed in the light of the Table given below with details of each inbank geometry.

Even though the main channel top widths are identical, the cross-sectional area of the trapezoidal channel is significantly greater than the natural channel, whereas the two natural channels at differing sinuosities have very similar cross-sectional areas.

Details of Main Channel Geometry

Shape	Sinuosity	Cross-Sectional Area m^2	Top Width m
trapez.	1.37	0.1575	1.2
nat.	1.37	0.0941	1.2
nat.	2.04	0.098	1.2

Concerning overbank flow regimes in **Fig (4.1)** the following general points can be made:

(i) Rough floodplain flows produce significantly less discharge than smooth floodplain flows. From **Fig (4.1)** the degree of flow reduction for rough cases increases with stage, reaching values of the order of 60-70% reduction compared to the smooth case.

(ii) An increase in sinuosity from 1.37 to 2.04 also reduces conveyance. This is particularly true in the smooth flood plain cases.

(iii) There is a different flow behaviour comparing trapezoidal and natural cross-sections, for the same value of sinuosity and flood plain smoothness. Comparing 1.37 NAT. SMOOTH with 1.37 TRAP. SMOOTH it is clear that up to stage 250.0 mm, the conveyance of the meandering channel with trapezoidal cross-section is slightly larger than the natural cross-section. However for stages higher than 250.00 mm, the stage-discharge curve of the natural case shows that its conveyance becomes greater than meandering channel with the trapezoidal cross-section. There are several possible reasons to explain this phenomenon. For depths smaller than 250.0 mm, the total conveyance of the meandering compound channel depends more on the contribution of the conveyance of the main channel. Because the trapezoidal cross-section has a 40% larger area than the natural cross-section, its conveyance is greater than the natural channel. Second, for stages higher than 250.00 mm, the floodplain streamlines are less affected by the main channel flow, and they become practically parallel with floodplain wall. In this case the trapezoidal cross-section, as evidenced by **Willetts and Hardwick(1990)**, produces more flow resistance than the natural cross-section. As well as this, an additional parameter, the aspect ratio(ratio between the main channel top width and the bankfull depth), may well influence the conveyance of meandering channels. The trapezoidal cross-section has an aspect ratio

(about 8.0) while than the aspect ratio of natural cross-section can reach as high as 13.0 at cross-over region, possibly producing some effects. This will be analysed in detail in section 4.5.

The effect of sinuosity, cross-section and floodplain roughness on the conveyance of the meandering channels of S.E.R.C. flume Series B (for the overbank case) was quantified as a percentage, considering the base for comparison as the discharge of the natural meander channel with sinuosity 1.37 and with smooth floodplains. The analysis, whose results are listed in **Table(4.1)**, was done for three different stages 200.00, 250.00 and 300.00 mm, respectively.

The results presented in **Table(4.1)** show that:

- As sinuosity increases from 1.37 to 2.04 and floodplain is smooth, the conveyance can be reduced by 20%; This effect diminishes with increases of stage.
- For a sinuosity of 1.37, if floodplain roughness is changed from the smooth case to the fully roughened case, the conveyance reduces significantly with the stage(the reduction for stage 300.00 mm was 65%).
- The trapezoidal cross-section, for stages less than 250.00 mm conveys more discharge than the natural cross-section; however, for stage 300.00 mm, the trapezoidal cross-section reduces the conveyance by 5%, in relation with the natural cross-section.
- Both roughened cases, for stages greater than 200.00 mm, exhibit similar results on the reduction of the conveyance.

Fig(4.2) shows the effect of five different kinds of obstacles placed on floodplain, on the stage-discharge curve for the overbank case of the natural meandering channel with sinuosity 1.37. The layout of these obstacles has been sketched in **Fig (3.3)** to **Fig (3.8)**. There is a substantial reduction on the capacity of the meandering compound channels as the floodplain roughness increases from smooth floodplain, floodplain with bridge piers, partly roughened floodplain, floodplain width reduced and smooth and finally, fully roughened floodplain.

Fig(4.3) shows the effect of five kinds of obstacles placed

on floodplain, on the stage-discharge curve for overbank case of the natural meandering channel with sinuosity 2.04. There is again a substantial reduction on the capacity of the meandering compound channel flow, as the floodplain roughness increases from smooth floodplain, floodplain with bridge piers, floodplain width reduced and smooth, fully roughened floodplain, and finally the floodplain with transverse walls. The conveyance of the bridge piers case and the floodplain width reduced case are practically the same. The case of walled floodplain shows a substantial reduction on the conveyance in comparison with the case of fully roughened floodplain. Thus it is expected that road embankments crossing river valleys will reduce significantly the discharge capacity of the meandering compound channel.

The effect of the different kind of obstacles placed on the floodplain of both meanders of S.E.R.C. flume Series B was quantified and expressed as a percentage, considering the base for comparison as discharge for the stage 250.00 mm of the meandering channel with sinuosity 1.37 and smooth floodplains. The results, presented in **Table(4.2)** show that:

- The bridge piers of the sinuosity 2.04 produce more effect in reducing the conveyance than the ones placed in the sinuosity 1.37.
- The two floodplain width reduced cases can not be compared directly because the meander belt width in both sinuosities is different.
- For sinuosity 1.37, the conveyance reduces significantly(26%) between the cases of partly roughened floodplain and fully roughened floodplain.
- For sinuosity 2.04, the floodplain wall introduces a great constriction to the flow(for example, for stage 250.0 mm the reduction reaches almost 90%), when compared with the smooth case.

The stage-discharge data from S.E.R.C. flume Series B are enclosed in **Appendix I**.

4.3 FLOW RESISTANCE IN MEANDERING COMPOUND CHANNELS

4.3.1. Approximate Friction Factors

The interpretation of the behaviour of the stage-discharge curves in open channel flows is often carried out through the analysis of the flow resistance coefficients. In this work the method of analysis of the flow resistance will be based on the determination of the resistance coefficient Manning's n with stage as well as and the Darcy-Weisbach friction factor with the Reynolds Number. For uniform flow the Manning's n resistance coefficient is expressed as

$$n = \frac{A\, R^{2/3} \sqrt{So}}{Q} \qquad (4.1)$$

where, A is the total cross-section area(which is equal to the sum of the main channel and floodplain areas), R is the hydraulic radius, So is the bed slope and Q is the discharge. The Darcy-Weisbach friction factor is expressed as,

$$f = \frac{A^2 8g\, R\, So}{Q^2} = \frac{8gRS_o}{V^2} \qquad (4.2)$$

Both resistance coefficients were calculated at the bend apex section of each meander studied, and the main channel and floodplain constitute a single unit. A problem arises immediately in the application of **Equations (4.1)** and **(4.2)** to meandering compound flow. The value of the bed slope S_0 is different from main channel to floodplain. Which bed slope is applied to which part of the flow, during overbank flow ? Clearly sub-division methods are required with resistance coefficients calculated for each sub-section of the flow. This will be discussed later. For the meantime it was decided to use the floodplain slope only in the determination of n and f, so that all the flow was assumed to have this slope. This means that the calculated resistance coefficients should be treated only as a rough guide until more sophisticated methods are discussed.

The other problem with **Equations (4.1)** and **(4.2)** applied to overbank flow is the definition of hydraulic radius R. Clearly at very shallow floodplain flow depths, the value of R(=A/P) suddenly decreases giving artificially low values of both Manning's 'n' and Darcy Weisbach, f.

With these restrictions in mind we may now turn to the results for the Series B S.E.R.C. flume.

Fig(4.4) shows the variation of Manning's n coefficient with depth (linear scale), for the following test conditions:

- Inbank and overbank cases(for both sinuosities)
- Trapezoidal cross-section(only for sinuosity 1.37)
- Natural cross-section (for both sinuosities)
- Smooth and fully roughened floodplain(for both sinuosities)

The following points may be noted from **Fig(4.4)** :

Inbank Case:

- As depth increases, Manning's 'n' tends to be constant.
- As sinuosity varies between 1.37 to 2.04, Manning's n increases approximately 14%. This is the result of the increase of the strength of the secondary currents.
- For low depths, the natural section with sinuosity 1.37 shows very high values of Manning's 'n', produced by the riffles and pools; as depth increases the Manning's n reduces below the values of the trapezoidal section.
- The Manning's n, calculated for the meandering channels with sinuosities 1.37 and 2.04, was 0.0115 and 0.0135 respectively. This includes the effects of skin friction and secondary flow; in Series A with the straight trapezoidal channel, the Manning's n value produced only by skin friction was about 0.01.
- For low depths the Manning's n value of the meandering channel with trapezoidal section was 0.01, behaving practically like a straight channel.

Overbank Flow:

- As the depth increases, the Manning's n of the smooth floodplain cases tend to be constant, while the Manning's n of the fully roughened floodplain cases increase with depth. The

latter is a function of the type of rod elements used for boundary roughness.

- Manning's n increases 25% as sinuosity changes from 1.37 to 2.04 for smooth floodplains, and by 55% for rough floodplains.
- Manning's n increases substantially with floodplain roughness. For example, for sinuosity 2.04, the Manning's n increases 63% at stage 200.0 mm, compared with the smooth case.
- Manning's n of the trapezoidal section is slightly larger than the one of the natural meander channel.
- The Manning's n for an overbank case, includes bed friction and additional losses produced by the lateral shear, secondary flow, horizontal shear and additional friction introduced by the floodplain roughness. These will be discussed in more detail later in the chapter.

Fig(4.5) and **Fig(4.6)** shows the effect of several different kinds of obstructions placed on the floodplain, on the variation of Manning's n coefficient with depth. On both figures, in the cases of smooth floodplain, floodplain width reduced and the floodplain with bridge piers, the Manning's n coefficient becomes almost constant with depth. In the other cases of the floodplain fully roughened, the partially roughened floodplain and the floodplain with transverse walls, the Manning's n coefficient increases substantially with the depth, even at a relative depth of 0.5 or stage 300 mm. This brings into question the use of vertical rods for floodplain roughness. In nature they would only represent trees, but not vegetation, weeds, grass and hedges which will bend in floodplain flows and in fact become submerged. The Darcy-Weisbach friction factor is plotted against the Reynolds number in **Fig(4.7(a))** and in **Fig(4.7(b)**, for the inbank and overbank cases and for the smooth and fully roughened floodplain cases of S.E.R.C. Series B.

Fig(4.7(a)) compares friction factors for inbank and overbank flows for smooth floodplain only. For inbank flows, friction factors tend to be almost constant with Reynolds Number, as the stage increases.

- Friction factor increases with sinuosity. For instance, as

sinuosity varies between 1.37 and 2.04, friction factors increase approximately 40%.

- Inbank flow friction factors are substantially less than those for overbank flow.
- For overbank flow, as sinuosity increases from 1.37 to 2.04, the friction factor may rise by 50%, for the smooth floodplain case.

Fig(4.7b) compares friction factors for smooth and rough cases for overbank flow only.

- As floodplain roughness changes from the smooth case to the fully roughened floodplain case, the friction factor increases dramatically.
- In both sinuosities, it was verified that: when the floodplain is smooth, the Darcy-Weisbach friction factor reduces with increasing of the Reynolds number; when the floodplain is fully roughened, the Darcy-Weisbach increases almost linearly with the Reynolds number. It is speculated that real floodplain behaviour will lie somewhere between these two extremes.
- The fully roughened case of the natural meandering channel with sinuosity 1.37 shows that for higher Reynolds numbers, the friction factors will eventually be greater than the ones of the meandering channel with sinuosity 2.0. For higher stages, the channel behaves like a single unit with a large rectangular cross-section. In this case, the loss of energy introduced by the main channel is very small in comparison with the loss produced by the floodplain roughness. Because the meander channel with sinuosity 2.0 has a roughened area smaller than the meandering channel with sinuosity 1.37, the friction factors will ultimately tend to be smaller for sinuosity 2.04.

Fig(4.8) and **Fig(4.9)** for sinuosities 1.37 and 2.04 respectively, show the effect of different types of floodplain obstructions on the variation of the Darcy-Weisbach friction factor with the Reynolds number. The test conditions were previously described in section 4.2. In **Fig(4.8)**, in the case of the floodplain with bridge piers, the friction factor is practically constant with the Reynolds number, defining a transition between the smooth floodplain case and the fully

roughened floodplain case. In **Fig(4.9)** the case of transverse floodplain wall shows very high values of friction factors. Thus it is predicted that river valleys crossed by road embankments, will produce great reductions in river conveyance. **Fig(4.8)** shows the appearance of a large gap between the friction factors of the cases of the fully roughened floodplain and the floodplain partly roughened. It seems that large energy losses occur outside of the meander belt in the fully roughened case.

Comparison between the results of the straight (Series A), the skew (Series A) and the meandering compound channel of S.E.R.C. Flume Series B are shown in **Fig(4.10)** in terms of the variation of the Darcy-Weisbach friction factor with the Reynolds number. The comparison is applied to an overbank case with smooth floodplain and the main channel with trapezoidal cross-section. **Table(4.3)** lists the geometric parameters of the straight and of the skew compound channel of S.E.R.C. flume Series A used in this comparative study. **Fig(4.10)** shows that as sinuosity rises from 1.0 to 1.37, the friction factor may increase 70%-100% although the size of the trapezoidal cross section of the main channel of S.E.R.C. Flume Series A and B were not exactly the same, as noted in **Table(4.3)**.

A similar effect is noted in **Fig(4.11)** for the case of the fully roughened floodplain. In both the Series A and B data there is a large increase in friction factor with Reynolds Number, as well as a large increase in friction factor comparing straight with sinuous. **Table(4.4)** lists the geometric parameters of the straight and of the skew compound channel of S.E.R.C. flume Series A used in this comparative study. The floodplain was roughened with 25.00 mm diameter rods with a triangular distribution, having a density of 12 per m^2 which was exactly the same as Series B tests.

Fig(4.8) has shown already the existence of a large gap between the friction factors of the fully roughened floodplain case and the one in which the floodplain was partly roughened at the limits of the meander belt width. The reason for this may be partly bound up in the original definition of bed slope and hence

friction factor; but it may also be partly explained with reference to **Fig(4.12)**. In this figure, the fully roughened cases studied with both sinuosities in S.E.R.C. Series B tests, is also presented together with a case tested in S.E.R.C. Series A, for an inbank condition of the straight compound channel(bottom width 1.5 m; side slope 1:2), in which the rod frames were placed inside the main channel. These rods roughness frames used in S.E.R.C. Series A had the same diameter and the same density distribution as the ones applied on the floodplain of Series B. The first conclusion is that the Series B cases with floodplain fully roughened are much nearer the inbank case of Series A with the main channel fully roughened than the other cases investigated in Series B. It seems that the flow resistance in Series B with floodplain fully roughened are highly influenced by the friction introduced by the rod frames placed outside the meander belt. This is apparently the reason that explains the large difference between the case of the floodplain partly roughened and the case of the floodplain fully roughened. **Fig(4.12)** shows also for the same Reynolds Number, the friction factors of the inbank case are: larger than the ones produced by sinuosity 1.37; smaller at the beginning and become again larger for higher Reynolds number than ones produced by sinuosity 2.04. The conclusion is that the friction effect, introduced by the sinuosity 1.37, is smaller than a case of a straight fully roughened channel. In relation to the meandering channel with sinuosity 2.04, the friction factors, for low depths on the floodplain, is dominated by the effect of sinuosity, in comparison with the case of a straight fully roughened channel; for higher stages, the meandering compound channel with 2.04 sinuosity and fully roughened will exhibit smaller friction factors than a fully roughened straight channel with same cross-section.

Another parameter that may affect the flow resistance of meandering compound channels is the ratio of the meander belt width(W_m) to the total channel width(W_t). Based on data from S.E.R.C. flume Series B and U.S. Army Corps of Engineers(1956),

an analysis of the effect of the ratio W_m/W_t on the flow resistance(expressed through the relationship between the Darcy-Weisbach friction factor and the Reynolds number) was carried out.

The best way to compare the effect of changing W_m/W_t is to consider data for one sinuosity where the only change has been to move the floodplain walls in, to the edge of the meander belt width. This was done for the smooth case at sinuosity 1.37, with W_m/W_t ratios below

S.E.R.C. Series B Floodplain Fully Roughened

Sinuosity	Total Channel Width m	Meander Belt Width m	W_m/W_t
1.37	10.0	6.1	0.61
1.37	6.1	6.1	1.0

Fig(4.13a) shows that the flow resistance tends to be approximately the same for both ratios W_m/W_t. This means that the flow resistance of meandering compound channels with smooth boundaries is practically not affected by the ratio W_m/W_t.

The analysis of the effect of the ratio W_m/W_t on the flow resistance of meandering compound channels was also carried out from data of U.S. Army Corps of Engineers(1956). The analysis was performed for meandering compound channels with sinuosities 1.33 and 1.57 both smooth and fully roughened floodplains. The geometric characteristics of the meandering compound channels were:

Sinuosity 1.33 and Floodplain Smooth

Total Channel Width m	Meander Belt Width m	Main Channel Top Width m	W_m'/W_t
4.88	3.05	0.457	0.63
9.1	3.05	0.457	0.33

- In the smooth case above, the floodplain roughness was brushed concrete with Manning's n approximately 0.012.

Details of the rough case are given below.

Sinuosity 1.57 and Floodplain Roughened

Total Channel Width m	Meander Belt Width m	Main Channel Top Width m	W_m/W_t
4.88	4.42	0.762	0.91
9.1	4.41	0.762	0.48

- The artificial roughness placed on the floodplain was reproduced through expanded metal with long dimension normal to the flow. The artificial roughness used is commercially designated as "Diamond Metal Lath, Wheeling 2.5 Bantam" with a quoted Manning's n approximately 0.025.
- The bed slope of the floodplain was $1*10^{-3}$, for both sinuosities.

The flow resistance was expressed in terms of the relationship between the Darcy-Weisbach friction factor against the Reynolds number. The calculation procedure followed was the same as the one adopted for the S.E.R.C. flume Series B. The results are plotted in **Fig(4.13b)**. This figure shows that for both smooth and fully roughened floodplain cases, the flow resistance reduces very slightly, as the ratio W_m/W_t diminishes. This confirms the previous findings of the S.E.R.C. flume Series B.

Another interesting finding of **Fig(4.13)** is the way the Darcy-Weisbach friction varies with the Reynolds number when the floodplain is fully roughened. These results show the Darcy-Weisbach friction factor reducing with the increase of the Reynolds number, whereas in the S.E.R.C. flume with vertical rod roughening the opposite occurs. A possible explanation for this different behaviour can be ascribed to the type of roughness used in both cases. In S.E.R.C. flume Series B the roughness was reproduced by vertical rod elements with 25.00 mm diameter, triangular distribution spacing 315.0 mm and always piercing the water surface. In U.S. Army Corps of Engineers(1956) case, the roughness was simulated through a metal mesh which was always submerged.

4.3.2. Refined Friction Factors

The flow behaviour in meandering compound channels, as previously noted, is highly three-dimensional. Therefore the calculation of the friction factor assuming a single section, is a simplified approach to a complex phenomenon. Another simplification of the above approach was, to assume in the calculation of the friction factor that the bed slope, So, was the floodplain slope. For inbank flows the bed slope was taken as the floodplain slope divided by the sinuosity. Even for inbank flows this assumption considered for the main channel region could not be true in the case of the natural cross section, because the cross-section geometry is changing longitudinally and transversely, and bottom slope is not necessarily the floodplain slope divided by sinuosity. In fact the main channel slope locally is sometimes adverse. In order to take into consideration the three-dimensionality of the flow, it was considered important to investigate the spatial variation of the Darcy-Weisbach friction factor in the main channel and on the floodplain regions of the meandering channels tested in S.E.R.C. flume Series B.

In order to calculate the local value of the friction factor, it is necessary first to introduce the expression that describes the boundary shear stress τ_0 exerted on a bed and banks of a straight open channel,

$$\tau_0 = R\ \rho\ g\ So \qquad (4.3)$$

Expressing the above equation in terms of g So and replacing these terms in equation (4.2), gives

$$f = \frac{8\ \tau_0}{\rho\ U^2} \qquad (4.4)$$

which is the equation that enables a calculation of the local value of the friction factor as a function of the boundary shear stress(τ_0) and of the depth averaged streamwise velocity(U). Equation (4.4) reveals that friction factor will be maximum where the depth averaged velocity reaches its minimum and the boundary shear reaches its maximum.

In order to calculate the local value of the friction factor it was necessary to determine first the values of the depth averaged velocity and the boundary shear stress at a particular vertical slice. As described in **Chapter 3**, measurements of flow velocities, stream angles and boundary shear stress were carried out in a grid that covered both the main channel and the floodplain region. In particular the boundary shear stress was measured by Preston tube in the local streamwise direction in the main channel and in the longitudinal direction on the floodplain. The steps followed in the calculation of the local value of the friction factor were to determine in each vertical the depth averaged velocity in streamwise direction in the main channel and in the longitudinal direction on the floodplain. Second, the measured shear stress was combined with depth-averaged velocity and the local value of the friction factor was obtained. From these values, contour levels of friction factor were generated by appropriate software called **UNIMAP**. Contour levels of friction factors were obtained in the following conditions:

a - Inbank Depth 140.0 mm and natural cross section(for both sinuosities)
b - Overbank Depth 165.0 mm and natural cross section(for sinuosity 1.37)
c - Overbank Depth 200.0 mm and natural cross section(for both sinuosities)

Fig(4.14) and **Fig(4.15)** show the contour levels of friction factors of an inbank case for sinuosities 1.37 and 2.04 respectively. Both figures reveal that the highest values of friction factor are located near the inner bank of the bend, reaching a maximum at the downstream end of the bend. In both cases the maximum value of the friction factor was approximately 0.04.

The reasons for this distribution of friction factors with peaks at the start of the cross over region may be connected with flow separation (in plan) with its attendant additional energy losses, or because of the region of flow deceleration in that

area where the channel bed has a strong downward gradient from the plateau region at the bend apex. Alternatively it may be a function of the formulation $f = 8\tau_0 / \rho U^2$ which may be appropriate for a full cross-section of the flow but of less relevance at local points in the flow.

Fig(4.16) shows the contour levels of the friction factors of an overbank case with a depth of 165.0 mm, as outlined in (b) above. The contour levels are plotted only in the main channel region because boundary shear stress and velocity measurements were not carried out in the floodplain region for this particular test. This figure reveals that the high values of the friction factors are still located near the inner bank of the bend, but the maximum value is moved slightly upstream compared to the inbank case. The maximum value of the friction factor was increased in relation to the inbank case, reaching approximately 0.05. The general range of friction factors are also increased, denoting greater resistance to flow in the main channel even at shallow depths of overbank flow) compared with the inbank case.

Fig(4.17) and **Fig(4.18)** show the contour levels of the friction factors of an overbank case with a depth of 200.0 mm, for both sinuosities as outlined in (c) above. On both figures the pattern of contour levels of the friction factors is totally different in relation to the one that develops for an inbank situation. For sinuosity 1.37 the maximum friction factor is located on the right downstream floodplain, at the cross over region. For sinuosity 2.04, there is a high peak of the friction factor at the right bank of the middle section of the cross-over. The reason for such high peaks in friction factor at this location is undoubtedly connected with regions of large acceleration where main channel flow "pours over" unto the floodplain. At this point the slope of the energy line is very steep in the longitudinal direction producing high values of $\rho g R S_f$ the local shear stress. In both cases the floodplain region, outside the influence of the area where the flow accelerates, exhibits a practically constant value of friction factor, being 0.02-0.025 for sinuosity 1.37 and 0.03 for

sinuosity 2.04.

4.4 BOUNDARY SHEAR STRESS DISTRIBUTION

The location of the maximum or the minimum values of the boundary shear stress in open channels will identify the zones where the flow will tend to cause erosion or deposition of sediments. Previous studies have shown that:

- In straight open channels with symmetric cross-section, the distribution of boundary shear tends to be symmetrical and reaches zero at the corners of the section, as the result of the presence of secondary currents(**Knight and Lai(1985)**).
- In the case of flow around a bend, the distribution of boundary shear stress is altered by the presence of secondary currents. At the bend entrance, the maximum values of boundary shear stress tend to be located near the inner bend. As the flow progresses downstream, the maximum value of boundary shear stress, as the result of the effect of secondary currents, moves gradually towards the outer bank(**Ippen and Drinker(1962)**.
- In a straight compound flow, **Knight(1991)**, the pattern of boundary shear stress is altered compared with an inbank case. As the result of momentum transfer from the main channel to the floodplain, the boundary shear stress reduces in the main channel in comparison with an inbank case, and increases in the floodplain region.
- In a meandering compound flow, both the bend and the cross-over regions, have enhanced strength of secondary currents, as pointed out by **Ervine and Jasem(1992)**). It is expected that these secondary currents will considerably affect the pattern of boundary shear stress, but there has not been until now, any studies on the effect of overbank flow on boundary shear stress distribution in meandering compound channels.

In the test program of S.E.R.C. Series B, the measurements of the boundary shear stress were carried out by the Preston tube in the streamwise direction in the main channel and in the

longitudinal direction in the smooth floodplain region. details of these measurements have been described in Chapter 3. Boundary shear measurements have been conducted for both sinuosities with natural cross section, for the following stages:

a) Inbank Case: Depth 140.0 mm
b) Overbank Case: Depth 165.0 mm
c) Overbank Case: Depth 200.0 mm

The Preston tube will give (at each grid point), the local value of the boundary shear stress. Based on these local values, contour levels were generated through software called **UNIMAP**.

Fig(4.19) and **Fig(4.20)** show the contours of boundary shear stress for the inbank case(a) for each sinuosity. On both figures the high values of boundary shear are located in opposite sides of the bend. For sinuosity 1.37, the high values are distributed along the inner bank of the bend, for sinuosity 2.0 they are located at the downstream end of the outer bend at the cross over section. For sinuosity 1.37 the maximum is reached approximately near the bend apex, while for the other sinuosity is at the cross-over section. The location of these high values of boundary shear are associated with the distribution of the highest velocities. This point will be discussed in **CHAPTER 5** during the analysis of the velocity distribution. It can be seen from **Fig (4.19)** and **Fig(4.20)** that the average values of shear stress are in the same region as an equivalent straight channel. Assuming a straight channel and considering the bed slopes of each sinuosity at the cross-over section, the boundary shear stress will be:

For sinuosity 1.37:

$$\tau_0 = \gamma\ h\ So = 10^4 * 0.079 * 0.996 * 10^{-3} * \cos 60^0 = 0.39\ N/m^2$$

For sinuosity 2.04:

$$\tau_0 = 10^4 * 0.079 * 1.02 * 10^{-3} * \cos 70^0 = 0.27\ N/m^2$$

Fig(4.21) and **Fig(4.22)** show the contours of boundary shear stress for overbank flow (stage 165 mm) and for both sinuosities. Both figures show a decrease of boundary shear stress in main

channel region compared with the inbank case. For sinuosity 1.37, in the main channel region, the high values are located near the inner bank of the bend and at the right bank of the cross-over. No values were available for the floodplain. For sinuosity 2.04, in the main channel region, the high values are located near the outer bank of the bend approximately 80-90 degrees downstream from the bend apex. For sinuosity 2.04, the maximum value of boundary shear is in fact located in the floodplain region, at the right bank, probably due to the effect of flow acceleration. At least 1/3 of the right floodplain is affected by the flow acceleration. Outside this region the distribution of the boundary shear is quite uniform(0.2 N/m^2) and similar to that which would occur in a straight channel.

Fig(4.23) and **Fig(4.24)** show the contours of boundary shear stress for the overbank flow, stage 200 mm and both sinuosities. Both figures show a reduction in the boundary shear stress value in the main channel region compared with the previous cases. For the meandering channel with sinuosity 2.04 in particular, a significant reduction in the boundary shear stress occurs compared with the values observed for the inbank case. This demonstrates that in meandering compound channels, as the flow goes from an inbank case to an overbank case, the main channel will start losing its capacity in carrying sediments downstream. As a result of this situation, the main channel will be a region where sediments will tend to deposit. **Fig(4.20)** and **Fig(4.22)** reveal also that the maximum boundary shear, as the result of flow acceleration, is located at the right floodplain at the edge of the main channel, at the downstream end of each bend. This area, where the high values of boundary shear were identified, extends from the main channel to the floodplain and could be subjected to scour and eventual migration of a meander.

4.5 PARAMETRIC ANALYSIS OF FLOW CONVEYANCE IN MEANDERING COMPOUND CHANNELS

4.5.1. Introduction

Assessment of discharge capacity in a compound channel is difficult, but even more so for a meandering compound channel. The difficulties are great because the relative influence of each parameter is unknown, and in meandering natural channels, the parameters extend to sinuosity, cross-sectional shape of the main channel, aspect ratio of the main channel, relative roughness between floodplain and main channel, relative width of meander belt to the full floodplain width, relative depth of flow on the floodplain, and so on. In this work, an investigation into the influence of each parameter is called, a parametric analysis. It is confined in the first instance to discharge assessment.

In the analysis it was decided to investigate only three non-dimensional terms for the discharge in a meandering compound flow. They are F_1 F_4 and F_5, and each one is a ratio of actual measured discharge to total computed discharge based on skin friction only.

F_1 = actual discharge/theoretical discharge for inbank flows

F_4 = actual discharge/theoretical discharge for overbank flows, with the theoretical discharge computed using imaginary vertical walls at the channel floodplain interface, using skin friction only.

F_5 = actual discharge/theoretical discharge for overbank flows, with the theoretical discharge computed by the **Ervine and Ellis(1987)** method, with a horizontal sub-division at bankfull level, and vertical sub-divisions at the edge of the meander belt width.

Because there is a range of other additional losses, apart from skin friction occurring in a meandering channel, the calculated value of discharge is always greater than the actual one, giving a ratio smaller than 1.0. Obviously in a straight inbank case of an open-channel, the value of those

functions will be near 1.0. As the flow becomes more heavily meandering, values of these functions depart further from unity because of a range of additional energy losses other than skin friction. Functions F_4 and F_5 were determined for the following cases: trapezoidal and natural sections; sinuosity 1.37 and 2.04; smooth and fully roughened floodplain. In the calculation of the theoretical discharge only skin friction was considered. **Fig(4.25)** illustrates the way that the floodplain and the main channel areas were split during the application of the division wall method for both smooth and rough floodplains.

As well as data from the S.E.R.C. flume, Series B data, this analysis of flow conveyance through the non-dimensional functions F_4 and F_5 also includes: data from S.E.R.C. flume Series A(straight and skew compound channels), whose geometric characteristics are listed in **Table(4.3)** and **Table(4.4)** as well as other experimental studies of meandering compound channels with smooth floodplains carried out worldwide, whose geometric characteristics are listed in **Table(4.5)**.

4.5.2 Computational Method for Inbank Function F_1

In the computation of the theoretical discharge, used in function F_1 the following assumptions were considered:

- The computation was performed at bend apex.
- The boundaries of the main channel were assumed smooth.
- The bed slope in the main channel was considered equal to the floodplain slope divided by the sinuosity.
- The turbulent resistance law for smooth boundaries applied in calculation of the loss of energy produced by skin friction was,

$$\frac{1}{\sqrt{f}} = 2.02 \log(Re \sqrt{f}) - 1.38 \qquad (4.5)$$

where f is the Darcy-Weisbach friction factor and Re is the Reynolds number. Equation **(4.5)** was derived by **Ackers(1991)**, from the results of the inbank case of a straight trapezoidal channel

of S.E.R.C. flume Series A. Considering these assumptions, the following method was adopted in the calculation of function F_1:

- By using equations 4.2 and 4.5 and through an iterative procedure, the friction factor, average velocity and discharge were calculated theoretically for a given stage.
- Function F_1 was calculated by dividing the actual discharge by the theoretical discharge.

4.5.3. Computational Method for Overbank Function F_4

As presented in **Fig(4.25)**, function F_4 was calculated at bend apex, for two different cases: in the first case, both main channel and floodplain were smooth; in the second case, the main channel was smooth and the floodplain was fully roughened. For smooth floodplain case, the procedure followed in the calculation of function F_4 was:

- By applying imaginary vertical walls(**Fig(4.25)**), at the edge of the main channel, the complete cross-section was divided in three main areas: main channel area; right floodplain area; and left floodplain area.
- For calculation of the main channel discharge the following assumptions were used:

. The bed slope was equal to the floodplain slope divided by the sinuosity.

. The friction factor applied was the one calculated by the method used for function F_1 at bankfull level.

. The wetted perimeter was the rigid boundary of the main channel up to bankfull level.

. The total area included the main channel area at bankfull level and the part above bankfull and limited by the vertical imaginary walls.

- Considering the above assumptions, the main channel discharge was computed by applying equation 4.2.
- By using equations 4.2 and 4.5 and applying an iterative procedure, the discharge of left floodplain for the smooth

floodplain case was calculated.
- By using a similar procedure the discharge for smooth case of the right floodplain was calculated, as well.
- The total theoretical discharge was equal to the sum of the main channel, left floodplain and right floodplain discharges.
- Dividing the actual discharge by the total theoretical discharge, function F_4 was obtained for the smooth floodplain case.

In order to calculate the friction loss introduced by the rod roughness elements used in the floodplains of the Series B tests, the **Author**, based on experimental data, has determined an empirical expression relating the Darcy-Weisbach friction factor with Reynolds number. The experimental data was obtained from S.E.R.C. Series A with frames identical to the ones used in Series B. The empirical relationship obtained was

$$\log f = -4.05 + 0.683 * \log Re \qquad (4.6)$$

This equation was determined by the application of the least squares method, with the correlation coefficient equal to 0.988, showing a very close level of agreement between the experimental and the calculated data. The experimental data and equation **(4.6)** are both plotted in **Fig(4.12)**. Once the turbulent equation was found, function F_4 for the fully roughened floodplain case was calculated in a similar way to the one described for the smooth case, the only difference being the application of equation 4.6 instead of equation 4.5.

Equation 4.6 represents the friction loss introduced by 25.0 mm rods with a density of 12.0 per m^2. Therefore it can not be used in any other circumstances. For general application, the **Author** recommends the equation devised by **Ackers(1991)** which determines the friction loss produced by any arrangement of rod elements.

4.5.4.. Computational Method for Overbank Function F_5

As shown in **Fig(4.25)**, function F_5 was also determined at bend apex for two cases namely the smooth and roughened floodplains. The method followed in the calculation of function F_5 was different. For the smooth floodplain case, the steps were the following:

- By applying imaginary vertical walls(**Fig(4.25)**) at the limits of the meander belt width and an imaginary horizontal plane at bankfull level, the complete cross-section was divided in four main areas: main channel area below bankfull; floodplain area inside of the meander belt and above bankfull level; right floodplain area; and left floodplain area. In regular meanders, which is the case in this research, the right and the left floodplain areas are equal.
- The main channel discharge at bankfull level was calculated by the method described for function F_1.
- A special procedure was adopted for the calculation of the discharge inside of the meander belt width above bankfull level:

. First, by considering only the meander belt area on the floodplains adjacent to the main channel and applying equations 4.2 and 4.5, the Darcy-Weisbach friction factor and the average velocity were calculated through an iterative procedure.

- Second, based in equation 4.1, the value of Manning's n resistance coefficient was calculated.
- Third, at this stage an additional equation was used for the calculation of the Manning's n parameter as a weighted averaged value across the total area inside the meander belt width, including both floodplains and flow above the main channel,

$$n = \left[\frac{\sum_{m=1}^{M} P_m n_m^2}{P} \right]^{1/2} \qquad (4.7)$$

where M is the number of segments across the section, the m^{th} segment having length P_m and roughness n_m. Equation **(4.7)** was

deduced by **Pavlovskii(1931)**, **Michhofer(1933)** and **Einstein and Banks(1950)** assuming that the total force resisting the flow was equal to the sum of the forces developed in the vertical subsections above the segments. In this particular case, some assumptions were considered in the calculation of the Manning's n as a composite roughness coefficient. P, the total perimeter, is the meander belt width less the main channel top width; the Manning's n of the main channel area above bankfull was assumed as zero; the only Manning's n considered in the calculation was the one determined for the floodplains within the meander belt region. The results applying **Equation (4.7)** is a composite Manning's 'n value for this region. The composite Manning's 'n was used to calculate the discharge inside the meander belt width.

- The discharge in each floodplain outside of the meander belt was calculated by a procedure similar to the one followed for function F_4.
- The total theoretical discharge was equal to the sum of the main channel discharge below bankfull, plus the meander belt discharge and plus the floodplain discharge outside of the meander belt.
- Function F_5 was obtained by dividing the actual discharge by the theoretical discharge.

4.5.5. Parametric Analysis of F_1 for Inbank Flows

A very brief analysis of inbank flow was carried out looking at the effect of cross-sectional shape of main channel, sinuosity, and comparison with other researchers.

It is clear that the amount the ratio F_1 is less than unity, is a measure of the degree of additional energy losses in inbank meandering flow. These losses are primarily due to bend losses not included in skin friction.

The effects of cross-section geometry and sinuosity on the inbank function F_1 plotted with depth ratio are shown in

Fig(4.26), and **Fig(4.27)**, for S.E.R.C. Series B data.

Fig(4.26) shows that for low depth ratios, the function F_1 of the trapezoidal cross-section is almost 1.0 which means that the meandering channel behaves like a straight channel. As the stage rises, the secondary currents start to develop and function F_1 diminishes. For instance, at depth ratio 0.8, 15% of losses of energy are produced probably by bend secondary currents. Comparing the effect of cross-section geometry, the same figure shows that, for low depth ratios, function F_1 of the natural cross-section is greater than the one obtained for the trapezoidal cross-section. This means that large losses of energy are occurring which are produced by the riffles and pools of the natural meandering channel. At depth ratio around 0.70, the function F_1 suddenly increases towards 1.0. This is a function of the sudden change of geometry at the bend apex when the main channel flow spreads on to a horizontal inner bend bar, when it behaves almost like compound flow within the main channel. At this point the hydraulic radius R is decreased, as its theoretical discharge.

As a general rule it is seen in **Fig (4.26)** that bend losses increase with stage up to bankfull level. This is to be expected as previous studies have shown bend losses to increase with Froude Number, which in this case increases up to bankfull level.

The effect of sinuosity is shown in **Fig(4.27)** for the case of sinuosities 1.37 and 2.04. As sinuosity rises from 1.37 to 2.04, the strength of secondary currents increases and energy losses may increase by 20%, as shown in **Fig(4.27)**.

The effect of sinuosity on inbank function F_1 was also determined for the small scale flumes of **Kiely(1988)** (sinuosity 1.25) and **Sooky(1967)** (sinuosity 1.13). The results are plotted in **Fig(4.28)** and are not very conclusive. This may be due to scale effects, to small inaccuracies in the measurements of water levels or discharge as the main channel was so small, or may be due to inaccurate estimates of friction factor for calculation of the theoretical discharge.

4.5.6. Parametric Analysis of F_4 for Overbank Flows

The function F_4 is for overbank flows and is based on a very simple vertical wall sub-division method. Again, the degree the function F_4 lies below unity, is a measure of the additional losses in the system other than skin friction.

Fig(4.29) to **Fig(4.32)** show the variation of function F_4 with depth ratio for overbank case of S.E.R.C. data, Series B tests.

Fig(4.29) presents the effect of the cross-section geometry on the variation of the function F_4 with the depth ratio. The study was done for sinuosity 1.37. It can be seen that the trapezoidal cross-section shows 10% lower values of function F_4 than the natural cross-section. This means additional energy losses produced by the trapezoidal cross-section compared with the natural cross section. This may be due to first, the smaller aspect ratio(ratio of top width of main channel divided by the bankfull depth) of the trapezoidal cross-section compared with the natural cross-section or it may be that the natural cross-section itself, as mentioned by **Willetts(1990)**, tends to disturb the flow less than the trapezoidal cross-section.

Fig(4.30) shows the effect of floodplain roughness on the variation of function F_4. The study was carried out for a meandering channel with sinuosity 1.37. It can be seen that by increasing the floodplain roughness dramatically, the function F_4 reduces only by 5%. In both cases function F_4 increases with depth ratio. For depth ratio of 0.5, 20% of total losses are produced by additional energy losses, but at depth ratio 0.1, 35% of losses are due to something other than skin friction.

Fig(4.31) shows the effect of sinuosity on the function F_4 when the floodplain is smooth. It is evident that by increasing sinuosity from 1.37 to 2.04, the function F_4 diminishes by about 15%. This means that the loss of energy produced by additional losses increases with sinuosity. It is clear that for depth ratio 0.1 at sinuosity 2.04, additional losses can make up 50% of the total, showing that bed friction is only one half of the total

losses.

Fig(4.32) shows the effect of sinuosity on the function F_4 when the floodplain is roughened. On both sinuosities function F_4 increases with depth ratio. For instance, for the depth ratio equal 0.4, 80% of total losses are produced by skin friction and friction induced by the rods whereas at depth ratio 0.1 this reduces to 50%-60%.

4.5.7. Parametric Analysis of F_5 for Overbank Flows

The function F_5 is based on a horizontal sub-division at bankfull level and vertical sub-division at the edge of the meander belt width.

Fig(4.33) to **Fig(4.36)** show the variation of function F_5 with depth ratio for overbank case of S.E.R.C. data, Series B tests.

Fig(4.33) shows the effect of the cross-section geometry on the variation of the function F_5 with the depth ratio. The study was carried out for sinuosity 1.37. It can be seen that function F_5 is similar to F_4 with the trapezoidal section producing greater energy losses apart from skin friction, as already discovered.

Fig(4.34) shows the effect of floodplain roughness on the variation of function F_5. The study was carried out for a meandering channel with sinuosity 1.37. It can be seen that with increasing flow depth ratio, function F_5 for the smooth case reduces slightly, while the same function for the roughened floodplain increases, reaching almost unity at higher flow depth ratio. This means that for a fully roughened floodplain case, for depth ratios greater than 0.4, the meandering compound channel behaves almost like a straight channel, with the skin friction losses and the losses induced by the rods producing 95% of total energy losses.

Comparing the F_4 Function on **Fig (4.32)** and the F_5 Function on **Fig (4.34)** for the same cases of sinuosity 1.37, and a

roughened floodplain, also reveals that F_5 is a much better measure, with its horizontal sub-division at bankfull level.

Fig(4.35) shows the effect of sinuosity in function F_5 when the floodplain is smooth. The conclusions are similar to that already presented to the corresponding function F_4, with the greater sinuosity producing a larger proportion of non-bed friction energy losses.

Fig(4.36) shows the effect of sinuosity with function F_5 when the floodplain is roughened. Here function F_5 tends to increase with depth ratio for both sinuosities. For higher stages both functions F_5 approach the value 1.0. With the increase of sinuosity function F_5 tends to increase slightly with depth ratio, but for depth ratios greater than 0.5, function F_5 is not affected by sinuosity.

From the results of F_4 and F_5 presented so far it seems that:

- Function F_4 shows more sensitivity to the effect of geometry of the main channel cross-section with smooth floodplains than function F_5.
- Both functions present identical behaviour for the effect of sinuosity when the floodplains were smooth.
- Function F_5 represents better the flow behaviour for the roughened floodplain case than function F_4.

4.5.8. Comparison with other Studies

Comparison of S.E.R.C. Series A(the skew and the straight compound channel), S.E.R.C. Series B(the meandering compound channel) and other world wide experimental studies on meandering compound channels was performed in terms of function F_4 and F_5.

Fig(4.37) and **Fig(4.38)** show the comparison of the functions F_4 and F_5 for the straight and skewed compound channel of S.E.R.C. Series A with the meandering compound channel with sinuosity 1.37 of S.E.R.C. Series B. In all flumes the floodplain was smooth and the main channel cross-section was trapezoidal.

Table(4.3) lists the geometric parameters of the Series A data used in this comparative study. Both figures show an increase in the functions F_4 and F_5 as the channel moves towards unity from meandering to skewed and to straight. Meandering channels have much more extensive non-friction energy losses. However the pattern of functions F_4 and F_5 of the straight and the skew compound channel is different. **Fig(4.37)** shows the function F_4 of the straight and the skew compound channel increasing with the depth ratio, while **Fig(4.38)** reveals the opposite. It is clear therefore that the F_4 function is much more appropriate for smooth floodplains than F_5. This is easily demonstrated in the case of the straight compound channel. As the depth ratio increases, the lateral shear stress that develops as the result of the gradient of velocities between the deeper main channel and the shallower floodplain should diminish. Therefore both functions should tend to value 1.0. However this happens only with function F_4. we may conclude that F_4 is suitable for smooth floodplain cases and F_5 for rough floodplain cases.

Fig(4.39) and **Fig(4.40)** shows the effect of sinuosity on the variation of functions F_4 and F_5 with data obtained from U.S.Army Corps of Engineers in two meandering channels with smooth floodplains. Both figures reveal that as sinuosity increases from 1.2 to 1.57 may produce a reduction of 15% in both functions. This data should be treated with some caution because of uncertainty over the value of Manning's 'n' value with depth.

Five different sets of data, obtained from other experimental studies in compound channels, and in small flumes with a range of sinuosities varying between 1.0 and 2.0 and with smooth floodplains are plotted in **Figs (4.41)** and **(4.42)**. Functions F_4 and F_5 were again calculated in relation to the depth ratio. These results are plotted, for function F_4, in **Fig(4.41)** and for function F_5, in **Fig(4.42)**. Again the significant reduction of function F_4 and F_5 with the increase of sinuosity is evident. For instance as sinuosity increases from 1.0 to 2.0, both functions reduce approximately 50% for higher depth ratios. Another interesting aspect of both figures is the

way both functions behave with depth ratio. For instance function F_4 shows that, for the skew and for the meander channels with sinuosities 1.13 and 1.25, F_4 increases with the depth ratio. The same function for meandering channels with sinuosities 1.41 and 2.06 increases slightly until a depth ratio around 0.3 and then starts to reduce. On the other hand, function F_5 shows that: for the skew channel it is almost constant with depth ratio, at least until a depth ratio around 0.3.

It should be noted that the data used in **Figs(4.41)** and **(4.42)** is for smaller scale model studies where the data of **Kiely**, **Sooky** and **Jasem** is for rectangular channels and that of **Willetts** for trapezoidal channels. In all cases the aspect ratio of the main channel is less than 3.5, which is a significant departure from the S.E.R.C. flume data with aspect ratios in the range 8 to 13.

The effect of sinuosity on the functions F_4 and F_5 for roughened floodplains is shown in **Figs(4.43)** and **(4.44)** comparing the skewed and straight compound channel of S.E.R.C. Series A with the meandering compound channel with sinuosity 1.37 of S.E.R.C. Series B. The results are plotted in **Fig(4.43)**, for function F_4 and in **Fig(4.44)**, for function F_5. Functions F_4 and F_5 show a different behaviour for the straight and the skew cases. Function F_4 for the straight and for the skew compound channel reduces with an increase in the depth ratio again showing F_4 to be unsuitable for rough floodplains, while function F_5 for the same cases is approximately 1.0. This confirms that function F_5 represents the fully roughened floodplain cases much better than function F_4.

Fig(4.45) is very interesting in the way it accurately predicts the discharge in the straight and 5.1^{o} skew Series A channels. This is because these channels are dominated by rod friction and bed friction with lateral shear a small component. Hence the horizontal sub-division method used in F_5 is most suitable.

In the Series B meandering data, the F_5 Function is still very suitable, but this time, additional energy losses other than

rod roughness and bed friction are apparent, with values up to 30% of the total energy loss.

Figs(4.45) and **(4.46)** investigate the effect of the aspect ratio of the main channel, which is defined as being the ratio of the top width of the main channel cross-section divided by the bankfull depth. Here, the study of the effect of aspect ratio on the conveyance of meandering channels will be done for meanders with same sinuosity. **Willetts and Hardwick(1990)** have carried out experiments in a small flume with meandering channels whose sinuosities were 1.41 and 2.06 which were almost identical to the ones tested in S.E.R.C. Series B. The difference between **Willetts and Hardwick(1990)** experimental data and data from S.E.R.C. Series B, smooth case was that the former were carried out at main channel aspect ratio 3.5 and the later at aspect ratio 8 to 13.6.

The effect of three aspect ratios in the variation of function F_4 with depth ratio are presented in **Fig(4.45)**, for sinuosity 1.37, and in **Fig(4.46)**, for sinuosity 2.04 both with smooth floodplains. The same analysis for function F_5 is shown in **Fig(4.47)** and **Fig(4.48)**. In all cases the reduction in the aspect ratio from 3.5 to 13.6 produces a decrease in function F_4 and F_5 between 15%-20%. Therefore in meandering channels with same sinuosity, geometry and roughness will produce smaller non-friction energy losses as the aspect ratio increases. These additional energy losses are produced by secondary currents. expansion-contraction phenomena and lateral shear and are therefore exaggerated in typical model studies with smaller aspect ratio. As the aspect ratio increases, the strength of these flow mechanisms will tend to diminish and subsequently additional energy loss reduces.

4.5.9. Summary of the Parametric Analysis

The results of this chapter thus far indicated that conveyance of meandering compound flows is a complex phenomenon

influenced by a range of parameters summarised below:

(i) The relative depth of flow (floodplain depth/main channel depth) obviously has an important influence on conveyance;.

(ii) The relative boundary roughness between main channel and floodplain is important.

(iii) The sinuosity of the main channel is very significant (this may also be characterised by the cross-over angle from one bend to the next).

(vi) The shape of the main channel (trapezoidal or natural) has an effect.

(v) The aspect ratio of the main channel (width/depth) has also proved to be significant.

(vi) The ratio of the meander belt width to the total width is also significant.

It is clear therefore that one possible approach in modelling the conveyance of such a complex system is by investigating the influence of each parameter above, and producing empirical best fit relationships in the manner of the Ackers (1991) Report for the Series A data. This approach is clearly outwits the scope of this thesis, but a first step has been taken in this chapter.

As a further step along this path, the author has investigated sinuosity, main channel aspect ratio, as well as the meander belt width/total width ratio, and included further details below.

Sinuosity effect

This parametric analysis has already demonstrated that sinuosity considerably affects the conveyance of meandering channels. In order to emphasize the importance of this parameter, two new set of graphs were prepared which show the variation of functions F_4 and F_5 with sinuosity maintaining constant flow depth ratio. **Fig(4.49)** and **Fig(4.50)** show the effect of sinuosity on functions F_4 and F_5, for the smooth floodplain case, and **Figs(4.51)** and **(4.52)** show the effect for the roughened

floodplain case. The data used in these plots was taken from S.E.R.C. Series A(the straight channel) and from S.E.R.C. Series B.

For smooth floodplains, the variation of sinuosity with function F_4, with flow depth ratio (Dr)is shown in **Fig(4.49)**. In the same test conditions, function F_5 is presented in **Fig(4.50)**. Both figures reveal that with increase of sinuosity from 1.0 to 2.1, function F_4 and function F_5 decrease by above 40% for the depth ratio of 0.10. However, as the depth ratio increases, sinuosity has less effect on both functions. For instance, for depth ratio of 0.40, the reduction on both functions varies between 20%-30%).

For roughened floodplains, the variation of sinuosity with function F_4, is shown in **Fig(4.51)**. For the same test conditions, function F_5 is presented in **Fig(4.52)**. **Fig(4.51)** reveals that for depth ratio equal to 0.10, function F_4 reduces with sinuosity as before for depth ratio greater than 0.3 function F_4 is practically not affected by sinuosity. **Fig(4.52)** shows that for low depth ratios, function F_5 reduces with sinuosity but as the depth ratio increases, sinuosity affect less and less function F_5. For depth ratios greater than 0.4, function F_5 is practically not affected by the sinuosity, reaching a value that is near 1.0.

Effect of Aspect Ratio

The variation of function F_4 with the aspect ratio, is shown in **Fig(4.53)**, for sinuosity 1.4 and smooth floodplains, in **Fig(4.54)**, for sinuosity 2.0 with smooth floodplains. For the same test conditions, **Fig(4.55)** and **Fig(4.56)** show the variation of function F_5 with aspect ratio for sinuosities 1.4 and 2.0, and again for smooth floodplains. In all four figures the pattern of the aspect ratio variation with function F_4 or function F_5 is similar although the graphs are somewhat tentative. An increase of aspect ratio is accompanied by an increase of both functions. However, the effect of the aspect ratio in both functions becomes more significant, as the depth ratio increases. For instance, for sinuosity 1.4, a variation of the aspect ratio between 3 and 15.0

will produce an increase of 5-10% in function F_4 for a depth ratio of 0.10, and an increase in the same function of 20%, for the depth ratio of 0.40. These graphs do illustrate that smaller scale model studies with low aspect ratio of the main channel exaggerate the energy losses that occur in real rivers with meandering compound flow.

Effect of the meander belt width

An other important parameter is the effect of the meander belt width(W_m) to the total floodway width(W_t) ratio. The ratio W_m/W_t will reach a maximum value 1.0 when the floodplain walls are located at the edge of meander belt. In the S.E.R.C. flume Series B with smooth floodplains, two test runs were carried out. In the first test run the total width of channel was 10.0 metres and the meander belt width was 6.1 m for sinuosity 1.37 and 8.6 m for sinuosity 2.04, giving ratios of Wm/Wt equal to 0.61 and 0.86. In the second test run the floodplain walls were brought in to the edge of the meander belt width, giving a ratio of Wm/Wt equal to 1.0.

The analysis of the effect of the ratio Wm/Wt on the conveyance of meandering compound channels of the S.E.R.C. flume Series B was carried out using the variation of functions F_4 and F_5 with depth ratio. Only sinuosity 1.37 with natural cross-section is considered here, with results plotted in **Fig(4.56a)**, for function F_4 and in **Fig(4.56b)**, for function F_5.

Fig(4.56a) shows that as the ratio Wm/Wt decreases from 1.0 to 0.6, there is additional loss of energy reaching a maximum of 10%, at the depth ratio of 0.15, and becoming almost zero at depth ratio equal to 0.3. For a depth ratio greater than 0.3, both functions F_4 tend to the value 82%. This means that for depth ratios greater than 0.3, the ratio Wm/Wt does not affect the additional loss of energy.

Fig(4.56b) shows again that as the ratio Wm/Wt decreases from 1.0 to 0.6, an additional loss of energy occurs reaching a maximum of 10%, at the depth ratio of 15% and becoming almost

zero at depth ratio equal to 0.3. This phenomenon indicates a degree of interaction between outer floodplain flow (Zone 3) and inner floodplain flow (Zone 2).

The analysis of the effect of the ratio W_m/W_t on the flow conveyance of meandering compound channels was complemented with data provided by the **U.S. Army Corps of Engineers Study (1956)** which allows a study of both the smooth floodplain case and the fully roughened floodplain case. The geometric characteristics of the meandering compound channels of the **U.S. Army Corps of Engineers Study (1956)** used in this analysis were described in Section 4.3.1.

The results of the **U.S. Army Corps of Engineers Study (1956)** are plotted in **Fig(4.56c)** and **Fig(4.56d)**, for sinuosity 1.33 with smooth floodplains and for Wm/Wt equal to 0.33 and 0.63, and in **Fig(4.56e)** and **Fig(4.56d)**, for sinuosity 1.57 with fully roughened floodplains and for Wm/Wt equal to 0.5 and 0.9. All four graphs reveal that, as the ratio W_m/W_t reduces from 0.63 to 0.33, functions F_4 and F_5 tend to increase slightly between 5%-10%.

Comparing the findings of the smooth cases of the S.E.R.C. flume Series B with the **U.S. Army Corps of Engineers Study (1956)**, it can be observed that they do not agree. These discrepancies could be caused by scale effects, different main channel aspect ratios or measurement errors. The most likely error might concern the computation of the resistance coefficients for the U.S.Army Corps of Engineers data, where only one Manning's n value was specified which could not be relevant to all the flow depths it was applied to. This means that the functions F_4 and F_5 values on **Fig(4.56c)** to **Fig(4.56f)** may not be accurate, because of inaccurate skin friction estimates.

Another possibility concerns the interaction between Zone 3 and Zone 2 floodplain flows which is related to the Wm/Wt ratio. (see Page 409) At Wm/Wt=1 the interaction between Zones 2 and 3 is removed and hence conveyance can be increased. As Wm/Wt is reduced by moving floodplains further out, the Zone 2/Zone 3 interaction may reach a peak at a given Wm/Wt value and decrease thereafter.

Fig(4.56c) shows also that for sinuosity 1.33 with smooth floodplains, for depth ratios greater 0.4, both functions F_4 tend to the same value 82%, therefore becoming independent of the variation of the ration Wm/Wt, confirming the trend shown by the results of the S.E.R.C. flume.

Fig(4.56e) and **Fig(4.56f)** reveal that, for sinuosity 1.57 with roughened floodplains, as the ratio Wm/Wt varies from 0.5 to 0.9, the additional energy loss increases.

4.6 SEPARATION OF MAIN CHANNEL LOSSES AND FLOODPLAIN ENERGY LOSSES

The parametric analysis of the flow conveyance in meandering channels carried out through the functions F_4 and F_5, from data obtained in S.E.R.C. flume Series B, has shown that in some cases the energy losses produced by boundary friction were as low as 50% of the total energy loss. This emphasises the importance of the other energy losses that occur in meandering compound flows as noted by **Ervine and Ellis(1987)**. They identified that besides skin friction, the following additional energy losses will occur in meandering compound flows:

Horizontal shear around bankfull level
Secondary currents
Flow expansion losses
Flow Contraction losses
Lateral shear

These may be termed as additional non-friction energy losses.

Based on the measurements of flow velocities, stream line angles and flow depths, performed in S.E.R.C. flume Series B, it was possible to separate the main channel discharge from the floodplain discharge in the meandering compound channel. Based in the knowledge of these separate discharges, a method was developed by the **Author**, which allows to separate the additional non-friction energy losses that occur in the main

channel from the additional non-friction losses that occur on the floodplain region. The additional loss of energy that occurs in the main channel was expressed in terms of function F_4 or F_5 in the following way:

$$\text{Function } F_4 \text{ or } F_5 = \frac{\text{Main Channel Theoretical Discharge} - \text{Main Channel Actual Discharge}}{\text{Total Theoretical Discharge}}$$

The additional loss of energy that occurs on the floodplain was expressed in terms of functions F_4 or F_5 in a similar way,

$$\text{Function } F_4 \text{ or } F_5 = \frac{\text{Floodplain Theoretical Discharge} - \text{Floodplain Actual Discharge}}{\text{Total Theoretical Discharge}}$$

This method was applied at bend apex section of both meandering compound channels. The results obtained for sinuosity 1.37 and 2.04, for trapezoidal and natural sections and for smooth floodplains are presented in **Fig(4.57)** to **Fig(4.59)**, for function F_4, and in **Fig(4.60)** to **Fig(4.62)**, for function F_5. In reading these graphs it is important to note that the area to the left of the graph (and up to the experimental data plotted points) represents the total bed friction losses. The area between the two curves on each graph represents non-friction energy losses in the main channel. The area to the right of both graphs represents the non-frictional energy losses on the floodplain. It should also be noted that the tentative nature of the right hand graph is due to detailed data being available at only 2 or 3 values of stage, namely 165 mm, 200 mm or 250mm.

All the graphs for the smooth floodplain case from **Fig(4.57)** to **(4.62)** reveal that the non friction energy losses in the main channel reduce with increasing flow depth ratio, while the opposite occurs with the non friction additional floodplain energy loss. The additional main channel energy losses, are essentially produced by the secondary currents and horizontal shear at bankfull level. Their role reduces with increasing flow

depth ratio because the streamlines become more parallel to the longitudinal direction and the main channel has less and less effect. The non friction energy losses in the floodplain region become greater because the flow contraction phenomenon increases with flow depth, but also because for smooth floodplains there is increasing momentum transfer from the floodplain into the main channel.

The results obtained for sinuosity 1.37 and 2.0, for the natural section and for roughened floodplains are presented in **Fig(4.63)** and **Fig(4.64)**, for function F_4, and in **Fig(4.65)** and **Fig(4.66)**, for function F_5. Here the pattern of the main channel and the floodplain additional energy losses is different compared to the smooth floodplain case. The non-friction floodplain energy losses reduce significantly with depth ratio, becoming almost zero for higher depth ratios. The non-friction main channel energy losses on the other hand seem to remain almost constant with increasing depth ratio. A likely explanation of this kind of behaviour in the main channel is the transference of very high friction resistance produced by rod elements on the floodplain, into the main channel. The reduction of the additional energy loss on the floodplain with increase of depth ratio is due to the fact that the lateral shear effect diminishes and the flow resistance is fully dominated by the turbulence and by the eddies created by the rods.

4.7 CONCLUSIONS

An analysis of flow conveyance in meandering compound channels was carried out this **Chapter 4**. This involved primarily the data from S.E.R.C. flume Series B, but also the study included comparisons from S.E.R.C. flume Series A(the straight and the skew compound channel) and data from other flumes(meandering channels with different sinuosities). The analysis was carried out in terms of:

- Stage-Discharge Relationship
- Flow Resistance
- Boundary Shear Stress Distribution
- A Parametric Analysis of Flow Conveyance in Meandering Compound Channels
- Separation of the Main Channel Energy Losses from Floodplain Energy Losses.

The main conclusions are as follows:

A) Stage-Discharge Curve

- In general, discharge reduces with the increasing sinuosity and increasing floodplain roughness, with vertical rod floodplain roughness causing the greatest degree of discharge reduction. For instance, an increase of sinuosity from 1.37 to 2.04 with smooth floodplains, reduces the discharge 23% at stage 200.00 mm. For the same stage and for sinuosity 1.37 and natural cross-section, produces a discharge reduction of 43% as the floodplain roughness changes from the smooth case to the fully roughened case.
- If the conveyance of two similar meandering compound channels with different main channel aspect ratios is compared, the one with larger aspect ratio will tend to convey more flow.
- Results obtained in the S.E.R.C. flume Series B confirms the findings of **Willetts and Hardwick** (1990) that meandering compound channels with natural cross-section tend to convey more discharge per unit area than a similar meandering compound channel with the trapezoidal cross-section.
- In meandering compound channels, the role of the main channel in conveying discharge is less important than the case of straight compound channels where the important role of the main channel in delivering discharge persists for higher stages. This is a result of meandering compound flows being orientated more in the longitudinal floodplain direction, than in the streamwise main channel direction.
- The ratio of the width of the meander belt(Wm) to the total channel width(W_t) has only a small effect on flow conveyance of

meandering compound channels with smooth floodplains.
- Any obstacle placed on the floodplain may reduce considerably the total conveyance of the meandering compound channel. In particular, the case of the transverse walled floodplain significantly constricted the conveyance of the meandering compound channel compared with a smooth floodplain case. For instance, at stage 250.0 mm, the reduction of discharge was 90%.

B) Flow Resistance

- Flow resistance was analysed in terms of the relationship of the Manning's n with stage, and the variation of the Darcy-Weisbach friction factor with the Reynolds number.
- For the overbank case as depth increases, Manning's 'n' tends towards a constant for smooth floodplain flow but increases significantly with stage for the fully roughened vertical rod floodplain case.
- Manning's n increases 25% as sinuosity increases from 1.37 to 2.04, for smooth floodplain case.
- The Darcy Weisbach friction factor tends to reduce for the smooth floodplain case and tends to increase almost linearly for the fully roughened floodplain case. The latter is a function of the use of vertical rods for roughening, producing an unrealistic increase in friction factor with depth.
- The Darcy-Weisbach friction factor (for smooth floodplain case) may rise 50% when the sinuosity of the meandering channel increases from 1.37 to 2.04.
- The relationship between the Darcy-Weisbach friction factor and the Reynolds Number was obtained for several kinds of obstacle (partly roughened floodplain; floodplain width reduced; floodplain with bridge piers). These (f- R)relationships usually lie between the smooth floodplain case and the fully roughened floodplain case.
- A significant difference in friction factor was identified between the fully roughened case and the partly roughened

floodplain case where the floodplain was roughened within the limits of the meander belt, but smooth outside the meander belt width. The friction factors for the fully roughened floodplain case were proportionately larger than the partially roughened floodplain case.

- Based on data from the S.E.R.C. flume Series B and the U.S. Army Corps of Engineers(1956), the effect of fully roughened floodplains on the flow resistance of the meandering compound channels was investigated. In the S.E.R.C. flume Series B, for a fully roughened floodplain case, the Darcy-Weisbach friction factor increases with an increase of Reynolds number, whereas in the U.S. Army Corps of Engineers(1956), the opposite occurs. The different behaviour exhibited by two models can be explained by the different type of "roughness" applied to the floodplains. In the first case, vertical rod elements were applied, while in the second case a metal mesh was used on the floodplain bed which reproduces more faithfully grass, stones or any kind of low obstacle that becomes submerged on river floodplains.
- Contour levels of friction factors show the regions where the flow experienced more flow resistance than normal. For overbank flow this region is located near the right downstream bank of the cross-over section.

C) Boundary Shear Stress Distribution

- The boundary shear stress distribution in the main channel is significantly affected by stage and sinuosity.
- As the stage passes from inbank to overbank, the boundary shear stress in the main channel reduces considerably. This effect is exacerbated if sinuosity is increased. Therefore, as a result the main channel will lose capacity in carrying sediments in the streamwise direction. However, its capacity in transporting sediments in the transverse direction of the main channel (as will be shown in Chapter 5), substantially increased in comparison with the inbank case.

- For the overbank case, the maximum values of boundary shear stress are located on right floodplain at the downstream end of the bend, near the cross-over section, where the flow on to the floodplain is accelerating. Therefore this is the region where scour will probably occur. For stage 200.0 mm with smooth floodplains, the peak of boundary shear stress can reach values between 1.5-2.0 times the value of the boundary shear stress that will occur in a straight channel.

D) Parametric analysis of conveyance in meandering compound channels

- By using non-dimensional functions F_1, for inbank flow, and F_4 and F_5, for overbank flow, a parametric analysis was initiated, and non-friction energy losses occurring in compound channels were quantified.
- The parametric analysis has shown that the following parameters affect the flow conveyance of meandering compound channels:

(i) The relative depth of flow (floodplain depth/main channel depth) obviously has an important influence on conveyance.

(ii) The relative boundary roughness ratio between main channel and floodplain is important.

(iii) The sinuosity of the main channel is very significant (this may also be characterised by the cross-over angle from one bend to the next).

(vi) The shape of the main channel (trapezoidal or natural) has an effect.

(v) The aspect ratio of the main channel (width/depth) has also proved to be significant.

(vi) The ratio of the meander belt width to the total width may also be significant especially for the case of fully roughened floodplains.

(vii) The ratio of the main channel top width to the total width of the channel is also an important parameter.

- Considering the inbank case and for very low depths of the flow, the function F_1 is practically 1.0, because the channel behaves like a straight channel. As the stage starts to increase, secondary flow develops, introducing additional losses to the flow, and function F_1 becomes smaller by 12% for sinuosity 1.37 and 23 % for sinuosity 2.04. This is due to bend losses.
- For the overbank case, functions F_4 and F_5 have shown that losses of energy produced by skin friction can be as low as 50% of total losses. The other additional losses were generated by the secondary currents, by flow expansion-contraction phenomena and by the lateral shear.
- Functions F_4 and F_5 reveal very clearly the effects of sinuosity, floodplain roughness, cross-section shape, aspect ratio and meander belt width on the non-friction energy losses experienced in meandering compound flows.
- By increasing the main channel sinuosity from 1.37 to 2.04, function F_4 reduces about 15%, for natural cross-section with smooth floodplains.
- The parametric analysis was extended for the straight, skewed and meandering compound channel with roughened floodplains has shown that, as the depth ratio increases, function F_5 reaches almost the unity for the higher stages. This means that for higher stages the losses of energy are entirely produced by skin friction and friction induced by floodplain rods.
- As depth ratio increases, the function F_4 for the straight and the skew compound channel with smooth floodplains tend to the unity.
- For smooth floodplains, the function F_4 shows more sensitivity to the effect of the geometry of the cross-section than function F_5.
- Function F_5 is a better indicator of roughened floodplain flows compared with F_4 which is a better indicator for smooth floodplain flows.
- Aspect ratio significantly affects the conveyance of meandering compound channels with smooth floodplains. As the aspect ratio decreases the additional losses of energy produced by the flow

expansion-contraction phenomena, secondary currents and flow separation will increase. This effect becomes more pronounced with the increase of the depth ratio.
- Simulation in a physical model of the loss of energy produced by meandering compound flow in nature, demands that the main channel aspect ratio should be kept the same as in nature. This means that distorted models with low aspect ratio of the main channel will exaggerate the loss of energy comparatively to that occur in actual rivers with meandering compound flows.
- The ratio of the meander belt width(Wm) to the total channel width(W_t) affects very slightly flow conveyance of meandering compound channels with smooth floodplains. For depth ratios greater than 0.3, there is practically no effect on conveyance. However in case of fully roughened floodplains the results from the **U.S. Army Corps of Engineers Study (1956)** have shown that ratio Wm/Wt affects the flow conveyance and its effect increases with depth ratio, although this data is of dubious value.

E) Separation of the Main Channel Additional Losses from Floodplain Additional Losses in Meandering Compound Flows.

- The main channel additional energy losses were separated from the floodplain additional energy losses. This analysis was carried out only for the S.E.R.C. flume Series B data.
- For the smooth floodplain case, the additional main channel energy losses reduce with depth ratio, while the opposite occurs with the additional floodplain energy losses.
- For the fully roughened floodplain case, the additional floodplain energy losses reduce with depth ratio, becoming practically zero for the higher flows, while the additional main channel energy losses tend to maintain approximately constant with depth ratio.

Table(4.1)

Effect of Cross-Section, Sinuosity, and Floodplain Roughness on The Conveyance of Meandering Channels. Comparison Made in Relation To The Meandering Channel with Sinuosity 1.37, Natural Cross-Section and Smooth Floodplains. Data from The S.E.R.C. Flume Series B.

Stage mm	Sinuosity	Cross-Section Type	Flood. Rough.	%
200	1.37	Trap.	smooth	+1.5
250	1.37	Trap.	smooth	+0.5
300	1.37	Trap.	smooth	-0.05
200	1.37	Nat.	smooth	0.0
250	1.37	Nat.	smooth	0.0
300	1.37	Nat.	smooth	0.0
200	1.37	Nat.	rough	-43
250	1.37	Nat.	rough	-58
300	1.37	Nat.	rough	-65
200	2.04	Nat.	smooth	-23
250	2.04	Nat.	smooth	-19
300	2.04	Nat.	smooth	-18
200	2.04	Nat.	rough	-46
250	2.04	Nat.	rough	-59
300	2.04	Nat.	rough	-64

The sign - means reduction while the sign + means increase.

Table(4.2)

Effect of Floodplain Roughness on The Conveyance of The Natural Meandering Channels

Data from The S.E.R.C. Flume Series B.

Stage mm	Sinuosity	Floodp. Roughness	%
250.0	1.37	Smooth	0.0
250.0	1.37	Bridge Piers	-13
250.0	1.37	Part. Rough.	-28
250.0	1.37	Floodp. Width Red.	-39
250.0	1.37	Fully Rough.	-57
250.0	2.04	Smooth	-19
250.0	2.04	Bridge Piers	-28
250.0	2.04	Floodp. Width Red.	-31
250.0	2.04	Fully Rough.	-59
250.0	2.04	Walled	-89

TABLE 4.3

GEOMETRIC CHARACTERISTICS OF S.E.R.C. FLUMES SERIES A USED IN THE COMPARATIVE STUDY OF OF THE CONVEYANCE OF COMPOUND CHANNELS - SMOOTH CASE.

TYPE OF CHANNEL	MAIN CHANNEL				FLOODPLAIN			B/b
	CROSS-SECTION	BOTTOM WIDTH B (m)	SIDE SLOPE	BANKF. DEPTH (m)	BOTTOM WIDTH b (m)	SLOPE 1/1000	SIDE SLOPE	
STRAIGHT	TRAPEZOIDAL	1.5	1 : 2	1.5	10.0	1.029	VERT.	6.67
SKEW	TRAPEZOIDAL	1.5	1 : 2	1.5	5.595	1.029	VERT.	3.73

TABLE 4.4

GEOMETRIC CHARACTERISTICS OF S.E.R.C. FLUMES SERIES A USED IN THE COMPARATIVE STUDY OF OF THE CONVEYANCE OF COMPOUND CHANNELS - FLOODPLAIN FULLY ROUGHENED

TYPE OF CHANNEL	MAIN CHANNEL				FLOODPLAIN			B/b
	CROSS-SECTION	BOTTOM WIDTH B (m)	SIDE SLOPE	BANKF. DEPTH (m)	BOTTOM WIDTH b (m)	SLOPE 1/1000	SIDE SLOPE	
STRAIGHT	TRAPEZOIDAL	1.5	1 : 2	1.5	6.9	1.029	VERT.	4.6
SKEW	TRAPEZOIDAL	1.5	1 : 2	1.5	5.595	1.029	VERT.	3.73

NOTE : THE FLOODPLAIN ROUGHNESS WAS REPRODUCED THROUGH 25.00 mm RODS WITH A DENSITY 12/m2.

TABLE 4.5

GEOMETRIC CHARACTERISTICS OF THE MEANDER COMPOUND CHANNELS USED IN THE PARAMETRIC ANALYSIS OF THE CONVEYANCE

AUTHOR	MAIN-CHANNEL CROSS-SECTION	FLOODPLAIN ROUGHNESS	SINUOSITY	SLOPE 1/1000	B/b	b/h	W/b
TOEBES SOOKY	RECTANGULAR	SMOOTH	1.13	1.6	5.65	5.5	2.24
KIELY	RECTANGULAR	SMOOTH	1.25	1.0	6.0	4.0	3.85
U.S.A. C. ENG.	TRAPEZOIDAL	SMOOTH	1.2	1.0	6.4	5.0	3.8
U.S.A. C. ENG.	TRAPEZOIDAL	SMOOTH	1.57	1.0	6.4	5.0	5.8
WILLETS HARDWICK	TRAPEZOIDAL	SMOOTH	1.41	1.0	6.89	3.48	5.7
WILLETS HARDWICK	TRAPEZOIDAL	SMOOTH	2.06	0.62	6.89	3.48	
S.E.R.C. SERIES B	TRAPEZOIDAL	SMOOTH	1.37	0.996	8.33	8.0	5.1
S.E.R.C. SERIES B	NATURAL	SMOOTH	1.37	0.996	8.33	13.5	5.1
S.E.R.C. SERIES B	NATURAL	SMOOTH	2.04	1.02	8.33	13.5	7.1

MEANING OF THE PARAMETERS:
B - TOTAL CHANNEL WIDTH
b - MAIN CHANNEL TOP WIDTH
h - BANKFULL DEPTH
W - MEANDER BELT WIDTH

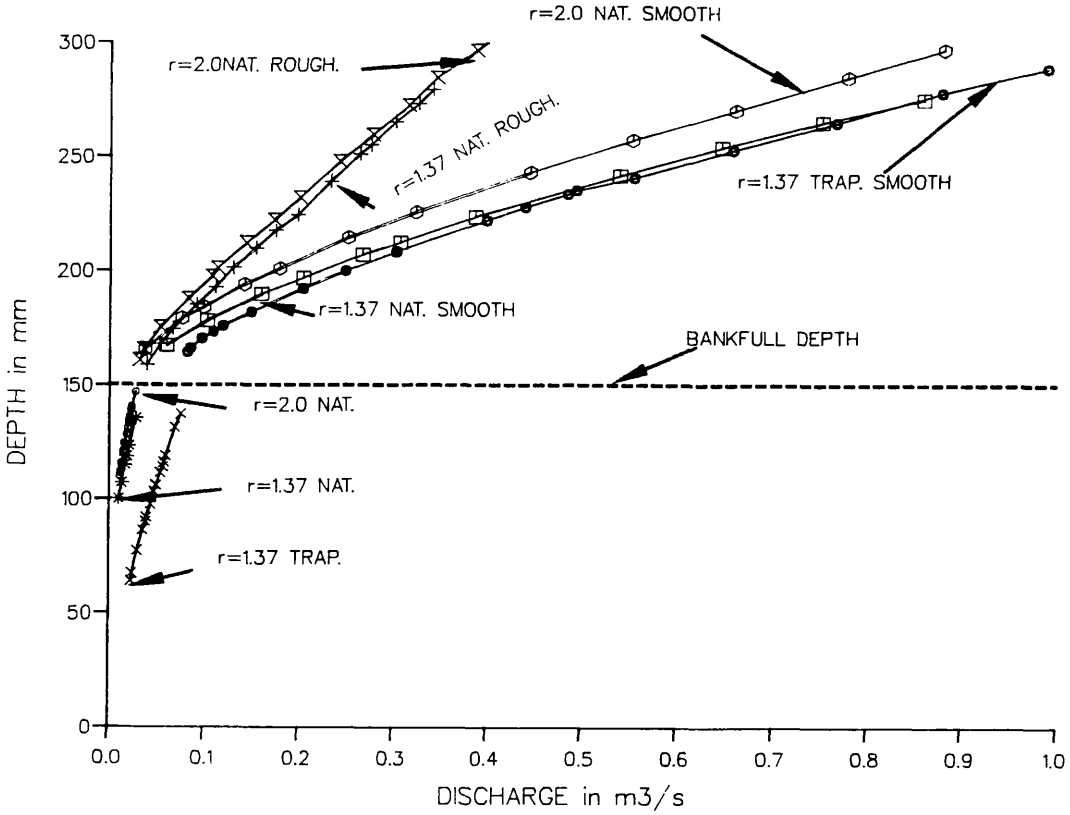

Fig (4.1) - Stage-Discharge Curve. S.E.R.C. Series B: Inbank and Overbank Cases; Sinuosities 1.37 and 2.04; Trapezoidal and Natural Cross-Sections; Smooth and Fully Roughened Floodplain.

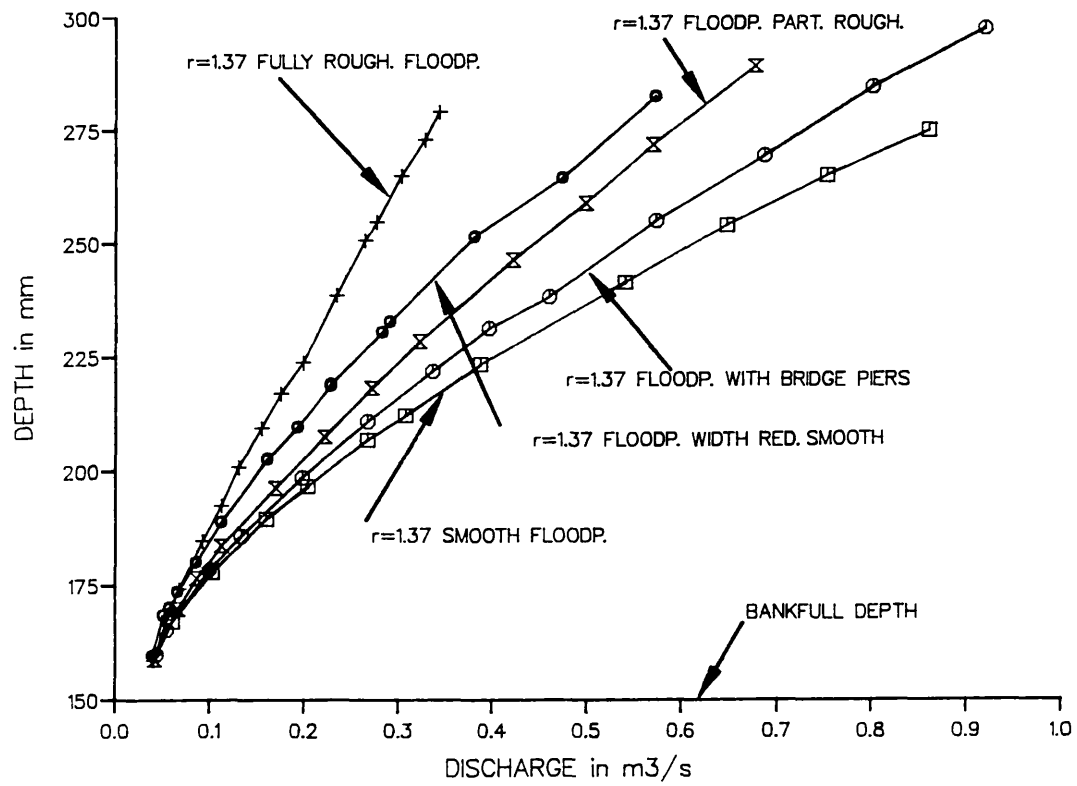

Fig (4.2) - Effect of The Floodplain Roughness on The Stage-Discharge Curve. S.E.R.C. Series B: Sinuosity 1.37.

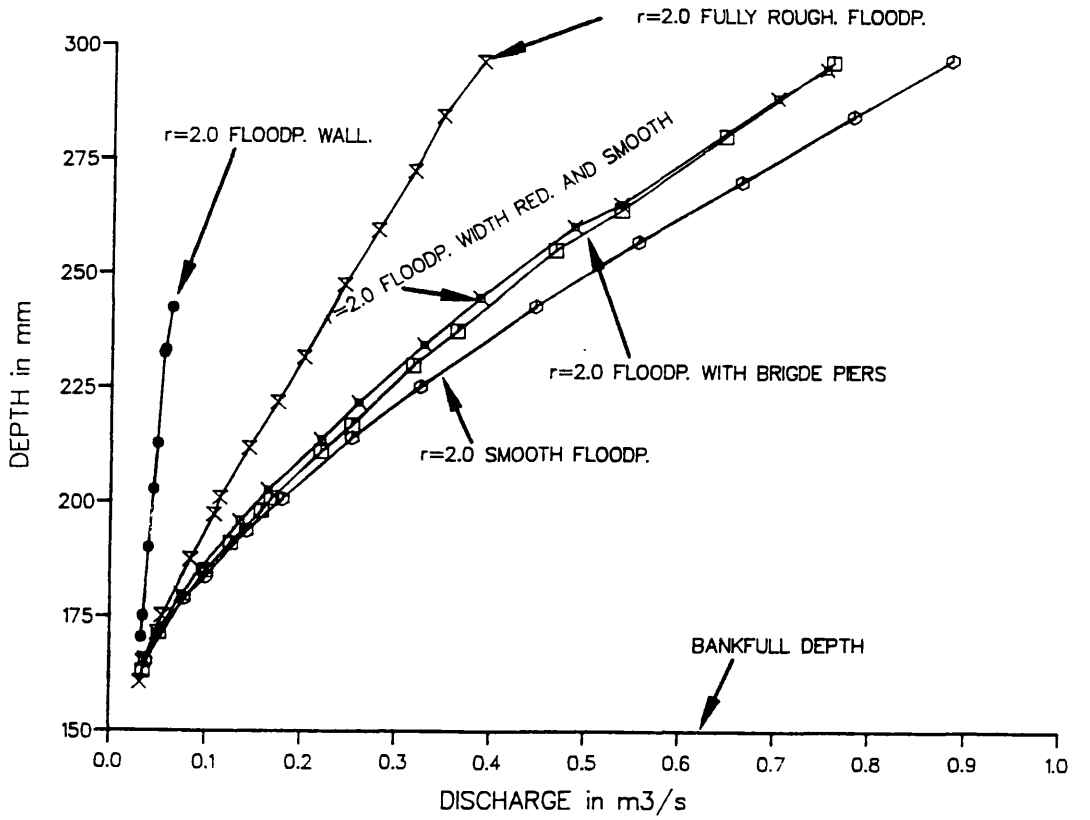

Fig (4.3) - Effect of The Floodplain Roughness on The Stage-Discharge Curve. S.E.R.C. Series B. Sinuosity 2.04.

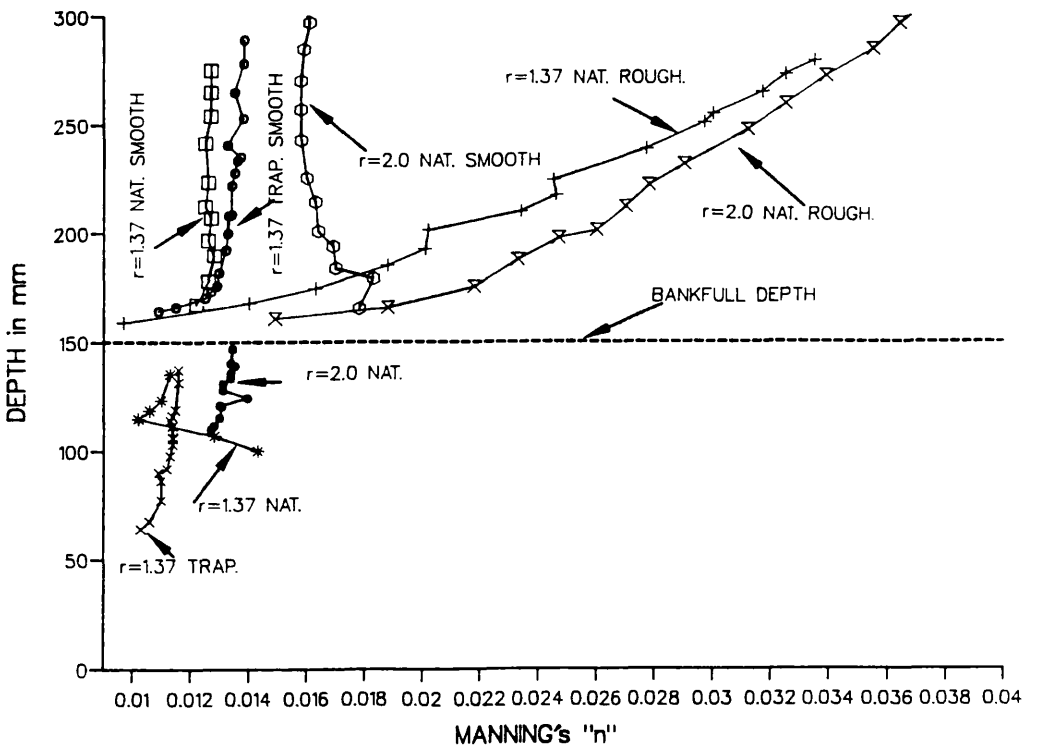

Fig (4.4) - Variation of Manning's n with Stage. S.E.R.C. Series B: Inbank and Overbank Cases; Sinuosities 1.37 and 2.04; Trapezoidal and Natural Cross-Sections; Smooth and Fully Roughened Floodplain.

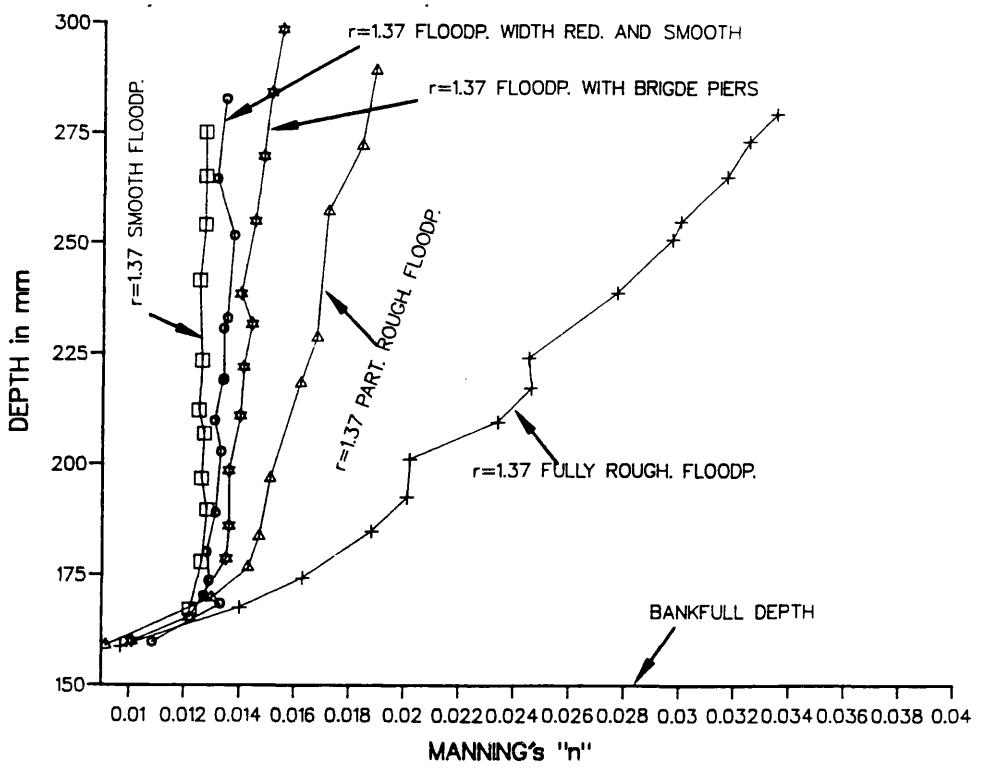

Fig (4.5) - Effect of Floodplain Roughness on Variation of Manning's n with Stage. S.E.R.C. Series B: Sinuosity 1.37.

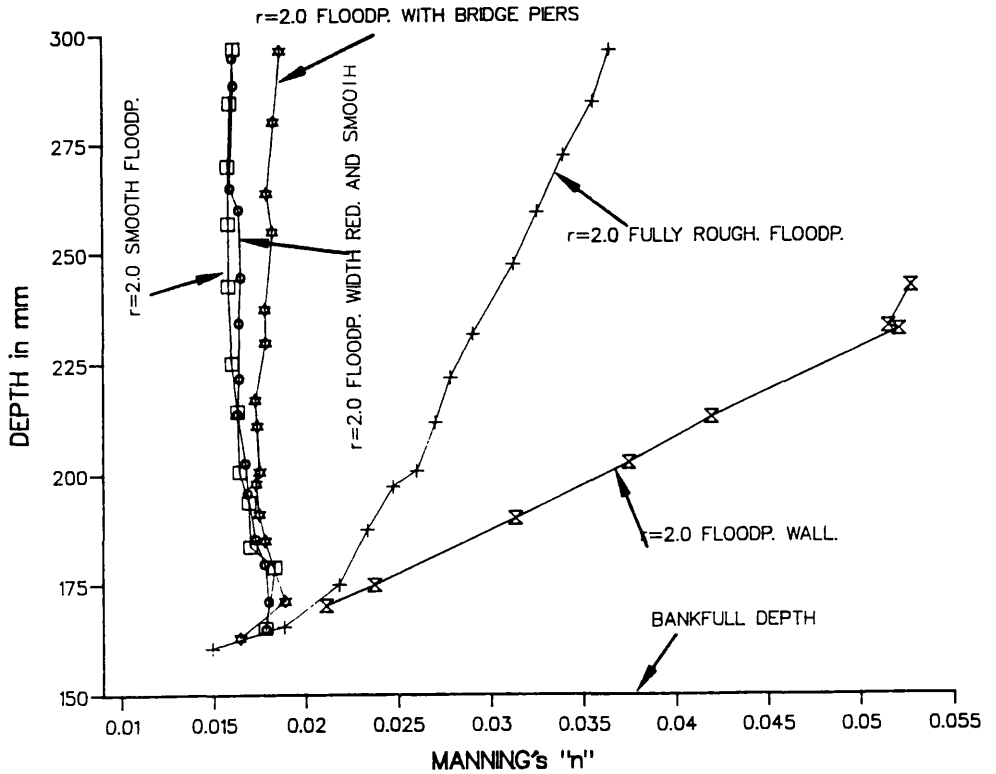

Fig (4.6) - Effect of Floodplain Roughness on Variation of Manning's n with Stage. S.E.R.C. Series B: Sinuosity 2.04.

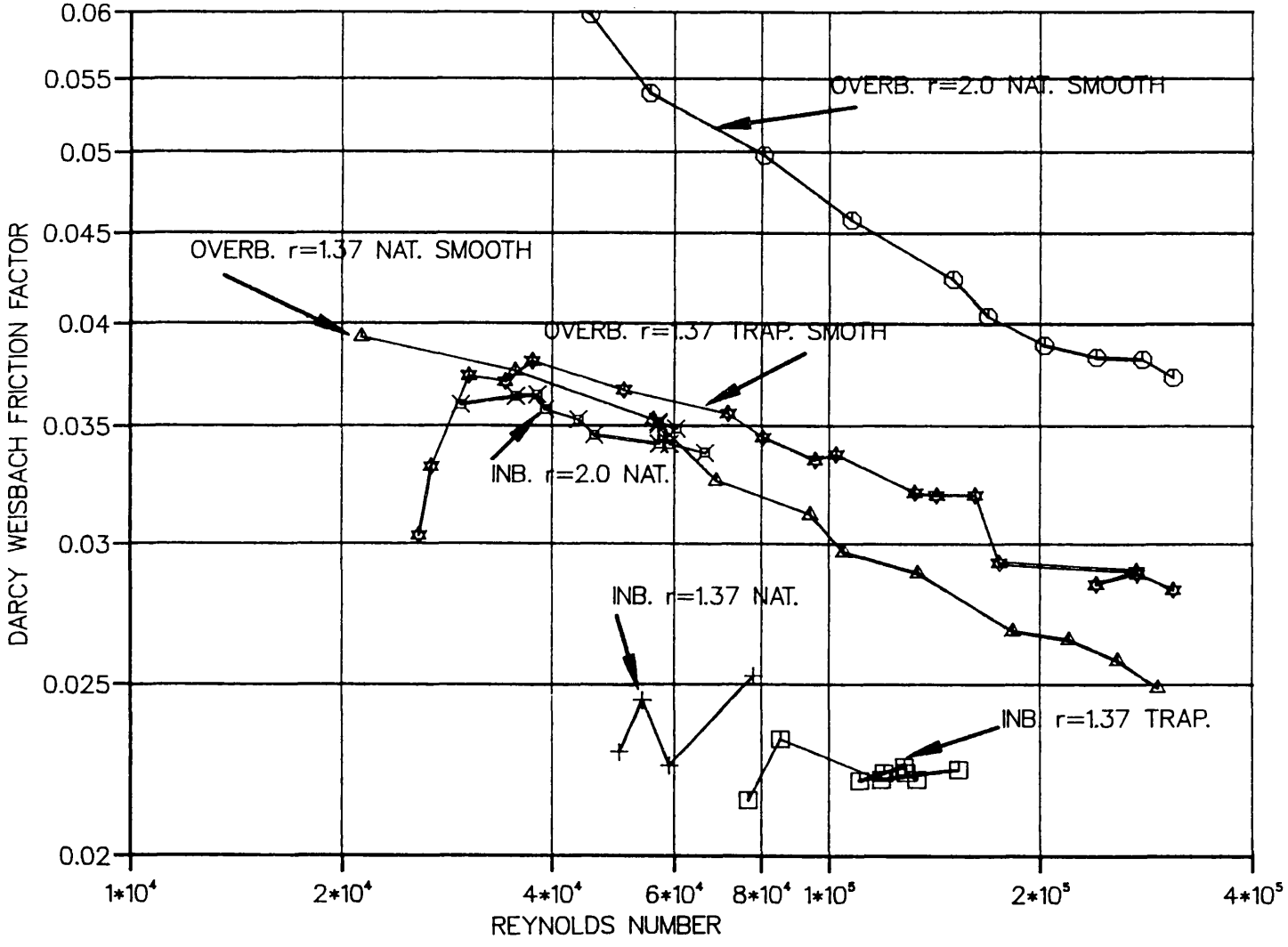

Fig (4.7a) - Variation of Darcy-Weisbach Friction Factor with Reynolds Number. S.E.R.C. Series B: Inbank and Overbank Cases; Sinuosities 1.37 and 2.04; Trapezoidal and Natural Cross-Sections; Smooth Floodplain.

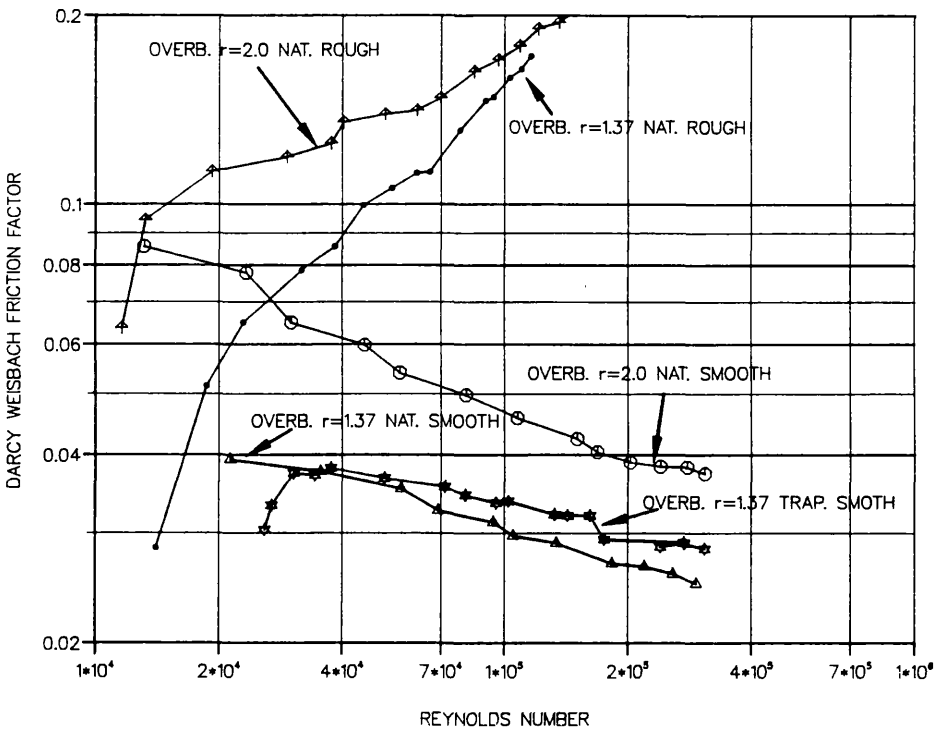

Fig (4.7b) - Variation of Darcy-Weisbach Friction Factor with Reynolds Number. S.E.R.C. Series B: Overbank Case; Sinuosities 1.37 and 2.04; Trapezoidal and Natural Cross-Sections; Smooth Floodplain.

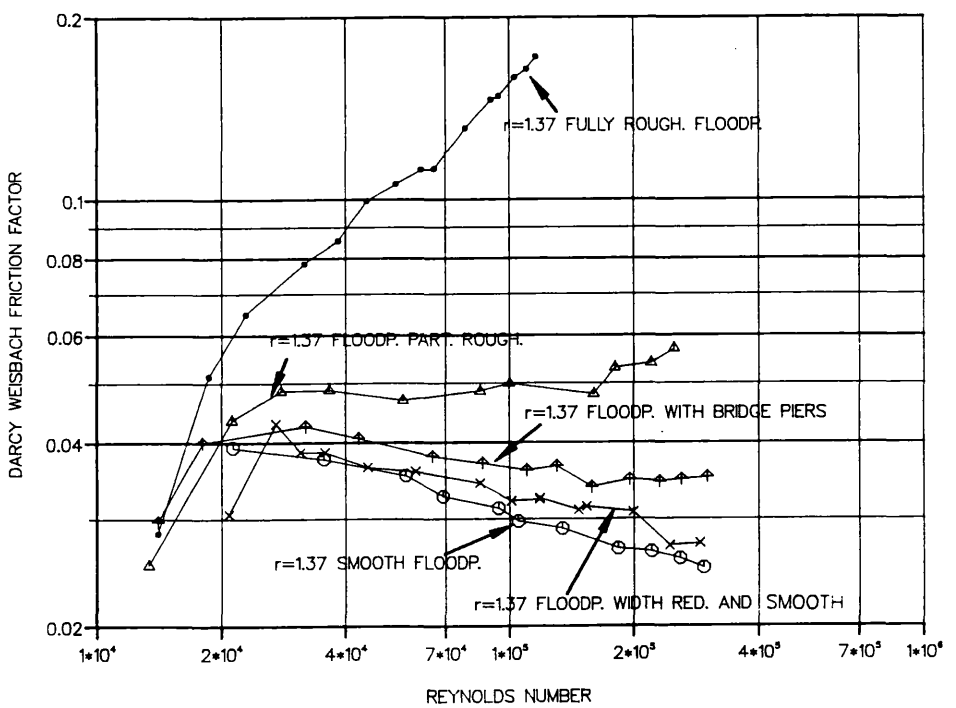

Fig (4.8) - Effect of The Floodplain Roughness on Variation of Darcy-Weisbach Friction Factor with Reynolds Number. S.E.R.C. Series B: Sinuosity 1.37.

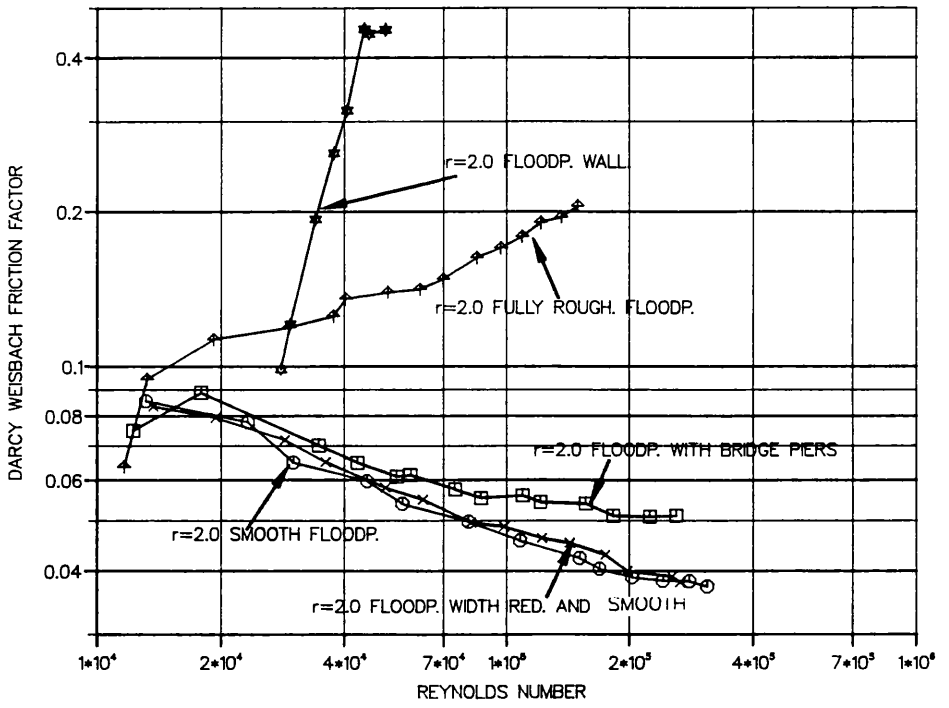

Fig (4.9) - Effect of Floodplain Roughness on Variation of Darcy-Weisbach Friction Factor with Reynolds Number. S.E.R.C. Series B: Sinuosity 2.04.

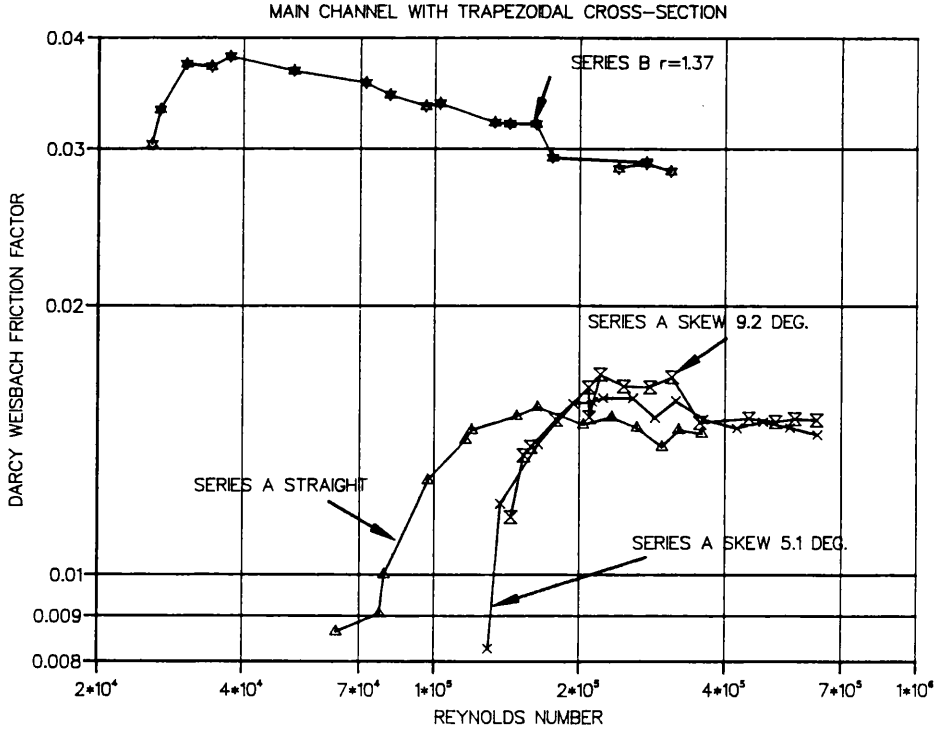

Fig (4.10) - Comparison of Friction Factors of The Straight, The Skew and The Meandering Compound Channel. S.E.R.C. Series B: Trapezoidal Cross-Section and Smooth Floodplains.

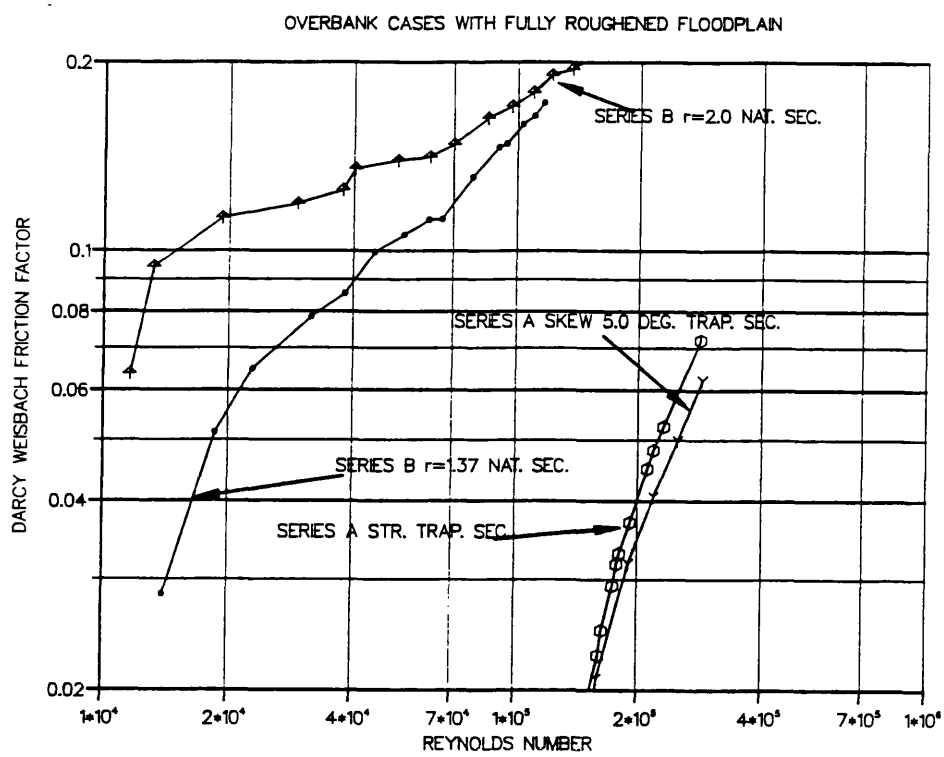

Fig (4.11) - Comparison of Friction Factors of The Straight, The Skew and The Meandering Compound Channel. S.E.R.C. Series B: Natural and Trapezoidal Cross-Sections and Fully Roughened Floodplains.

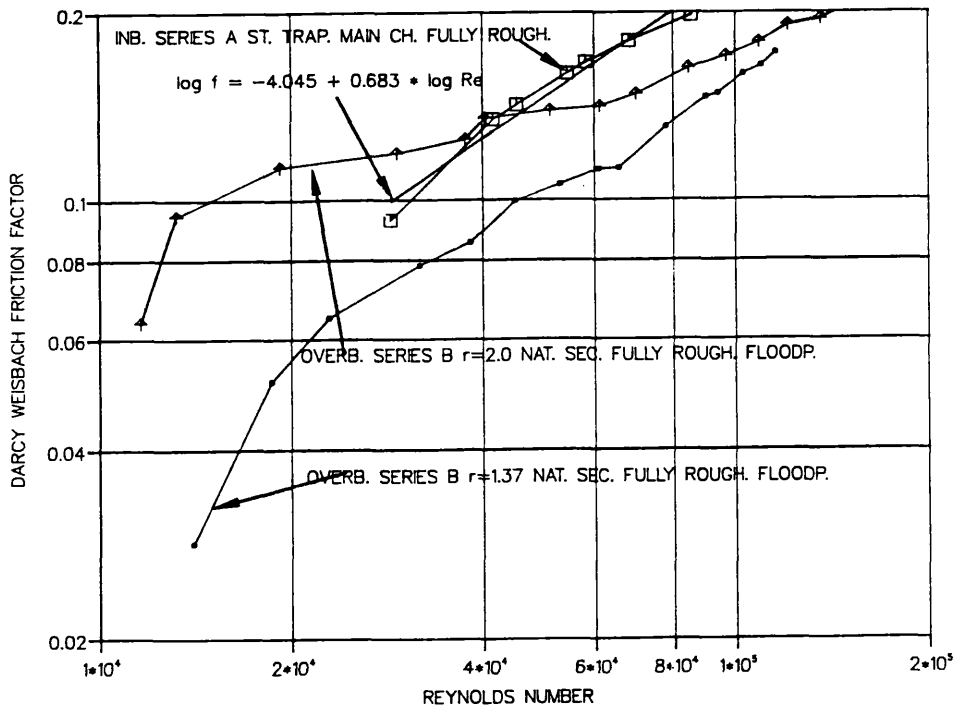

Fig (4.12) - Comparison of Friction Factors of The Inbank Case of The Straight Channel Fully Roughened with The Overbank Case of Meandering Channel with Fully Roughened Floodplain. S.E.R.C. Series A and B.

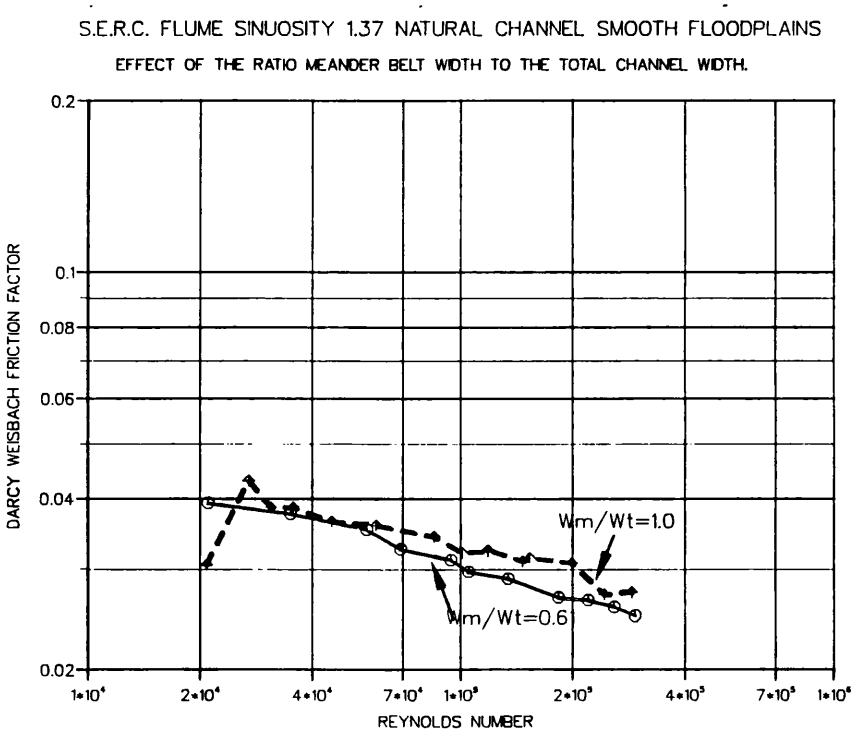

Fig (4.13a) - Analysis of the Effect of the Ratio Meander Belt Width to the Total Channel Width on the Conveyance of Meandering Compound Channels. Data from the S.E.R.C. Flume Series B Sinusity 1.37, Natural Meandering Channel with Smooth Floodplains.

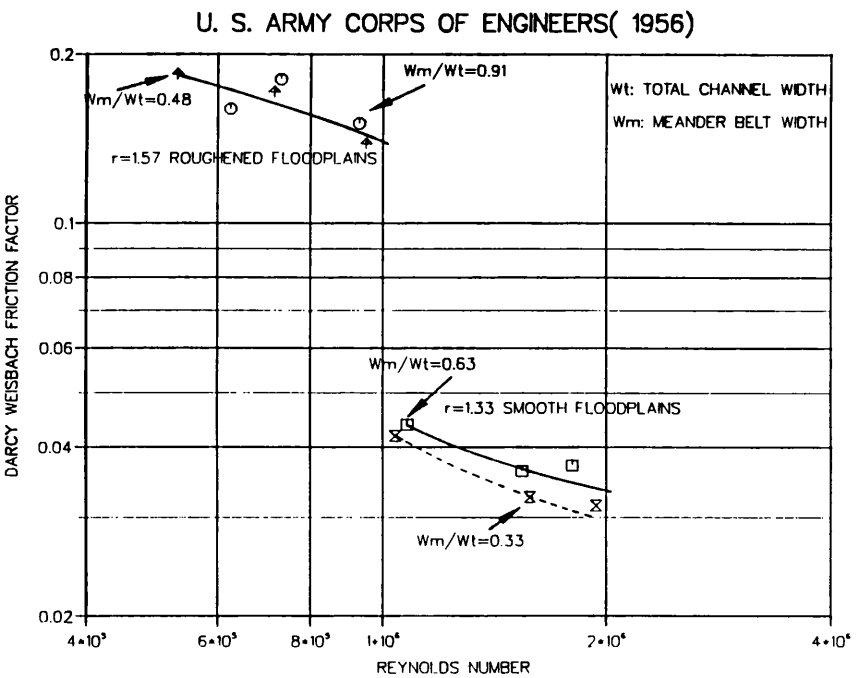

Fig (4.13b) - Analysis of the Effect of the Ratio Meander Belt Width to the Total Channel Width on the Conveyance of Meandering Compound Channels. Data from U.S. Army Corps of Engineers(1956).

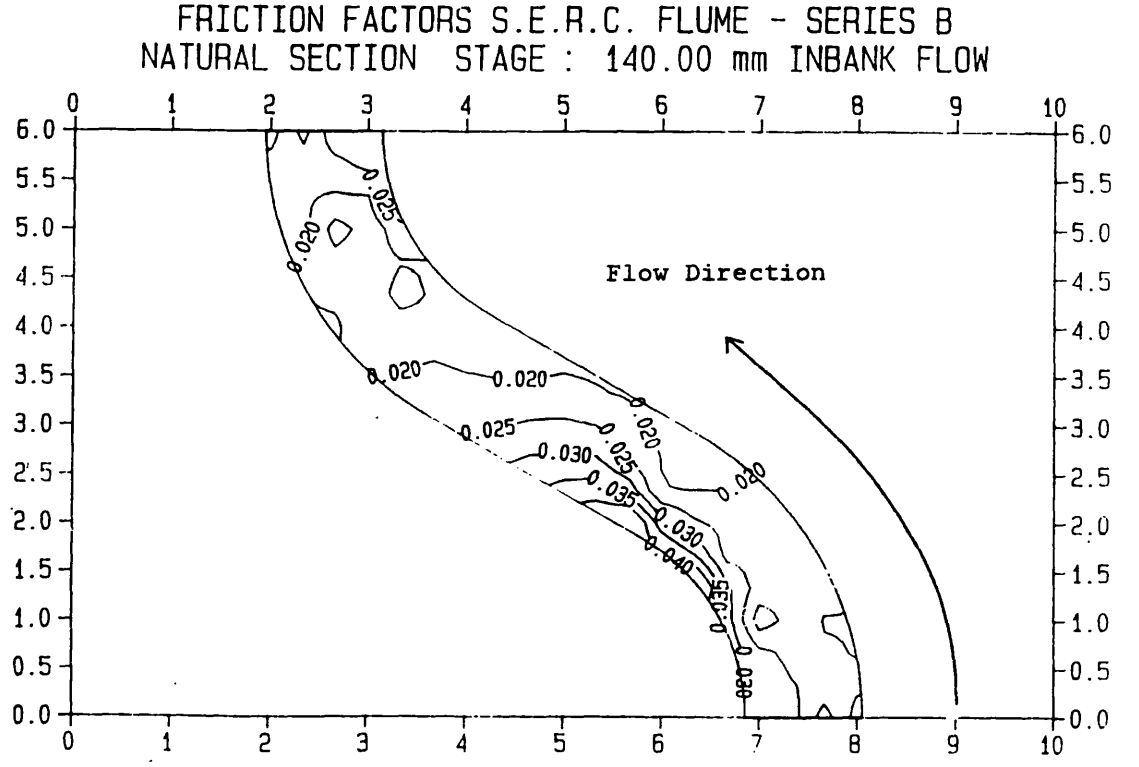

Fig (4.14) - Contour Levels of Friction Factors. S.E.R.C. Series B: Sinuosity 1.37; Inbank Case; Natural Cross-Section; Stage 140.00 mm.

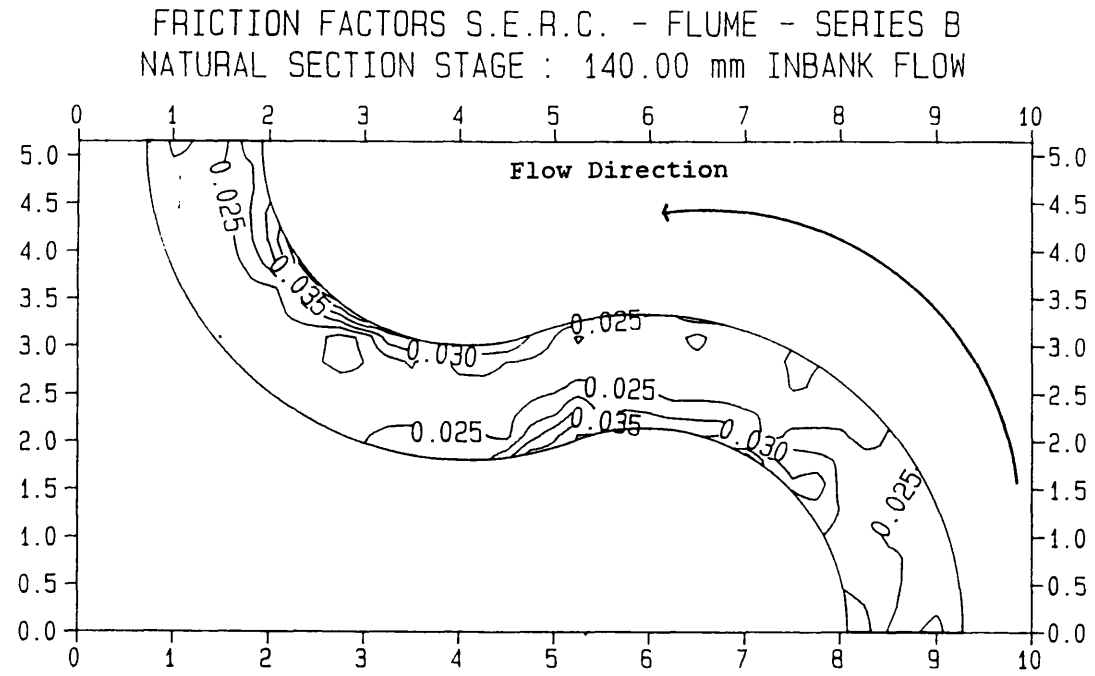

Fig (4.15) - Contour Levels of Friction Factors. S.E.R.C. Series B: Sinuosity 2.04; Inbank Case; Natural Cross-Section; Stage 140.00 mm.

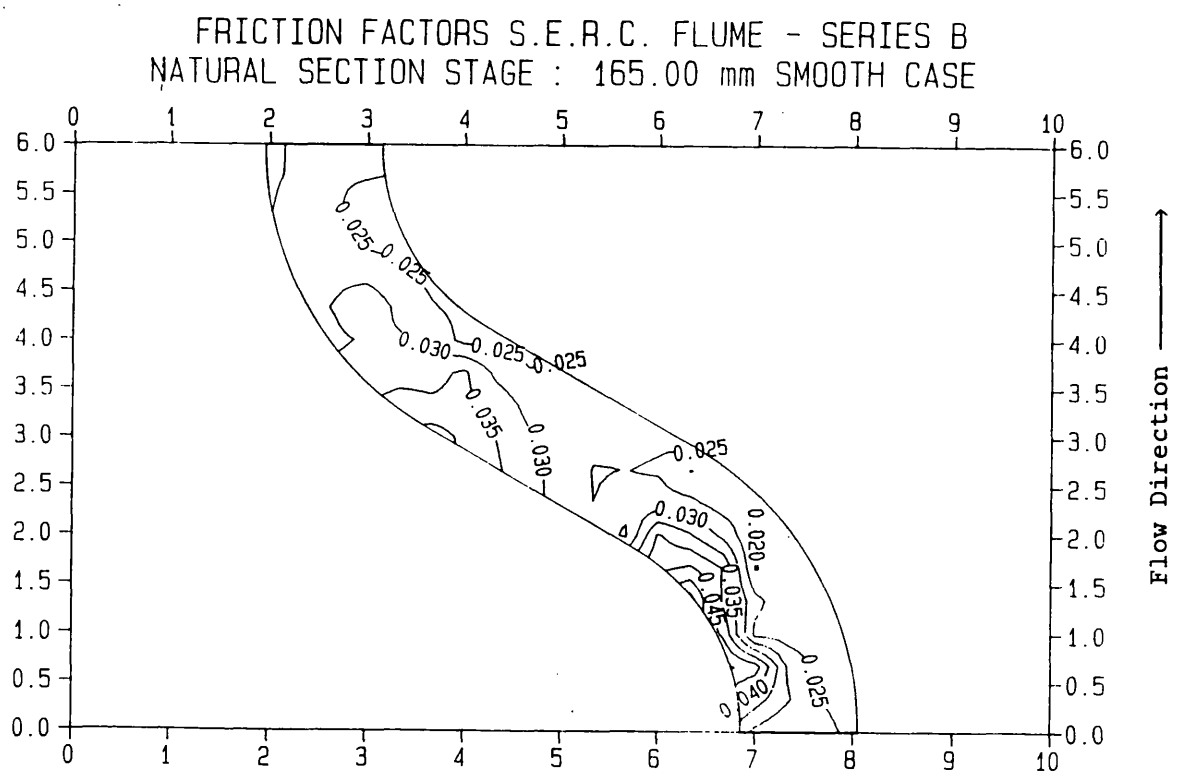

Fig (4.16) - Contour Levels of Friction Factors. S.E.R.C. Series B: Sinuosity 1.37; Overbank Case; Natural Cross-Section; Stage 165.00 mm; Smooth Floodplains.

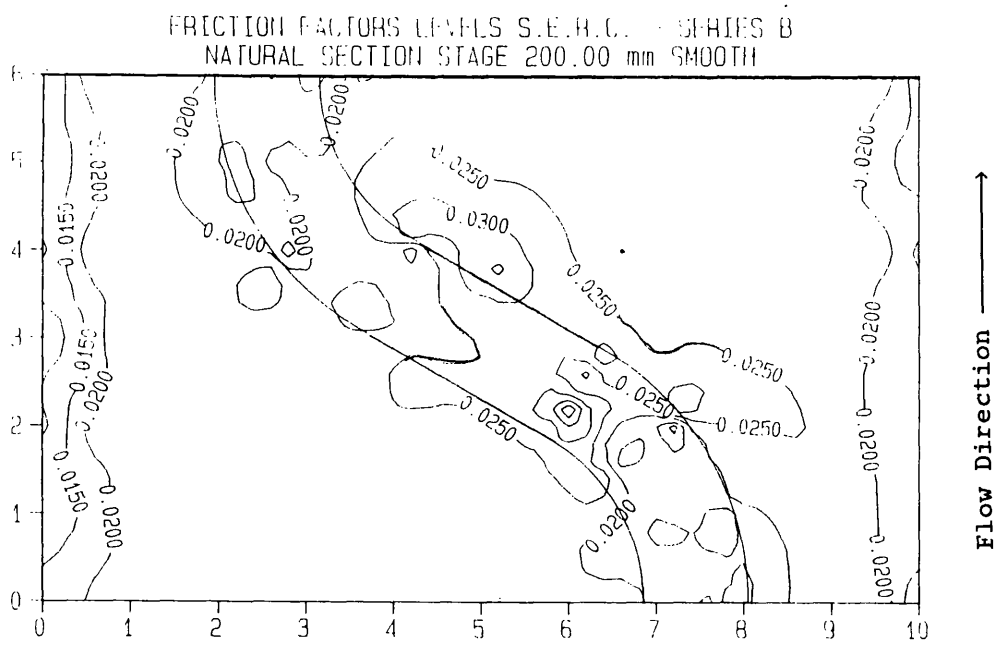

Fig (4.17) - Contour Levels of Friction Factors. S.E.R.C. Series B: Sinuosity 1.37; Overbank Case; Natural Cross-Section; Stage 200.00 mm; Smooth Floodplains.

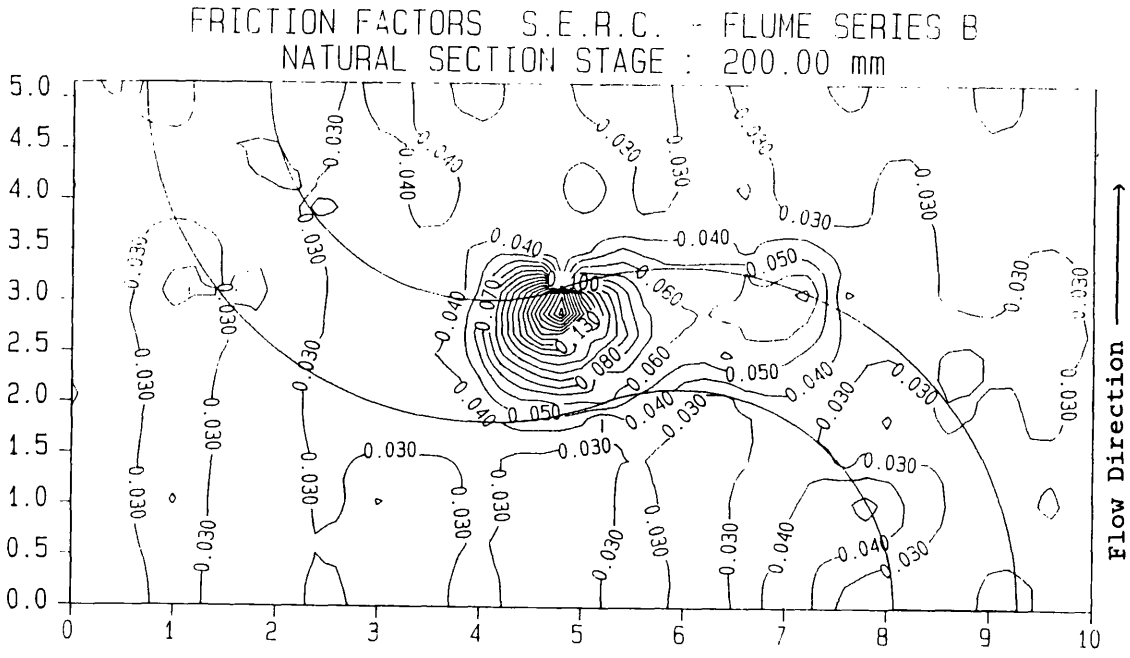

Fig (4.18) - Contour Levels of Friction Factors. S.E.R.C. Series B: Sinuosity 2.04; Overbank Case; Natural Cross-Section; Stage 200.00 mm; Smooth Floodplains.

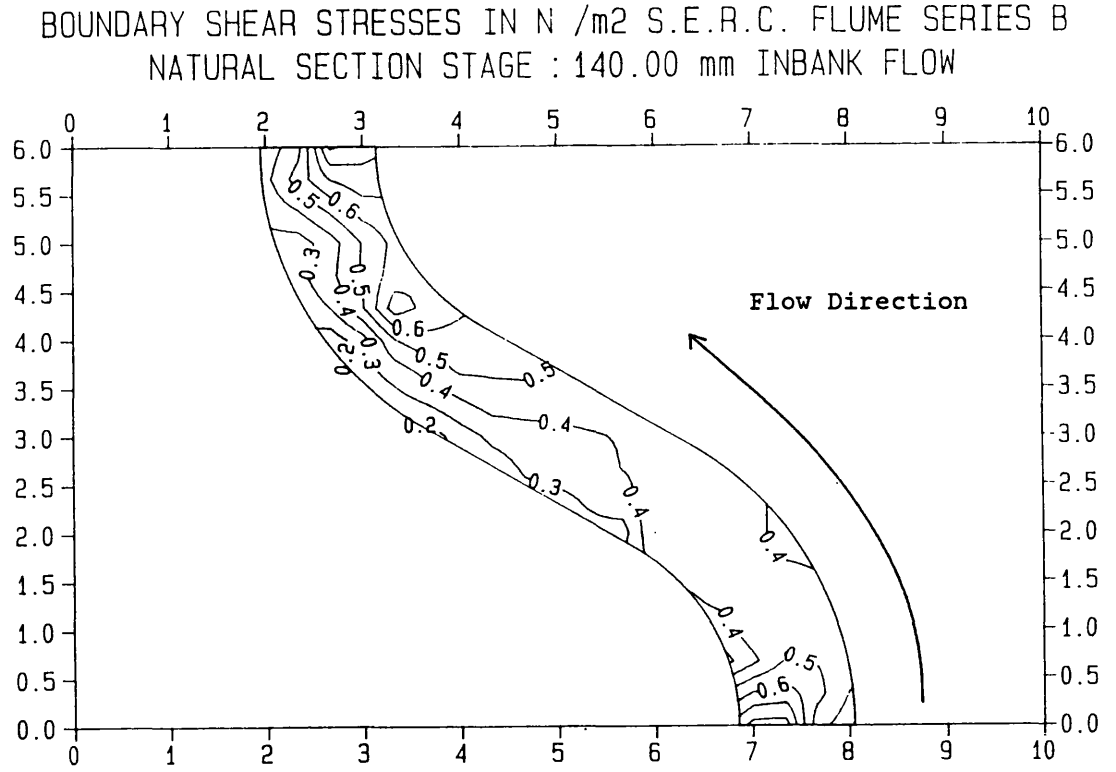

Fig (4.19) - Contour Levels of Boundary Shear Stress. S.E.R.C. Series B: Sinuosity 1.37; Inbank Case; Natural Cross-Section; Stage 140.00 mm.

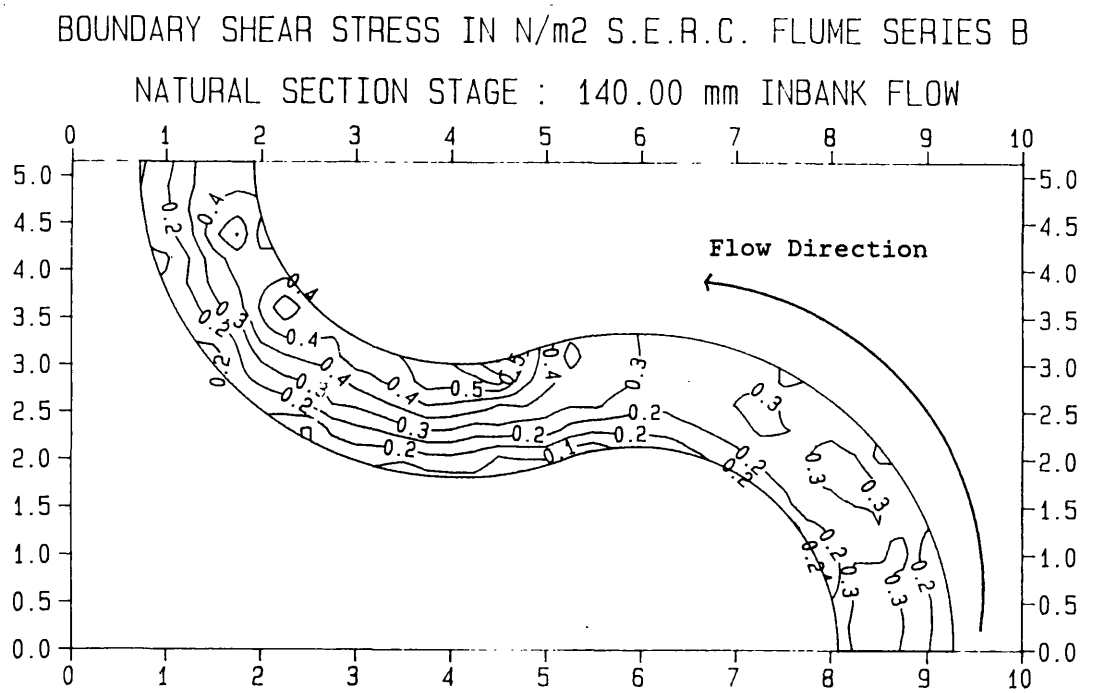

Fig (4.20) - Contour Levels of Boundary Shear Stress. S.E.R.C. Series B: Sinuosity 2.04; Inbank Case; Natural Cross-Section; Stage 140.00 mm.

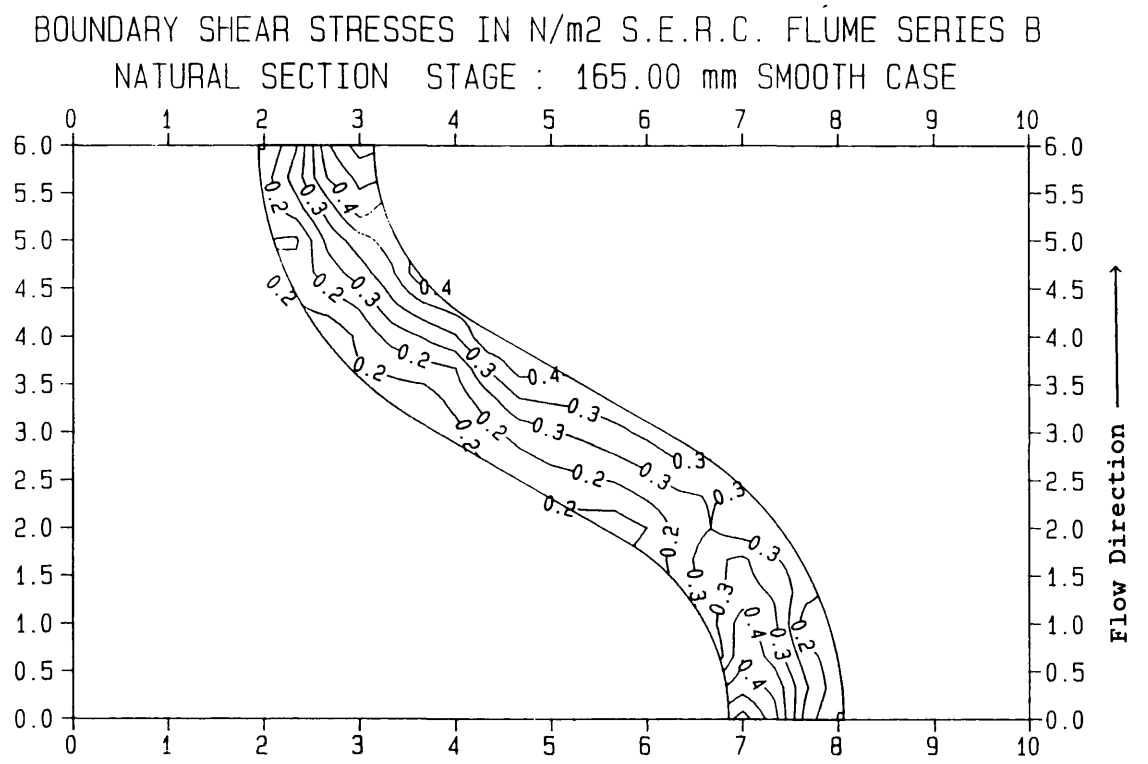

Fig (4.21) - Contour Levels of Boundary Shear Stress. S.E.R.C. Series B: Sinuosity 1.37; Overbank Case; Natural Cross-Section; Stage 165.00 mm; Smooth Floodplains.

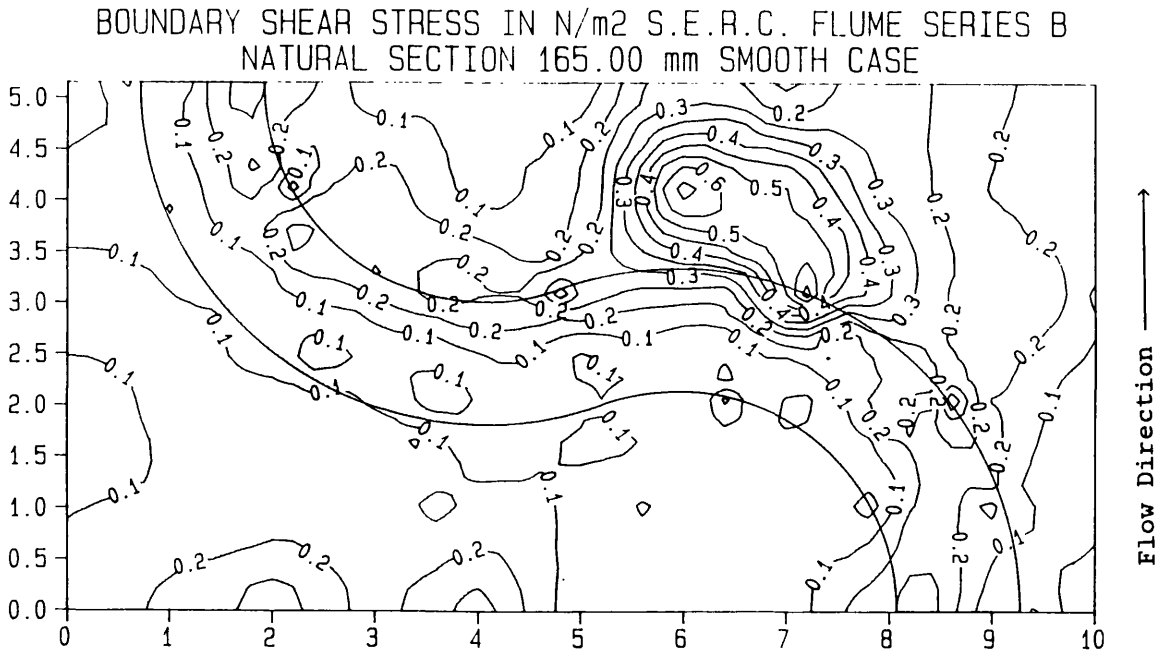

Fig (4.22) - Contour Levels of Boundary Shear Stress. S.E.R.C. Series B: Sinuosity 2.04; Overbank Case; Natural Cross-Section; Stage 165.00 mm; Smooth Floodplains.

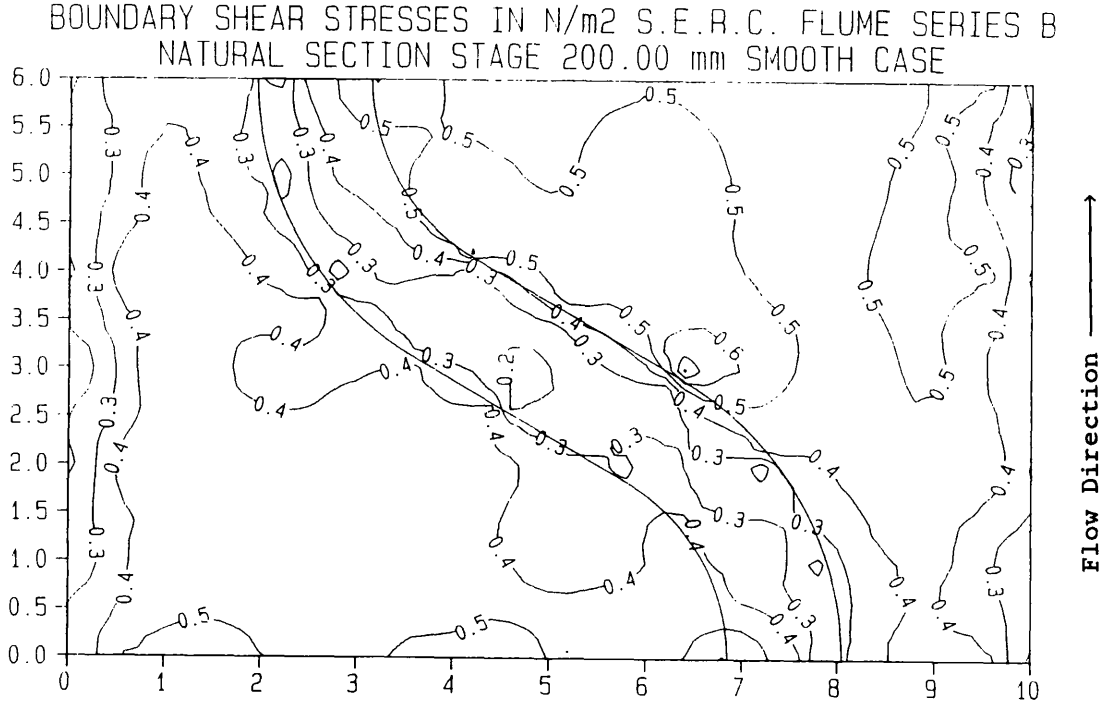

Fig (4.23) - Contour Levels of Boundary Shear Stress. S.E.R.C. Series B: Sinuosity 1.37; Overbank Case; Natural Cross-Section; Stage 200.00 mm; Smooth Floodplains.

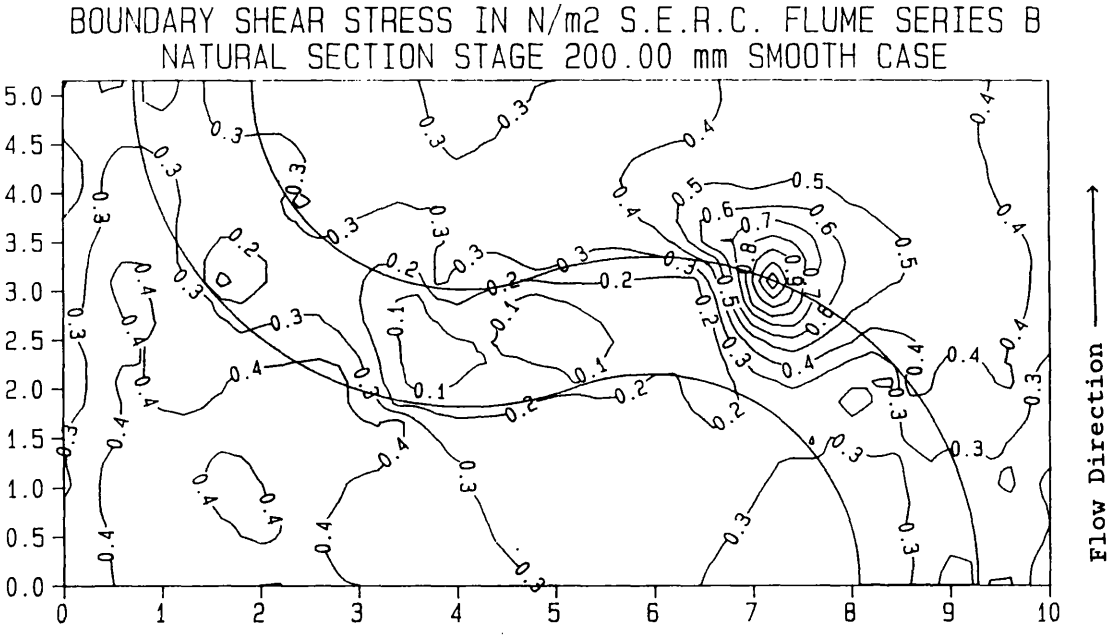

Fig (4.24) - Contour Levels of Boundary Shear Stress. S.E.R.C. Series B: Sinuosity 2.04; Overbank Case; Natural Cross-Section; Stage 200.00 mm; Smooth Floodplains.

Fig. 4.25 - ANALYSIS OF CONVEYANCE IN MEANDERING COMPOUND CHANNELS

METHOD OF CALCULATION FUNCTIONS F4 AND F5

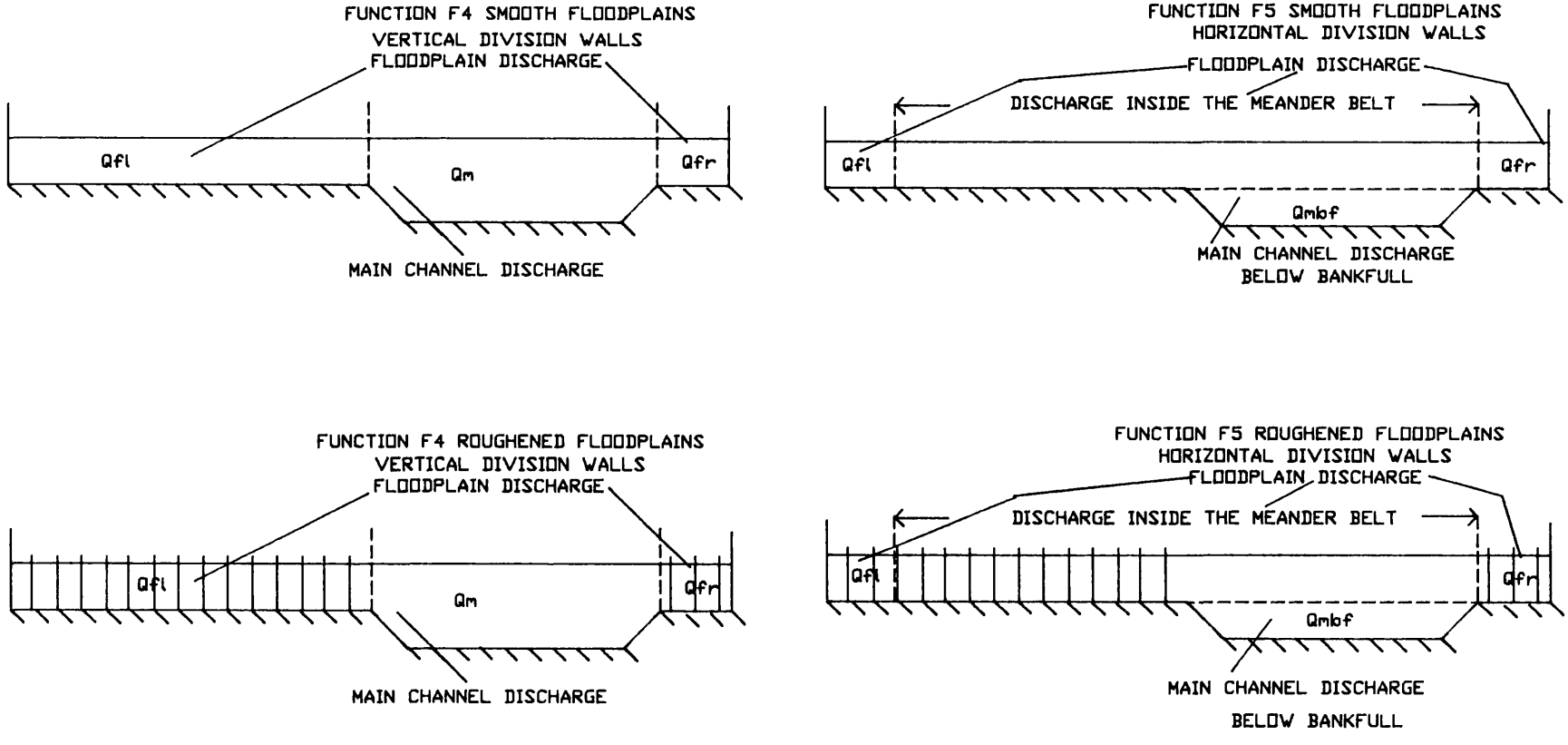

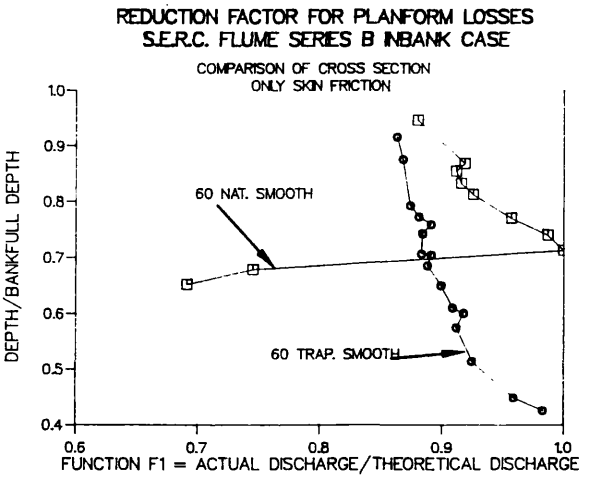

Fig (4.26) - Variation of Function F_1 with Depth Ratio. Comparison of Cross-Sections. S.E.R.C. Series B: Inbank Case; Sinuosity 1.37; Natural and Trapezoidal Cross-Section.

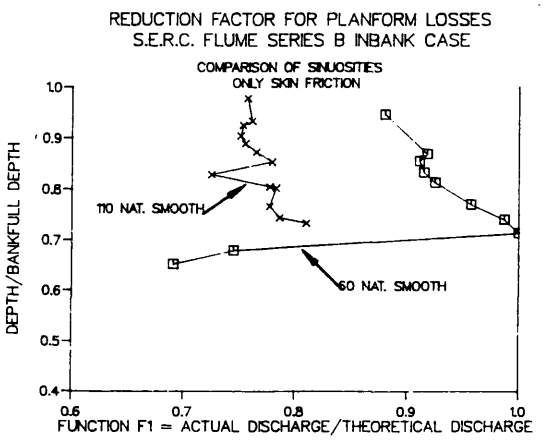

Fig (4.27) - Variation of Function F_1 with Depth Ratio. Comparison of Sinuosities. S.E.R.C. Series B: Inbank Case; Sinuosity 1.37 and 2.04; Natural Cross-Section.

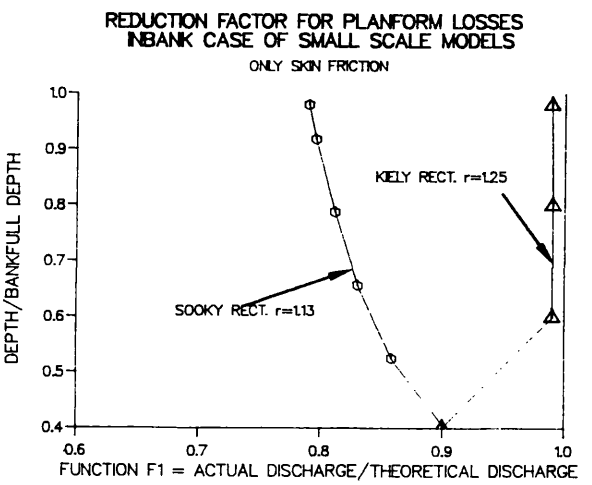

Fig (4.28) - Variation of Function F_1 with Depth Ratio. Comparison Between Kiely's and Toebes and Sooky 's Results.

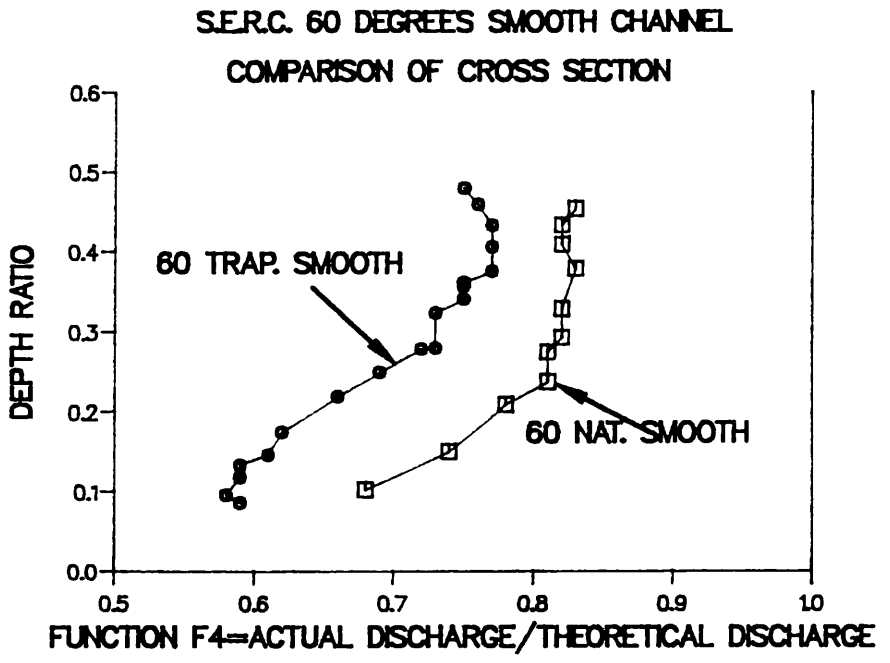

Fig (4.29) - Variation of Function F_4 with Depth Ratio. Comparison of Cross-Sections. S.E.R.C. Series B: Sinuosity 1.37; Natural and Trapezoidal Cross-Section; Smooth Floodplains.

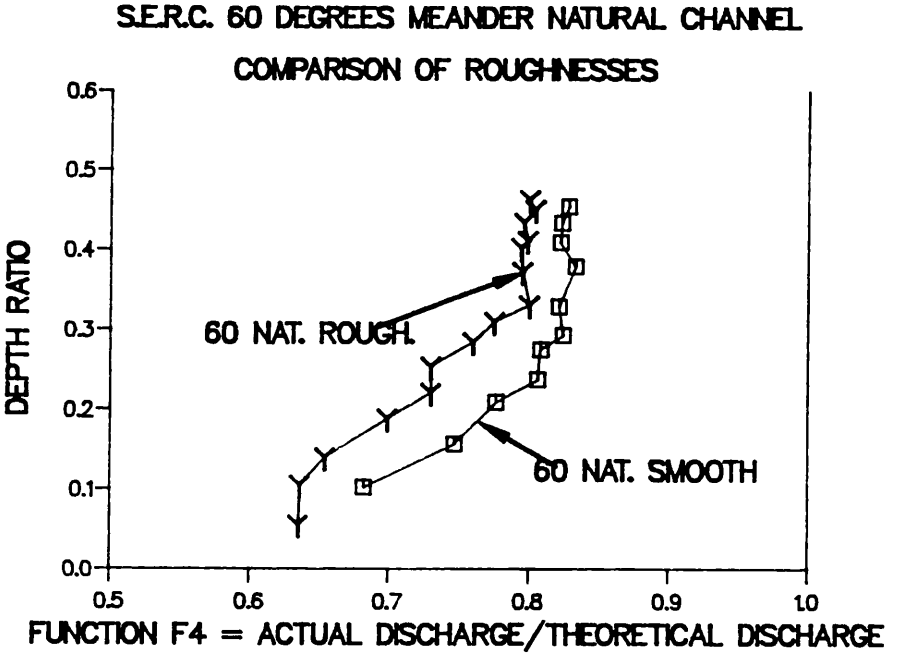

Fig (4.30) - Variation of Function F_4 with Depth Ratio. Comparison of Roughnesses. S.E.R.C. Series B: Sinuosity 1.37; Natural Cross-Section; Smooth and Fully Roughened Floodplains.

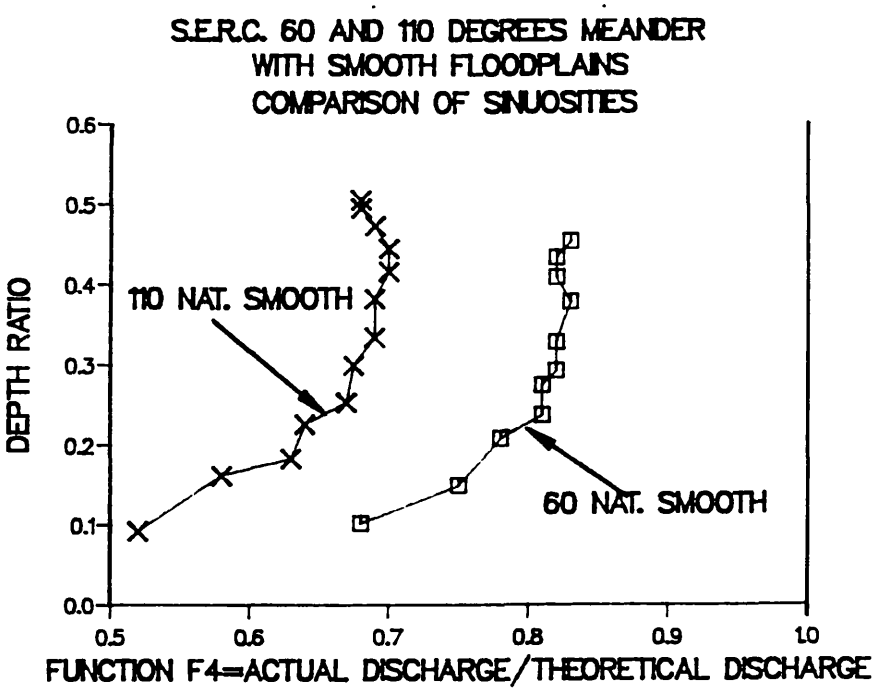

Fig (4.31) - Variation of Function F_4 with Depth Ratio. Comparison of Sinuosities. S.E.R.C. Series B: Sinuosity 1.37 and 2.04; Natural Cross-Section; Smooth Floodplains.

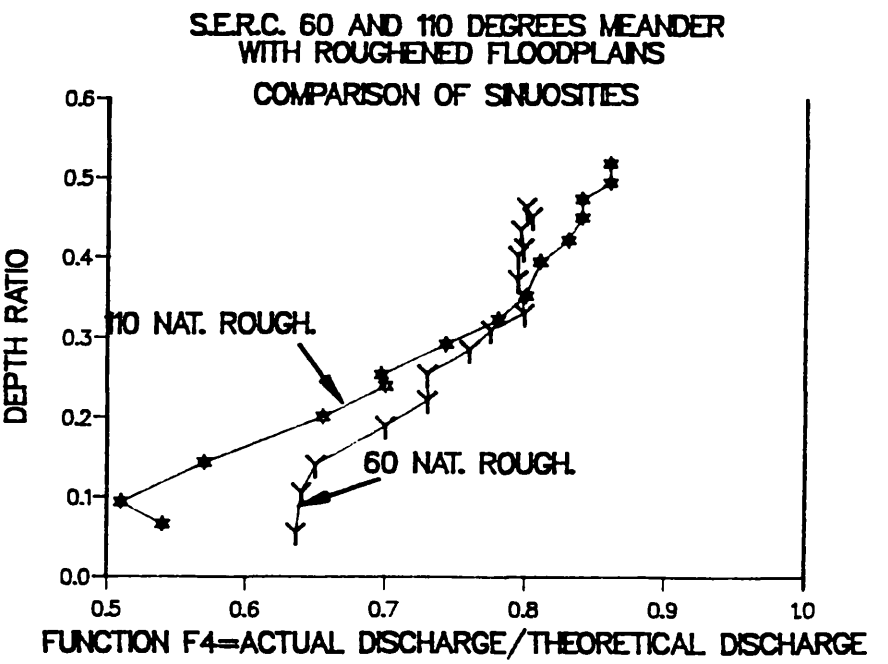

Fig (4.32) - Variation of Function F_4 with Depth Ratio. Comparison of Sinuosities. S.E.R.C. Series B: Sinuosity 1.37 and 2.04; Natural Cross-Section; Fully Roughened Floodplains.

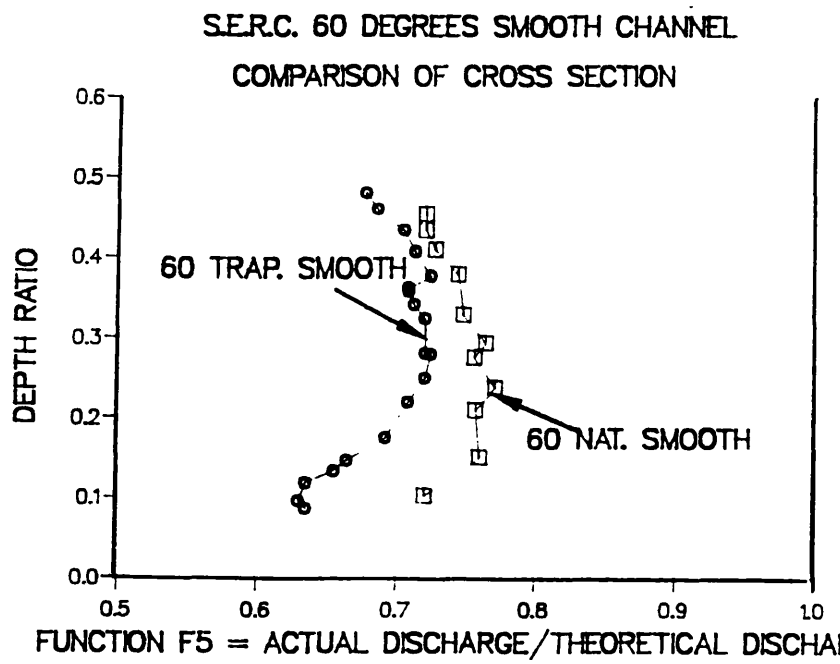

Fig (4.33) - Variation of Function F_5 with Depth Ratio. Comparison of Cross-Sections. S.E.R.C. Series B: Sinuosity 1.37; Natural and Trapezoidal Cross-Section; Smooth Floodplains.

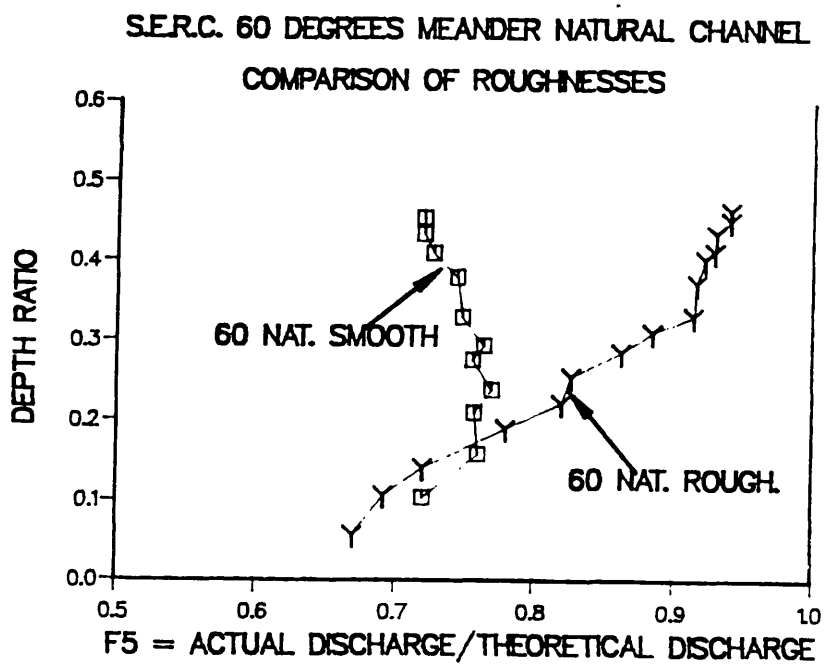

Fig (4.34) - Variation of Function F_5 with Depth Ratio. Comparison of Roughnesses. S.E.R.C. Series B: Sinuosity 1.37; Natural Cross-Section; Smooth and Fully Roughened Floodplains.

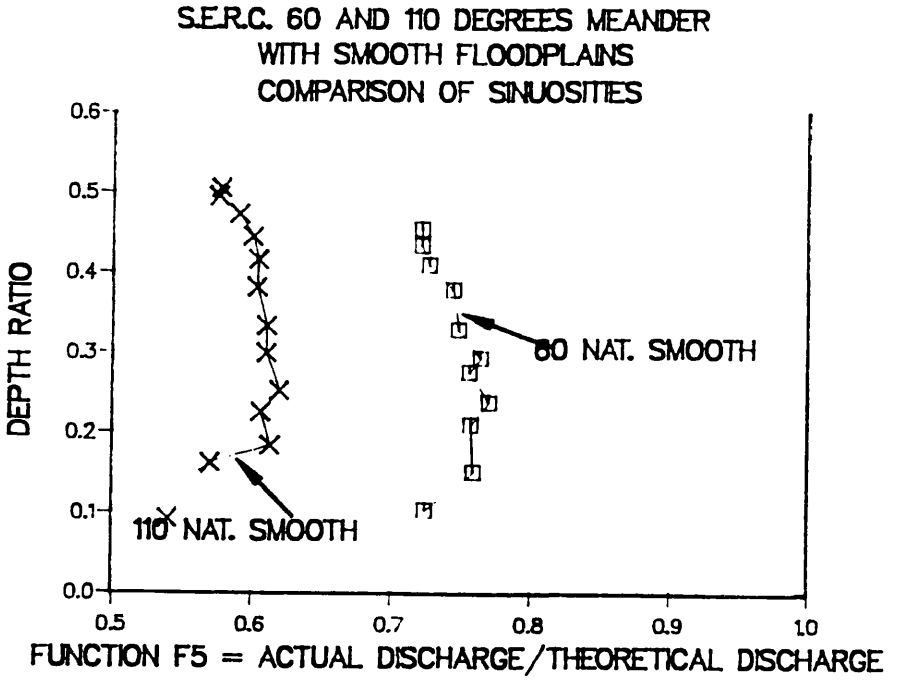

Fig (4.35) - Variation of Function F_5 with Depth Ratio. Comparison of Sinuosities. S.E.R.C. Series B: Sinuosity 1.37 and 2.04; Natural Cross-Section; Smooth Floodplains.

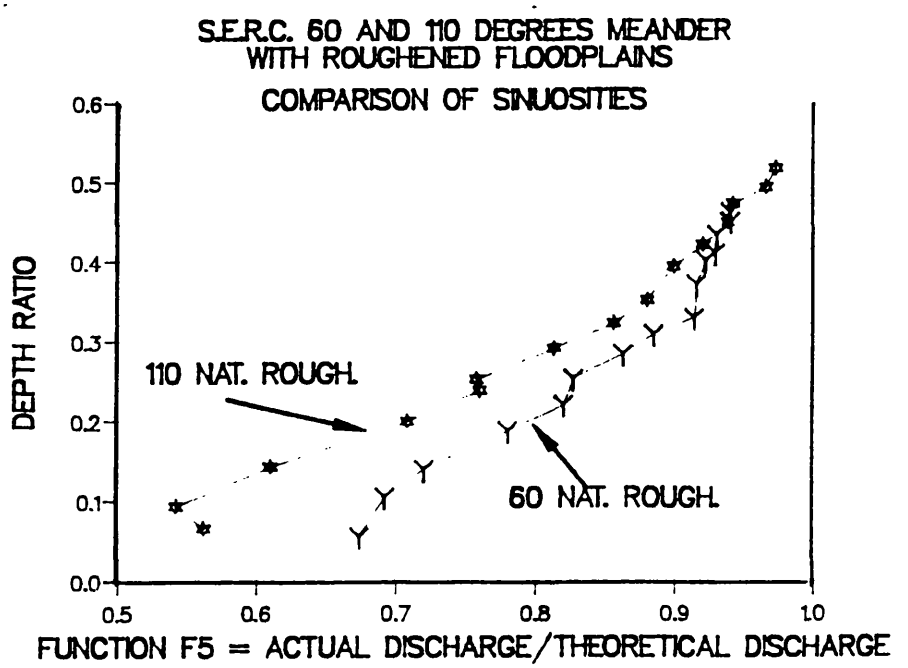

Fig (4.36) - Variation of Function F_5 with Depth Ratio. Comparison of Sinuosities. S.E.R.C. Series B: Sinuosity 1.37 and 2.04; Natural Cross-Section; Fully Roughened Floodplains.

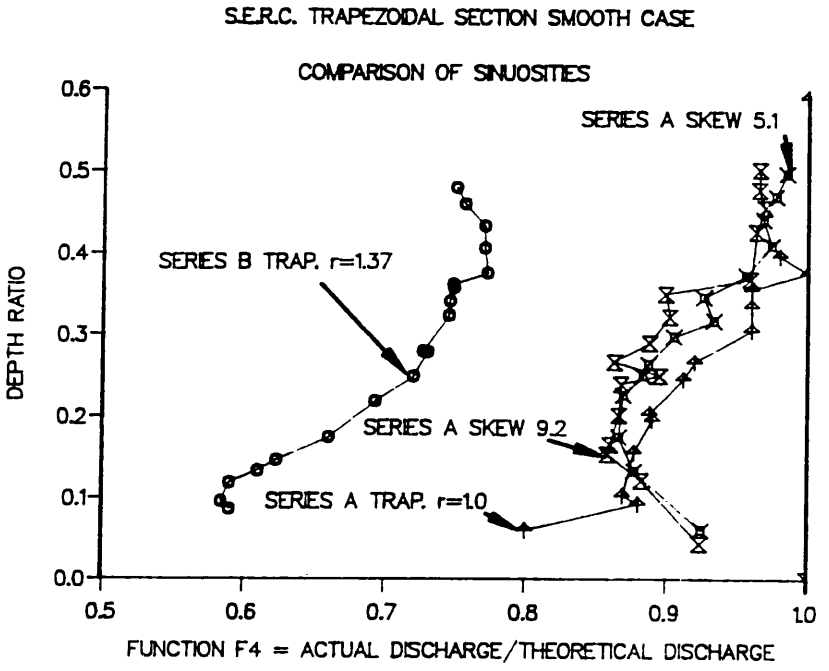

Fig (4.37) - Variation of Function F_4 with Depth Ratio. Comparison of Sinuosities. S.E.R.C. Series A and B. The Straight, The Skew and The Meandering Channel. Smooth Floodplains.

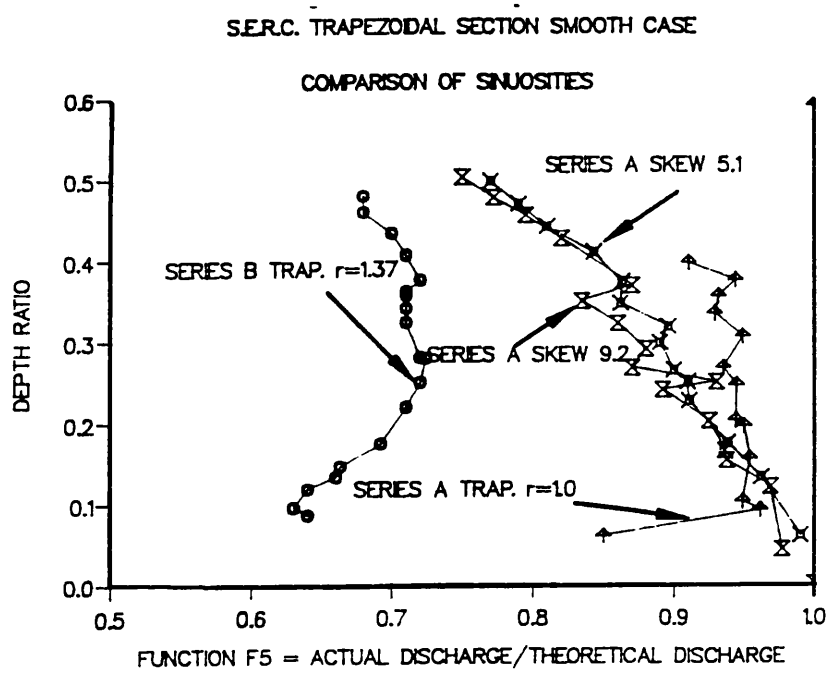

Fig (4.38) - Variation of Function F_5 with Depth Ratio. Comparison of Sinuosities. S.E.R.C. Series A and B. The Straight, The Skew and The Meandering Channel. Smooth Floodplains.

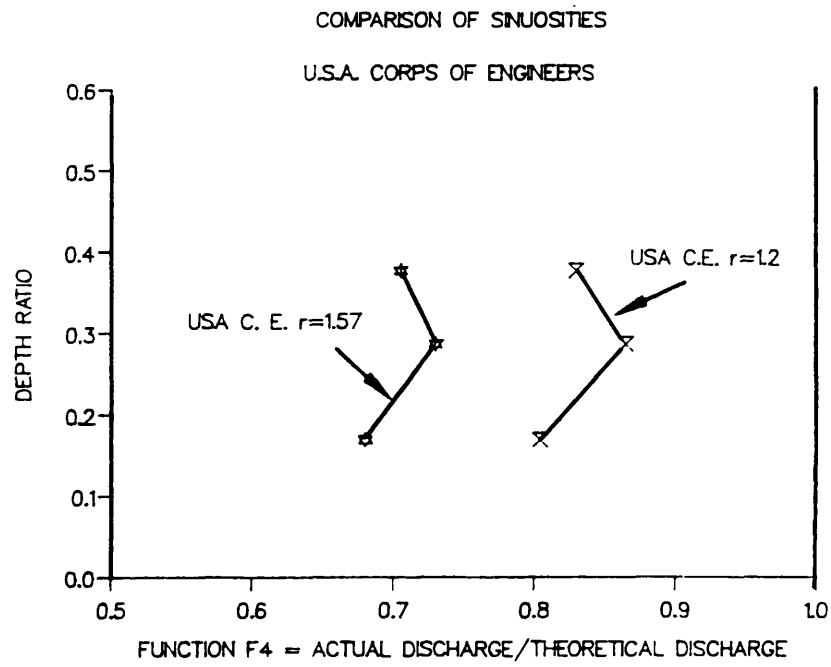

Fig (4.39) - Variation of Function F_4 with Depth Ratio. Comparison of Sinuosities. Results from U.S.A. Corps of Engineers. Smooth Floodplains.

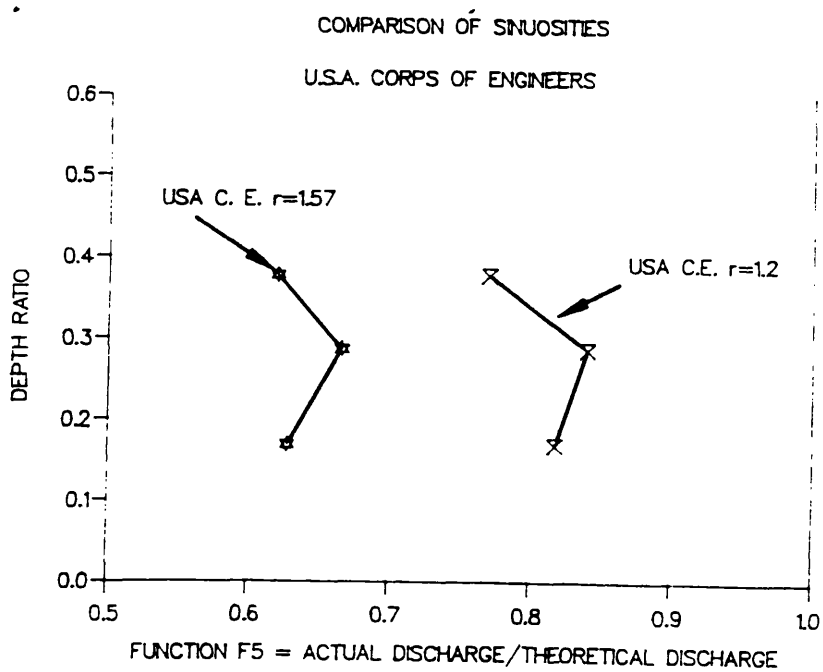

Fig (4.40) - Variation of Function F_5 with Depth Ratio. Comparison of Sinuosities. Results from U.S.A. Corps of Engineers. Smooth Floodplains.

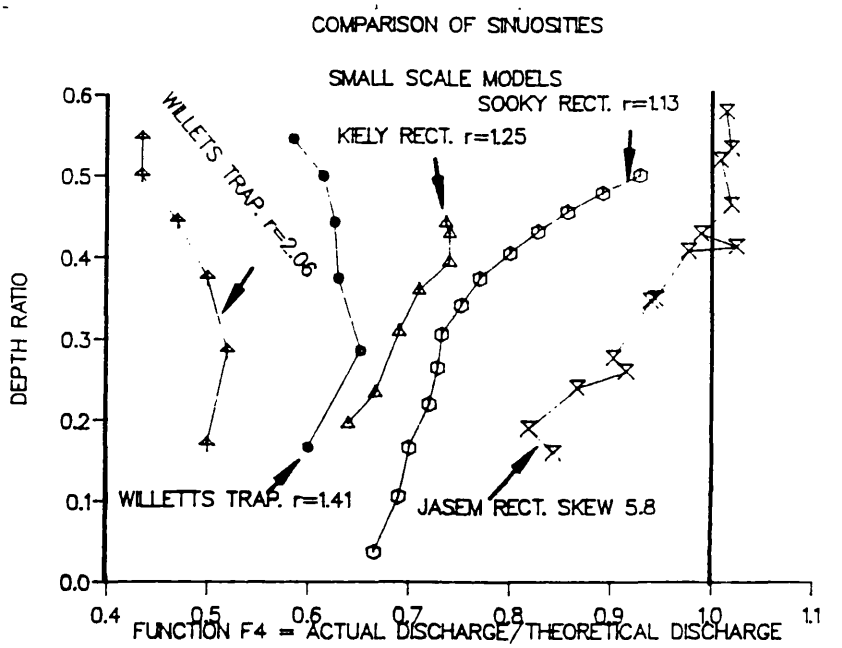

Fig (4.41) - Variation of Function F_4 with Depth Ratio. Comparison of Sinuosities. Results from Kiely, Sooky, Jasem and Willetts. Smooth Floodplains.

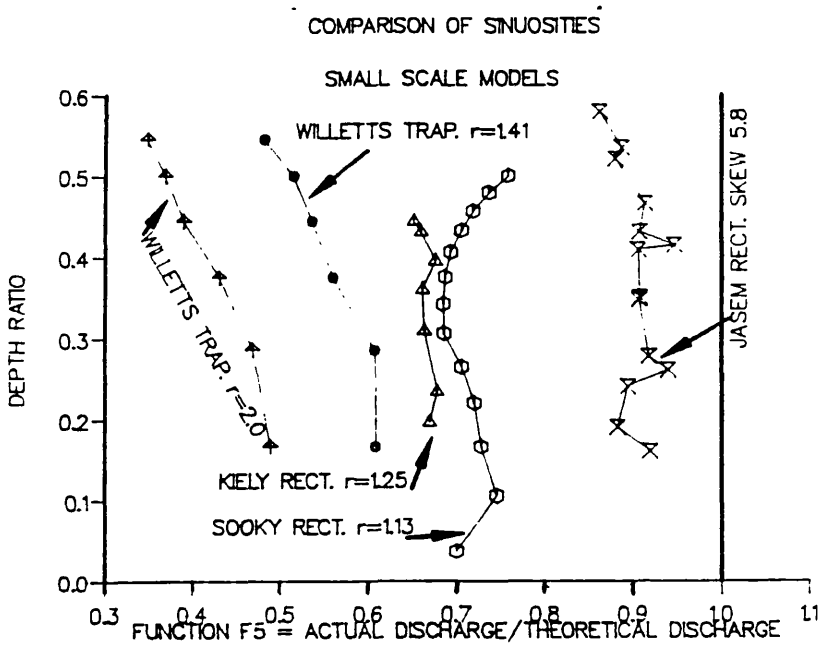

Fig (4.42) - Variation of Function F_5 with Depth Ratio. Comparison of Sinuosities. Results from Kiely, Sooky, Jasem and Willetts. Smooth Floodplains.

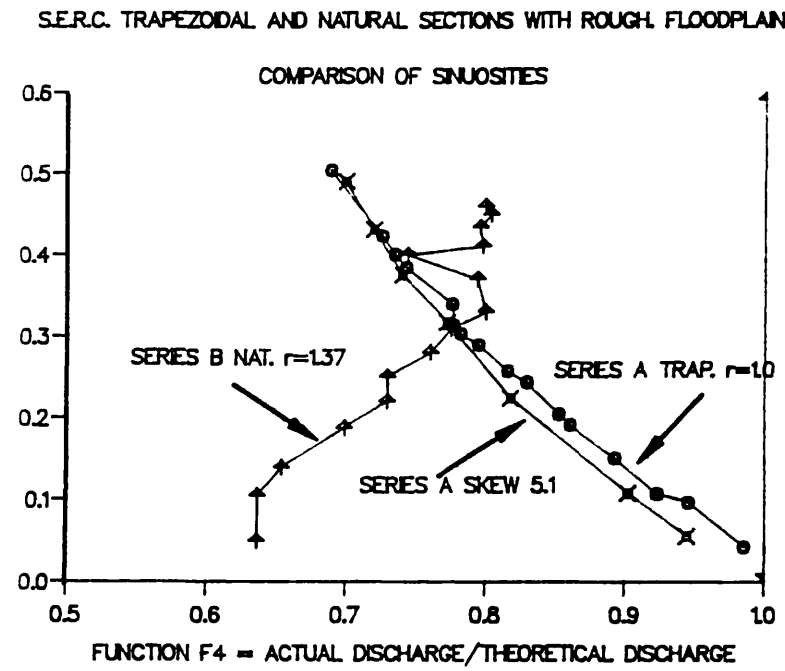

Fig (4.43) - Variation of Function F_4 with Depth Ratio. Comparison of Sinuosities. S.E.R.C. Series A and B. The Straight, The Skew and The Meandering Compound Channel. Roughened Floodplains.

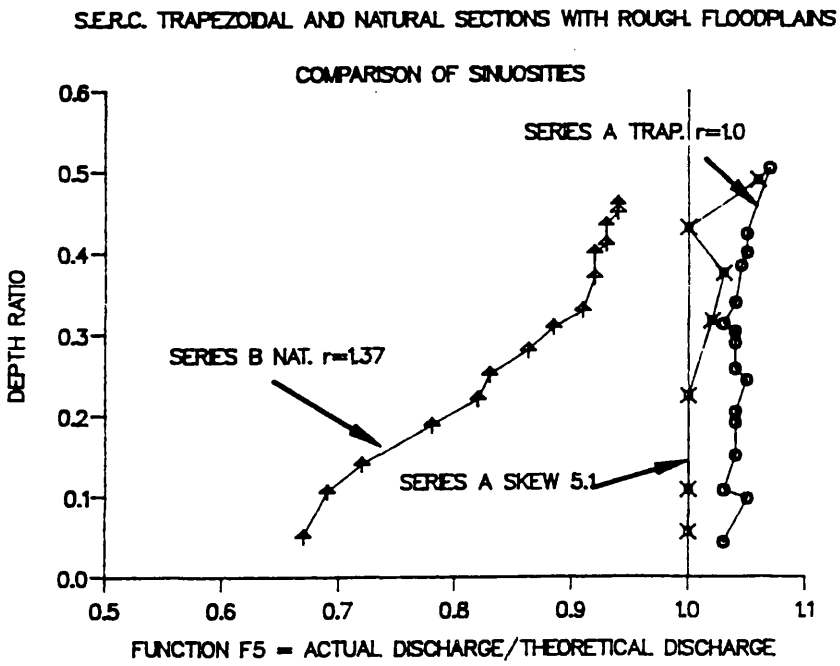

Fig (4.44) - Variation of Function F_5 with Depth Ratio. Comparison of Sinuosities. S.E.R.C. Series A and B. The Straight, The Skew and The Meandering Compound Channel. Roughened Floodplains.

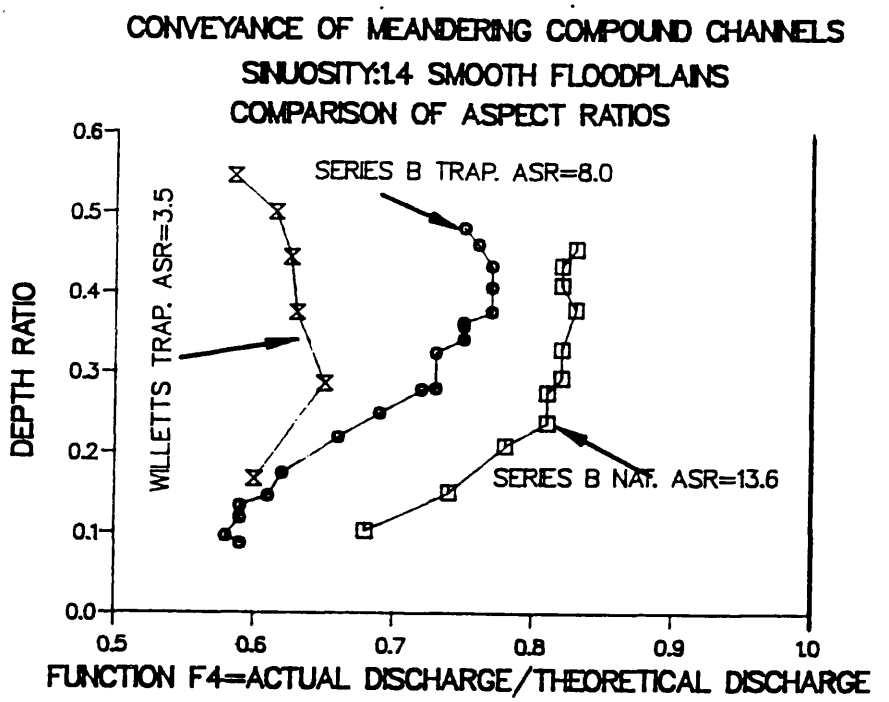

Fig (4.45) - Variation of Function F_4 with Depth Ratio. Comparison of Aspect Ratios. Results from S.E.R.C. Series B and from Willetts. Sinuosity 1.37. Smooth Floodplains.

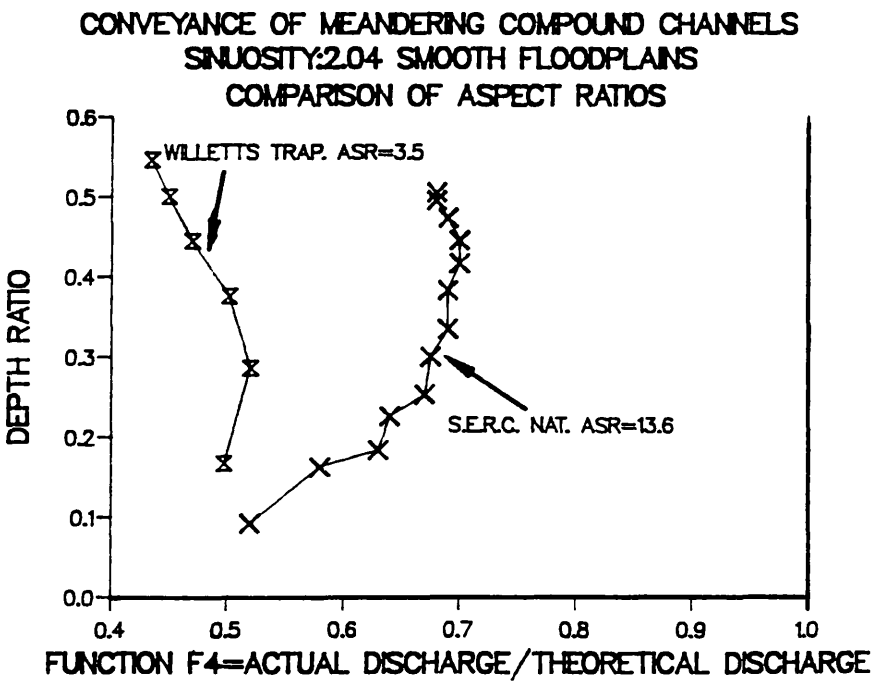

Fig (4.46) - Variation of Function F_4 with Depth Ratio. Comparison of Aspect Ratios. Results from S.E.R.C. Series B and from Willets. Sinuosity 2.0. Smooth Floodplains.

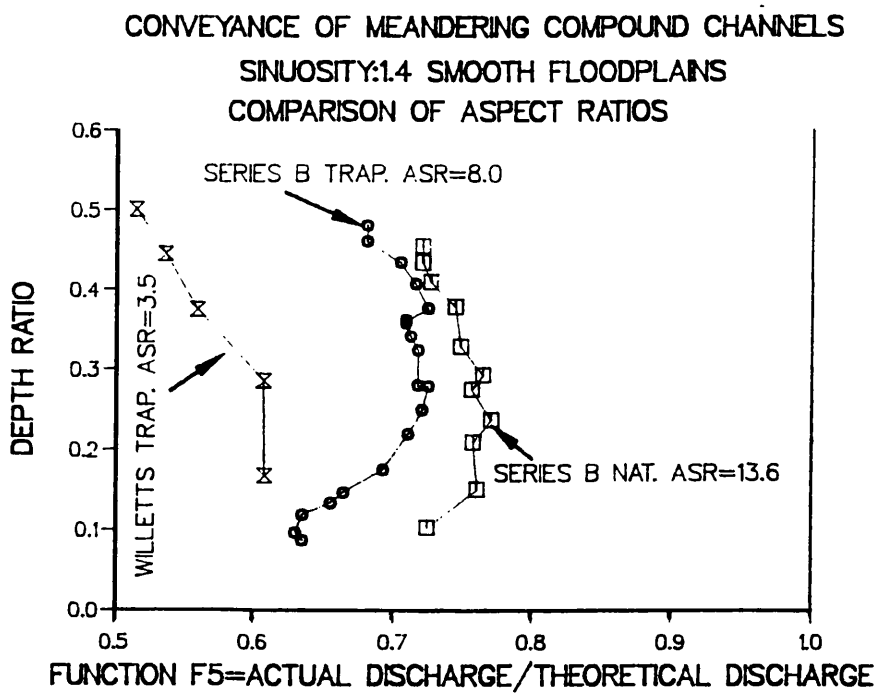

Fig (4.47) - Variation of Function F_5 with Depth Ratio. Comparison of Aspect Ratios. Results from S.E.R.C. Series B and from Willetts. Sinuosity 1.37. Smooth Floodplains.

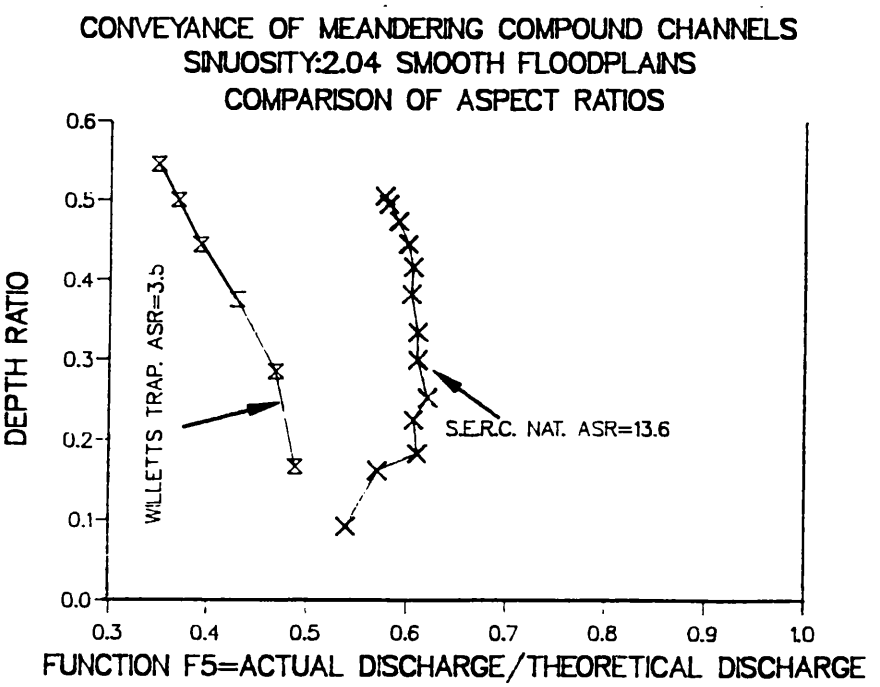

Fig (4.48) - Variation of Function F_5 with Depth Ratio. Comparison of Aspect Ratios. Results from S.E.R.C. Series B and from Willetts. Sinuosity 2.0. Smooth Floodplains.

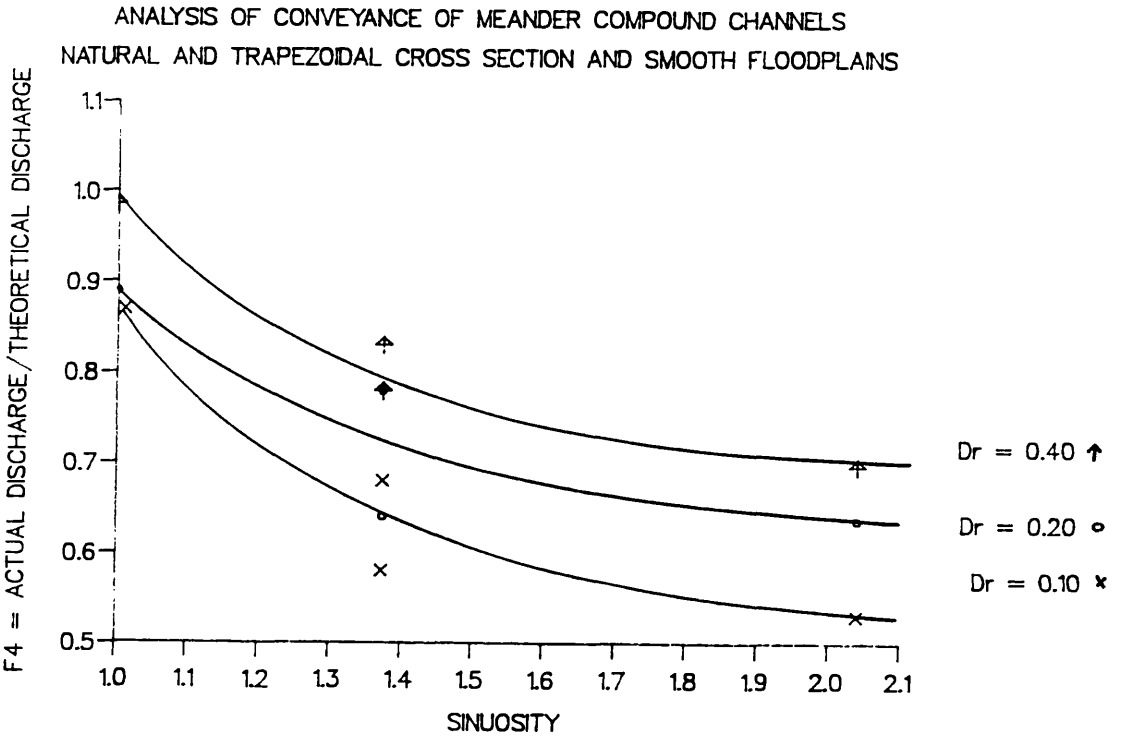

Fig (4.49) - Parametric Analysis of the Conveyance in Meandering Compound Channels. Variation of Function F_4 with Sinuosity for Constant Values of Depth Ratio. S.E.R.C. Series A and B. Smooth Floodplains.

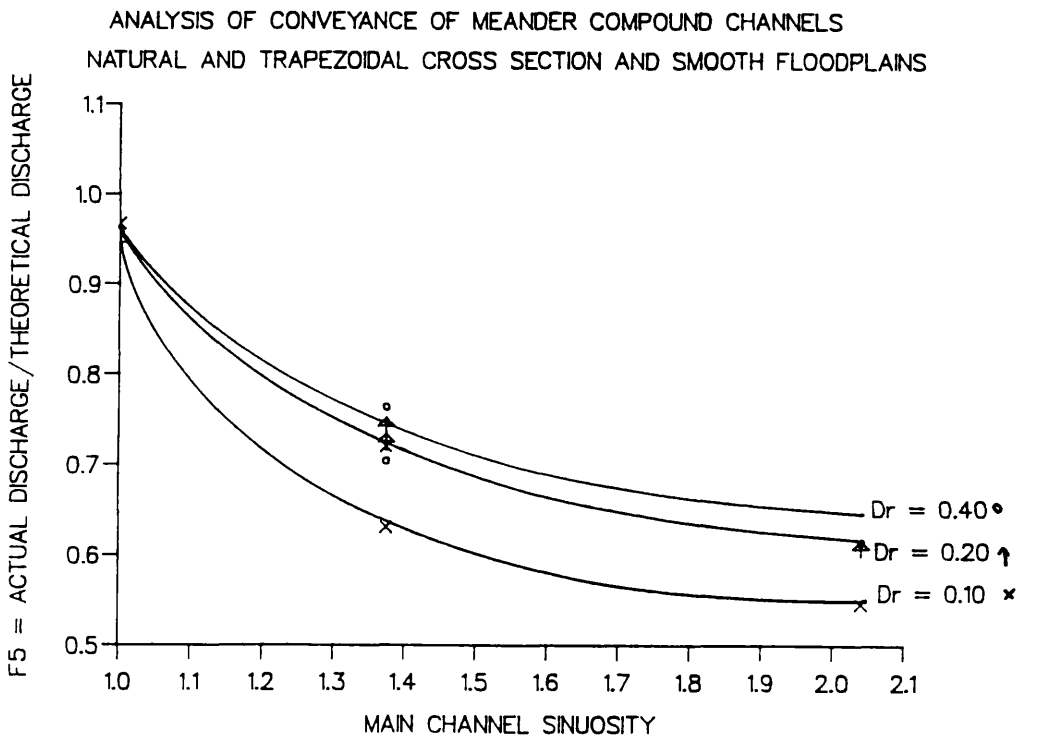

Fig (4.50) - Parametric Analysis of the Conveyance in Meandering Compound Channels. Variation of Function F_5 with Sinuosity, for Constant Values of Depth Ratio. S.E.R.C. Series A and B. Smooth Floodplains.

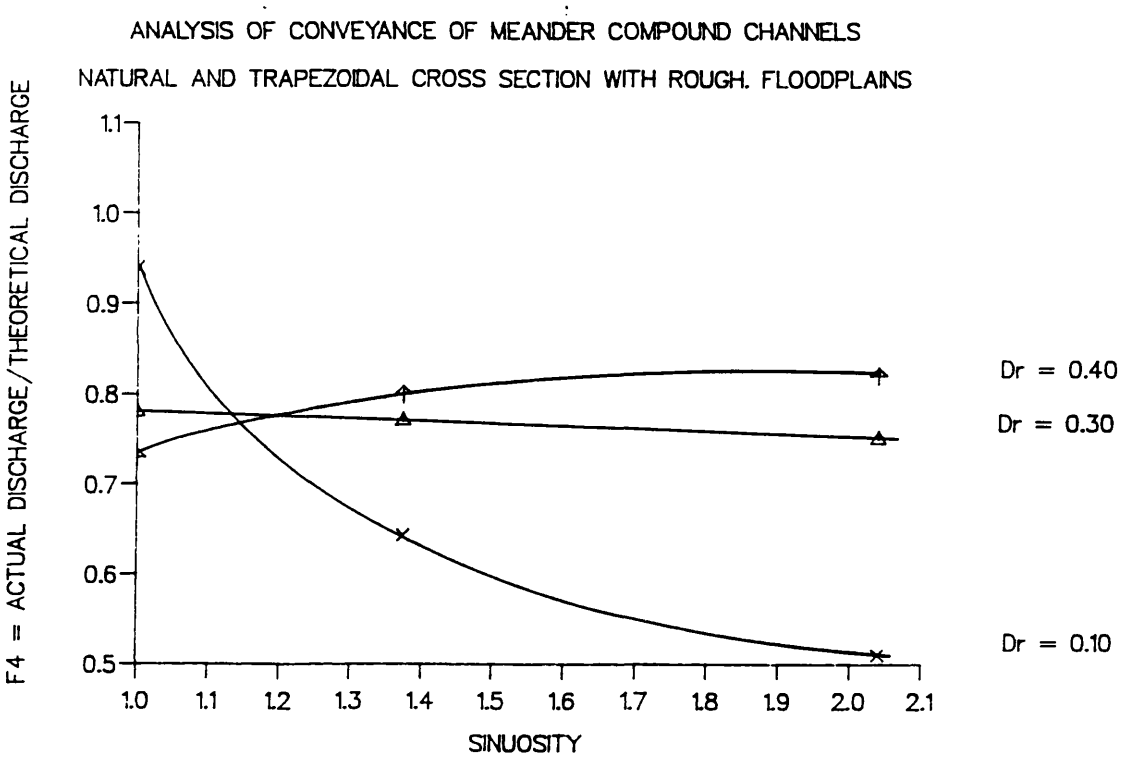

Fig (4.51) - Parametric Analysis of the Conveyance in Meandering Compound Channels. Variation of Function F_4 with Sinuosity, for Constant Values of Depth Ratio. S.E.R.C. Series A and B. Roughened Floodplains.

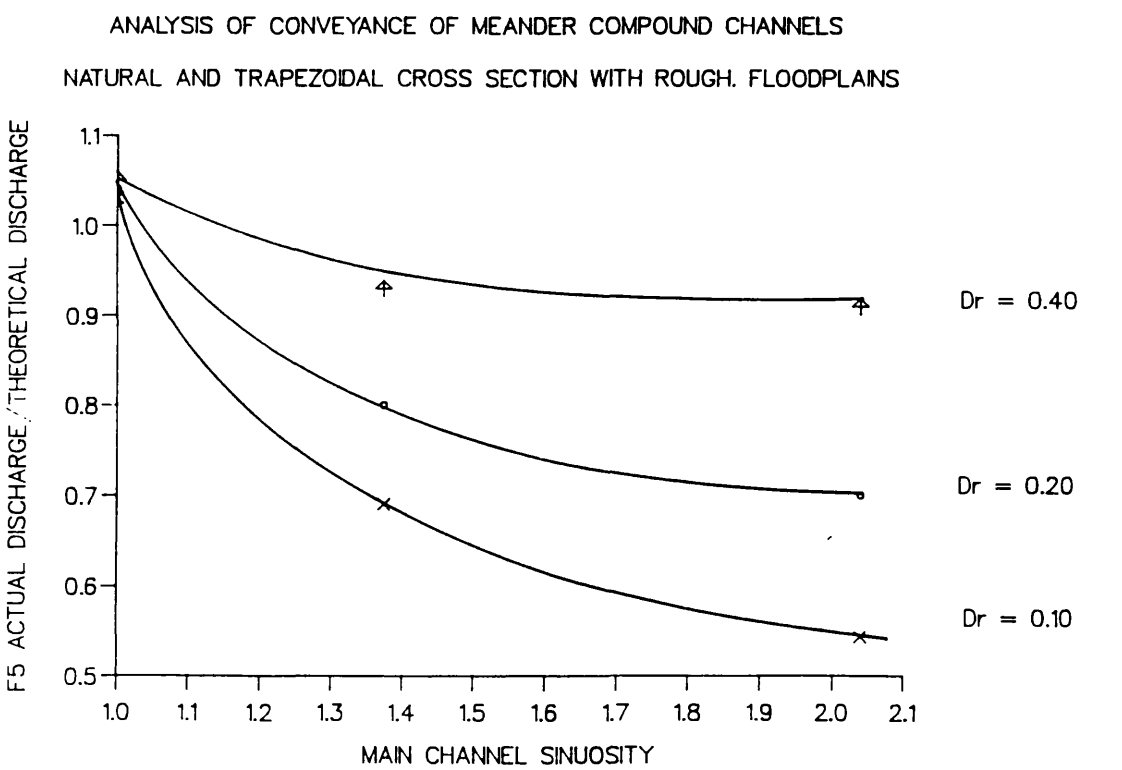

Fig (4.52) - Parametric Analysis of the Conveyance in Meandering Compound Channels. Variation of Function F_5 with Sinuosity, for Constant Values of Depth Ratio. S.E.R.C. Series A and B. Roughened Floodplains.

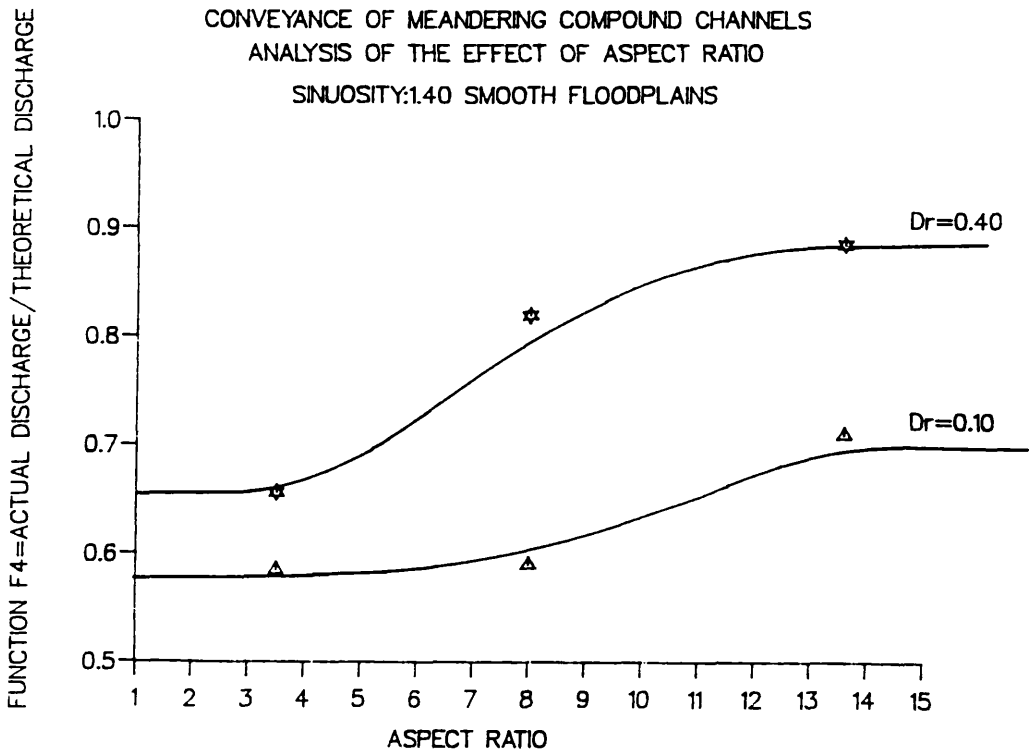

Fig (4.53) - Parametric Analysis of the Conveyance in Meandering Compound Channels. Variation of The Aspect Ratio with Function F4 for Constant Values of The Depth Ratio. Results from S.E.R.C. Series B and from Willetts.(1990) Sinuosity 1.4. Smooth Floodplains.

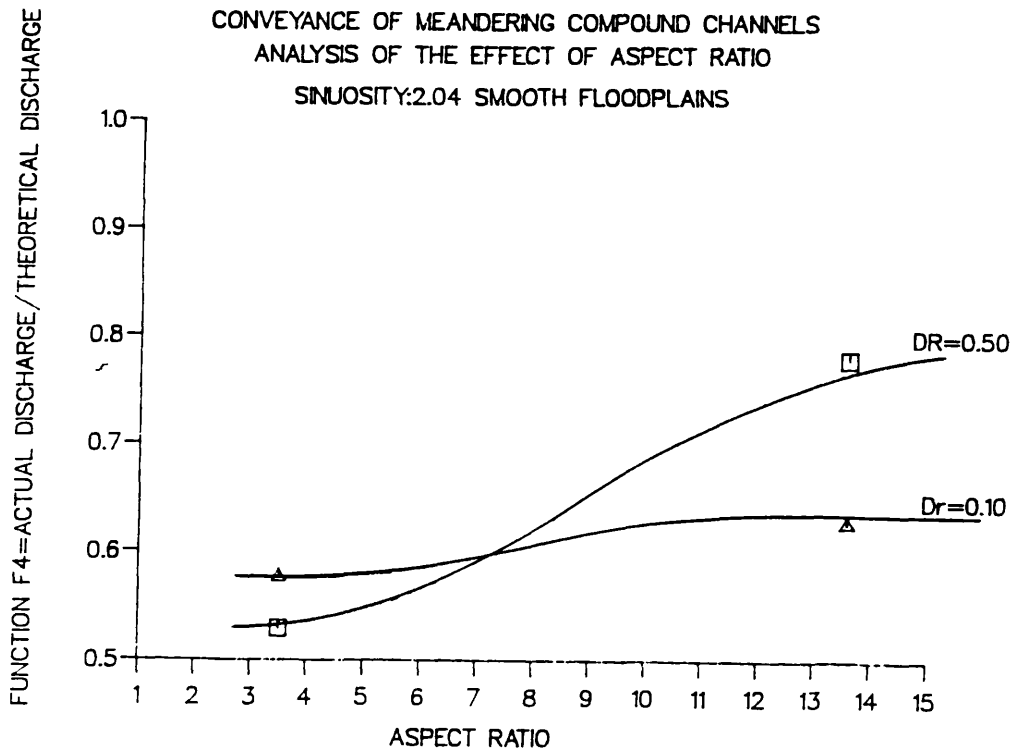

Fig (4.54) - Parametric Analysis of the Conveyance in Meandering Compound Channels. Variation of Function F4 with the Aspect Ratio, for Constant Values of The Depth Ratio. Results from S.E.R.C. Series B and from Willets.(1990) Sinuosity 2.0. Smooth Floodplains.

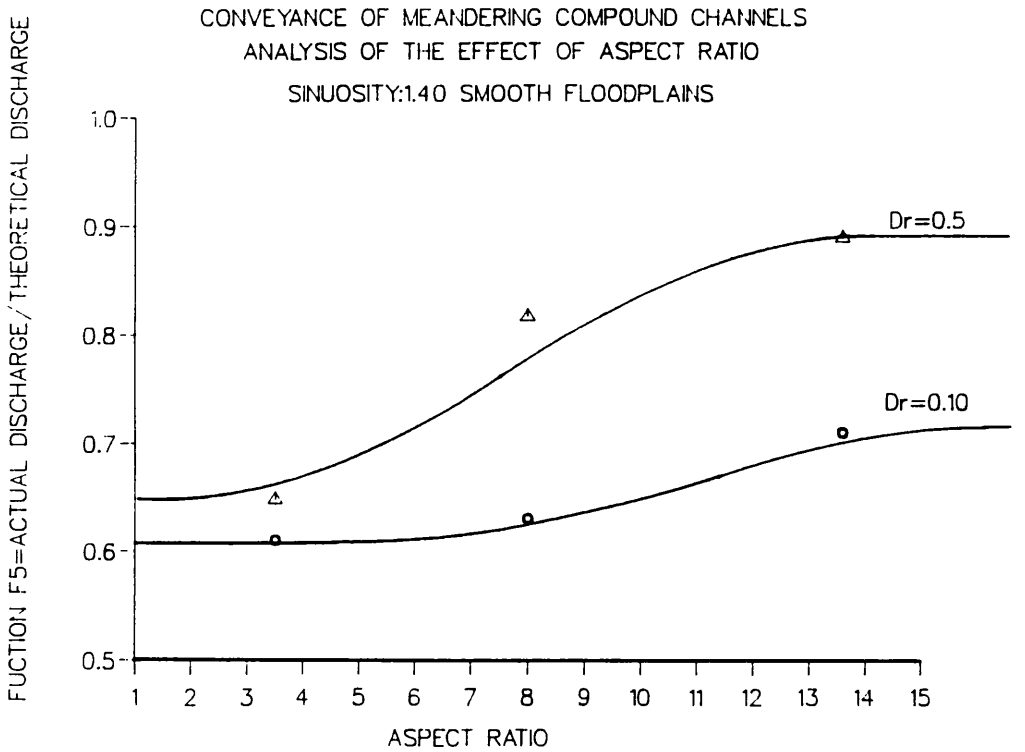

Fig (4.55) - Parametric Analysis of the Conveyance in Meandering Compound Channels. Variation of Function F_5 with the Aspect Ratio, for Constant Values of The Depth Ratio. Results from S.E.R.C. Series B and from Willets (1990). Sinuosity 1.4. Smooth Floodplains.

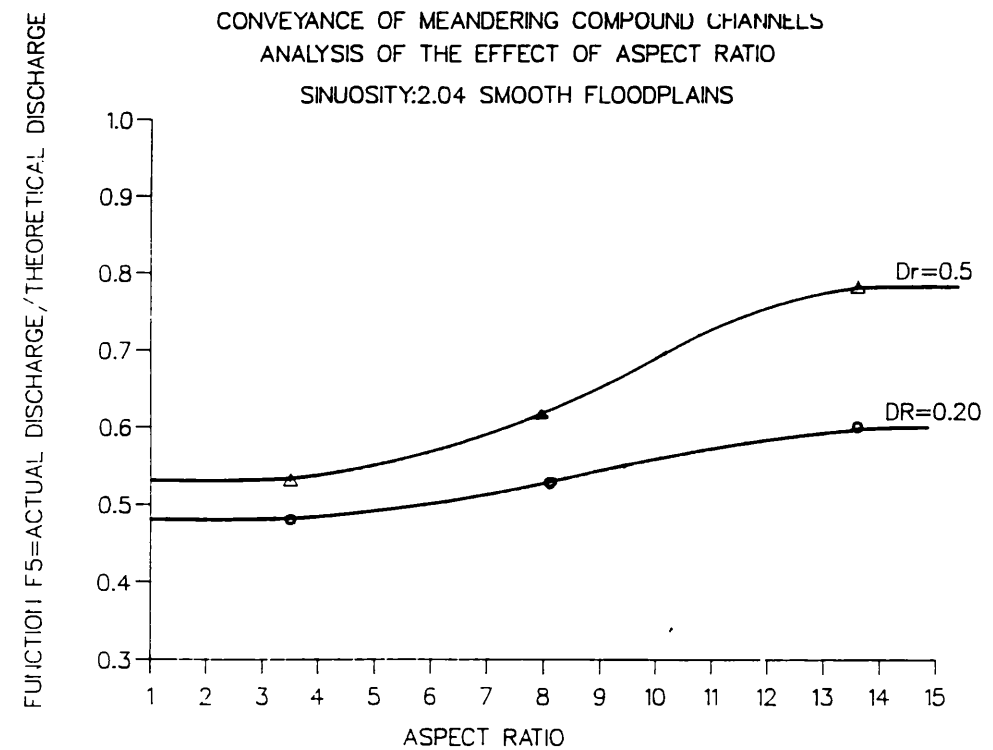

Fig (4.56) - Parametric Analysis of the Conveyance in Meandering Compound Channels. Variation of Function F_5 with The Aspect Ratio, for Constant Values of The Depth Ratio. Results from S.E.R.C. Series B and from Willetts (1990). Sinuosity 2.0. Smooth Floodplains.

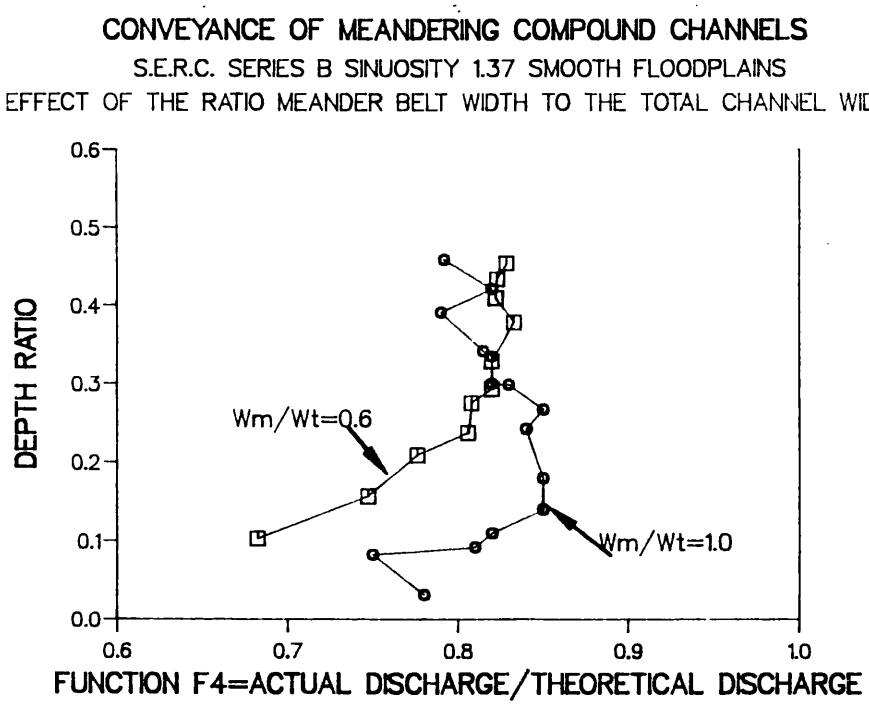

Fig (4.56a) - Variation of Function F_4 with the Ratio of the Meander Belt Width(W_m) to the total Width of the Channel(W_t). Results from S.E.R.C. Series B. Sinuosity 1.37 and Smooth Floodplains. W_m/W_t=1.0 and 0.6.

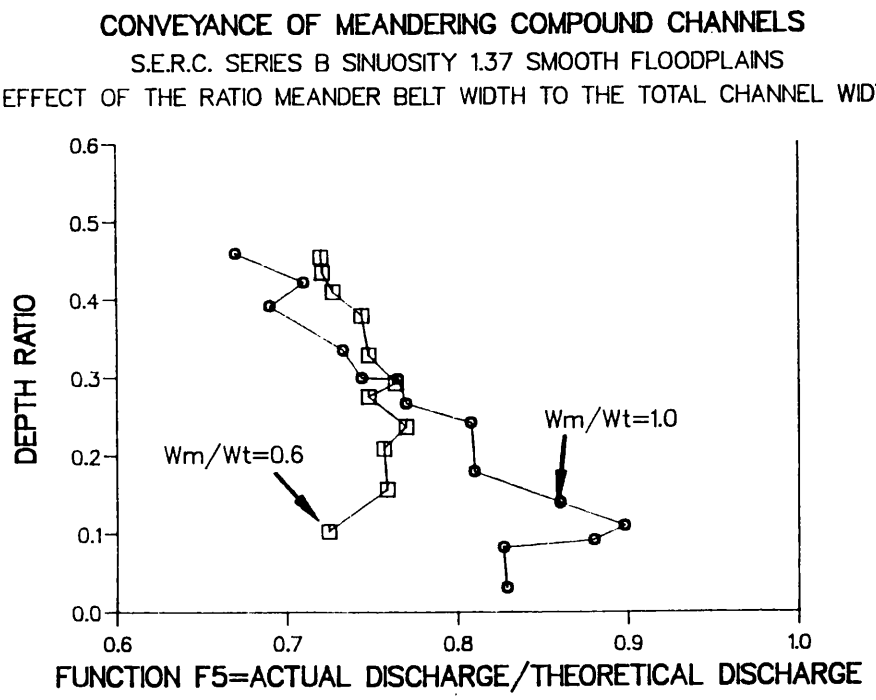

Fig (4.56b) - Variation of Function F_5 with the Ratio of the Meander Belt Width(W_m) to the total Width of the Channel(W_t). Results from S.E.R.C. Series B. Sinuosity 1.37 and Smooth Floodplains. W_m/W_t=1.0 and 0.6.

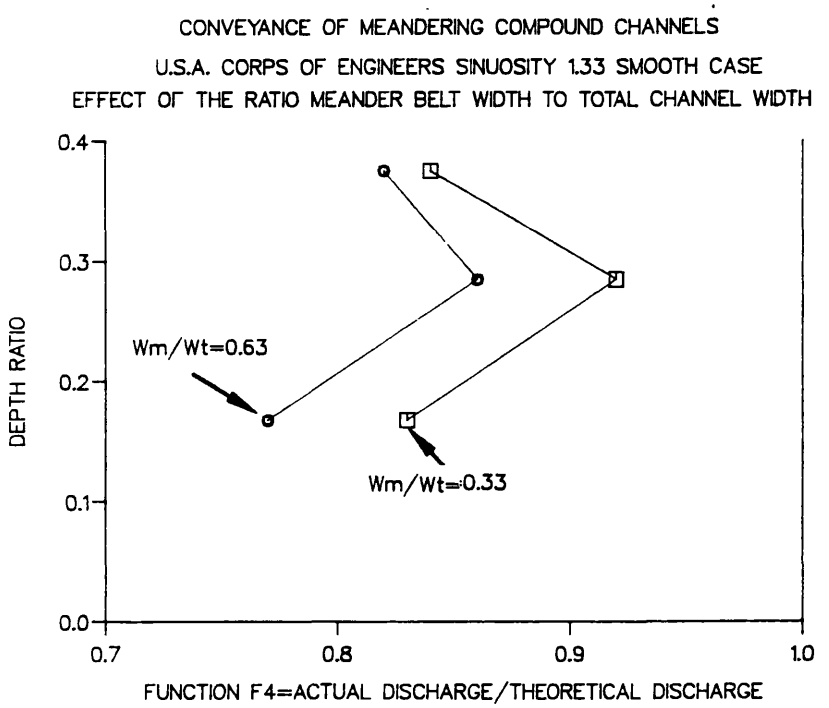

Fig (4.56c) - Variation of Function F_4 with the Ratio of the Meander Belt Width(W_m) to the total Width of the Channel(W_t). Results from U.S. Army Corps of Engineers (1956). Sinuosity 1.33. Smooth Floodplains.

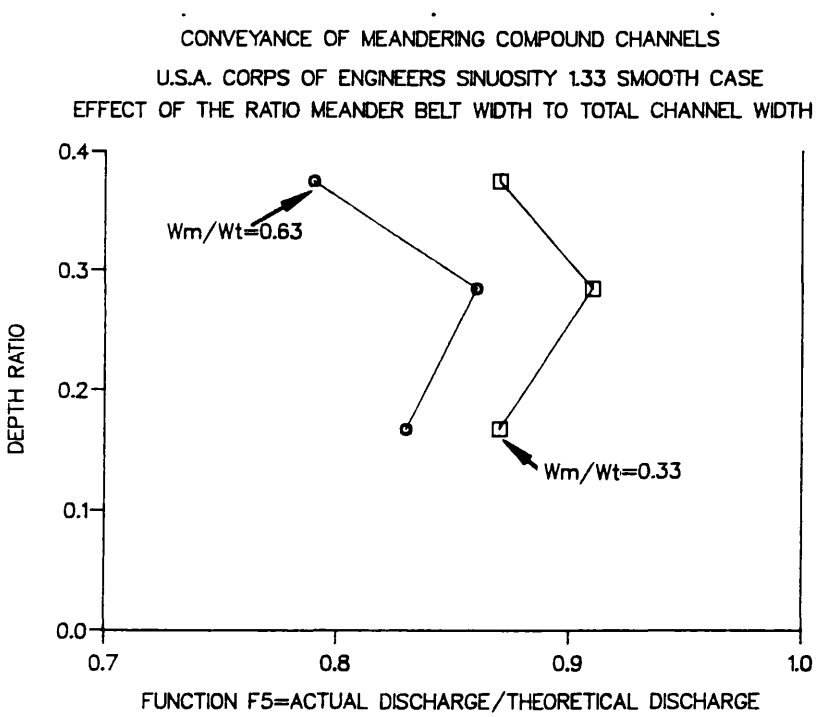

Fig (4.56d) - Variation of Function F_5 with the Ratio of the Meander Belt Width(W_m) to the total Width of the Channel(W_t). Results from U.S. Army Corps of Engineers (1956). Sinuosity 1.33. Smooth Floodplains.

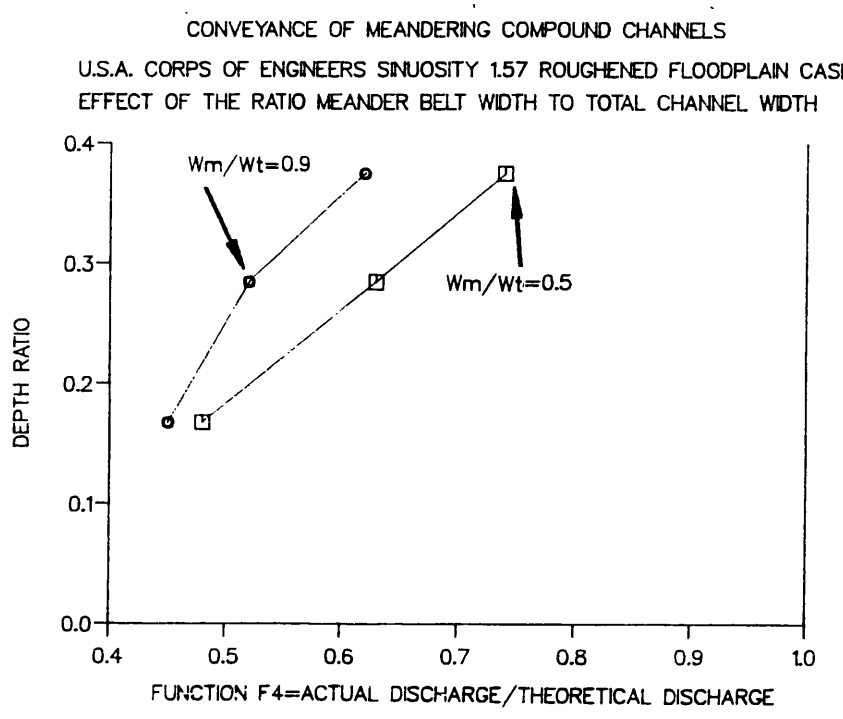

Fig (4.56e) - Variation of Function F_4 with the Ratio of the Meander Belt Width(W_m) to the total Width of the Channel(W_t). Results from U.S. Army Corps of Engineers (1956). Sinuosity 1.57. Fully Roughened Floodplains.

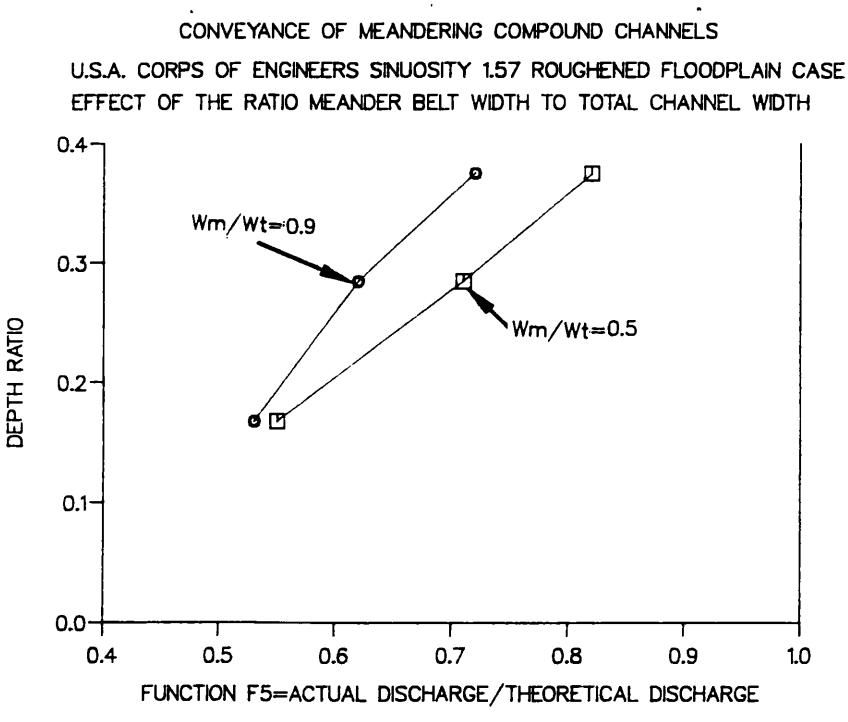

Fig (4.56f) - Variation of Function F_5 with the Ratio of the Meander Belt Width(W_m) to the total Width of the Channel(W_t). Results from U.S. Army Corps of Engineers (1956). Sinuosity 1.57. Fully Roughened Floodplains.

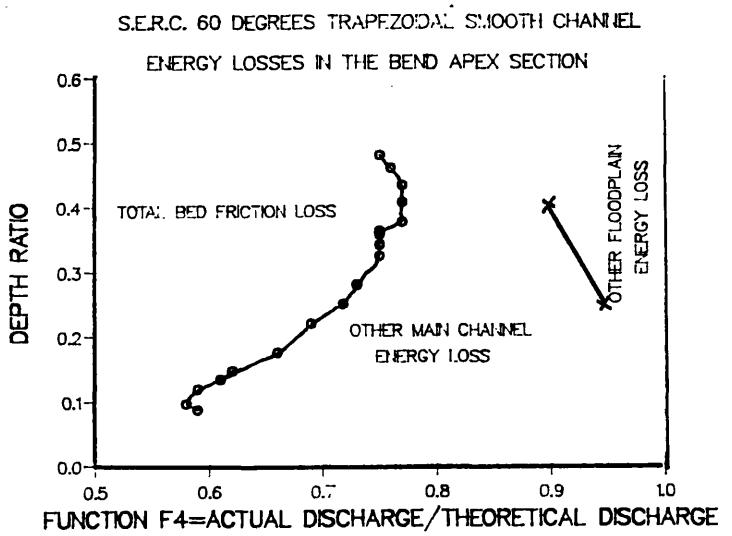

Fig (4.57) - Separation of The Main Channel Energy Losses from Floodplain Energy Losses. Variation of Function F_4 with Depth Ratio. S.E.R.C. Series B: Sinuosity 1.37; Trapezoidal Cross-Section; Smooth Floodplains.

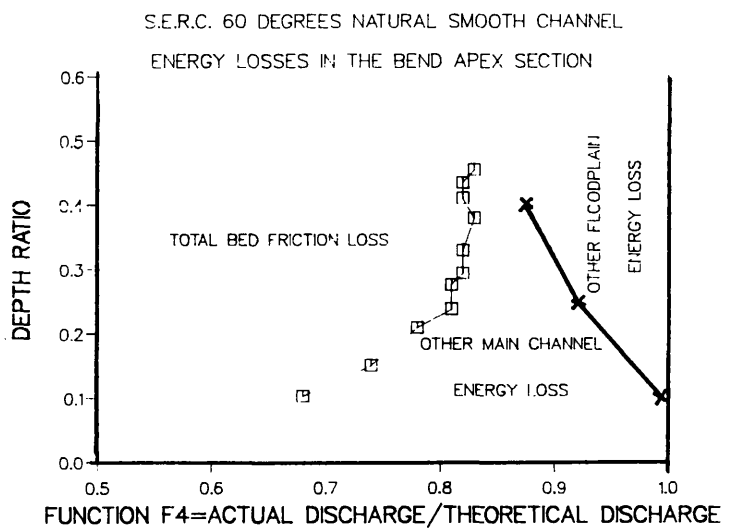

Fig (4.58) - Separation of The Main Channel Energy Losses from Floodplain Energy Losses. Variation of Function F_4 with Depth Ratio. S.E.R.C. Series B: Sinuosity 1.37; Natural Cross-Section; Smooth Floodplains.

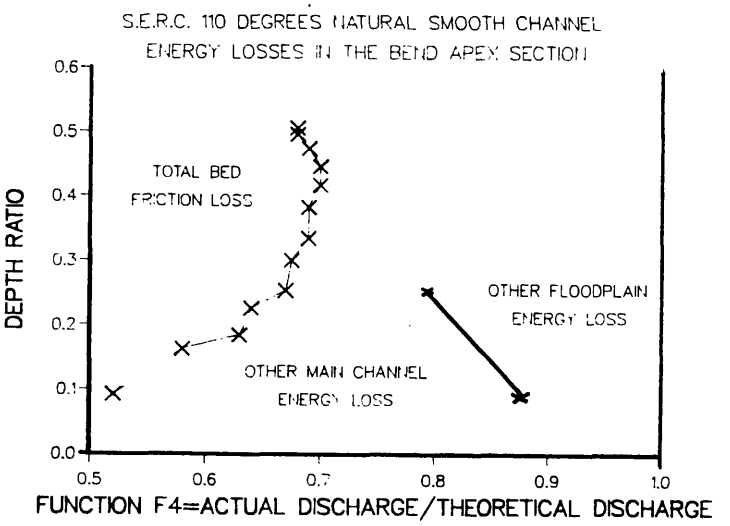

Fig (4.59) - Separation of The Main Channel Energy Losses from Floodplain Energy Losses. Variation of Function F_4 with Depth Ratio. S.E.R.C. Series B: Sinuosity 2.04; Natural Cross-Section; Smooth Floodplains.

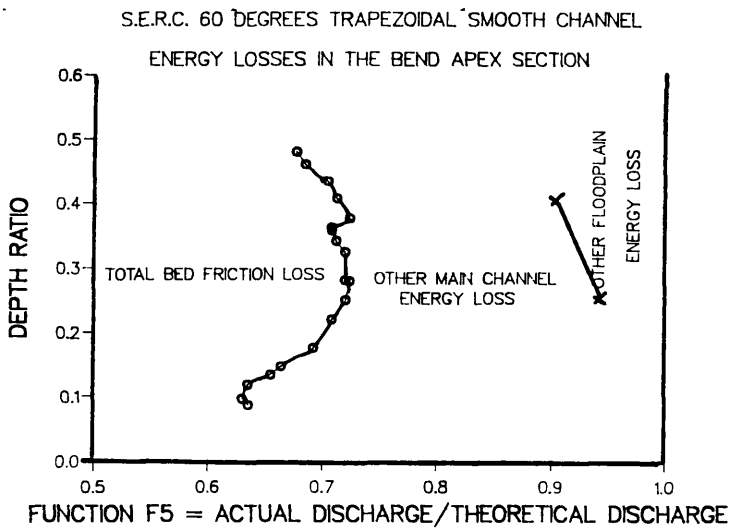

Fig (4.60) - Separation of The Main Channel Energy Losses from Floodplain Energy Losses. Variation of Function F_5 with Depth Ratio. S.E.R.C. Series B: Sinuosity 1.37; Trapezoidal Cross-Section; Smooth Floodplains.

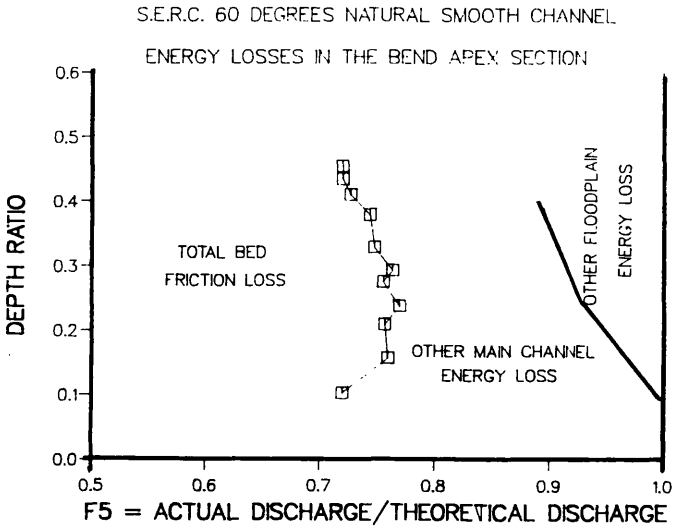

Fig (4.61) - Separation of The Main Channel Energy Losses from Floodplain Energy Losses. Variation of Function F_5 with Depth Ratio. S.E.R.C. Series B: Sinuosity 1.37; Natural Cross-Section; Smooth Floodplains.

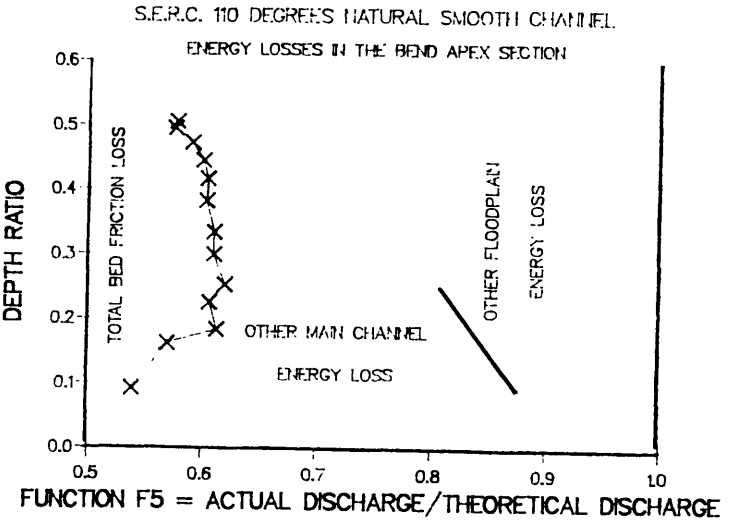

Fig (4.62) - Separation of The Main Channel Energy Losses from Floodplain Energy Losses. Variation of Function F_5 with Depth Ratio. S.E.R.C. Series B: Sinuosity 2.04; Natural Cross-Section; Smooth Floodplains.

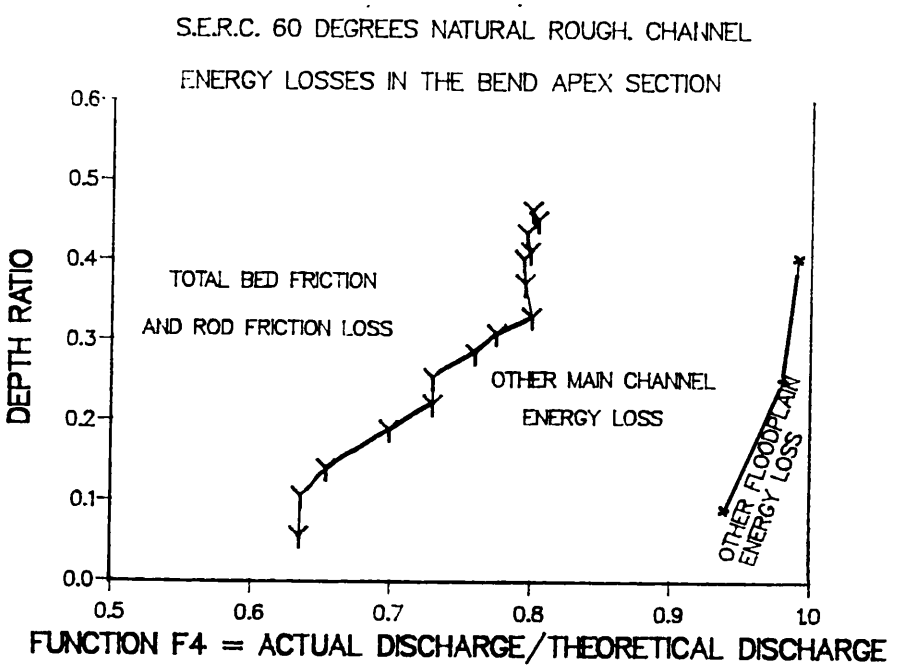

Fig (4.63) - Separation of The Main Channel Energy Losses from Floodplain Energy Losses. Variation of Function F_4 with Depth Ratio. S.E.R.C. Series B: Sinuosity 1.37; Natural Cross-Section; Roughened Floodplains.

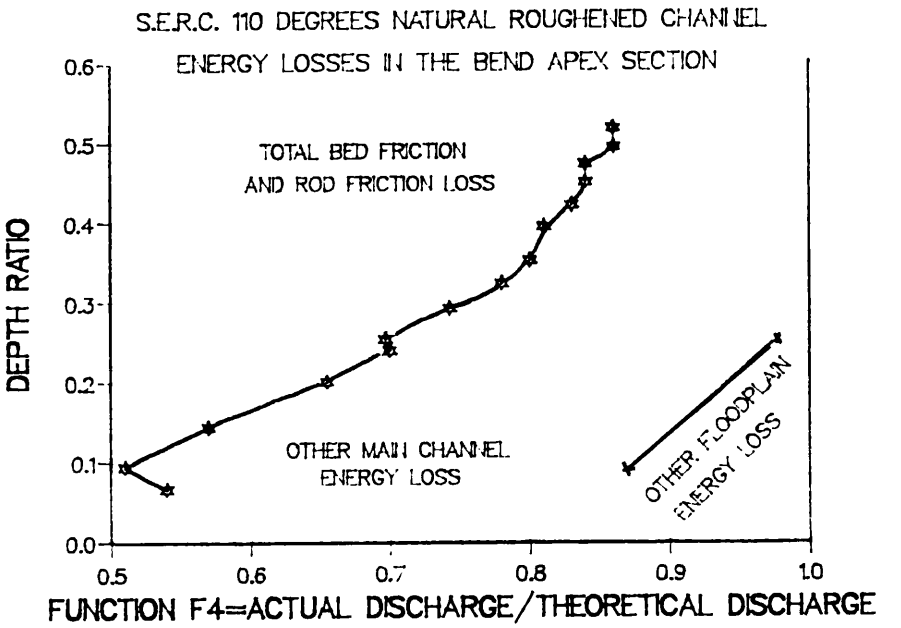

Fig (4.64) - Separation of The Main Channel Energy Losses from Floodplain Energy Losses. Variation of Function F_4 with Depth Ratio. S.E.R.C. Series B: Sinuosity 2.04; Natural Cross-Section; Roughened Floodplains.

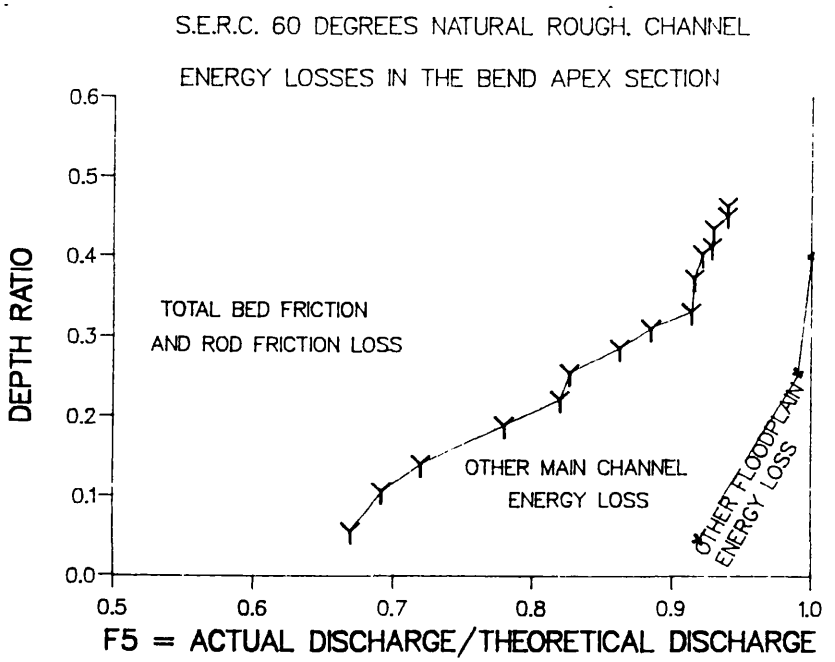

Fig (4.65) - Separation of The Main Channel Energy Losses from Floodplain Energy Losses. Variation of Function F_5 with Depth Ratio. S.E.R.C. Series B: Sinuosity 1.37; Natural Cross-Section; Roughened Floodplains.

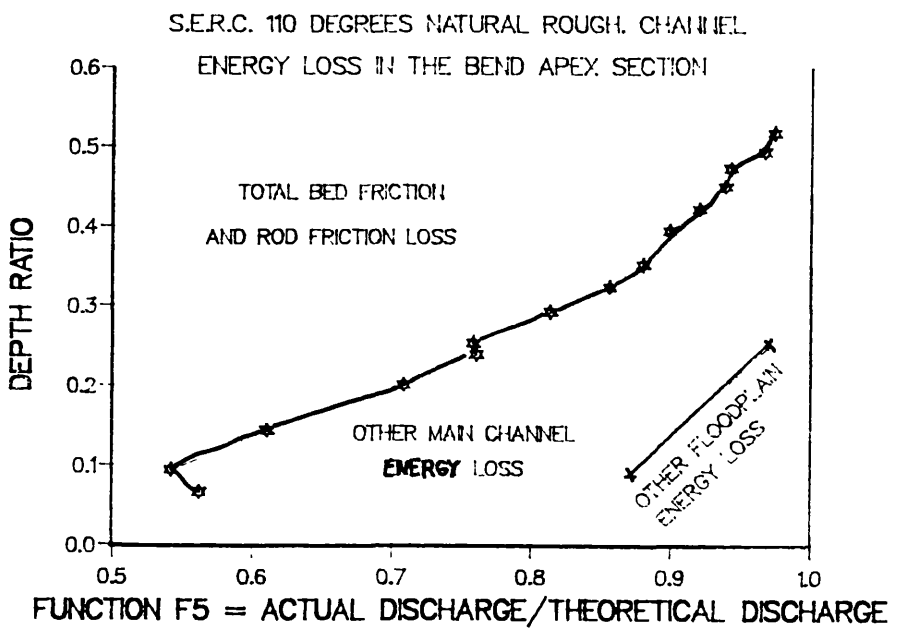

Fig (4.66) - Separation of The Main Channel Energy Losses from Floodplain Energy Losses. Variation of Function F_5 with Depth Ratio. S.E.R.C. Series B: Sinuosity 2.04; Natural Cross-Section; Roughened Floodplains.

CHAPTER 5

VELOCITY DISTRIBUTION AND FLOW STRUCTURES IN MEANDERING COMPOUND CHANNEL

CHAPTER 5

VELOCITY DISTRIBUTION AND FLOW STRUCTURES IN MEANDERING COMPOUND CHANNEL

5.1. INTRODUCTION

The purpose of this Chapter is simply to investigate the velocity distribution for meandering compound flows, both in the streamwise and transverse directions, for both inbank and overbank flows, and from these results to deduce, or infer, the most important features or flow mechanisms. This is essential before any realistic model of the flow can be formulated.

Previous studies carried out in small scale flumes have already identified the existence of significant flow structures and flow mechanisms in meandering compound flows which are not present in straight compound flows or inbank meandering flows. These findings can be summarised as follows:

- At a bend apex section, for overbank flow, the secondary cell is rotating in the opposite direction to that for an inbank case. This was pointed out by **Toebes and Sooky(1967)**, **Stein and Rouve(1989)** and **Kiely(1989)**.
- As the stage rises from the inbank case to the overbank case, the strength of the secondary currents increases significantly especially in the cross-over region. **Ervine and Jasem(1992)** mentioned that the strength of the secondary currents is defined as being the ratio of the transverse velocity to the streamwise velocity.
- The appearance in meandering compound flows of a kind of expansion-contraction phenomena(**Ervine and Ellis(1987)**). This is the result of floodplain flow approaching in the deeper main channel where the flow expands, and afterwards, when returning to the shallower floodplain, flow experiences contraction. This might be considered as an horizontal shearing in the main channel region, at the bankfull level, as referred to by **Ervine and Ellis(1987)** and **Kiely(1990)**. As the essential flow direction

above bankfull level is parallel with floodplain walls and below bankfull, flow tends to follow the boundaries of the main channel, a skewed horizontal shearing at bankfull level will occur.

Smaller scale studies at Aberdeen **(Willetts and Hardwick, 1989)** also revealed that downstream of the bend apex, and part of the way towards the bend exit, there is a large efflux of flow from the main channel and on to the floodplain.

- **Rajaratnam and Ahmadi(1989)** showed that the maximum velocity near the surface occurred just outside the limits of the meandering main channel, in the region of the inner bend.

5.2 VELOCITY DISTRIBUTION IN THE S.E.R.C. FLUME

5.2.1. Introduction

It has already been discussed in some detail in Chapter 2, Sections 3.3.4 and 3.3.5, that velocity measurements in the S.E.R.C. flume were carried out using a combination of miniature propeller, and vane with potentiometer for streamline angle measurement.

From the measurements of the resultant velocity (U_R) and the stream angle of the current ($\oplus$) carried out in S.E.R.C. flume Series B, the streamwise and the longitudinal velocity(U) components were calculated through the equation,

$$U = U_R * \text{Cos} \oplus \qquad (5.1)$$

and the transverse velocity by applying the following equation,

$$V = U_R * \text{Sin} \oplus \qquad (5.2)$$

The velocity and angle measurements were conducted at the same grid points in the flow. **Fig(5.1a)** and **Fig(5.1b)** show the location of the eleven cross-sections and the vertical slice

locations (inbank and overbank) for sinuosity 1.37 and cross-over angle 60^0.

Fig(5.2a) and **Fig(5.2b)** show the location of the cross-sections and the vertical slice location (inbank and overbank) for the larger sinuosity 2.04 with cross-over angle 110^0.

Measurements on the floodplain outwith the detailed grid shown in **Figs(5.1a)** and **Figs(5.2a)** were carried out on a rectangular grid pattern parallel to the walls of the flume (longitudinal direction) at intervals of 0.5 m.

5.2.2. Streamwise Velocities for Inbank Flows

The results of the streamwise component of velocity are plotted in **Figs(5.3a)** to **(5.3k)**, for all eleven cross-sections of the meandering channel of S.E.R.C. Series B with sinuosity 1.37, for the trapezoidal cross-section for 100.0 mm water depth and for a discharge of 0.047 m^3/s. **Fig(5.3a)** corresponds to Section 1, **Fig(5.3b)** to Section 2, and so on until **Fig(5.3k)** which corresponds to Section 11. At the top of each page the cross-section is shown with vertical slices for inbank trapezoidal flow. There are twelve slices per cross section named f to q, and each slice is presented with its data of streamwise velocity plotted with depth.

It is clear from **Figs(5.3a)** and **(5.3k)** that the velocity distribution is not evenly distributed cross the channel width. In **Fig(5.3a)** velocity is concentrated at the left inner bank where as in **Fig(5.3k)** velocity is concentrated at the right bank which is at Section 11 and is the inner bank of the next bend.

It is also of interest to note that at the bend region Sections 2, 3, 4, the inner bend produces velocities which are greatly reduced nearer the free surface and hence not obeying any logarithmic distribution with depth. This distortion may be due to the strength of secondary cells in that region and/or flow separation at the inner bend.

A summary of these eleven graphs is shown in **Fig(5.4)** which shows the variation of the depth averaged streamwise velocity along the meandering channel of S.E.R.C. Series B (sinuosity 1.37, trapezoidal cross-section and for stage 100.0 mm). It is clear that: along the bend(between sections 0 and 6), the maximum value of the depth averaged velocity is gradually moving from the inner bank of bend to the centre of the cross-section. The maximum value of the depth averaged velocity, in the cross-over region, moves from the centre of the cross-section towards the outer bank. Since the flow is steady, in each cross-section, the total discharge in the streamwise direction should be the same. Therefore the movement of the maximum velocity from the inner bank of the main channel to the outer bank produces a net transverse discharge. This point will be detailed in section 5.2.3.

Exactly the same detailed measurements have been conducted at sinuosity 2.04 for the natural cross section geometry. The mass of data collected is too extensive for this thesis, so it was decided in the interests of brevity to present just one graph on **Fig(5.5)**. This shows the contour levels of the streamwise component of velocity of the meandering channel of S.E.R.C. Series B with sinuosity 2.04 for the natural cross-section and stage 140.0 mm. The pattern of the streamwise component of velocity is similar to the previous one although the effect is not as pronounced.

It should be remembered that the apex of each bend in **Fig(5.5)** has a 'natural' cross section as shown in **Fig(5.2b)**. This means that the inner part of the flow has the shallowest flow depth and the other part the deepest flow depth. This would tend to produce higher velocities nearer the outer bend at each apex.

This phenomenon, however, is counterbalanced by the free vortex phenomenon at bends Ur = constant which would produce much higher velocities at the inner bend as seen in **Fig(5.4)** for the trapezoidal case.

Thus **Fig(5.5)** is a product of these two phenomena, revealing

at both bend apices there is no pronounced cross distribution of velocity.

However, where the cross-section becomes almost trapezoidal in the cross-over region there is a gross re-distribution of flow velocity, also partly caused by flow separation at the inner bend, where the flow is concentrated along the right side of the channel. The line of the maximum velocity filament is shown dashed.

5.2.3. Transverse Velocities for Inbank Flows

Returning again to sinuosity 1.37, and to the trapezoidal cross-sectional shape, we may now investigate the transverse (normal to main channel walls) velocity components for the case discussed in Section 5.2.2. with flow depth 100 mm and discharge 0.047 m^3/s.

The results are again presented for all eleven cross sections, and for each cross section, twelve vertical slices, f to q, are shown with transverse velocity data.

There are a few points to note:

(i) At Section 1 **Fig(5.6a)** still remains some anti clockwise secondary motion which is a remnant of a cell developed at the previous bend.

(ii) By Section 3 at the bend apex **Fig(5.6c)** this motion is eliminated and replaced by the conventional in-bank clockwise bend cell. This transverse velocity component can reach values in excess of 0.05 m/s, when compared to longitudinal velocities around 0.5 m/s (trapezoidal case) giving a ratio of the two values around 10% maximum. This was compared with theoretical estimates by **Fares(1989)**, giving good agreement.

(iii) The bend cell continues with some strength and only begins significant decay in the cross over region Sections 6 to 10, with just a remnant left at section 11 at the entrance to the next bend.

(iv) It will be noted that the transverse velocity components are

not always symmetrical about the axis with equal flows to left and right. This is because the transverse discharge is not in balance over a half meander wavelength as measured in the S.E.R.C. flume. As already noted in **Fig(5.4)** there is a net transverse discharge from left to right in moving from Section 1 to section 2. This means that the transverse velocities are composed of <u>two</u> components; one for secondary cells and one for net transverse discharge(**Goncharov(1957)**).

5.2.4. Streamwise and Longitudinal Velocities for Overbank Flow

Again the great mass of velocity data collected for overbank flows in the S.E.R.C. flume means that the **Author** of this thesis has needed to be very selective, in just presenting a flavour of the results. The velocity data has been collected by **Mrs Greenhill(1989, 1990, 1991)**, in five volumes under the aegis of Bristol University.

The results of the streamwise velocity for the meandering compound flow of S.E.R.C. Series B are plotted in **Fig(5.7)**, for sinuosity 1.37, for trapezoidal cross-section, stage 200.0 mm and smooth floodplains.

Fig(5.7a) and **Fig(5.7b)** again cover all eleven cross-sections, with each cross section containing velocity data for twenty-two vertical slices as shown. Each velocity data point is denoted by a small cross to the right of the vertical slice axis.

Some points can be noted from **Fig(5.7a)** and **Fig(5.7b)**:

(i) In the main channel region the streamwise velocity profiles are highly distorted. For instance at section 1, in the region between the bankfull level and the water surface, the streamwise component of the velocity is significantly reduced from the conventional log distribution. Above bankfull level the velocity vectors do not flow parallel to the sidewalls of the main channel, but instead are deflected by floodplain flow and tend to

run more parallel with the direction of the floodplain walls. It will be noted in **Fig(5.7a)** Section 1, the large velocity gradients near bank-full level which produce large turbulent shearing in that region as predicted by **Ervine and Ellis(1987)**. Large velocity gradients and high turbulent shearing can also be observed at Sections 6,7, and 8 of **Fig(5.7a)** and **Fig(5.7b)**, corresponding to the cross over region. It will be shown in section 5.3.2, that when overbank flow occurs in meandering compound channels, the floodplain flow on reaching the main channel region, tends to separate from the bank, creating strong secondary currents and turbulent shearing. The abrupt changes in the gradients of the streamwise velocity profile observed in sections 5, 6 and 7 of **Fig(5.7a)** and **Fig(5.7b)**, are in agreement with the location of the surface where separation is occurring. As it is expected, flow separation will introduce significant energy losses in the meandering compound flow, reducing the total conveyance of the channel.

(ii) **Fig(5.7a)** and **Fig(5.7b)**, also reveal that the streamwise velocity (parallel to the main channel walls) tends to reduce between section 3(bend apex) and section 8(cross-over). This confirms the findings about the variation of the streamwise discharge in the main channel region, presented in **Chapter 4**. The flow in the main channel is steady but not uniform. There is a significant reduction of streamwise discharge between the bend apex section(maximum discharge) and the cross-over section No. 8(minimum discharge). This is because of a net efflux discharge out of the main channel and on to the downstream floodplain, along this length.

(iii) In the floodplain region, the velocity profiles in the verticals located at the edge of the right bank of the cross-over region(section Nos. 6-11) reveal that the greater streamwise velocities are located near the bottom and the smaller velocities are near the water surface, as shown in **Fig(5.7a)** and **Fig(5.7b)**. This points to the existence of a contraction phenomenon when the flow depth reduces considerably and the velocity accelerates. Outside this region, the profiles of streamwise velocity in the

floodplain region tend to be practically log shape. This, in fact, will be shown to be a very significant flow mechanism. Flow in the main channel tends to leave the main channel and be transported on to the floodplain downstream of each bend apex, around the region of the bend exit. This region corresponds to the region of maximum shear stress, as shown in **Fig(4.23)**, for the case of the natural cross-section with the same test conditions. Because of this net efflux, velocities of the cross over region are reduced. However, the fluid lost out of the main channel is now replaced by a net influx into the main channel before the next bend apex, in the region of the start of the next bend.

This overbank data is shown summarised in **Fig(5.8)**, with the floodplain velocities excluded for clarity.

The depth averaged velocity in the main channel region for the meandering channel with sinuosity 1.37, stage 200.0 trapezoidal cross-section and smooth floodplains is presented. This figure reveals that the behaviour of the maximum streamwise velocity is similar to the inbank case but much less pronounced. At the bend entrance, the maximum of the streamwise velocity is located near the inner bank and gradually it moves towards the centre of the section and finally, in the cross-over region to the outer bank of the main channel.

The depth averaged streamwise velocity in the main channel and in the floodplain regions, for the meandering channel with sinuosity 1.37, stage 250.0 mm, trapezoidal cross-section and smooth floodplains is shown in **Fig(5.9)**. In the main channel region, the maximum streamwise velocity, at bend entrance is located at inner bank and moves gradually towards the outer bank along the length of the main channel. The same figure reveals also that the distribution of the streamwise velocity in the floodplain region, outside the area where the flow is accelerating, is quite uniform. This is partly because of the small scale of **Fig(5.9)** which conceals the fact that higher floodplain velocities exist near the inner bend, and also outwith the meander belt width near the flume side walls.

Fig(5.10) takes one cross-section in the flow at the cross over region and shows in more detail the depth averaged longitudinal velocity on the floodplain and the depth averaged streamwise direction in the main channel. This is a significant graph as it shows a dip in velocity near the centre of the flume. This drawing shows also the mean velocity for an equivalent straight channel and equivalent straight floodplain. It can be seen immediately in **Fig(5.10)** the large difference between the straight equivalent and the actual compound meandering case.

The distribution of the streamwise velocity of S.E.R.C. Series B, for sinuosity 2.04 with smooth floodplains and natural cross-section is presented in **Fig(5.11)**, for stage 165.00 mm and in **Fig(5.12)**, for stage 200.0 mm. The floodplain velocities are omitted for stage 165.00 mm, the pattern of the location of the maximum velocity is similar to the patterns observed for the sinuosity 1.37 with significant streamwise velocity reduction at the cross-over region. **Fig(5.12)** shows that the streamwise velocity, at cross-over section reduces by over 80% to one sixth of the streamwise velocity values observed at the bend apex. This shows that as sinuosity increases from 1.37 to the 2.04, the streamwise component velocity, at the cross-over section, will tend to diminish substantially. This is not surprising in the sense that longitudinal velocity components become more dominant.

It is useful also to compare the distribution of depth averaged velocity for different types of compound flow.

Fig(5.13a) shows the distribution of the longitudinal velocity obtained by **Kiely(1989)** for a straight parallel compound flow. This figure reveals that the maximum longitudinal velocities are always located in the main channel region; the presence of a strong lateral velocity gradient which increases significantly the floodplain velocity and produces strong lateral shear. The case of a skewed compound flow is shown in **Fig(5.13b)** from work on a 5.8^{0} skew, done by **Ervine** and **Jasem (1992)**. In this case the depth averaged velocity is still highest in the main channel, there is no shear layer on the right (converging) upstream floodplain and there is a significant shear layer on the

left receiving floodplain. This is typical of a slightly skewed compound flow.

The case of a meandering compound flow is shown in **Fig(5.13c)** from this work revealing an entirely different scenario with high velocities on the floodplain outwith the meander belt and lower velocities in the main channel.

As it will be demonstrated in **Chapter 6**, the streamwise velocities in the main channel will reduce when the floodplain roughness increases from the smooth case to the fully roughened case.

5.2.5. Transverse Velocities for Overbank Flow

The earliest experiments on the S.E.R.C. meander compound flume were very crude dye tests conducted by **Dr. Ervine** and **Professor Willetts**. These consisted of injecting dye at various local points in the flow, and following the subsequent dye path. one of the findings is sketched in **Fig(5.14a)** where dye is injected into the floodplain flow at the edge of the main channel at the cross-over region. When injected near the floodplain bed, the dye can be swept down into an expanding swirl flow in the main channel. When injected a little further up, the dye can be transported with deviation to the opposite side of the main channel to the opposite floodplain. This means that oncoming floodplain flow can bifurcate.

Another key finding from the crude dye tests concerns dye injecting at almost any point near the bend apex as shown in **Fig(5.14b)**. Dye injected at almost any depth or at any point on the apex cross-section appeared to end up on the floodplain opposite producing a great "slackness" in the flow in the shaded region. There was a substantial exflux out of the main channel along this length, roughly from Section 4 to Section 6.

Photographic evidence of the dye tests taken at bend apex and near the cross-over region for sinuosity 2.04 are shown in **Fig(5.14c)** and **Fig(5.14d)**, for stage 200.0 mm, natural

cross-section and smooth floodplains. The dye was injected at the bed level, near the outer bend(section 4), in the first case and near the cross-over(section No 8), in the second case. Both graphs reveals that the flow streamlines in the main channel sections Nos. 4 and 8 tend to be longitudinal, that is parallel with the floodplain walls. Another important finding is that the main channel is supplying discharge to the receiving floodplain. As the result of this the discharge in the main channel should be dramatically reducing in downstream direction. These dye tests corroborate the Author's findings presented in Chapter 6 about discharge distribution in sinuosity 2.04 of S.E.R.C. flume Series B.

The dye tests performed in the meandering compound flows of sinuosities 1.37 and 2.04 of S.E.R.C. flume Series B evidenced that the two sinuosities will tend to develop different flow mechanisms.

The flow visualization was also performed through float photographs, which are presented in **Fig(5.14e)** and **Fig(5.14f)**, for sinuosity 1.37, trapezoidal cross-section with smooth floodplains and for stage 200.0 mm and 250.0 mm, respectively. These figures evidence that, inside the meander belt, as the stage increases, the float deflection induced by the main channel meandering flow tend to diminish. Another important finding is that the floats, outside the meander belt, are parallel to the floodplain walls, as it is expected. These findings confirm the experimental results obtained by **Goncharov(1957)**.

The dominant flow mechanism proved to be due to floodplain flow passing over the main channel flow below, especially in the cross over region. As it approaches the main channel it experiences an abrupt variation of water depth which creates along the side bank an adverse pressure gradient. This adverse pressure gradient leads to flow separation. The velocity profile is significantly changed with the appearance of strong circulating currents whose strength is much greater than the ones that occur in the bend region for the inbank case. The existence of these secondary currents has been reported by several

researchers such as **Toebes and Sooky(1967)**, **Ervine and Ellis(1987)**, **Stein and Rouve(1989)**, **McKeogh and Kiely(1989)**; **Schroder, Stein and Rouve(1991)**, and **Sellin(1991)**.

Fig(5.15a) and **Fig(5.15b)** show the growth and the decay of the secondary currents in the main channel region of the meandering compound channel of S.E.R.C. Series B with sinuosity 1.37, for stage 200.0 mm, for the trapezoidal cross-section and for smooth floodplains.

It should be noted that **Fig(5.15a)** and **Fig(5.15b)** presents the transverse data components for all eleven cross-over sections and for the twenty two vertical slices at each cross-section. Transverse velocity is plotted as a cross, and the secondary cells and cross-flows are interpreted by the Author for each cross section as well.

Between sections 1 and 3 and below bankfull, **Fig(5.15a)** reveals the appearance of a large anti-clockwise cell occupying the entire width of the section as well as a small clockwise cell in right low corner of the section. Between sections 1 and 3, the strength of the large cell is decaying while the small cell is increasing in size. The large cell is generated by the floodplain flow which separates from the bank along the previous (just upstream) cross-over region. At bend apex(section 3), the sense of rotation of the large cell is anti-clockwise, which is the opposite to that for inbank bend flows. This fact was also reported by **Toebes and Sooky(1967)**, **McKeogh and Kiely(1989)**, **Schroder, Stein and Rouve(1991)**. The presence of the small cell was also noticed by the above researchers. However the size of the small cell was greater in the rectangular cross-section of the meandering compound channel model of **McKeogh and Kiely(1989)**, than in the trapezoidal cross-section of S.E.R.C. Series B. A possible explanation for this is probably due to the side slope of bank which influences the development of the cell.

Section 4 downstream of the bend apex has a peculiar transverse velocity distribution in the sense that the remnant of the bend cell is still there, but the whole flow is dominated by a strong cross-flow to the opposite floodplain. This corroborates

the result of the crude dye tests noted above.

Downstream of section 4, **Fig(5.15a)** and **Fig(5.15b)** show that, as the result of floodplain flow coming from the left bank and impinging in the main channel, a new clockwise cell starts to develop gradually increasing in width over Sections 5,6,7,8, and 9. The old anti-clockwise cell, formed upstream of the bend apex, decays very rapidly. At section 6, the new clockwise cell is not yet fully developed and the old anti-clockwise cell has practically vanished. These sections 6-9 also show a strong cross-flow in the upper regions of the main channel.

At section No. 9 of the cross-over region, the large clockwise cell is fully developed, occupying the full width of the section, as shown in **Fig(5.15b)**. The width(L) of the large secondary cell is approximately 0.9 m, which is six times the bankfull depth(0.15 m). This result agrees with the shear layer length $L \cong 6$ h, proposed by **Lean and Wear(1979)** for secondary circulations at backward steps.

These observations bear out the observations from the crude dye tests noted above.

Fig(5.15a) and **Fig(5.15b)** also reveal that, at the bend apex(section 3) and in the cross-over regions, the recirculating velocities, can reach 25-30% of the streamwise velocity component. These results show that the strength of the secondary currents for the overbank case is greater than the ones that develop for the inbank case, where the recirculating velocities were only 5-10% of the streamwise component of velocity. For an overbank case of a meandering channel with rectangular cross-section, **Kiely(1989)** has obtained magnitudes, for the strength of secondary circulation, in the order of 30% of the streamwise velocity. **Kiely's** tests were performed in a meandering channel with sinuosity 1.25, with a rectangular main channel cross-section and smooth floodplains. **Kiely's** findings lead to the conclusion that a rectangular cross-section increases the strength of secondary currents in comparison with trapezoidal cross-section. In the rectangular cross-section, the depth variation between the shallower floodplain and the deeper main

channel, is much more abrupt compared with the trapezoidal cross-section. Consequently the separation phenomenon produced by the floodplain flow when it impinges in the main channel will be exacerbated with a rectangular cross-section in comparison with the trapezoidal cross-section.

It should also be noted that the aspect ratio of **Kiely's** main channel was around 4, compared to 8 in the S.E.R.C. flume, giving a further reason for differences in recirculating velocity.

In any case it is becoming clear that meandering compound flows possess very strong transverse velocities and secondary currents both in the cross-over region and at the bend apex region. The magnitudes of these secondary cells is around 25-30% of streamwise velocity and therefore several times greater than equivalent inbank flows.

As demonstrated in **Chapter 4,** secondary currents that grow and decay in the main channel region, introduce significant energy losses to the flow, reducing the overall conveyance of the meandering compound channel. **Fig(5.15b)** shows that the secondary cells become fully developed downstream of the middle section of the cross-over region. Therefore it is in this area of the cross-over that a substantial part of energy losses should occur.

5.2.6. Further Analysis of Secondary Currents in Meandering Compound Flow

The results presented in **Fig(5.15a)** and **Fig(5.15b)** were for only one geometry tested in the S.E.R.C. flume. Space does not permit a full presentation of all transverse velocities for all geometries and flow depths.

It will be appreciated that the S.E.R.C. flume data covered:

- two sinuosities 1.37 and 2.04
- two floodplain roughnesses (smooth and rough)
- two main channel cross-sectional shapes, trapezoidal and natural, at least for sinuosity 1.37.

. one or two inbank flow depths 100 mm/140 mm
. up to three overbank flow depths 165 mm, 200 mm, and 250 mm

As well as the basic geometries listed above, transverse velocities were measured over an intricate grid for half a meander wave length, including all the cross-sections and over twenty vertical slices per cross section.

In the interests of brevity we will consider only the bend apex cross-section in this analysis. This was chosen because the data at that cross-section was also extensively measured by LDV techniques and also because there are no transverse currents due to floodplain flow passing over the main channel below, as in the cross-over regions.

The strength of secondary currents is usually presented as being the ratio of the transverse velocity(V) divided by the longitudinal velocity(U). The value of the strength is not only affected by geometry of the cross-section but also by main channel sinuosity, main channel aspect ratio, the relative flow depth and by floodplain roughness. **Tables 5.1** to **5.3** present the value of maximum strength of the secondary cells, $|V/U|_{max}$, calculated as an absolute value at the bend apex section, for all test cases of S.E.R.C. Series B. In the trapezoidal cross-section the maximum values of the strength were located in the middle part of the section, while in the natural cross-section, they were found in the deepest part of the section, thus near the outer bank of the bend. The data is also structured in **Fig(5.16a)** and **(5.16b)**. The following conclusions can be drawn from the Tables and graphs:

- For the inbank case, both natural cross-sections exhibit a value of maximum strength of secondary circulation that is greater than the one for the trapezoidal cross-section.
- As stage rises from the inbank case to the overbank case, in all cases, the maximum strength of secondary cells increases substantially especially in the trapezoidal case. However, as the overbank stage continues to rise the trend generally is to

diminish the maximum strength.

- Comparing the fully roughened cases with the smooth case, the maximum strength, itself, seems to be almost the same at least for sinuosity 1.37. For sinuosity 2.04 the roughened case produces greater relative strength of secondary cells. It is important to note that, when the floodplain is fully roughened, both the resultant velocity and the stream angle diminish in comparison with the smooth floodplain case.
- As sinuosity changes from 1.37 to 2.04, the maximum strength of the secondary currents tends to increase, both for the smooth floodplain case and for the fully roughened floodplain case.

Further confirmation of the differences between inbank and overbank flows are shown in **Fig(5.17)** for the bend apex section and **Fig(5.18)** for the cross-over region. Both figures pertain to the 1.37 sinuosity, smooth floodplains and trapezoidal cross-section of main channel.

Fig(5.17) compares the cases of inbank flow (depth 100 mm) and overbank flow (depth 200 mm). The magnitude of transverse velocities are clearly shown as it is the interpretation of secondary cell behaviour. Please note the very different velocity scales based on 0.03m/s per centimetre for inbank and 0.1m/s per centimetre for overbank.

For overbank flow the cell is clockwise with strengths around 5-10%, whereas for overbank the cell is anti-clockwise with strength around 20-30%. In the latter case the direction of this cell is solely due to floodplain flow shearing over the main channel flow at the previous cross-over region.

Fig(5.18) compares the same inbank and overbank flow regimes at the cross-over region between bends. It is important to note this time the large difference in velocity scales between the two diagrams, being 0.03 m/s for inbank flows and 0.5 m/s overbank flows, a difference of over sixteen times.

In this case the direction of the cells is the same, in both cases both the flow mechanisms are different. For the inbank case the cell is due to the previous bend and shows a relative strength almost as great as the bend apex. For the overbank case

the cell is below bankfull and driven by floodplain flow shearing over flow in the main channel below. Considering only recirculating transverse velocities below bankfull level, the relative strength can reach 30-35%, about 5 times greater than the inbank case.

5.2.7. A Summary of Flow Mechanisms and Implications for Sediment Transport

Fig(5.19) represents an attempt to include many of the flow mechanisms, already discussed, on one diagram of meandering compound flow. **Fig(5.19)** shows:

- The expanding cell in the main channel region driven by cross-over floodplain flow.
- Cell rotation at bend and decay beyond bend.
- Efflux of main channel flow on to the floodplain beyond the bend apex and at the outer bend.
- High velocity distribution at inner bend and on floodplain outside meander belt width.
- Deviation of floodplain streamlines on crossing over main channel.
- 'Slack' region beyond each bend where old cell is decaying, plus new cell is beginning.

The effect of all these flow mechanisms may be significant for sediment transport and river channel morphology. This may be true for natural rivers with occasional overbank flow, and will certainly be true for artificially designed two-stage channels.

The appearance of secondary currents in meandering compound flows will induce also an increase of levels of turbulence, mainly in the cross-over region where the large cells are fully developed. Experimental results(not yet published), obtained by M. Schoreer, from the Institute of Hydraulic Engineering and Water Resources Development(IWW) from Aachen, University of Technology(Germany), haveshown that the Reynolds shear stresses are greater in the cross-over region, where the cells are fully

developed, and smaller near the bend apex, where the secondary circulation changes its sense of rotation. In rivers, the transport of suspended load is highly dependent on turbulence. It is expected that, as turbulence increases, the transport of suspended load should increases as well. Probably the transport will be from the main channel to the floodplain part of sediment will tend to deposit on the floodplain where the levels of turbulence may be lower than in the main channel.

The pattern of scour and deposition in meandering compound channels will be greatly affected by these secondary circulations. As the stage rises from an inbank case to an overbank case, the strength of the secondary currents increases considerably, and the boundary shear stress in the transverse direction will also become significantly greater. Based in the profiles of transverse velocities, obtained in S.E.R.C. Series B, for the meandering channel with sinuosity 1.37, the main channel with trapezoidal cross-section and smooth floodplains, it is possible qualitatively to make a rough prediction of the pattern of scour and deposition that will occur in this meandering compound channel. This is sketched on **Fig(5.20)**.

Between sections 3 and 6 downstream of bend apex:

- This is a transition zone where the old anti-clockwise cell is decaying and the new clockwise cell will start to develop.
- In the main channel region, scour will move from the inner bank to the outer bank, while the region of deposition will change from the outer bank to the inner bank.
- In the floodplain region, scour may start to occur near the outer bank in the region of significant efflux out of the main channel where very high boundary shear stresses have been measured. This is shown in **Fig(5.20)**.

Between sections 6 and 11(cross-over region):

- The strength of the secondary circulation reaches its maximum in the cross-over region.
- In the main channel, scour may occur along the downstream bank

and deposition along the upstream bank.
- In the floodplain, deep scour will occur along the outer (downstream) bank. In this region boundary shear stress measurements in S.E.R.C. Series B, as presented in **Chapter 4**, reached very high values.
- Boundary shear stress measurements are reduced in the main channel during overbank flow, at least in the streamwise direction. Transverse shear stress is however likely to be greater during overbank flow as is the level of turbulence. This will lead to more transverse sediment movements and more sediment held in suspension.

The general pattern will be scour at the outer bends (downstream) of the cross over region and deposition at the inner cross over region leading to longer term meander migration downstream. This pattern of scour and deposition will need time to develop. In natural river meanders that seldom are in flood, this pattern of scour and deposition probably does not have sufficient time to develop. However in the case of two-stage meandering channels, where overbank flows could often occur, this pattern may have time to be fully developed.

A detailed experimental investigation of sediment transport in meandering compound flows is expected to be carried out in the third phase of S.E.R.C. Project, which will be entitled Series C.

5.3 VELOCITY DISTRIBUTION AND FLOW STRUCTURES IN THE GLASGOW FLUME.

5.3.1. Introduction

Details of the design and philosophy of the Glasgow flume are given in Chapter 3, section 3.7. A plan view sketch is given again in **Fig(5.21)** to serve as a reminder of the unique features of this flume, which is really two flumes in one. The ratio of the main channel discharge to floodplain discharge can be set at any ratio from zero to infinity, and the flume is much more

flexible in changing geometry, than the S.E.R.C. flume, Walllingford.

Unfortunately, time constraints did not permit detailed bend and floodplain measurements over a wide range of flow depths, bend radii, cross over angles, bend apex cross-sectional shapes, floodplain roughness and ratios of main channel to floodplain flows. This type of programme would require at least three years full-time work which was not available in this case because of work at Wallingford.

It was decided therefore in this section to provide detailed measurements of bend and floodplain behaviour for a specific case of great practical interest. That is, with main channel flow at a depth above bankfull, but with zero floodplain flow. In this case the water on the floodplain is essentially stationary, and represents a situation which often occurs in nature, where co-flowing main channel and floodplain flows do not occur because the geometry of the river valley or obstruction prevents floodplain water from moving.

The other reason for presenting this case in detail is the behaviour of bends during overbank flow, but with zero velocity in the floodplain flow. It has been noted in Section 5.2. that the bend cell changes rotation during overbank flow because of floodplain flow passing over the main channel flow in the upstream cross over region. This is not the case with stationary floodplain water, so there is considerable interest in the strength and direction of bend secondary cells in this case.

5.3.2. Flow Resistance Coefficients for the Glasgow Flume

As a precursor to measurements of velocity, streamline angles and water surface slopes, it was necessary first to determine the basic flow resistance characteristics of both parts of the Glasgow flume.

This was carried out first for inbank flow in the main channel with the bend in terms of stage-discharge as plotted in

Fig(5.22). Only five points on the curve have been determined, and difficulty was experienced in obtaining uniform flow in a channel with a bend.

The same procedure was carried out for flow along the floodplain only with the main channel completely closed off. This represents bed friction on the flood plain but also floodplain flow passing over the main channel bend. The stage-discharge curve for this scenario is shown in **Fig(5.23)**.

The resistance coefficients were determined for both cases outlined above, in terms of variation of Manning's 'n' value with depth, but also in terms of the variation of the Darcy-Weisbach friction factor with Reynolds Number.

Fig(5.24a) shows the variation of Manning's 'n' with depth for the inbank flow in the main channel. In general the Manning's n coefficient is approximately constant(0.010) with depth.

Fig(5.24b) shows the variation of Manning's 'n' with depth for flow on the floodplain only and it was compared with S.E.R.C. Series B, the meandering case with sinuosity 1.37 with trapezoidal cross-section and smooth floodplains. The Manning's of Glasgow flume increases with depth ratio and is smaller than the S.E.R.C. Series B values.

Fig(5.25) shows the variation of Darcy-Weisbach friction factor with Reynolds Number for the case in **Fig(5.24b)** with floodplain only. The Darcy-Weisbach friction factor reduces with Reynolds number and tend to values obtained in S.E.R.C. Series B.

5.3.3. Velocity Measurements in the Glasgow Flume

The detailed measurements described below are for an experiment carried out for a discharge in the main channel 0.0175 m^3/s with uniform depth of 88 mm and no floodplain discharge. The bankfull level is 67 mm, so this is an overbank flow condition. These test conditions simulate an overbank case of a meandering channel, and although the floodplains are inundated, the floodplain discharge is zero simulating the presence of an

infinite roughness(eg. trees, transverse walls, etc).

The velocity was measured in the streamwise direction through a Pitot static tube connected to a very sensitive pressure transducer. The stream angles of the current were taken by a vane linked to a potentiometer. The manner of testing was the same as the S.E.R.C. flume study. The water depths were taken by pointer gauge. Therefore the velocity readings obtained from the Pitot static tube gave directly the streamwise velocity component(U). The transverse velocity(V) component was obtained by applying the following expression:

$$V = U \tan \Theta \qquad (5.3)$$

where Θ is the stream angle in relation to the streamwise direction. Velocity and angle measurements were taken in a depth range, varying between 10.0 mm and 72 mm, from the main channel bottom .

Measurements were taken over the five cross sections shown in **Fig(5.27)** and for each cross section, measurements were taken over ten vertical slices as shown in **Fig(5.26)**.

5.3.4. Streamwise Velocity Components

The results of the streamwise velocity in each vertical and in each section of Glasgow flume are plotted in **Fig(5.26)**, for an uniform depth equal to 88.0 mm and a main channel discharge equals to 0.0175 m^3/s. The profile of the streamwise velocity is not affected by the flow above bankfull(depth) 65.0 mm). The distribution of velocity in each vertical seems to be reasonably uniform although distortions in the vertical velocity profile begin to appear at section 0^0 (slices 1 and 2), section $+20^0$ (slices 1 to 5) and at section $+45^0$ (slices 1 to 7). These distortions appear in the upper reaches of the flow and indicate very clearly turbulent shearing and momentum transfer, either on to the adjacent floodplain or to the opposite side of the main channel.

The fact that this phenomenon occurs in the upper reaches of

the flow, suggests the cause to be an interaction between main channel and floodplain, rather than flow separation at the inner bend (in plan view) which would have caused velocity profile distortion over the full flow depth.

The depth averaged velocity in the streamwise direction is shown in **Fig(5.27)**. At the entrance of the bend, the maximum depth averaged velocity is located near the inner bank and gradually moves towards the outer bank. At bend exit the maximum depth averaged velocity is already located near the outer bank of the bend. It is interesting to compare **Fig(5.27)** with **Fig(5.8)** for the S.E.R.C. flume behaviour at the same relative flow depth of 0.25. The lateral transfer of the highest velocity filament from inner to outer takes much longer in the S.E.R.C. flume. In fact it takes until the entrance to the subsequent bend. The behaviour in **Fig (5.27)** on the other hand is much similar to inbank flow characteristics.

5.3.5. Transverse Velocity Components

The transverse velocity for each cross section and vertical slice of the Glasgow flume are presented in **Fig(5.28)**. The test conditions were the same as those defined for the streamwise velocity component above. **Fig(5.28)** shows that at bend entrance, a clockwise secondary cell just starts to develop.

The following points can be noted from **Fig(5.28)**:

(i) Transverse velocity components and secondary cell strength reach a maximum just downstream of the bend apex at section $+20^{o}$.

(ii) The maximum ratio of transverse to streamwise velocity is around 20-30% which is similar to the S.E.R.C. flume data for overbank flow, although the sense of rotation of the secondary cell at the bend is opposite in these two cases. Rough measurements of the secondary cell strength for inbank flows in the Glasgow flume give values around 15% which is 1.5 times inbank case of S.E.R.C. Series B. The strength of secondary currents of a flow around a bend increases as flow depth-central

radius of the bend h/r increases. In Glasgow flume this ratio was 6.7% whereas in S.E.R.C. Series B it was 5.5%.
(iii) The major finding from **Fig(5.28)** is that, in all bend region, the cell maintains the same sense of rotation(clockwise) as conventional inbank flows. In the S.E.R.C. flume Series B, for the overbank cases, the secondary cell at bend apex changed its sense of rotation completely.

Although the floodplains are inundated, the secondary cell that appears at bend apex section of Glasgow flume is rotating exactly in the same way as a typical clockwise cell generated for an inbank case of a flow around the bend. As the system that delivers floodplain flow to the Glasgow flume is closed, then the phenomenon of floodplain flow shearing over the main channel flow below does not occur and the anti-clockwise cell observed at bend apex, for the overbank cases of S.E.R.C. Series B, does not occur. This proves conclusively that floodplain flow shearing over the main channel flow is responsible to bend cells changing rotation direction.

5.3.6. Transverse Water Surface Slope

The water surface level results for each vertical and for all five sections of Glasgow flume, for mean water depth 88.0 mm and discharge 0.0175 m^3/s are plotted in **Fig(5.29)**. This figure shows the smaller depths are located near the inner bank of the bend while the greater depths are placed in the opposite bank.

Based in the water depths measurements, the water surface slope for each section was calculated and plotted for each of the five sections in **Fig(5.30)**. This figure shows that the transverse slope gradually increases from the bend entrance until the apex section where it reaches its maximum value of $2* 10^{-2}$. Then, it starts to decay until the bend exit. The profile of transverse slope against section number seems to be symmetrical in relation to the bend apex.

In a flow around the bend, the mean transverse slope($\bar{S}_r$) of

the water surface can be approximately calculated by the following equation

$$\bar{S}_r = \frac{\bar{U}^2}{g\ Rc} \qquad (5.4)$$

where $\bar{U}$ is the depth averaged streamwise velocity component; Rc is the central radius of the bend; and g is the acceleration of gravity. If the above equation is applied to Glasgow flume data, the transverse slope obtained was:

$$S_r = \frac{0.44^2}{9.8 * 1.0} = 0.0198$$

which is very similar to the maximum transverse slope value, determined at the bend apex section of Glasgow flume, shown in **Fig(5.17)**. This result reconfirms that the flow, in Glasgow flume, although it is an overbank case, is behaving like an inbank case and the floodplain water does not act a great deal to repress the magnitude of transverse water slope.

A summary of the rotational nature of bend secondary cells is given in **Fig(5.31)** for inbank; overbank with floodplain flow; overbank with no floodplain flow.

This clearly shows cell reversal for case 2 of overbank flow and no flow reversal for case 3 with overbank floodplain water.

5.4 CONCLUSIONS

Based on experimental data, obtained in the S.E.R.C. flume Series B and in the Glasgow flume, a detailed analysis of velocities and flow structures in meandering compound flows was carried out. The main conclusions obtained were:

(i) The mechanism that creates secondary currents for an inbank case of a flow around the bend is totally different from the one that develops secondary circulation at a bend, for an overbank case of meandering compound channel. For the inbank case, the secondary circulation appears in consequence of the imbalance

between the body weight component and the centrifugal force combined with non-uniform distribution of velocity. For the overbank case, the secondary circulation is generated by floodplain flow shearing over the main channel flow driving secondary cells on to the next bend.

(ii) Floodplain flow approaching the main channel can bifurcate with part of the flow entering the main channel swirl and part crossing the main channel to the opposite floodplain.

(iii) Just downstream of the bend apex a large efflux of flow leaves the main channel and flows on to the floodplain.

(iv) For inbank flows the highest velocity filament at the inner region of one bend moves across the channel to be at the inner region of the next bend.

(v) At bend apex, inbank transverse velocities reach relative magnitudes of 5-10% for trapezoidal and 15-20% for natural. This is the ratio between transverse/longitudinal velocities.

(vi) For overbank flows the distribution of streamwise velocity, in the main channel region, is highly distorted. Above bankfull level the streamwise velocity is significantly reduced from the conventional log distribution. In particular, the cross-over region at bankfull level exhibits large velocity gradients which will produce large turbulent shearing.

(vii) For overbank flows the distribution of transverse velocities produces at bend apex ratios of transverse/longitudinal around 20-30%.

- At the bend apex the cell is anti clockwise of strength.
- At the cross over region the cell is driven by floodplain flow shearing over main channel flow giving relative strengths 30%-35%, 5 times greater than inbank case.

(viii) In the main channel region, between bend apex section and cross-over region, the streamwise and the transverse velocities diminish, while between the cross-over and apex section of the next bend the opposite occurs.

(ix) In S.E.R.C. flume Series B, it was demonstrated that the strength of secondary circulation is affected by depth of flow, geometry of the cross-section, the stage, sinuosity and

floodplain roughness. The natural cross-section tends to increase the strength of secondary currents in comparison with the trapezoidal cross-section, for the inbank case, while the opposite occurs for the overbank case. The strength of secondary cells increases significantly as the stage rises, from the inbank to the overbank case. However, further increases in the overbank stage tends to reduce the strength of the secondary flow. As the floodplain roughness increases from the smooth case to the fully roughened case, the resultant velocity and the stream angle both diminish. However, the strength of the secondary flow tends to maintain approximately the same value, at least in the smooth case.

(x) It is expected that the levels of turbulence and the Reynolds shear stress will increase considerably, in meandering compound flow, as the flow goes from the inbank case to an overbank case.

(xi) The boundary shear stress field in the streamwise direction and in the transverse direction will be affected by the secondary flow. On one hand, the measurements of the streamwise boundary shear stress, presented in **Chapter 4**, have shown that a reduction will occur in the main channel and a substantial increase of boundary shear values will appear, at the edge of the floodplain at the exit of each bend. On the other hand, the considerable increase of the strength of the secondary currents in the cross-over region will induce the increase of the transverse boundary shear. A qualitative pattern of scour and deposition, for the meandering compound channel of S.E.R.C. flume with sinuosity 1.37, was presented.

(xii) The flow expansion-contraction phenomena, pointed out by **Ervine and Ellis(1987)**, was also observed in the meandering compound flows of S.E.R.C. Series B.

(xiii) Observations from the Glasgow flume indicate that:

- In the overbank case, although the floodplains are inundated, the secondary cell that appears at bend apex section is rotating exactly in same way as a typical clockwise cell generated for an inbank case of flow around the bend. This proves conclusively that floodplain flow shearing over the main channel flow is

responsible to develop bend cells changing rotation direction.
- In the overbank case, the secondary currents reach its maximum downstream of the bend apex and the maximum ratio of transverse velocity to the streamwise velocity was around 20%-30%, which is similar to S.E.R.C. flume data although the sense of rotation of the secondary current at the bend is opposite in theses two cases.

Table 5.1

ANALYSIS OF THE STRENGTH OF SECONDARY CURRENTS AT BEND APEX
S.E.R.C. SERIES B. SINUOSITY 1.37. TRAPEZOIDAL CROSS-SECTION

Stage mm	Floodplain case	$(V/U)_{max.}$ %
100.0		7
200.0	Smooth	27
250.0	Smooth	19

Table 5.2

ANALYSIS OF THE STRENGTH OF SECONDARY CURRENTS AT BEND APEX
S.E.R.C. SERIES B. SINUOSITY 1.37. NATURAL CROSS-SECTION

Stage mm	Floodplain case	$(V/U)_{max.}$ %
140.0		14
165.0	Smooth	25
200.0	Smooth	20
250.0	Smooth	18
165.0	Rough.	30
200.0	Rough.	19
250.0	Rough.	18

Table 5.3

ANALYSIS OF THE STRENGTH OF SECONDARY CURRENTS AT BEND APEX
S.E.R.C. SERIES B. SINUOSITY 2.04. NATURAL CROSS-SECTION

Stage mm	Floodplain case	$(V/U)_{max.}$ %
140.0		18
165.0	Smooth	25
200.0	Smooth	22
165.0	Rough.	29
200.0	Rough.	30

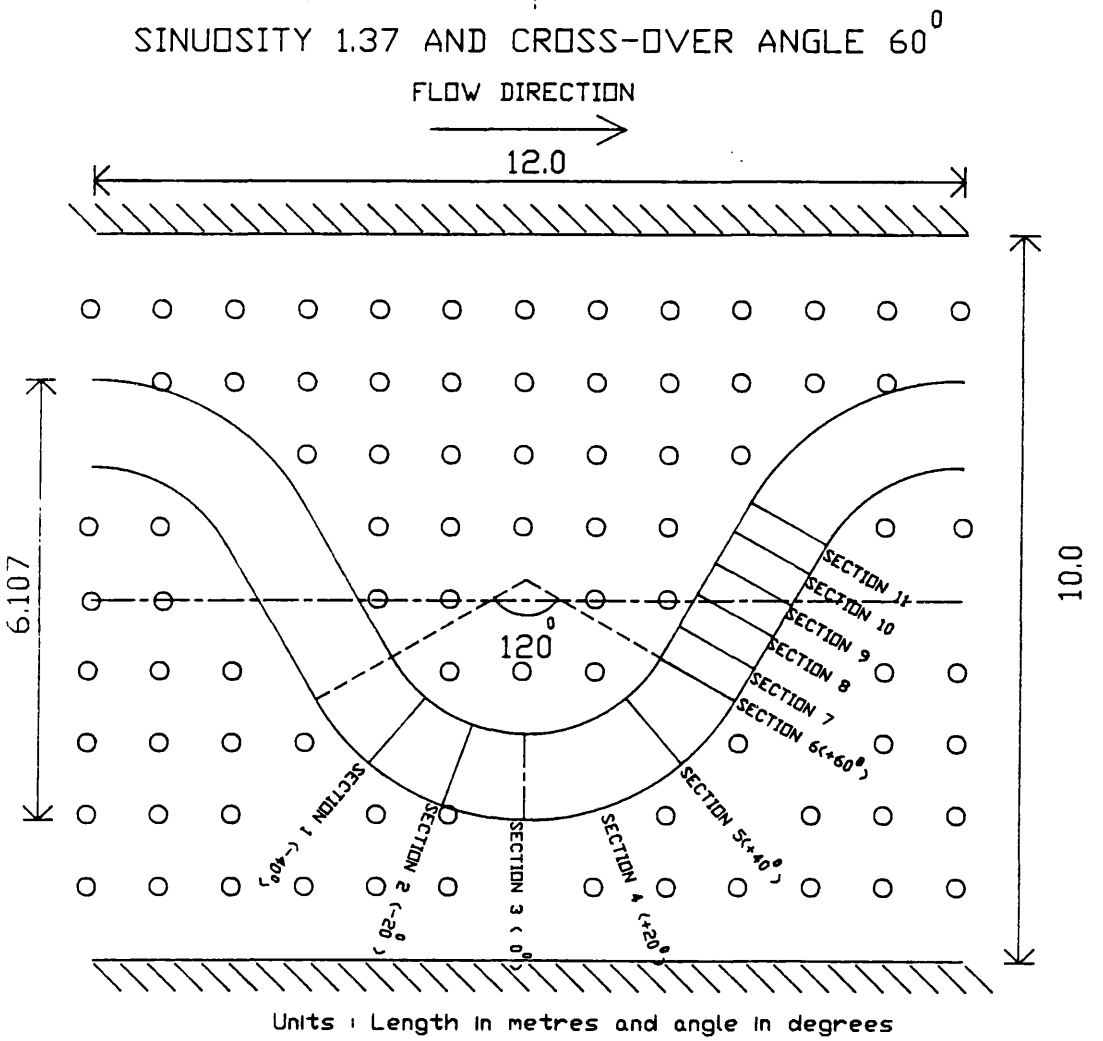

Fig (5.1a) - Plan View of the One Wave-Length of Sinuosity 1.374 of S.E.R.C. Flume Series B with the Location of the Measurement Sections.

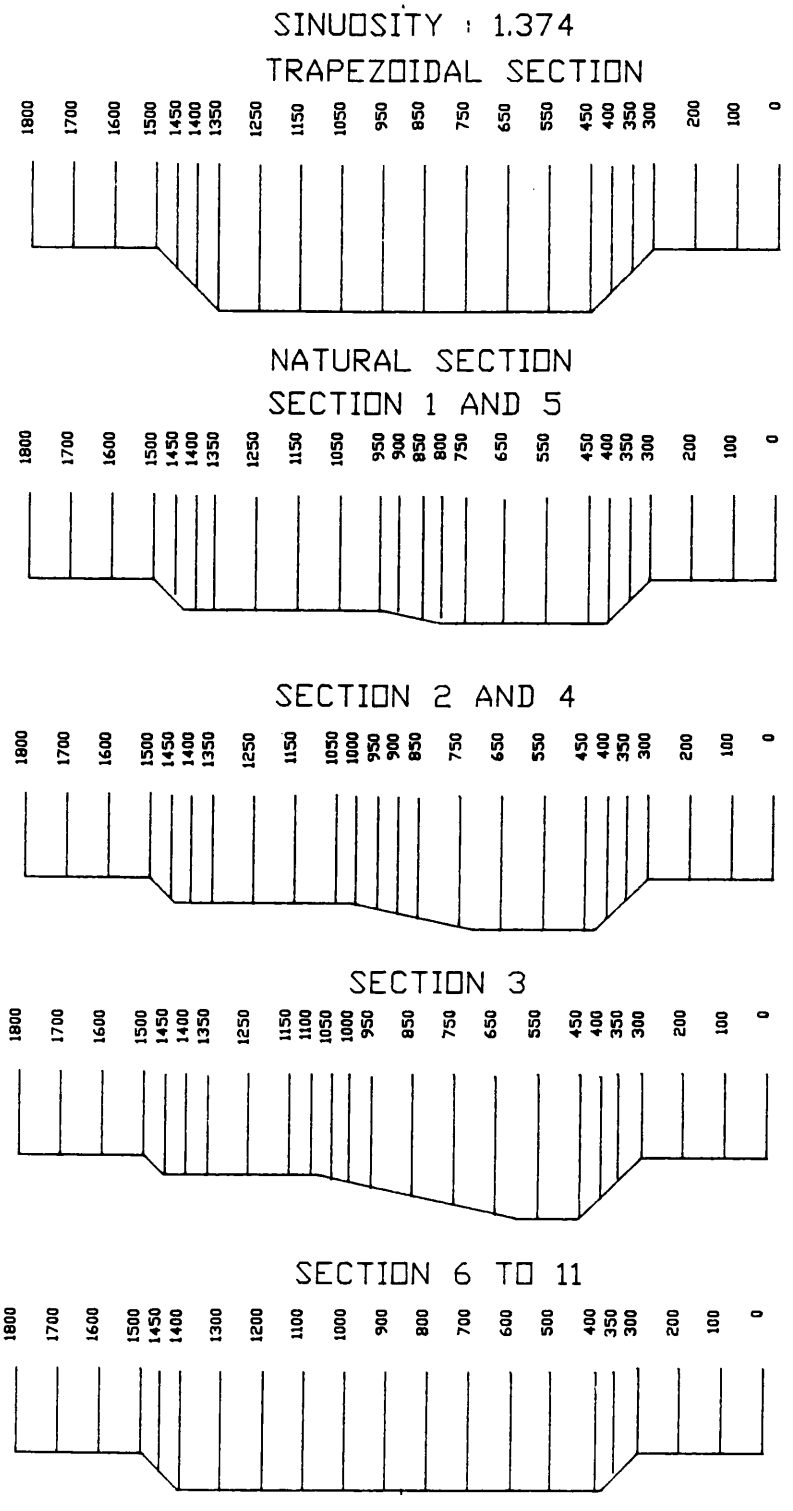

Fig (5.1b) - Location of Vertical Slices Where Measurements Took Place for Sinuosity 1.37 of S.E.R.C. Flume Series B.

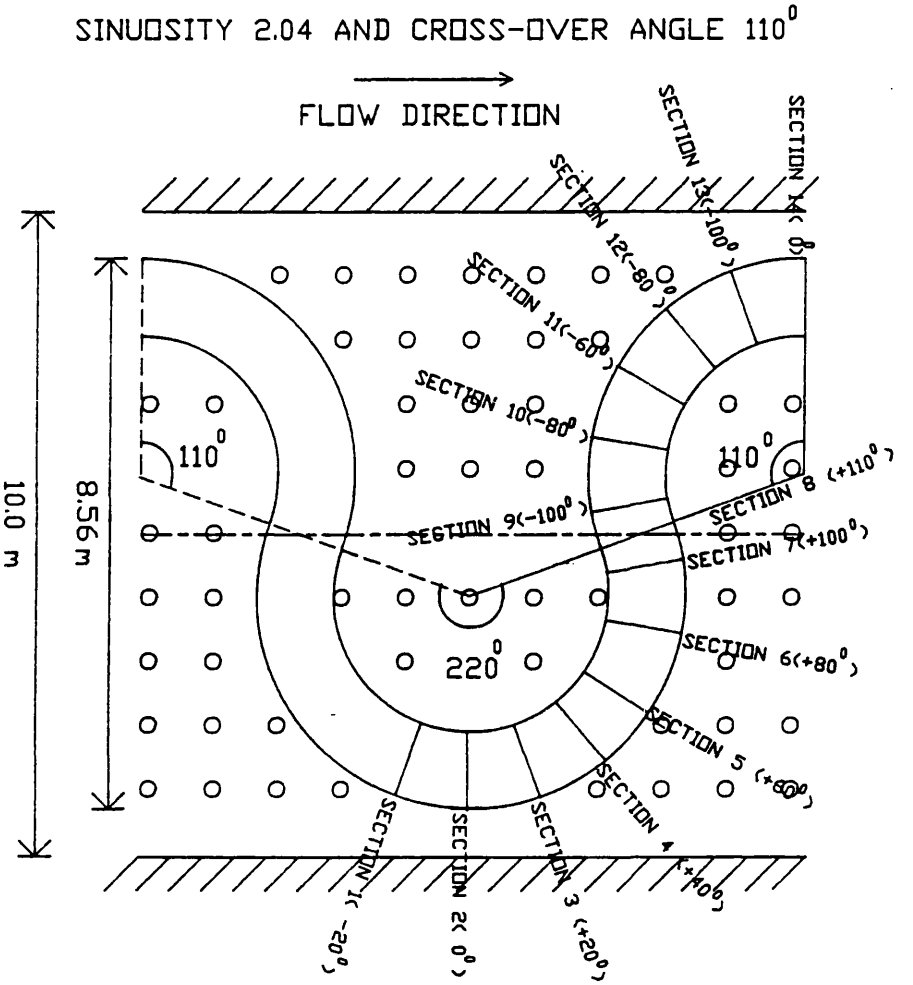

Fig (5.2a) - Plan View of the One Wave-Length of Sinuosity 2.04 of S.E.R.C. Flume Series B with the Location of the Measurement Sections.

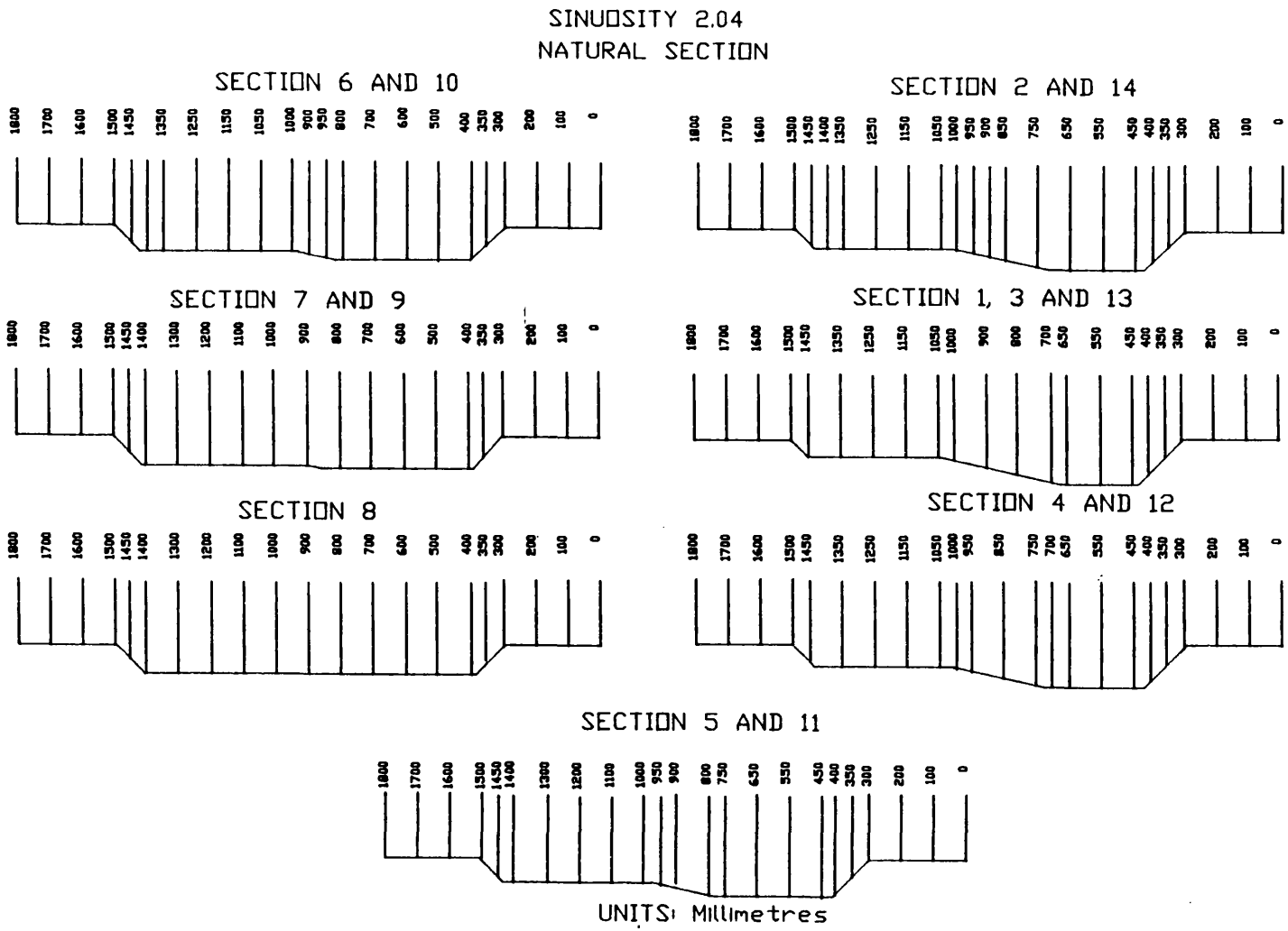

Fig (5.2b) - Location of Vertical Slices Where Measurements Took Place for Sinuosity 2.04 of S.E.R.C. Flume Series B.

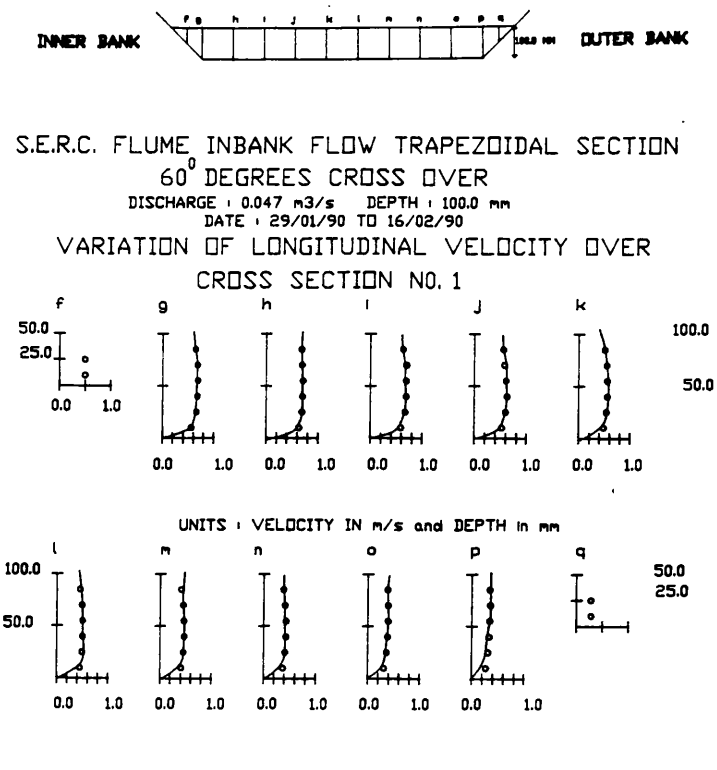

Fig (5.3a) - Variation of The Streamwise Velocity in Section No.1 for The Inbank Case. S.E.R.C. Series B. Meandering Channel With Sinuosity 1.37. Trapezoidal Cross-Section. Stage 100.0 mm. Discharge 0.047 m^3/s.

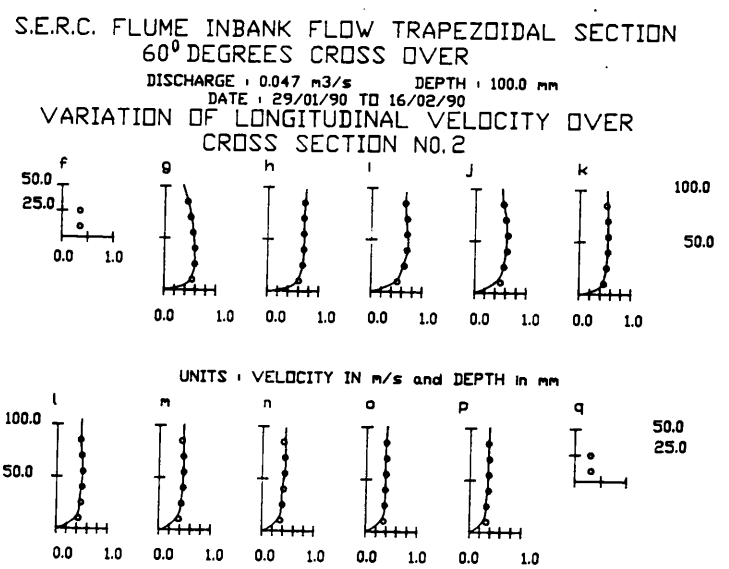

Fig (5.3b) - Variation of The Streamwise Velocity in Section No.2 for The Inbank Case. S.E.R.C. Series B. Meandering Channel With Sinuosity 1.37. Trapezoidal Cross-Section. Stage 100.0 mm. Discharge 0.047 m^3/s.

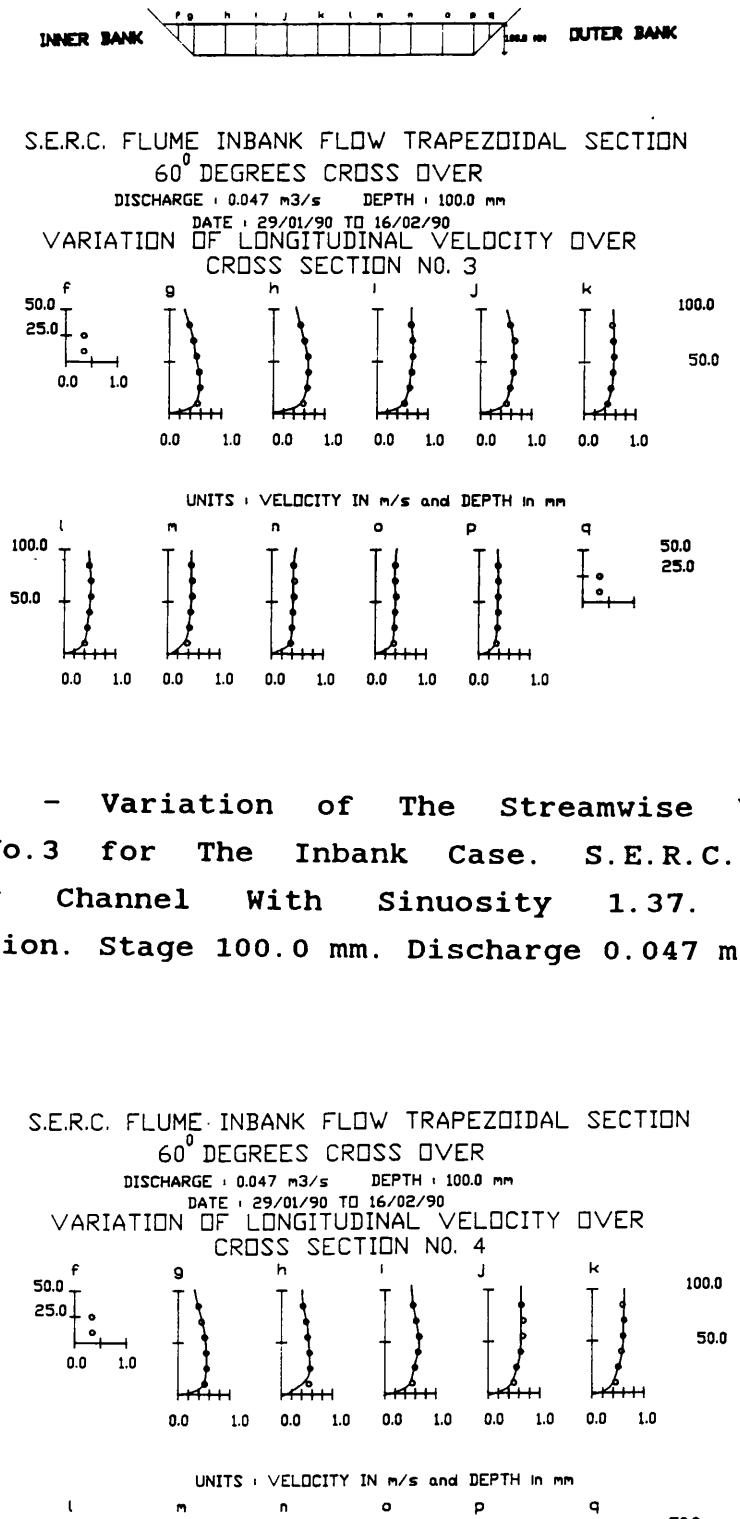

Fig (5.3c) - Variation of The Streamwise Velocity in Section No.3 for The Inbank Case. S.E.R.C. Series B. Meandering Channel With Sinuosity 1.37. Trapezoidal Cross-Section. Stage 100.0 mm. Discharge 0.047 m^3/s.

Fig (5.3d) - Variation of The Streamwise Velocity in Section No.4 for The Inbank Case. S.E.R.C. Series B. Meandering Channel With Sinuosity 1.37. Trapezoidal Cross-Section. Stage 100.0 mm. Discharge 0.047 m^3/s.

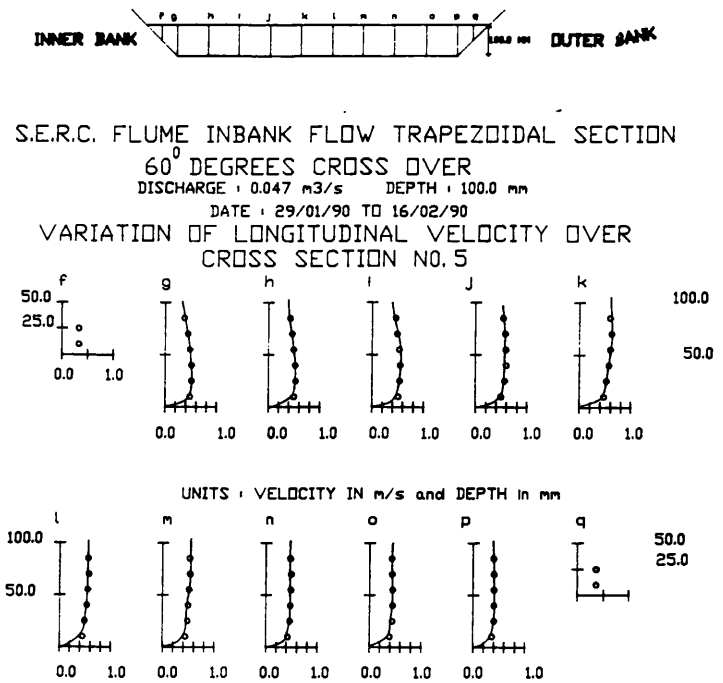

Fig (5.3e) - Variation of The Streamwise Velocity in Section No.5 for The Inbank Case. S.E.R.C. Series B. Meandering Channel With Sinuosity 1.37. Trapezoidal Cross-Section. Stage 100.0 mm. Discharge 0.047 m^3/s.

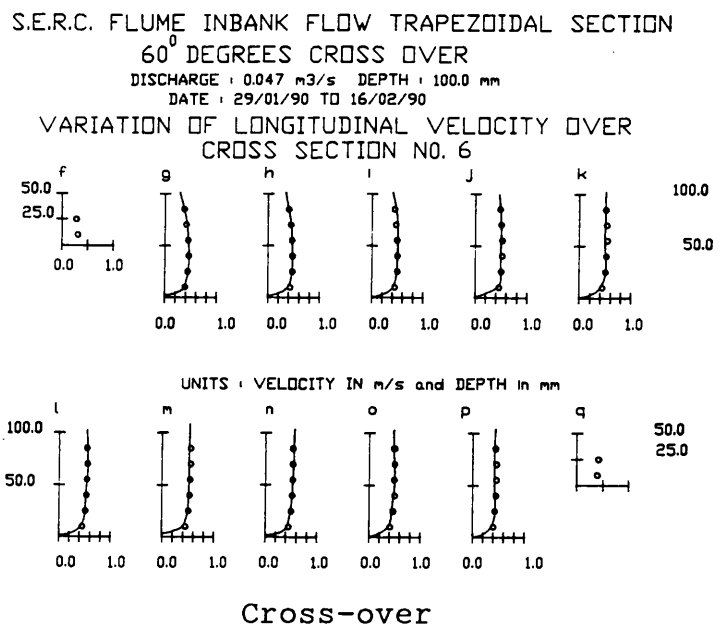

Fig (5.3f) - Variation of The Streamwise Velocity in Section No.6 for The Inbank Case. S.E.R.C. Series B. Meandering Channel With Sinuosity 1.37. Trapezoidal Cross-Section. Stage 100.0 mm. Discharge 0.047 m^3/s.

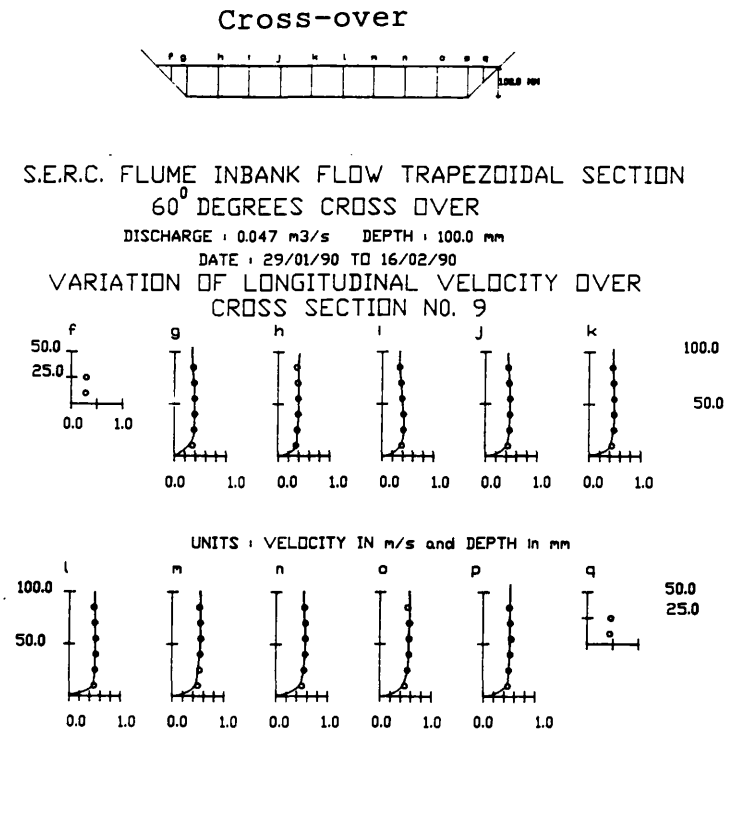

Fig (5.3i) - Variation of The Streamwise Velocity in Section No.9 for The Inbank Case. S.E.R.C. Series B. Meandering Channel With Sinuosity 1.37. Trapezoidal Cross-Section. Stage 100.0 mm. Discharge 0.047 m^3/s.

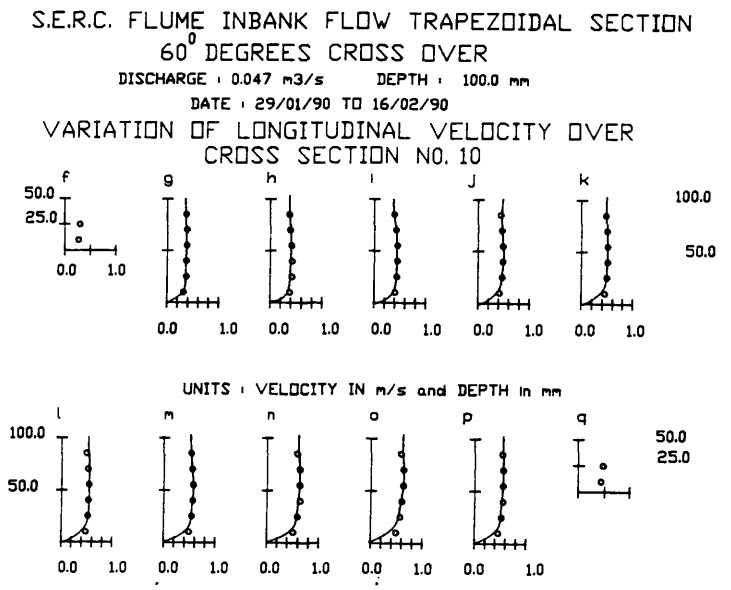

Fig (5.3j) - Variation of The Streamwise Velocity in Section No.10 for The Inbank Case. S.E.R.C. Series B. Meandering Channel With Sinuosity 1.37. Trapezoidal Cross-Section. Stage 100.0 mm. Discharge 0.047 m^3/s.

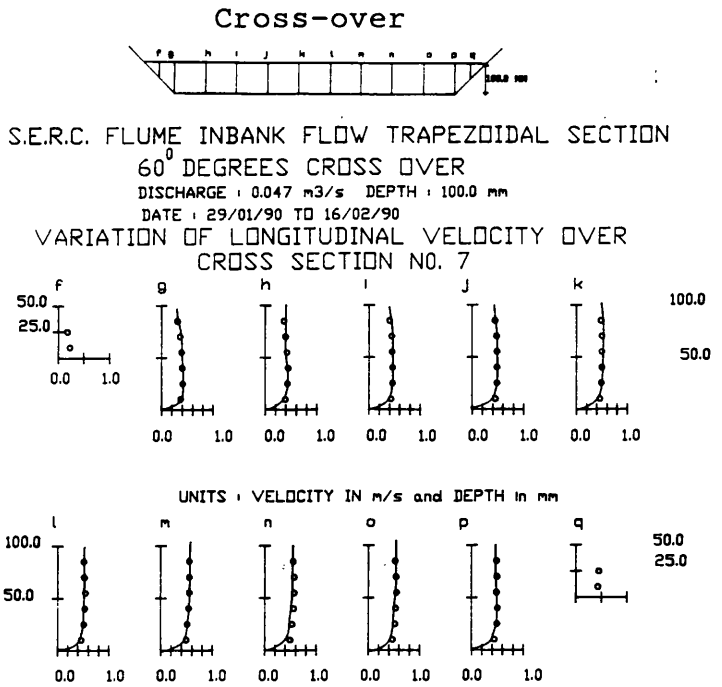

Fig (5.3g) - Variation of The Streamwise Velocity in Section No.7 for The Inbank Case. S.E.R.C. Series B. Meandering Channel With Sinuosity 1.37. Trapezoidal Cross-Section. Stage 100.0 mm. Discharge 0.047 m^3/s.

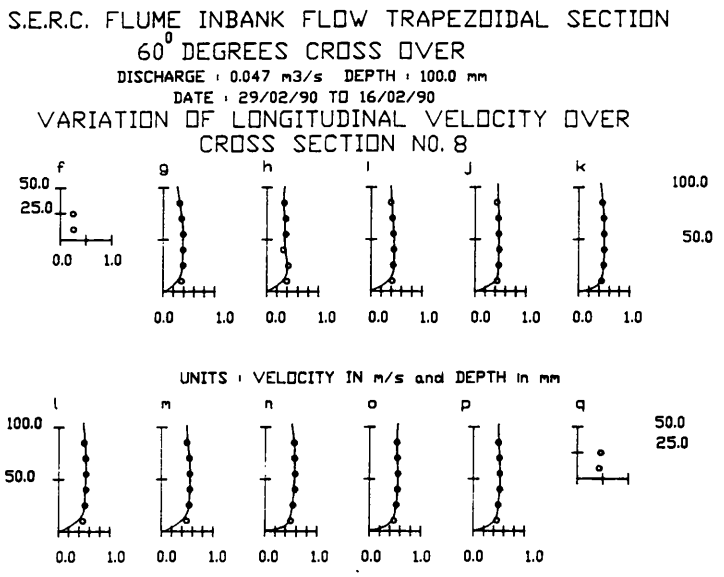

Fig (5.3h) - Variation of The Streamwise Velocity in Section No.8 for The Inbank Case. S.E.R.C. Series B. Meandering Channel With Sinuosity 1.37. Trapezoidal Cross-Section. Stage 100.0 mm. Discharge 0.047 m^3/s.

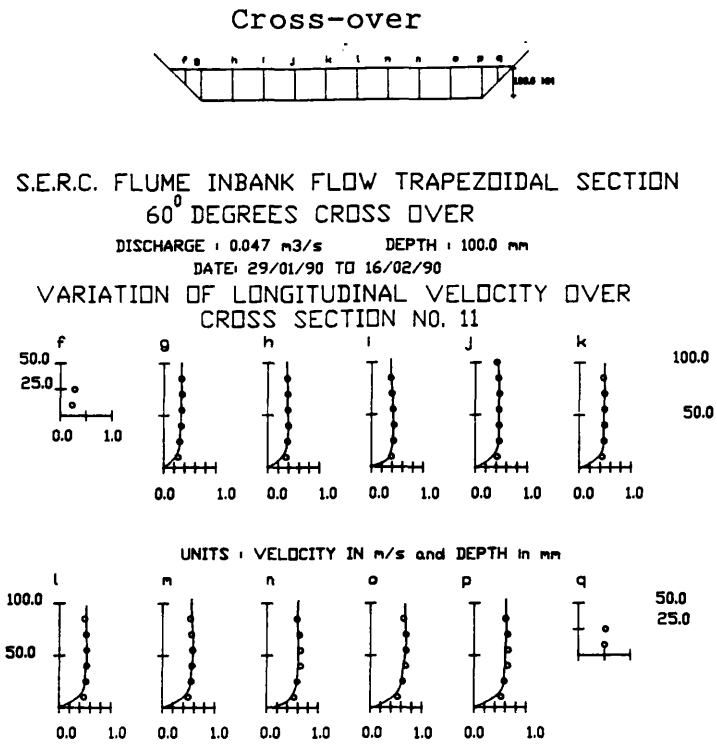

Fig (5.3k) - Variation of The Streamwise Velocity in Section No.11 for The Inbank Case. S.E.R.C. Series B. Meandering Channel With Sinuosity 1.37. Trapezoidal Cross-Section. Stage 100.0 mm. Discharge 0.047 m^3/s.

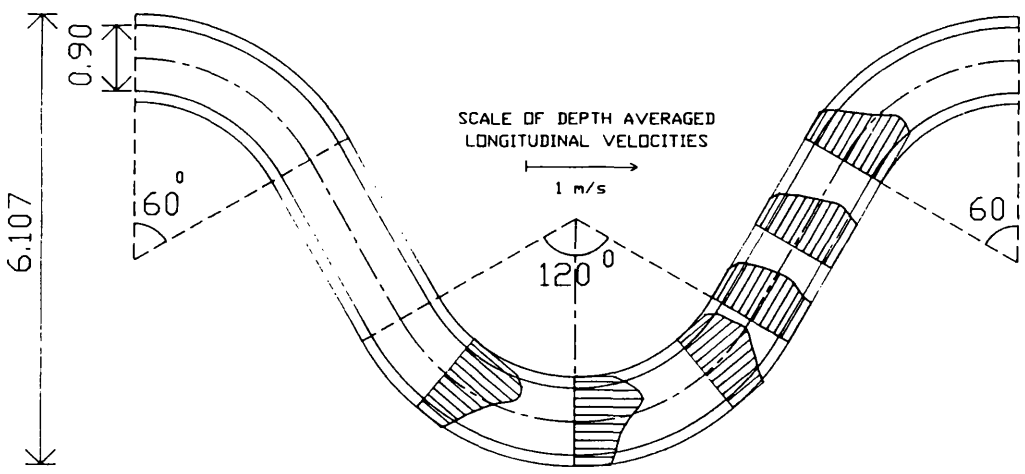

Fig (5.4) - Variation of The Depth Averaged Velocity For The Inbank Case. S.E.R.C. Series B. Meandering Channel With Sinuosity 1.37. Trapezoidal Cross-Section. Stage 100.0 mm. Discharge 0.047 m^3/s.

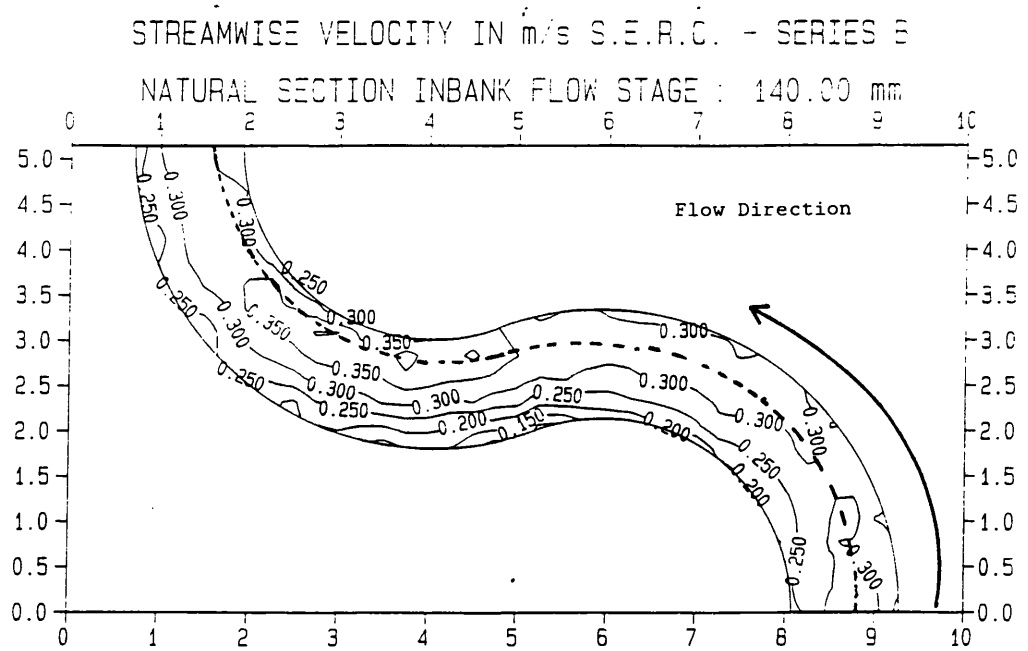

Fig (5.5) - Contour Levels of The Streamwise Velocity. Inbank Case. S.E.R.C. Series B. Meandering Channel With Sinuosity 2.04. Natural Cross-Section. Stage 140.0 mm.

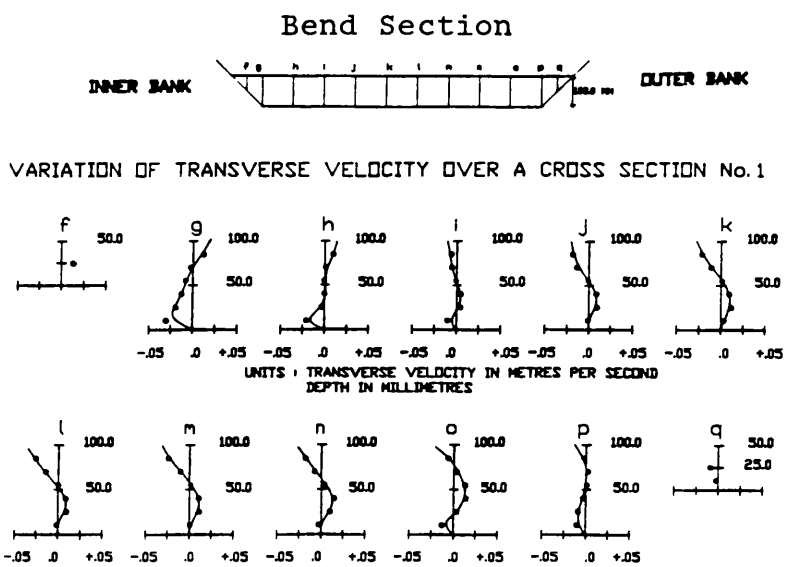

Fig (5.6a) - Variation of The Transverse Velocity in Section No.1 for the Inbank Case. S.E.R.C. Series B. Meandering Channel With Sinuosity 1.37. Trapezoidal Cross-Section. Stage 100.0 mm. Discharge 0.047 m^3/s.

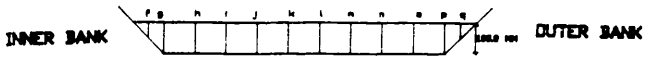

Bend Section

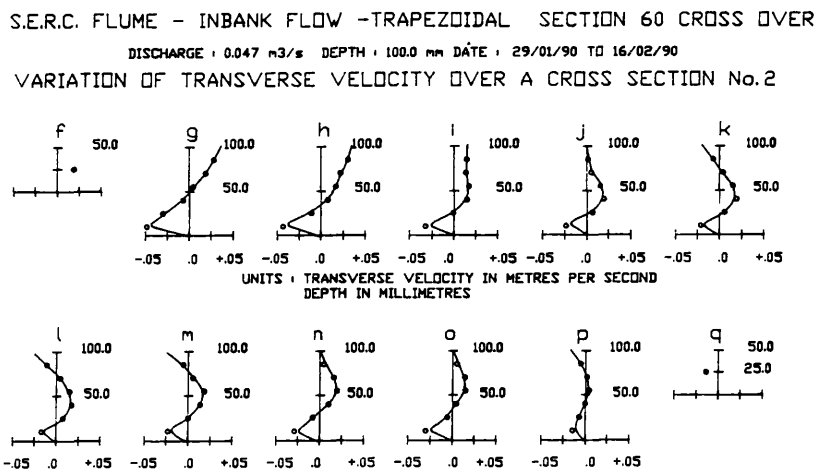

Fig (5.6b) - Variation of The Transverse Velocity in Section No.2 for the Inbank Case. S.E.R.C. Series B. Meandering Channel With Sinuosity 1.37. Trapezoidal Cross-Section. Stage 100.0 mm. Discharge 0.047 m^3/s.

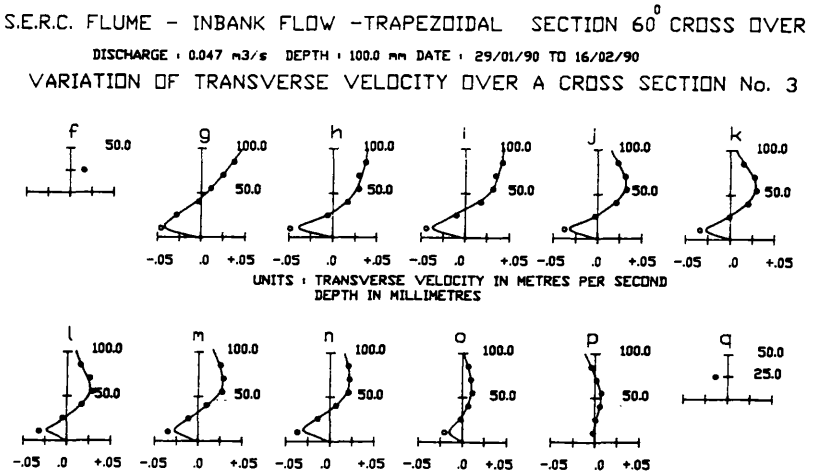

Fig (5.6c) - Variation of The Transverse Velocity in Section No.3 for the Inbank Case. S.E.R.C. Series B. Meandering Channel With Sinuosity 1.37. Trapezoidal Cross-Section. Stage 100.0 mm. Discharge 0.047 m^3/s.

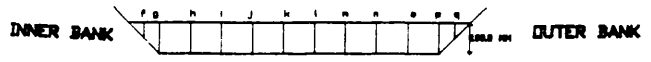

Bend Section

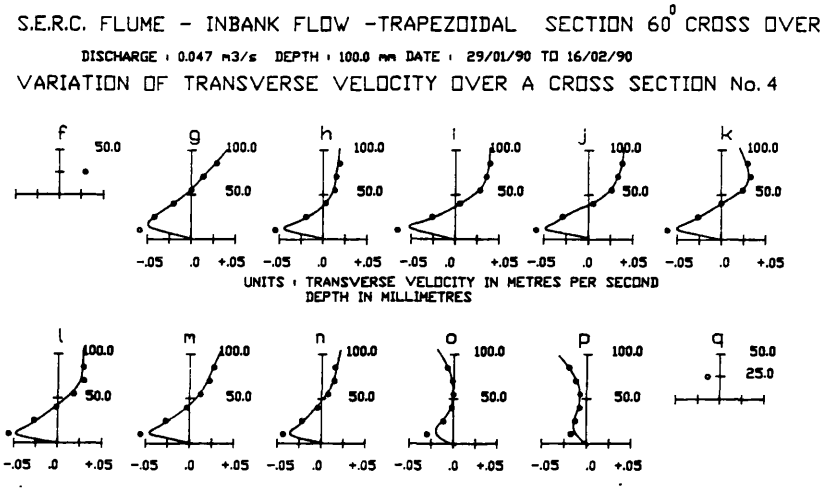

Fig (5.6d) - Variation of The Transverse Velocity in Section No.4 for the Inbank Case. S.E.R.C. Series B. Meandering Channel With Sinuosity 1.37. Trapezoidal Cross-Section. Stage 100.0 mm. Discharge 0.047 m^3/s.

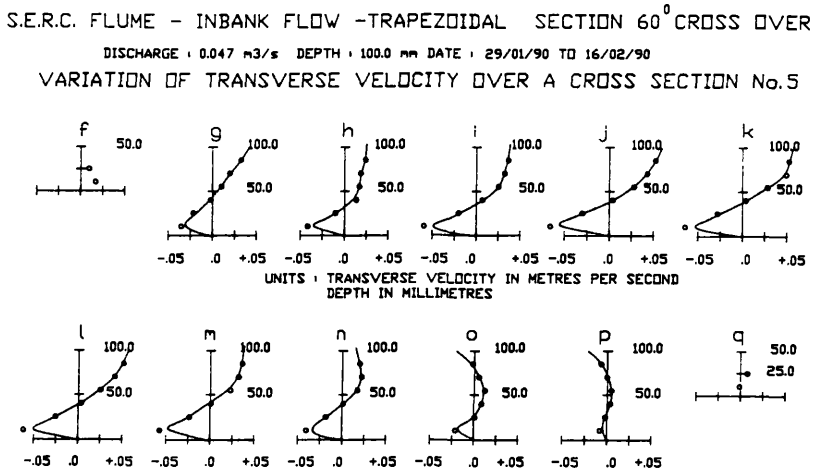

Fig (5.6e) - Variation of The Transverse Velocity in Section No.5 for the Inbank Case. S.E.R.C. Series B. Meandering Channel With Sinuosity 1.37. Trapezoidal Cross-Section. Stage 100.0 mm. Discharge 0.047 m^3/s.

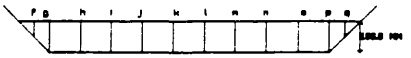

Cross-Over Section

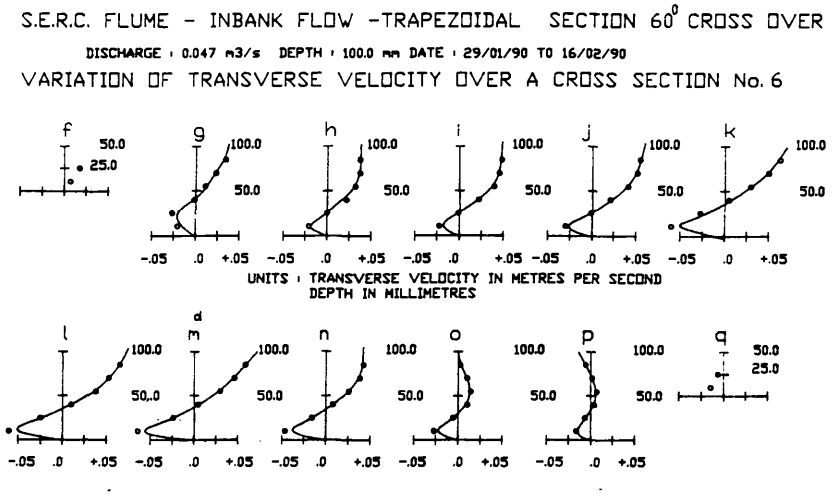

Fig (5.6f) - Variation of The Transverse Velocity in Section No.6 for the Inbank Case. S.E.R.C. Series B. Meandering Channel With Sinuosity 1.37. Trapezoidal Cross-Section. Stage 100.0 mm. Discharge 0.047 m^3/s.

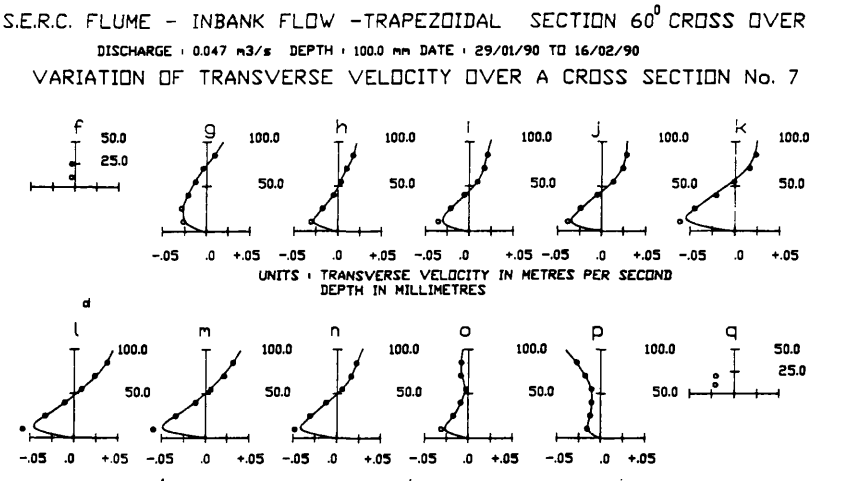

Fig (5.6g) - Variation of The Transverse Velocity in Section No.7 for the Inbank Case. S.E.R.C. Series B. Meandering Channel With Sinuosity 1.37. Trapezoidal Cross-Section. Stage 100.0 mm. Discharge 0.047 m^3/s.

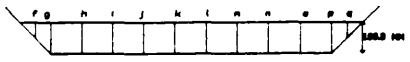

Cross-Over Section

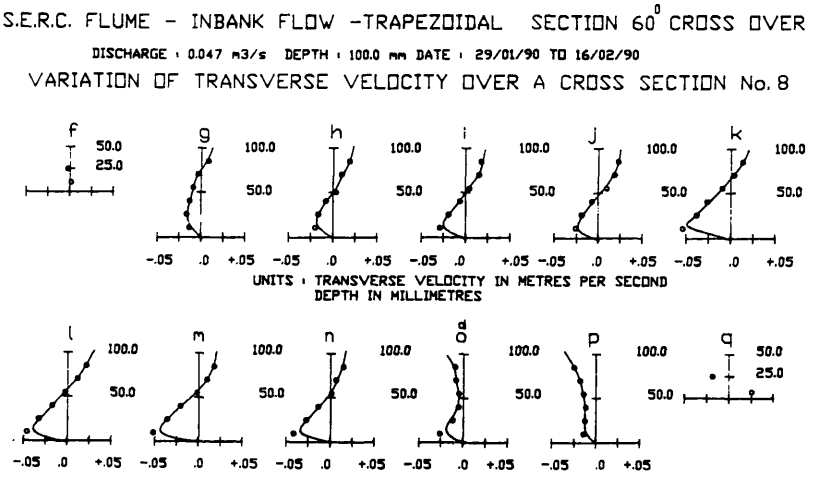

Fig (5.6h) - Variation of The Transverse Velocity in Section No.8 for the Inbank Case. S.E.R.C. Series B. Meandering Channel With Sinuosity 1.37. Trapezoidal Cross-Section. Stage 100.0 mm. Discharge 0.047 m^3/s.

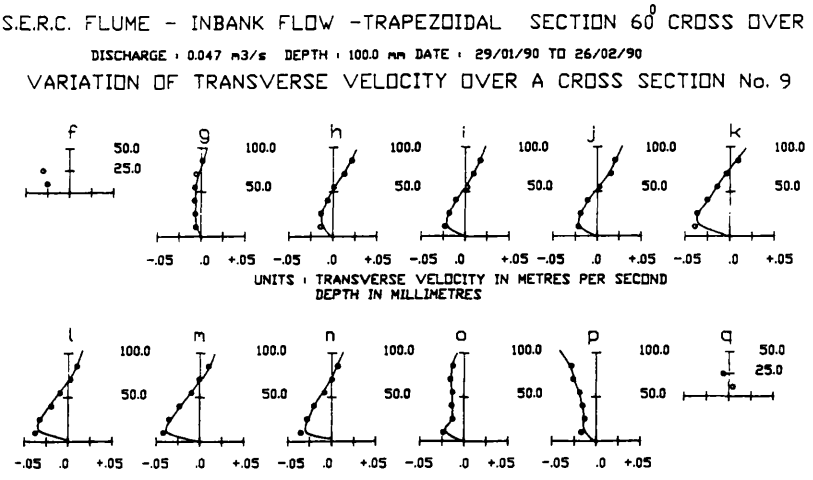

Fig (5.6i) - Variation of The Transverse Velocity in Section No.9 for the Inbank Case. S.E.R.C. Series B. Meandering Channel With Sinuosity 1.37. Trapezoidal Cross-Section. Stage 100.0 mm. Discharge 0.047 m^3/s.

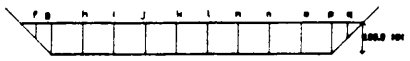

Cross-Over Section

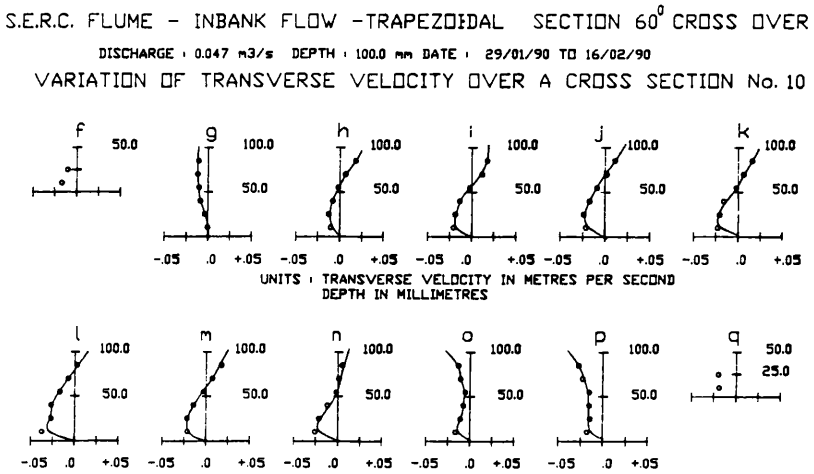

Fig (5.6j) - Variation of The Transverse Velocity in Section No.10 for the Inbank Case. S.E.R.C. Series B. Meandering Channel With Sinuosity 1.37. Trapezoidal Cross-Section. Stage 100.0 mm. Discharge 0.047 m^3/s.

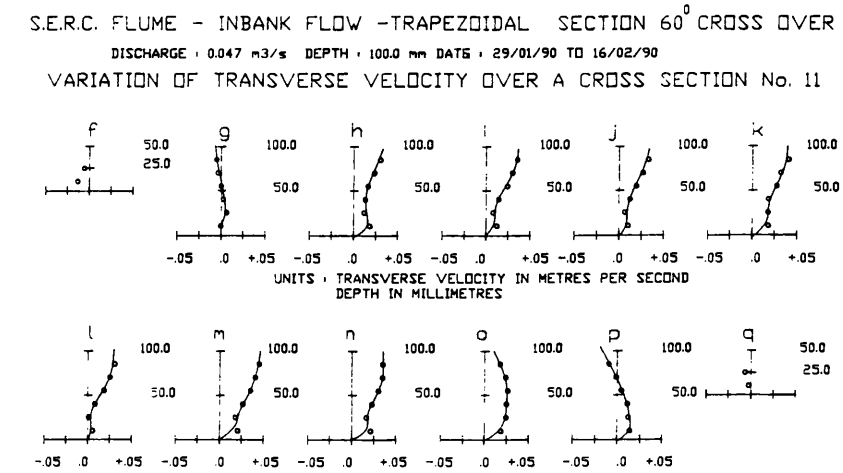

Fig (5.6k) - Variation of The Transverse Velocity in Section No.11 for the Inbank Case. S.E.R.C. Series B. Meandering Channel With Sinuosity 1.37. Trapezoidal Cross-Section. Stage 100.0 mm. Discharge 0.047 m^3/s.

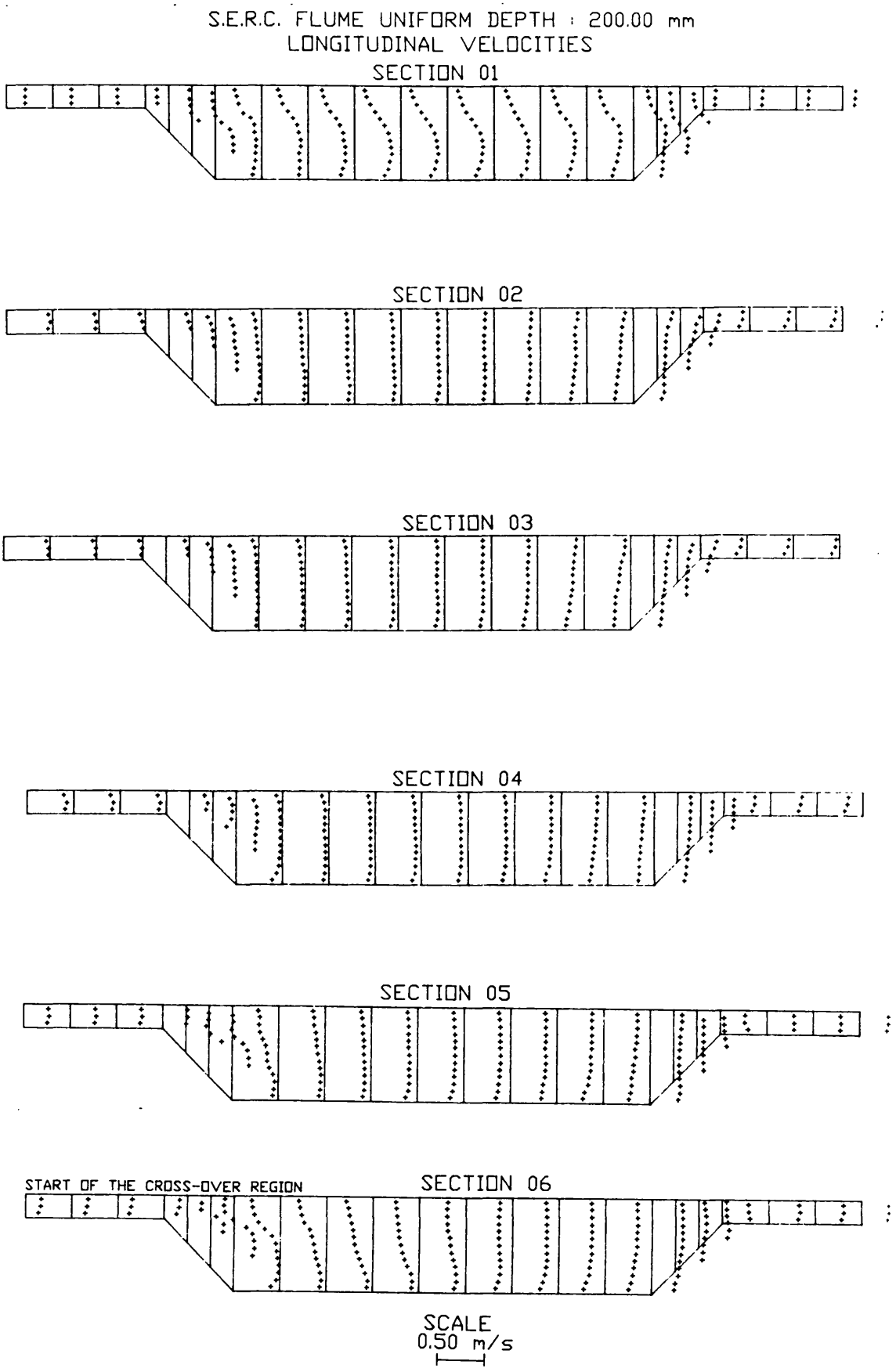

Fig (5.7a) - Variation of The Streamwise Velocity in Section Nos.1 to 6 for The Overbank Case. S.E.R.C. Series B. Meandering Channel With Sinuosity 1.37. Trapezoidal Cross-Section. Stage 200.0 mm. Smooth Floodplains.

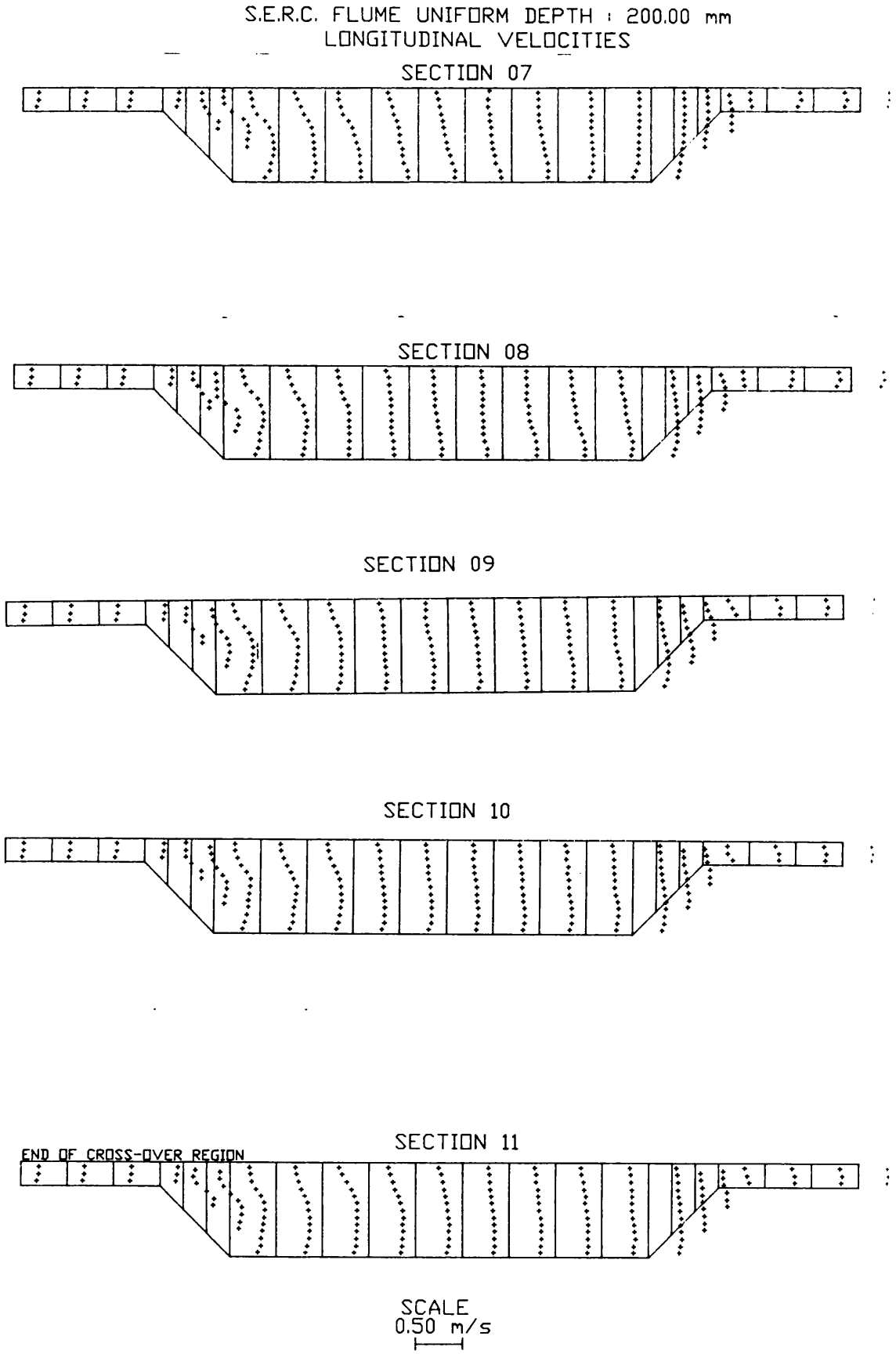

Fig (5.7b) - Variation of The Streamwise Velocity in Section Nos.7 to 11 for The Overbank Case. S.E.R.C. Series B. Meandering Channel With Sinuosity 1.37. Trapezoidal Cross-Section. Stage 200.0 mm. Smooth Floodplains.

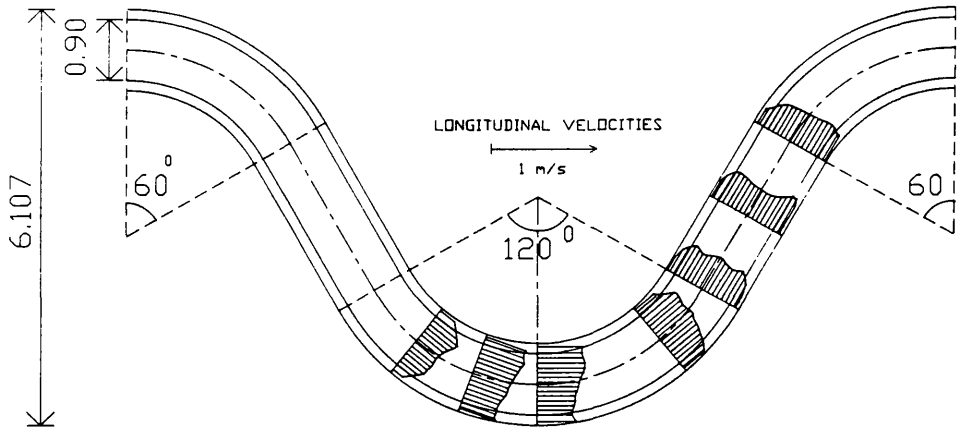

Fig (5.8) - Variation of The Depth Averaged Velocity For The Overbank Case. S.E.R.C. Series B. Meandering Channel With Sinuosity 1.37. Trapezoidal Cross-Section. Stage 200.0 mm. Smooth Floodplains.

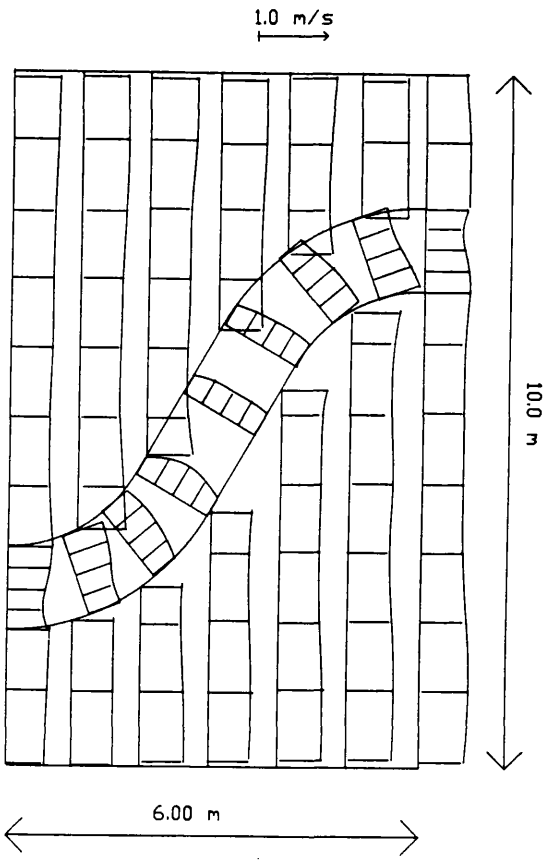

Fig (5.9) - Variation of The Depth Averaged Velocity For The Overbank Case. S.E.R.C. Series B. Meandering Channel With Sinuosity 1.37. Trapezoidal Cross-Section. Stage 250.0 mm. Smooth Floodplains.

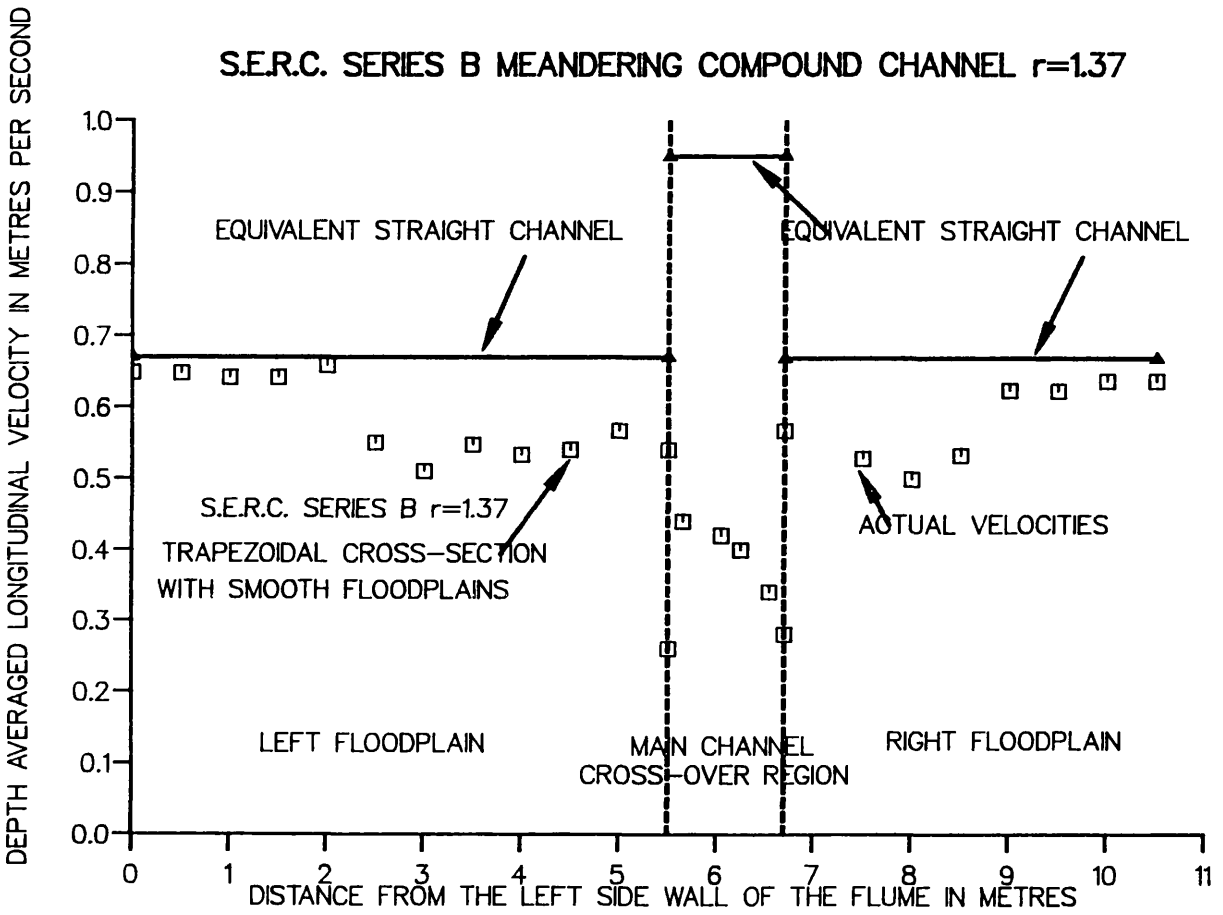

Fig (5.10) - Typical Distribution of the Depth Averaged Longitudinal Velocity on the Floodplain and the Depth Averaged Streamwise Velocity in the Main Channel of a Meandering Compound Flow. Data Taken from S.E.R.C.Series B with Sinousity 1.37, Stage 250.0 mm, Trapezoidal Cross-Section and Smooth Floodplains.

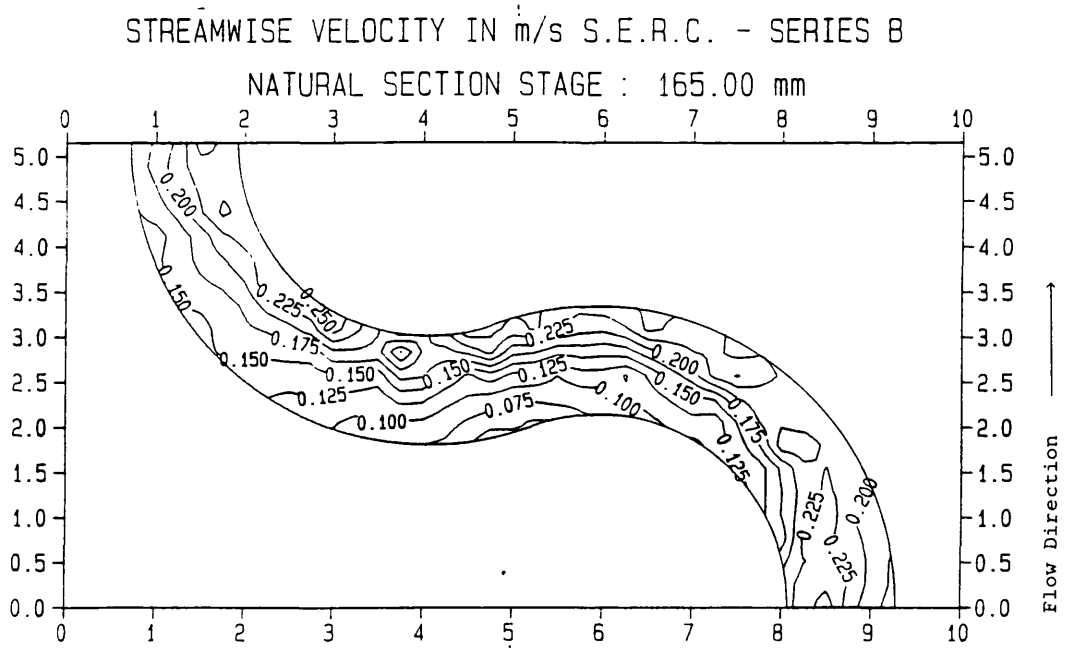

Fig (5.11) - Contour Levels of The Streamwise Velocity. Overbank Case. S.E.R.C. Series B. Meandering Channel With Sinuosity 2.04. Natural Cross-Section. Stage 165.0 mm. Smooth Floodplains.

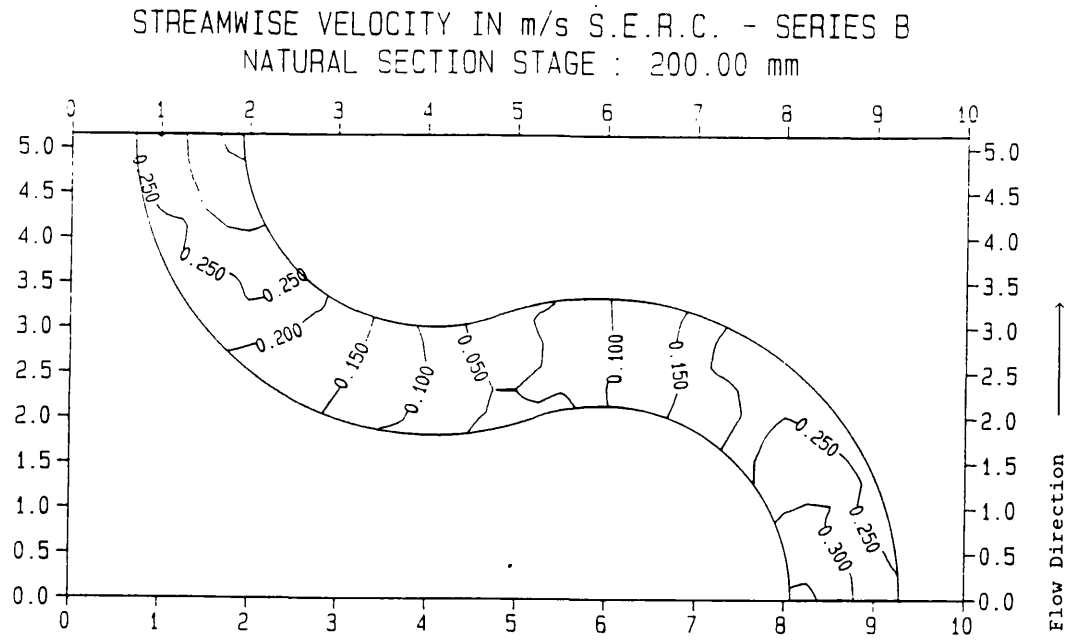

Fig (5.12) - Contour Levels of The Streamwise Velocity. Overbank Case. S.E.R.C. Series B. Meandering Channel With Sinuosity 2.04. Natural Cross-Section. Stage 200.0 mm. Smooth Floodplains.

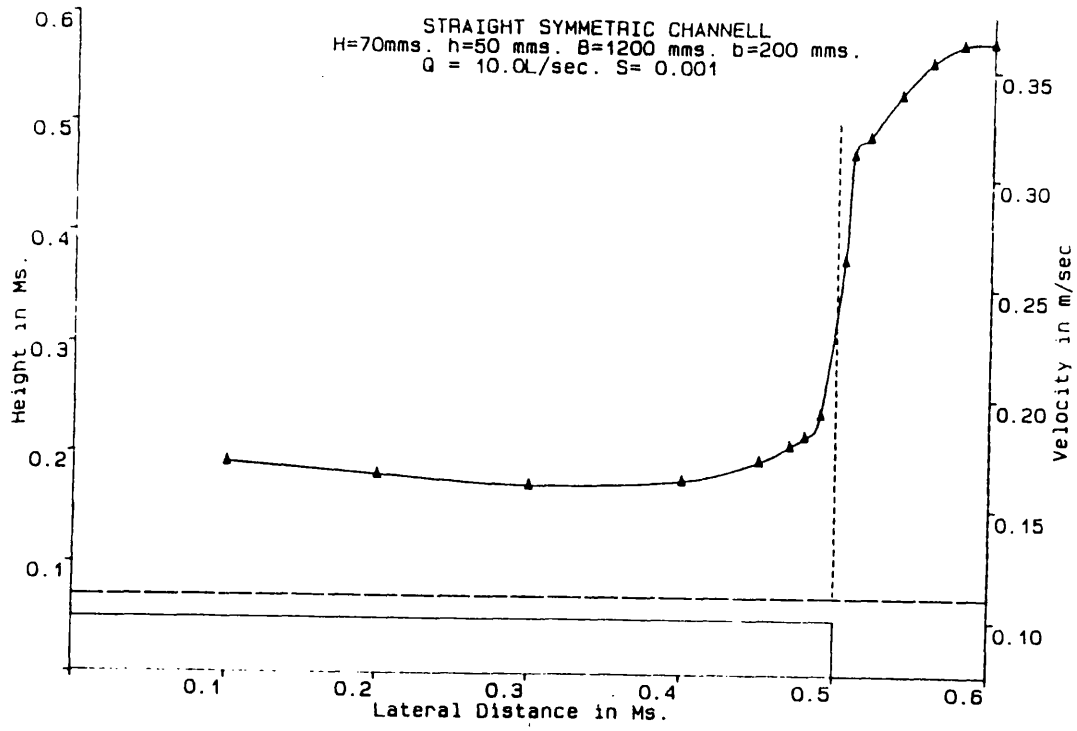

Fig (5.13a) - Typical Distribution of the Depth Averaged Longitudinal Velocity on the Floodplain and the Depth Averaged Streamwise Velocity in the Main Channel of a Straigth Compound Flow from Kiely(1989).

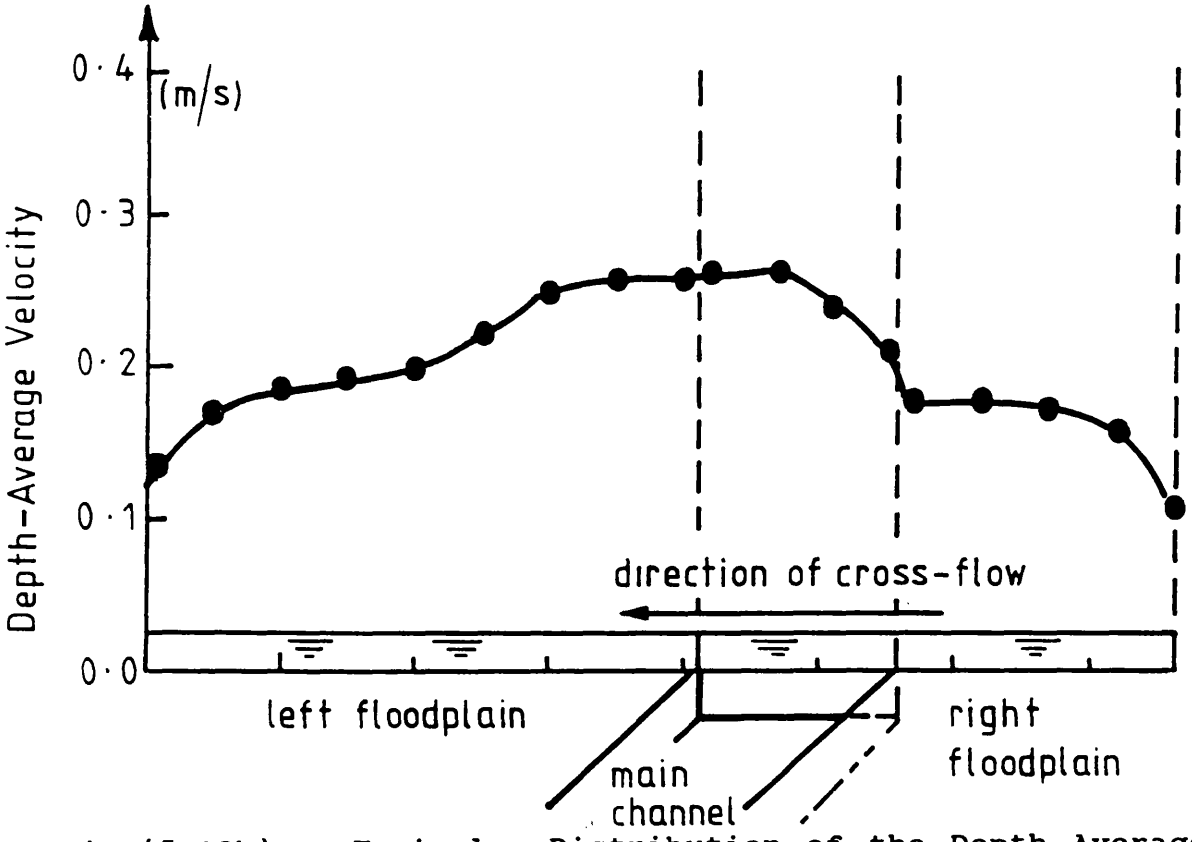

Fig (5.13b) - Typical Distribution of the Depth Averaged Longitudinal Velocity on the Floodplain and the Depth Averaged Streamwise Velocity in the Main Channel of a Skewed Compound Flow from Ervine and Jasem(1992).

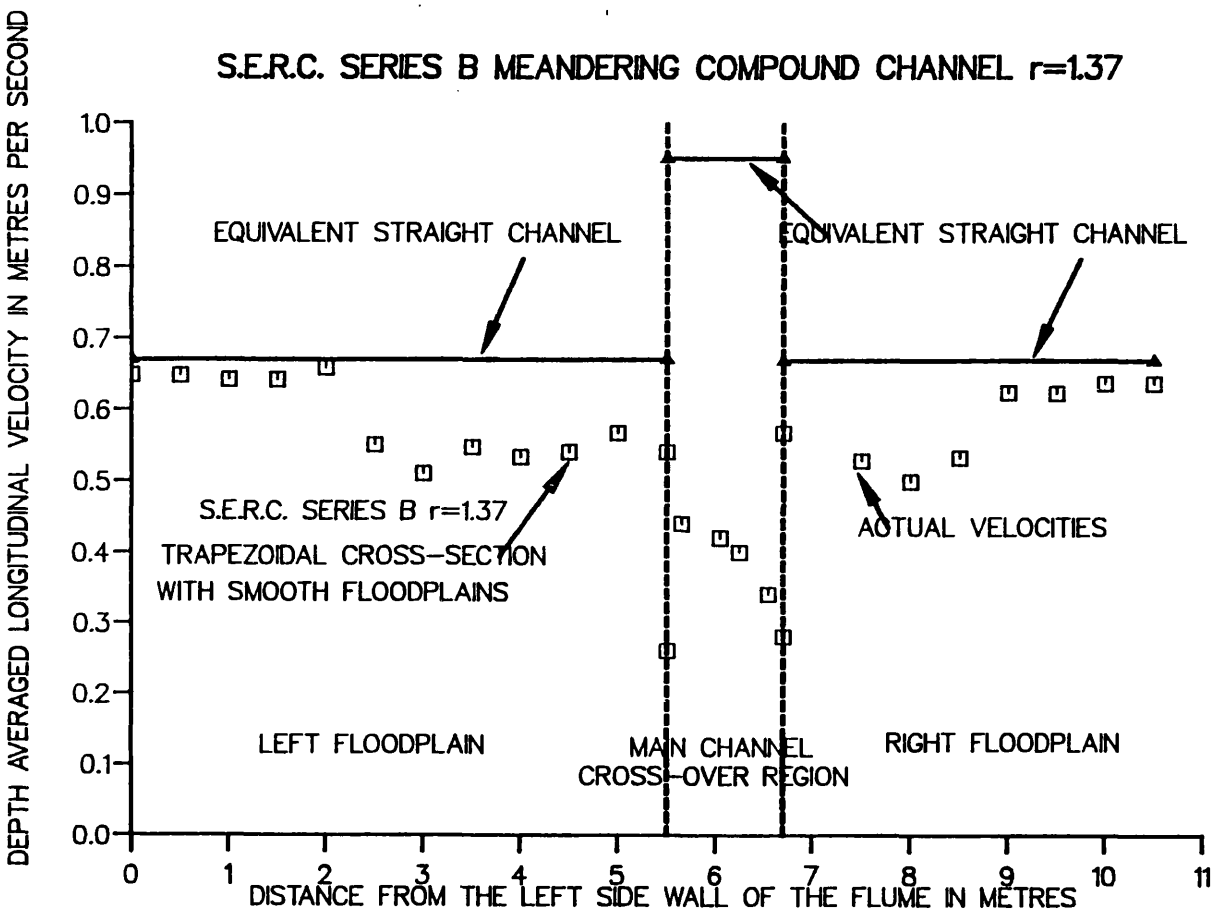

Fig (5.13c) - Typical Distribution of the Depth Averaged Longitudinal Velocity on the Floodplain and the Depth Averaged Streamwise Velocity in the Main Channel of a Meandering Compound Flow.

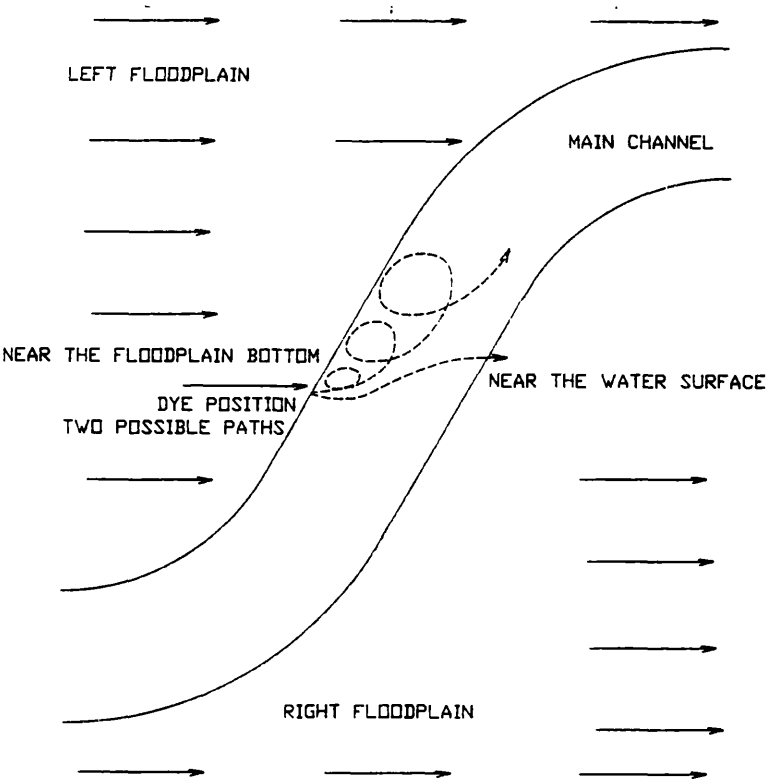

Fig (5.14a) - Paths Followed by The Water Particles in the Cross-Over Region of a Meandering Compound Flow.

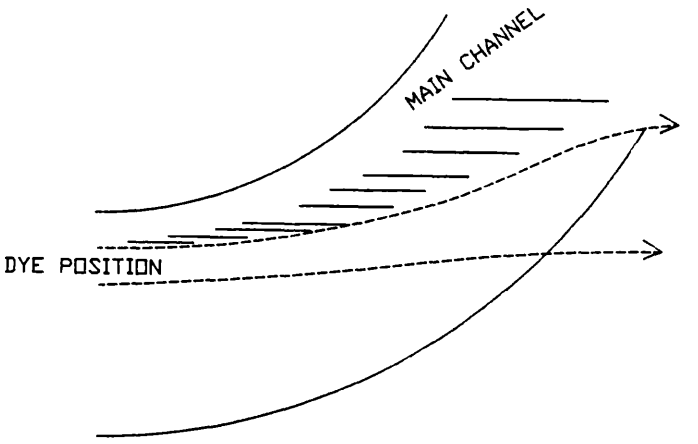

Fig (5.14b) - Paths Followed by The Water Particles in the Bend Region of a Meandering Compound Flow.

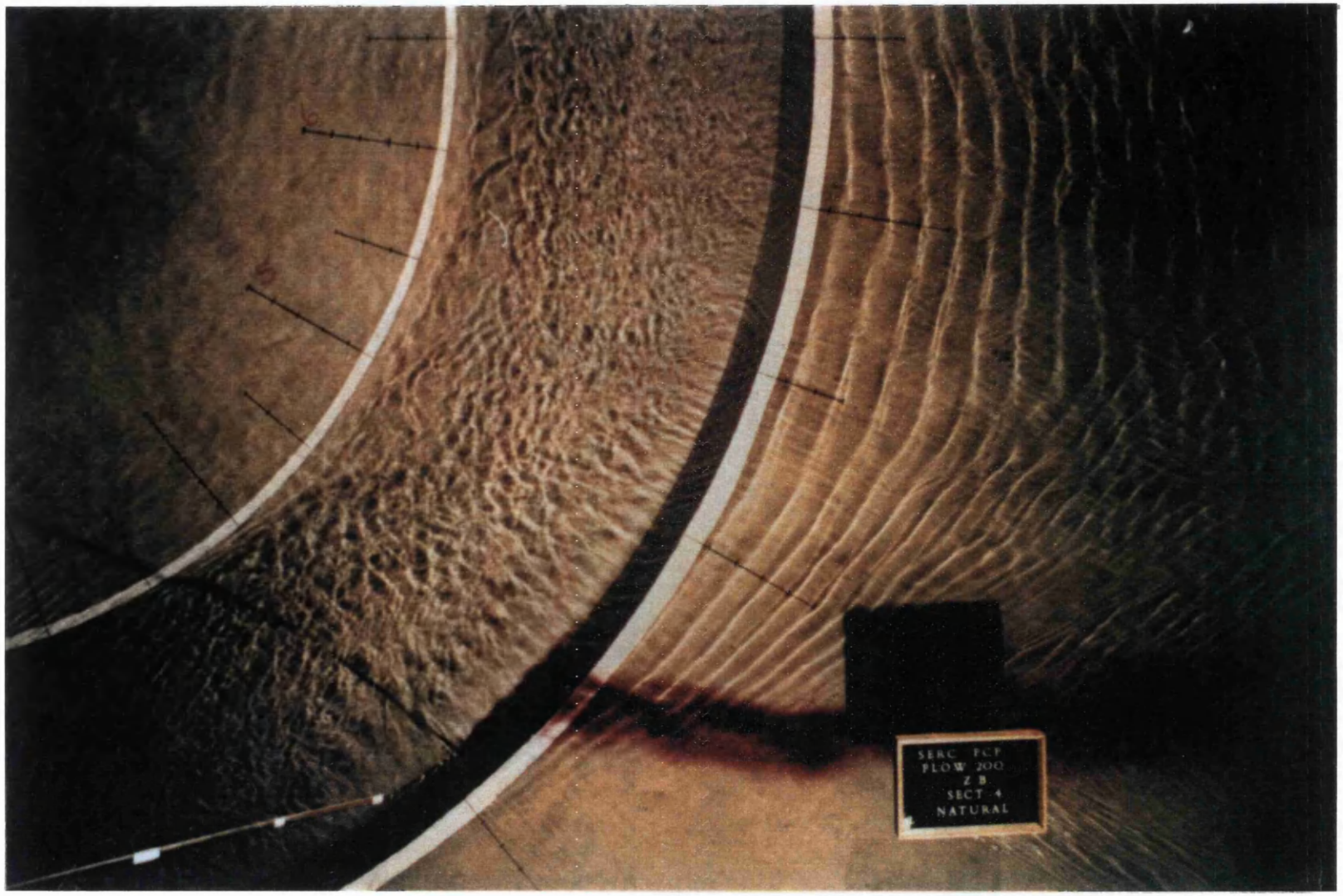

Fig (5.14c) - Dye Tests at Bed Level at the outer Bend of S.E.R.C. Flume Series B, Sinuosity 2.04, Natural Cross-Section, Stage 200.0 mm, Smooth Floodplains.

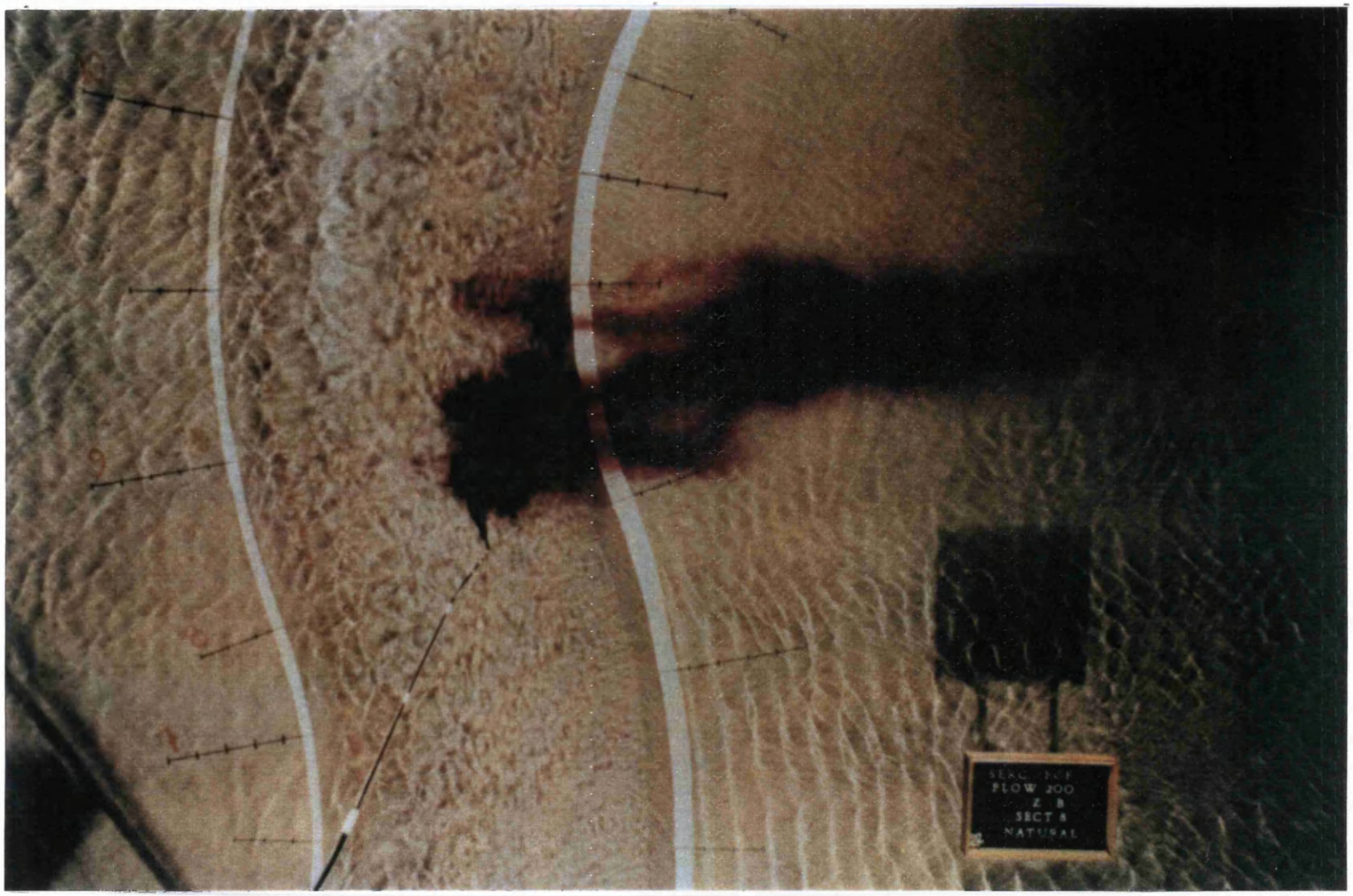

Fig (5.14d) - Dye Tests at Bed Level at the Cross-Over of S.E.R.C. Flume Series B, Sinuosity 2.04, Natural Cross-Section, Stage 200.0 mm, Smooth Floodplains.

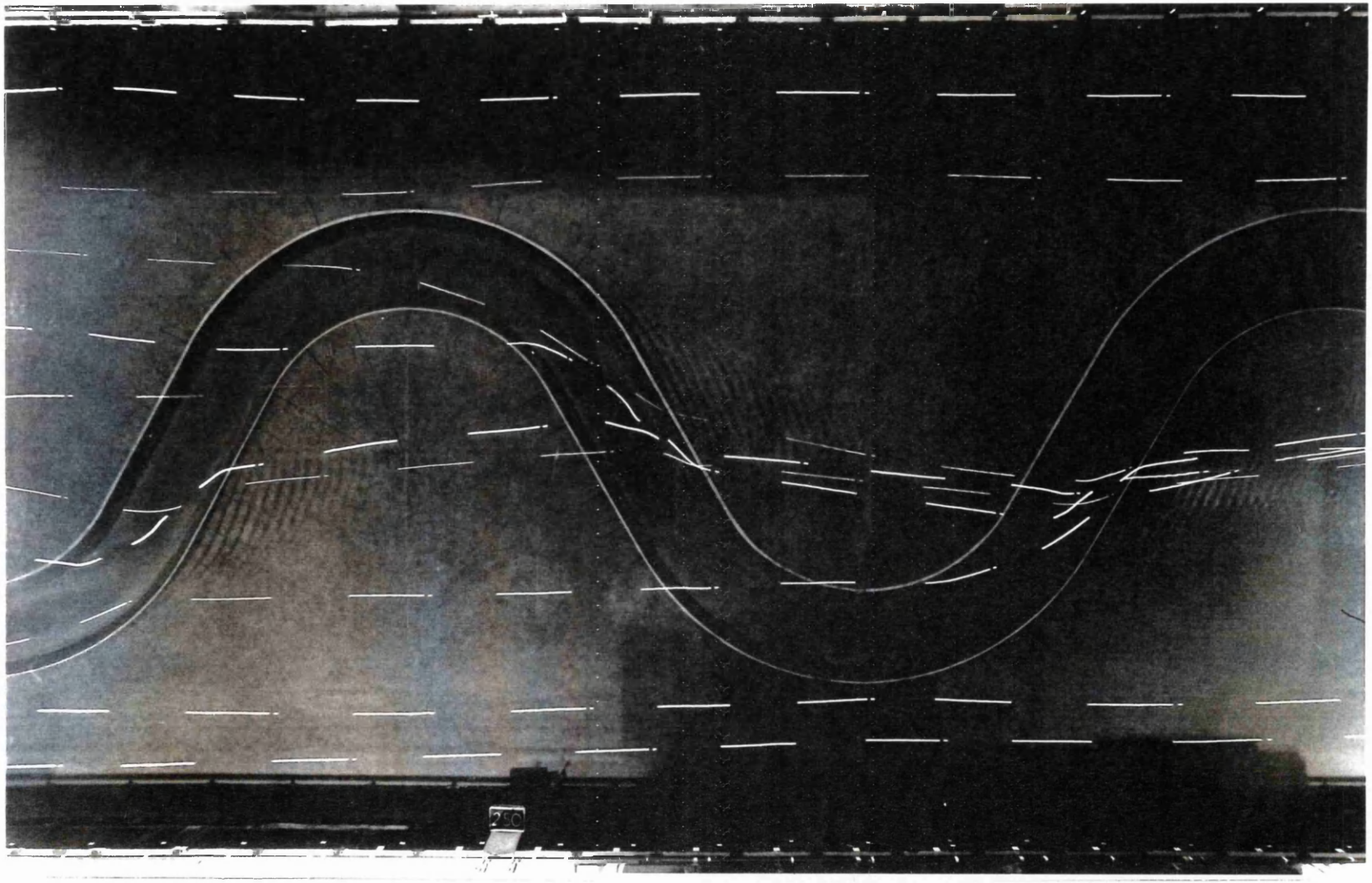

Fig (5.14e) - Float Photographs in S.E.R.C. Flume Series B, Sinuosity 1.37, Trapezoidal Cross-Section, Stage 200.0 mm, Smooth Floodplains.

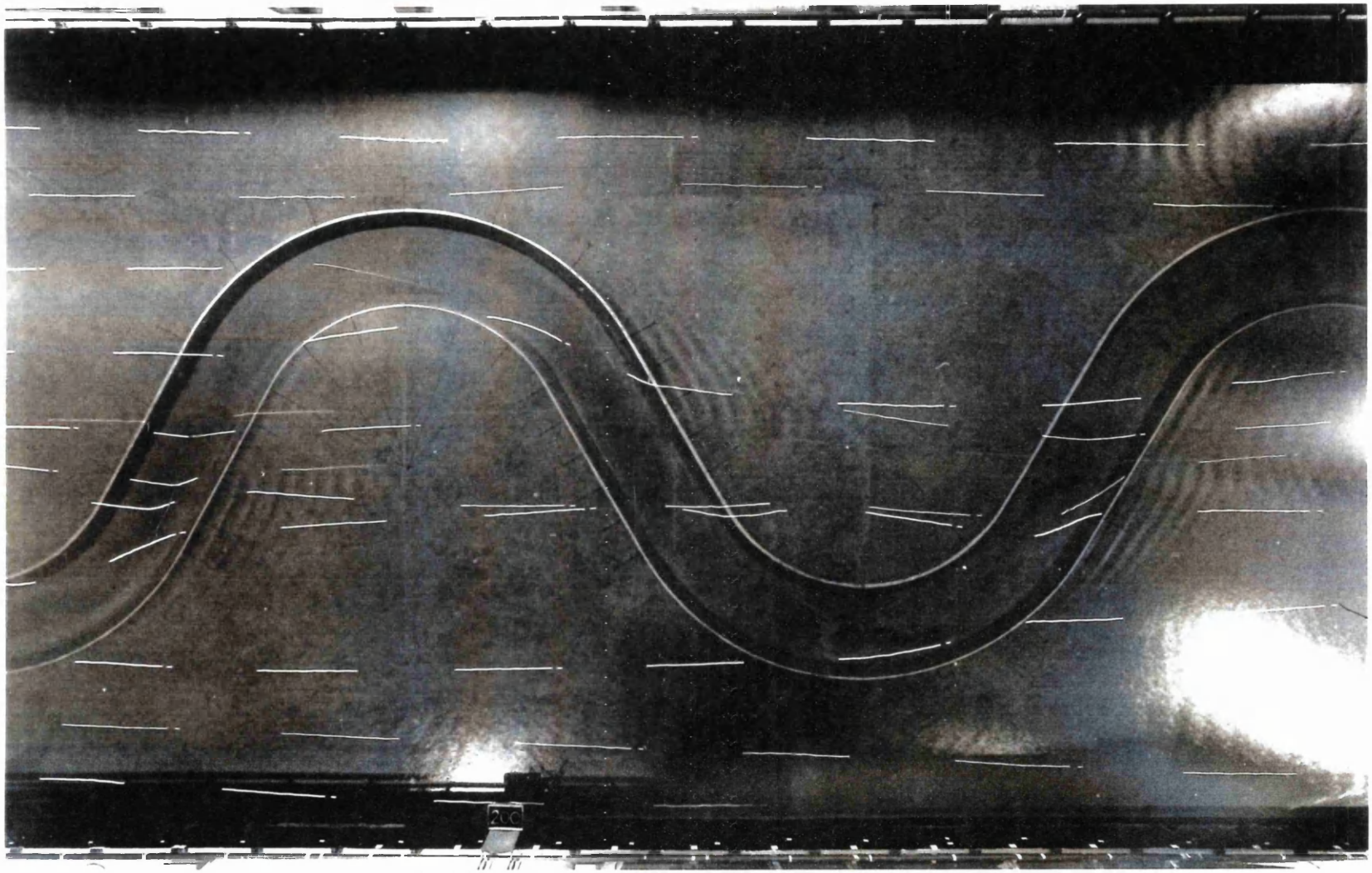

Fig (5.14f) - Float Photographs in S.E.R.C. Flume Series B, Sinuosity 1.37, Trapezoidal Cross-Section, Stage 250.0 mm, Smooth Floodplains.

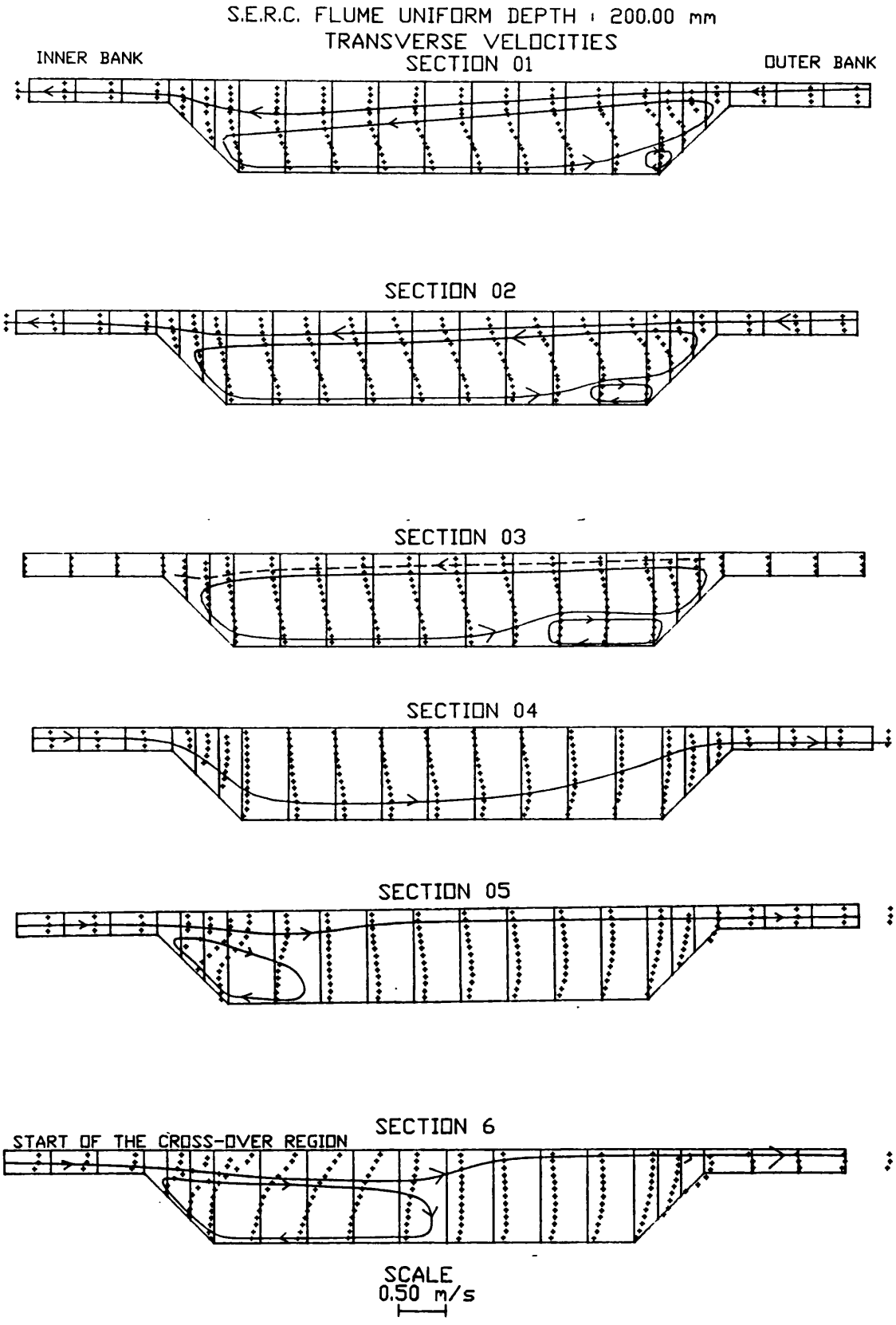

Fig (5.15a) - Variation of The Transverse Velocity in Sections Nos.1 to 6. For The Overbank Case. S.E.R.C. Series B. Meandering Channel With Sinuosity 1.37. Trapezoidal Cross-Section. Stage 200.0 mm. Smooth Floodplains.

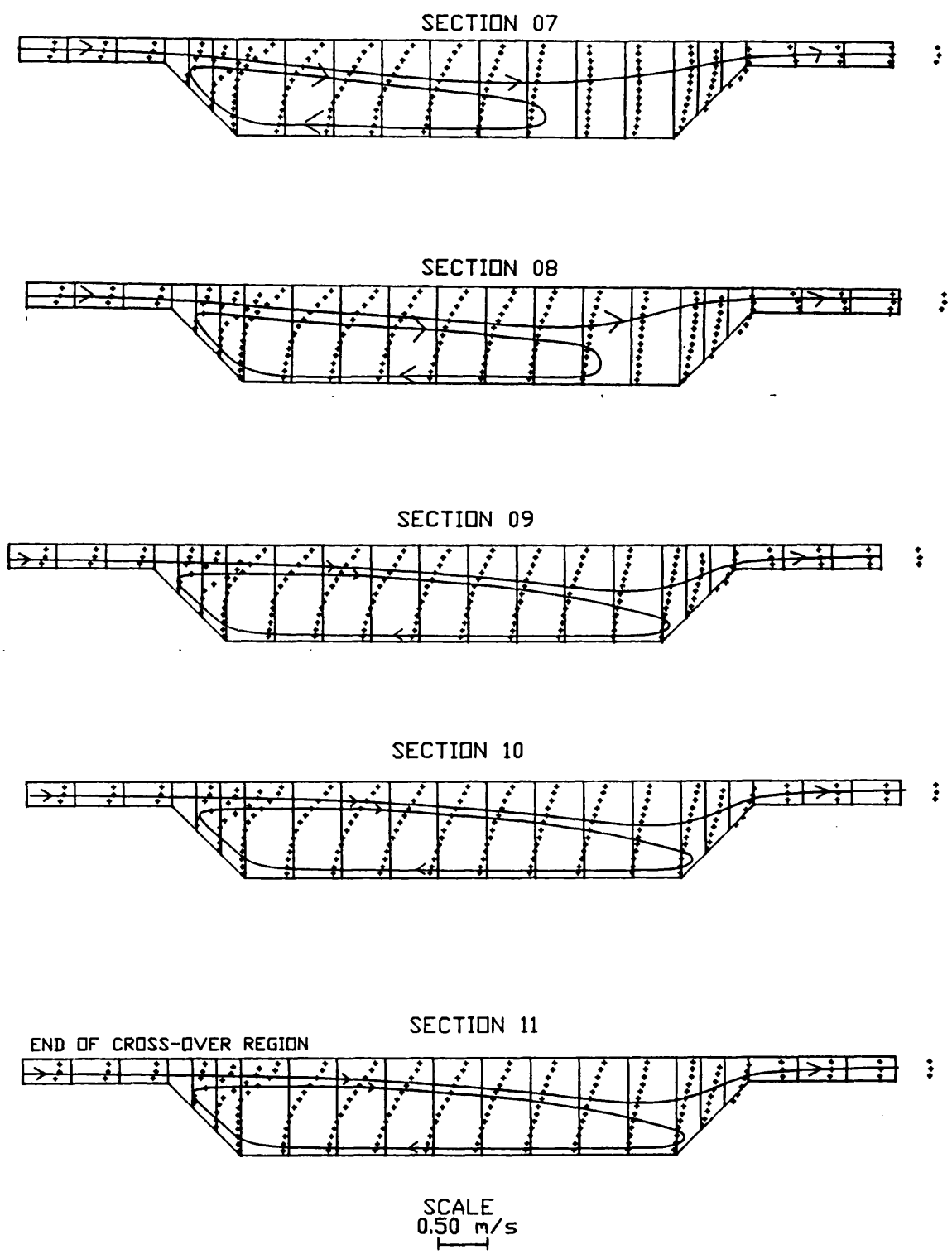

Fig (5.15b) - Variation of The Transverse Velocity in Sections Nos.7 to 11. For The Overbank Case. S.E.R.C. Series B. Meandering Channel With Sinuosity 1.37. Trapezoidal Cross-Section. Stage 200.0 mm. Smooth Floodplains.

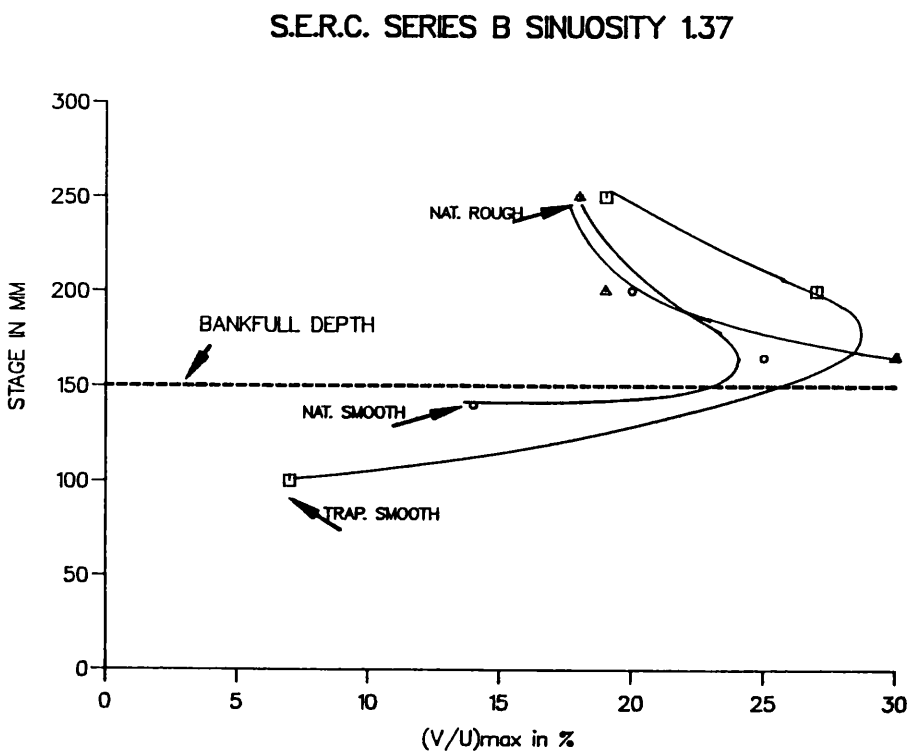

Fig (5.16a) - Variation of the Strength of Secondary Currents[$(V/U)_{max.}$] with Stage for Sinuosity 1.37 of S.E.R.C. Series B.

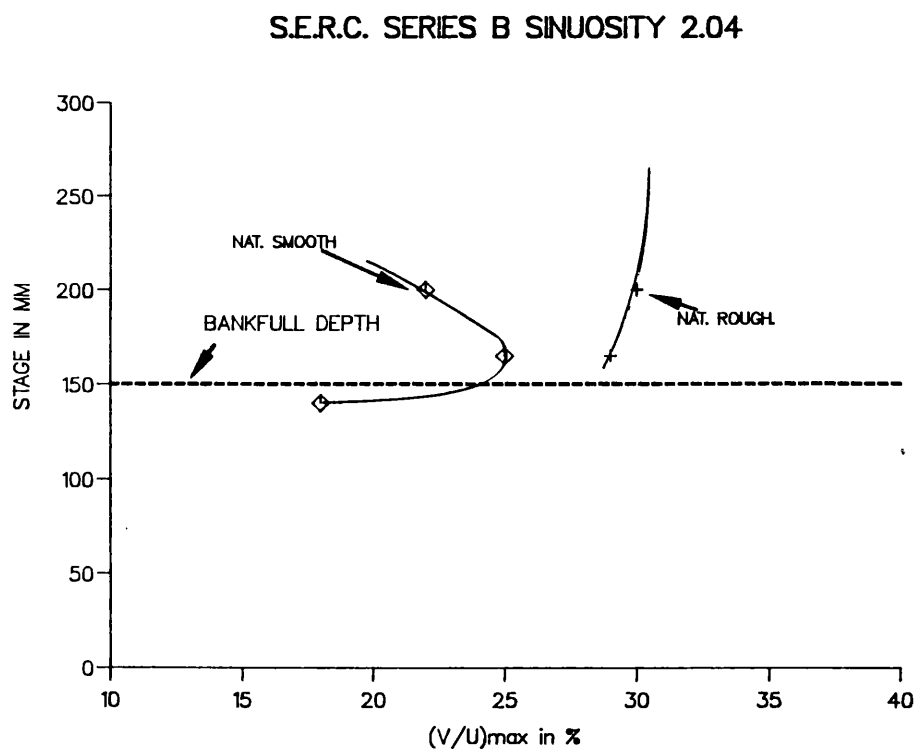

Fig (5.16b) - Variation of the Strength of Secondary Currents[$(V/U)_{max.}$] with Stage for Sinuosity 2.04 of S.E.R.C. Series B.

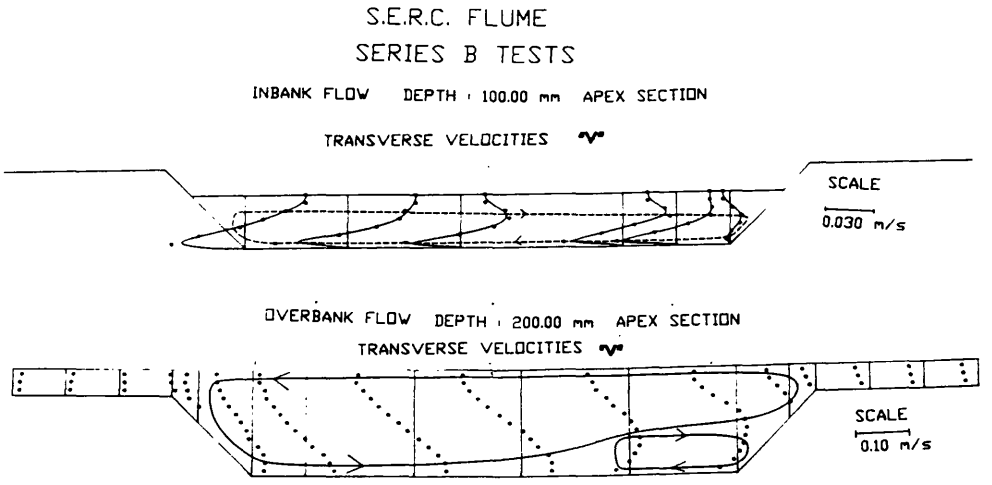

Fig (5.17) - Secondary Circulation at Bend Apex of the Meandering Compound Channel of S.E.R.C. Flume. Sinuosity 1.37. Trapezoidal Cross-Section. Smooth Floodplains. Comparison of the Inbank Case(Stage 100.0 mm) with the Overbank Case(Stage 200.0 mm).

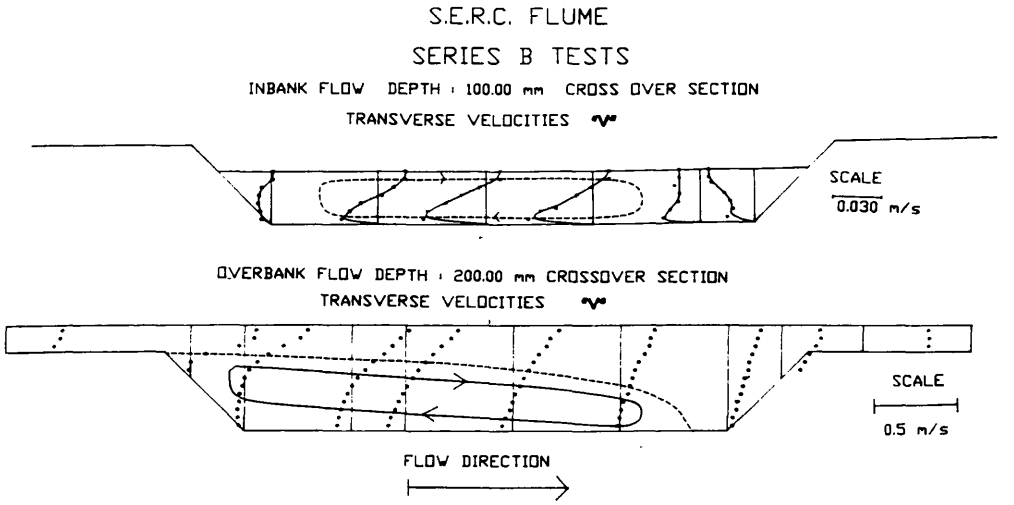

Fig (5.18) - Secondary Circulation at Cross-Over Section of the Meandering Compound Channel of S.E.R.C. Flume. Sinuosity 1.37. Trapezoidal Cross-Section. Smooth Floodplains. Comparison of the Inbank Case(Stage 100.0 mm) with the Overbank Case(Stage 200.0 mm).

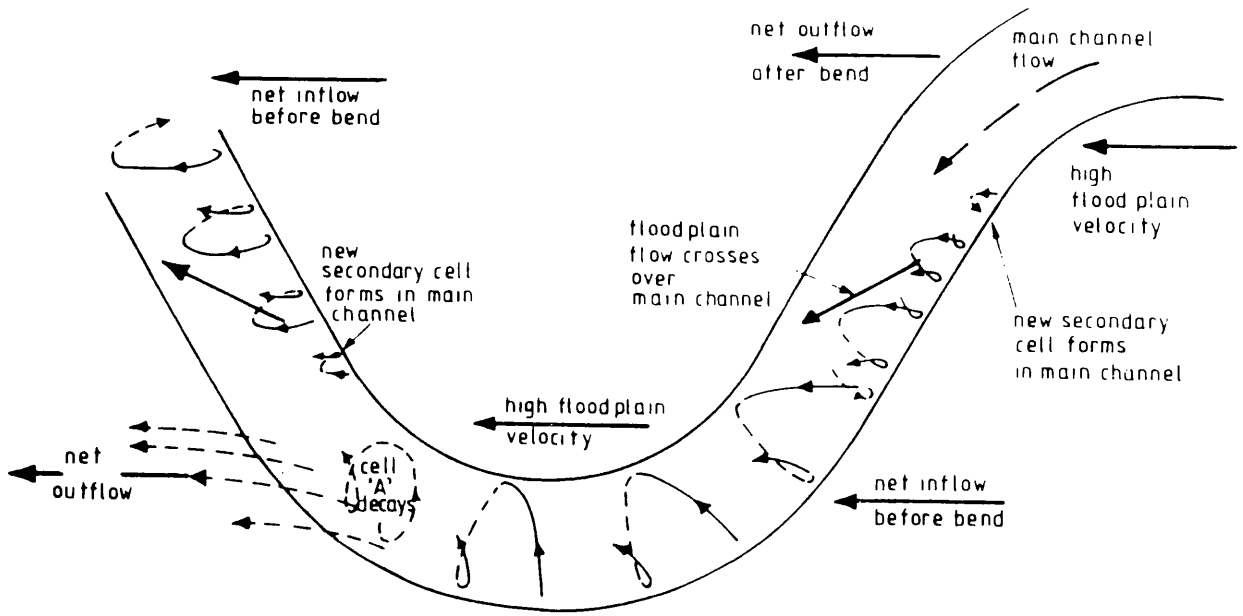

Fig (5.19) - Flow Mechanisms and Flow Structures in Meandering Compound Flows.

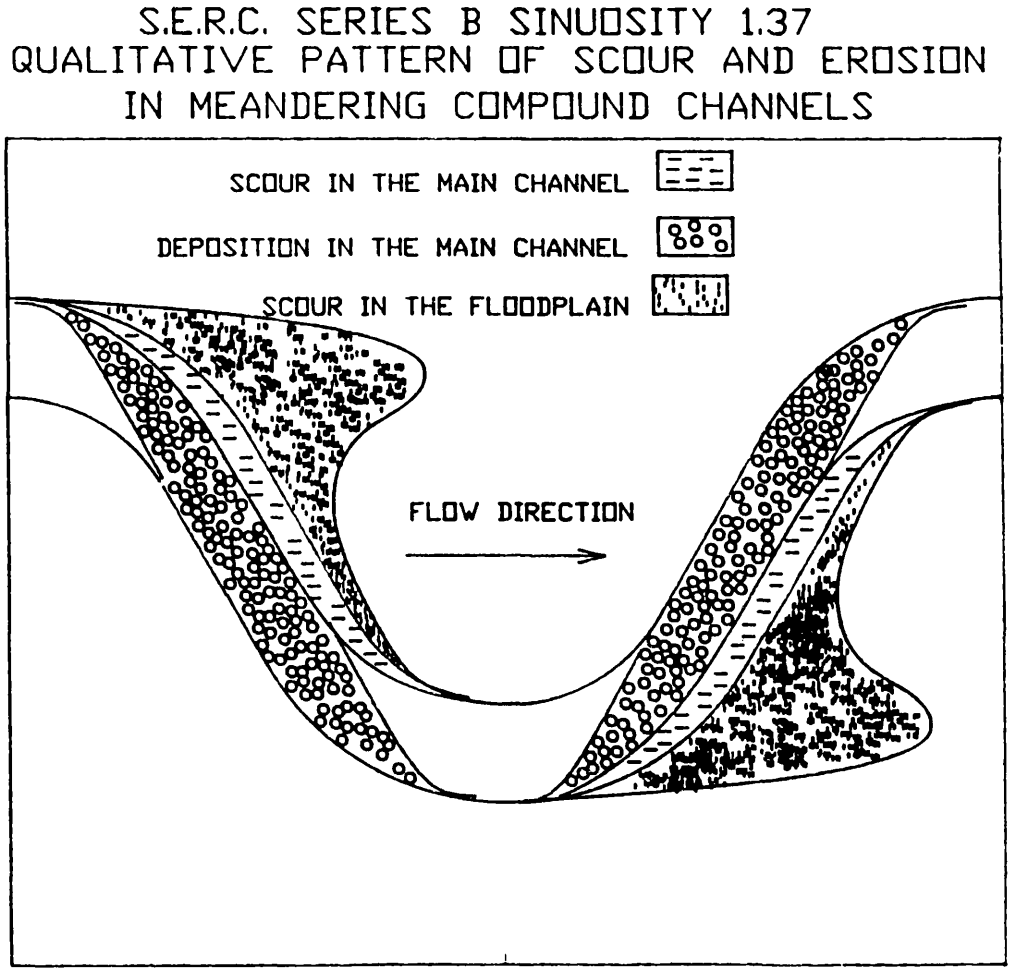

Fig (5.20) - Pattern of Scour and Erosion in The Meandering Compound Channel of S.E.R.C. Series B with Sinuosity 1.37. Qualitative Approach.

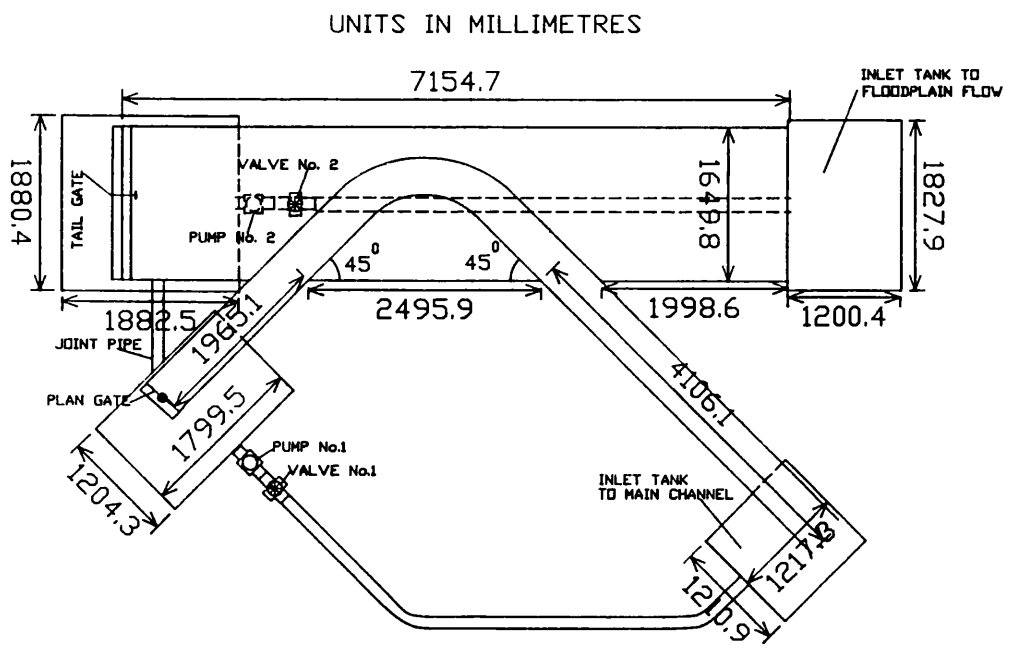

Fig (5.21a) - Plan View of Glasgow Flume.

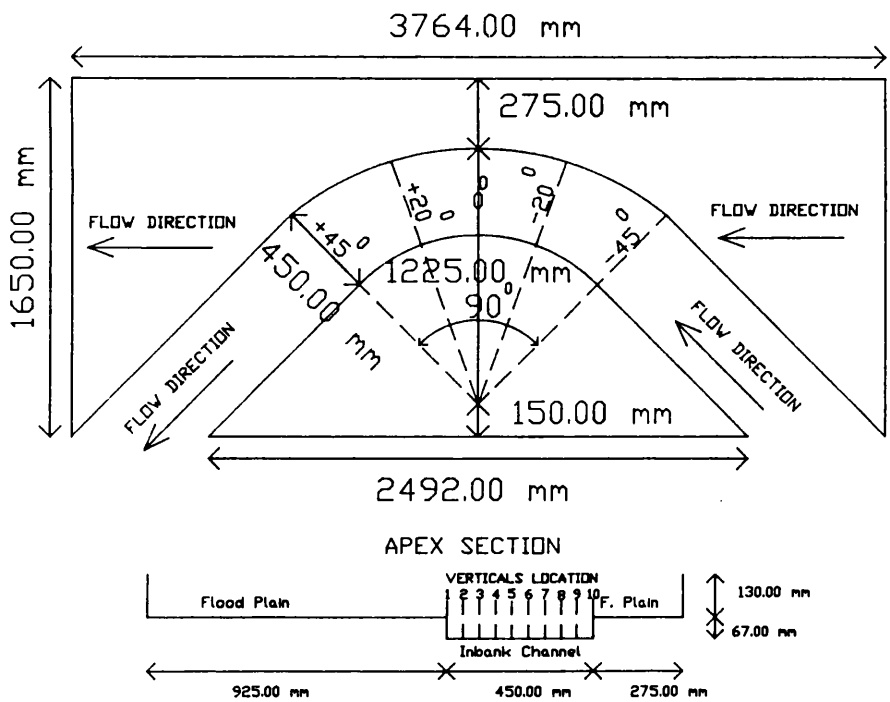

Fig (5.21b) - Test Sections and Measurement Verticals of Glasgow Flume.

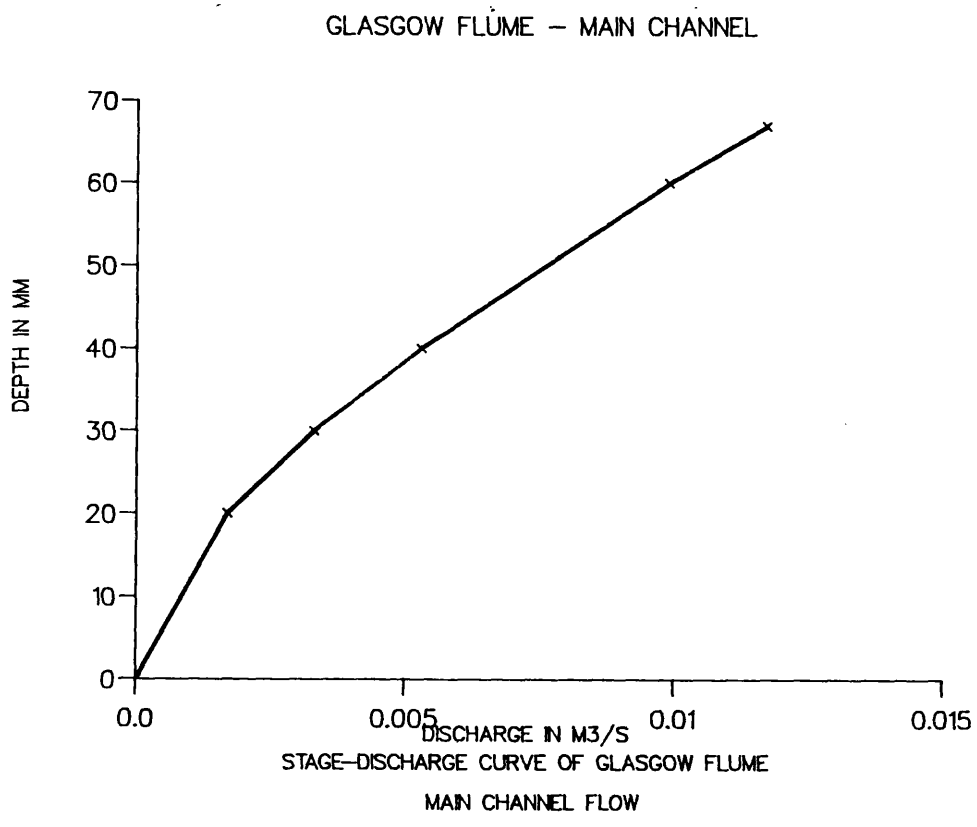

Fig (5.22) - Stage-Discharge Curve of the Main Channel of Glasgow Flume.

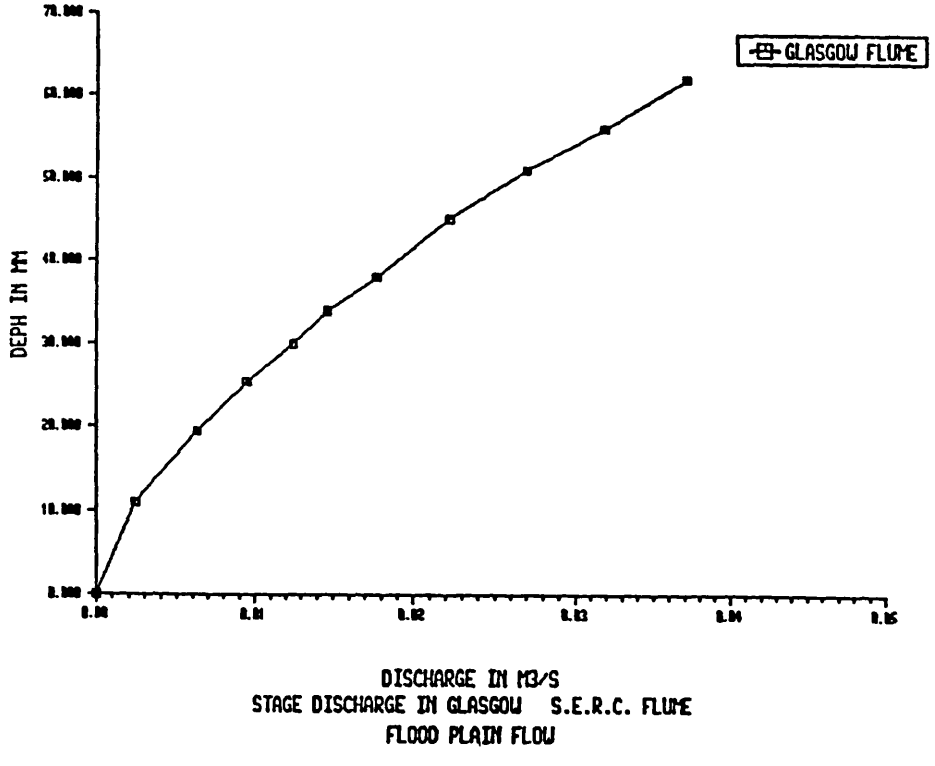

Fig (5.23) - Stage-Discharge Curve of the Floodplain Channel of Glasgow Flume.

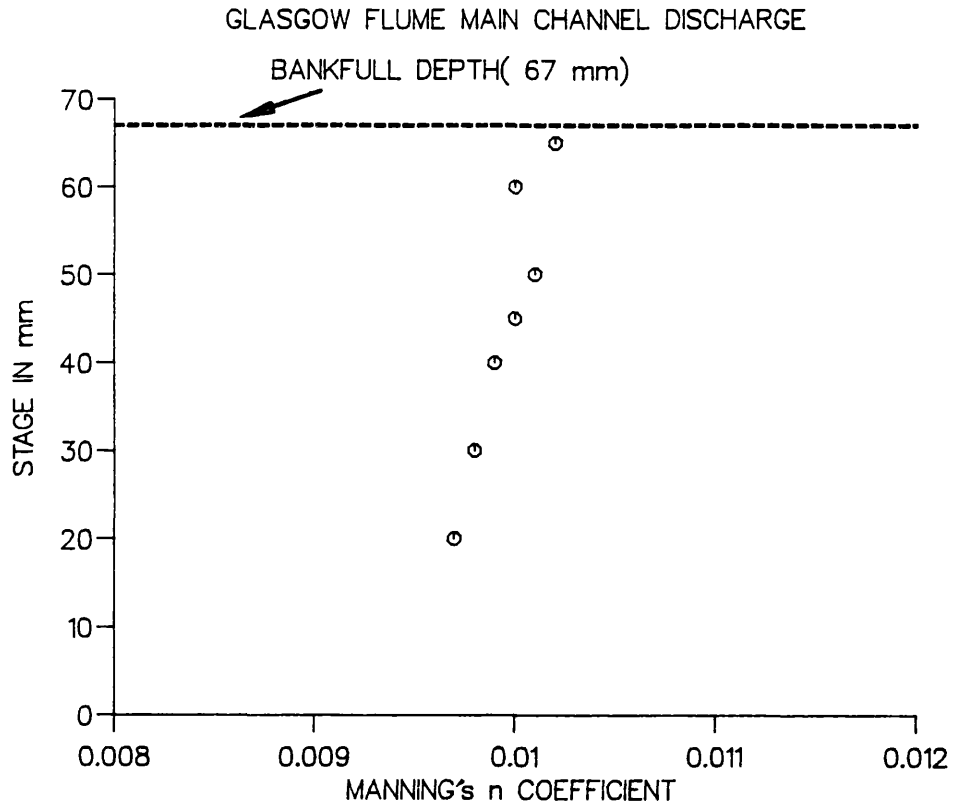

Fig (5.24a) - Variation of Manning's n with Stage for Inbank Case of the Main Channel Flow of Glasgow Flume.

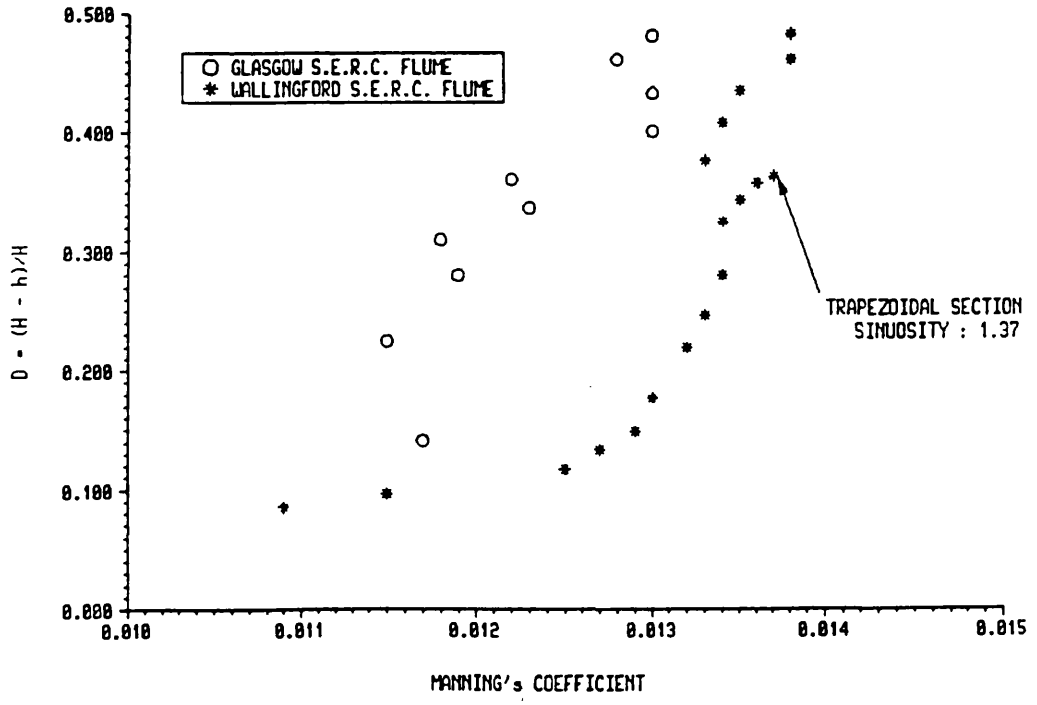

Fig (5.24b) - Variation of Manning's n with Stage for the Floodplain Flow of Glasgow Flume.

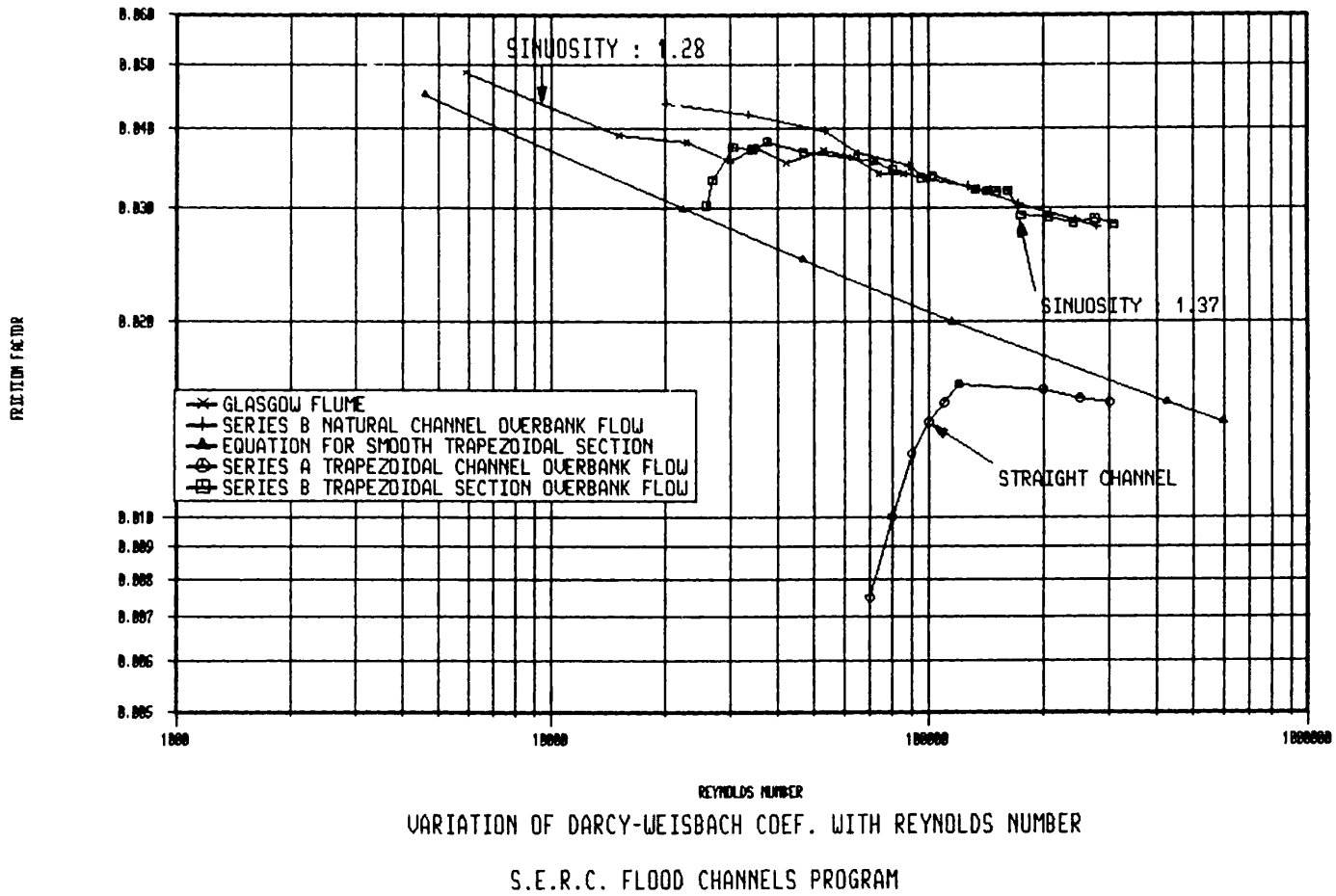

Fig (5.25) - Variation of The Darcy-Weisbach Friction Factor with Reynolds Number for the Floodplain Flow of Glasgow Flume and Comparison with S.E.R.C. Series B.

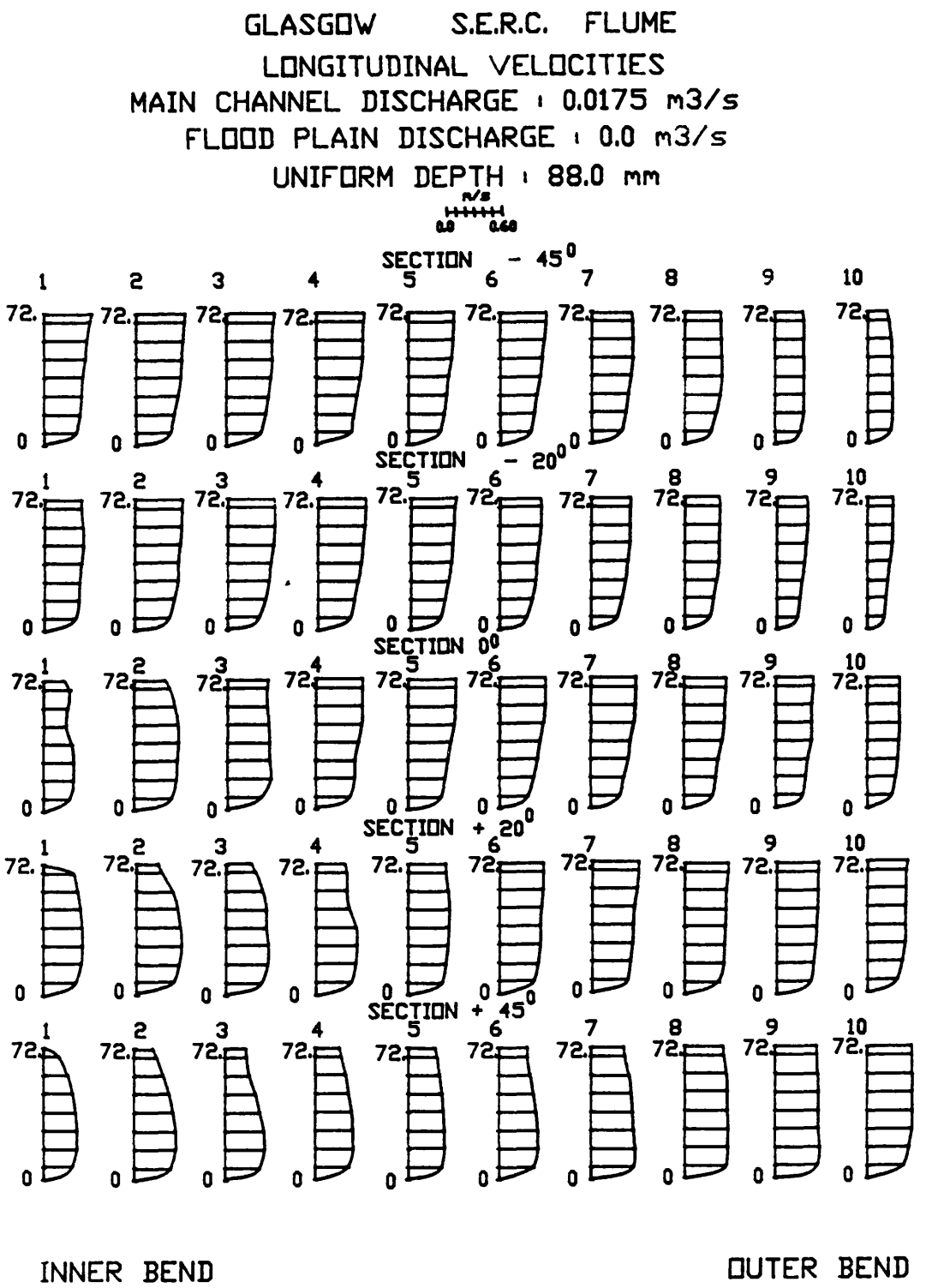

Fig (5.26) - Variation of The Streamwise Velocity For The Overbank Case. Glasgow Flume. Uniform Depth 88.0 mm. Main Channel Discharge 0.0175 m^3/s. Floodplain Discharge 0.0 m^3/s.

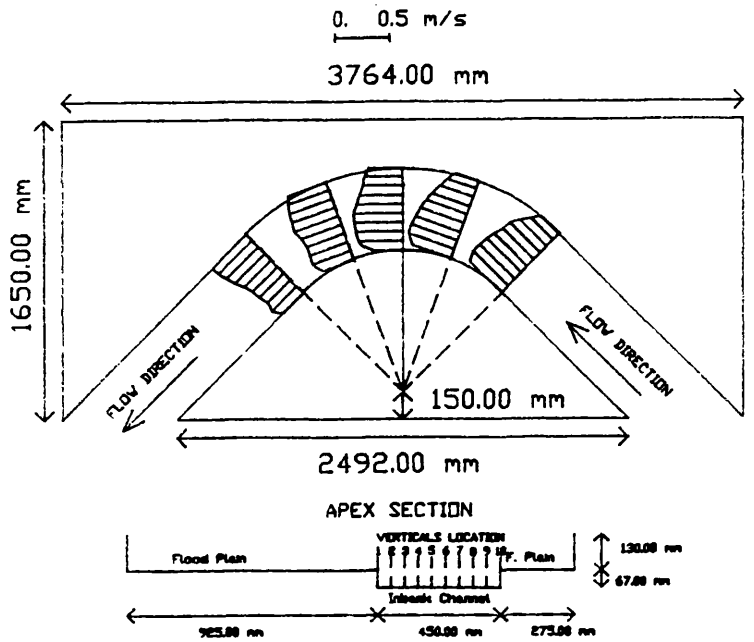

Fig (5.27) - Variation of The Depth Averaged Velocity For The Overbank Case. Glasgow Flume. Uniform Depth 88.0 mm. Main Channel Discharge 0.0175 m^3/s. Floodplain Discharge 0.0 m^3/s.

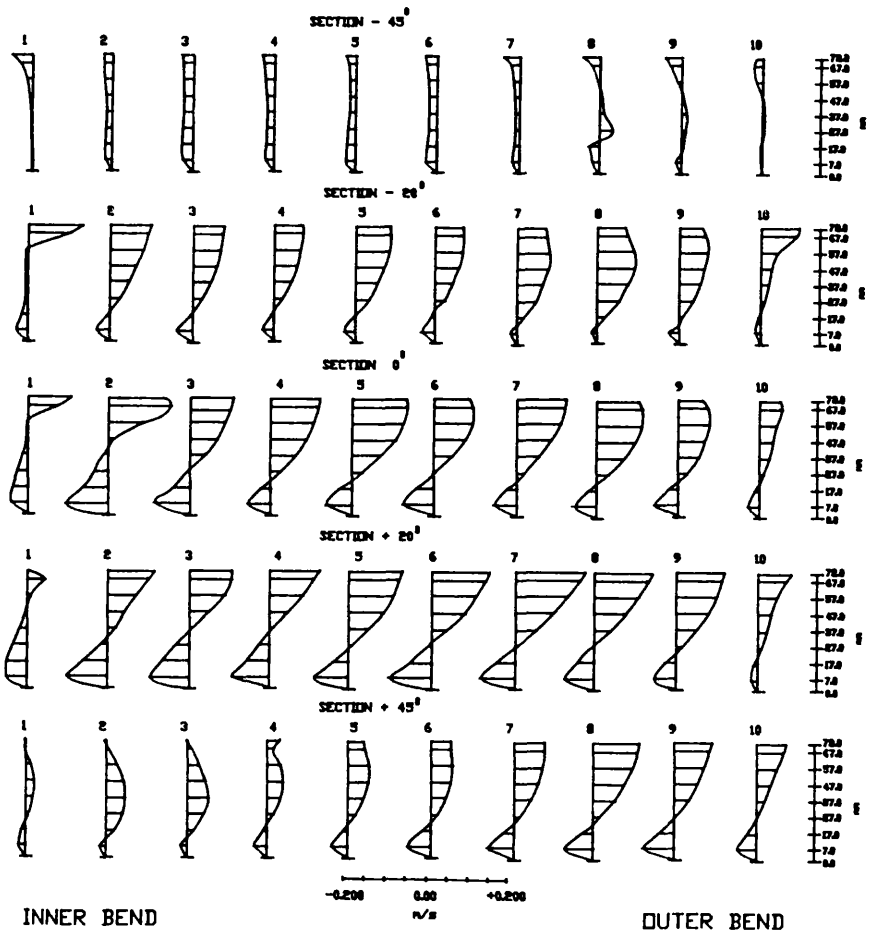

Fig (5.28) - Variation of The Transverse Velocity For The Overbank Case. Glasgow Flume. Uniform Depth 88.0 mm. Main Channel Discharge 0.0175 m^3/s. Floodplain Discharge 0.0 m^3/s.

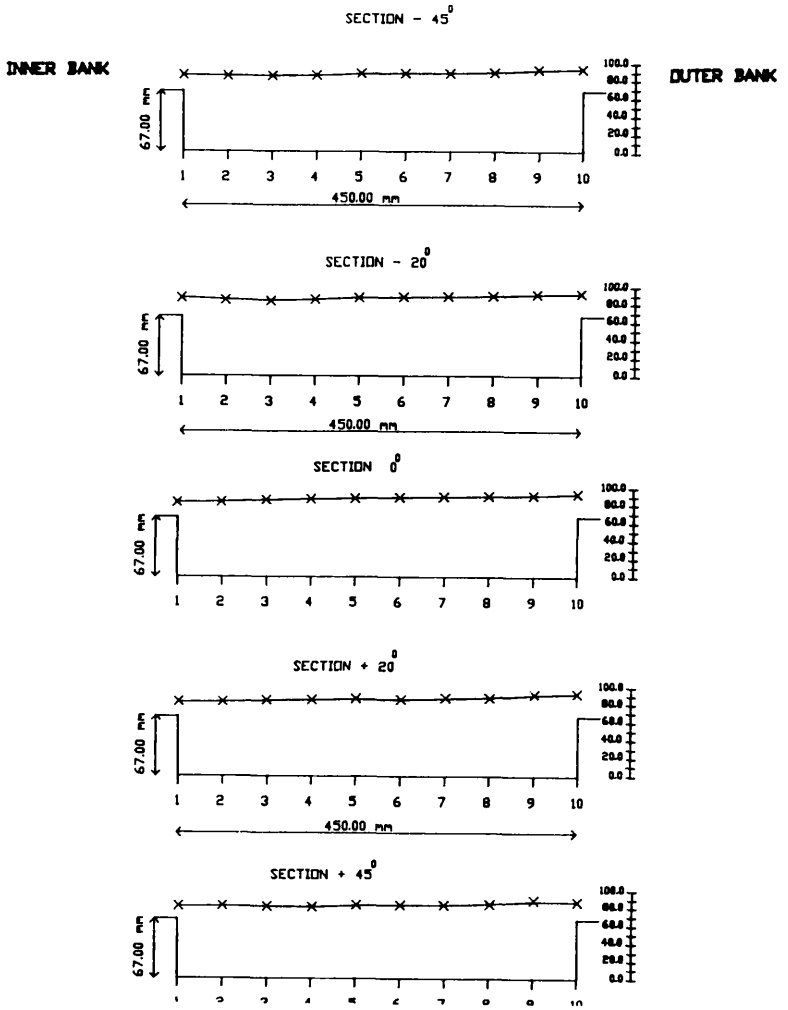

Fig (5.29) - Water Depths For The Overbank Case. Glasgow Flume. Uniform Depth 88.0 mm. Main Channel Discharge 0.0175 m^3/s. Floodplain Discharge 0.0 m^3/s.

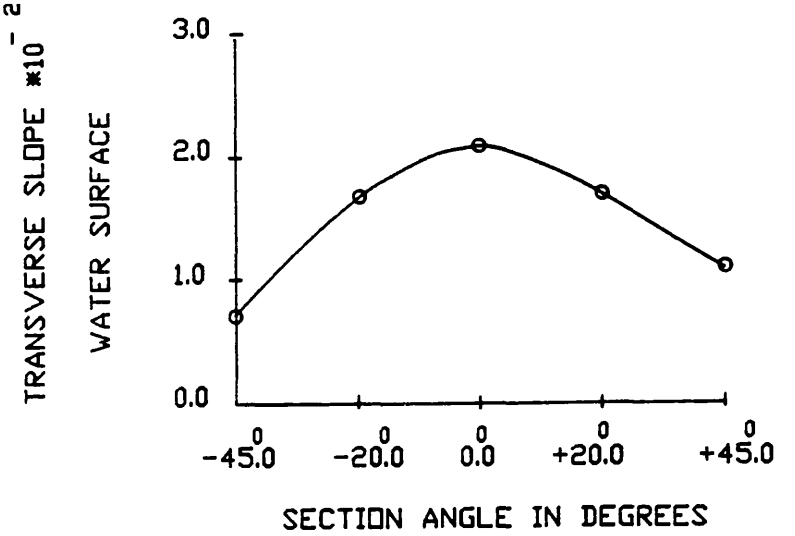

Fig (5.30) - Variation Along The Bend of The Water Surface Slope For The Overbank Case. Glasgow Flume. Uniform Depth 88.0 mm. Main Channel Discharge 0.0175 m^3/s. Floodplain Discharge 0.0 m^3/s.

S.E.R.C. INBANK FLOW IN A MEANDERING CHANNEL

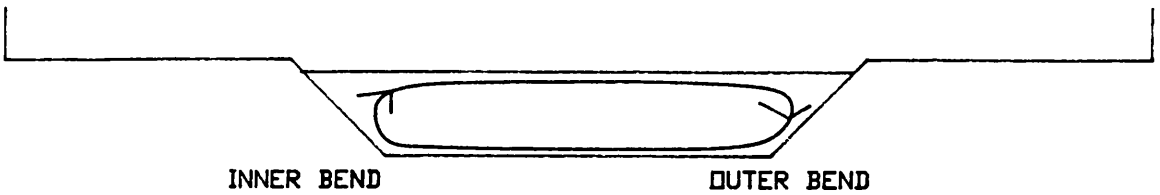

S.E.R.C. OVERBANK FLOW IN A MEANDERING CHANNEL
OVERBANK FLOW IN A MEANDER CHANNEL

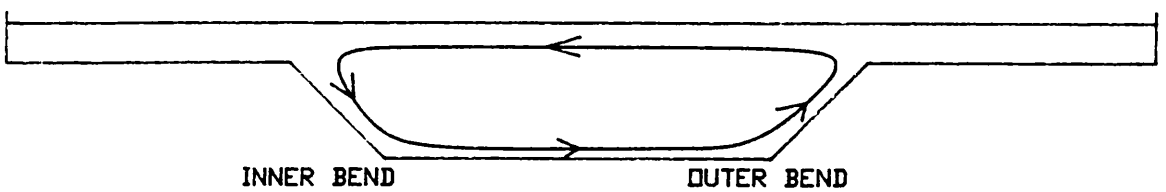

OVERBANK FLOW WITH A STATIONARY FLOODPLAIN WATER
IN GLASGOW FLUME

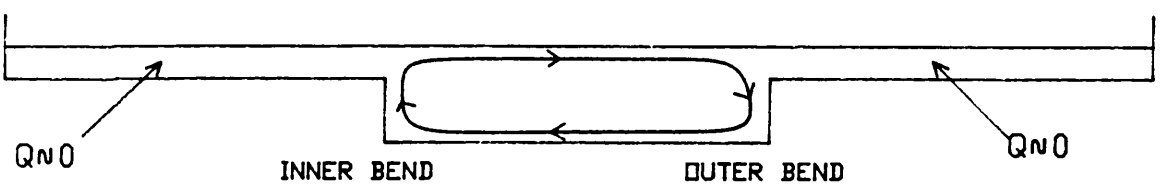

Fig (5.31) - Sketch of The Sense of Rotation of The Secondary Currents in The Bend Apex For The Inbank and The Overbank Cases of S.E.R.C. Series B and For the Overbank Case of Glasgow Flume.

CHAPTER 6

CONTINUITY, ENERGY AND MOMENTUM EQUATIONS APPLIED TO MEANDERING COMPOUND CHANNELS

CHAPTER 6

CONTINUITY, ENERGY AND MOMENTUM EQUATIONS APPLIED TO MEANDERING COMPOUND CHANNELS

6.1 INTRODUCTION

The experimental work on compound meandering flows at the S.E.R.C. flume Wallingford, investigated a series of idealised cases which may bear some reality to nature. The value of the detailed measurements on the S.E.R.C. flume can only be optimised if the data is used to produce a MODEL which can be applied to any situation, and not just the limited range tested. The most suitable model is a subject of debate at the present and can vary from the sophisticated range 3-D numerical models incorporating turbulence models, to a simplified quasi-one dimensional model such as used by **Ervine and Ellis(1987)**. Any modelling technique will ultimately make use of the concepts of continuity of mass, force-momentum and/or conservation of energy.

The purpose of this **Chapter**, however is not to produce a model, but rather as a first step, to investigate by using a two-dimensional approach, the continuity equation, energy equation and momentum equation can be applied to the test cases studied in the meandering channels of S.E.R.C. flume(Series B). The aim of this analysis is to explain how both discharge and energy are distributed and how momentum is exchanged between the main channel and the floodplain. The continuity and energy equations were applied to both S.E.R.C. flume sinuosities(1.374 and 2.04), both floodplain boundary roughnesses(smooth case and fully roughened case) for all test cases, while the momentum equation was applied only to sinuosity 1.37 but both floodplain roughnesses cases(smooth case and fully roughened case).

6.2 CONTINUITY EQUATION APPLIED TO MEANDERING COMPOUND CHANNELS.

6.2.1 Introduction

In open-channel flows, the flow regime is usually turbulent and the instantaneous velocities are defined as a sum of the time averaged velocity and a fluctuating random component. In a cartesian coordinates system, the instantaneous velocities in X, Y and Z directions are

$$u = \overline{U} + u' \tag{6.1}$$

$$v = \overline{V} + v' \tag{6.2}$$

$$w = \overline{W} + w' \tag{6.3}$$

No matter of whether a flow is in laminar or turbulent regime, every fluid must satisfy the equation of conservation of mass or, as it is commonly termed the equation of continuity. For the time-averaged motion and considering the flow incompressible, the equation of continuity in cartesian coordinates is expressed as being,

$$\frac{\partial \overline{U}}{\partial x} + \frac{\partial \overline{V}}{\partial y} + \frac{\partial \overline{W}}{\partial z} = 0 \tag{6.4}$$

where $\overline{U}$, $\overline{V}$, and $\overline{W}$ are the depth-averaged longitudinal, transverse and vertical velocity components in x, y and z directions, respectively.

For a flow around a curved channel, such as in the bend region of meandering channels, the continuity equation is better expressed by using a cylindrical coordinate system. For a steady and incompressible flow, the continuity equation in cylindrical coordinates is

$$\frac{\partial \overline{U}s}{\partial s} + \frac{\overline{V}R}{r} + \frac{\partial \overline{V}R}{\partial r} + \frac{\partial \overline{W}}{\partial z} = 0 \tag{6.5}$$

where $\overline{U}s$ is the depth averaged tangential component of velocity

in direction s, $\overline{V}_R$ is the depth averaged radial component of the velocity in normal direction n, and $\overline{W}$ is the depth averaged vertical component of velocity in direction z.

Nelson and Smith(1989) expressed the continuity equation in curvilinear coordinates. The equation proposed was

$$\frac{\partial \overline{U}}{\partial s} + \frac{1}{r}\frac{\partial(\overline{V} r)}{\partial n} + \frac{\partial \overline{W}}{\partial z} = 0 \qquad (6.6)$$

where $\overline{U}$, $\overline{V}$ and $\overline{W}$ are the depth averaged velocity components in s, n, and z directions.

Equations 6.4 and 6.6 were applied to the meandering flow of S.E.R.C. flume Series B. In both equations, the control volume considered was limited by the water surface and by the channel bottom, and hence the vertical component of velocity $\overline{W}$ could be eliminated in the two-dimensional case. Equations 6.4 and 6.5 become,

$$\frac{\partial \overline{U}}{\partial x} + \frac{\partial \overline{V}}{\partial y} = 0 \qquad (6.7)$$

$$\frac{\partial \overline{U}}{\partial s} + \frac{\partial \overline{V}}{\partial n} = 0 \qquad (6.8)$$

Equation 6.7 was applied on the floodplain while equation 6.8 was applied in the main channel region.

6.2.2. Discharge Distribution of The Meandering Compound Channels of S.E.R.C. Series B.

One of the key questions about mass exchange in meandering compound flows is the distribution of flow(discharge) throughout the flow field, and how much is exchanged between main channel and floodplain, and vice-versa. How much discharge is carried in the main channel and on the floodplain, and how does this value vary along meander length.

Chapter 5 has already revealed significant flow mechanisms which involve mass exchange. Beyond each bend apex, main channel

discharge is substantially diverted to the floodplain. In each cross-over region, floodplain flow can bifurcate, with a proportion entering the main channel flow below bankfull level.

Other flow mechanisms, such as secondary cells, considerably affect the discharge distribution. These cells, whose strength increases substantially in overbank case compared with an inbank case, has an important role in transporting discharge from the main channel to floodplain and vice-versa. **Toebes and Sooky(1967)** pointed out the existence of significant mass exchange between the meander and the floodplain flows. The discharge distribution obtained by these two researchers was presented in **Fig(2.58)**.

In this work two different methods were used to determine mass exchange and the discharge distribution in the main channel and floodplain of the S.E.R.C. flume Series B data.

(i) Method 1 used the two component velocity data and water depth data to calculate the radial discharge received by the main channel from the left upstream floodplain; the radial discharge supplied by the main channel to the right bank floodplain; the variation of the streamwise discharge along the main channel; the determination of the right floodplain and the left floodplain longitudinal discharges at the bend apex section. These components are shown in **Fig(6.1)**.

(ii) Method 2 used velocity and depth to analyse the discharge distribution using the known " Dog Leg System", where the cross-sections are defined as perpendicular to the longitudinal direction in the floodplain and perpendicular to the streamwise direction in the main channel. In this case, the longitudinal discharge on both sides of the floodplain and the main channel streamwise discharge were determined. A typical example is shown in **Fig(6.6)**.

The method used for the calculation of the streamwise discharge in the main channel(parallel to the main channel walls) and the longitudinal discharge(parallel to flume side walls) in the both floodplains was as follows:

- Based on the measurements of the resultant flow velocity U_R and the stream angle of the current Θ , the streamwise velocity in the main channel and the longitudinal velocity on the floodplain was determined from equation

$$U_i = U_R \cos \Theta \qquad (6.9)$$

where the index i refers to the particular point of the vertical where measurements took place.
It should be noted that streamwise in the main channel means parallel to main channel walls and integrated over the full depth of the main channel flow.
- In each vertical the depth averaged velocity was calculated from the following equation,

$$\overline{U}_J = \frac{\sum_{i=1}^{i=n-1} (U_i + U_{i+1})(H_i - H_{i+1})/2}{H_J} \qquad (6.10)$$

where i is the index of the point on the vertical, n is the number of velocity measurements on the vertical, J is the index of the vertical and H_J is the total depth of the vertical J.
- Once the values of depth averaged velocities have been calculated, the discharge was integrated, for each section of the main channel and on several sections of the floodplain, using the following equation,

$$Q_K = \frac{\sum_{J=1}^{J=m-1} \left[\left(\overline{U}_J + \overline{U}_{J+1} \right) * \left(H_J + H_{J+1} \right) * \Delta l_{J-J+1} \right]}{4} \qquad (6.11)$$

where K is the index of the section, Δl is the width between the verticals J and $J+1$ and m is the number of verticals of the section under consideration.

The method developed for the calculation of the radial discharge entering and leaving by the main channel was as

follows:

- Based on measurements of the resultant flow velocity U_R and the streamline angle of the current Θ, the transverse velocity(normal to banks) at a point of a vertical located on the boundaries of the main channel with the floodplain was determined by

$$V_i = U_R \sin \Theta \qquad (6.12)$$

where the index i refers to a particular point of the vertical where measurements took place.

- All the other steps are similar to the ones described for the streamwise discharge of the main channel and the longitudinal discharge of the floodplain. The only difference was that, the radial discharge was integrated along the edge of the main channel, at the main channel/floodplain interface.

The results of the discharge distribution following the Method 1 are shown in:

Fig(6.1) for sinuosity 1.37, stages 200.0 and 250.0 mm, trapezoidal section and with smooth floodplains.

Fig(6.2) for sinuosity 1.37, stages 165.00, 200.0 and 250.0 mm and natural section and with smooth floodplains.

Fig(6.3) for sinuosity 1.37, for stages 165.00, 200.0 and 250.0 mm, natural section and with fully roughened floodplains.

Fig(6.4) for sinuosity 2.04, stages 200.0 and 250.0 mm, natural section and with smooth floodplains.

Fig(6.5) for sinuosity 2.04, for stages 200.0 and 250.0 mm, natural section and with fully roughened floodplains.

Fig(6.1) to **Fig(6.5)** express discharge as an absolute value. In the particular cases of the fully roughened floodplain, the floodplain discharge at the bend apex could not be computed because of the absence of velocity data. It was decided in these particular cases to estimate the floodplain discharge from,

$$Q_1 - Q_2 = Q_3 \qquad (6.13)$$

$$Q_1 + Q_2 + Q_4 = Q_5 \quad (6.14)$$

where:

- Q_1 is the left/upstream floodplain discharge(unknown)
- Q_2 is the right/downstream floodplain discharge(unknown)
- Q_3 is the radial discharge received by the main channel from the left bank which can be calculated from the measurements(known).
- Q_4 is streamwise main channel discharge at bend apex which can be computed from the measurements(known).
- Q_5 is the total discharge(streamwise main channel discharge plus the floodplain discharge at the bend apex) measured by the orifice meter(known).

Equations (6.13) and (6.14) are solved simultaneously to provide estimates of roughened floodplains discharges.

The results of the discharge distribution, following Method 2 ("Dog-Leg System") are shown in:

Fig(6.6) and **Fig(6.7)** for sinuosity 1.37, stages 200.0 and 250.0 mm, trapezoidal section and with smooth floodplains.

Fig(6.8) and **Fig(6.9)** for sinuosity 1.37, for stages 200.0 and 250.0 mm, natural section and with smooth floodplains.

Fig(6.10) for sinuosity 2.04, stage 200.0 mm, natural section and with smooth floodplains.

The main channel discharge and the floodplain discharge are expressed as a percentage of the total discharge along the flume passing each bend apex section.

The following points can be noted from **Fig(6.1)** to **Fig(6.10)**:

- The discharge distribution in meandering compound channels is highly three-dimensional, with significant longitudinal and lateral movements revealed.
- As expected, the maximum streamwise component of discharge occurs at the bend apex in all cases, whereas at the cross-over region, the streamwise discharge reaches its minimum. This effect is more pronounced in the more highly sinuous case in **Fig(6.5)**.

- The main channel streamwise discharge variation agrees well with the radial discharge variation. Confirming the excellent quality of the experimental data.
- The discharge distribution in both sinuosities has a similar pattern. Between the bend apex and the cross-over section the main channel discharge in the streamwise direction reduces by delivering discharge to the right downstream floodplain. Between the cross-over section and the next bend apex, the main channel discharge in the streamwise direction increases, by receiving discharge from the left upstream floodplain.
- The flow is steady but it is not uniform either in the main channel or the floodplain. For one-dimensional case, uniform flow means a constant discharge and a constant flow depth along the channel length. Here the flow is three-dimensional with the discharge varying in the main channel and floodplain region with water depths varying as well. However the flow can be considered quasi-uniform in this particular case of regular meanders if the criterion of uniformity is applied to sections that are mirror images on each meander wave length.

The key findings in **Fig(6.1)** to **Fig(6.10)** can also be summarised in more detail in terms of the effect of flow depth, boundary roughness, sinuosity and main channel cross-sectional shape.

- The effect of flow depth can be seen on **Fig(6.2)** for example. At stage 165.0 mm, the reduction in the main channel discharge(in the main channel direction) is 10% comparing apex and cross-over regions. The corresponding values are 30% and 34% for stages 200.0 mm and 250.0 mm. More of the main channel flow is diverted longitudinally as the stage increases. The percentage of flow remaining in the main channel reduces with stage. As stage increases from 165.0 mm to 250.0 mm the basic orientation of the flow changes from the main channel direction to the longitudinal direction. This can be seen vividly in the cross-over region of Fig(6.2). At the stage 165.0 mm, the transverse discharge is 6.0 to 8.0 l/s corresponding to 27.0 to 29.0 l/s in the main channel direction. This is a ratio of 0.25 transverse to streamwise main

channel. At stage 250.0 mm, this ratio is now 110/81=1.35, a difference of over five fold. This greater transverse movement with stage drives stronger secondary cells in the main channel and causes greater fluid transfer from main channel on floodplain.

- The effect of the floodplain roughness can be seen by comparing **Fig(6.2)** and **Fig(6.3)**, comparing smooth and fully roughened floodplain cases. As the floodplain roughness changes to the fully roughened case, the discharge reduces in both the floodplain and the main channel regions. That is rough floodplains reduce the discharge in the main channel even though the main channel has smooth boundaries. The retardation effect of the floodplain roughness is thus transmitted into the main channel. Comparing **Fig(6.2)** and **Fig(6.3)** at stage 165.0 mm, shows that floodplain roughness has very little effect on the main channel discharge, at the stage 200.0 mm the main channel discharge is reduced by 35%, whereas at stage 250.0 mm, the main channel discharge reduces by 50% simply by increasing floodplain roughness. This has important implications for the management of two-stage channels and vegetation removal.

- The effect of sinuosity can be seen by comparing **Fig(6.2)** with **Fig(6.4)**, at stages 165.0 mm and 200.0 mm. This is the smooth floodplain case. As expected, the reduction in discharge in the main channel direction is much more pronounced in the higher sinuosity case **Fig(6.4)** and is much more pronounced at the higher stages as well. The effect is also seen vividly comparing **Fig(6.8)** with **Fig(6.10**, both with stage 200.0 mm, smooth floodplains and natural cross-sections in the main channel. First, the total discharge is reduced from 222 l/s to 183 l/s simply by increasing sinuosity from 1.37 to 2.04. Thus a reduction of almost 20%. Second the percentage of flow held in the main channel alone decreases with an increase in sinuosity even at the bend apex section. This means that sinuosity has a retarding effect on both main channel and floodplain flows, and hence must be producing significant energy losses simply due to plan form shape.

- The effect of main channel cross-sectional shape comparing the trapezoidal and the natural cross-section can be seen by comparing **Fig(6.6)** with **Fig(6.8)**. In these two cases everything is identical apart from main channel cross-section shape(and area). The total flow is reduced from 251 l/s to 222 l/s in moving from trapezoidal to natural case. For the main channel alone, at bend apex, the percentage held in the main channel falls from 34% to 27%, a fall of 20% but the main channel cross-sectional area has fallen by 40%, showing that per unit area of flow the natural cross is more efficient at conveying flow. This was verified in the experiments of **Willetts and Hardwick(1990)** who showed greater efficiencies in natural cross-section conveyance compared with the trapezoidal.

6.2.3. Analysis of The Total Main Channel Discharge in the Streamwise Direction of The S.E.R.C. Flume Series B.

A slightly different mode of analysis is given in **Fig(6.11)** to **Fig(6.13)** for discharge variation in the main channel in the streamwise direction . This includes flow below bankfull level as well as flow above bankfull level resolved in the main channel direction. The graphs in general are a plot of the flow in the main channel region plotted with the distance around a half meander from bend apex to the next bend apex. The bend apex is section 3 for sinuosity 1.37 and section 2 for sinuosity 2.04.

The variation of the total main channel with distance around the meander and stage is presented in:

- **Fig(6.11)** for sinuosity 1.37, for trapezoidal and for natural main channel cross-sections with smooth floodplains.
- **Fig(6.12)** for sinuosity 1.37, with natural main channel cross-sections, comparing smooth floodplains with fully roughened floodplains.
- **Fig(6.13)** for sinuosity 2.04, with natural main channel cross-sections, again comparing smooth floodplains with fully roughened floodplains.

The tabulated data of the total main channel discharge in the streamwise direction are enclosed in **Appendix II**.

Fig(6.11) shows that the variation of the streamwise main channel discharge occurs practically outside the cross-over region and between the bend apex and the cross-over region.

- Discharge reduces from apex to start of the cross-over and increases in symmetrical way from the end of the cross-over region to next bend.
- There is very little variation in discharge along the cross-over length.
- The reduction/increase pattern is more pronounced at higher stages of flow.
- There is little difference in this effect comparing natural and trapezoidal cross sections.

Fig(6.12) shows the effects of stage and of floodplain roughness on the variation of the total streamwise main channel discharge of the meander with sinuosity 1.37.

- At stage 165.0 mm there is no difference in behaviour between smooth and rough floodplain cases.
- Even at the highest stage 250.0 mm the pattern is very similar for smooth and rough cases, apart from the fact that the main channel discharge is reduced by around 50% for the rough case. The 250.0 mm smooth case has a reduction in discharge around one third from the bend apex to cross-over. and 250.0 mm rough case also has a reduction around one third from bend apex to cross-over region.

Floodplain roughness has powerful retarding effect on the main channel flow, but the relative variations around the a meander wave length are not affected much by roughness. They are affected by stage, as seen in **Fig(6.11)** and they are affected by sinuosity by comparing **Fig(6.12)** and **Fig(6.13)**.

The effect of the floodplain roughness (and of stage) on the variation of the streamwise discharge in the main channel is shown in **Fig(6.13)** for the case of sinuosity 2.04.

- For stage 165.0 mm both smooth floodplain and fully roughened floodplain shows a behaviour similar to the previous sinuosity,

where the variation of the main channel discharge is not influenced by the floodplain roughness.
- For stage 200.0 mm, rough and smooth floodplain behaviour was again very similar, but the effect of increasing stage from 165.0 mm to 200.0 mm was to produce very much larger reductions in the main channel discharge. That is, very much larger sweeping out of the main channel on to the floodplain before the cross-over region, and vice-versa after the cross-over region.

The origin of such a large reduction is simply not just variations in stage, but variations in sinuosity as can be judged by comparing **Fig(6.12)** at stage 200.0 mm and **Fig(6.13)** at stage 200.0 mm. The increase in sinuosity has a significant effect on the flow in the main channel direction, as expected.

6.2.4. Analysis of The Main Channel Discharge Below Bankfull of The S.E.R.C. Flume Series B.

The variation of the main channel discharge below bankfull level is even greater interest because the streamlines should be in the main channel direction irrespective of sinuosity or other parameters. The results are given in **Fig(6.14)** to **Fig(6.16)** and compared in each case with the inbank bankfull discharge with no overbank flow.
- **Fig(6.14)** is for the trapezoidal section with smooth floodplains and meander sinuosity 1.37.
- **Fig(6.15)** is for the natural section main channel, sinuosity 1.37 and with smooth and fully roughened floodplains.
- **Fig(6.16)** is for the natural section main channel, sinuosity 2.04 and with smooth and fully roughened floodplains.

All the tabulated data of the main channel discharge below bankfull level in the streamwise direction are presented in **Appendix III**.

As a general rule, the discharge held in the main channel below bankfull level is significantly lower than the discharge held in the main channel with no overbank flows. In other words,

overbank flows impose a massive reduction in the discharge capacity of the main channel compared to no overbank flows. This is a clear measure of the interaction effect as it affects flows below bankfull level.

- In **Fig(6.14)** the effect is less with increasing stage.
- In **Fig(6.15)** the effect is significant for rough floodplains and practically non-existence for high stage(250.0 mm) and smooth floodplains.

This is a most important phenomenon in modelling flow behaviour below bankfull level during overbank flow.

The discharge which results below bankfull level is severely disturbed by the floodplain flow above especially at higher sinuosities, higher floodplain roughness and lower stages.

6.2.5. Analysis of The Balance of The Vertical Discharge

In **Chapter 4**, it was shown that in meandering channels the growth and decay of secondary cells introduce significant energy losses to flow. The strength of these cells should become greater when sinuosity increases. Secondary cells transport flow in the streamwise, in the transverse and in the vertical directions. One possible way to evaluate, if the strength of these cells is increasing, is to determine the vertical discharge. Here the vertical discharge will be computed at imaginary horizontal slice located at bankfull level.

During the test programme of S.E.R.C. flume Series B, the vertical component of velocity was only measured in some sections of the main channel. However, based in the calculations made for the discharge distribution in the main channel, it will be possible to calculate, at bankfull level, the balance of vertical discharge comparing the bend apex section and the cross-over section. The discharge below bankfull level, at bend apex, is greater than at the cross-over section. Therefore there must be a net upward balance of the vertical discharge between bend apex and cross-over region which means that the discharge balance is

going in upward direction. Between the cross-over section and the next bend apex section the opposite occurs.

It is important to emphasise that a difference exists between the vertical velocities and the net balance of vertical discharge. There are vertical velocities going up and vertical velocities going down along the secondary cells. However the integration of these velocities along the imaginary horizontal slice, located at bankfull level, will give the balance of vertical discharge. This was calculated by the **Author** from the values of streamwise discharge below bankfull level at bend apex and cross-over sections.

The results of the balance of vertical discharge with the depth ratio(h/(H-h)) are presented in **Table(6.1)** and are plotted in **Fig(6.17)**. In general, the balance of vertical discharge increases with depth ratio(or stage), with sinuosity, with trapezoidal compared with natural, and reduces with the increase of the floodplain roughness. For example, if the case of the natural section with smooth floodplains and stage 200.0 mm is chosen, the results show that the balance of vertical discharge at bankfull level is 5.0 l/s for sinuosity 1.37 and 17.5 l/s for sinuosity 2.04. Both natural cross-sections have the same geometry and the only difference is the length of the channel. This significant increase in the vertical discharge(3.5 times) is reflected also by substantial rise in the resistance experienced by the flow when main channel sinuosity is changed from 1.37 to 2.04.

6.2.6 Modelling Discharges Distributions.

Modelling the complex three dimensional discharge distribution will eventually be achieved either with a full three-dimensional numerical model at one end of the spectrum, or a quasi one-dimensional model, at the other end of the spectrum. Any one dimensional approximation involves sub-division of the meandering compound flow into zones sketched below and

discussed in **Chapter 4.**

Zone 1 is below bankfull level, Zone 2 is above bankfull level

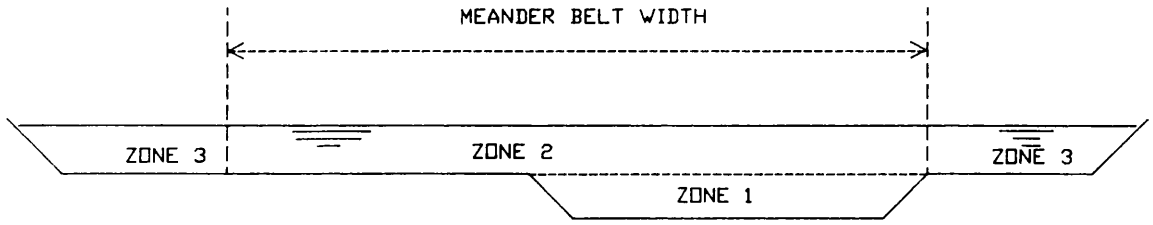

but contained within the meander belt width, and Zone 3 is above bankfull level outside the meander belt width.

Sections(6.2.4) and (6.2.5) have already discussed the distribution of discharge below bankfull level during overbank flow, and have already demonstrated that there is a great reduction of discharge in Zone 1 compared with an inbank flow. The reduction in Zone 1 discharge depends on stage, sinuosity, geometry of main channel cross-section and floodplain roughness.

What is the corresponding discharge distribution in Zone 2 and 3? To simplify matters, it was decided to compute the discharge in Zone 2 and in Zone 3 in the longitudinal x - direction only, bounded by imaginary vertical walls at the outer edge of the meandering main channel and a horizontal slice at bankfull level as shown above. This is shown in **Fig(6.18a)** to **Fig(6.18e)** and compared with discharge that would result in an equivalent straight channel at the same width and depth with same degree of boundary roughness. These plots show the variation of discharge from bend apex to next bend apex, for the following specific case all of which involve smooth floodplains:

- **Fig(6.18a)** and **Fig(6.18b)** are for sinuosity 1.37, trapezoidal cross-section, stage 200.0 mm, for zones 2 and 3, and zone 1, respectively.
- **Fig(6.18c)** and **Fig(6.18d)** are for sinuosity 1.37, natural cross-section, stage 200.0 mm, for zones 2 and 3, and zone 1, respectively.
- **Fig(6.18e)** and **Fig(6.18f)** are for sinuosity 1.37, trapezoidal cross-section, stage 250.0 mm, for zones 2 and 3, and zone 1, respectively.
- **Fig(6.18g)** and **Fig(6.18h)** are for sinuosity 1.37, natural

cross-section, stage 250.0 mm, for zones 2 and 3, and zone 1, respectively.

- **Fig(6.18i)** and **Fig(6.18j)** is for sinuosity 2.04, natural cross-section, stage 200.0 mm, , for zones 2 and 3, and zone 1, respectively.

All the figures show that in Zone 2, the actual discharge varies very little between bend apex, cross-over and next bend apex. On other hand, the actual value of discharge is always smaller than its theoretical value(corresponding to a straight channel). This is the result of an interaction mechanism between the main channel flow and the floodplain flow. Another interesting aspect revealed by these graphs is the effect of stage, main channel cross-section geometry and sinuosity on the ratio between actual discharge(Q_{ac}) and theoretical discharge(Q_{th}), which could be an indicator of the degree of interaction mechanism. Values of the ratio Q_{ac}/Q_{th} are given in the table below for Zone 2 floodplain flows.

Analysis of Discharge of Zone 2

Sinuosity	Stage	Cross-section	$\frac{\text{Actual Discharge}}{\text{Theoretical Discharge}}$
	mm		
1.37	200.0	Trapezoidal	0.95
1.37	200.0	Natural	0.86
1.37	250.0	Trapezoidal	0.84
1.37	250.0	Natural	0.87
2.04	200	Natural	0.74

It can be noted that the result for sinuosity 1.37, for trapezoidal cross-section with stage 200.0 mm may be in doubt because of lack of consistency with other data. As a broad generalization, it is clear that sinuosity 1.37 floodplain flow losses about 15% discharge due to interaction, and at sinuosities 2.04 this figure is more like 25%.

- As stage rises, the natural cross-section reveals that the

discharge ratio to be almost constant.
- Comparing the natural cross-section case with trapezoidal case, for stage 250.0 mm, above table shows the discharge ratio for natural case is 3% greater than trapezoidal, as expected. This confirms the findings presented in **Chapter 4** and 5 about the effect of the main channel aspect ratio on the conveyance of meandering compound channels.
- Sinuosity is undoubtly the parameter that most affects the discharge of Zone 2. Comparing sinuosity 1.37 and 2.04, for natural cross-section and stage 200.0 mm reveals a substantial difference of 12%. Sinuosity increases substantially the interaction mechanisms in Zone 2.

Concerning the discharge in Zone 3, **Fig(6.18a)** to **Fig(6.18c)** show that the actual discharge is approximately equal to the theoretical discharge value in all cases, independently of stage, sinuosity and main channel cross-section shape. Hence it was a correct assumption, considered by **Ervine and Ellis(1987)** in their one-dimensional model that the flow on the floodplain, outside the meander belt is influenced mainly by the bed friction.

6.3 ENERGY EQUATION APPLIED TO MEANDERING COMPOUND CHANNELS.

6.3.1 Introduction.

Further insight into the behaviour of meandering compound flows can be achieved by investigating the distribution of energy throughout the flow field. This will point directly to the distribution of energy loss through the flow field and hence will give a clear idea as to the sources and magnitudes of energy loss, over and above boundary friction.

In order to predict the local energy level at every point in the flow, accurate depths and at least 2 components of velocity are required.

The law of conservation of energy for one-dimensional flow

was defined by **Bernoulli** with the equation

$$H = z + \frac{p}{\gamma} + \alpha \frac{u^2}{2g} \qquad (6.15)$$

where H is the total energy; z the elevation above a datum; p is the pressure; γ is the fluid specific weight; p/γ is the pressure head; u is the streamline velocity; $u^2/2g$ is the kinetic energy; g is the acceleration of gravity; and α is the energy coefficient for the over-all effect of the nonuniform velocity distribution. If the pressure distribution is considered hydrostatic, equation 6.15 becomes

$$H = z + d \cos \ominus + \alpha \frac{u^2}{2g} \qquad (6.16)$$

where d is the flow depth and $\ominus$ is the slope angle of the channel bottom. For a channel of small slope $\ominus \cong 0^{\ll}$ the total energy at the channel section is approximated to,

$$H = z + d + \alpha \frac{u^2}{2g} \qquad (6.17)$$

Extending equation 6.17 to a three-dimensional case, as in the case of flow in meandering channels,

$$H = z + d + \alpha_1 \frac{u^2}{2g} + \alpha_2 \frac{v^2}{2g} + \alpha_3 \frac{w^2}{2g} \qquad (6.18)$$

where v is the transverse component of the velocity, w is the vertical component of velocity; and α_1, α_2 and α_3 are the energy coefficients to correct the non-uniform distribution of velocity in streamwise, in the transverse and in the vertical directions.

As mentioned in **Chapter 3**, in S.E.R.C. Series B the measurements of the resultant flow velocity and of the stream angle were carried out only in X-Y plan. Based on these measurements it was possible to calculate only the streamwise component and the transverse component of the flow velocity.

The energy equation applied by the **Author** to the S.E.R.C. Series B data was equation 6.18, but neglecting the effect of the

kinetic energy produced by the vertical component of velocity,

$$H = z + d + \alpha_1 \frac{u^2}{2g} + \alpha_2 \frac{v^2}{2g} \qquad (6.19)$$

The datum was a slice parallel with the bottom of the floodplain and distanced 150.0 mm below the floodplain. In general this level corresponds to the base of the main channel at the bend apex deepest section.

Mitchell and Griffiths(1980) in their book entitled " The Finite Difference Method in Partial Differential Equations"(page 253) derived an energy equation for a two-dimensional flow case which was similar to equation 6.15, applied by the **Author**.

Although the vertical component of the kinetic energy was not taken into account, the **Author** considers that its effect is very small in comparison with the importance of other terms of the equation.

The method followed in the calculation of each term of the energy equation was as follows:

a) The Sum of The Elevation (relative to datum) and of the Flow Depth;(z + d) called the surface level, was performed by a Churchill probe, and measured locally throughout the grid for the flow field, as described in **Chapter 3** Section 3.3.6.

b) Streamwise Component of the kinetic energy: $\alpha_1 \frac{u}{2g}$
Equation 6.9 calculates the value of the streamwise component of the velocity at each grid point of each the vertical slice and at all cross sections in the flow. At each vertical of the main channel and floodplain, the depth-averaged kinetic energy was calculated by the following equation,

$$\frac{\overline{U}^2}{2g}_J = \frac{\int_0^H U_i^2 \, dh}{2g \; H_J} \qquad (6.20)$$

where J is the index of the vertical and H is the total depth of

the vertical J. The value of α_1 was computed from the distribution of velocity with depth over each vertical slice.

c) Transverse Component of the kinetic energy: $\alpha 2 \frac{v^2}{2g}$

Equation 6.12 calculates the value of the transverse component of the velocity at each grid point of each vertical slice. In each vertical of the main channel and of the floodplain, the depth averaged kinetic energy was calculated by the following equation,

$$\frac{\overline{V}^2}{2g}_J = \frac{\int_0^H V_i^2 \, dh}{2g \; H_J} \qquad (6.21)$$

where J is the index of the vertical and H is the total depth of the vertical J. α_2 was computed in a similar manner to α_1. The calculation of the kinetic energy and total energy was carried out by a computer program written in Basic.

6.3.2. Contours of Locally Measured Water Surface Levels

Hardwick(1990/1991) has measured and plotted the contours of the local water surface levels for all the case studies of S.E.R.C. Series B. Some examples are shown in **Fig(6.19a), Fig(6.19b) and Fig(6.20)** for inbank flows of sinuosity 1.37 and 2.04, and for stages 100.0 mm and 140.0 mm.

- **Fig(6.21)** to **Fig(6.23)** for overbank cases with smooth floodplains, for sinuosity 1.37 and 2.04 and for stage 200.0 mm. A complete data set has been produced by **Hardwick(1990/1991)** and is shown here only as one or two examples.
- For the inbank case in **Fig(6.19a)** and **Fig(6.19b)**, the higher surface levels are located near the outer bank beyond the bend apex and the lower surface levels are near the inner bank of the bend around the bend apex. These findings corroborate the results obtained by others researchers.
- In the cross-over region the water surface levels are

approximately constant.

- **Fig(6.20)** for sinuosity 2.04 also reveals very high water levels at the outer bend close to the cross-over point.
- For the overbank cases in **Fig(6.21)** and **Fig(6.23)** the highest water levels were recorded in the main channel beyond the bend apex, before the cross-over region.
- The lowest water levels were recorded on the floodplain beyond the bend apex, before the cross-over region and just downstream of the highest main channel water levels.

This means that very substantial water surface gradients exist in this region, straddling the main channel and the floodplain junction and behaving almost like a weir type flow with water level variations upwards of 10.0 mm over a short distances of 1.0 to 2.0 metres. This is very similar to the expansion contraction phenomenon described by **Jasem(1990)** in his research into flow over slots in a channel bed.

- Comparing the effect of the cross-section geometry on the water surface levels of sinuosity 1.37, in **Fig(6.21)** and **Fig(6.22)**, it is observed that this phenomenon is less pronounced in the natural section case. A significant part of the energy losses that occur in the main channel of the meander will be produced by this type of expansion-contraction phenomenon, which may mean that there will be less loss of energy as the aspect ratio of the section increases, as was the case of the natural cross-section.

- **Fig(6.22)** and **Fig(6.23)** reveal the effect of changing sinuosity from 1.37 to 2.04 on the water surface levels. There are much steeper water level gradients at the higher sinuosity, and occurring over greater areas, implying greater energy losses due to this phenomenon.

In general the water surface levels produced by **Hardwick** were invaluable in computing the local energy levels.

6.3.3 Contours of The Total Energy Levels for Meandering Compound Channels.

Contours of the total energy levels in the meandering channels of S.E.R.C. Series B were plotted for the following conditions:

- For sinuosity 1.374, for trapezoidal cross section with smooth floodplains in **Fig(6.24)**(for stage 200.0 mm) and in **Fig(6.25)**(for stage 250.0 mm).
- For sinuosity 1.374, for natural cross section with smooth floodplains in **Fig(6.26)**(for stage 140.0 mm), in **Fig(6.27)** (for stage 165.0 mm), in **Fig(6.28)**(for stage 200.0 mm) and in **Fig(6.29)**(for stage 250.0 mm).
- For sinuosity 1.374, for natural cross section with fully roughened floodplains in **Fig(6.30)**(for stage 165.0 mm).
- For sinuosity 2.04, for natural section with smooth floodplains in **Fig(6.31)**(for stage 140.0 mm) and in **Fig(6.32)**(for stage 200.0 mm).

A cursory glance at these graphs reveals immediately that the highest energy levels during overbank flow are to be found in the inner bend apex region, Zone 3 outside the meander belt width, and also at the edge of the downstream floodplain near the start of the cross-over region.

Detailed comments on the contours of total energy levels will be presented in terms of each parameter, namely:

a) Cross-section geometry of the main channel.
b) Sinuosity.
c) Stage.
d) Floodplain Roughness.

a) Effect of the Cross-Section Geometry:

- Comparison of the trapezoidal cross-section with the natural cross-section for sinuosity 1.37 with smooth floodplains and for stage 200.0 mm and 250.0 mm, can be seen by comparing **Fig(6.24)** and **Fig(6.25)** with **Fig(6.28)** and **Fig(6.29)**.
- The pattern of the contours of the energy levels in both cases

is very similar. However, comparing **Fig(6.24)** and **Fig(6.28)** for stage 200.0 mm, the trapezoidal section exhibits slightly higher energy levels on the downstream floodplain, near the cross-over section, reaching 215.0 mm, compared with a value of 211.0 mm for the natural cross section in the same region. Flow is accelerating in this region and it is characterized by high levels of energy.

- Again comparing **Fig(6.24)** and **Fig(6.28)** for stage 200.0 mm, the main channel cross-over region, where the flow is decelerating, the levels of total energy reach a minimum value of 206.0 mm for the trapezoidal cross-section and 204.0 mm for the natural cross-section.
- In the floodplain area apart from, the zone where flow is accelerating, the natural cross-section case and the trapezoidal cross-section case exhibit contours of total energy that are very similar with an average value between 206.00 mm and 207.0 mm, in both cases.

Comparison of the two cross sectional geometries at stage 250.0 mm can be seen in **Fig(6.25)** and **Fig(6.27)**. The pattern is very similar to the 200.0 mm stage except that higher energy levels are now also to be found on the floodplain completely outside the meander belt width. This phenomenon is so pronounced in **Fig(6.25)** and **Fig(6.27)** that the longitudinal contour lines of energy appear concentrated exactly along the imaginary edges of Zone 2(meander belt width) indicating that this sub-division is good at least for higher flow stages.

b) Effect of the Sinuosity:

- Comparison is made first for inbank stage 140.0 mm of the sinuosity 1.37 and 2.04 and for the natural cross-section, as shown in **Fig(6.26)** and **Fig(6.31)**.
- In both cases the highest levels of total energy, in the main channel region, are located near the cross-over section, along the outer downstream bank, being 152.0 mm for sinuosity 1.37 and 149.0 mm for sinuosity 2.04.
- The sinuosity 1.37 gives higher general energy levels because

of greater velocities than the sinuosity 2.04, at the same flow depth.
- Comparison is made for the stage 200.0 mm of the sinuosity 1.37 and 2.04 for the natural cross-section with smooth floodplains, as shown in **Fig(6.28)** and **Fig(6.32)**.
- The meander channel with sinuosity 2.04 shows much lower levels of total energy than the meander with sinuosity 1.37. This is primarily due to lower velocities in the 2.04 case, but may also be due to inaccuracies in the datum level.
- As result of flow acceleration, there is an increase of the total energy on the downstream bank of the meander channel with sinuosity 1.37(214.0 mm). This phenomenon is less evident in the meander channel with sinuosity 2.04(205.0 mm).
- In both cases the highest levels of total energy in the main channel region are located in the bend apex section, near the inner bank.

c) Effect of the Stage:
- Comparison is made between stages 140.0 mm(an inbank case) and 165.0 mm(an overbank case), for a natural cross-section with sinuosity 1.37 and with smooth floodplains, as shown in **Fig(6.26)** and **Fig(6.27)**.
- In both cases the pattern of contours of the total energy in main channel region is similar, with the maximum values located along the outer bank of the cross-over region.
- In the bend region, for both stages, the maximum levels are located along the outer bank of the meander.
- Comparison of stages 165.0 mm and 200.0 mm, for the meander channel with sinuosity 1.37, natural cross-section and smooth floodplains, is shown **Fig(6.27)** and **Fig(6.28)**.
- In the main channel region, the pattern of contours of the total energy for stage 200.0 mm is different from the one for stage 165.0 mm. For stage 200.0 mm, the maximum levels of total energy are reached in the bend region, near the inner bank, while for the stage 165.0 mm, maximum values are near the outer bank of the cross-over. Therefore, it seems for stages greater than 165.0

mm, the flow behaviour in the bend region changes considerably.
- Comparison between stages 200.0 mm and 250.0 mm, for the meander channel with sinuosity 1.37, natural cross-section and smooth floodplains, is shown **Fig(6.28)** and **Fig(6.29)**.
- In the main channel both stages show the maximum total energy levels at the bend apex near the inner bank.
- On the downstream floodplain, the increase of total energy produced by the flow acceleration phenomenon is very clear for the stage 200.0 mm, but becomes less evident for the stage 250.0 mm.
- For stage 250.0 mm, the maximum levels of total energy are located on both floodplains, outside of the meander belt(266.0 mm). This is also a function of the floodplain being as smooth as the main channel, which may also occasionally occur in nature.

d) Effect of the Floodplain Roughness.
- Comparison is made for stage 165.0 mm, for sinuosity 1.37, for natural cross-section and with smooth floodplains and fully roughened floodplains, is given in **Fig(6.27)** and **Fig(6.30)**. In the main channel region, the contour levels of energy are the same for both floodplain roughness cases. Therefore, for stage 165.0, the contour levels of total energy are not affected by the floodplain roughness.
- For stage 200.0 mm, for meander channel with sinuosity 1.37, with natural cross-section, with increasing floodplain roughness from smooth to fully roughened case, it is expected that the levels of total energy will diminish in the main channel and in the floodplain region, as the floodplain roughness changes from smooth case to fully roughened case. These figures are not presented in the interests of brevity.

6.3.4. Implications of the Energy Study.

A one-dimensional model of meandering compound flows might be achieved by combining the force-momentum equation with

continuity. This approach will contain several simplifying assumptions and approximations.

Another less rigorous approach is to provide estimates for the energy loss in each zone of the flow, including friction and non-friction terms, relating to the energy gradient available, solving for the velocity in each sub-section of the flow and integrating to obtain the total discharge for any given stage. This approach was used by **Ervine and Ellis(1987)** and is now being developed further at the University of Glasgow, but with a more accurate knowledge of the non-friction losses in each part of the flow.

6.4 THE MOMENTUM EQUATION APPLIED TO MEANDERING COMPOUND CHANNELS.

6.4.1 Introduction.

In this section, however, it was decided to investigate the possibility of a two-dimensional force-momentum method applied to sub-sections(Blocks) of the meandering compound flow. The purpose of this approach is to quantify momentum fluxes, pressure forces, body weight forces and boundary shear forces in each sub-section, with a view to analysing the net out of balance force(known as the apparent shear force) for any trends or patterns in a typical meandering compound flow. Clearly, if the apparent shear force can be predicted, in general, then the force-momentum method can be applied to any case of meandering compound.

The measurements in the S.E.R.C. flume were two-dimensional (U-V) in general, and hence a two-dimensional approach is taken in the application of the force-momentum equation.

In turbulent flows, the conservation of momentum is governed by a set of equations known as Reynolds equations which were derived from the Navier-Stokes equations. Considering the flow to be steady and neglecting the effect of viscosity, these equations

expressed in cartesian coordinate system are,

- In the X direction

$$\rho\left(U \frac{\partial U}{\partial x} + V \frac{\partial U}{\partial y} + W \frac{\partial U}{\partial z} \right) = - \frac{\partial}{\partial x} (\bar{p} + \gamma h) -$$

$$-\rho\left(\frac{\partial u'^2}{\partial x} + \frac{\partial u'v'}{\partial y} + \frac{\partial u'w'}{\partial z} \right) \qquad (6.22)$$

- In the Y direction

$$\rho\left(U \frac{\partial V}{\partial x} + V \frac{\partial V}{\partial y} + W \frac{\partial V}{\partial z} \right) = - \frac{\partial}{\partial y} (\bar{p} + \gamma h) -$$

$$-\rho\left(\frac{\partial u'v'}{\partial x} + \frac{\partial v'^2}{\partial y} + \frac{\partial v'w'}{\partial z} \right) \qquad (6.23)$$

- In the Z direction

$$\rho\left(U \frac{\partial W}{\partial x} + V \frac{\partial W}{\partial y} + W \frac{\partial W}{\partial z} \right) = - \frac{\partial}{\partial z} (\bar{p} + \gamma h) -$$

$$-\rho\left(\frac{\partial u'w'}{\partial x} + \frac{\partial w'v'}{\partial y} + \frac{\partial w'^2}{\partial z} \right) \qquad (6.24)$$

where:

U, V, and W are the velocity components X, Y and Z directions.

h is the vertical distance.

ρ is the fluid density.

p is the pressure.

u', v', and w' are the components of turbulence in X, Y and Z directions.

The same momentum equations expressed in curvilinear coordinates system and in terms of instantaneous velocities can be written as

- In s streamwise direction

$$\left(u \frac{\partial u}{\partial s} + v \frac{\partial u}{\partial n} + w \frac{\partial u}{\partial z} \right) + \frac{u v}{r} = - \frac{1}{\rho} \frac{\partial p}{\partial x} + Fs \qquad (6.25)$$

- In n transverse direction

$$\left(u \frac{\partial v}{\partial s} + v \frac{\partial v}{\partial n} + w \frac{\partial v}{\partial z} \right) - \frac{u^2}{r} = - \frac{1}{\rho} \frac{\partial p}{\partial y} + F_N \qquad (6.26)$$

- In w vertical direction

$$\left(u \frac{\partial w}{\partial s} + v \frac{\partial w}{\partial n} + w \frac{\partial w}{\partial z} \right) + g = - \frac{1}{\rho} \frac{\partial p}{\partial z} + Fz \qquad (6.27)$$

where u, v and w are the instantaneous components of velocity in s, n and w directions; Fs, F_N and Fz are the friction terms applied in the three directions; r is the local radius of curvature.

Equations 6.25 and 6.26 were further developed by **Nelson and Smith(1989)**.

Consider first the momentum equation applied in s direction, defined in equation (6.25). Also multiplying the continuity equation (6.6) by u

$$u \frac{\partial u}{\partial s} + \frac{u}{r} \frac{\partial (v r)}{\partial n} + u \frac{\partial w}{\partial z} = 0 \qquad (6.6a)$$

Calculating the derivatives gives

$$u \frac{\partial u}{\partial s} + u \frac{\partial (v r)}{\partial n} + \frac{u v}{r} + u \frac{\partial w}{\partial z} = 0 \qquad (6.6b)$$

Adding this equation to momentum equation in the s direction yields

$$2u \frac{\partial u}{\partial s} + v \frac{\partial u}{\partial n} + w \frac{\partial u}{\partial z} + 2 \frac{u v}{r} + u \frac{\partial v}{\partial n} + u \frac{\partial w}{\partial z} =$$

$$= - \frac{1}{\rho} \frac{\partial p}{\partial x} + Fs \qquad (6.25a)$$

Regrouping the partial derivatives of equation (6.25a), gives

$$\frac{\partial (u)^2}{\partial s} + \frac{\partial (u\,v)}{\partial n} + \frac{\partial (u\,w)}{\partial z} + 2\,\frac{u\,v}{r} = -\frac{1}{\rho}\,\frac{\partial p}{\partial x} + Fs \qquad (6.25b)$$

Taking long time averages,

$$\overline{\frac{\partial (\bar{U} + u')^2}{\partial s}} + \overline{\frac{\partial (\bar{U} + u')(\bar{V} + v')}{\partial n}} + \overline{\frac{\partial (\bar{U} + u')(\bar{W} + w')}{\partial z}}$$

$$+ 2\,\overline{\frac{(\bar{U} + u')(\bar{V} + v')}{r}} = -\frac{1}{\rho}\,\overline{\frac{\partial (\bar{p} + p')}{\partial s}} + Fs \qquad (6.25c)$$

Simplifying equation 6.25c gives,

$$\frac{\partial \bar{U}^2}{\partial s} + \frac{\partial (\bar{U}\,\bar{V})}{\partial n} + \frac{\partial (\bar{U}\,\bar{W})}{\partial z} + 2\,\frac{\bar{U}\,\bar{V}}{r} = -\frac{1}{\rho}\,\frac{\partial \bar{p}}{\partial s} + Fs$$

$$- \overline{\frac{\partial (u'^2)}{\partial s}} - \overline{\frac{\partial u'v'}{\partial n}} - \overline{\frac{\partial u'w'}{\partial z}} - 2\,\overline{\frac{u'v'}{r}} \qquad (6.25d)$$

Comparing the cartesian frame(equation 6.22) with the curvilinear system(equation 6.25d) in the s direction, there are two additional terms: $2(\overline{UV})/r$ on the left hand side and $2(\overline{u'v'})/r$ on the right hand side.

Similarly, if the continuity equation was multiplied by v and applying a similar procedure to the momentum equation in n direction, the following equation will be obtained

$$\frac{\partial (\overline{UV})}{\partial s} + \frac{\partial \bar{V}^2}{\partial n} + \frac{\partial (\bar{U}\,\bar{W})}{\partial z} + \frac{\bar{V}^2 - \bar{U}^2}{r} = -\frac{1}{\rho}\,\frac{\partial \bar{p}}{\partial s} + Fs$$

$$- \overline{\frac{\partial u'v'}{\partial s}} - \overline{\frac{\partial (u')^2}{\partial n}} - \overline{\frac{\partial v'w'}{\partial z}} - \overline{\frac{(v')^2 - (u')^2}{r}} \qquad (6.26a)$$

Comparing the cartesian frame(equation 6.23) with the curvilinear system(equation 6.26A) in the n direction, it can be seen that there is two additional terms: $(\bar{V}^2 - \bar{U}^2)/r$ on left hand side and $-[(\bar{v}')^2 - (\bar{u}')^2]/r$ on the right hand side.

The reason for deriving both sets of equations is connected with the fact that a lot of the floodplain flow follows the standard cartesian frame work, whereas the bend flow especially in the main channel are better suited to the curvilinear flows system.

6.4.2 The Momentum Equation Applied to the S.E.R.C. Flume Series B Data with Sinuosity 1.374.

The momentum equations defined by equations (6.22) in the x direction, equation (6.23) in the y direction and equation (6.25d) in the S direction were applied to the meandering channel of the S.E.R.C. flume with sinuosity 1.374. The momentum equations in the X and Y directions were applied in the floodplain region whereas the momentum equation in the S direction was applied in the main channel region. To ease the calculations of the several terms of the momentum equation, half of the wave length of the meander channel shown in **Fig(6.33)** was divided into nine blocks, six on the floodplain and three in the main channel region. Blocks 1, 2 and 3 are on the upstream floodplain, 4 ,5, and 6 on the downstream floodplain, and 7,8, and 9 in the main channel. The U, velocity component, represent the longitudinal component on the floodplain and the streamwise component in the main channel. The velocity component V represents the transverse velocity on the floodplain or the spanwise component in the main channel, normal to the main channel walls.

Although the application of the force-momentum equation was applied only for one sinuosity, it was decided to apply it to as broad a range of tests as possible, including the trapezoidal and natural main channel cross-sections, smooth and rough floodplains, inbank and overbank flows, as well as full range of stages up to 250.0 mm tested in detail.

As a minimum condition, the application of the force-momentum equation in this form requires a knowledge of

local water levels, accurate bed slopes, boundary shear stress measurements, velocity components in two directions and other relevant data.

6.4.3. The Momentum Equation Applied to the Floodplain Region in The X Direction.

The floodplain region of the meandering channel with sinuosity 1.37 is shown in **Fig(6.33)** divided into six blocks. In each block the momentum equation in the X direction, defined by equation (6.22), was applied. The upper and the lower limits of the equation were the channel bottom and the free water surface. These boundary conditions allow a simplification of some of the terms of equation (6.22). For instance the term $W \frac{\partial U}{\partial z}$ is eliminated because the W component of velocity is zero at the channel bottom and at the water surface. The turbulent term $\frac{\partial u'w'}{\partial z}$, when integrated between the channel bottom and the water surface reduces to the bottom shear stress τ_o which was measured in detail by the Preston tube. The turbulent intensities on the floodplain are very small, thus terms that contain the turbulent intensities($\frac{\partial u'^2}{\partial x}$) can be neglected. The second turbulent term $(\frac{\partial u'v'}{\partial y})$ when depth integrated will produce the lateral shear term τ_{xy}, which, as evidenced by **Knight(1999)**, is very significant for straight compound channels. Considering these simplifications, equation (6.22) reduces to

$$\rho\left(U \frac{\partial U}{\partial x} + V \frac{\partial U}{\partial y} \right) = - \frac{\partial}{\partial x} (\bar{p} + \gamma h) - \tau_o - \tau_{xy} \qquad (6.22a)$$

Based on the measurements of the resultant flow velocity, streamline angles, boundary shear stress and local water levels carried out in the S.E.R.C. flume, the following terms of the momentum equation above are known:

. $U \frac{\partial U}{\partial x}$ and $V \frac{\partial U}{\partial y}$ are the momentum flux terms. These terms are sketched in **Fig(6.34)**. In meandering channels with overbank flow both terms are important. The second term was calculated at the boundaries of the main channel with the floodplain and represents the effect of secondary flow. The component V(the spanwise component of velocity) for overbank flow becomes very significant, as the strength of the secondary cells in the main channel region increases considerably in comparison with an inbank case.

. $- \frac{\partial \gamma h}{\partial x}$ is the body weight component term. From accurate measurements of local water levels, knowing the cross-section geometry and the bottom slope of the floodplain, the body weight component force can be easily computed. **Fig(6.35)** shows the body weight component for each block.

. $- \tau_o$ is the boundary shear stress component which has been measured on the floodplain over various cross-sections. Integrating these values over each block area, the total boundary shear force can be calculated, for each block. **Fig(6.35)** shows the boundary shear forces for each block.

. $- \frac{\partial p}{\partial x}$ is the pressure component term. From measurements of local water levels and assuming that the pressure distribution is hydrostatic, the pressure forces can be calculated. **Fig(6.36)** shows the pressure forces for each block, and a hydrostatic pressure distribution with depth is assumed reasonable at least for floodplain flows.

. τ_{xy} is the lateral shear stress and the only unknown term in the momentum equation in the x direction, applied to the floodplain region. Integrating the lateral shear stress in the vertical plane will produce the lateral shear force. This term will be included under the umbrella of a general term called "Apparent Shear Force". Previous researchers have used this

concept to include unknown terms of the momentum equation, applied to straight and to skewed compound channels. **Fig(6.37)** shows the apparent shear force terms for each block assumed to be operating in the boundaries of the main channel/floodplain junction, in a vertical plane and in the x direction

A detailed description of the method followed in the computation of each term of the momentum equation will be demonstrated for the case of block 1. The method followed for the other blocks was identical. The demonstration will be made for the test conditions: stage 200.0 mm; natural cross-section; and smooth floodplain.

Momentum Equation applied in BLOCK 1

(i) Calculation of the momentum flux at the upstream side,

$M_{11} = \rho\, U_{11} U_{11} A_{11}$

Based on actual data, the water depths were averaged.

$A_{11} = 6.854 * 0.0468 = 0.32\ m^2$

$U_{11} = 0.1275/0.32 = 0.398\ m/s$

$M_{11} = 1000 * 0.398 * 0.1275 = 50.7\ N$

(ii) Calculation of the momentum flux at the downstream side,

$M_{12} = \rho\, U_{12} U_{12} A_{12}$

$A_{12} = 6.24 * 0.0445 = 0.2778\ m^2$

$U_{12} = 0.104/0.2778 = 0.374\ m/s$

$M_{12} = 1000 * 0.374 * 0.104 = 38.9\ N$

It should be pointed out

(iii) Calculation of the momentum flux M_{13}

It should be pointed out in the clearest possible terms that M_{13} is the momentum flux leaving the curved boundary of Block 1(at the junction with the main channel), and resolved in the longitudinal x direction.

This term was computed from a knowledge of the velocity V_i normal to this curved boundary and normal to the main channel local direction.

M_{13} was calculated by applying the following method:
- The radial component of velocity $\overline{V}_i$ in each vertical along the boundary of the floodplain and main channel was calculated using equation (6.12).
- The term $(V_i^2)$was depth-averaged in each vertical located around the perimeter of the bend for Block 1.

$$\overline{V_J^2} = \frac{\sum_{i=1}^{i=n-1} (V_i^2+V_{i+1}^2)(H_i-H_{i+1})/2}{H_J} \qquad (6.28)$$

- The momentum flux $M_{13}= \rho\, V_{13}V_{13}A_{13}$ was calculated using

$$\rho\, V_{13}^2 A_{13} = \sum_{J=1}^{J=\,m-1} \left(\overline{V^2}_J + \overline{V^2}_{J+1} \right) \left(\Delta\, Y_J - {}_{J+1} \right) \left(H_J + H_{J+1} \right)/4 \qquad (6.29)$$

where $\Delta\, Y_{J-J+1}$is the projection on y axis of the curve between vertical J and J+1, H_J and $H_{J+1}$are the depths of verticals J and J+1. **Fig(6.38)** illustrates the procedure followed in the calculation of ΔY.
In essence $\rho\, V_{13}^2 A_{13}$is the momentum flux leaving the floodplain Block 1, along the curved length, and projected on to an area A_{13} which from **Fig(6.38)** is equal to Δy times the floodplain depth. For this particular block 1,
$M_{13}= \rho\, V_{13}V_{13}A_{13}= 3.46$ N

(iv) Calculation of the momentum flux M_{14}
M_{14} is the momentum flux from $V \frac{\partial U}{\partial y}$ term, in the x direction and applied again at the main channel/floodplain junction. It was calculated by a method similar to one used for M_{13}above.
- The velocity components U_i and V_i in each point on the verticals, located at the boundaries of the floodplain/main channel, were calculated using equations (6.9) and (6.12).
- The term $(\overline{UV})$ was depth averaged for each vertical, located around the perimeter of the bend,

$$\overline{V_J U_J} = \frac{\sum_{i=1}^{i=n-1} (V_i U_i + V_{i+1} U_{i+1})(H_i - H_{i+1})/2}{H_J} \qquad (6.30)$$

- The momentum flux $M_{14} = \rho\, V_{14} U_{14} A_{14}$ was calculated by

$$\sum_{J=1}^{J=m-1} \left(\overline{VU}_J + \overline{VU}_{J+1} \right) \left(\Delta X_{J - J+1} \right) \left(H_J + H_{J+1} \right)/4 \qquad (6.31)$$

where ΔX_{J-J+1} is the projection on x axis of the curve between vertical J and J+1, H_J and H_{J+1} are the depths of verticals J and J+1. **Fig(6.38)** illustrates the procedure followed in the calculation of ΔX. A_{14} represents the length Δx times the floodplain depth.

For Block 1,

$M_{14} = \rho\, V_{14} V_{14} A_{14} = 5.0$ N

(v) Calculation of the Body Weight in Block 1.

Average Depth = 0.047 m

Area = 12.13 m^2

Slope = $0.996 * 10^{-3}$

$BW_1 = 12.13 * 0.047 * 0.996 * 10^{-3} * 10^4 = 5.7$ N

(vi) Calculation of Boundary Shear Force in Block 1.

The boundary shear stress was measured by the Preston tube in a staggered grid(1 metre intervals). In each section the average value was calculated and averaged again by the value obtained in the next section. This average value was multiplied by the area between the two sections giving the boundary shear force for that particular region. Finally, the procedure was extended to the others regions until the entire area of block 1 was completed.

The equation used for the calculation of the average value of the boundary shear stress of a particular section was:

$$\bar{\tau}_S = \frac{\sum_{K=1}^{K=p-1} (\tau_K + \tau_{K+1})(\Delta l_{K-K+1})}{2 L_S} \qquad (6.32)$$

where k is the index of the vertical where the measurements took place; p is the number of verticals of the section; τ_K the boundary shear stress measured at the vertical k; - Δl_{K-K+1} is the distance between the vertical k and k+1; L_S is the total length of the section s; and $\bar{\tau}_S$ is the average boundary shear stress of section s.

The equation used for the calculation of the boundary shear force applied in block 1 was

$$BSF_1 = \frac{\sum_{S=1}^{S=R-1} (\bar{\tau}_S + \bar{\tau}_{S+1})(\Delta A_{S-S+1})}{2} \qquad (6.33)$$

where s is the index of the section and R is the total number of sections of block 1; ΔA_{S-S+1} is the area between sections k and k+1.

The boundary shear force for this particular case was calculated using a computer programme with the result,

$BSF_1 = 5.2$ N

(vii) Calculation of Pressure Force:

The pressure distribution was considered hydrostatic and the pressure force was calculated based on actual water depths. The results obtained were:

$PF_{11} = 76.6$ N ; $PF_{12} = 66.8$ N ; $PF_{13} = 12.8$ N

(viii) The Momentum Equation Applied to Block 1

Having considered all the terms in the force-momentum equation which can be computed from the data, it is now possible to write the equation of the momentum balance for Block 1. This is given by

$$M_{12} + M_{13} + M_{14} - M_{11} = BW_1 - BSF_1 + PF_{11} - PF_{12} - PF_{13} + ASFX_1 \qquad (6.22b)$$

$$38.9 + 3.5 + 5.0 - 50.7 = 5.7 - 5.2 + 76.6 - 66.8 - 12.8 + ASFX_1$$

$-3.3 = -2.5 + ASFX_1$

$ASFX_1 = -0.8$ N

where $ASFX_1$ is the apparent shear force(out of balance force) in the x direction.

Exactly the same procedure was carried out for all six flood plain blocks, Block 1 to 6 shown in **Fig(6.33)** in the **x** direction. The results are given below for the apparent shear force in the x direction. The results are given below for the apparent shear force in the **x** direction for each block

Upstream Flood Plain	Downstream Floodplain
Block 1 ASFx = -0.8 N	Block 4 ASFx = 2.7 N
Block 2 ASFx = 2.2 N	Block 5 ASFx = -5.3 N
Block 3 ASFx = 1.0 N	Block 6 ASFx = -5.5 N

The values above for the particular case of sinuosity 1.37, natural cross-section, smooth floodplains and stage 200.0 mm, reveal

(i) Apparent shear force at a maximum at Block 5 and 6 indicating areas of greatest momentum transfer.

(ii) Positive ASFx terms indicate momentum transfer in the downstream direction and negative in the upstream direction.

(iii) The apparent shear force for blocks 1, 3, 4, and 6 included not only the turbulence terms(not measured) but also the acceleration term +2UV/r which is difficult to estimate. The apparent shear force of blocks 2 and 5 is essentially the Reynolds shear stress term τ_{xy}.

6.4.4. General Application of the Force-Momentum Equation in the X-Direction on the Floodplains.

The calculation and discussion above was carried out for a very specific case where the boundary shear force was measured at every point on the floodplain hence was able to provide accurate

integrations of boundary shear force. This was not the case for all other geometries tested and hence a difficult method would need to be found to estimate boundary shear.

An inspection of the data in 6.4.3, above, revealed that on the upstream floodplain, the boundary shear forces were almost in balance with the body weight, whereas on the downstream floodplain the boundary shear force was usually slightly greater than the body weight. This phenomenon could be reflected in other geometries estimates of the boundary shear force. However, it was decided for all other geometries to equate body weight with boundary shear force on the floodplain, this being the most rational approach to any model being developed.

Exactly the same approach was taken for the pressure terms P_1, P_2 and P_3. Although these terms are very large for each block as seen by inspection of equation(6.22b), they would require an a priori knowledge of local flow depth at every point in the flow for accurate estimate. It was found that the hydrostatic pressure terms usually balanced on the floodplain and hence any force-momentum model could reflect this.

With this in mind, the full data set for the application of force-momentum to the floodplains, for all geometries is given in detail in **Appendix IV** and in summary form in **Table (6.2)**. The detailed data in **Appendix IV** gives the magnitude of each term in the force momentum equation.

The following conclusions can be noted from **Appendix IV**:

(i) In the interest of clarity it was decided to plot the apparent shear force graphically from **Appendix IV** thus enabling a visualization of any trends in ASFx. This procedure is plotted in **Fig(6.38a)** for Block 1 and 4 together and in **Fig(6.38b)** for Block 2 and 5 together.

(ii) The figures reveal no discernible trend in Apparent shear force with stage. This is disappointing because if no trend is apparent, then there is no way to systematically estimate apparent shear , and hence its magnitude is unknown for any given meander

geometry.

(iii) Comparing Block 1 with Block 4 reveals greater apparent shear forces at Block 1 inner bend and less at the outer bend. This is to be expected. Also the trapezoidal cross-section section appears to generate much greater Apparent shear force than natural cross-section.

(iv) Block 2 at the cross-over region produces little apparent shear force compared with Block 5 at the downstream cross-over region.

(v) In general, rough floodplains tend to produce more positive apparent shear forces implying momentum transfer from main channel to floodplain as might be expected.

(vi) It seems therefore that apparent shear stress varies considerably with the distance around the meander from apex to apex, with no discernible pattern.

(vii) The first conclusion, therefore is that this form of force-momentum equation is not satisfactory for high three dimensional compound flows. It can only be applied accurately knowing boundary shear stress, local flow depths, local velocities body weight, and from a knowledge of the turbulence terms involved in the apparent shear force term. The later is unknown and has no discernible trend.

(ix) This leaves the stark conclusion, that full three-dimensional numerical modelling is probably required including estimates of turbulence terms.

Two dimensional depth averaged modelling will miss some important features of the flow, although may be adjusted to provide reasonable answers.

One-dimensional modelling may be possible using the approach of **Ervine and Ellis(1987)** but will require an accurate

distribution of energy losses in each part of the flow field.

A one-dimensional force-momentum model might have pressures in balance, body weight equal to boundary shear force but will require the knowledge of turbulence term which not being predicted can only be provided by accurate measurement. Therefore not knowing flow depth or discharge as well as the effect of turbulence term, this approach is not suitable to model meandering compound flows.

6.4.5. The Momentum Equation Applied to the Floodplain Region in The Y Direction.

The known terms in the momentum equation applied in the y direction are:

- the momentum fluxes, shown in **Fig(6.39)**, are referred to as M_5 and M_6.
- the body weight which does not have any effect in the y direction.
- the boundary shear force that is very small in the y direction.
- the effect of pressure force that was considered negligible in y direction. This assumes small variations in the local water level laterally on the floodplain.

The unknown term is again the turbulent shear which will be included inside the apparent shear force in Y direction. The apparent shear force term of each block in the y-direction is sketched in **Fig(6.37)**. The momentum equation was applied between the bottom of the floodplain and the water surface. Neglecting the effect of the body weight, the boundary shear stress, and pressure force and considering turbulent shear to be contained in the apparent shear force term, Equation 6.23 was simplified, giving

$$\rho\left(\bar{u}\,\frac{\partial\,\bar{v}}{\partial\,x} + \bar{v}\,\frac{\partial\,\bar{v}}{\partial\,y} \right) = ASF_y \qquad (6.23a)$$

where ASF_y is the apparent shear force in y direction.

The demonstration of the application of momentum equation in Y direction will be made for the block 1 for the same test conditions as before, namely a sinuosity 1.374, smooth floodplains, natural cross-section and stage 200.0 mm.

Momentum Equation applied to BLOCK 1

(i) Calculation of the Momentum Flux leaving the Curved Boundary in the y-direction,

$M_{15} = \rho V_{15} V_{15} A_{15}$

M_{15} was calculated by applying the following method:

- The spanwise component of velocity V_i in each vertical along the boundaries of the main channel was calculated using equation (6.12).
- The term $\overline{(V_J^2)}$ was depth-averaged for each vertical, located around the perimeter of the bend using equation (6.28).
- The momentum flux $M_{15} = \rho V_{15} V_{15} A_{15}$ was calculated from the following equation

$$\rho \overline{V}_{15}^2 A_{15} = \sum_{J=1}^{J=m-1} \left(\overline{V^2}_J + \overline{V^2}_{J+1} \right) \left(\Delta X_J - {}_{J+1} \right) \left(H_J + H_{J+1} \right) / 4 \qquad (6.34)$$

where ΔX_{J-J+1} is the projection on x axis of the curve between vertical J and J+1, H_J and H_{J+1} are the depths of verticals J and J+1. **Fig(6.38)** illustrates the procedure followed in the calculation of ΔX shows the projected area A_{15}. All the calculations were carried out by a computer programme.

$M_{15} = \rho V_{15} V_{15} A_{15} = 3.8$ N

(ii) M_{16} is the momentum flux at the curved boundary due to the term $U(\partial V/\partial x)$ and resolved in the y direction.

$M_{16} = \rho V_{16} U_{16} A_{16}$

M_{16} was calculated by a method similar to the one used for M_{15}:

- The velocity components U_i and V_i at each point of the verticals, located at the boundaries of the main channel, were calculated from equations (6.9) and (6.12).

- From equation (6.30), the term ($\overline{UV}$) was depth averaged at each vertical around the perimeter of the bend.
- The momentum flux $M_{16} = \rho V_{16} U_{16} A_{16}$ was calculated from the following equation

$$\rho V_{16} U_{16} A_{16} = \sum_{J=1}^{J=m-1} \left(\overline{VU}_J + \overline{VU}_{J+1} \right) \left(\Delta Y_{J-J+1} \right) \left(H_J + H_{J+1} \right) / 4 \qquad (6.35)$$

where ΔY_{J-J+1} is the projection on y axis of the curve between vertical J and J+1, H_J and H_{J+1} are the depths of verticals J and J+1. **Fig(6.38)** illustrates the procedure followed in the calculation of ΔY and shows the projected area A16.

$M_{16} = \rho V_{16} V_{16} A_{16} = 3.5$ N

(iii) The Momentum Equation Applied to Block 1 becomes,

$M_{15} + (- M_{16}) = ASFY_1$

$3.8 - 3.5 = ASFY_1$

$0.3 = ASFY_1$

$ASFY_1 = 0.3$ N

There is an explanation for the signs used in the momentum equation applied on the left floodplain in the y direction. The momentum flux ρVVA(M_{15}) is leaving the block and its projection in the y direction is positive. Therefore its sign is positive. The momentum flux ρUVA(M_{16}) is leaving the block as well but its projection in the y direction is negative. Therefore its sign is negative. On the left floodplain ρVVA is positive and ρUVA is negative. On the right floodplain ρVVA is negative and ρUVA is positive.

Exactly the same procedure has been carried out for all six floodplain blocks for this particular test run. Their values of apparent shear stress in the y direction are summarised as follows

Upstream Floodplain		Downstream Floodplain	
Block	ASFy	Block	ASFy
1	0.3 N	4	-0.9 N
2	-1.8	5	2.3 N
3	-0.3	6	1.2 N

These findings show that the maximum values of the apparent shear force in y the direction are located in the cross-over regions(Block 2 and 5).

Appendix V shows the results in detail for the force momentum equation in y direction. These results are also presented in summary in **Table (6.2)** highlighting values of apparent shear force.

It is interesting again with the data of **Appendix V** to plot the results of ASFy with stage, for each block and test condition. The result is shown in **Fig(6.39a)** with Blocks 1 and 4 plotted and in **Fig(6.39b)** with Blocks 2 and 5 plotted together.

The following points can be noted:

(i) Again there is no real pattern to the emerging values of apparent shear force with depth.

(ii) Blocks 2 and 5 at the cross-over region give high values of apparent shear force for all geometries and boundary roughness and especially at greater flow depths.

(iii) Block 1 produces small apparent shear forces generally whereas Block 4 on the opposite outer bank produces large forces for the rough case(momentum to the floodplain) and large forces for the trapezoidal case(momentum from the floodplain).

(iv) Again there is no systematic pattern emerging which means that the apparent shear force will be difficult to estimate for each geometry and flow depth, and hence full three-dimensional numerical modelling with a turbulence model may be required.

Again the one-dimensional energy method may be worthwhile pursuing for crude estimates of discharge capacity.

6.4.6. The Momentum Equation Applied to the Main Channel

The momentum equation was also applied in the S direction of the main channel region of the S.E.R.C. flume, sinuosity 1.37.

The main channel region, as shown in **Fig(6.33)**, was split into three blocks, 7, 8 and 9 respectively. The momentum equation applied was defined by Equation (6.25d), Considering each term of equation (6.25d) in turn:

$- \overline{U} \frac{\partial \overline{U}}{\partial s}$ This term is very significant and was computed based on measurements of resultant velocity and stream angles. U is the streamwise component of velocity parallel to main channel walls in the main channel. This momentum flux is sketched in **Fig(6.40)** and denoted as M_{71}, M_{72}, etc.

$- \overline{V} \frac{\partial \overline{U}}{\partial n}$ This term represents the effect of secondary currents in the main channel region. The spanwise component(normal to main channel walls) of velocity, V, becomes very significant for overbank flow, as the strength of secondary currents increases substantially compared with an inbank case. This momentum flux is sketched in **Fig(6.40)**.

$- \overline{W} \frac{\partial \overline{U}}{\partial s}$ As the momentum equation was integrated between the channel bottom and the water surface and the net vertical component of velocity, $\overline{W}$, in those limits is zero. Therefore, this term can be eliminated.

$- 2 \frac{\overline{U}\,\overline{V}}{r}$ This term represents the convective acceleration and it is very important in overbank flows in the bend region where the velocity component $\overline{V}$ can be significant and the radius of the streamlines r is small. In the cross-over region this term is zero because $r = \infty$.

$- \frac{1}{\rho} \frac{\partial \overline{p}}{\partial s}$ The pressure term is very important in meandering compound flows because local water levels are changing as

result of the effects of flow deceleration, acceleration and centrifugal force. The pressure term includes the pressure force and the body weight. The pressure distribution is not necessarily hydrostatic. For instance in the cross-over region the floodplain flow can separate from the upstream bank, forming a strong circulation and plunging flows in the main channel. This can rise to non-hydrostatic flows but because the effect is difficult to quantify as the floodplain flow and the vertical components of velocities are very small, the pressure field was assumed hydrostatic.

Another aspect that affects the calculation of the pressure force of the natural meander channel, in the s direction, is the geometric shape of the cross-section and longitudinal bed slope over the pool(bend) and riffle(cross-over) sequences. For the natural case, the geometry of the cross-section is changing along the bend, between a pronounced asymmetric shape, at bend apex, with large depths near the outer bank and shallow depths near the inner bank and a trapezoidal section, at cross-over section. This is a pool to riffle length and is characterised by a local adverse bed slope. The body weight component in the s direction, sketched in **Fig(6.41)**, is very complicated. The complication is primarily that in moving from bend apex section to cross-over region, the outer part of the bend moves from a depth of 150.0 mm to 89.0 mm an adverse gradient, whereas at the inner part of the bend, the bed moves from a depth 45.0 mm to a depth of 89.0 mm at the cross-over, giving a positive slope. A range of bed slopes exist over this length, although the overall main channel bed slope from apex to apex remains constant at 0.001/1.374. A method was developed by the **Author** to calculate not only the body weight component in the s direction at the bend region but also the cross-over slope. This method will be described later in section 6.4.7.

$-\frac{\partial \overline{u'^2}}{\partial s}$ Turbulent intensities in general vary only slightly in the streamwise direction. In meandering compound flows however this may not necessarily be the case. **Ervine and Jasem(1992)**,

based on **Kiely(1989)'s** results, pointed out that $u' \frac{\partial u'}{\partial s}$ is approximately 10% of $\bar{U} \frac{\partial \bar{U}}{\partial S}$. This term was neglected in the Author's analysis.

$- \frac{\partial \overline{u'v'}}{\partial n}$ This term is the Reynolds lateral shear usually represented by τ_{xy}. It has been shown by **Knight(1999)**, to be important in straight compound channels. **Elliot and Sellin(1990)** have shown that for skew compound flows with Θ less than 10^0 cross-over angle that τ_{xy} is less significant than the straight compound cases. Here τ_{xy} term will be considered unknown and included in the apparent shear force.

$- \frac{\partial \overline{u'w'}}{\partial z}$ As the momentum equation was integrated between the channel bottom and the water surface, this term reduces to bottom shear stress, usually represented by τ_0. The bottom shear stress was measured by a Preston tube in the s direction. The integration of the boundary shear stress over the block area will produce a boundary shear force in the s direction, sketched in **Fig(6.41)**.

$- 2 \frac{\overline{u'v'}}{r}$ This term is important in the bend region and will be included as an unknown term in the apparent shear force. In the cross-over region this term is zero because $r = \infty$. The value of radius r used in the calculation was the local radius of each vertical slice where measurements of velocities and streamlines were taken.

Considering the above simplifications, equation (6.25d) reduces to

$$\frac{\partial \bar{U}^2}{\partial s} + \frac{\partial(\bar{U}\,\bar{V})}{\partial n} + 2\frac{\bar{U}\,\bar{V}}{r} = -\frac{1}{\rho}\frac{\partial \bar{p}}{\partial s} - \frac{\partial \overline{u'v'}}{\partial n} - \tau_0 - 2\frac{\overline{u'v'}}{r} \qquad (6.25e)$$

Considering that AST_s is the apparent shear term for the bend region which includes the unknown lateral shear term, and the

term 2 $\frac{\overline{u'v'}}{r}$, then equation (6.25e) becomes

$$\frac{\partial \overline{U}^2}{\partial s} + \frac{\partial(\overline{U}\,\overline{V})}{\partial n} + 2\,\frac{\overline{U}\,\overline{V}}{r} = -\frac{1}{\rho}\,\frac{\partial \overline{p}}{\partial s} - \tau_0 - AST_s \qquad (6.25f)$$

For the cross-over region the bend radius $r = \infty$, then the apparent shear stress in this region includes only the lateral shear term.

6.4.7. Application of Force-Momentum Equation to an Inbank Flow in the Natural Main Channel.

To apply the momentum equation in the s direction in the main channel region, for the particular case of the natural meander channel, presents a difficulty concerning the calculation of the body weight component. The natural main channel cross-section geometry is changing longitudinally and transversely, as already explained, and therefore it is very complicated to calculate the body weight from measurements of water levels and from estimated values of bed slope. In order to overcame this difficulty, the momentum equation in the s direction was applied first to an inbank case where the only unknown is the body weight. The demonstration will be made for stage 140.00 mm, and details will be given for blocks 7 (upstream bend region) and 8(cross-over region). Application of the momentum equation in the s direction to an inbank case has another advantage, namely is the calibration of the bed slope in the cross-over section, as well.

Inbank Case of the natural meander channel : Stage 140.00 mm

Momentum Equation Applied to Block 7(Upstream Bend Region)

(i) Calculation of Momentum Flux:

$M_{71} = \rho\, U_{71}\, U_{71}\, A_{71}$

This momentum flux, as shown in **Fig(6.40)**, was calculated by applying the following procedure:

- The main channel streamwise component was calculated by equation (6.9) at each point of the vertical measurement slice.
- The square of the streamwise component U_i was depth averaged in each vertical of the section by

$$\overline{U_J^2} = \frac{\sum_{i=1}^{i=n-1} (U_i^2+U_{i+1}^2)(H_i-H_{i+1})/2}{H_J} \qquad (6.36)$$

- The momentum flux $M_{71}= \rho\ U_{71}\ U_{71}\ A_{71}$ was computed through

$$\rho\ U_{71}^2 A_{71}= \sum_{J=1}^{J= m-1} \left(\overline{U^2}_J + \overline{U^2}_{J+1} \right) \left(\Delta\ l_J - {}_{J+1} \right) \left(H_J + H_{J+1} \right)/4 \qquad (6.37)$$

where $\Delta\ l_{J-J+1}$ is the distance between the verticals of the main channel cross-section and the meaning of the remaining parameters were previous described.

All the calculations were performed through a computer program written in Basic. The results were

$M_{71}= \rho\ U_{71}\ U_{71}\ A_{71} = 14.8$ N

(ii) The momentum flux at the downstream end of the block is M_{72}(**Fig(6.42)**).

M_{72} was calculated by a method similar to the one described for M_{71}.

$M_{72}= \rho\ U_{72}\ U_{72}\ A_{72}= 13.9$ N

(iii) The Force Produced by the Acceleration $2\ \frac{UV}{r}\ \rho$ was calculated using the expression $2\ \frac{UV}{r}\rho$Vol in two steps. First it was calculated for each section,

$$2\rho \frac{\overline{UV}}{\overline{r}} A = 2\rho \sum_{J=1}^{J=m-1} \left(\frac{\overline{VU}_J}{r_J} + \frac{\overline{VU}_{J+1}}{r_{J+1}} \right) \left(\Delta X_J - {}_{J+1} \right) \left(H_J + H_{J+1} \right) /4 \quad (6.38)$$

where A is the cross-section area, r_J is the central radius of the vertical J; ΔX_{J-J+1} is the distance between verticals; H_J is the water depth of vertical J.

Once the term $2\rho \frac{\overline{UV}}{r} A$ was calculated for each main channel cross-section and averaged between two consecutive cross-sections, it was multiplied by an average perimeter, producing the force between these two cross-sections. This procedure was extended to entire bend. The result for Block 7 was

$$2 \frac{UV}{r} \rho \text{ Vol.} = 1.12 \text{ N}$$

(iv) Calculation of the Boundary Shear Force.
The perimeter of each main channel cross-section was split into five reaches. In each reach, the boundary shear stress, measured by the Preston tube, was averaged and multiplied by the corresponding length of the reach. This value was averaged again with the corresponding one of the next section and multiplied by the average perimeter, giving the average boundary shear force of that area between two sections. The procedure was extended to the full bottom and sides wall area of the main channel region, yielding the boundary shear force in the s direction. For this particular example, the result gave
$BSF_7 = 1.58$ N

(v) Calculation of Pressure Force.
Based on the detailed water level measurements, and assuming that the pressure distribution is hydrostatic, the pressure forces that acts perpendicular to the main channel cross-sections at the limits of the blocks were calculated by a computer program and the results were:
$PF_{71} = 41$ N ; $PF_{72} = 34.5$ N

(vi) Finally the momentum equation applied to Block 7 for the inbank case became,

$M_{72} - M_{71} + 2\ \rho\ \frac{U\ V}{r}\ Vol. = BW_7 - BSF_7 + PF_{71} - PF_{72}$

$13.9 - 14.8 - 1.12 = BW_7 - 1.58 + 41 - 34.5$

$-2.02 = 4.9 + BW_7$

$BW_7 = -6.94$ N, where BW_7 is the net body weight in the streamwise direction.

There is a good explanation why the body weight component in the s direction is negative. In the deep areas of the bend(near the outer bank) the channel bottom slope is negative(adverse slope) towards the cross-over region(pool $\longrightarrow$ riffle) while in the shallower areas(near the inner bank) the bottom slope is positive. As the negative slope is much greater than the positive slope, the negative component is greater than the positive component of the body weight, giving a net negative value for the resultant body weight.

(vii) Momentum Equation applied to Block 8 at the Cross-Over Region

The same procedure as (i) to (vi), above, was carried out for the cross-over region, for the same case of inbank flow, depth of 140.0 mm and natural cross-section.

Boundary shear forces, pressure forces and momentum fluxes were again computed to produce a final net estimate of the body weight, BW_8, in the cross-over region.

The final answer was $BW_8 = 1.27$ N.

This is a positive value in the streamwise direction, which is very feasible in view of the fact in the upstream part of Block 8 the bed slope is adverse, in downstream part it is positive and also the whole main channel region is on a net positive slope of $0.00096/1.374 = 7.2*10^{-4}$.

In fact knowing the body weight component over Block 8 it is possible to compute its effective bed slope from the total water volume and length of Block 8. The equivalent bed slope is

$1.27/\ (0.217*10^4) = 5.85*10^{-4}$

This is a little less than the overall average for the main

channel slope from apex to apex, namely $7*10^{-4}$m, but is also a little greater than the other estimate for the cross-over region(floodplain slope* 60^{0}) giving $4.98*10^{-4}$.

(viii) Momentum Equation Applied at Block 9(Downstream Bend Region)

Finally the force-momentum equation was applied to Block 9 for the same inbank flow.

The momentum equation applied to Block 9 is:

$$M_{92} - M_{91} + 2\,\rho\,\frac{U\,V}{r}\,\text{Vol.} = BW_9 - BSF_9 + PF_{91} - PF_{92}$$

$$14.8 - 13.9 - 0.95 = BW_9 - 1.65 + 34.5 - 41.0$$

$$-0.05 = -8.15 + BW_9$$

$$BW_9 = +8.1 \text{ N}$$

In this case the shallower part and the deeper part of bend both have a positive slope, and combining with the overall main channel positive slope gives a body weight component which is greater in absolute value than the one obtained for the upstream bend(in block 7 the body weight component was equal to -6.94 N).

It should be noted that body weights computed by this method for inbank flows, provided a very useful method to estimate and compute body weights for the over bank case described below.

6.4.8. Force Momentum Equation for the Main Channel Region During Overbank Flow.

This procedure was carried out for the same scenario as the floodplains in sections 6.4.4 and 6.4.6, for the case of a 1.37 sinuosity, depth of 200.0 mm, smooth floodplains and natural cross-section.

Again Blocks 7, 8 and 9 were involved, with the calculation for Block 7 in detail below.

Calculation of Momentum Fluxes in and out of Block 7:

(i) $M_{71} = \rho\, U_{71}\, U_{71}\, A_{71} = 25.1$ N

(ii) $M_{72} = \rho\, U_{72}\, U_{72}\, A_{72} = 12.1$ N

These momentum fluxes were calculated following a procedure similar to the one described for the inbank case.

(iii) $M_{73} = \rho\, U_{73}\, V_{73}\, A_{73}$

This is shown in **Fig(6.40)**, and is the momentum flux that acts tangentially at the limits of the inner bank of the bend. The procedure followed in its calculation was as follows,

- This main channel streamwise and spanwise components were calculated by equation (6.9) and (6.12) at each point of each vertical slice.
- Using equation (6.30), the term $(\overline{UV})$ was depth averaged at each vertical, located around the perimeter of the inner bend.
- The momentum flux $M_{73} = \rho\, V_{73} U_{73} A_{73}$ was calculated from

$$\rho V_{73} U_{73} A_{73} = \sum_{J=1}^{J=\,m-1} \left(\overline{VU}_J + \overline{VU}_{J+1} \right) \left(\Delta\, P_{J\,-\,J+1} \right) \left(H_J + H_{J+1} \right) / 4 \qquad (6.35)$$

where $\Delta\, P_{J-J+1}$ is the perimeter of the inner bank curve between vertical J and J+1, H_J and H_{J+1} are the depths of verticals J and J+1. The calculations were carried out by a computer programme and the result was

$$M_{73} = \rho\, V_{73} U_{73} A_{73} = 6.4 \text{ N}$$

(iv) $M_{74} = \rho\, V_{74} U_{74} A_{74}$

This momentum flux, as sketched in **Fig(6.42)**, acts as well tangentially at the limits of the outer bank of the bend. The procedure followed in its calculation was similar to the one made for M_{73}. The result obtained was

$M_{74} = \rho\, V_{74} U_{74} A_{74} = 10.8$ N

(v) Calculation of the Force Produced by the Acceleration $2\frac{UV}{r}\rho$:

A procedure similar to one used for the inbank case was used and the result was

$2 \frac{UV}{r} \rho$ Vol. = 9.2 N

(vi) Calculation of the Boundary Shear Force from Boundary Shear Stress Measurements:

BSF_7 = 1.1 N

(vii) Calculation of Pressure Force:

PF_{71} = 107.8 N ; PF_{72} = 102.4 N

(viii) Calculation of the Body Weight Force:

The body weight force between the channel bottom and stage 140.0 mm is -6.94 N as discussed in section 6.4.7.

The body weight force between the stage 140.0 mm and stage 200.0 mm is therefore:

$(2.87 * 1.2 * 0.06) * 0.996*10^{-3}* 10^4/1.37 = 1.77$ N

Total Body Weight Force: -6.94 + 1.77 = -5.17 N

(ix) The momentum equation applied in Block 7 is:

$M_{72} - M_{71} + M_{74} - M_{73} + 2 \rho \frac{U V}{r}$ Vol. = $BW_7 - BSF_7 + PF_{71} - PF_{72} + ASF_S$

12.1 - 25.1 + 10.8 - 6.4 + 9.2 = -5.17 - 1.1 + 107.8 - 102.4 + ASF_S

+0.6 = -0.87 + ASF_S

ASF_S = +1.47 N, which is the resulting apparent shear force for Block 7.

(x) Similarly the momentum equation applied to Block 8 is:

$M_{82} - M_{81} + M_{84} - M_{83} = BW_8 - BSF_8 + ASF_S$

12.6 - 12.1 + 12.1 - 5.7 = 2.5 - 0.8 + ASF_S

6.9 = 1.7 + ASF_S

ASF_S = 5.2 N

which is the apparent shear force for Block 8. **Fig(6.42)** shows the apparent shear force in the cross-over region and is basically the lateral shear force produced by the Reynolds shear stress τ_{SN} projected in the S direction and integrated along the vertical plan. An identical result should be achieved if the apparent shear force, computed in X direction and in Y direction,

on Blocks 2 and 5 of the floodplain, was projected in the s direction. In order to project in S direction the apparent shear force obtained in X direction should be multiplied by COS $60^0$and the apparent shear force in Y direction should be multiplied by COS 30^0.

$-2.2 \cos 60^0$	$+1.8 \cos 30^0$
$+5.3 \cos 60^0$	$+2.3 \cos 30^0$
+1.55 N	+3.5 N

This gives a total apparent shear force for the floodplains of 5.05 N, which when compared with 5.2 N of the main channel calculation shows very good agreement.

(xi) The momentum equation applied to Block 9 is:

$$M_{92} - M_{91} + M_{94} - M_{93} - 2\rho \frac{U\,V}{r} \text{Vol.} = BW_9 - BSF_9 + PF_{91} - PF_{92} + ASF_s$$

$$+ 25.1 - 12.1 + 7.3 - 11.0 - 9.2 = 9.97 - 1.0 + 102.4 - 107.8 + ASF_s$$

$$+0.1 = +3.57 + ASF_s$$

$$ASF_s = -3.47 \text{ N}$$

The residual error obtained in cross-over region(block 8) for the overbank cases is very small. Therefore it can be said that the momentum equation was closed and the simplifications considered by the Author in the momentum equation were correct.

6.4.9. Summary of Apparent Shear Force in the Main Channel Region only.

All the results of the apparent shear force in the s direction for the main channel region only, with sinuosity 1.374, are presented in **Table (6.3)** for stages 140.0 mm, 165.0 mm and 200.0 mm. The apparent shear force for stage 140.0 mm is the body weight component while for stages 165.0 mm and 200.0 mm, the apparent shear force includes the lateral shear force and the term $2(\overline{u'v'})/\pi$ for Blocks 7 and 9, and the lateral shear force only for Block No. 8. More precise details are shown in **Appendix VI**.

The results from **Appendix VI** and **Table (6.3)** reveal:

(a) Comparing Blocks 7 and 9 for overbank flow it appears that both bend regions have similar magnitudes of apparent shear force but in opposite directions. For Block 7 just downstream of each bend apex, the momentum transfer is positive indicating transfer from the floodplain to the main channel. For Block 9, just before each bend apex the opposite is the case with momentum transfer to the floodplain.

(b) The apparent shear force in the cross-over region is the lateral shear force, which acts on both sides of the element, shown in **Fig(6.42)**. This lateral shear force is produced by turbulence($\overline{u'v'}$) and corresponds to the lateral Reynolds shear stress τ_{SN}, when integrated along the vertical plan. **Table(6.3)** shows that the balance of the lateral shear force is positive and increases significantly with depth. For 20% rise in depth, the lateral shear force increases 8.3 times. This represents a momentum transfer from the floodplain to the main channel in the cross-over region.

It is also interesting in view of the very close agreement of floodplain apparent shear forces resolved in the s direction, at least at the cross-over region, to further develop this theme. That is, to take all various geometries presented in **Table (6.2)**, and to compute s direction components, as a likely measure of main channel apparent shear forces for a range of geometries.

The apparent shear force in X and Y directions obtained in Blocks 2 and 5 of the floodplain region of the meandering channel, with sinuosity 1.37 were converted into apparent shear force in the s direction through the following relationship:

$$ASF_S = ASF_X * COS\ 60^0 - ASF_Y * COS\ 30^0$$

Table(6.4) lists all the results obtained. This table shows that:

- The lateral shear force on the downstream main channel/floodplain(block 5) is always negative, increases with depth, is smaller with natural cross-section compared with trapezoidal cross-section; reduces with the change of the floodplain roughness from smooth to the fully roughened case. For

instance comparing the results obtained for stage 200.0 mm and the apparent shear force in the natural cross section with smooth floodplains is significantly less than the trapezoidal section with smooth floodplains. Again at stage 200.0 mm the natural section with fully roughened floodplains is 32% smaller than the natural smooth case.

- In all cases the apparent shear force for Block 5 is negative which means a strong transfer of momentum into the main channel at that point.
- The lateral shear force in left floodplain(block 2) does not show a very consistent pattern. However it is smaller than the lateral shear of the other bank and in most cases tends to be positive, indicating momentum transfer to the floodplain at that point.

The results from **Table(6.4)** are plotted in **Fig(6.42a)** showing the differences between the upstream(Block 2) and downstream (Block 5) sides of the main channel cross-over region.

In order to compare these results with those obtained by **Elliot and Sellin(1990)** in the S.E.R.C. Series A tests, in a skewed compound channel, the **Author's** results of the lateral shear force in the S-direction of blocks 2 and 5 of the floodplain were non-dimensionalised by the body weight component in the S-direction. The values obtained are also presented in **Table(6.4)**, as $ASFS_2/BWS_2$.

Elliot and Sellin(1990) carried out experiments in a skewed compound channel with the main channel skewed 5^0 and 9^0 to the floodplain direction. A schematic diagram of their flume geometry is presented in **Fig(6.43)**. They also applied the momentum equation, in X direction, in the sub-volumes II and III of the skew channel and determined the lateral shear force at the interface between the main channel and the floodplain. This is equivalent to the apparent shear force at the edge of Blocks 2 and 5, in this work.

In order to compare with the **Author's** results, the lateral shear force obtained by **Elliot and Sellin(1990)** was also

non-dimensionalised by the body weight component. **Elliot and Sellin(1990)** results are presented in **Table(6.5)**, for both skew angles.

Both sets of data are plotted in **Fig(6.44)**, for Block 2 and **Fig(6.45)**, for Block 5. Blocks 2 and 5 of the meandering compound channel correspond to sub-volumes III and II of the **Elliot and Sellin(1990)** skewed case. **Fig(6.44)** and **Fig(6.45)** show that the lateral shear force in Block 2 and sub-volume III (both on the left/upstream side of the main channel) is smaller than those obtained in block 5 and sub-volume II, the right downstream side of the main channel. **Fig(6.45)** shows that the non-dimensional lateral shear force becomes negative and increases substantially as the cross-over angle changes from 5^{o}, 9^{o} and 60^{o}, going from the Series A to the Series B case. The lateral shear force in block 5 and sub-volume II(on the right/downstream side of the main channel) is produced by the effect of flow contraction and acceleration as the main channel flow enters the downstream floodplain, where the flow depth reduces considerably, like a weir flow, and simultaneously the flow is accelerated. This phenomenon becomes more intense as the skew angle increases.

The flow mechanism that generates this negative lateral shear force, at the vertical interface in skewed and meandering compound flows, is totally different to the positive one that produces lateral shear force in straight compound channels. As mentioned in **Chapter** 2, in straight compound channels, the lateral shear force is produced by the velocity gradient that develops between the main channel and the floodplain.

6.5 CONCLUSIONS

By using a two-dimensional approach, the continuity equation, energy equation and momentum equations were applied to meandering compound channels. From this analysis, the main conclusions were as follows:

Continuity Equation:

- The analysis of discharge distribution in meandering compound channels carried out in the S.E.R.C. flume Series B has shown that mass exchange between the main channel flow and the floodplain flow is highly three-dimensional and is affected by flow depth, boundary roughness, sinuosity, and main channel cross-section shape.
- As the stage increases, the basic orientation of the flow changes from the main channel direction to the longitudinal direction. More main channel flow is diverted longitudinally, and the percentage of flow moving in the main channel streamwise direction reduces.
- As the floodplain roughness changes to the fully roughened case, discharges reduces in both main channel and floodplain regions. Comparing the smooth and the fully roughened cases of sinuosity 1.37 with natural cross-section, the results show that for stage 165.0 mm no discharge reduction occurred in the main channel but for stages 200.0 mm and 250.0 mm a discharge reduction of 35% and 50% was observed in the main channel.
- The effect of sinuosity in the conveyance of meandering compound channels is more pronounced in the case of smooth floodplains. Comparing the effect of increasing sinuosity from 1.37 to 2.04 with smooth floodplains and natural cross-section, the total discharge for stage 200.0 mm is reduced from 222.0 l/s to 183.0 l/s, a reduction of 20%.
- The main channel cross-section affects also the conveyance of meandering compound channels. The tests carried out in the S.E.R.C. flume has shown that a natural cross-section presents a greater hydraulic efficiency in conveyance than a trapezoidal cross-section. This corroborates the findings of **Willets and Hardwick(1990)**.
- The main channel discharge reduces from bend apex to start of the cross-over and increases in symmetrical fashion from the end of cross-over region to the next bend.
- The discharge held in the main channel below bankfull is significantly lower than the discharge held in the main channel with no overbank flows. This is clearly a measure of the

interaction effect as it affects the flow below bankfull. This effect increases significantly with sinuosity.
- The cross-section area of the meandering compound channel was divided into three Zones and the actual discharge of each zone was compared with the theoretical discharge that will occur in a straight channel with same boundary roughness, area and bed slope. The results show that

(i) the discharge outside the meander belt width (Zone 3) is approximately equal to the theoretical discharge, from skin friction.

(ii) the discharge within the meander belt and above bankfull(Zone2) is less than the theoretical discharge, by 15%-25%.

(iii) the discharge in the main channel but below bankfull (Zone 1) is much smaller than the theoretical value. For instance, for trapezoidal cross-section with sinuosity 1.37, smooth floodplains and stage 200.0 mm, the reduction reaches 40%.

Energy Equation

- A trapezoidal cross-section with smooth floodplains increases the contour levels of energy on the right downstream floodplain compared with a natural cross-section. As the stage rises, this effect diminishes.
- The highest energy levels for overbank flow are found at the cross-over region on the edge of the downstream floodplain and also outside the meander belt width.
- For stage 165.0 mm, the pattern of energy levels contours(in the main channel region for both sinuosities), is not affected much by the floodplain roughness.
- Energy levels in the main channel and floodplain region diminish with increasing sinuosity and floodplain roughness. For instance an increase of sinuosity 1.37 to 2.04, the maximum energy level in the main channel reduces from 208.0 mm to 204.0

mm.

Momentum Equation Applied to Meandering Channel with Sinuosity 1.37.

- The momentum equation applied in the X-direction in the floodplain region has shown that:

. In the upstream floodplain region(blocks Nos. 1, 2 and 3) the body weight component is practically in balance with the boundary shear force, whereas in the downstream floodplain (blocks Nos. 4, 5 and 6), the body weight component was slightly smaller than the boundary shear force.

. The maximum values of the apparent shear force are located, near the cross-over region, in block Nos. 5 and 6, indicating areas of greatest out of balance forces.

. Although the apparent shear force in the x direction reduces with floodplain roughness and increases with stage, no apparent trend with stage was discernible.

. The two-dimensional force-momentum equation in this work is not satisfactory for highly three-dimensional compound flows. The force-momentum equation can only be applied accurately if the boundary shear stress is known as well as local velocities, local flow depths, body weight and the turbulence components. Hence, these complex flows can only be modelled by three-dimensional models with the turbulence terms modelled.

- The momentum equation applied in Y direction in the floodplain region has shown that:

. Again there are no real patterns of variation of apparent shear force in the y direction with stage. Hence there is no way to predict systematically the apparent shear force in the y direction.

. Blocks 2 and 5 give high values of apparent shear force for all geometries.

- The momentum equation applied in the main channel region has shown that:

. In cross-over region, there is a close agreement of floodplain apparent shear forces resolved in the S direction with those of the main channel in the S direction.
. The balance of the lateral shear force in the cross-over region in the S direction is produced by the turbulence term ($\overline{u'v'}$) and is positive for Block 8 which represents a momentum transfer from the floodplain to the main channel.

- Comparison between the **Author's** results with **Elliot and Sellin(1990)** findings showed that the apparent shear force which develops at the interface of the cross-over region with the downstream floodplain(where flow is accelerating)and increases substantially with the skew angle. For instance as the skew angle increases from 9^0 to 60^0, the ratio of lateral shear force/body weight increases from 0.5 to about 5.0, for stage 250.0 mm with trapezoidal cross-section and smooth floodplains. This phenomenon becomes less pronounced if the aspect ratio increases.
- In skew and in meandering channels with overbank flow, the apparent shear force that develops at the interface of the cross-over region with the downstream floodplain is produced by the flow contraction phenomenon, which accelerates. Whereas in straight compound channels, the flow mechanism that generates the lateral shear force is the large velocity gradient, between the higher velocities at the main channel that is deeper and smaller velocities on the floodplain that is shallower.

TABLE 6.1

ANALYSIS OF VERTICAL DISCHARGE AT BANKFULL LEVEL OF THE MEANDERING CHANNELS OF S.E.R.C. FLUME SERIES B

SINUOSITY	CROSS-SECTION TYPE	FLOODPLAIN ROUGHNESS	STAGE mm	MAIN CHANNEL DISCHARGE BELOW BANKFULL IN l/s		VERTICAL DISCHARGE IN l/s
				BEND APEX	CROSS-OVER	
1.374	TRAPEZOIDAL	SMOOTH	200.0	61.0	51.0	10.0
1.374	TRAPEZOIDAL	SMOOTH	250.0	71.0	60.0	11.0
1.374	NATURAL	SMOOTH	165.0	28.5	26.0	2.5
1.374	NATURAL	SMOOTH	200.0	31.0	26.0	5.0
1.374	NATURAL	SMOOTH	250.0	40.0	32.0	8.0
1.374	NATURAL	FULLY ROUGH.	165.0	29.0	25.0	4.0
1.374	NATURAL	FULLY ROUGH.	200.0	21.0	17.0	3.0
1.374	NATURAL	FULLY ROUGH.	250.0	24.0	15.0	9.0
2.04	NATURAL	SMOOTH	165.0	18.0	14.0	4.0
2.04	NATURAL	SMOOTH	200.0	24.0	6.5	17.5
2.04	NATURAL	FULLY ROUGH.	165.0	18.0	13.0	5.0
2.04	NATURAL	FULLY ROUGH.	200.0	17.0	6.5	10.5

TABLE 6.2

APPARENT SHEAR FORCE IN X AND Y DIRECTIONS IN THE FLOODPLAIN

S.E.R.C. SERIES B SINUOSITY 1.37

CROSS-SECTION TYPE	FLOODPLAIN ROUGHNESS	STAGE mm	BLOCK 1 UNITS: NEWTONS		BLOCK 2 UNITS: NEWTONS		BLOCK 3 UNITS: NEWTONS		BLOCK 4 UNITS: NEWTONS		BLOCK 5 UNITS: NEWTONS		BLOCK 6 UNITS: NEWTONS	
			ASFX1	ASFY1	ASFX2	ASFY2	ASFX3	ASFY3	ASFX4	ASFY4	ASFX5	ASFY5	ASFX6	ASFY6
TRAPEZOIDAL	SMOOTH	200.0	-5.5	+1.0	+1.4	+0.2	+2.4	+0.3	+0.9	-1.7	-7.9	+3.9	-2.0	+1.6
TRAPEZOIDAL	SMOOTH	250.0	-6.4	+0.4	+0.7	-3.4	-1.3	-0.6	+2.3	-4.0	-9.4	+5.1	-5.5	+3.0
NATURAL	SMOOTH	165.0	-0.5	+0.8	-0.3	-0.4	-0.57	-0.6	+0.82	+1.3	-1.07	+1.0	-0.5	+0.46
NATURAL	SMOOTH	200.0	-3.8 (-0.8)	+0.3	-0.5 (+2.2)	+1.8	+0.7 (+1.0)	-0.3	-0.2 (-2.7)	-0.9	-3.6 (-5.3)	+2.3	-1.2 (-5.5)	+1.2
NATURAL	SMOOTH	250.0	-0.6	-1.7	+1.6	-4.8	-1.5	-0.8	-4.6	+0.2	-7.8	+7.8	-2.5	+2.9
NATURAL	FULLY ROUGH.	165.0	-0.3	+0.11	+0.3	-0.3	+0.52	-0.4	-0.25	+1.2	-0.98	+1.0	+0.2	+0.10
NATURAL	FULLY ROUGH.	200.0	-2.4	+0.4	-2.4	-0.8	+1.2	-0.8	+0.10	+2.4	+1.5	+4.5	-0.1	+1.0
NATURAL	FULLY ROUGH.	250.0	-1.7	-0.6	+0.3	-1.8	-2.2	-0.9	+1.1	+3.5	+1.7	+5.7	+0.2	+2.0

THE VALUES BETWEEN BRACKETS ARE THE APPARENT SHEAR FORCE IN X DIRECTION WITH THE EFFECT OF PRESSURE FORCE

Table(6.3)

Apparent Shear Force in S Direction in the Meandering Channel. S.E.R.C. Series B. Sinuosity 1.37. Smooth Floodplains.

Apparent Shear Force in S direction in Newtons

Stage	Block No.7	Block No.8	Block No.9
mm	$ASFS_7$	$ASFS_8$	$ASFS_9$
140.0	-6.94	+1.27	+8.1
165.0	+3.11	+0.63	-1.3
200.0	+1.47	+5.2	-3.47

TABLE 6.4

APPARENT SHEAR FORCE IN S DIRECTION IN BLOCKS Nos. 2 AND 5 OF THE FLOODPLAIN
S.E.R.C. SERIES B SINUOSITY 1.37

CROSS-SECTION TYPE	FLOODPLAIN ROUGHNESS	STAGE mm	$ASFS_2$ NEWTONS	BWS_2 NEWTONS	$\frac{ASFS_2}{BWS_2}$	$ASFS_5$ NEWTONS	BWS_5 NEWTONS	$\frac{ASFS_5}{BWS_5}$
TRAPEZOIDAL	SMOOTH	200.0	+0.33	1.42	+0.23	-6.98	1.42	-4.9
TRAPEZOIDAL	SMOOTH	250.0	+3.04	2.8	+1.1	-8.7	2.8	-3.7
NATURAL	SMOOTH	165.0	+0.20	0.45	+0.44	-1.4	0.45	-3.1
NATURAL	SMOOTH	200.0	-0.46	1.42	-0.32	-4.64	1.42	-3.27
NATURAL	SMOOTH	250.0	+4.8	2.8	+1.7	-10.2	2.8	-3.64
NATURAL	FULLY ROUGH.	165.0	+0.41	0.45	+0.91	-1.36	0.45	-3.0
NATURAL	FULLY ROUGH.	200.0	-0.51	1.42	-0.36	-3.15	1.42	-2.2
NATURAL	FULLY ROUGH.	250.0	+1.0	2.8	+0.36	-4.1	2.8	-1.46

TABLE 6.5

APPARENT SHEAR FORCE IN X DIRECTION IN THE SUB-VOLUMES II AND III OF THE FLOODPLAIN. S.E.R.C. SERIES A. SKEW CHANNEL. (FROM ELLIOT AND SELLIN (1990))

SKEW ANGLE : 5 DEGREES

FLOODPLAIN DEPTH mm	STAGE mm	$ASFS_{II}$ NEWTONS	BWS_{II} NEWTONS	$\frac{ASFS_{II}}{BWS_{II}}$	$ASFS_{III}$ NEWTONS	BWS_{III} NEWTONS	$\frac{ASFS_{III}}{BWS_{III}}$
50.0	200.0	+4.75	11.1	+0.43	+2.1	8.3	+0.25
100.0	250.0	-0.56	22.4	-0.025	-2.4	16.9	-0.14
150.0	300.0	+12.65	34.0	+0.37	-6.03	25.73	-0.23

SKEW ANGLE: 9 DEGREES

FLOODPLAIN DEPTH mm	STAGE mm	$ASFS_{II}$ NEWTONS	BWS_{II} NEWTONS	$\frac{ASFS_{II}}{BWS_{II}}$	$ASFS_{III}$ NEWTONS	BWS_{III} NEWTONS	$\frac{ASFS_{III}}{BWS_{III}}$
50.0	200.0	+1.14	6.98	+0.16	+3.11	10.47	+0.30
100.0	250.0	-5.06	14.2	-0.356	+4.67	21.17	+0.22
150.0	300.0	-10.92	21.63	-0.5	+4.92	32.1	+0.15

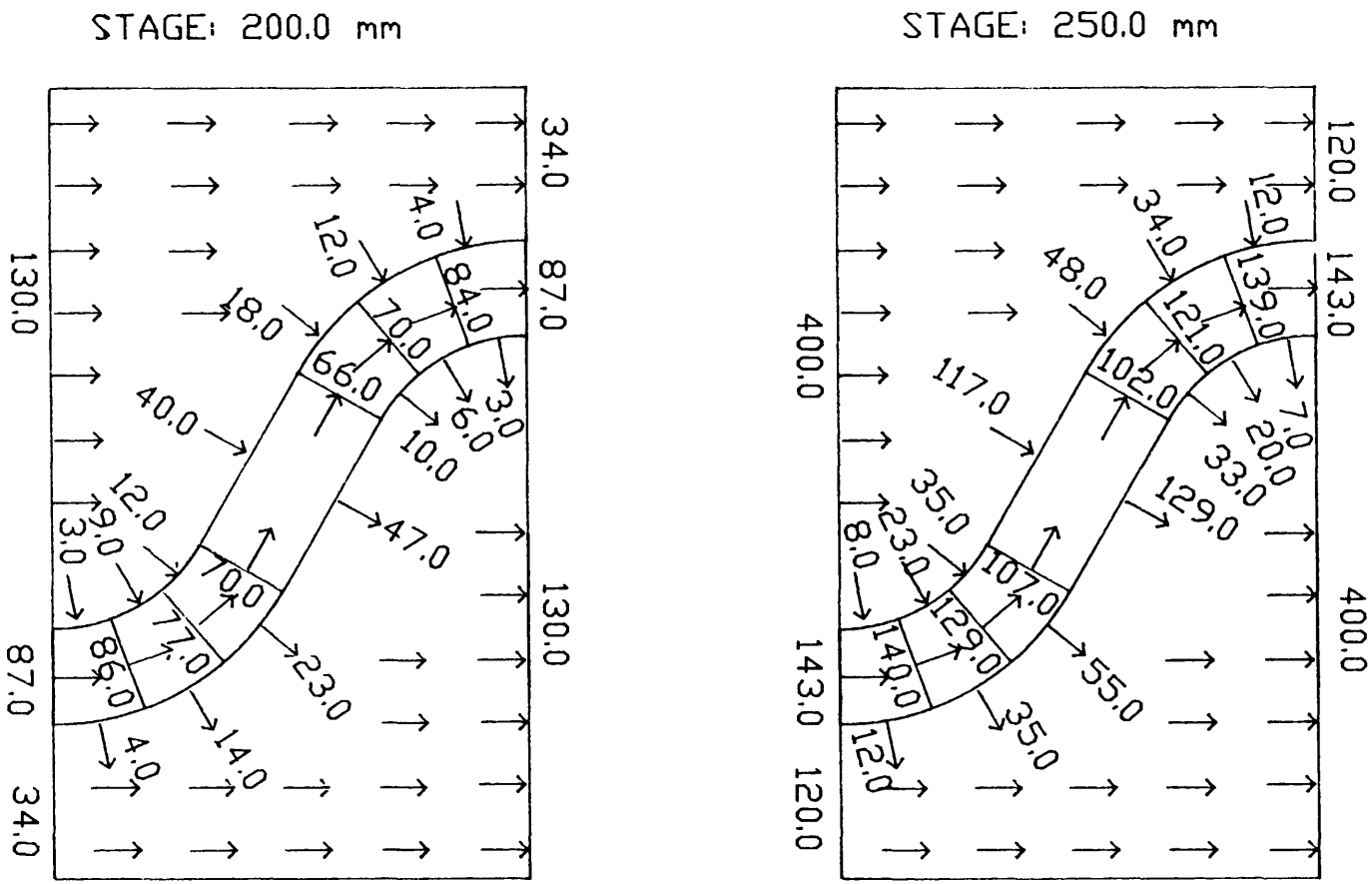

Fig 6.1 - DISCHARGE DISTRIBUTION. S.E.R.C. SERIES B. SINUOSITY 1.37. MAIN CHANNEL WITH TRAPEZOIDAL CROSS-SECTION. SMOOTH FLOODPLAINS. DISCHARGE IN l/s

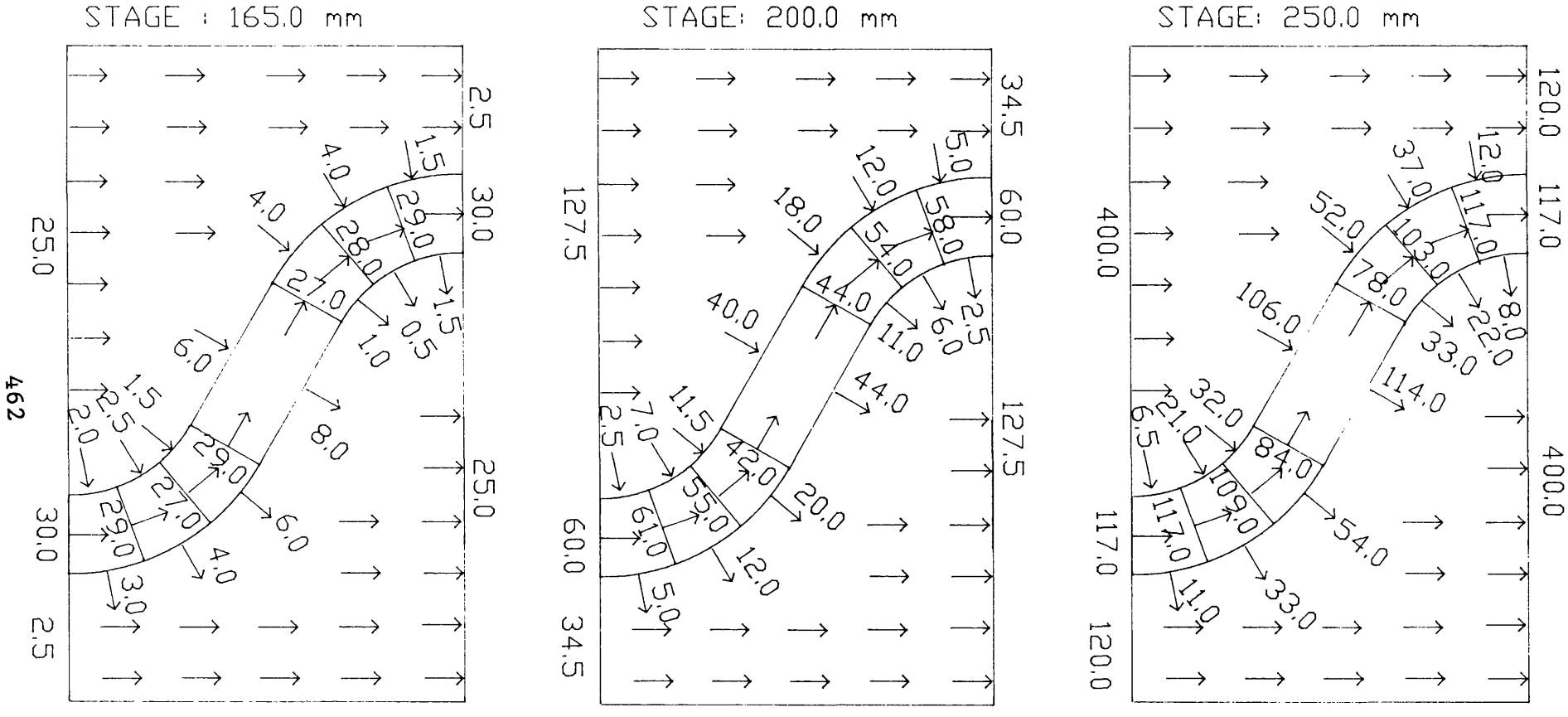

FIG 6.2 - DISCHARGE DISTRIBUTION. S.E.R.C. SERIES B SINUOSITY 1.37. MAIN CHANNEL WITH NATURAL CROSS-SECTION. SMOOTH FLOODPLAINS. DISCHARGE IN l/s

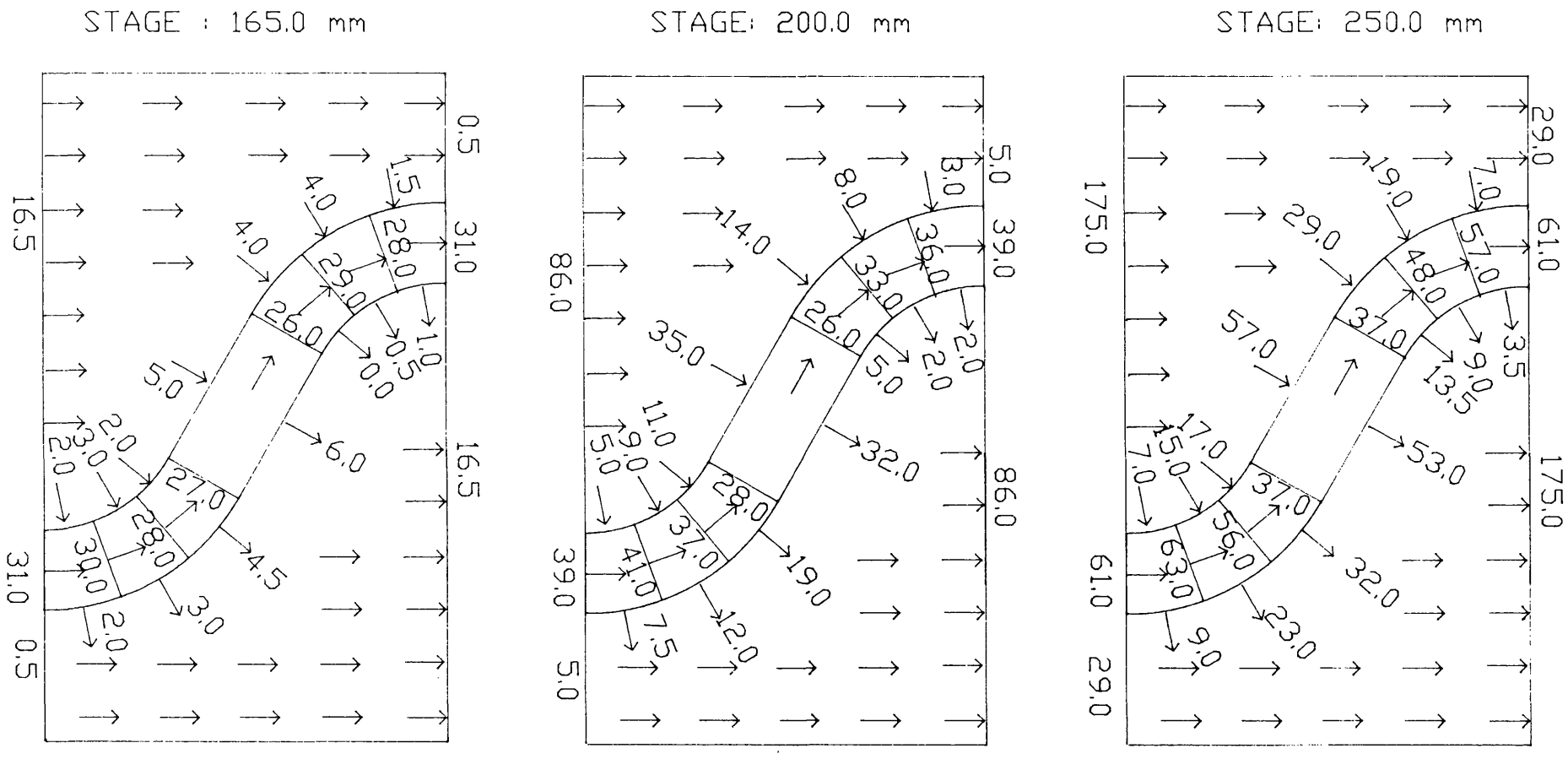

Fig. 6.3 - DISCHARGE DISTRIBUTION. S.E.R.C. SERIES B. SINUOSITY 1.37.
MAIN CHANNEL WITH NATURAL CROSS-SECTION. FULLY ROUGHENED FLOODPLAIN.
DISCHARGE IN l/s

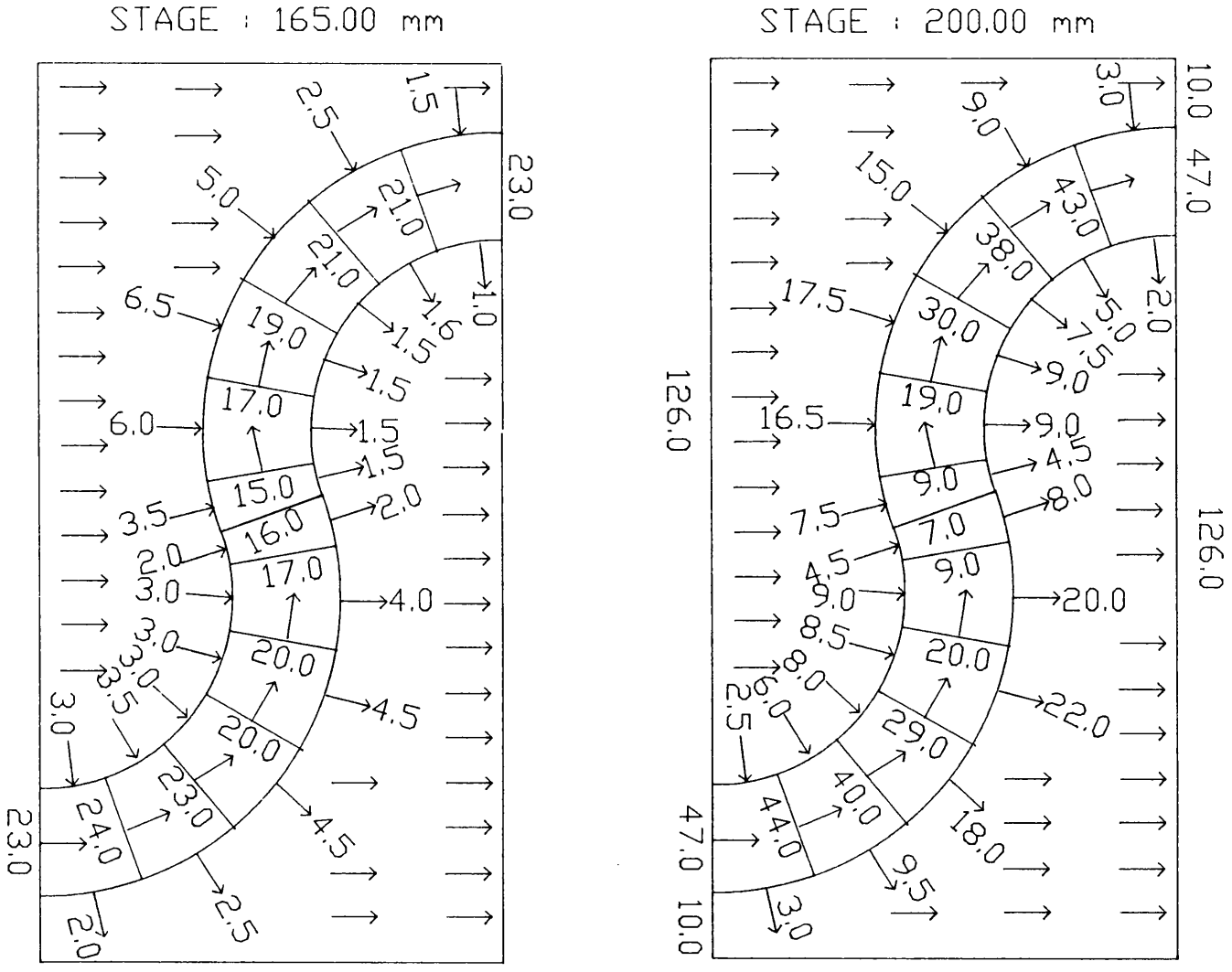

Fig. 6.4 - DISCHARGE DISTRIBUTION. S.E.R.C. SERIES B. SINUOSITY 2.04. MAIN CHANNEL WITH NATURAL CROSS-SECTION. SMOOTH FLOODPLAINS. DISCHARGE IN l/s.

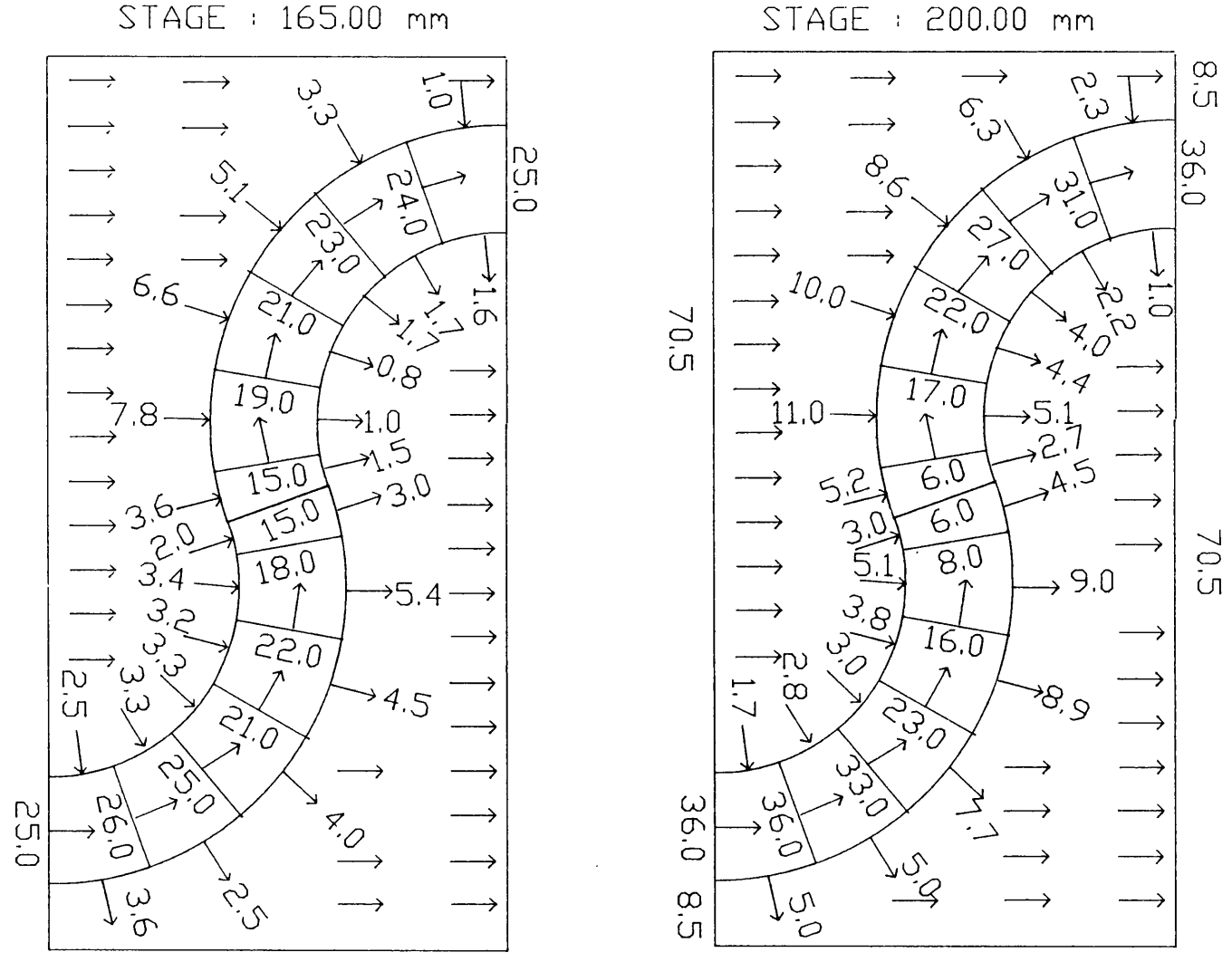

Fig. 6.5 - DISCHARGE DISTRIBUTION. S.E.R.C. SERIES B.. SINUOSITY 2.04. MAIN CHANNEL WITH NATURAL CROSS-SECTION. FULLY ROUGHENED FLOODPLAINS. DISCHARGE l/s

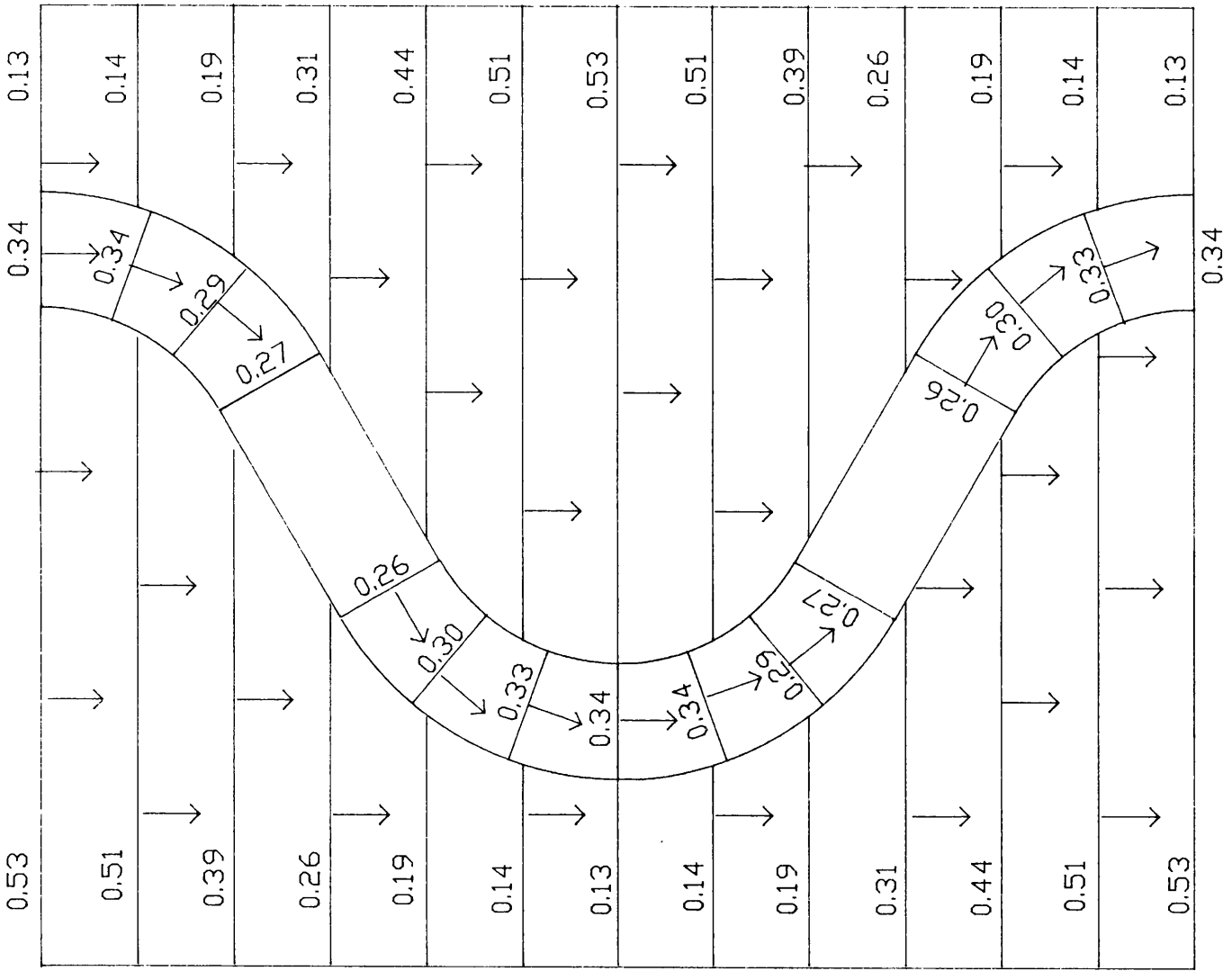

Fig. 6.6 - DISCHARGE DISTRIBUTION IN PERCENTAGE OF TOTAL DISCHARGE. S.E.R.C. SERIES B. SINUOSITY 1.37. MAIN CHANNEL WITH TRAPEZOIDAL CROSS-SECTION. SMOOTH FLOODPLAINS. STAGE 200.0 mm. Q: 251.0 l/s.

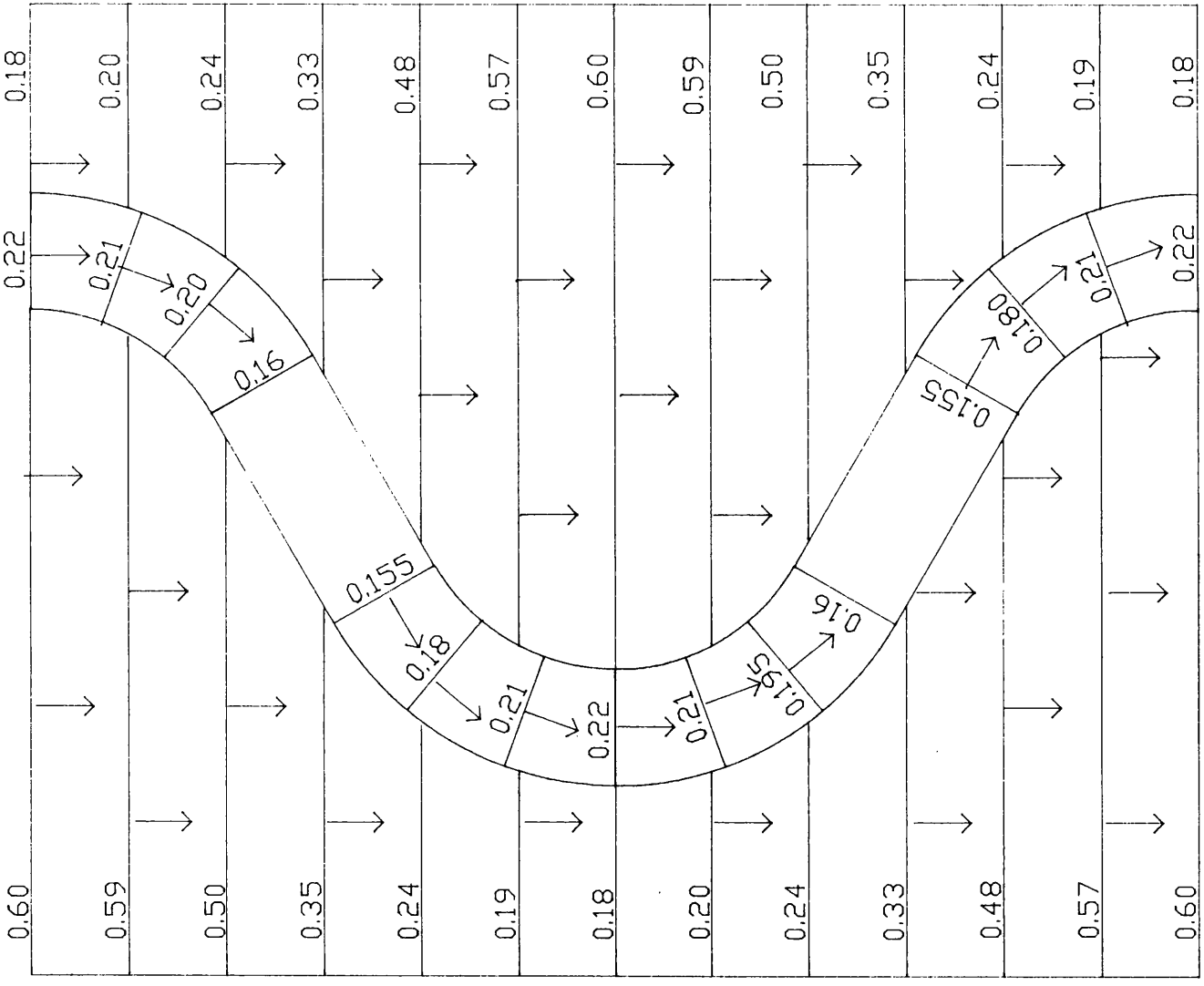

Fig 6.7 - DISCHARGE DISTRIBUTION IN PERCENTAGE OF TOTAL DISCHARGE. S.E.R.C. SERIES B. SINUOSITY 1.37. MAIN CHANNEL WITH TRAPEZOIDAL CROSS-SECTION. SMOOTH FLOODPLAINS. STAGE 250.0 mm. Q: 663.0 l/s.

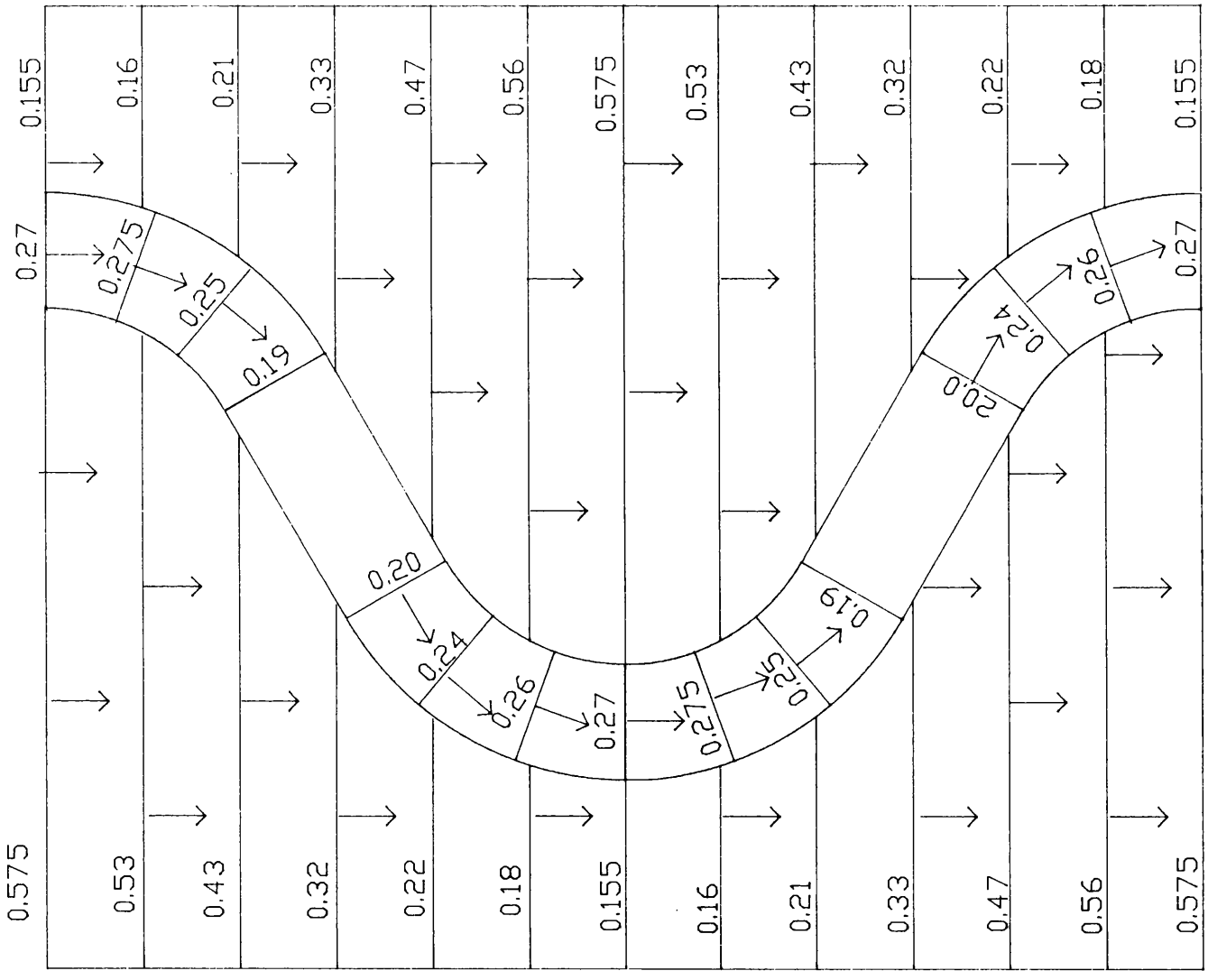

Fig. 6.8 - DISCHARGE DISTRIBUTION IN PERCENTAGE OF TOTAL DISCHARGE. S.E.R.C. SERIES B. SINUOSITY 1.37. MAIN CHANNEL WITH NATURAL CROSS-SECTION. SMOOTH FLOODPLAINS. STAGE 200.0 mm. Q: 222 l/s.

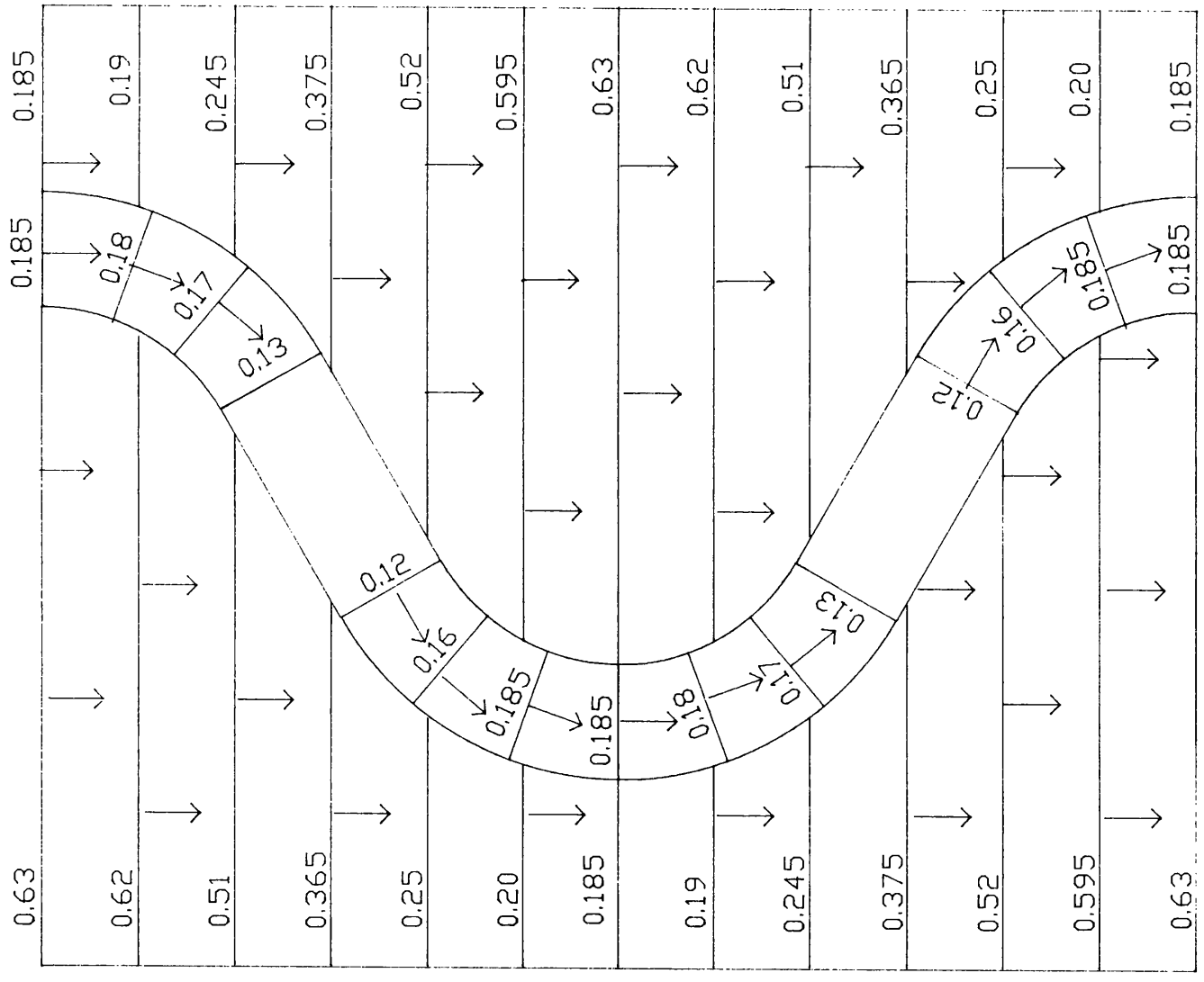

Fig. 6.9 - DISCHARGE DISSTRIBUTION IN PERCENTAGE OF TOTAL DISCHARGE. S.E.R.C. SERIES B. SINUOSITY 1.37. MAIN CHANNEL WITH NATURAL CROSS-SECTION. SMOOTH FLOODPLAINS. STAGE 250.0 mm. Q: 637.0 l/s.

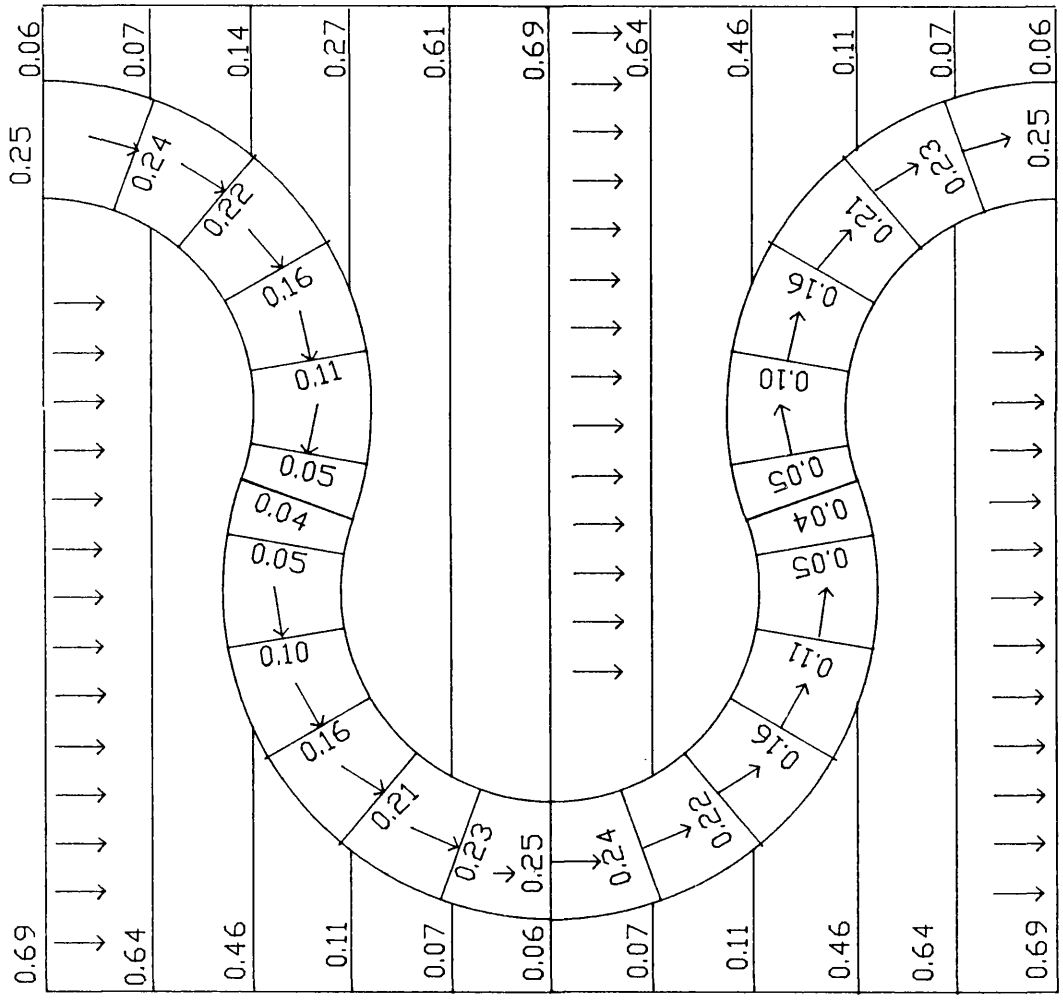

Fig. 6.10 - DISCHARGE DISTRIBUTION IN PERCENTAGE OF TOTAL DISCHARGE. S.E.R.C. SERIES B. SINUOSITY 2.04. MAIN CHANNEL WITH NATURAL CROSS-SECTION. SMOOTH FLOODPLAINS. STAGE 200.0 mm. Q: 183.0 l/s.

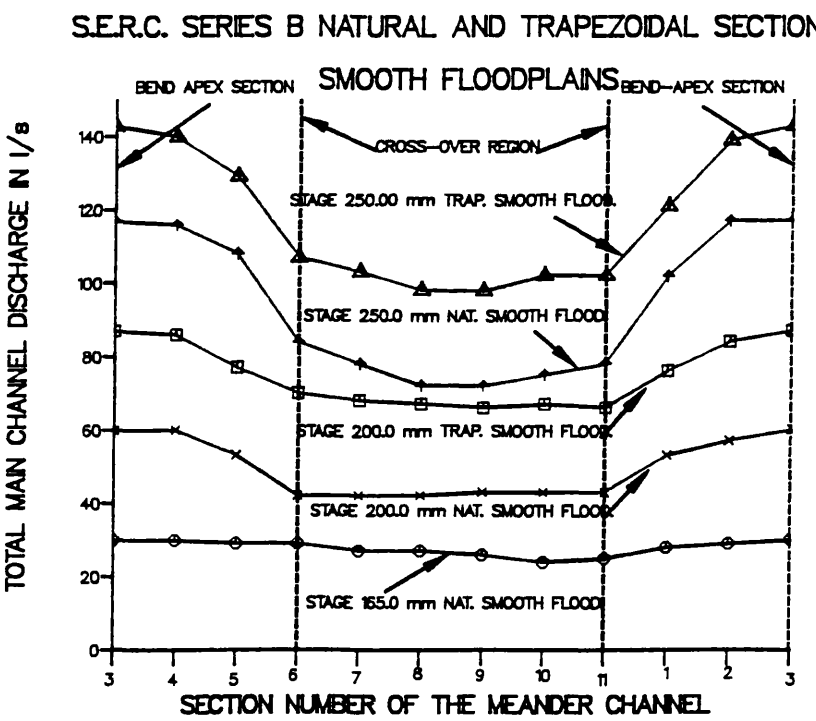

Fig (6.11) - Variation of Total Main Channel Discharge in the Streamwise Direction. S.E.R.C. Series B. Sinuosity 1.37. Trapezoidal and Natural Cross-Sections. Smooth Floodplains.

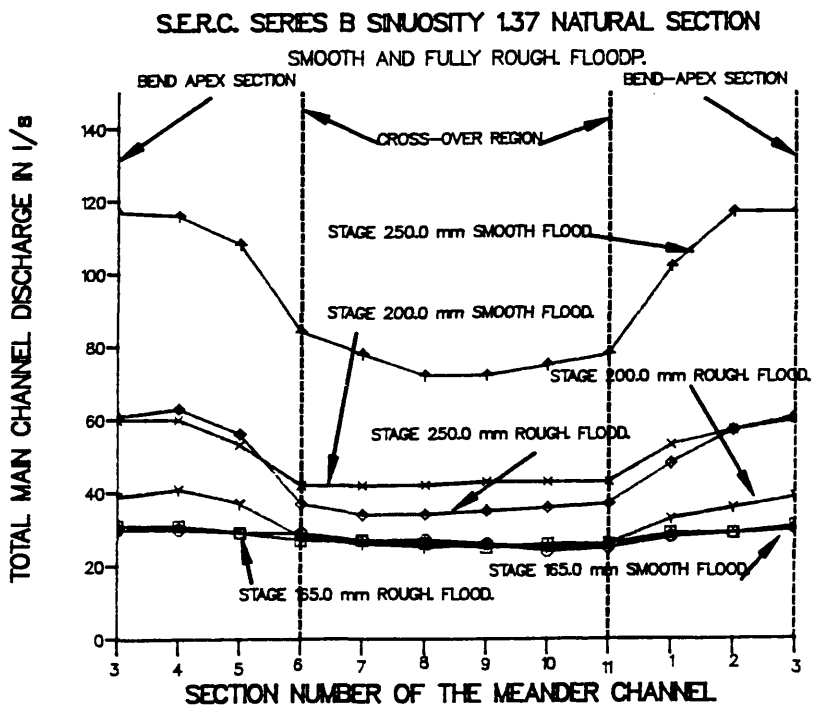

Fig (6.12) - Variation of Total Main Channel Discharge in the Streamwise Direction. S.E.R.C. Series B. Sinuosity 1.37. Natural Cross-Section. Smooth and Fully Roughened Floodplains Cases.

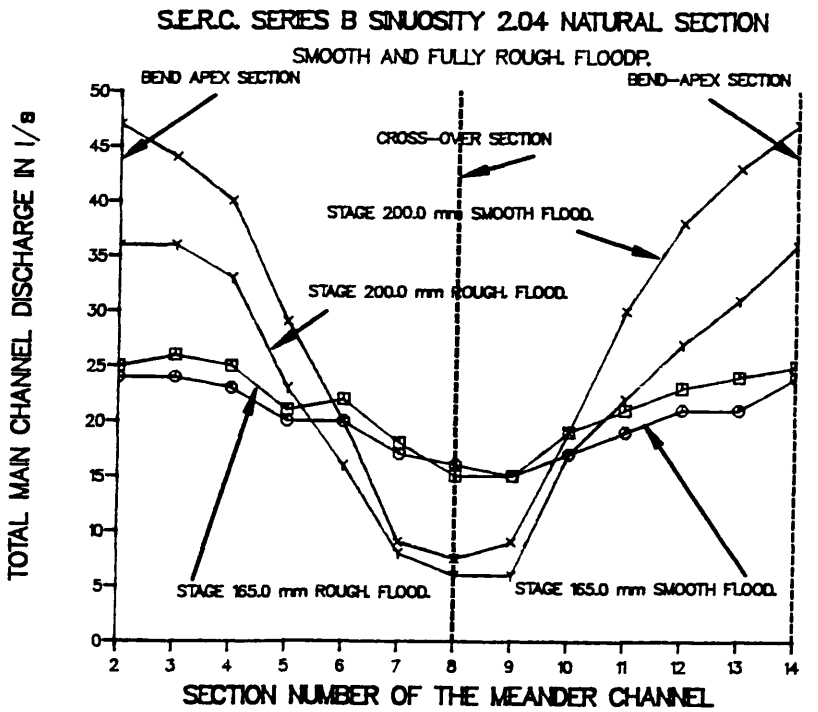

Fig (6.13) - Variation of Total Main Channel Discharge in the Streamwise Direction. S.E.R.C. Series B. Sinuosity 2.04. Natural Cross-Section. Smooth and Fully Roughened Floodplains Cases.

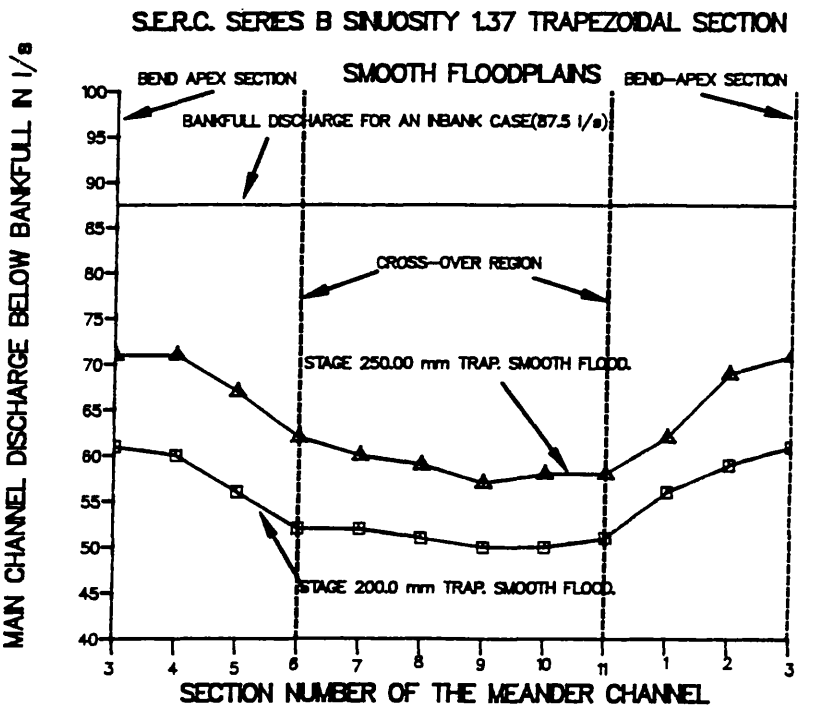

Fig (6.14) - Variation of Main Channel Discharge Below Bankfull in the Streamwise Direction. S.E.R.C. Series B. Sinuosity 1.37. Trapezoidal Cross-Section. Smooth Floodplains.

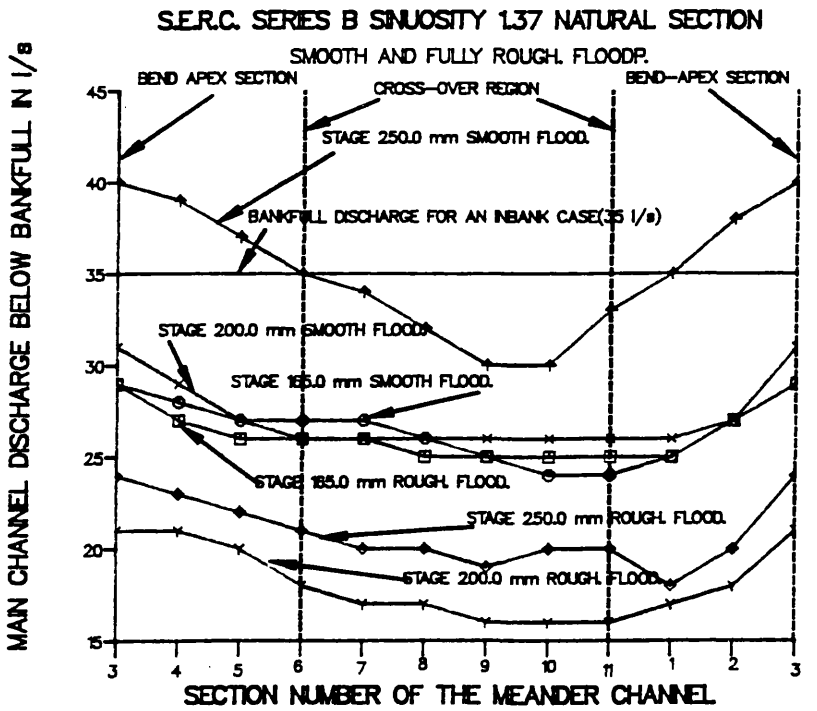

Fig (6.15) - Variation of Main Channel Discharge Below Bankfull in the Streamwise Direction. S.E.R.C. Series B. Sinuosity 1.37. Natural Cross-Section. Smooth and Fully Roughened Floodplains.

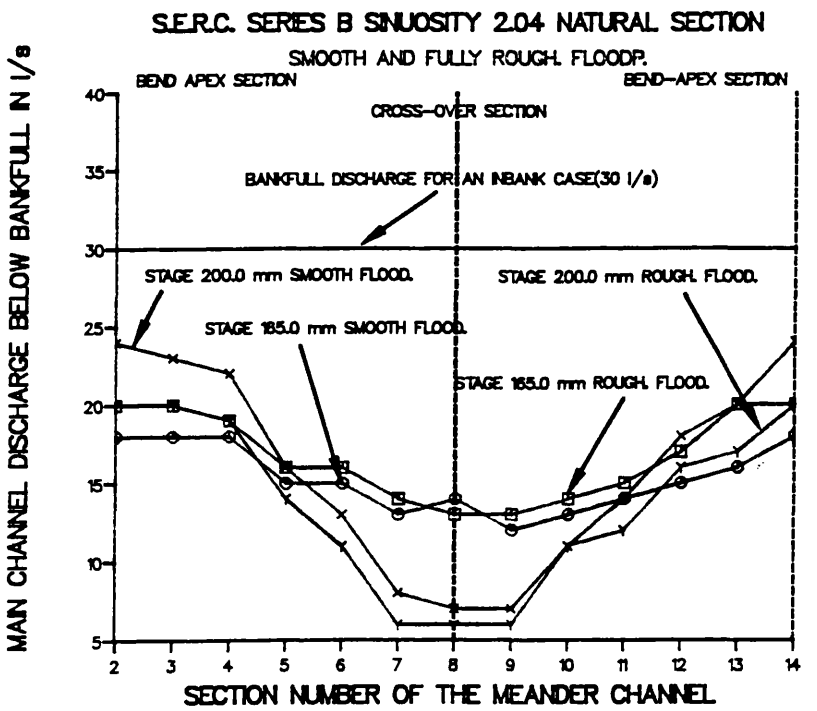

Fig (6.16) - Variation of Main Channel Discharge Below Bankfull in the Streamwise Direction. S.E.R.C. Series B. Sinuosity 2.04. Natural Cross-Section. Smooth and Fully Roughened Floodplains.

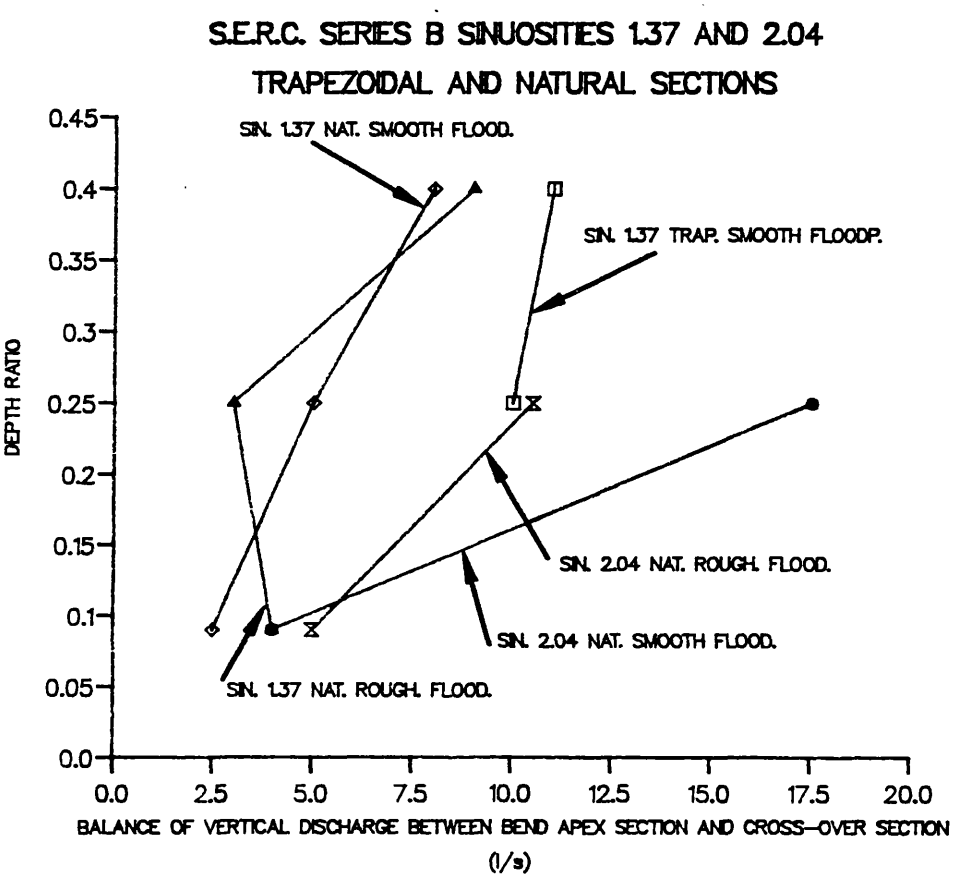

Fig (6.17) - Variation of Vertical Flow at Bankfull Level with Depth Ratio. S.E.R.C. Series B.

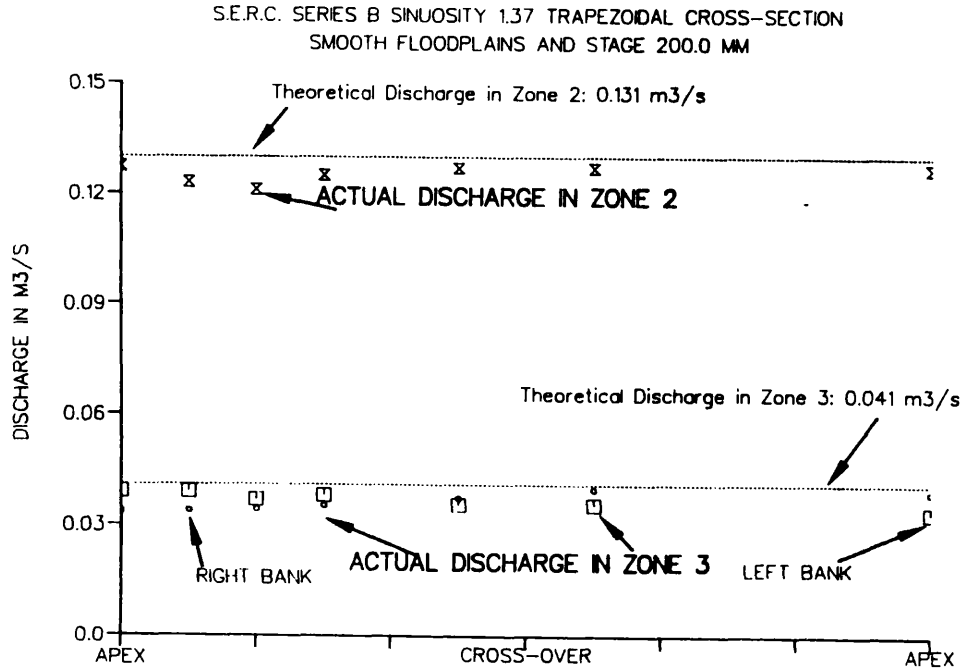

Fig (6.18a) - Actual Discharge in Zones 2 and 3 of the Meandering Channel of S.E.R.C. Flume Series B with Sinuosity 1.37, Trapezoidal Cross-Section, Smooth Floodplains and Stage 200.0 mm. Comparison with the Theoretical Discharge Produced by a Straight Channel with same Boundary Roughness, Area, and Bed Slope.

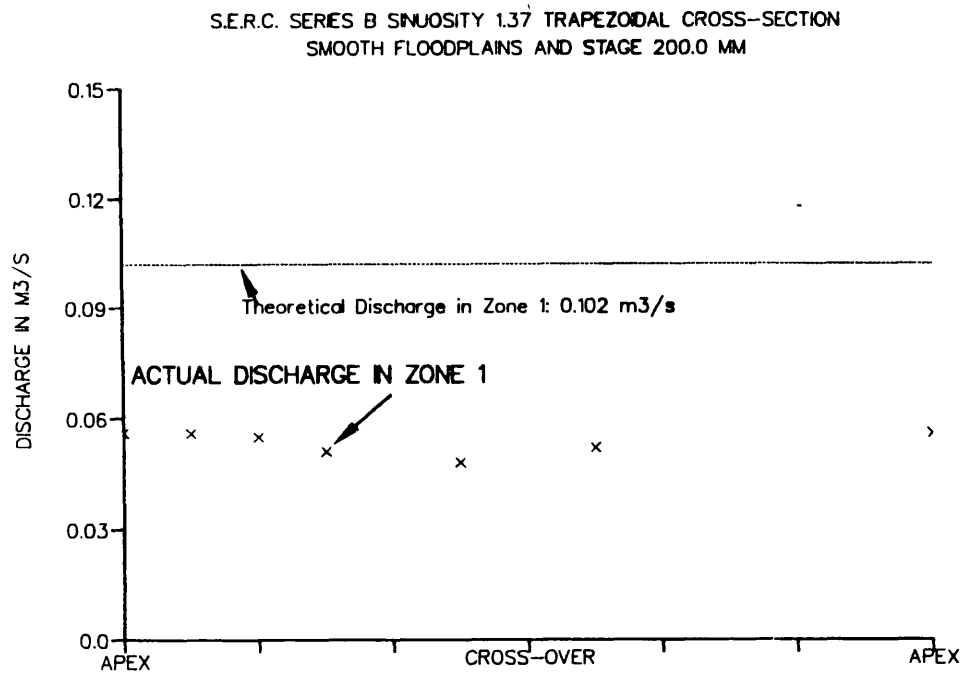

Fig (6.18b) - Actual Discharge in Zone 1 of the Meandering Channel of S.E.R.C. Flume Series B with Sinuosity 1.37, Trapezoidal Cross-Section, Smooth Floodplains and Stage 200.0 mm. Comparison with the Theoretical Discharge Produced by a Straight Channel with same Boundary Roughness, Area, and Bed Slope.

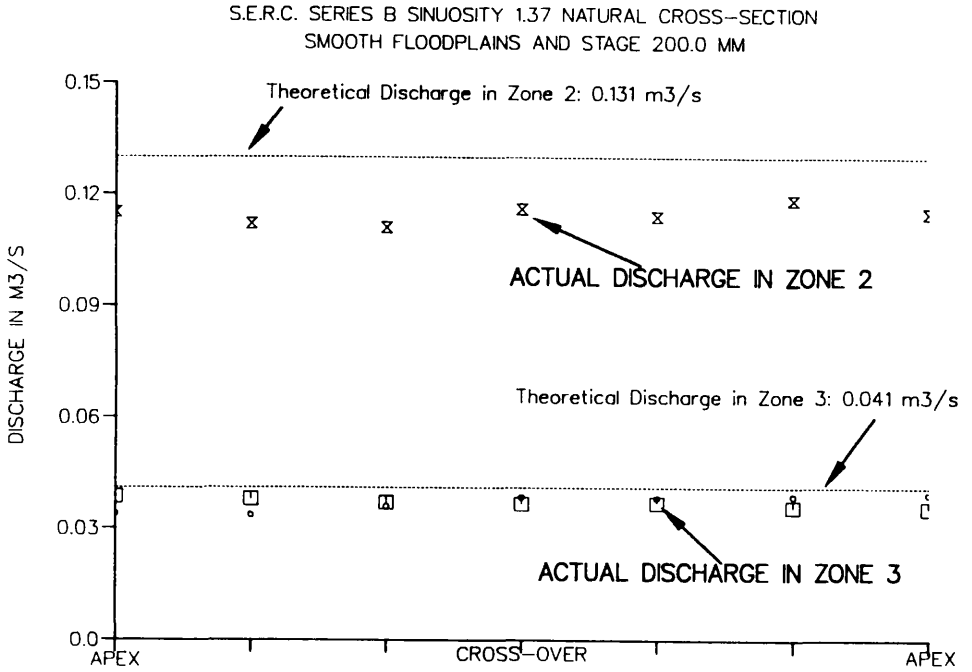

Fig (6.18c) - Actual Discharge in Zones 2 and 3 of the Meandering Channel of S.E.R.C. Flume Series B with Sinuosity 1.37, Natural Cross-Section, Smooth Floodplains and Stage 200.0 mm. Comparison with the Theoretical Discharge Produced by a Straight Channel with same Boundary Roughness, Area, and Bed Slope.

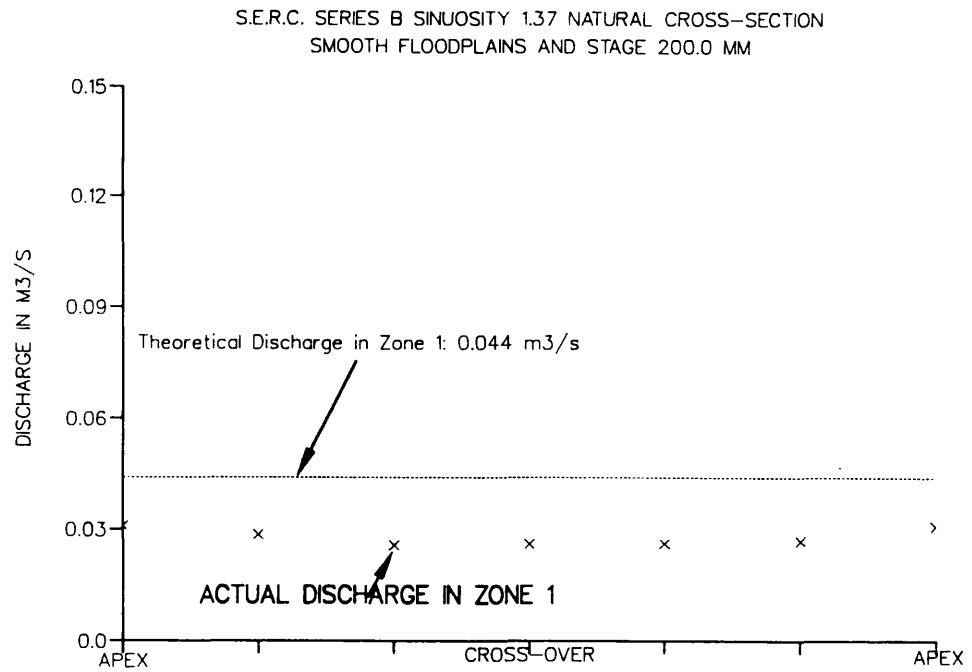

Fig (6.18d) - Actual Discharge in Zone 1 of the Meandering Channel of S.E.R.C. Flume Series B with Sinuosity 1.37, Natural Cross-Section, Smooth Floodplains and Stage 200.0 mm. Comparison with the Theoretical Discharge Produced by a Straight Channel with same Boundary Roughness, Area, and Bed Slope.

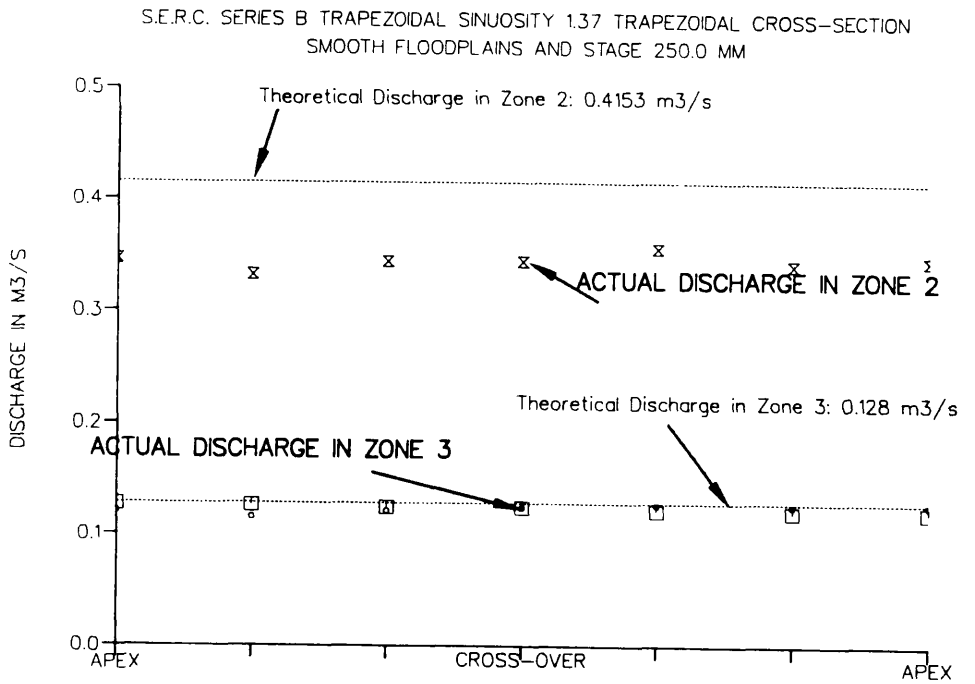

Fig (6.18e) - Actual Discharge in Zones 2 and 3 of the Meandering Channel of S.E.R.C. Flume Series B with Sinuosity 1.37, Trapezoidal Cross-Section, Smooth Floodplains and Stage 250.0 mm. Comparison with the Theoretical Discharge Produced by a Straight Channel with same Boundary Roughness, Area, and Bed Slope.

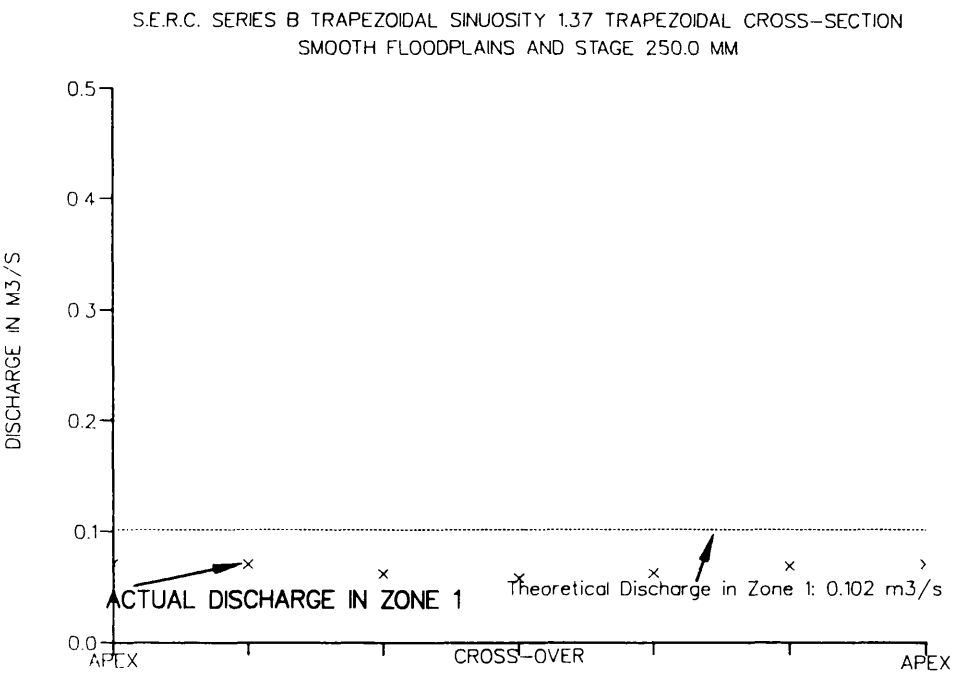

Fig (6.18f) - Actual Discharge in Zone 1 of the Meandering Channel of S.E.R.C. Flume Series B with Sinuosity 1.37, Trapezoidal Cross-Section, Smooth Floodplains and Stage 250.0 mm. Comparison with the Theoretical Discharge Produced by a Straight Channel with same Boundary Roughness, Area, and Bed Slope.

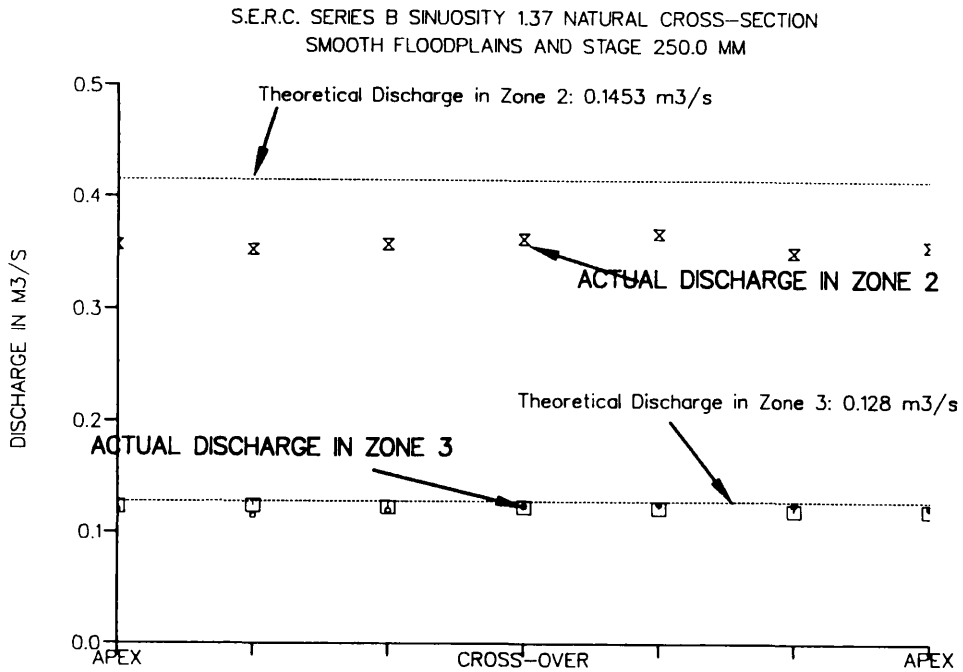

Fig (6.18g) - Actual Discharge in Zones 2 and 3 of the Meandering Channel of S.E.R.C. Flume Series B with Sinuosity 1.37, Natural Cross-Section, Smooth Floodplains and Stage 250.0 mm. Comparison with the Theoretical Discharge Produced by a Straight Channel with same Boundary Roughness, Area, and Bed Slope.

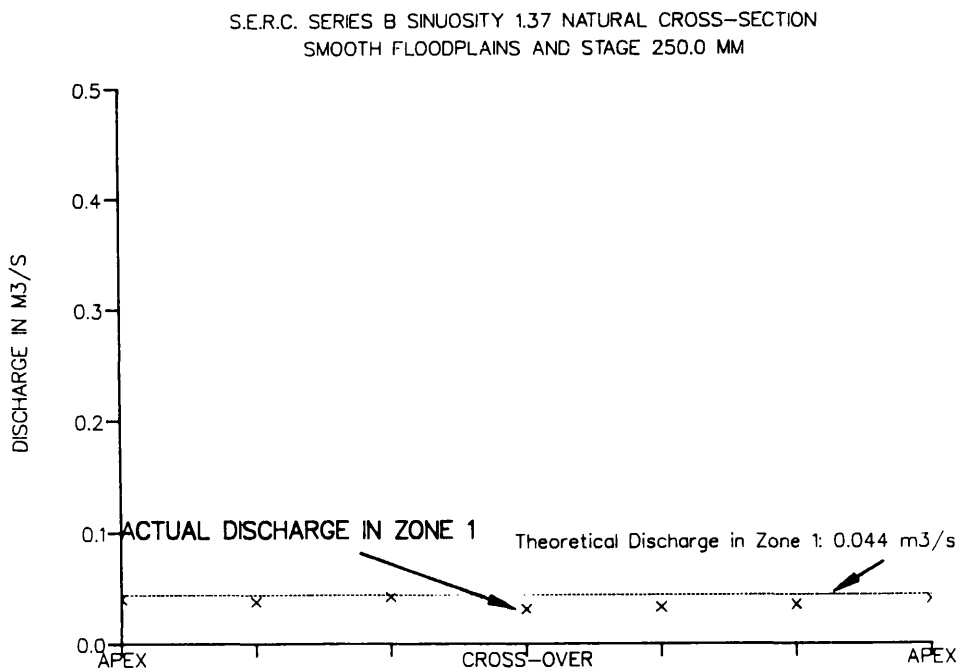

Fig (6.18h) - Actual Discharge in Zone 1 of the Meandering Channel of S.E.R.C. Flume Series B with Sinuosity 1.37, Natural Cross-Section, Smooth Floodplains and Stage 250.0 mm. Comparison with the Theoretical Discharge Produced by a Straight Channel with same Boundary Roughness, Area, and Bed Slope.

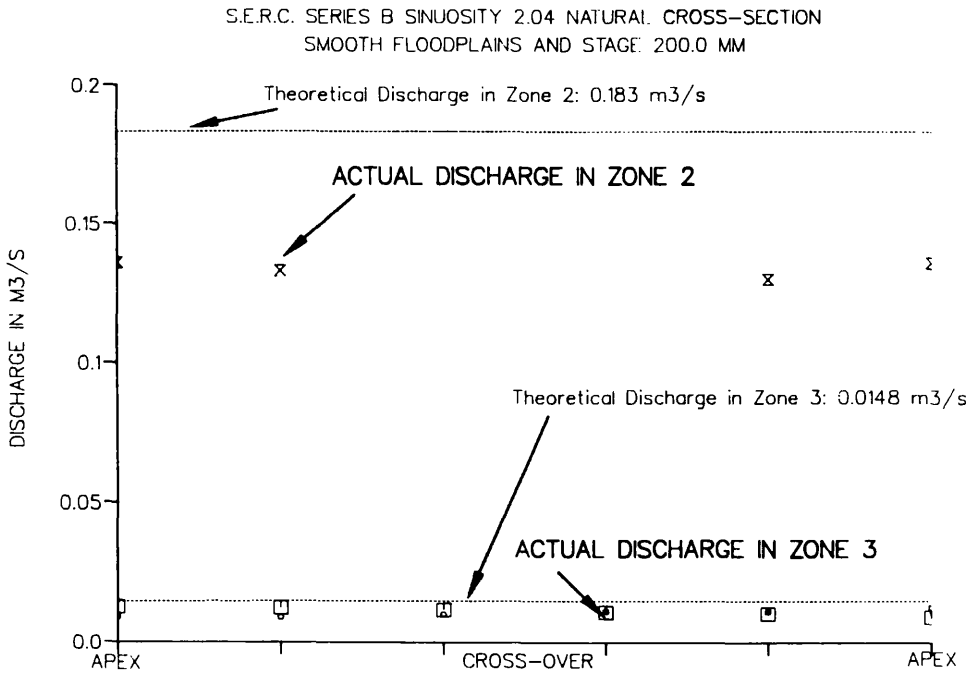

Fig (6.18i) - Actual Discharge in Zones 2 and 3 of the Meandering Channel of S.E.R.C. Flume Series B with Sinuosity 2.04, Natural Cross-Section, Smooth Floodplains and Stage 200.0 mm. Comparison with the Theoretical Discharge Produced by a Straight Channel with same Boundary Roughness, Area, and Bed Slope.

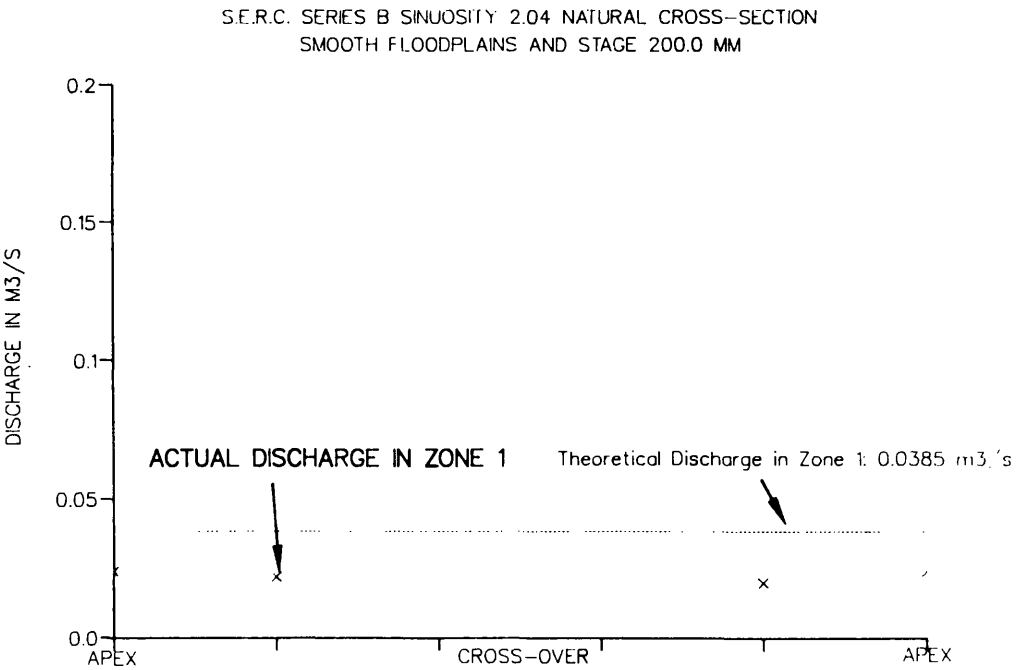

Fig (6.18j) - Actual Discharge in Zone 1 of the Meandering Channel of S.E.R.C. Flume Series B with Sinuosity 2.04, Natural Cross-Section, Smooth Floodplains and Stage 200.0 mm. Comparison with the Theoretical Discharge Produced by a Straight Channel with same Boundary Roughness, Area, and Bed Slope.

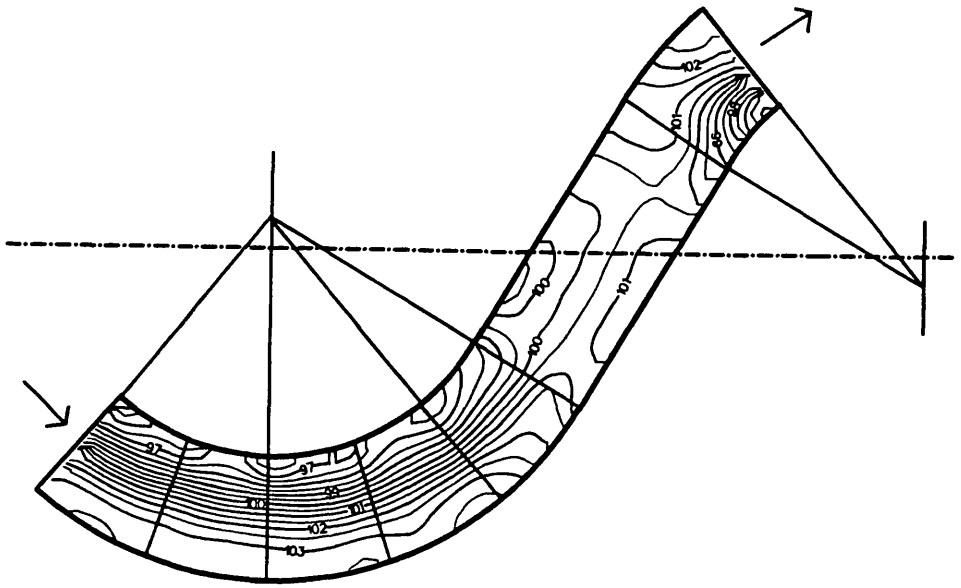

Fig (6.19a) - Contour of Surface Levels. S.E.R.C. Series B. Sinuosity 1.37. Trapezoidal Cross-Section. Stage 100.0 mm. (from Hardwick(1991))

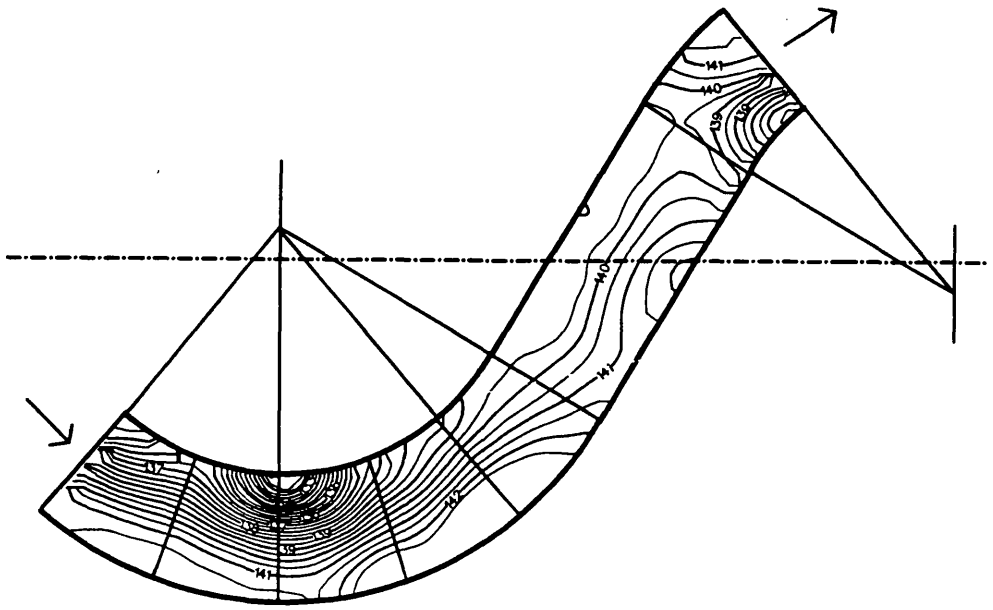

Fig (6.19b) - Contour of Surface Levels. S.E.R.C. Series B. Sinuosity 1.37. Natural Cross-Section. Stage 140.0 mm. (from Hardwick(1991))

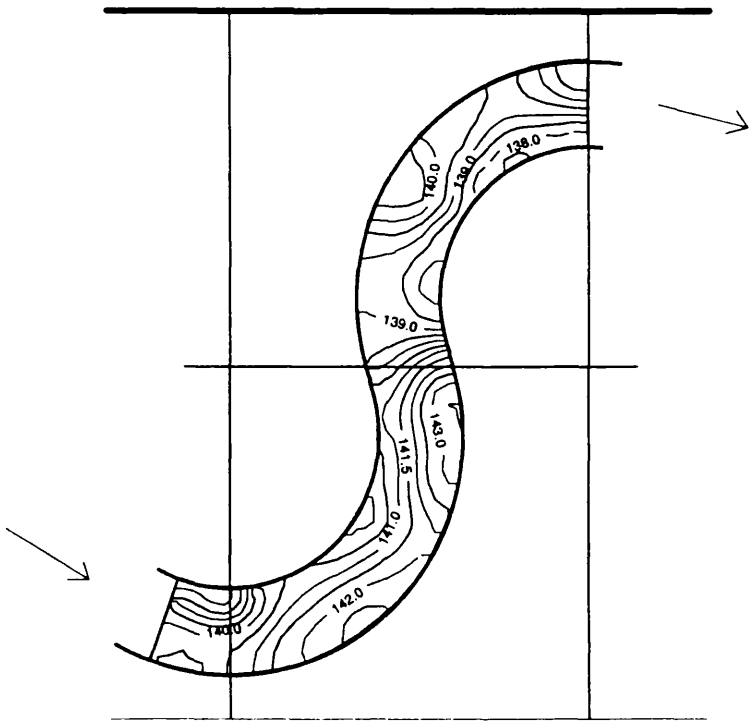

Fig (6.20) - Contour of Surface Levels. S.E.R.C. Series B. Sinuosity 2.04. Natural Cross-Section. Stage 140.0 mm.(from Hardwick(1991))

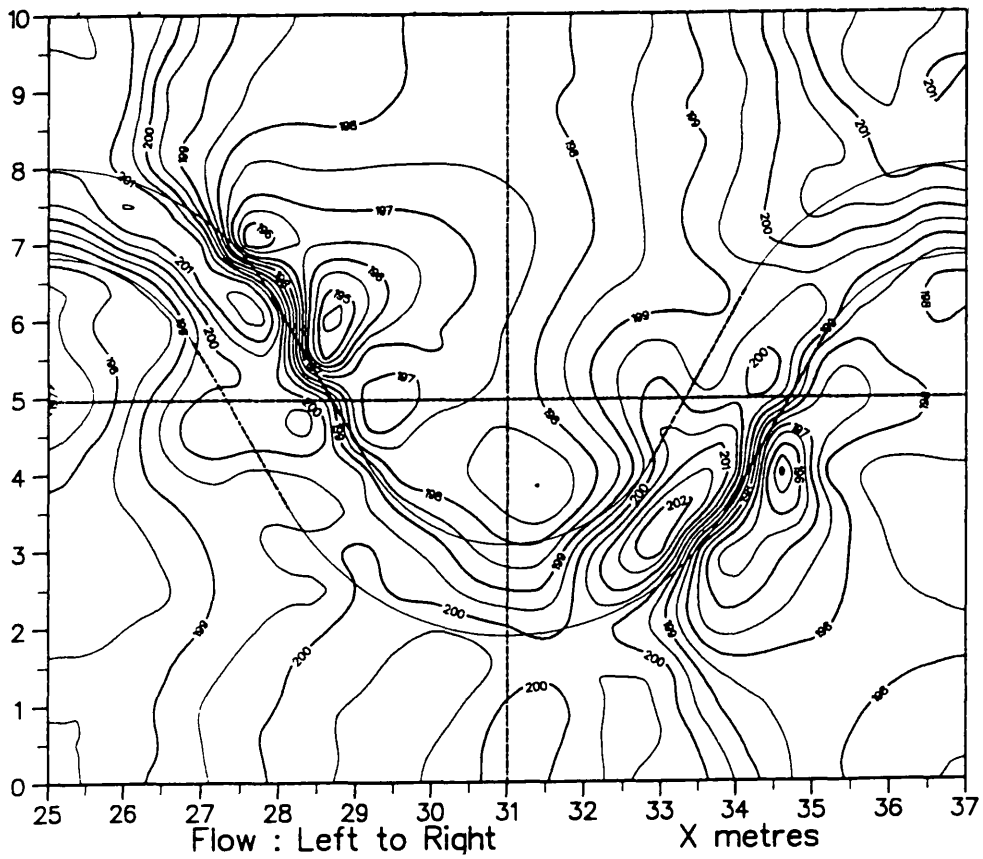

Fig (6.21) - Contour of Surface Levels. S.E.R.C. Series B. Sinuosity 1.37. Trapezoidal Cross-Section. Stage 200.0 mm. Smooth Floodplains (from Hardwick(1990))

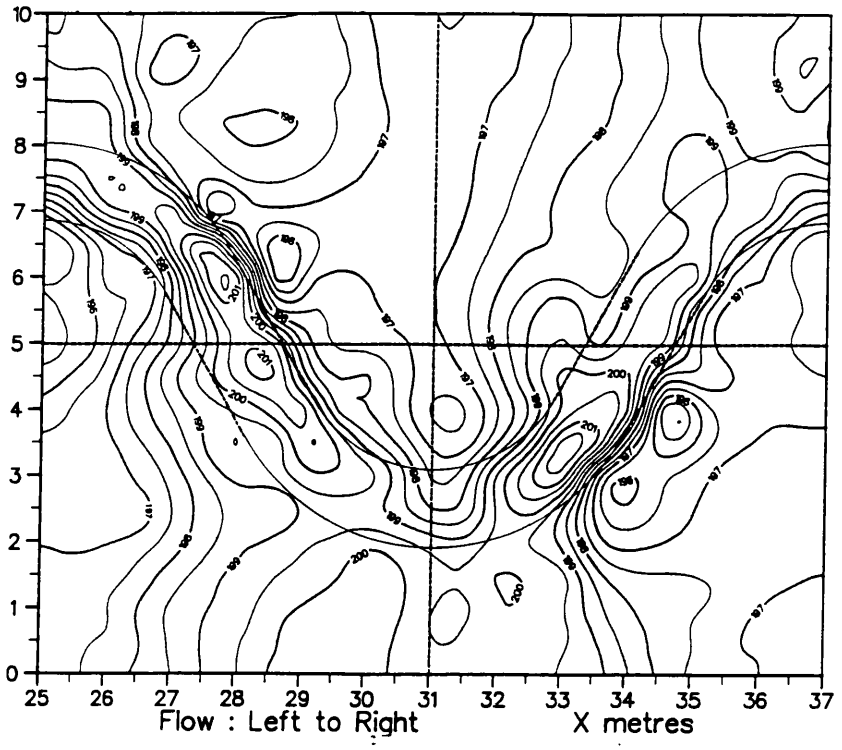

Fig (6.22) - Contour of Surface Levels. S.E.R.C. Series B. Sinuosity 1.37. Natural Cross-Section. Stage 200.0 mm. Smooth Floodplains(from Hardwick(1990))

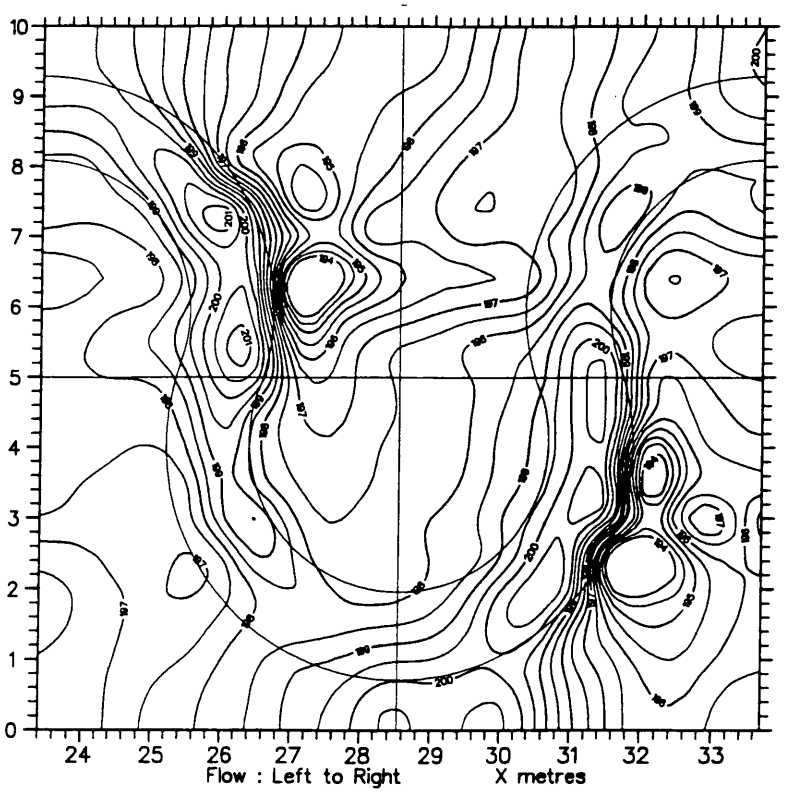

Fig (6.23) - Contour of Surface Levels. S.E.R.C. Series B. Sinuosity 2.04. Natural Cross-Section. Stage 200.0 mm. Smooth Floodplains(from Hardwick(1991))

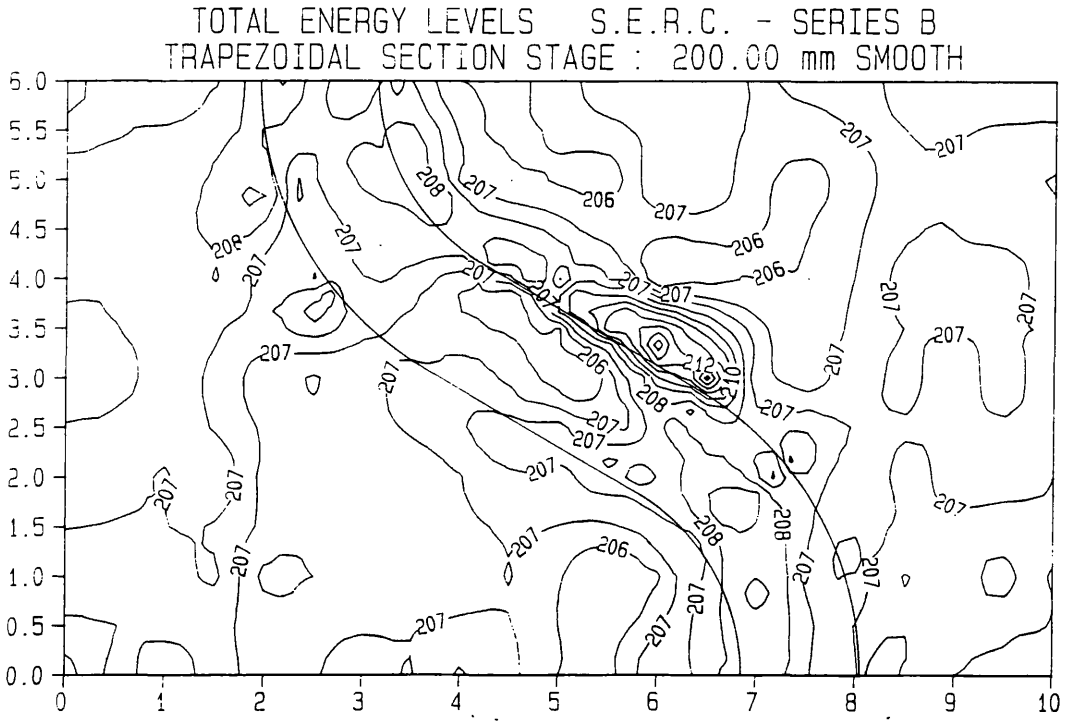

Fig (6.24) - Contour Levels of Energy. S.E.R.C. Series B. Sinuosity 1.37. Trapezoidal Cross-Section. Stage 200.0 mm. Smooth Floodplains

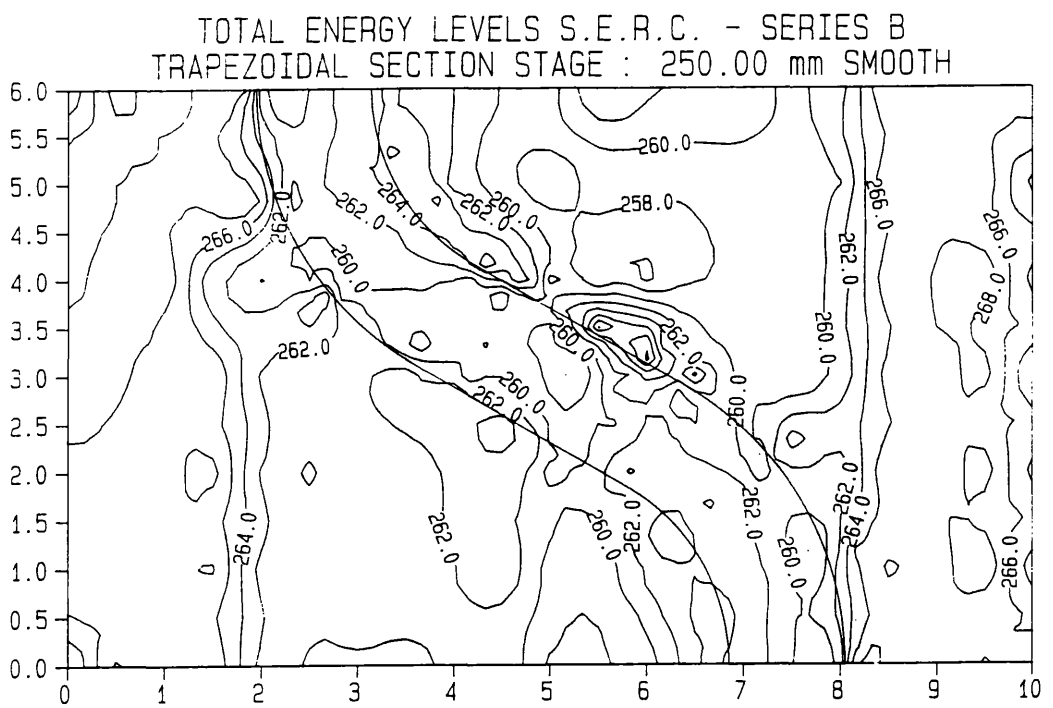

Fig (6.25) - Contour Levels of Energy. S.E.R.C. Series B. Sinuosity 1.37. Trapezoidal Cross-Section. Stage 250.0 mm. Smooth Floodplains

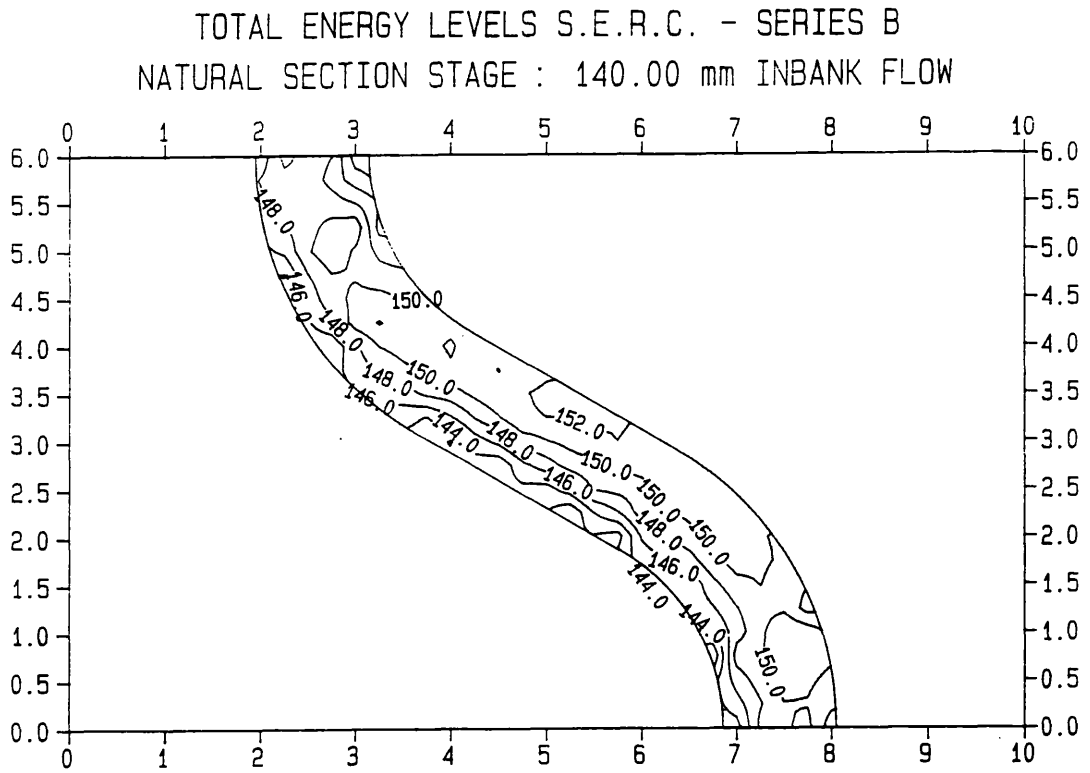

Fig (6.26) - Contour Levels of Energy. S.E.R.C. Series B. Sinuosity 1.37. Natural Cross-Section. Stage 140.0 mm.

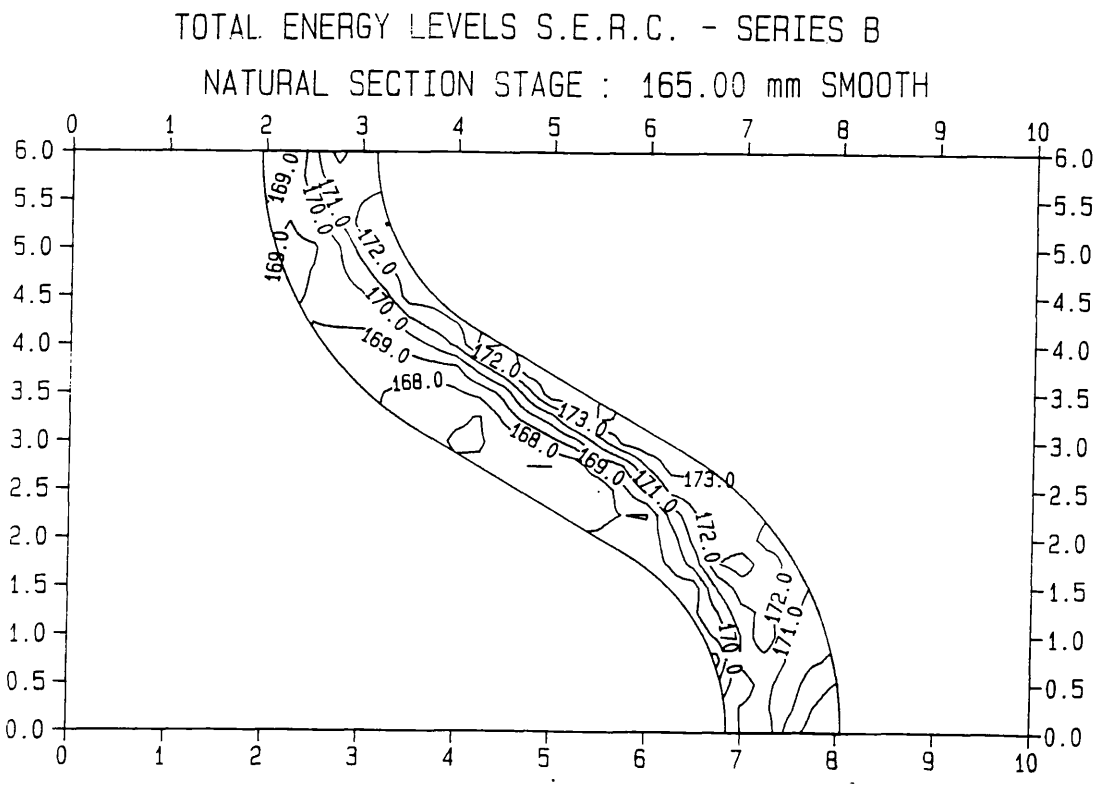

Fig (6.27) - Contour Levels of Energy. S.E.R.C. Series B. Sinuosity 1.37. Natural Cross-Section. Stage 165.0 mm. Smooth Floodplains

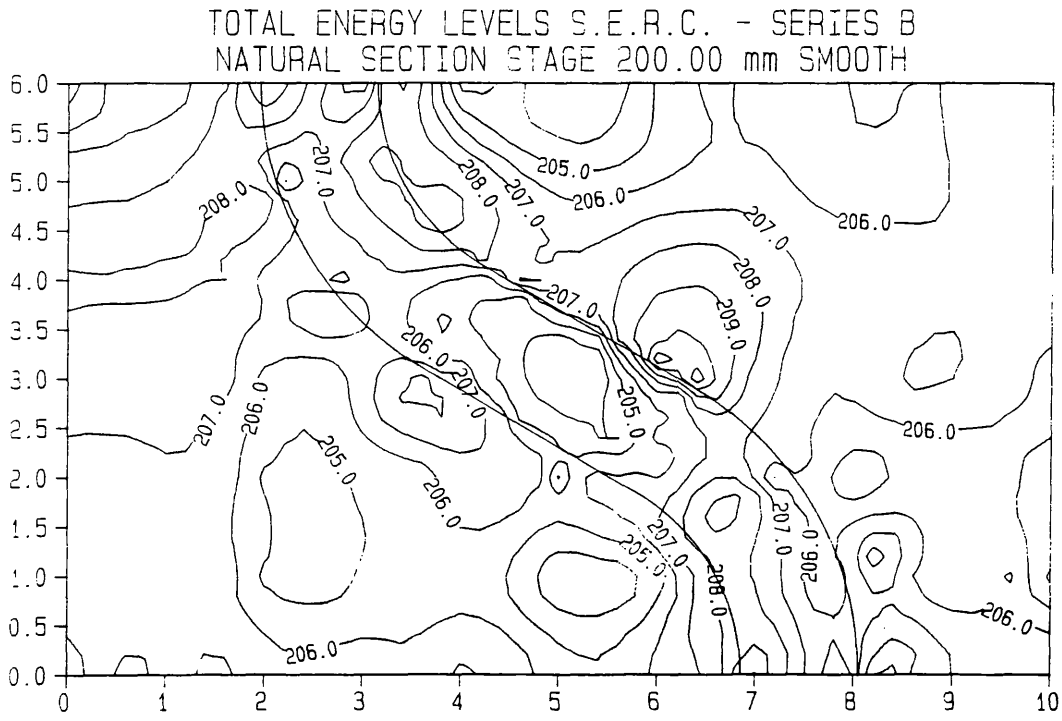

Fig (6.28) - Contour Levels of Energy. S.E.R.C. Series B. Sinuosity 1.37. Natural Cross-Section. Stage 200.0 mm. Smooth Floodplains

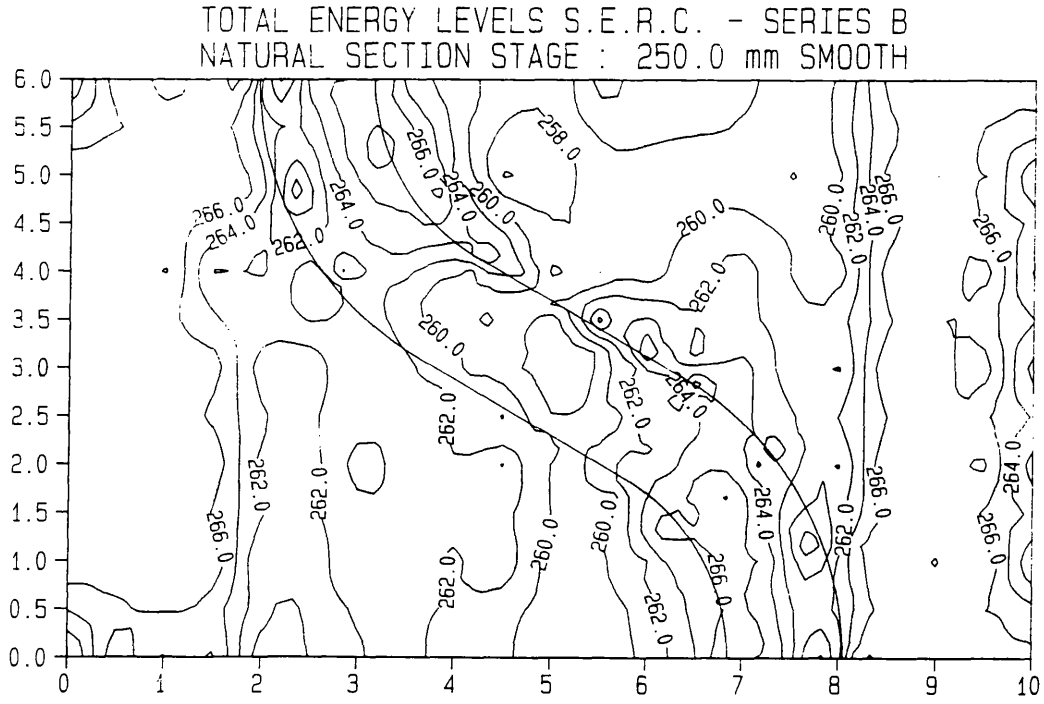

Fig (6.29) - Contour Levels of Energy. S.E.R.C. Series B. Sinuosity 1.37. Natural Cross-Section. Stage 250.0 mm. Smooth Floodplains

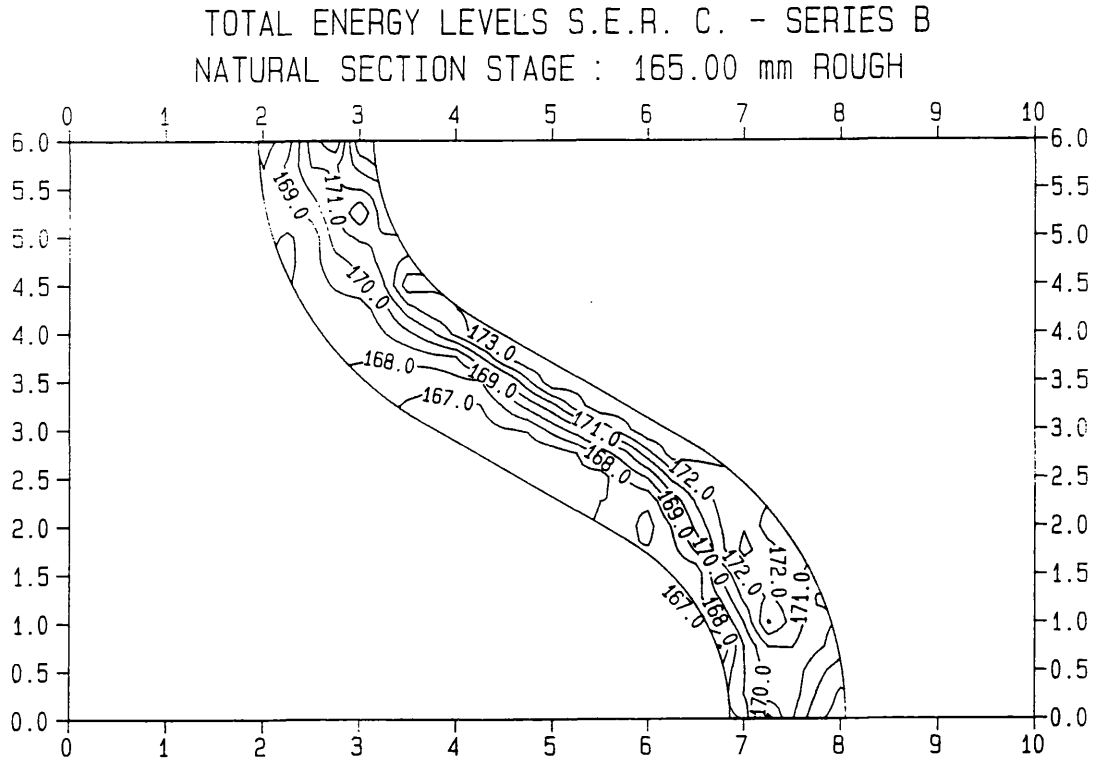

Fig (6.30) - Contour Levels of Energy. S.E.R.C. Series B. Sinuosity 1.37. Natural Cross-Section. Stage 165.0 mm. Fully Roughened Floodplain.

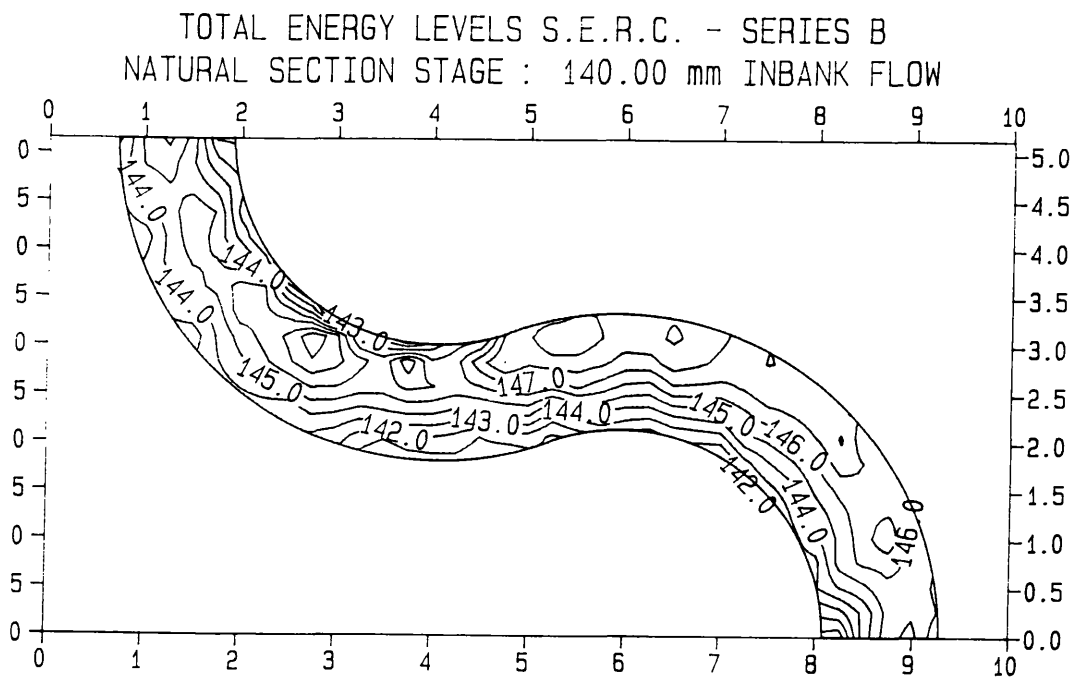

Fig (6.31) - Contour Levels of Energy. S.E.R.C. Series B. Sinuosity 2.04. Natural Cross-Section. Stage 140.0 mm.

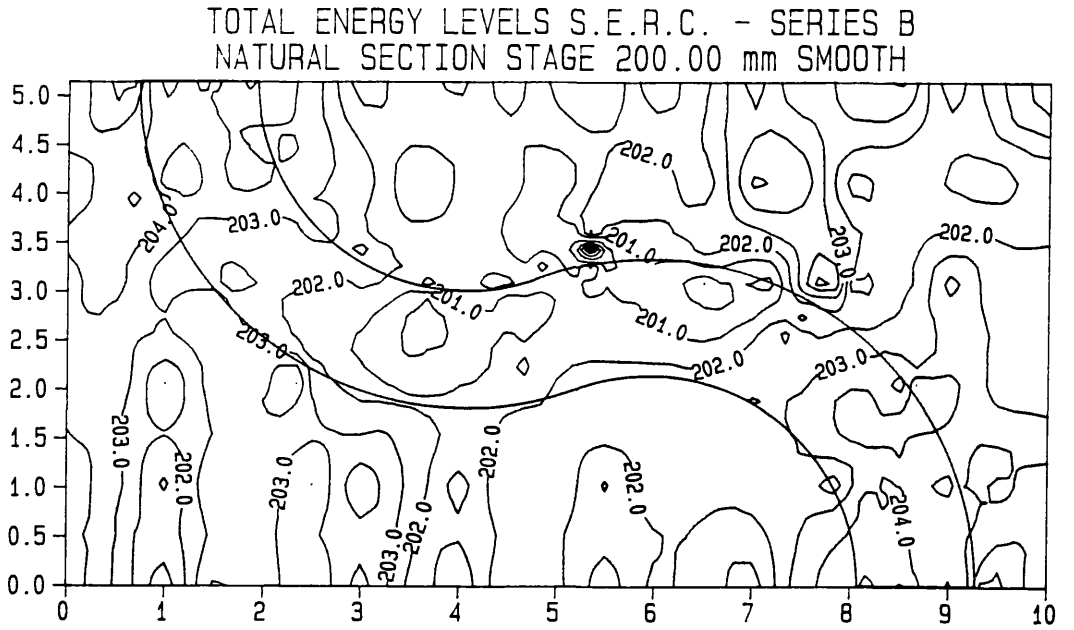

Fig (6.32) - Contour Levels of Energy. S.E.R.C. Series B. Sinuosity 2.04. Natural Cross-Section. Stage 200.0 mm. Smooth Floodplains

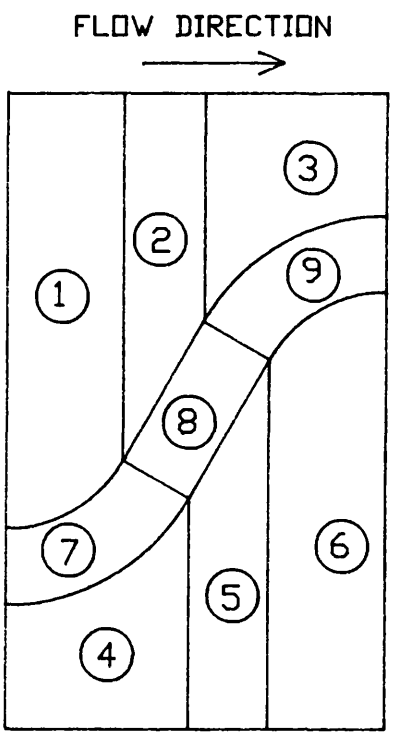

Fig 6.33 - MOMENTUM EQUATION APPLIED TO MEANDERING CHANNELS S.E.R.C. SERIES B. SINUOSITY 1.37. DEFINITION OF THE BLOCKS.

Fig 6.34 - MOMENTUM EQUATION APPLIED IN X DIRECTION IN THE FLOODPLAIN.
S.E.R.C. SERIES B. SINUOSITY 1.37. DEFINITION OF THE MOMENTUM FLUX TERMS.

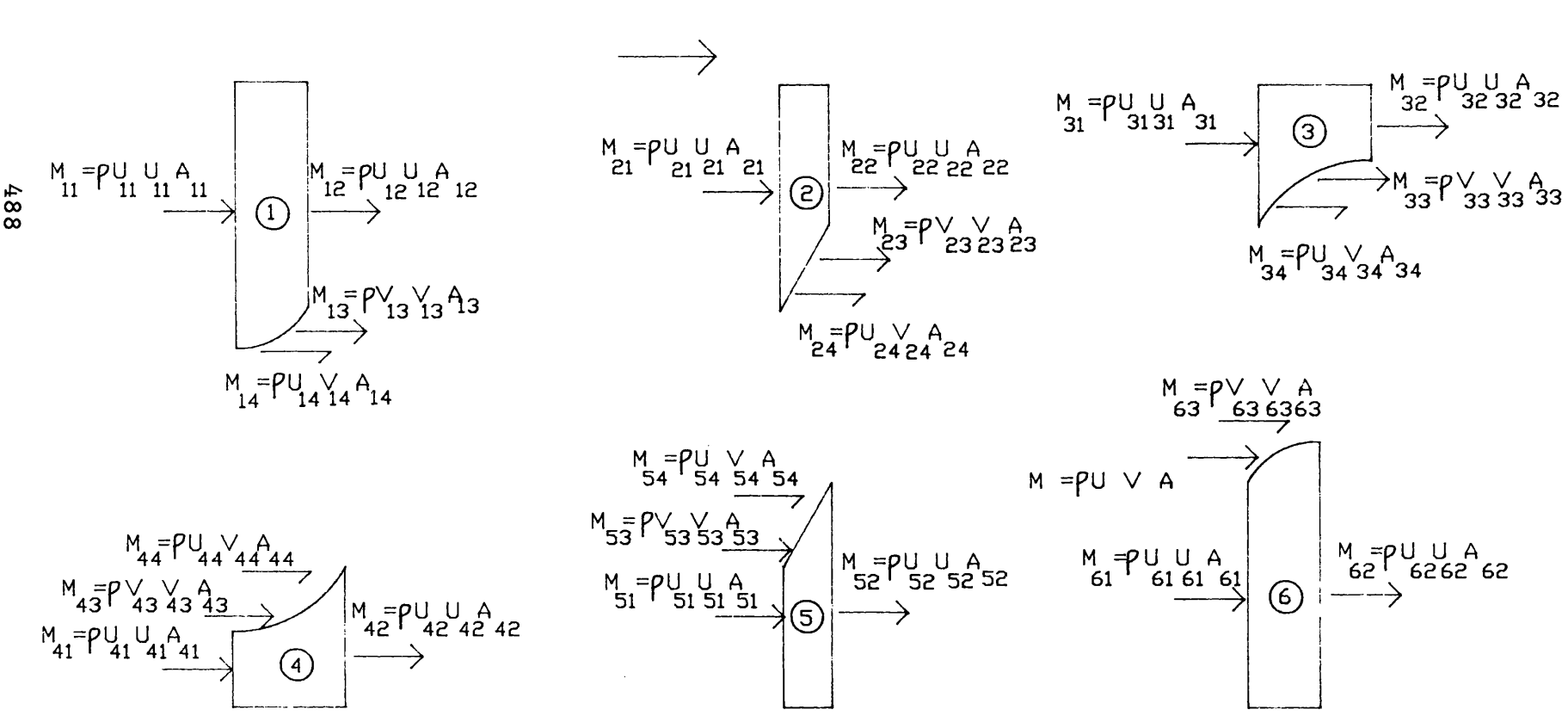

Fig 6.35 - MOMENTUM EQUATION APPLIED IN X DIRECTION IN THE FLOODPLAIN. S.E.R.C. SERIES B. SINUOSITY 1.37. DEFINITION OF THE BODY WEIGHT AND BOUNDARY SHEAR FORCE TERMS.

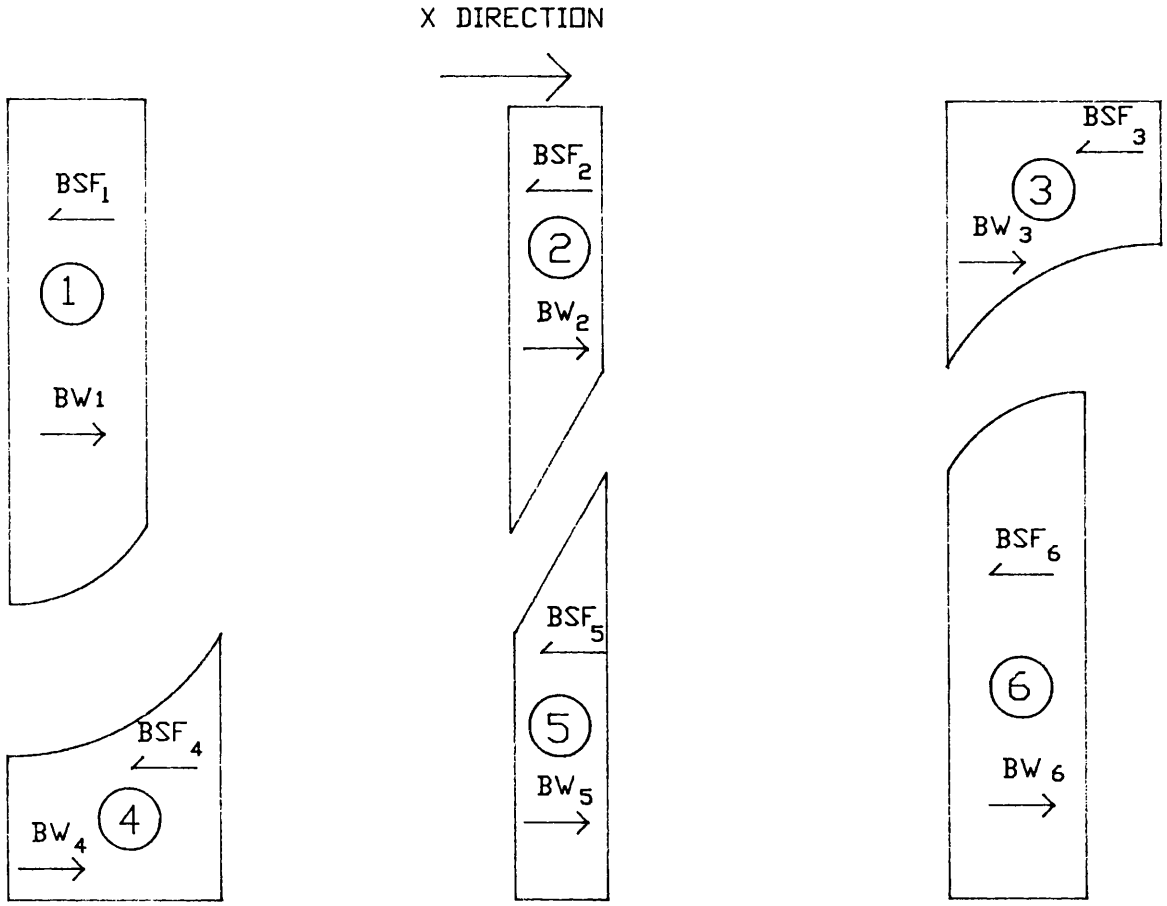

Fig 6.36 - MOMENTUM EQUATION APPLIED IN X DIRECTION IN THE FLOODPLAIN. S.E.R.C. SERIES B. SINUOSITY 1.37. DEFINITION OF THE PRESSURE FORCE.

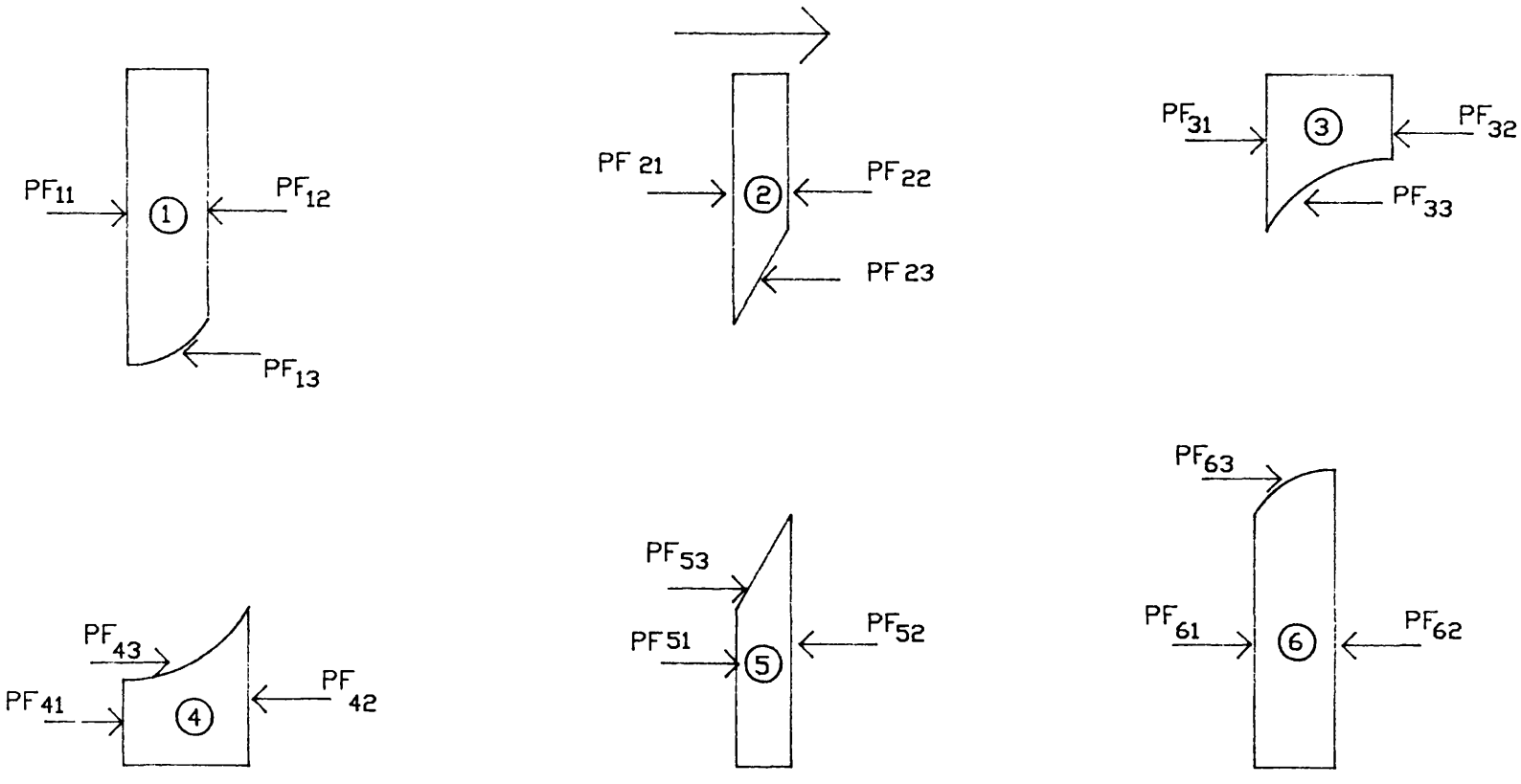

Fig 6.37 - MOMENTUM EQUATION APPLIED IN X DIRECTION IN THE FLOODPLAIN.
S.E.R.C. SERIES B. DEFINITION OF THE APPARENT SHEAR FORCE IN X AND IN Y DIRECTIONS.

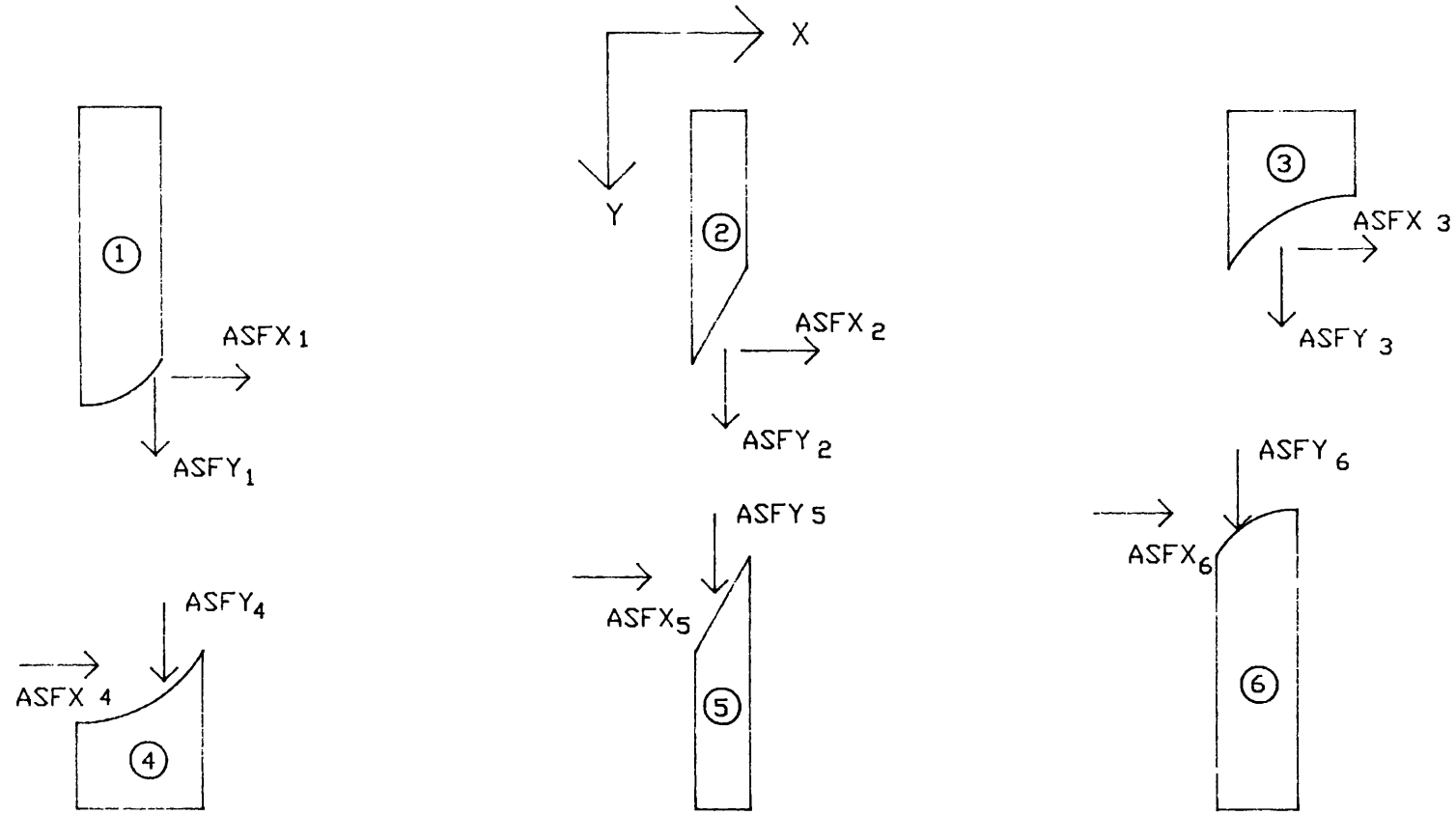

Fig 6.38 - MOMENTUM EQUATION APPLIED IN X AND Y DIRECTIONS IN THE FLOODPLAIN.

S.E.R.C. SERIES B. SINUOSITY 1.37. DEFINITION OF THE COORDINATE SYSTEM FOR THE COMPUTATION OF THE MOMENTUM FLUX M_{13}, M_{14}, M_{15} AND M_{16} OF BLOCK No. 1.

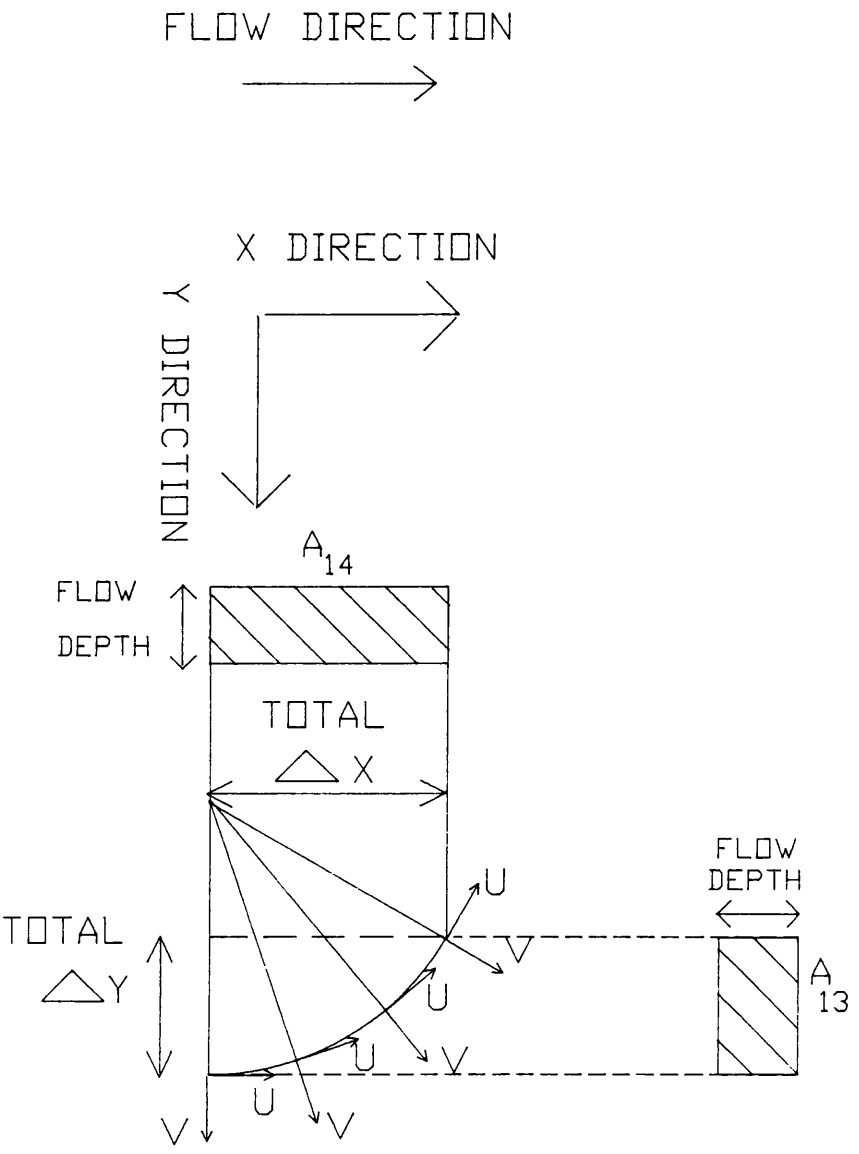

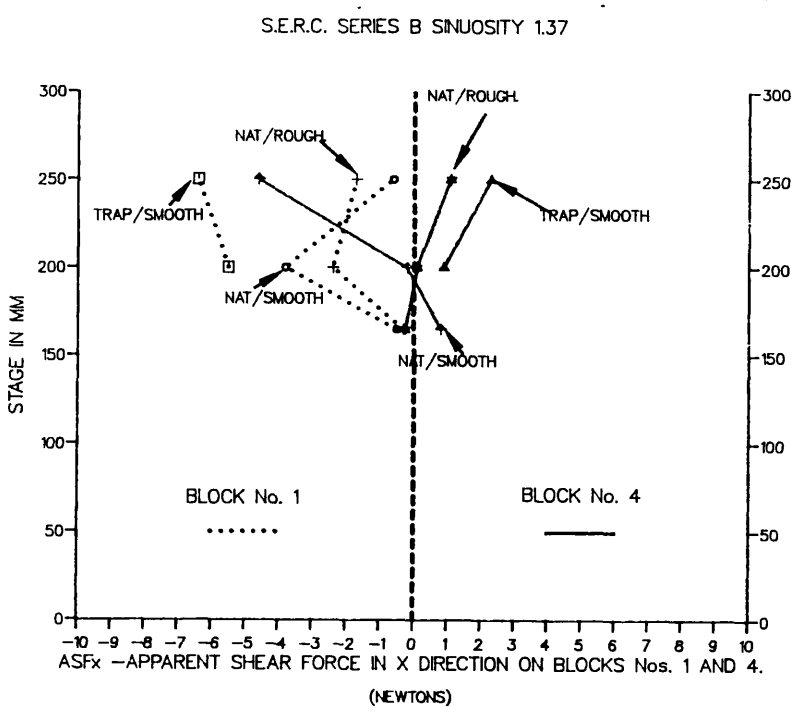

Fig (6.38a) - Apparent Shear Force in the X Direction in Blocks 1 and 4 of S.E.R.C. Flume Series B with Sinuosity 1.37.

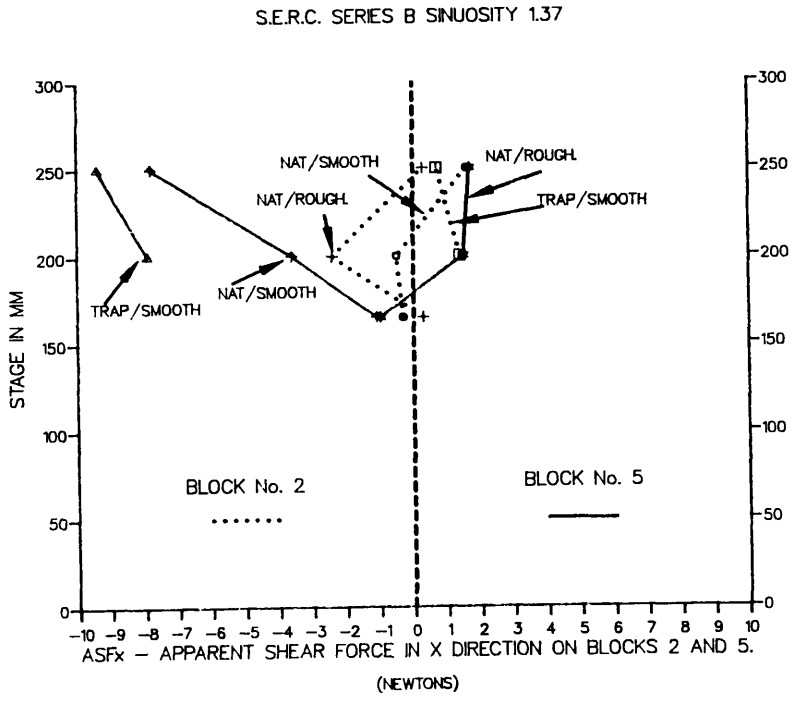

Fig (6.38b) - Apparent Shear Force in the X Direction in Blocks 2 and 5 of S.E.R.C. Flume Series B with Sinuosity 1.37.

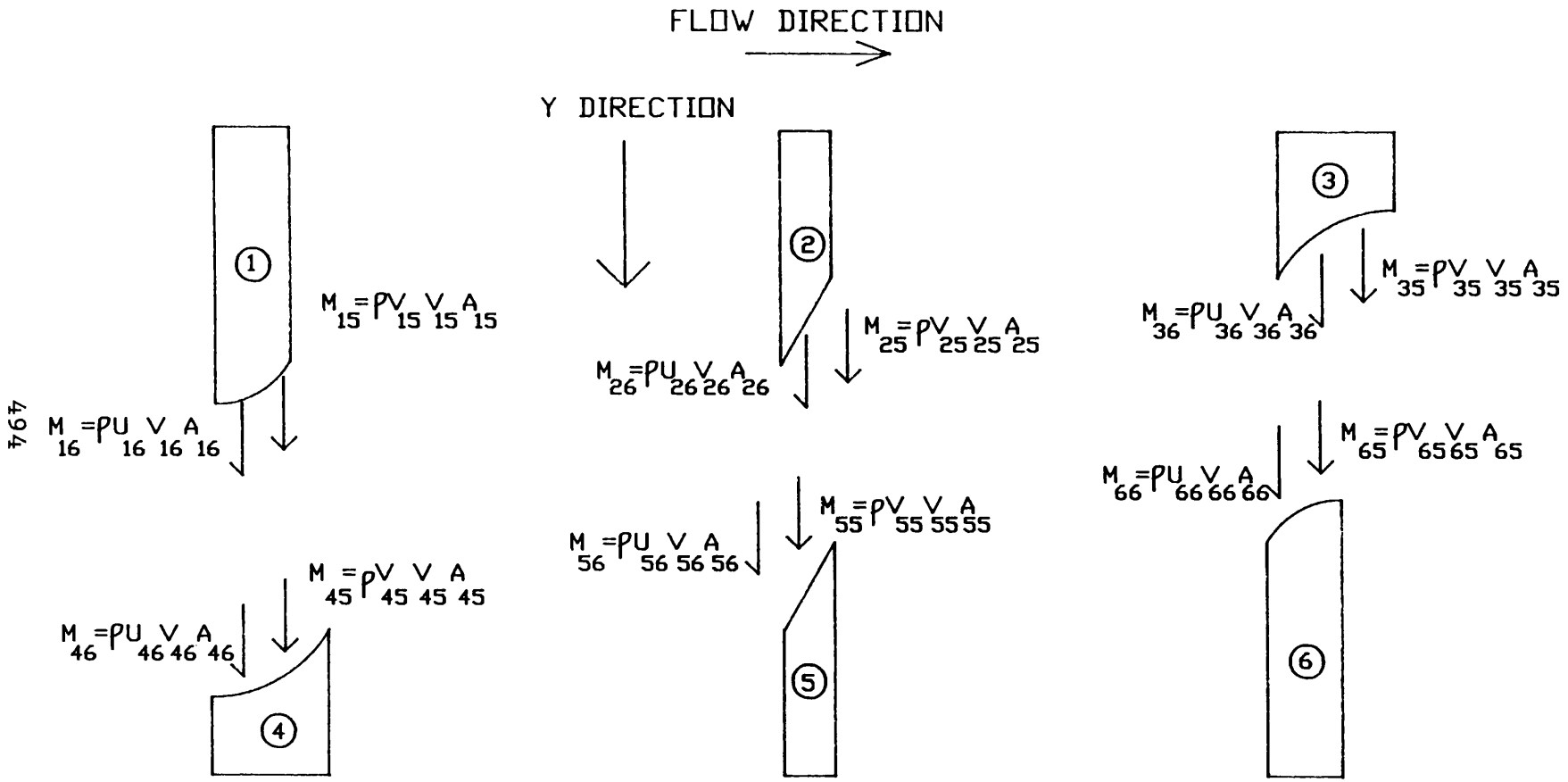

Fig. 6.39 - MOMENTUM EQUATION APPLIED IN Y DIRECTION IN THE FLOODPLAIN S.E.R.C. SERIES B. SINUOSITY 1.37. DEFINITION OF MOMENTUM FLUX TERMS.

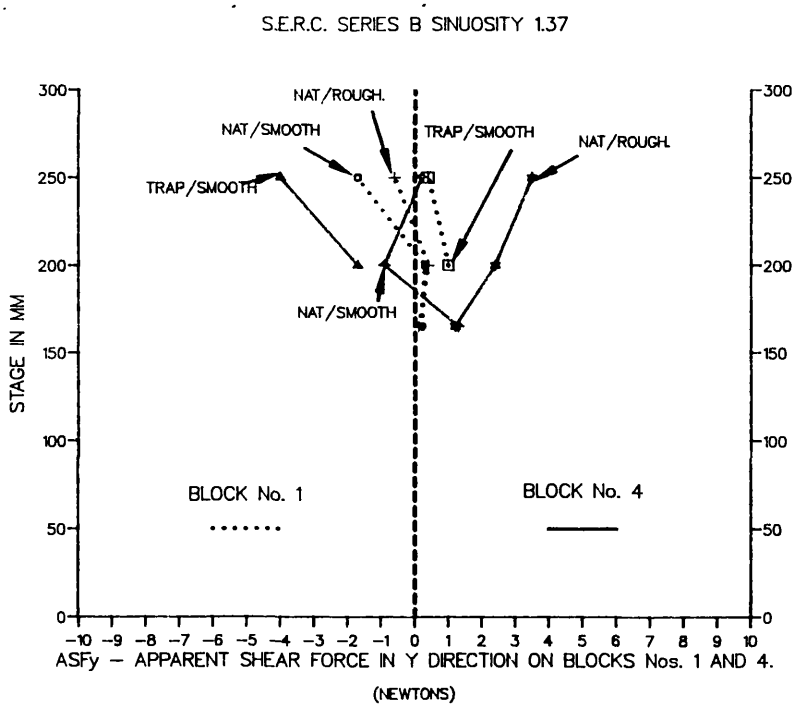

Fig (6.39a) - Apparent Shear Force in the Y Direction in Blocks 1 and 4 of S.E.R.C. Flume Series B with Sinuosity 1.37.

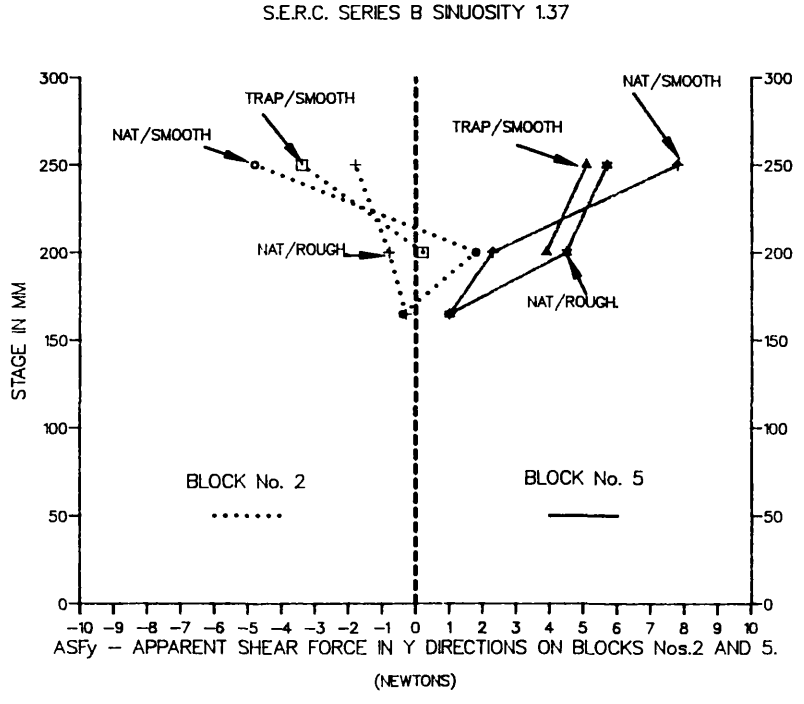

Fig (6.39b) - Apparent Shear Force in the Y Direction in Blocks 2 and 5 of S.E.R.C. Flume Series B with Sinuosity 1.37.

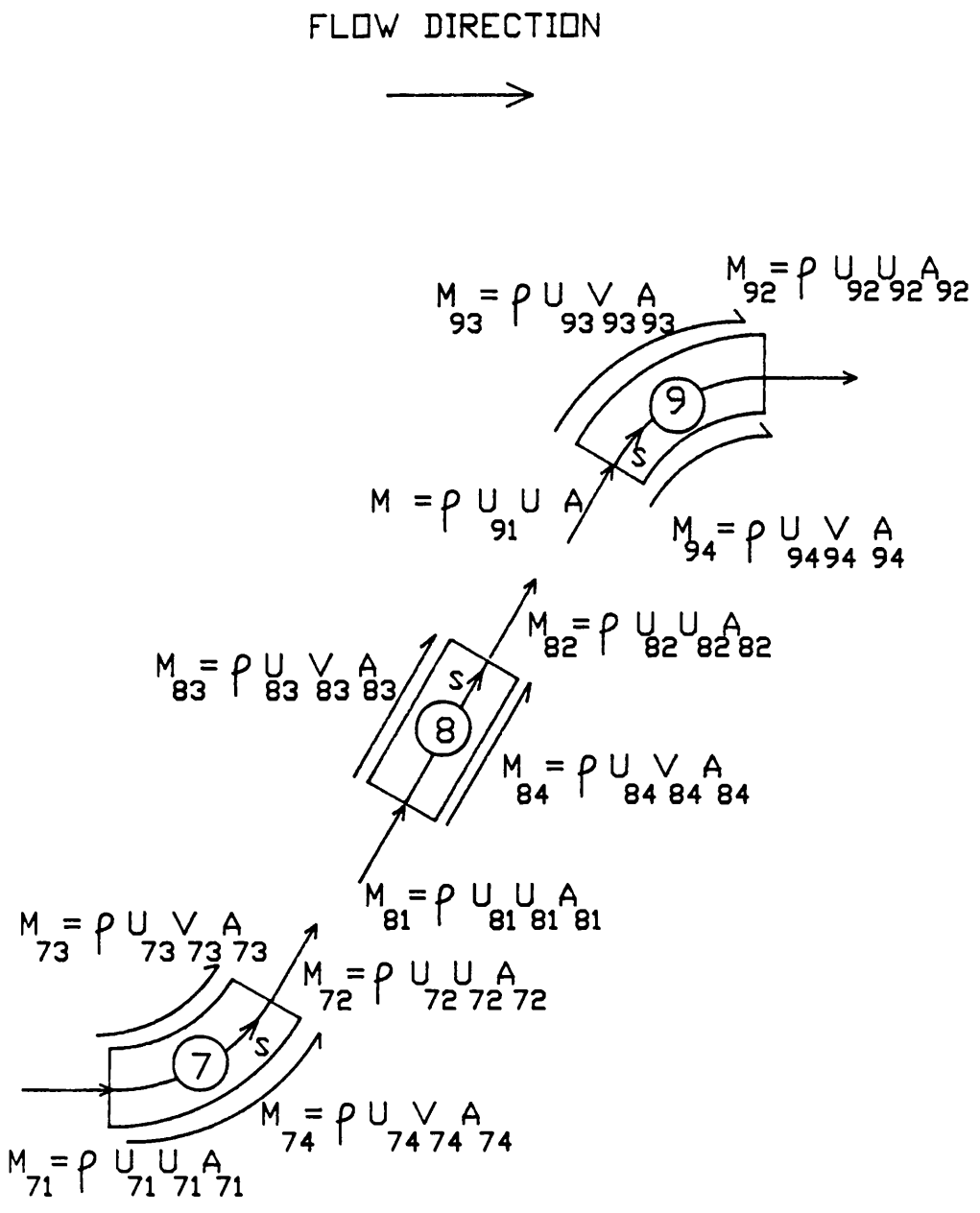

Fig. 6.40 – MOMENTUM EQUATION APPLIED IN S DIRECTION IN THE MEANDERING CHANNEL WITH SINUOSITY 1.37. S.E.R.C. SERIES B. DEFINITION OF THE MOMENTUM FLUX.

Fig. 6.41 - MOMENTUM EQUATION APPLIED IN S DIRECTION IN THE MEANDERING CHANNEL WITH SINUOSITY 1.37. S.E.R.C. SERIES B. DEFINITION OF THE BODY WEIGHT AND BOUNDARY SHEAR FORCE TERMS.

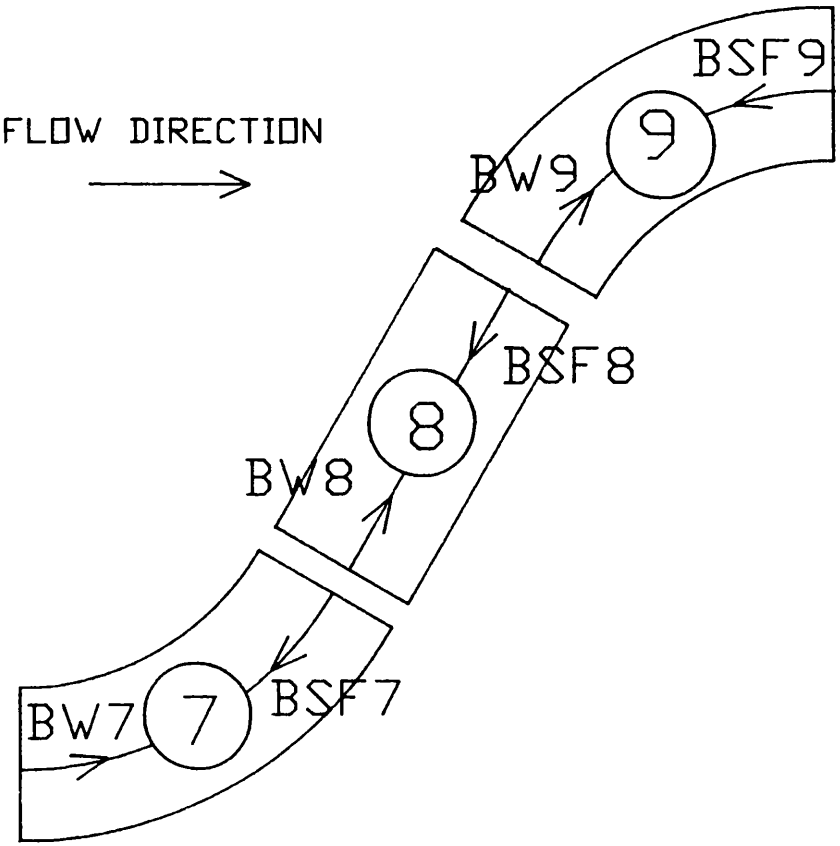

Fig. 6.42 - MOMENTUM EQUATION APPLIED IN S DIRECTION

IN THE CROSS-OVER REGION.

S.E.R.C. SERIES B. SINUOSITY 1.37.

DEFINITION OF THE LATERAL SHEAR STRESS

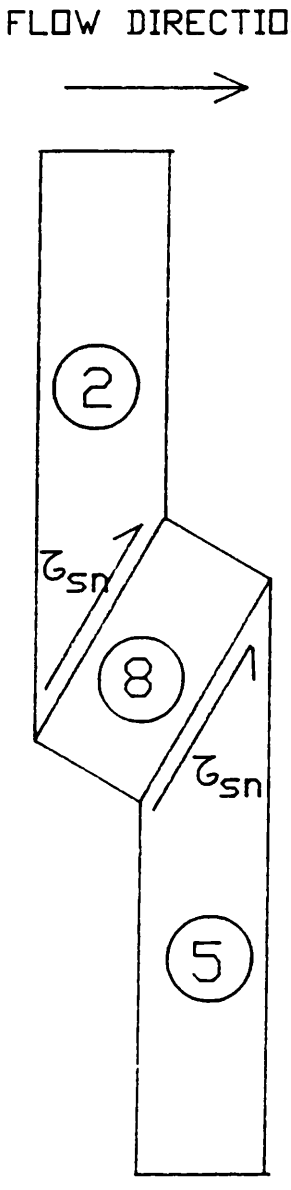

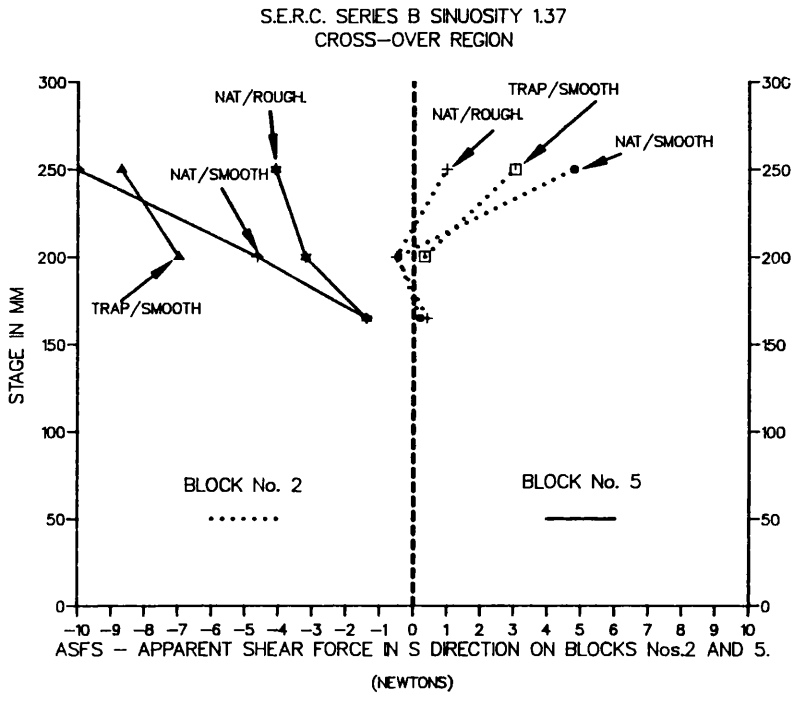

Fig (6.42a) - Apparent Shear Force in the S Direction in Blocks 2 and 5 of S.E.R.C. Flume Series B with Sinuosity 1.37.

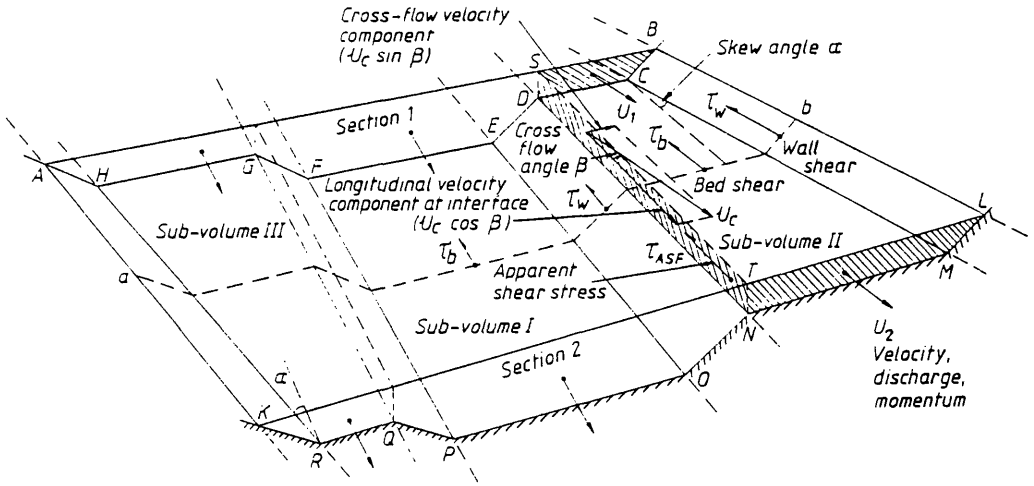

Fig (6.43) - Perspective View of the Control Volume in the Skew Channel of Elliot and Sellin(1990).

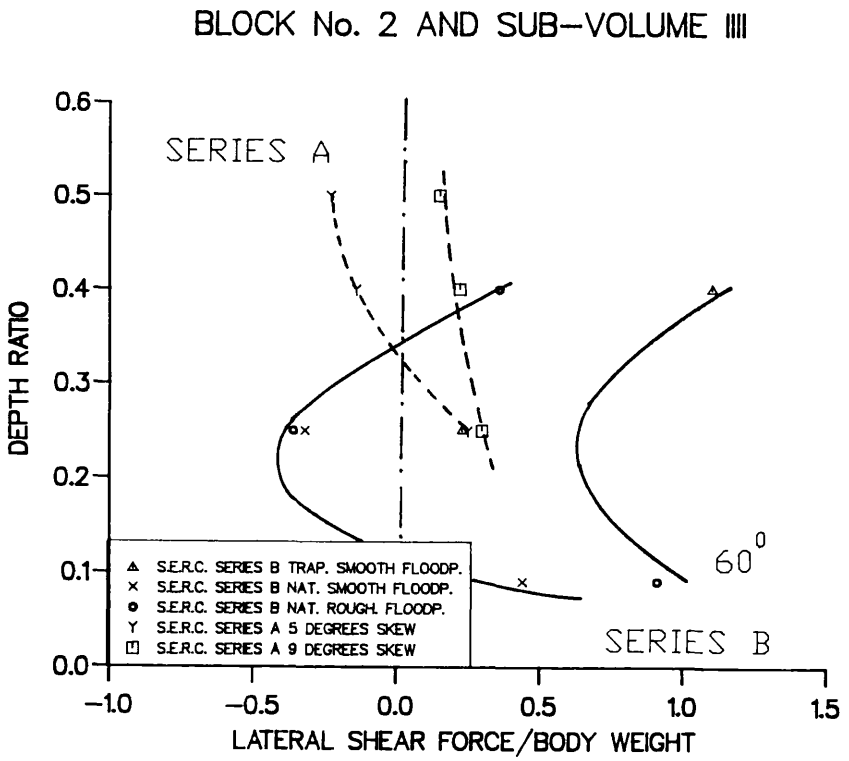

Fig (6.44) - Variation of Non-Dimensional Lateral Shear Force with Depth Ratio. Block No. 2 of the Meandering Channel with Sinuosity 1.37 of S.E.R.C. Series B and Sub-Volume III of the Skew Flume of Elliot and Sellin(1990).

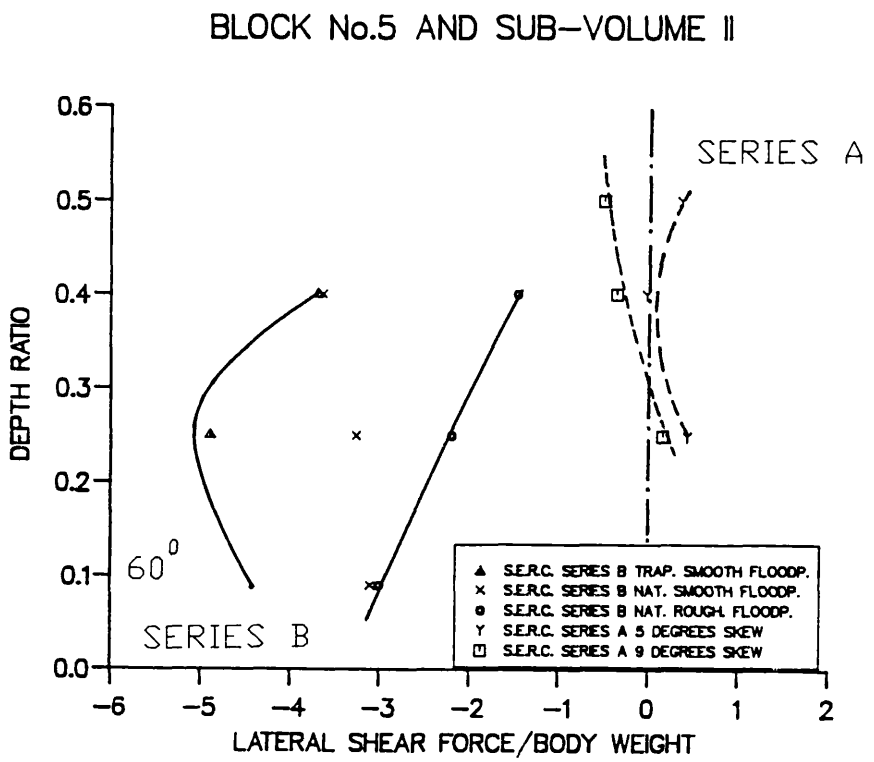

Fig (6.45) - Variation of Non-Dimensional Lateral Shear Force with Depth Ratio. Block No. 5 of the Meandering Channel with Sinuosity 1.37 of S.E.R.C. Series B and Sub-Volume II of the Skew Flume of Elliot and Sellin(1990).

CHAPTER 7

MODELLING, CONCLUSIONS AND FUTURE RESEARCH

CHAPTER 7

MODELLING, CONCLUSIONS AND FUTURE RESEARCH

7.1 Towards a Model of Meandering Compound Flow

7.1.1. Introduction.

Perhaps the most important aim of the physical modelling studies at S.E.R.C. Flood Channel Facility, H.R. Wallingford, is the evolution to a model which will be generalised enough to apply to any meandering compound flow.

The type of model to adopt is the subject of intense debate at present, but the choice will invariably depend on the type of output desired from the model. For instance, approximate estimates of stage-discharges can be obtained from a quasi-one dimensional model. If the output required is stage-discharge as well as lateral distributions of velocity on the floodplains, then a lateral distribution method(LDM) of the type developed by **Wark et al(1990)** might be applied. If the output requires details of secondary currents, larger flow structures, bed forms and distribution of sediment transport, then a full three dimensional model may be required including simulation of turbulence. This type of model is being developed by **Manson(1991)** (section 7.1.3) using k-ε turbulence model, and also by **Younis(1992)** using a Reynolds shear stress model. In the field of dispersion of pollutants, a random walk model may be more appropriate.

There is a range of modelling techniques available and the most appropriate choice must reflect the desired output from the model.

The physical modelling programme described in this thesis was therefore required to produce data for some of the range of models described above. On one hand, stage and discharge were measured at the S.E.R.C. flume to provide basic data for simple one-dimensional models. At the other end of the spectrum, sophisticates laser measurements provided data on turbulent

velocities and Reynolds shear stress, which will be enormous benefit in the turbulence modelling field.

In a sense, limiting the S.E.R.C. flume to only two basic planforms sinuosities, large the model scale, effectively limited a detailed parametric analysis due to sparse data. The data from this study pertains only to the few geometries tested, and hence extrapolation and generalization to other geometries can be done only through other model studies or field studies. The numbers of other model studies is also small in meandering compound flows, and hence a wide-ranging parametric type analysis such as carried out by **Ackers(1991)** for Series A data is rather more limited in this Series B case. The first step in this direction has been taken in **Chapter 4** of this thesis, and will be followed later in 1992 by an analysis by James and **Wark** at H. R. Wallingford.

In the event of such sparse parametric study it is advocated by the **Author** that the simplest initial approach is the further development of a one-dimensional energy method produced by **Ervine and Ellis(1987)**. This is preferable to a force-momentum type balance as outline in Section 7.1.2 below.

For more refined flow modelling the **Author** also recommends the development of three-dimensional numerical models with turbulence modelling. This approach has been the basis of work of **Manson** under the supervision of **Drs. Pender and Ervine** which commenced in 1990 and is intended to eventually simulate flow conditions in meandering compound flows. Details are provided in Section 7.1.3.

7.1.2 A One Dimensional Energy Method.

The reader is referred in the first instance to a paper by **Ervine and Ellis(1987)** outlining the simplified energy loss method. The ideas in this paper required to be up-dated in the light of all measurements at the S.E.R.C. flume and Glasgow flume. This process is now an ongoing project at the University of Glasgow but some tentative ideas are noted below.

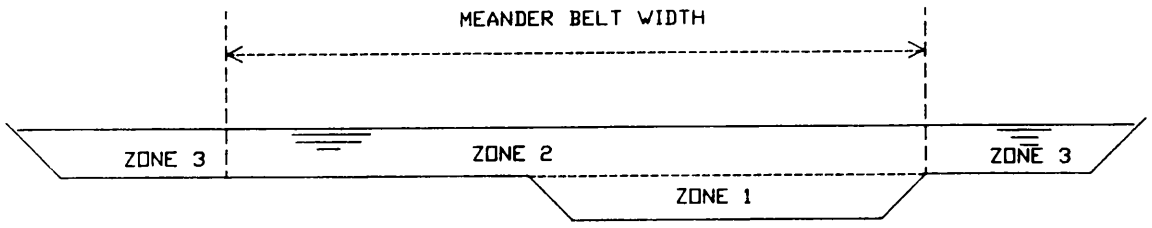

(i) The method involves sub-divisions of the meander geometry into three zones, in the same manner as sketched above.

The manner of the sub-division above has been discussed in detail in **Chapter 4**. It became apparent that this method is particularly appropriate for rough floodplains cases and for larger aspect ratios of the main channel. This usually the case in the nature with floodplain roughness typically twice that of the main channel. It is argued therefore that this method is the most appropriate for the widest possible application, although others methods may be slightly more appropriate for the specialised cases of smooth floodplains boundaries.

(ii) Zone 1 - From the sketch above refers to the main channel region below bankfull level.

In the original model, the main channel energy losses were computed by assuming bed friction, bed form losses, and secondary cells energy losses, which were computed assumed to be generated by the bends. The later assumption is now shown to be in error for compound meandering flows, except for the specific cases of zero floodplain flow velocity(stagnant floodplain water) as shown in the Glasgow flume model studies.

In fact it is now evident that the main mechanism for secondary cells in this type of flow is floodplain flow shearing over the main channel below. This process sets up the secondary cell, and in fact energy is added to the main channel flow through this mechanism.

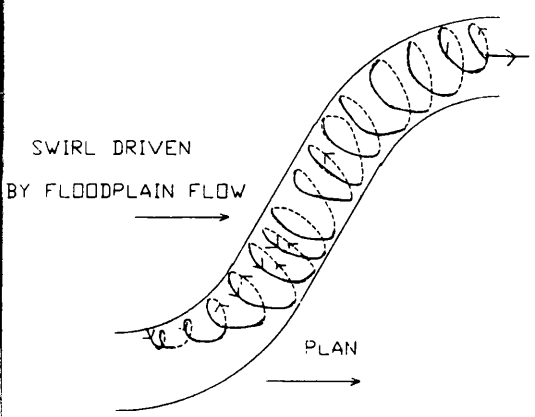

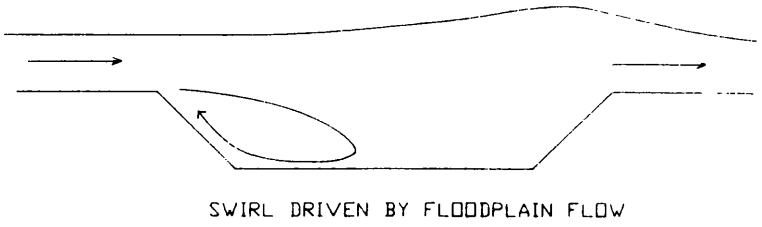

The addition of energy to the main channel from the floodplain, occurs mainly from cross-over region to the next bend apex.

If we consider also the flow mechanisms at the work from bend apex to the cross-over region, the opposite occurs.

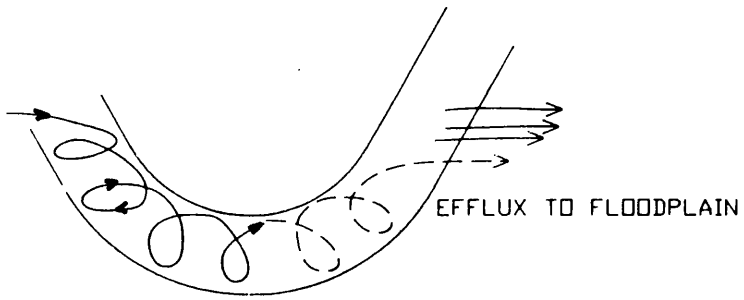

At the bend apex the driving cell suddenly decays due to lack of floodplain flow shearing over the main channel. The fluid from the bend apex appears to be dumped on to the floodplain as shown above producing a great reduction of flow in Zone 1(main channel) from apex to cross-over region.

This is a loss of fluid flowing in the main channel to the floodplain and hence can be interpreted as a loss of energy out of main channel to the floodplain flow. This phenomenon is amply illustrated in a plot of the discharge in the main channel(below bankfull level) from apex to apex.

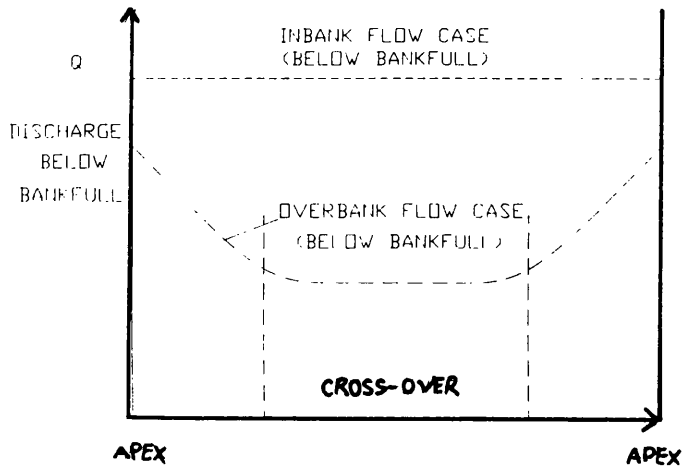

Maximum discharge at a bend apex is reduced on moving to the cross-over region and increases again from the cross-over region to the next apex. This must be a reflection of the energy distribution loss along a meander as well.

The problem in Zone 1 in modelling terms, is not necessarily to estimate energy loss from apex to cross-over and energy gain from cross-over to bend apex, but rather how to model the fact that there is much less flow in the main channel during overbank flow than there is during inbank flow. This is sketched above, where two inbank flows can be modelled quite easily from bed friction and bend losses.

What is causing a sudden reduction in the main channel flow during the overbank regime? Can this be quantified as an energy loss?

There are two ways of modelling such flow reduction

(a) to assume that an extra retarding force acts on the main channel flow below bankfull, which can be quantified as an additional shear on a horizontal plane at bankfull level.

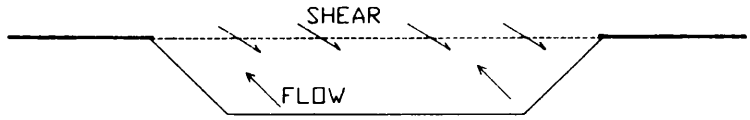

The physical justification for this lies in the fact that floodplain flow on the top of the main channel is decelerated or accelerated or deviated as sketched below, all of which require work done and hence an energy loss is expended. This additional shear may greatest at the cross-over region. Such a shear would be difficult to estimate would certainly require calibration for data of S.E.R.C. flume, but it does represent one possible way forward.

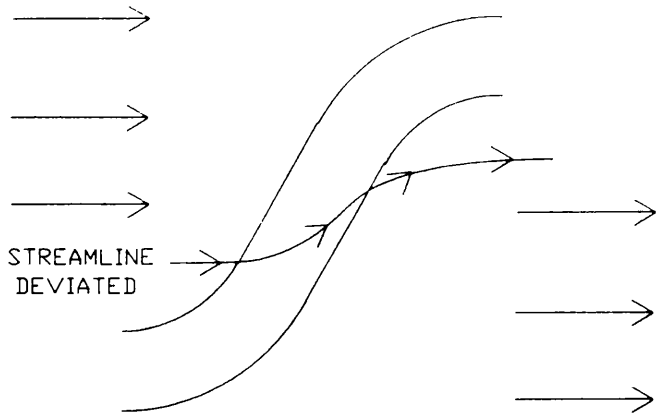

(b) Another way of approaching this problem is that the flow in main channel can be considered to have greatly reduced cross-sectional area flowing in the streamwise direction. This is demonstrated in the sketch below where plunging floodplain flows plunge into the main channel, occupying a large proportion of the cross-sectional area available and effectively leaving only the shaded area for the main channel flow to pass through.

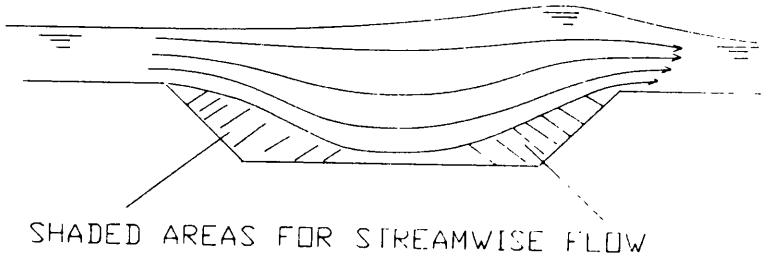

This idea would require also calibration from S.E.R.C. flume data.

(ii) Zone 2 of the energy loss model is above bankfull level and within the limits of the meander belt width. this represents the section of the floodplain flow which is continuously passing over the main channel, floodplain, main channel in sequence. From the energy contour plots in **Fig (6.24)** it is clear that this zone of separation is a good choice.

The flow retardation experienced by this flow mechanism has two components:

- Flowing over the floodplain.
- Flowing over the main channel where it also experiences horizontal retarding effect shear previously quantified by an expansion-contraction loss.

(a) The flow retardation on the floodplain is quantified simply from a knowledge of the floodplain roughness friction factor. This is a problematic with vegetation roughness which can bend in the flow or become flattened. Accurate estimates of floodplain roughness coefficients are notoriously difficult to estimate and constitute a substantial research programme alone. The S.E.R.C. flume data at least provides an accurate knowledge of the roughness coefficients for the smooth and rough cases, and hence can be used in testing a new energy loss model.

(b) The flow retardation of floodplain passing over the main channel might be treated like an expansion-contraction phenomenon. Flow visualisation studies in **Chapter 5** reveal that this is not exactly the case although many of the transverse velocities profiles especially in the cross-over region exhibit expansion-contraction type flow patterns as sketched below.

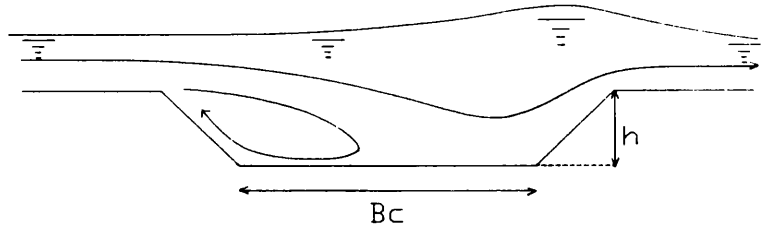

There are several flow features which are very similar to flow over a slot, namely,

- a recirculating cell forming below bankfull level, extending up to 6 times h into main channel.
- a plunging of the floodplain streamlines into the main channel and rising back out of the main channel at the opposite bank.
- a raising of the free water surface level at the downstream side of the main channel, flowed by a type of weir flow accelerating on the adjacent floodplain.

With this in mind there seems every justification for an expansion energy loss of the form

$$(1-y_f/y_c)^2 \quad U_{f2}^2/2g$$

Where y_f/y_c is the ratio of the floodplain depth to the main channel depth and U_{f2} is the floodplain velocity in Zone 2. Similarly a contraction loss can be estimated in the form.

$$C_L \, U_{f2}^2/2g$$

where C_L is the loss coefficient.
Jasem(1990) has carried out extensive tests on slot energy losses, with the aspect ratio of the main channel varying from Bc/h = 2.0 to 20.0. This was found to be a significant parameter, and **Jasem data(1990)** can be usefully added to an energy loss model.

The losses from this mechanism require to be integrated over a meander wave length and hence will be operating over a continually varying skew angle. The losses are applied only to the flood plain flow in Zone 2.

In a sense, applying expansion and contraction losses to Zone 2 flow is a gross over-simplification and requires detailed calibration with resulting velocities in Zone 2 as measured in the S.E.R.C. flume.

(iv) Zone 3 flows are completely outside the meander belt width and subject only to the boundary roughness in that zone. This area can be modelled from a knowledge of the outer floodplain roughness.

7.1.3 A Three Dimensional Numerical Model

The latest efforts at numerical modelling of complex three dimensional flows at the University of Glasgow have been conducted by **Manson(1991/1992) and Pender**, with an intention of simulating flows in the S.E.R.C. flume Series B, using the refined flow data available.

According to **Manson(1991)**, the model is intended to incorporate the following physical flow features:

. The flows are strongly three dimensional.
. The flow field may possess a non-stationary free surface.
. There may be local and global flow reversals.
. There may be significant turbulent stress fluxes.
. There may be external body forces such as Coriolis, buoyancy in addition to gravity.

The co-ordinate system used by **Manson(1992)** is shown in **Fig(7.1)** and the equations of Continuity and Conservation of Momentum shown in **Equations (7.1)** and **(7.2)**.

The equation of continuity in Tensor notation is given by

$$\frac{\partial U_j}{\partial X_j} = 0 \qquad (7.1)$$

and force-momentum by

$$\frac{\partial U_i}{\partial t} + \frac{\partial (U_j U_i)}{\partial x_j} = -\frac{1}{\rho}\frac{\partial P}{\partial x_i} + \frac{1}{\rho}\frac{\partial \tau_{ij}}{\partial x_j} + G_i \qquad (7.2)$$

where $U_{i,j,k}$ is the mean velocity in the x,y and z directions, G_i the body weight component, ρ density, t time, $x_{i,j}$ Cartesian coordinate system and τ_{ij} the interfacial shear stress.
The interfacial shear stress τ_{ij} is the stress exerted by fluid on fluid and may be represented by the expression

$$\tau_{ij} = \nu \left(\frac{\partial \bar{U}_i}{\partial X_j} + \frac{\partial \bar{U}_j}{\partial X_i} \right) - \rho \overline{u'_i u'_j} \qquad (7.3)$$

where ν is the kinematic viscosity.
The $\overline{u'_i u'_j}$ terms are known as the Reynold's stresses. There are now more unknowns than there are equations. The provision of a closure condition is a matter for the current research carried out by **Manson(1992)**.

Equation (7.3) shows that the interfacial stress is composed by two parts. For fully turbulent flow the first part of equation 7.3 becomes negligible compared to the second part throughout

most of the fluid. The problem of representing the interfacial stress becomes one of representing the Reynold's stress

Manson(1992) has adopted the Boussinesq's assumption which considers the Reynold's stress may be modelled as linearly proportionally to the mean strain rate with the constant of proportionality, ν_t, the eddy viscosity.

$$-\overline{u_i' u_j'} = \nu_t \left(\frac{\partial U_i}{\partial x_i} + \frac{\partial U_j}{\partial x_j} \right) - \frac{2}{3} k \delta_{ij} \qquad (7.4)$$

Manson(1992) has represented the eddy viscosity by a linear two equation model of turbulence consisting of transport equations for the turbulent kinetic energy per unit mass k :

$$k = \frac{1}{2} \overline{u_i' u_i'} \qquad (7.5)$$

and its rate of dissipation ε :

$$\varepsilon = \nu \overline{\frac{\partial U_i}{\partial x_i} \frac{\partial U_j}{\partial x_j}} \qquad (7.6)$$

Dimensional analysis suggests that,

$$\nu_t = c_\mu \frac{k^2}{\varepsilon} \qquad (7.7)$$

The transport equations for k and ε are,

$$\frac{\partial k}{\partial t} + \frac{\partial (U_i k)}{\partial x_i} = \frac{\partial}{\partial x_i} \left(\frac{\nu_t}{\sigma_k} \frac{\partial k}{\partial x_i} \right) + P - \varepsilon \qquad (7.8)$$

$$\frac{\partial \varepsilon}{\partial t} + \frac{\partial (U_i \varepsilon)}{\partial x_i} = \frac{\partial}{\partial x_i}\left(\frac{\nu_t}{\sigma_\varepsilon}\frac{\partial \varepsilon}{\partial x_i}\right) + c_1 \frac{\varepsilon}{k} P -$$

$$- c_2 \frac{\varepsilon^2}{k} \qquad (7.9)$$

where,

$$P = \overline{u_i' u_j'} \frac{\partial U_i}{\partial x_j}$$

The constants are assigned values 'standard values',

$c_\mu = 0.09$

$\sigma_k = 1.0$

$\sigma_t = 1.3$

$c_1 = 1.44$

$c_2 = 1.92$

The k-ε turbulence model will reproduce turbulent production, dissipation and transport process in the flow and will at least simulate prominent turbulent shear features in the flow, such as the floodplain flow passing over a main channel.

The k-ε turbulence model is not perfect however, in particular it poorly predicts the normal Reynold's stresses which are sometimes important in the analysis of secondary flows in straight compound channels.

The research at the University of Glasgow has led to a three dimensional model with a k-ε turbulence model, and has been

applied in the first instance to flow over the slot in a channel bed. This is similar to floodplain flow passing over a main channel flow below, as occurs to some extent in the cross-over region of meandering compound flows. Typical output from the computer model is shown in **Fig(7.2)** with velocities vectors predicted in the slot region. This work is expected to be extended to skewed and meandering compound flows, and represents a very promising method for accurate simulations of the main channel flows features.

7.2 CONCLUSIONS

In this section the Author summarises the conclusions of the experimental research in meandering compound flows performed by him and presented in this thesis. This includes the more general and the most important conclusions presented in **Chapters 4, 5 and 6**, which were the chapters where the analysis of the results of S.E.R.C. Series A and B and data of other small flumes was carried out.

7.2.1. General Conclusions

(1) Meandering Compound Flow behaviour bears little or no resemblance to straight parallel compound flow.
(2) The following flow mechanisms were identified in meandering compound flows:
- The expanding cell in the main channel region driven by cross-over floodplain flow.
- Cell rotation at bend apex and decay beyond bend.
- Efflux of main channel flow on to floodplain beyond the bend apex at the outer bend.
- High velocity distribution at the inner bend and at the edge of the cross-over region with the downstream floodplain as well as on floodplain outside the meander belt width.

- Deviation of floodplain streamlines on crossing over main channel.
- " Slack " region beyond each bend where old cell is decaying and new cell is beginning.

(3) The parametric analysis has shown that conveyance of meandering compound channels is affected by the relative flow depth(floodplain depth/main channel depth), relative boundary roughness(main channel boundary roughness/floodplain boundary roughness), main channel sinuosity, main channel cross-section shape, main channel aspect ratio and the ratio of meander belt width to the total floodplain width.

(4) The flow mechanisms and flow structures, in particular the secondary currents will affect the sediment transport and the pattern of scour and deposition in meandering compound channels. Measurements of the streamwise boundary shear stress conducted in the S.E.R.C. flume Series B have revealed a significant reduction of boundary shear will occur in the main channel and a substantial increase of boundary shear will appear, at the edge of the floodplain.

(5) The discharge held in the meandering main channel below bankfull is significantly lower than the discharge held in the main channel with no overbank flow. This is clearly a measure of the interaction effect as it affects the flow below bankfull. This effect increases substantially with sinuosity.

(6) The cross-section area of the meandering compound channel was divided into three zones and actual discharge of each zone was compared with the theoretical discharge that will occur in a straight channel with same boundary roughness, area and bed slope. The results show that:
- The discharge outside the meander belt width(Zone 3) is approximately equal to the theoretical discharge from skin friction.

- The discharge within the meander belt and above bankfull (Zone 2) is less than the theoretical discharge by 15% - 25%.
- The discharge in the main channel but below bankfull(Zone 1) is much smaller than the theoretical value. For instance, for trapezoidal cross-section with sinuosity 1.37, smooth floodplains and stage 200.0 mm, the reduction reaches 40%.

(7) The two-dimensional force-momentum equation applied in this work is not satisfactory for highly three-dimensional compound flows. The variation of the apparent shear force with stage and floodplain roughness has show no real trend.

7.2.2. Conclusions on Flow Resistance of Meandering Compound Flows.

(i) Flow resistance in meandering compound flows was analysed in terms of the relationship of the Manning's n with stage and the variation of the Darcy-Weisbach friction factor with Reynolds number.

(ii) For the overbank case, as depth increases, Manning's n tends to be almost constant for smooth floodplain but increases significantly with stage for the fully roughened floodplain case.
(iii) The Darcy-Weisbach friction factor tends to reduce with the Reynolds number for smooth floodplain case and increases almost linearly for the fully roughened floodplain case.

(iv) The Darcy-Weisbach friction, for smooth floodplain case, may rise 50% when main channel sinuosity increases from 1.37 to 2.04.

(v) In meandering compound channels with smooth floodplains and floodplain walls parallel, the flow resistance is controlled by main channel sinuosity, main channel aspect ratio and main channel cross-section shape, whereas in case of the fully

roughened floodplains the flow resistance is dominated by the effect of the floodplain roughness.

7.2.3. Conclusions on Conveyance of Meandering Compound Channels.

(i) Through non-dimensional functions F_1(for inbank case), and F_4 and F_5(for overbank cases), a parametric analysis of meandering compound flow was initiated and the non-friction energy losses were quantified.

(ii) Functions F_4 and F_5 reveal very clear the effects of main channel sinuosity, aspect ratio, floodplain roughness, main channel aspect ratio, main channel cross-section shape and the ratio meander belt width to the total channel width on the non-friction energy losses experienced by meandering compound flows.

(iii) Functions F_4 and F_5 have shown that losses of energy produced by skin friction can be low as 50% of total energy losses.

(iv) By increasing the main channel sinuosity from 1.37 to 2.04, function F_4 reduces about 15% for natural cross-section with smooth floodplains.

(v) For smooth floodplain case function F_4 shows more sensitivity to the effect of geometry of the cross-section. However for the fully roughened floodplain function F_5 is a better indicator.

(vi) Experimental studies of meandering compound flow should be conducted in physical models where the main channel aspect ratio is same as in nature. Therefore distorted models with low aspect ratios will exaggerate the losses of energy that occur in nature.

7.2.4 Conclusions on Flow Mechanisms and Flow Structures in Meandering Compound Flows.

(i) Floodplain flow approaching the main channel can bifurcate with part of the flow entering the main channel swirl and part crossing the main channel to the opposite floodplain.

(ii) The strength of secondary currents(transverse velocity/ streamwise velocity) in meandering compound flows is affected by depth of flow, geometry of cross-section, sinuosity and floodplain roughness. In particular the strength of secondary cells increases substantially as the stage rises from the inbank case to the overbank case.

(iii) It is expected that the levels of turbulence and the Reynolds shear stress will increase considerably, in meandering compound, as the flow goes from the inbank case to an overbank case.

(iv) Research performed at the Glasgow flume demonstrated that the large secondary cells observed in the main channel of the S.E.R.C. Series B are produced by floodplain flow shearing over the main channel below bankfull. In case that the floodplain possesses an infinite roughness, the secondary cell that appears at the bend apex will rotate clockwise for both inbank and overbank cases.

7.2.5. Conclusions on The Continuity, Energy and Momentum Equations Applied to Meandering Compound Flow.

(i) The analysis of discharge distribution in meandering compound channels carried out in the S.E.R.C. flume Series B has shown that mass exchange between the main channel and the floodplain flow is highly three-dimensional and is affected by the flow depth, boundary roughness, sinuosity and main channel aspect

7.2.6. Restatement of Conclusions of Interest to Two-Stage Channel Designers.

(i) Accurate Prediction of Stage Discharge Curve

The one-dimensional energy method proposed by **Ervine and Ellis(1987)** offers the simplest method for the calculation of stage-discharge relationship of meandering compound channels. The Series B data will allow this model to be calibrated for each zone of the flow field. Some proposals for the calibration procedure were presented in Section 7.1.1.. Further developments of a similar method are presently being undertaken by **Prof. Cris James and Mr. James Wark(1992)** at Hydraulics Research Ltd, Wallingford.

(ii) Significant Main Channel/Floodplain Interactions

The following flow mechanisms were identified in **Chapter 5**:

- An expanding cell in the main channel region driven by cross-over floodplain flow.
- Cell rotation at bend and decay beyond bend.
- Efflux of main channel flow on to the floodplain beyond the bend apex and at the outer bend.
- High velocity distribution at the inner bend and on the floodplain outside the meander belt width.
- Deviation of floodplain streamlines on crossing over main channel.
- A "Slack " region beyond each bend where old cell is decaying and the new cell is beginning.

(iii) Parametric Analysis of Conveyance of Meandering Compound Channels.

The parametric analysis carried out by the **Author** in **Chapter 4** shows that the following parameters affect the flow conveyance of meandering compound channels:

- The relative depth of flow(Section 4.5).
- Ratio between main channel and floodplain roughness (Section 4.5).

- The sinuosity of the main channel(Section 4.5.9).
- The shape of the main channel(Section 4.5.9).
- The aspect ratio of the main channel(Section 4.5.9).
- The ratio of meander belt width to the total floodway width(Section 4.5.9).
- The ratio of main channel top width to the total width of the floodway(Section 4.5.).

(iv) Boundary Shear Stress Distribution in Meandering Compound Channels.

In meandering compound channels, the boundary shear stress distribution in the main channel region is significantly affected by stage and by sinuosity.

As the stage passes from inbank to overbank, the boundary shear stress in the main channel reduces considerably. This effect increases with sinuosity. As a result the main channel will loses capacity to carry sediments in the streamwise direction. However, its capacity in transporting sediments in the transverse direction of the main channel will be substantially increased in comparison with the inbank case.

The maximum values of boundary shear stress are located on the downstream floodplain at the downstream end of the bend, near the cross-over region, where the flow is accelerating. In this region where scour will problably occur. The peaks of boundary reach between 1.5-2.0 times the values that occur in straight channels.

ratio as well as main channel cross-section shape.

(ii) The effect of sinuosity and main channel aspect ratio as well as main channel cross-section shape on the conveyance of meandering compound channels is more pronounced in the case of smooth floodplains.

(iii) The main channel discharge reduces from bend apex to start of the cross-over and increases in symmetrical fashion from the end of the cross-over region to the next bend.

(iv) Energy levels in the main channel and floodplain region diminish with increasing sinuosity and floodplain roughness.

(v) Momentum equation applied in X direction in the floodplain region has revealed that the body weight component is approximately in balance with the boundary shear force and the maximum values of the apparent shear force are located near the cross-over region, in blocks Nos. 5 and 6.

(vi) The balance of the lateral shear force in the cross-over region in the S direction is produced by the turbulence term ($\overline{u'v'}$) and is positive.

(vii) Comparison between the Author's results and **Elliot and Sellin(1990)** findings showed that the apparent shear force which develops at the interface of the cross-over region with downstream floodplain increases substantially with the skew angle.

7.3 FURTHER RESEARCH

The following topics are suggested for further research in meandering compound flows:

(i) Physical modelling of other compound meander geometries

The S.E.R.C. flume Series B study, although at a large scale, investigated only a narow range of basic meandering compound geometries. This now needs to be extended to a systematic physical study of a range of other key parameters, small or large scale, so that a detailed parametric analysis of meandering compound flow can be performed.

(ii) A physical modelling programme for boundary roughness

Energy losses in a river channel are dependent on bed material size (d_{50}), bed form losses(pools and riffles), planform losses(bends and cross-overs) vegetation(grass, weeds and trees) and biomass loss due to algae growth. A comprehensive study of estimating the magnitude of each component loss should be performed.

This could be extended to floodplain boundary roughness, where the best method of simulation by using rods, flexible elements, mesh has not been yet established.

(iii) Scale effect data study

A detailed study of scale effect in meandering compound flows needed to be carried out. This research should be started by comparing prototype real rivers data against data obtained in reduced models. **Higginson(1992)** has already initiated the research in this area by comparing results obtained in the river Maine in Northern Ireland against data produced by a physical model. The investigation could be complemented by comparing results of the S.E.R.C. flume Series B with data obtained in small scale flumes.

The study of scale effect in meandering compound flows should be performed by analysing the variation of the Reynolds

Number with the Darcy-Weisbach friction factor.

(iv) Interaction of channel flow structures and bed topography in two-stage channels.

The time has come for a study of compound flows using mobile beds. The general purpose of the experimental work would be to conduct an investigation of sediment transport and morphology in a river/floodplain system during overbank flow. The work would cover both straight and meandering compound channels, coarse and fine sediments, with some inbank studies as well as overbank. The investigation should analyse the changes in sediment transport and deposition during overbank flow, as well as changes in the pattern of large flow structures for natural channels with overbank flow. This constitutes the research programme proposed by the Universities of Aberdeen, Glasgow and Newcastle upon Tyne for S.E.R.C. Series C which was supposed to follow the S.E.R.C. Series B study.

(v) Numerical modelling of meandering compound flows by the mixing length determination of ε(eddy viscosity).

A simplified quasi-three dimensional numerical model of the type initiated by **Hardwick(Aberdeen)** requires further development.

Numerical simulation of meandering compound flows should be carried out using the mixing length approach for eddy viscosity. One wave length of the meander is divided into rectilinear finite elements on the floodplain and elements conforming to the channel(plan) curvature in the main channel and above it. Equations of momentum and continuity are solved for the elements over a wavelength. This research programme has been initiated by **Mr. R. Hardwick** from Aberdeen University. **Fig(7.3)** shows on the y-z plane(tranverse direction) comparisons of secondary currents

predicted by the model and observed in FCF at Wallingford for sinuosity ≅ 1.4, for the apex and the middle of the cross-over reach. The observations show only horizontal components of the y-z plane velocities. Dye visualisations, however suggest that the model lacks some important features found in the flow. The model could be improved by refining the spatial schematisation and by varying the water surface level which at present was considered (artificially) parallel to the floodplain with no local water surface variations.

(vi) Numerical simulation of meandering compound flows by one-dimensional energy method suggested by **Ervine and Ellis(1987)**.

The one-dimensional energy method proposed by **Ervine and Ellis(1987)** for the calculation of stage-discharge relationship in meandering compound flows should be improved. Data obtained in S.E.R.C. Series B will allow a calibration of the discharge calculated for each zone of the flow field. Some proposals for the calibration procedure were presented by the Author in Section 7.1.1., and developments of this nature are presently being undertaken by **Prof. Chris James and Mr. James Wark** at Hydraulic Research Ltd, Wallingford.

(vii) Three-dimensional models of meandering compound flows with two equation models of turbulence.

A research project on the numerical simulation of meandering compound flows by a three-dimensional model with two equation turbulence model has been presently undertaken at Glasgow University by **Mr. Russell Manson** under the supervision of **Drs. G. Pender and A. Ervine**. The model was first used to simulate flow passing over a slot in a channel bed, which is similar to floodplain flow passing over the cross-over region of a

meandering compound flow. The model will be extended to skew and meandering compound flows, and represents a very promising method for accurate simulations of three-dimensional flow features.

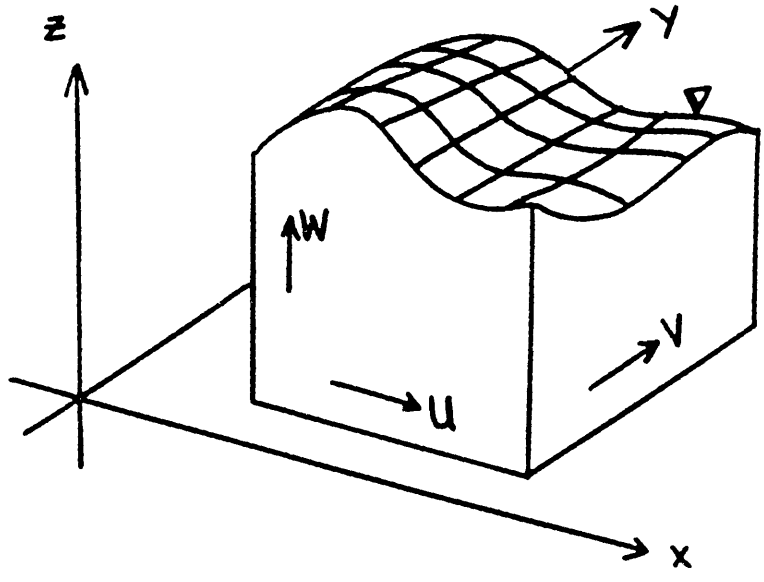

Fig (7.1) - The Coordinate System Used by Manson(1992).

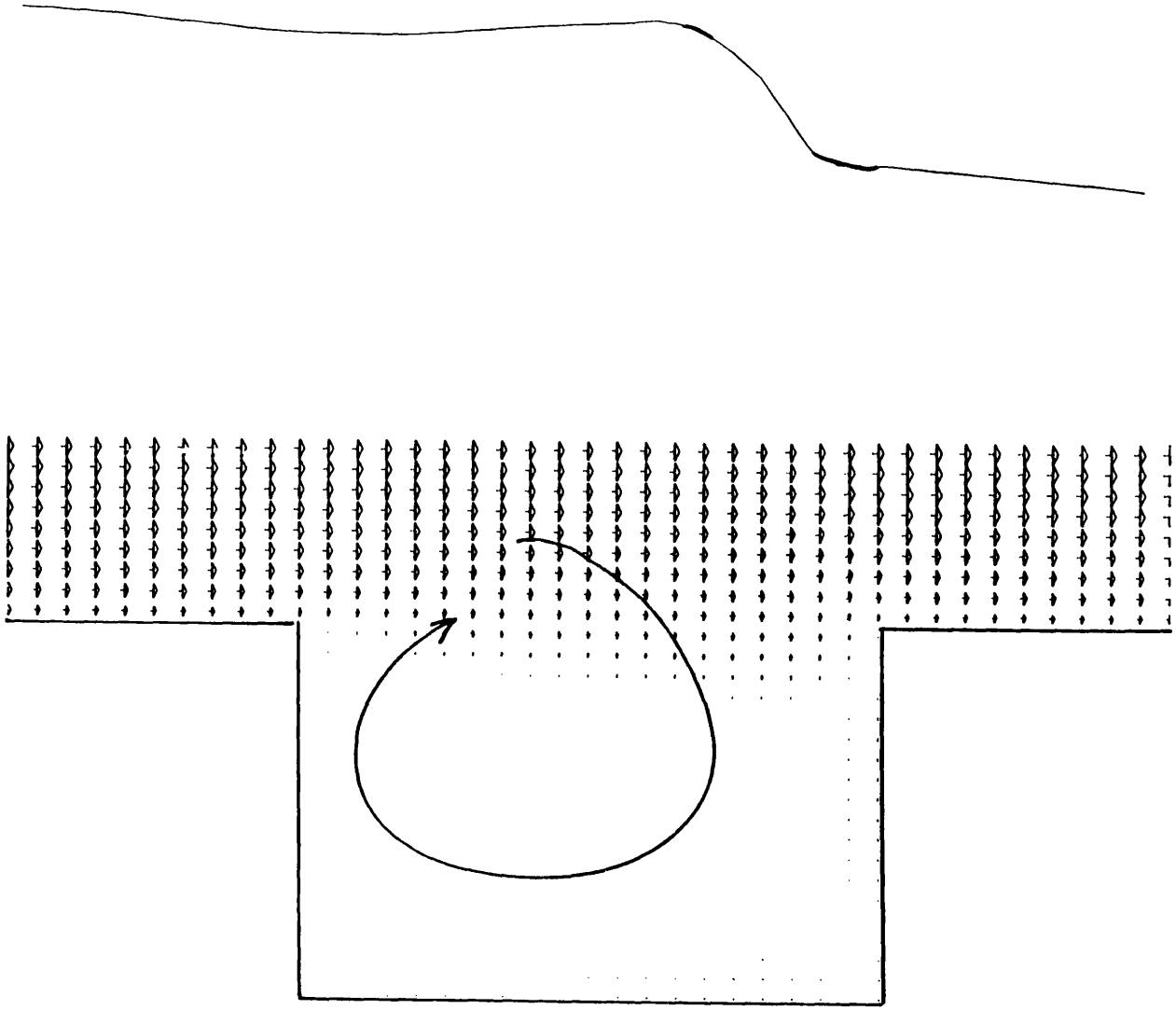

Fig (7.2) - Water Surface Profile and Velocity Vectors of a Flow over a Slot(from Manson (1992)).

ABERDEEN MODEL RESULTS

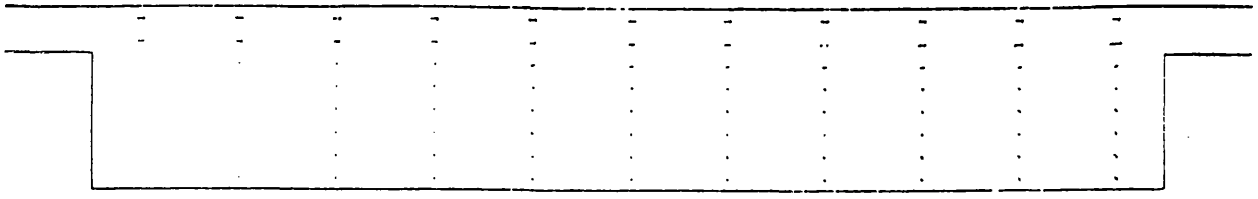

APEX

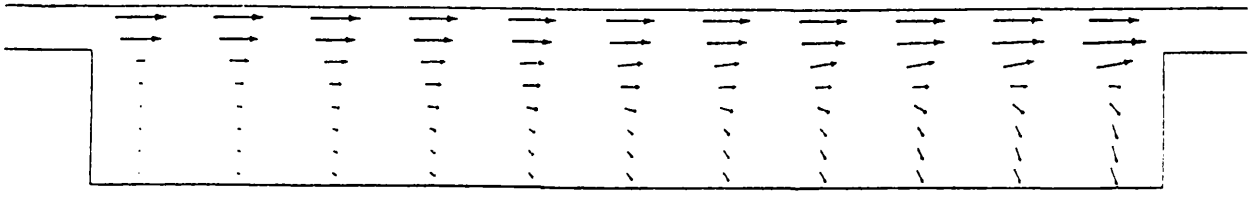

CROSSOVER

S.E.R.C. - F.C.F. FLUME RESULTS

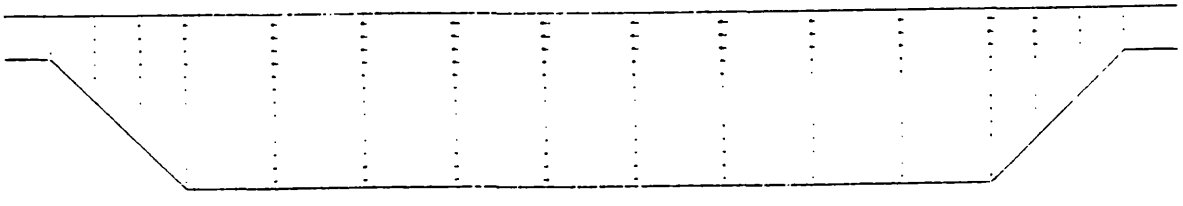

APEX

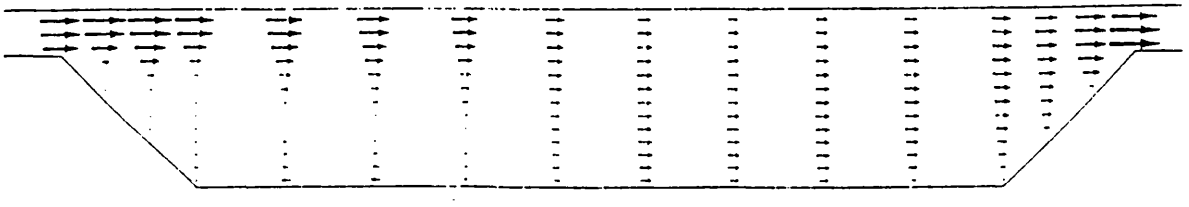

CROSSOVER

Fig (7.3) Comparison of Hardwick's Numerical Model and Experimental Velocities from S.E.R.C. Series B, Sinuosity 1.37, Trapezoidal Cross-Section and Smooth Floodplains.

BIBLIOGRAPHIC REFERENCES

Ackers P. and White R. " Feasibility study of tests with sediment ". S.E.R.C. PHASE " C " EXPERIMENTS, June **1990.**

Ackers P. "Hydraulic design of straight compound channels ". H. R. Wallingford. Report SR 281 October **1991.**

Ahmadhi R. "Experimental study of the interaction between main channel and floodplain flows." Phd University of Alberta, Edmonton, Canada, **1979.**

Baird J.I. and Ervine D.A." Resistance to flow in channels with overbank floodplain flow." Proc. of the first Int. Conf. on Hydraulic Design in Water Resources Engineering: channels and channels control structures, University of Southampton, p. 4.135-4.150 **April 1984.**

Bathurst, J.C. , Thorne C. R. and Hey R.D. " Secondary flow and shear stress at river bends." Jnl of Hydraulic Division pp 1277-1295 A.S.C.E. HY 10 **October 1961.**

Bhowmik N. G. and Demissie M. " Carrying capacity of floodplains " Proc. of A.S.C.E. Jnl of Hydraulic Division Vol. 108, no. Hy3, March **1982.**

Chang, H. "Fluvial processes in river engineering." John Wiley "& Sons **1987.**

Chow V.T. "Open Channel Hydraulics" New York Mcgraw Hill,**1959.**

Cunge J., Holly F. and Verwey A.,"Practical Aspects of Computational River Hydraulics", Pitman, London **1980.**

Elliot S. and Sellin R. " SERC Flood channel facility : Skew flow experiments ", J. Hydraulic Research, Vol. 28, no.2, IAHR, Delft, pp 197-214,**1990.**

Einstein H. A. and Banks R.B., "Fluid resistance of composite roughness", Trans America Geophysical Union, 31, No. 4, pp 603-610 **August 1950.**

Ervine D. A. and Baird J.I."Rating curves for rivers with overbank flow ." Proc. I.C.E. Part 2, Vol. 73, **June 1982.**

Ervine D. A.and Ellis J. "Experimental and computational aspects of overbank floodplain flow " Trans. Royal Society of Edinburgh, vol. 78, 315-325, **1987.**

Ervine D. A.and Jasem H.K. " Two-Stage channels with skewed compound flow." (for publication in A.S.C.E.) **1992.**

Fares, Y. R. "Effects of cut-off(flood relief) channel intersection on bend flow characteristics" Thesis submitted in Fulfilment of the Requirements for the degree of Doctor of Philosophy, Department of Civil Engineering University of Glasgow, Glasgow, **1989.**

Goncharov V. N. " Dynamic of channel flow " Israel Program for Scientific Translation, Jerusalem, **1964.**

Greenhill, R. " S.E.R.C. Series B Data, Measurements of Stream Angles and Resultant Velocities and Stage-Discharge Data for Sinuosity 1.37, Trapezoidal Cross-Section, Smooth Floodplains, Inbank and Overbank Cases", Report published by The Department of Civil Engineering of Bristol University. **Volume I, 19/10/89 to 5/3/90.**

Greenhill, R. " S.E.R.C. Series B Data, Measurements of Stream Angles and Resultant Velocities and Stage-Discharge Data for Sinuosity 1.37, Natural Cross-Section, Smooth Floodplains, Inbank and Overbank Cases", Report published by The Department of Civil Engineering of Bristol University. **Volume II, July to October 1990.**

Greenhill, R. " S.E.R.C. Series B Data, Measurements of Stream Angles and Resultant Velocities and Stage-Discharge Data for Sinuosity 1.37, Natural Cross-Section, Roughened Floodplains, Overbank Case", Report published by The Department of Civil Engineering of Bristol University. **Volume III, October 1990 to January 1991.**

Greenhill, R. " S.E.R.C. Series B Data, Measurements of Stream Angles and Resultant Velocities and Stage-Discharge Data for Sinuosity 2.04, Natural Cross-Section, Smooth Floodplains, Inbank and Overbank Cases", Report published by The Department of Civil Engineering of Bristol University. **Volume IV, April 1991 to June 1991.**

Greenhill, R. " S.E.R.C. Series B Data, Measurements of Stream Angles and Resultant Velocities and Stage-Discharge Data for Sinuosity 2.04, Natural Cross-Section, Roughened Floodplains,

Inbank and Overbank Cases", Report published by The Department of Civil Engineering of Bristol University. **Volume V, August 1991 to October 1991.**

Hardwick, R. "Measurements of local surface levels in the S.E.R.C. flume Series B ". Technical Report from Civil Engineering Department of University of Aberdeen. S.E.R.C. Series B. October. **1990.**

Hardwick, R. "Measurements of local surface levels in the S.E.R.C. flume Series B "Technical Report from Civil Engineering Department of University of Aberdeen. S.E.R.C. Series B. July. **1991.**

Hardwick, R. "Velocity and Angle easurements on the floodplains of the S.E.R.C. flume Series B ". Technical Report from Civil Engineering Department of University of Aberdeen. S.E.R.C. Series B. February. **1991.**

Hey, R.D., " Geometry of river meanders." Nature, 262, pp 482-484, **August 1976.**

Ippen, A. T. and Drinker, P.A. " Boundary shear stress in curved trapezoidal channels." J. Hydraulics Division A.S.C.E., 88 HY5, pp 143-180, **September 1962.**

Jansen, P.Ph.," Principles of River Engineering",Pitman, **1979.**

James, M. and Brown J. " Geometric parameters that influence floodplain flow."U.S.A. Army Corps of Engineers Waterways Experiment Station Viksburgh Report H-77-1, **June 1977.**

Jasem, H. K. "Flow in two-stage channels with main channel skewed to the floodplain direction" Thesis submitted in Fulfilment of the Requirements for the degree of Doctor of Philosophy, Department of Civil Engineering University of Glasgow, Glasgow, **June 1990.**

Kalkwwijk, J. P. and De Vriend, H. J. "Computation of the flow in shallow river bends." Jnl. of Hydraulics Research No.4, pp 327-342, **1980.**

Kawara Y. and Tamai N. "Numerical calculation of turbulent flows in compound channels with an algebraic stress turbulence model" Proc. 3rd Symposium Refined Flow Modelling and Turbulence Measurements Tokyo, Japan, p. 527-536, **1988.**

Kawara Y. and Tamai N. "Mechanism of lateral momentum transfer in compound channel flows " 23rd I.A.R.H. Congress, Ottawa **August** 1989.

Keller R. J. and Rodi W. "Prediction of main channel/floodplain flows." J.Hydraulic Research, Vol.26, no.4, p 425-441,**1988.**

Kiely R. J. "An experimental study of overbank flow in straight and in meandering compound channels." Ph.D. Thesis submitted to Civil Engineering Department of Unversity College, Cork, Republic of Ireland **September 1989.Kikkawa, H. , Ikeda , I. and Kitagawa, A.,** " Flow and bed topography in curved open channels." J. Hydraulic Div. A.S.C.E., 102 HY9, pp 1327-1342, **September 1976.**

Knight D.W., Shiono K.and Pirt J, "Prediction of depth mean velocity and discharge in natural rivers with overbank flow, Conf. on Hydraulic and Environmental Modelling of Coastal, Estuarine and Rivers Waters, ed. Falconer, Goodwin and Matthew Gower Tecnical Press, 419-428, **1989.**

Kondrat'ev, N. E. ed. "River flow and river and river channel formation."**1959** Transl. from Russian and published by the Israel Program for Scientific Translations, Jerusalem, **1962.**

Leopold L. B. and Wolman M.G." River channel patterns; braided, meandering and straight. " USGS Profissional Paper 282-B, pp 45-62, **1957.**

Leopold L. B. and Wolman M.G." River meanders" Geol. Soc. Am. Bull. ,71 pp 769-794 **1960.**

Leschziner, M. and Rodi, W. "Calculations of strongly curved open channel flow." Jnl. of Hydraulic Division A.S.C.E., Vol. 105, No. Hy 10, **October 1979.**

Mckeogh E.J. and Kiely G. K. " A comparison of velocity measurements in straight, single meander and multiple meander compound channels " Int. Conf. on Channel Flow and Catchment Runnoff, Centennial of Manning's n formula and Kuichling's Rational Formula. University of Virginia **May 1989.**

Mckeogh E.J., Kiely G. K. and Javan M." Velocity and turbulence measurements in a straight channel with interacting floodplains using laser Doppler anemometry" Int. Conf. on Hydraulics and Environment Modelling of Coastal, Estuarine and River Waters,

Bradford U.K. September 1989.
Manson, R. " The Development and application of a numerical model for simulating free surface turbulent flows". Internal Report No. 1, Glasgow University, 1991.
Manson, R. " PhD. research in computational hydraulics ". Internal Report No. 2. Glasgow University, May, 1992.
Mitchell, A. R. and Griffiths, D. F." The finite difference method in partial differential equations". Published by John Wiley & Sons. 1980.
Mockmore C.E. " Flow around bends in stable channels ." Transactions A.S.C.E. Vol. 109,1944.
Myers W. R. C. "Velocity and discharge in compound channels." Proc. of Jnl. Hydraulic Eng. A.S.C.E., Vol. 113, no. Hy6 June 1987.
Michhofer L., "Roughness investigations in with concrete bottom and unlined walls". Wasserhraft und Wasserwirtschaft, Munich, 28, No. 8, pp 85-88, 1933.
Myers W. R. C. and Elsawy E.M. "Boundary shear in channel with floodplain." Proc. of Jnl Hyd. Eng., A.S.C.E., Vol. 101, no. HY7 1975.
Myers W. R. C. and Brennan E.K. "Flow resistance in compound channels " J. Hydraulic Research, vol. 28, no.2, 1990, I.A.H.R., Delft 141-156 1990.
Nalluri C. and Judy N. D. " Interaction between main channel and flood plain", Proc. 21st Congress I.A.R.H., Melbourne, Australia p 377-382 1985.
Nelson, J.M. and Smith, J. D. " Flow in meandering channels with natural topography",(pages 69-101), River Meandering. Water Resources Monograph 12. Edited by S. Ikeda and G. Parker. 1989.
Patel, V. C." Calibration of the Preston tube and its limitations on its use in pressure gradients", J. Fluid Mechanics, part 1, p.p. 185-208, 1965.
Pavlovski, N.N., "On a design formula for uniform movement in channels with non-homogeneous walls". Trans All Union Scientific Research Institute of Hydraulics Enginnering, Leningrad, 3, pp 157-164, 1931.

Pender, G. "The numerical modelling of tide and flood movement in two-dimensional space using implicit finite difference methods" Thesis submitted in Fulfilment of the Requirements for the degree of Doctor of Philosophy, Department of Civil Engineering University of Strathclyde Glasgow, 1985.

Posey C.J.F. "Computation of discharge including overbank flow." Civil Engineering A.S.C.E. No.CE4, Vol.37, April 1967.

Prinos P., Townsend R. and Tavoularis S. " Structure of turbulence in compound channel flows " J. Hydr. Eng.,A.S.C.E. 111, 1246-1261 1985.

Preston, J.H. "The determination of turbulent skin friction by means of Pitot tubes. J. Roy. Aer. Soc. 58,109,1954.

Radojkovic M. "Mathematical modelling of rivers with floodplains." 3rd Annual Symp. Water Ways Harbours and Coastal Div. A.S.C.E. Vol.1,1976.

Radojkovic M. and Djordjevic S. " Computational of discharge distribution in compound channels" 21st I.A.R.H. Congress, Melbourne 1985.

Rajaratnam N. and Ahmadi R. " Hydraulics of channels with floodplains I.A.R.H. Jnl of Hydr. Res. Vol. 19 no. 1 1981

Rajaratnam N. and Ahmadi R. "Three notes on hydraulics of channels with floodplains". Proc. Hydrocomp, Dubrovnik, published, published by Elsevier Applied Science as " Computational modelling and experimental methods in hydraulics."pp 224-233 1989.

Raju S. P., "Resistance to flow in curved open channels." abridged translations of hydraulics papers, Proceedings A.S.C.E. p 49 November 1937.

Ramsbottom D.R."Flood discharge assessment." Interim Report Hydraulics Research Ltd., Report SR 195

Rouse, H. ed. " Advanced mechanics of fluids." John Wiley & Sons New York,1959.

Rozovskii, I. L. " Flow of water in bends of open channels." The Academy of Sciences of The Ukrainian SSR 1957, Translated from Russian by the Israel program for Scientific Translations, Jerusalem, Israel 1961.

Samuels P.G. " Modelling of river and floodplain flow using the finite element method." ,Hydraulic Research Ltd. Report SR 61.1985.

Samuels P.G. " The hydraulics of two stage channels- review of current knowledge- Conference of Rivers Engineers University of Loughborough July 1989.

Sellin R.H.J." A laboratory investigation into the interaction between the flow in the channel of river and over its floodplains. " La Houille Blanche, 7, 1964.

Sellin R.H.J. and Giles A. "Two-Stage channel flow". Publication of University of Bristol, Department of Civil Engineering July 1988.

Sellin R.H.J. and Searle D.J. "Flow mechanisms in spilling meander channels. " 23rd I.A.R.H. Congress Ottawa, August 1989.

Shiono K. and Knight D. W. " Two dimensional analytical solution for a compound channel." Proc. 3rd Int. Symp. on Refined Flow Modelling and Turbulence Measurements, Tokyo, July 1988.

Shiono K. and Knight D. W. " Transverse and vertical Reynolds stress measurements in a shear layer region of a compound channel " 7th Symposium on Turbulent Shear Flows Stantford August 1989.

Shiono K. and Knight D. W. " Turbulent open-channels flows with variable depth across the channel." J. Fluid Mechanics Vol. 222, p. 617-646 1991.

Shukry A. " Flow around bends in stable channels". Transactions A.S.C.E. Vol. 115 1950.

Stein C.J. and Rouve' G. "2D Depth averaged numerical predictions of flow in a meandering channel with compound cross section." Computational Mechanics Publication Hydrosoft Vol.2, No. 1, 1989.

Thompson J. " On the origin of winding of rivers in alluvial plains, with remarks in the flow of water around the bends in pipes." Proc. Royal Soc. London, England Vol. 25, 1876

Toebes G.H..and Sooky A.A. "The hydraulics of meandering rivers with floodplain". Proc. A.S.C.E. Jnl. of Waterways and Harbours". Div. Vol. 73 pp. 213-236,1967.

Tominaga A. and Nezu I. " Turbulent structure in compound open channels flows " Jnl of Hyd. Eng., A.S.C.E., 1991

U.S.A. Corps of Engineers "Hydraulic capacity of Meandering channels in straight floodways." Technical Memorandum, No.2-429, March 1956.

Vreugdenhill, C.B. and Wijbenga, J.H.A. "Computation of flow patterns on rivers", J. Hydr. Div., A.S.C.E. Vol. 108 No. 11 1982.

Wark J., Samuels P. G. and Ervine D. A. " A pratical method of estimating velocity and discharge in compound channels." Int. Conf. on River Hydraulics, Wallingford, England, September 1990.

Willetts B.B., Hardwick R.I. and Maclean, A.G. "Model studies of overbank flow from a meandering channel". International Conference on River Hydraulics, edited by W.R. White Hydraulics Research Limited, Published by John Wiley & Sons Ltd pp 197-205 September 1990.

Wark J., Slade J. and Ramsbottom D., "Flood Discharge Assessment by the Lateral Distribution Method", Report Sr 277, Hydraulics Research Ltd, Wallingford, December, 1991.

Williams, J.J., " Large eddy simulations", Symposium of I.A.H.R. Is turbulence modelling of any use. London, April, 1992.

Webber, N. B." Fluid mechanics for Civil Engineers ", Published by Chapman and Hall Ltd. 1971.

Wormleaton P.R. "Determination of discharge in compound channels using the dynamic equation for lateral velocity distribution" Proc. Int. Conf. on Fluvial Hydraulics, Vitaki, Budapeste, 1988.

Wormleaton P.R. and Merret D. "An improved method of calculation for steady uniform flow in prismatic main channel/floodplain sections, Jnl of Hydraulic Research, Vol. 28 No.2 I.A.H.R., Delft 157-174 1990.

Yalin, M. S. " On the formation of dunes and meanders" Proceedings of 14th. International Congress of the Hydraulics Reseaarch Association, Paris pp 1-8 1971.

Yen, B. "Characteristics of sub-critical flow in in meandering channels." Institute of Hydraulic Research University of Iowa, Iowa City, 1965.

Yen, B. "Flood flow over meandering channels." River Meandering Conference, Louisiana, 1983.

Younis, B. " Some Turbulence Models", Symposium of I.A.H.R. Is Turbulence Modelling of any Use. London, April, 1992.

Zeller,J. "Meandering Channels in Switzerland." Publication International Association of Scientific Hydrology, 75, 174-86, 1967.

Zheleznyakov G.V. " Relative deficit of mean velocity of unstable river beds with floodplain." Proc. 11th International Congress I.A.H.R. Leningrad, 1965.

James, C. and Wark J., "Assessment to flows in meandering compound channels". Report No. E.X. 2606 from Hydraulics Research Ltd, Wallingford, September, 1992.

Pursglove, J. "Taming the flood" A History and Natural History of Rivers and Wetlands. Oxford University Press with Channel 4. Television Company, 1989.

Sellin, R.H. "Environmental and hydraulic aspects of compound channel design". One-Day Seminar on River & floodplain management. Sponsored by the Scottish Hydraulics Study Group. Glasgow. 22nd March, 1992.

UNIMAP, UNIRAS, VERSION 5, UNIRAS LTD, Slough, August 1988.

Willetts, B.B. and Hardwick, R.I. "Model studies of overbank flow from a meandering compound channel". In White, W.R. (Ed.) River Flood Hydraulics. Wiley & Sons, London. 1990.

APPENDIX Ia

PROGRAMME AND SCHEDULE OF THE S.E.R.C. PROJECT
PERIOD 1988/91
SERIES B MEANDER GROUP

SERIES B : MEANDER GROUP | Revision date: 25/06/91 | Circulation date: 17/07/91 | Resident RA at HR

item no.	FCF - PROGRAMME AND RA SCHEDULE: Geometry	Test details	Week No	week 1989	Rosemary Greenhill	Manuel Lorena	Richard Hardwick	Birmingham Univ.
1	Trapezoidal 60° meander	Commissioning of flume and completion	1	11/9	√			
			2	18/9	√			
			3	25/9	√			
			4	2/10	√	√	√	
			5	9/10	√		√	
2		H v Q data inbank	6	16/10	√	√		
		and H v Q data overbank	7	23/10	(12?)	√		
			8	30/10		√	√	
		Completion of traverser	9	6/11	√		√	
		and data collection	10	13/11	√			
		software	11	20/11	½	√		
			12	27/11		√		
			13	4/12	½	√	½	
			14	11/12			√	
			15	18/12			√	
		Christmas Closure 9 days	16	25/12				
3				1990				
		Inbank U+θ data	17	1/1	½			
		depth = 100mm	18	8/1	√	√		
			19	15/1		√		
			20	22/1		√	½	
			21	29/1			√	
4		Overbank U+O data	22	5/2			√	
		depth = 200mm	23	12/2			√	
		U + θ DATA Depth = 200mm	24	19/2	√			
		U + θ DATA Depth = 200mm	25	26/2	√			
5		Laser measurements	26	5/3	√			√
		and boundary shear	27	12/3			√	√
			28	19/3			√	√
			29	26/3			√	√
			30	2/4				√
			31	9/4	√			√
		U + θ DATA Depth = 250mm	32	16/4	√			
		½ week U + 0 DATA	33	23/4	½			
6		Dispersion	34	30/4				
		Heriott Watt and	35	7/5				
		Sheffield Universities	36	14/5				
			37	21/5				
		Flow visualisation	38	28/5			√	
		Profiles and U + 0 DATA	39	4/6	½		√	
		U + θ DATA Depth = 250mm	40	11/6	√			
7	Natural 60° meander	Remould of Main Channel (Natural Inserts)	41	18/6	HR staff			
			42	25/6				

					Ro	Ma	Ri	B'ham
	Natural	survey of main channel	43	2/7		√		
8	60° meander	H v Q : overbank	44	9/7		√		
		H v Q : inbank	45	16/7	½			
		Water surface profiles	46	23/7			√	
		Flow visualisation	47	30/7			√	
9		U + θ DATA Depth = 200mm	48	6/8			√	
		U + θ DATA Depth = 200mm	49	13/8	√			
10		U + θ DATA Depth = 250mm	50	20/8	√			
		U + θ DATA Depth = 250mm	51	27/8	√			
		Laser Measurements	52	3/9				√
			53	10/9		√		√
11	Narrow fp	H v Q : overbank	54	17/9		√	√	√
		Laser Measurements	55	24/9		√		√
			56	1/10				√
			57	8/10				√
12		U + θ DATA Depth = 165mm	58	15/10	√			
		U + θ DATA Depth = 140mm	59	22/10	√			
		H v Q semi rough	60	29/10	√			
	semi-rough	H v Q overbank	61	5/11				
13	fully roughened flood plain	H v Q overbank	62	12/11				
		U + θ DATA Depth = 200mm	63	19/11		√		
		U + θ DATA Depth = 200mm	64	26/11		√		
		Flow visualisation	65	3/12			√	
		U + θ DATA Depth = 250mm	66	10/12			√	
		U + θ DATA Depth = 250mm	67	17/12			√	
		Christmas Closure	68	24/12				
		U + θ Data Depth = 165mm	69	31/12	½			
				1991				
		extra H v Q DATA	70	7/1	√			
14	Smooth	Laser Measurements at	71	14/1		√		√
		Section 3 +40°	72	21/1		√		√
			73	28/1		√	√	
15		Photographs, H v Q blocks	74	4/2			√	
16	110° Natural meander	Construction of 110° meander system	75	11/2	HR staff			
			76	18/2				
			77	25/2				
			78	4/3				
			79	11/3				
			80	18/3				
			81	25/3				
17		SURVEY NEW CHANNEL	82	1/4	√			
18	Smooth flood plain	H v Q : inbank	83	8/4				
		H v Q : overbank	84	15/4				

19		H v Q and U + θ at 200mm U + θ DATA Depth = 200mm+fp U + θ DATA Depth = 140mm Water surface profiles Flow visualisation U + θ DATA Depth = 140mm U + θ DATA Depth = 165mm Boundary Shear Measurements	85 86 87 88 89 90 91 92	22/4 29/4 29/4 6/5 13/5 27/5 3/6 10/6	√ √ √	 √ √ √	 √ √ 	
20		Laser Measurements	93 94 95 96 97	17/6 24/6 1/7 8/7 15/7				√ √ √ √ √
21		Dispersion Sheffield University	98 99 100	22/7 29/7 5/8			✓	
22		Vertical Vels and 250mm	101	12/8	√			
23 24		H v Q Semi-Rough H v Q Fully Roughened	102 103	19/8 26/8				
25	Fully Roughened Flood plain	U + θ Depth = 165mm U + θ Depth = 200mm Water Surface Profiles Flow visualisation	104 105 106 107	2/9 9/9 16/9 23/9	√	 √ 	 √ √	
26 27 28		H v Q Breeze block piers H v Q Narrow Flood plain H v Q with Sand Bags? Contingency	108 109 110 111	30/9 7/10 14/10 21/10				

APPENDIX I

STAGE-DISCHARGE DATA FROM THE S.E.R.C. FLUME SERIES B

AND FROM THE GLASGOW FLUME

APPENDIX I

STAGE-DISCHARGE DATA FROM THE S.E.R.C. FLUME SERIES B

Sinuosity 1.37

Inbank case

Slope: $0.7249 * 10^{-3}$

Main Channel Cross-Section: Trapezoidal

Depth mm	Discharge m^3/s	Temperature ^{o} C
63.76	0.0238	14.7
67.24	0.0251	11.0
77.15	0.0305	10.8
86.18	0.0363	11.6
90.08	0.0397	14.5
91.7	0.0402	11.5
97.7	0.044	11.6
103.0	0.0478	11.5
105.8	0.050	11.7
106.0	0.0497	10.9
111.5	0.0547	13.7
114.0	0.057	12.7
115.95	0.0583	14.2
118.97	0.0604	14.1
131.5	0.0707	12.9
137.37	0.076	14.5

APPENDIX I

STAGE-DISCHARGE DATA FROM THE S.E.R.C. FLUME SERIES B

(Continued)

Sinuosity 1.37

Inbank case

Slope: $0.7249 * 10^{-3}$

Main Channel Cross-Section: Natural

Depth mm	Discharge m^3/s	Temperature ^{o}C
94.9	0.0105	13.8
102	0.01368	13.8
109.7	0.01765	13.7
113.5	0.0191	13.8
118.3	0.0214	13.7
130.6	0.0286	13.8

Sinuosity 2.04

Inbank case

Slope: $0.5 * 10^{-3}$

Main Channel Cross-Section: Natural

Depth mm	Discharge m^3/s	Temperature ^{o}C
109.8	0.01135	10.4
111.49	0.01189	16.1
115.16	0.0132	15.0
120.3	0.0153	10.5
120.7	0.0156	14.4
124.2	0.01699	14.1
127.91	0.01873	10.3
130.7	0.02006	15.9
133.46	0.02102	14.2
135.66	0.02206	14.9
138.82	0.02342	10.3
140.08	0.0243	10.5
146.7	0.02778	10.4

APPENDIX I

STAGE-DISCHARGE DATA FROM THE S.E.R.C. FLUME SERIES B

(Continued)

Sinuosity 1.37

Overbank case

Smooth Floodplains

Slope: $0.996 * 10^{-3}$

Main Channel Cross-Section: Trapezoidal

Depth mm	Discharge m^3/s	Temperature ^{o} C
164.1	0.0824	11.5
165.88	0.08576	11.5
170.1	0.0975	11.4
175.67	0.1198	11.6
181.67	0.1494	14.6
192.05	0.2039	14.0
199.75	0.2496	12.8
207.96	0.302	12.2
208.28	0.303	14.5
221.8	0.399	14.1
227.65	0.440	13.2
233.3	0.485	14.4
235.0	0.494	11.0
240.49	0.555	12.3
252.8	0.658	12.3
264.8	0.766	12.3
277.97	0.878	12.3

APPENDIX I

STAGE-DISCHARGE DATA FROM THE S.E.R.C. FLUME SERIES B

(Continued)

Sinuosity 1.37

Overbank case

Smooth Floodplains

Slope: $0.996 * 10^{-3}$

Main Channel Cross-Section: Natural

Depth mm	Discharge m^3/s	Temperature ^{o}C
162.1	0.0605	15.9
175.9	0.1031	14.7
184.6	0.160	15.9
191.7	0.204	14.4
201.9	0.2674	16.0
207.2	0.3073	14.7
218.4	0.387	15.5
236.4	0.5396	14.9
249.0	0.6465	15.5
260.0	0.752	15.6
270.0	0.8587	15.7

APPENDIX I

STAGE-DISCHARGE DATA FROM THE S.E.R.C. FLUME SERIES B

(Continued)

Sinuosity 1.37

Overbank case

Fully Roughened Floodplains

Slope: $0.996 * 10^{-3}$

Main Channel Cross-Section: Natural

Depth mm	Discharge m^3/s	Temperature ^{o}C
153.7	0.0402	15.1
162.6	0.0544	14.5
169.3	0.0674	14.4
179.8	0.092	15.0
187.5	0.112	14.7
196.0	0.130	15.1
204.6	0.1544	14.8
212.2	0.1749	15.4
219.0	0.1985	13.8
233.7	0.2339	14.1
245.8	0.264	15.0
249.8	0.276	14.8
260.0	0.302	15.0
268.0	0.327	14.6
274.2	0.342	14.8
287.0	0.376	14.6
297.0	0.410	15.4
312.6	0.455	15.0

APPENDIX I

STAGE-DISCHARGE DATA FROM THE S.E.R.C. FLUME SERIES B

Sinuosity 1.37

(Continued)

Overbank case

Partly Roughened Floodplains

Slope: $0.996 * 10^{-3}$

Main Channel Cross-Section: Natural

Depth mm	Discharge m^3/s	Temperature ^{o}C
153.9	0.0416	12.2
164.8	0.0665	12.2
172.6	0.086	12.4
178.6	0.112	13.0
191.7	0.170	13.0
213.2	0.271	11.8
223.5	0.322	11.6
252.0	0.498	13.4
267.0	0.5694	13.0
284.0	0.6756	13.3
300.0	0.765	13.3

APPENDIX I

STAGE-DISCHARGE DATA FROM THE S.E.R.C. FLUME SERIES B

(Continued)

Sinuosity 1.37

Overbank case

Floodplain with Bridge Piers

Slope: $0.996 * 10^{-3}$

Main Channel Cross-Section: Natural

Depth mm	Discharge m^3/s	Temperature ^{o} C
155.0	0.0433	12.8
160.4	0.0543	12.8
173.6	0.0996	12.8
181.0	0.133	12.8
193.5	0.198	13.4
205.9	0.267	13.4
216.9	0.336	13.0
226.6	0.396	13.3
233.4	0.459	15.2
249.8	0.572	15.0
264.5	0.685	14.5
279.0	0.800	13.9
293.4	0.918	13.9

APPENDIX I

STAGE-DISCHARGE DATA FROM THE S.E.R.C. FLUME SERIES B

(Continued)

Sinuosity 1.37

Overbank case

Floodplain Width Reduced but Smooth

Slope: $0.996 * 10^{-3}$

Main Channel Cross-Section: Natural

Depth mm	Discharge m^3/s	Temperature ^{o} C
154.8	0.0387	14.0
163.51	0.05079	13.9
165.21	0.05766	14.4
168.64	0.06616	14.4
175.03	0.08538	14.1
183.91	0.1123	14.1
197.76	0.1612	14.4
204.76	0.1929	14.4
213.89	0.2283	14.3
214.16	0.2285	14.3
225.53	0.282	14.7
227.86	0.2903	15.4
246.55	0.380	15.6
259.45	0.473	15.3
277.52	0.5714	15.0

APPENDIX I

STAGE-DISCHARGE DATA FROM THE S.E.R.C. FLUME SERIES B

(Continued)

Sinuosity 2.04

Overbank case

Smooth Floodplain

Slope: $1.021 * 10^{-3}$

Main Channel Cross-Section: Natural

Depth mm	Discharge m^3/s	Temperature ^{o} C
165.14	0.0382	15.5
178.92	0.07693	10.3
183.58	0.09972	10.3
193.65	0.1421	12.7
200.61	0.1793	11.4
214.07	0.2528	12.9
225.21	0.3246	14.5
235.01	0.391	15.4
242.66	0.4452	15.3
256.86	0.5535	11.2
270.05	0.6614	11.6
284.5	0.7799	12.0
296.88	0.8813	13.2
302.82	0.9435	14.5

APPENDIX I

STAGE-DISCHARGE DATA FROM THE S.E.R.C. FLUME SERIES B

(Continued)

Sinuosity 2.04

Overbank case

Fully Roughened Floodplain

Slope: $1.021 * 10^{-3}$

Main Channel Cross-Section: Natural

Depth mm	Discharge m^3/s	Temperature ^{o} C
160.54	0.03254	16.6
165.5	0.037	16.7
175.02	0.0545	16.3
187.39	0.0836	16.3
197.19	0.108	16.1
200.85	0.1146	16.7
211.73	0.1439	16.9
221.75	0.1738	16.7
231.55	0.2011	16.3
247.4	0.2434	16.4
259.26	0.2785	16.5
272.21	0.3162	16.3
284.4	0.3494	16.5
296.3	0.3885	17.0
311.2	0.4333	16.4

APPENDIX I

STAGE-DISCHARGE DATA FROM THE S.E.R.C. FLUME SERIES B

(Continued)

Sinuosity 2.04

Overbank case

Floodplain with Bridge Piers

Slope: $1.021 * 10^{-3}$

Main Channel Cross-Section: Natural

Depth mm	Discharge m^3/s	Temperature ^{o} C
162.9	0.0353	15.7
171.3	0.0519	15.7
185.0	0.10064	15.7
190.98	0.1262	15.4
197.86	0.1578	15.3
200.65	0.168	15.8
210.65	0.2199	15.4
216.64	0.2525	15.7
229.81	0.3169	16.0
237.38	0.363	14.7
254.9	0.466	15.0
263.78	0.535	15.8
280.09	0.645	16.6
296.3	0.757	16.3

APPENDIX I

STAGE-DISCHARGE DATA FROM THE S.E.R.C. FLUME SERIES B (Continued)

Sinuosity 2.04

Overbank case

Floodplain Width Reduced but Smooth

Slope: $1.021 * 10^{-3}$

Main Channel Cross-Section: Natural

Depth mm	Discharge m^3/s	Temperature ^{o} C
164.84	0.03559	13.9
171.12	0.05023	14.3
179.6	0.07456	14.2
185.23	0.09496	13.8
195.66	0.13586	13.2
202.48	0.165	14.0
213.55	0.2205	13.6
221.65	0.2593	14.7
234.2	0.3279	14.1
244.55	0.3865	14.0
259.96	0.4855	13.3
264.95	0.534	14.5
288.42	0.6985	14.3
294.75	0.7506	13.4

APPENDIX I

STAGE-DISCHARGE DATA FROM THE S.E.R.C. FLUME SERIES B

(Continued)

Sinuosity 2.04

Overbank case

Walled Floodplain

Slope: $1.021 * 10^{-3}$

Main Channel Cross-Section: Natural

Depth mm	Discharge m^3/s	Temperature ^{o}C
170.3	0.03353	13.5
174.95	0.035	14.0
189.95	0.04065	14.0
202.6	0.0454	13.9
212.68	0.04945	13.7
232.44	0.05538	13.4
233.15	0.0566	13.6
242.35	0.06312	13.2

APPENDIX I

STAGE-DISCHARGE DATA FROM THE GLASGOW FLUME

(Continued)

Overbank case

Only Floodplain System

Slope: $1.0 * 10^{-3}$

Main Channel Cross-Section: Rectangular

Depth	Discharge	Temperature
mm	l/s	^{o} C
11.0	2.4	21.5
19.5	6.3	21.5
25.5	9.5	21.5
30.0	12.5	21.5
34.0	14.7	21.5
38.0	17.8	21.5
45.0	22.3	21.5
51.0	27.1	21.5
56.0	31.9	21.5
62.0	37.1	21.5

APPENDIX II

DATA FROM THE S.E.R.C. FLUME SERIES B

Total Main Channel Discharge In The Streamwise Direction

APPENDIX II

DATA FROM THE S.E.R.C. FLUME SERIES B

Total Main Channel Discharge In The Streamwise Direction (l/s)

Sinuosity 1.37 Trapezoidal Section Smooth Floodplains

Section Number	Stage 200.0mm	Stage 250.0 mm
1	76.0	121.0
2	84.0	139.0
3	87.0	143.0
4	86.0	140.0
5	77.0	129.0
6	70.0	107.0
7	68.0	103.0
8	67.0	98.0
9	66.0	98.0
10	67.0	102.0
11	66.0	102.0

Sinuosity 1.37 Natural Section Smooth Floodplains

Section Number	Stage 165.0 mm	Stage 200.0mm	Stage 250.0 mm
1	28.0	53.0	102.0
2	29.0	57.0	117.0
3	30.0	60.0	117.0
4	30.0	60.0	116.0
5	29.0	53.0	108.0
6	29.0	42.0	84.0
7	27.0	42.0	78.0
8	27.0	42.0	72.0
9	26.0	43.0	72.0
10	24.0	43.0	75.0
11	25.0	43.0	78.0

APPENDIX II

DATA FROM THE S.E.R.C. FLUME SERIES B

(Continued)

Total Main Channel Discharge In The Streamwise Direction

(l/s)

Sinuosity 1.37 Natural Section Fully Rough. Floodplains

Section Number	Stage 165.0 mm	Stage 200.0mm	Stage 250.0 mm
1	29.0	33.0	48.0
2	29.0	36.0	57.0
3	31.0	39.0	61.0
4	31.0	41.0	63.0
5	29.0	37.0	56.0
6	27.0	28.0	37.0
7	27.0	26.0	34.0
8	26.0	25.0	34.0
9	25.0	26.0	35.0
10	26.0	25.0	36.0
11	26.0	26.0	37.0

APPENDIX II

DATA FROM THE S.E.R.C. FLUME SERIES B

(Continued)

Total Main Channel Discharge In The Streamwise Direction

(l/s)

Sinuosity 2.04 Natural Section Smooth Floodplains

Section Number	Stage 165.0 mm	Stage 200.0mm
2	24.0	47.0
3	24.0	44.0
4	23.0	40.0
5	20.0	29.0
6	20.0	20.0
7	17.0	9.0
8	16.0	7.5
9	15.0	9.0
10	17.0	19.0
11	19.0	30.0
12	21.0	38.0
13	21.0	43.0
14	24.0	47.0

APPENDIX II

DATA FROM THE S.E.R.C. FLUME SERIES B

(Continued)

Total Main Channel Discharge In The Streamwise Direction (l/s)

Sinuosity 2.04 Natural Section Fully Rough. Floodplains

Section Number	Stage 165.0 mm	Stage 200.0mm
2	25.0	36.0
3	26.0	36.0
4	25.0	33.0
5	21.0	23.0
6	22.0	16.0
7	18.0	8.0
8	15.0	6.0
9	15.0	6.0
10	19.0	17.0
11	21.0	22.0
12	23.0	27.0
13	24.0	31.0
14	25.0	36.0

APPENDIX III

DATA FROM THE S.E.R.C. FLUME SERIES B

Main Channel Discharge In The Streamwise Direction Below Bankfull

APPENDIX III

DATA FROM THE S.E.R.C. FLUME SERIES B

Main Channel Discharge In The Streamwise Direction Below Bankfull

(l/s)

Sinuosity 1.37 Trapezoidal Section Smooth Floodplains

Section Number	Stage 200.0mm	Stage 250.0 mm
1	56.0	62.0
2	59.0	69.0
3	61.0	71.0
4	60.0	71.0
5	56.0	67.0
6	52.0	62.0
7	52.0	60.0
8	51.0	59.0
9	50.0	57.0
10	50.0	58.0
11	51.0	58.0

APPENDIX III

DATA FROM THE S.E.R.C. FLUME SERIES B

(Continued)

Main Channel Discharge In The Streamwise Direction Below Bankfull

(l/s)

Sinuosity 1.37 Natural Section Smooth Floodplains

Section Number	Stage 165.0 mm	Stage 200.0mm	Stage 250.0 mm
1	25.0	26.0	35.0
2	27.0	27.0	38.0
3	29.0	31.0	40.0
4	28.0	29.0	39.0
5	27.0	27.0	37.0
6	27.0	26.0	35.0
7	27.0	26.0	34.0
8	26.0	26.0	32.0
9	25.0	26.0	30.0
10	26.0	26.0	30.0
11	26.0	26.0	33.0

APPENDIX III

DATA FROM THE S.E.R.C. FLUME SERIES B

(Continued)

Main Channel Discharge In The Streamwise Direction Below Bankfull

(l/s)

Sinuosity 1.37 Natural Section Fully Rough. Floodplains

Section Number	Stage 165.0 mm	Stage 200.0mm	Stage 250.0 mm
1	25.0	17.0	18.0
2	27.0	18.0	20.0
3	29.0	21.0	24.0
4	27.0	21.0	23.0
5	26.0	20.0	22.0
6	26.0	18.0	21.0
7	26.0	17.0	20.0
8	25.0	17.0	20.0
9	25.0	16.0	19.0
10	25.0	16.0	20.0
11	25.0	16.0	20.0

APPENDIX III

DATA FROM THE S.E.R.C. FLUME SERIES B

(Continued)

Main Channel Discharge In The Streamwise Direction Below Bankfull (l/s)

Sinuosity 2.04 Natural Section Smooth Floodplains

Section Number	Stage 165.0 mm	Stage 200.0mm
2	18.0	24.0
3	18.0	23.0
4	18.0	22.0
5	15.0	16.0
6	15.0	13.0
7	13.0	8.0
8	14.0	7.0
9	12.0	7.0
10	13.0	11.0
11	14.0	14.0
12	15.0	18.0
13	16.0	20.0
14	18.0	24.0

APPENDIX III

DATA FROM THE S.E.R.C. FLUME SERIES B

(Continued)

Main Channel Discharge In The Streamwise Direction Below Bankfull

(l/s)

Sinuosity 2.04 Natural Section Fully Rough. Floodplains

Section Number	Stage 165.0 mm	Stage 200.0mm
2	20.0	20.0
3	20.0	20.0
4	19.0	19.0
5	16.0	14.0
6	16.0	11.0
7	14.0	6.0
8	13.0	6.0
9	13.0	6.0
10	14.0	11.0
11	15.0	12.0
12	17.0	16.0
13	20.0	17.0
14	20.0	20.0

APPENDIX IV

S.E.R.C. Flume Series B Sinuosity 1.374.

Momentum Equation Applied in X Direction in the Floodplain

APPEXDIX IV

S.E.R.C. FLUME SERIES B SINUOSITY 1.374

MOMENTUM EQUATION APPLIED IN X DIRECTION IN THE FLOODPLAIN

BLOCK No. : 1

SINUOSITY	CROSS-SECTION TYPE	FLOODPLAIN ROUGHNESS	STAGE mm	M_{11} NEWTONS	M_{12} NEWTONS	M_{13} NEWTONS	M_{14} NEWTONS	BODY WEIGHT NEWTONS	BOUND. SHEAR FORCE NEWTONS	APPARENT SHEAR FORCE NEWTONS
1.374	TRAPEZOIDAL	SMOOTH	200.0	52.0	37.2	4.0	5.3	6.0	6.0	-5.5
1.374	TRAPEZOIDAL	SMOOTH	250.0	234.0	191.8	16.1	23.8	12.0	12.0	-6.4
1.374	NATURAL	SMOOTH	165.0	6.1	3.7	1.4	0.5	1.8	1.8	-0.5
1.374	NATURAL	SMOOTH	200.0	50.7	38.9	3.5	5.0	5.7	5.2	-3.8
1.374	NATURAL	SMOOTH	250.0	222.0	186.0	13.3	22.0	12.0	12.0	-0.6
1.374	NATURAL	FULLY ROUGH.	165.0	2.6	1.1	0.87	0.33	1.8	1.8	-0.3
1.374	NATURAL	FULLY ROUGH.	200.0	21.6	13.3	1.9	4.0	6.0	6.0	-2.4
1.374	NATURAL	FULLY ROUGH.	250.0	44.8	33.1	1.9	6.8	12.0	12.0	-1.7

APPEXDIX IV

S.E.R.C. FLUME SERIES B SINUOSITY 1.374

MOMENTUM EQUATION APPLIED IN X DIRECTION IN THE FLOODPLAIN

BLOCK No. : 2

SINUOSITY	CROSS-SECTION TYPE	FLOODPLAIN ROUGHNESS	STAGE mm	M_{21} NEWTONS	M_{22} NEWTONS	M_{23} NEWTONS	M_{24} NEWTONS	BODY WEIGHT NEWTONS	BOUND. SHEAR FORCE NEWTONS	APPARENT SHEAR FORCE NEWTONS
1.374	TRAPEZOIDAL	SMOOTH	200.0	37.2	22.6	12.0	4.0	2.9	2.9	+1.4
1.374	TRAPEZOIDAL	SMOOTH	250.0	191.7	127.7	47.2	17.5	6.0	6.0	+0.7
1.374	NATURAL	SMOOTH	165.0	3.7	2.9	0.2	0.3	0.9	0.9	-0.3
1.374	NATURAL	SMOOTH	200.0	38.9	24.8	11.3	2.8	2.84	2.34	-0.5
1.374	NATURAL	SMOOTH	250.0	186.1	132.5	38.6	16.6	6.0	6.0	+1.6
1.374	NATURAL	FULLY ROUGH.	165.0	1.1	1.0	0.2	0.24	0.9	0.9	+0.3
1.374	NATURAL	FULLY ROUGH.	200.0	13.1	4.6	4.2	1.9	2.9	2.9	-2.4
1.374	NATURAL	FULLY ROUGH.	250.0	33.1	19.0	19.0	3.5	6.0	6.0	+0.3

APPEXDIXIV

S.E.R.C. FLUME SERIES B SINUOSITY 1.374

MOMENTUM EQUATION APPLIED IN X DIRECTION IN THE FLOODPLAIN

BLOCK No. : 3

SINUOSITY	CROSS-SECTION TYPE	FLOODPLAIN ROUGHNESS	STAGE mm	M_{31} NEWTONS	M_{32} NEWTONS	M_{33} NEWTONS	M_{34} NEWTONS	BODY WEIGHT NEWTONS	BOUND. SHEAR FORCE NEWTONS	APPARENT SHEAR FORCE NEWTONS
1.374	TRAPEZOIDAL	SMOOTH	200.0	22.6	11.6	5.5	7.9	3.5	3.5	+2.4
1.374	TRAPEZOIDAL	SMOOTH	250.0	127.7	74.4	19.3	32.7	7.0	7.0	-1.3
1.374	NATURAL	SMOOTH	165.0	2.9	0.23	0.3	1.8	1.0	1.0	-0.57
1.374	NATURAL	SMOOTH	200.0	24.8	12.4	5.3	8.5	3.5	2.8	+0.7
1.374	NATURAL	SMOOTH	250.0	132.5	68.0	26.0	37.0	7.0	7.0	-1.5
1.374	NATURAL	FULLY ROUGH.	165.0	0.98	0.0	0.3	1.2	1.0	1.0	+0.52
1.374	NATURAL	FULLY ROUGH.	200.0	4.6	0.5	1.5	3.8	3.5	3.5	+1.2
1.374	NATURAL	FULLY ROUGH.	250.0	19.0	4.3	4.6	7.9	7.0	7.0	-2.2

APPEXDIXIV

S.E.R.C. FLUME SERIES B SINUOSITY 1.374

MOMENTUM EQUATION APPLIED IN X DIRECTION IN THE FLOODPLAIN

BLOCK No. : 4

SINUOSITY	CROSS-SECTION TYPE	FLOODPLAIN ROUGHNESS	STAGE mm	M_{41} NEWTONS	M_{42} NEWTONS	M_{43} NEWTONS	M_{44} NEWTONS	BODY WEIGHT NEWTONS	BOUND. SHEAR FORCE NEWTONS	APPARENT SHEAR FORCE NEWTONS
1.374	TRAPEZOIDAL	SMOOTH	200.0	11.6	30.0	8.4	9.1	3.4	3.4	+0.9
1.374	TRAPEZOIDAL	SMOOTH	250.0	74.4	132.6	25.3	30.6	6.8	6.8	+2.3
1.374	NATURAL	SMOOTH	165.0	0.23	3.95	0.5	2.4	1.0	1.0	+0.82
1.374	NATURAL	SMOOTH	200.0	12.4	28.0	6.9	8.2	3.4	3.1	+0.2
1.374	NATURAL	SMOOTH	250.0	74.0	125.6	24.3	31.9	6.9	6.9	-4.6
1.374	NATURAL	FULLY ROUGH.	165.0	0.0	1.95	0.3	1.9	1.0	1.0	-0.25
1.374	NATURAL	FULLY ROUGH.	200.0	0.5	10.8	3.0	7.2	3.5	3.5	+0.10
1.374	NATURAL	FULLY ROUGH.	250.0	4.3	24.7	6.0	13.3	7.0	7.0	+1.1

APPEXDIX IV

S.E.R.C. FLUME SERIES B SINUOSITY 1.374

MOMENTUM EQUATION APPLIED IN X DIRECTION IN THE FLOODPLAIN

BLOCK No. : 5

SINUOSITY	CROSS-SECTION TYPE	FLOODPLAIN ROUGHNESS	STAGE mm	M_{S1} NEWTONS	M_{S2} NEWTONS	M_{S3} NEWTONS	M_{S4} NEWTONS	BODY WEIGHT NEWTONS	BOUND. SHEAR FORCE NEWTONS	APPARENT SHEAR FORCE NEWTONS
1.374	TRAPEZOIDAL	SMOOTH	200.0	30.0	44.7	15.3	7.3	2.8	2.8	-7.9
1.374	TRAPEZOIDAL	SMOOTH	250.0	132.6	203.3	57.9	22.2	5.6	5.6	-9.4
1.374	NATURAL	SMOOTH	165.0	3.95	4.8	0.2	0.8	0.9	0.9	-1.07
1.374	NATURAL	SMOOTH	200.0	28.0	43.8	13.8	5.9	2.8	3.1	-3.6
1.374	NATURAL	SMOOTH	250.0	125.6	185.0	45.2	22.0	5.6	5.6	-7.8
1.374	NATURAL	FULLY ROUGH.	165.0	1.95	1.97	0.2	0.8	0.9	0.9	-0.98
1.374	NATURAL	FULLY ROUGH.	200.0	10.8	20.0	3.8	3.9	2.9	2.9	+1.5
1.374	NATURAL	FULLY ROUGH.	250.0	24.7	38.2	6.4	5.4	5.9	5.9	+1.7

APPEXDIX IV

S.E.R.C. FLUME SERIES B SINUOSITY 1.374

MOMENTUM EQUATION APPLIED IN X DIRECTION IN THE FLOODPLAIN

BLOCK No. : 6

SINUOSITY	CROSS-SECTION TYPE	FLOODPLAIN ROUGHNESS	STAGE mm	M_{61} NEWTONS	M_{62} NEWTONS	M_{63} NEWTONS	M_{64} NEWTONS	BODY WEIGHT NEWTONS	BOUND. SHEAR FORCE NEWTONS	APPARENT SHEAR FORCE NEWTONS
1.374	TRAPEZOIDAL	SMOOTH	200.0	44.7	52.0	2.6	6.7	6.0	6.0	-2.0
1.374	TRAPEZOIDAL	SMOOTH	250.0	203.3	234.0	13.3	22.9	12.0	12.0	-5.5
1.374	NATURAL	SMOOTH	165.0	4.8	6.1	0.0	0.8	1.8	1.8	-0.5
1.374	NATURAL	SMOOTH	200.0	43.8	50.7	3.0	5.5	5.8	6.2	-1.2
1.374	NATURAL	SMOOTH	250.0	185.0	222.0	14.2	25.3	12.0	12.0	-2.5
1.374	NATURAL	FULLY ROUGH.	165.0	1.97	2.6	0	0.4	1.8	1.8	+0.2
1.374	NATURAL	FULLY ROUGH.	200.0	20.0	21.6	0.3	1.4	6.0	6.0	-0.1
1.374	NATURAL	FULLY ROUGH.	250.0	38.2	44.8	1.5	4.9	12.0	12.0	+0.2

APPENDIX V

The S.E.R.C. Flume Series B Sinuosity 1.374.

Momentum Equation Applied in The Y Direction on the Floodplain

APPEXDIX V

S.E.R.C. FLUME SERIES B SINUOSITY 1.374

MOMENTUM EQUATION APPLIED IN Y DIRECTION IN THE FLOODPLAIN

BLOCK No. : 1, 2, AND 3.

CROSS-SECTION TYPE	FLOODPLAIN ROUGHNESS	STAGE mm	BLOCK 1			BLOCK 2			BLOCK 3		
			M_{15} NEWTONS	M_{16} NEWTONS	$ASFY_1$ NEWTONS	M_{25} NEWTONS	M_{26} NEWTONS	$ASFY_2$ NEWTONS	M_{35} NEWTONS	M_{36} NEWTONS	$ASFY_3$ NEWTONS
TRAPEZOIDAL	SMOOTH	200.0	4.5	3.5	+1.0	6.9	6.7	+0.2	5.9	5.6	+0.3
TRAPEZOIDAL	SMOOTH	250.0	17.3	16.9	+0.4	27.2	30.6	-3.4	22.8	26.7	-3.9
NATURAL	SMOOTH	165.0	0.8	0.6	+0.2	0.1	0.5	-0.4	0.4	1.0	-0.6
NATURAL	SMOOTH	200.0	3.8	3.5	+0.3	6.7	4.9	+1.8	5.8	6.1	-0.3
NATURAL	SMOOTH	250.0	14.3	16.0	-1.7	24.0	28.7	-4.8	25.4	26.3	-0.9
NATURAL	FULLY ROUGH.	165.0	0.54	0.43	+0.11	0.1	0.4	-0.3	0.4	0.8	-0.4
NATURAL	FULLY ROUGH.	200.0	2.5	2.1	+0.4	2.4	3.2	-0.8	1.6	2.4	-0.8
NATURAL	FULLY ROUGH.	250.0	3.7	4.3	-0.6	4.3	6.1	-1.8	4.9	5.8	-0.9

APPEXDIX V

S.E.R.C. FLUME SERIES B SINUOSITY 1.374

MOMENTUM EQUATION APPLIED IN Y DIRECTION IN THE FLOODPLAIN

BLOCK No. : 4, 5 AND 6.

CROSS-SECTION TYPE	FLOODPLAIN ROUGHNESS	STAGE mm	BLOCK 4			BLOCK 5			BLOCK 6		
			M_{45} NEWTONS	M_{46} NEWTONS	$ASFY_4$ NEWTONS	M_{55} NEWTONS	M_{56} NEWTONS	$ASFY_5$ NEWTONS	M_{65} NEWTONS	M_{66} NEWTONS	$ASFY_6$ NEWTONS
TRAPEZOIDAL	SMOOTH	200.0	8.8	7.1	-1.7	8.8	12.7	+3.9	2.7	4.3	+1.6
TRAPEZOIDAL	SMOOTH	250.0	26.7	22.7	-4.0	33.4	38.5	+5.1	14.0	17.1	+3.0
NATURAL	SMOOTH	165.0	0.6	1.7	+1.1	0.2	1.1	+1.1	0.0	0.5	+0.5
NATURAL	SMOOTH	200.0	7.3	6.4	-0.9	8.2	10.5	+2.3	3.2	4.4	+1.2
NATURAL	SMOOTH	250.0	25.3	25.5	+0.2	30.1	37.9	+7.8	15.4	18.3	+2.9
NATURAL	FULLY ROUGH.	165.0	0.3	1.5	+1.2	0.1	1.1	+1.0	0.0	0.1	0.1
NATURAL	FULLY ROUGH.	200.0	3.3	5.7	+2.4	2.2	6.7	+4.5	0.3	1.3	+1.0
NATURAL	FULLY ROUGH.	250.0	6.7	10.2	+3.5	3.7	9.4	+5.7	1.6	3.6	+2.0

APPENDIX VI

Momentum Equation Applied in The S Direction in the Meandering Channel of The S.E.R.C. Flume Series B with Sinuosity 1.374

APPENDIX VI

MOMENTUM EQUATION APPLIED IN S DIRECTION IN THE MEANDERING CHANNEL
S.E.R.C. SERIES B. SINUOSITY 1.37. SMOOTH FLOODPLAINS.

BLOCK No. 7

STAGE mm	M_{71} NEWTONS	M_{72} NEWTONS	M_{73} NEWTONS	M_{74} NEWTONS	$2\rho\frac{UV}{R}Vol$	BW_7 NEWTONS	BSF_7 NEWTONS	PF_{71} NEWTONS	PF_{72} NEWTONS	$ASFS_7$ NEWTONS
140.0	14.8	13.9			1.12	-6.94	1.58	41.0	34.5	-6.94
165.0	9.4	8.7	1.5	3.25	1.8	-6.32	0.94	66.0	59.0	+3.11
200.0	25.1	12.1	6.4	10.8	9.2	-5.17	1.1	107.8	102.4	+1.47

BLOCK No. 8

STAGE mm	M_{81} NEWTONS	M_{82} NEWTONS	M_{83} NEWTONS	M_{84} NEWTONS	$2\rho\frac{UV}{R}Vol$	BW_8 NEWTONS	BSF_8 NEWTONS	PF_8 NEWTONS	PF_8 NEWTONS	$ASFS_8$ NEWTONS
140.0	13.9	13.9				+1.27	1.27			+1.27
165.0	8.7	7.9	0.6	3.0		1.69	0.72			+0.63
200.0	12.1	12.6	5.7	12.1		2.5	0.8			+5.2

BLOCK No. 9

STAGE mm	M_{91} NEWTONS	M_{92} NEWTONS	M_{93} NEWTONS	M_{94} NEWTONS	$2\rho\frac{UV}{R}Vol$	BW_9 NEWTONS	BSF_9 NEWTONS	PF_{91} NEWTONS	PF_{92} NEWTONS	$ASFS_9$ NEWTONS
140.0	13.9	14.8			0.95	+8.1	1.65	34.5	41.0	+8.1
165.0	7.9	9.4	2.4	1.0	0.7	+8.7	1.0	59.0	66.0	-1.32
200.0	12.1	25.1	11.0	7.3	9.2	+9.97	1.0	102.4	107.8	-3.47